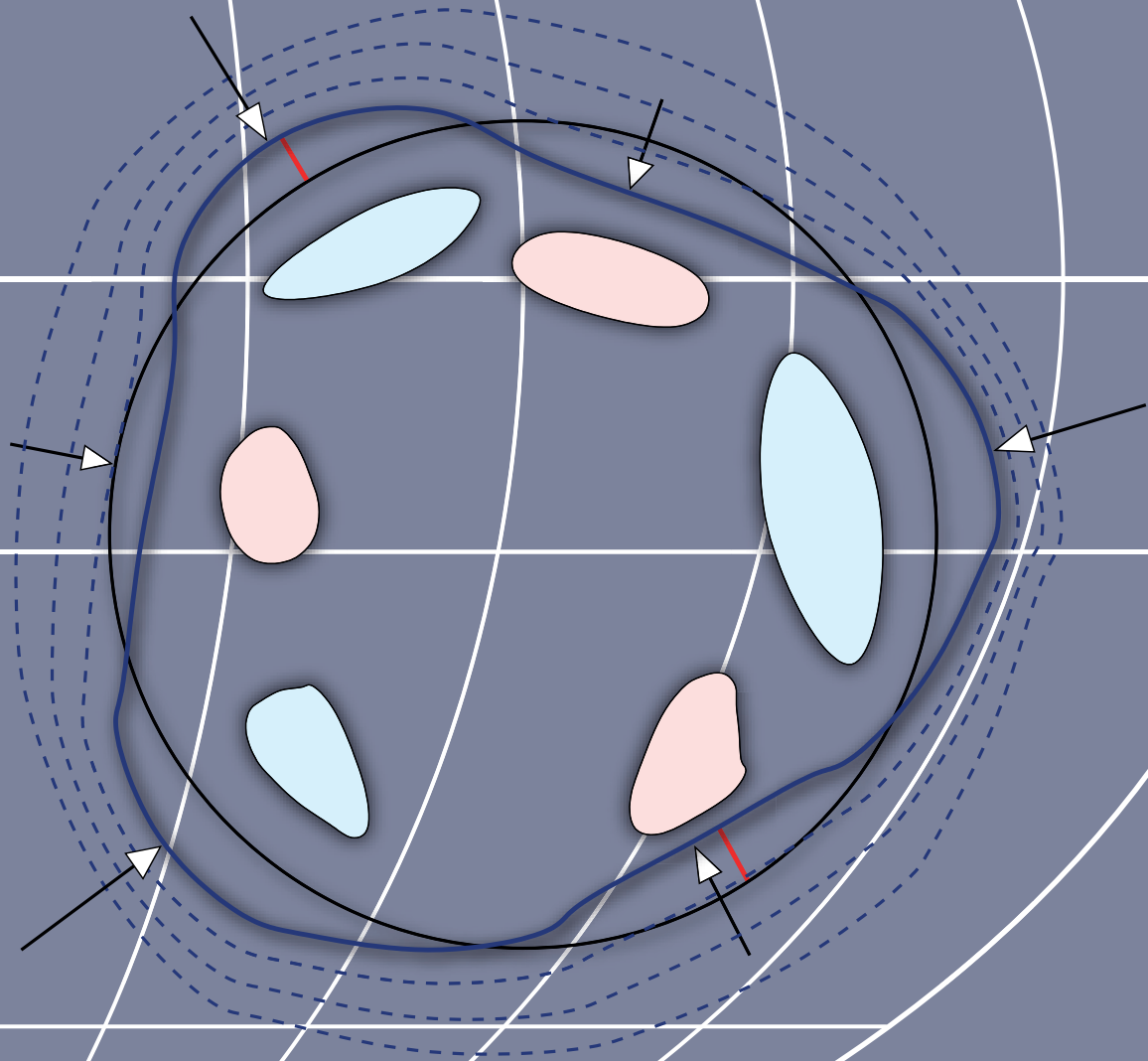


Martin Vermeer

PHYSICAL GEODESY



Aalto University publication series

SCIENCE + TECHNOLOGY 2/2020

Physical geodesy

Martin Vermeer

**Aalto University
School of Engineering
Department of Built Environment**

Aalto University publication series
SCIENCE + TECHNOLOGY 2/2020

© 2020 Martin Vermeer

ISBN (pdf) 978-952-60-8940-9

ISSN 1799-490X (pdf)

<http://urn.fi/URN:ISBN:978-952-60-8940-9>

Graphic design: Cover: Tarja Paalanen

Helsinki 2020

Finland

Author

Martin Vermeer

Name of the publication

Physical geodesy

Publisher School of Engineering**Unit** Department of Built Environment**Series** Aalto University publication series SCIENCE + TECHNOLOGY 2/2020**Field of research** Geodesy**Language** English**Abstract**

Physical geodesy studies the large-scale figure and gravity field of the Earth, which are closely related. Our understanding of the gravity field is based on Newton's theory of gravitation. We present field theory, with partial differential equations describing the behaviour of the field throughout space. Techniques for solving these equations using boundary conditions on the Earth's surface are explained. A central concept is the geopotential.

The figure of the Earth is approximated by an ellipsoid of revolution, after which the precise figure is described by small deviations from this ellipsoid. Vertical reference systems are discussed in this context. Extending the approach to the Earth's gravity field yields small difference quantities, such as the disturbing potential and gravity anomalies.

Approaches to modelling the gravity field explained are spectral development of the field using spherical harmonics, the Stokes equation, numerical techniques based on the Fast Fourier Transform, the remove-restore technique, and least-squares collocation. Gravity measurement techniques are discussed, as are the multiple links with geophysics, such as terrain effects, isostasy, mean sea level and the sea level equation, and the tides.

Keywords figure of the Earth, gravity field, geopotential, reference ellipsoid, normal field, disturbing potential, gravity anomaly, geoid, height system, spherical harmonics, Stokes equation, remove-restore, least-squares collocation, gravimetry, isostasy, mean sea level, tides

ISBN (pdf) 978-952-60-8940-9

ISSN (PDF) 1799-490X

Location of publisher Helsinki

Location of printing Helsinki

Year 2020

Pages 516

urn <http://urn.fi/URN:ISBN:978-952-60-8940-9>

Preface

This book aims to present an overview of the current state of the study of the Earth's gravity field and those parts of geophysics closely related to it, especially geodynamics, the study of the changing Earth. It has grown out of over two decades of teaching at Helsinki's two universities: the Helsinki University of Technology — today absorbed into Aalto University — and the University of Helsinki. As such, it presents a somewhat Fennoscandian perspective on a very global subject. In addition, the author's own research on gravimetric geoid determination helped shape the presentation. While there exist excellent textbooks on all the different parts of what is presented here, I may still hope that this text will find a niche to fill.

Helsinki, 27th March 2020,

Martin Vermeer

Acknowledgements

Thanks are due to the many students and colleagues, both in academia and at the Finnish Geodetic Institute, who have given useful comments and corrections over the course of many years of lecturing both at the University of Helsinki and at the Helsinki University of Technology, today Aalto University.

Special thanks are due to the foreign students at Aalto University, who forced me during recent years to provide an English version of this text. The translation work also prompted a basic revision of the Finnish text, which was long overdue as parts were written in the 1990s before the author had had the benefit of pedagogical training. Thanks are thus also due to Aalto University's pedagogical training programme.

Olivier Francis is gratefully acknowledged for contributing figure 11.8.



































The English language was competently checked by the Finnish Translation Agency Aakkosto Oy. Laura Mure and Matti Yrjölä helped with the practicalities of publishing.







This content is licenced under the *Creative Commons Attribution 4.0 International* (CC BY 4.0) licence, except as noted in the text or otherwise apparent.



Contents

Chapters

| | | |
|--|---|-----|
|   | 1. Fundamentals of the theory of gravitation | 1 |
|   | 2. The Laplace equation and its solutions | 41 |
|   | 3. Legendre functions and spherical harmonics | 55 |
|   | 4. The normal gravity field | 85 |
|   | 5. Anomalous quantities of the gravity field | 109 |
|   | 6. Geophysical reductions | 127 |
|   | 7. Vertical reference systems | 161 |
|   | 8. The Stokes equation and other integral equations | 189 |
|   | 9. Spectral techniques, FFT | 229 |
|   | 10. Statistical methods | 251 |
|   | 11. Gravimetric measurement devices | 295 |
|   | 12. The geoid, mean sea level, and sea-surface topography | 323 |
|   | 13. Satellite altimetry and satellite gravity missions | 343 |
|   | 14. Tides, the atmosphere, and Earth crustal movements | 377 |
|   | 15. Earth gravity field research | 391 |
|   | A. Field theory and vector calculus — core knowledge | 395 |
|   | B. Function spaces | 413 |

| | | |
|---|---|-------------|
|   | C. Why does FFT work? | 429 |
|   | D. Helmert condensation | 433 |
|   | E. The Laplace equation in spherical co-ordinates | 443 |
| Preface | | i |
| List of Tables | | xii |
| List of Figures | | xiii |
| Acronyms | | xix |
| 1. Fundamentals of the theory of gravitation | | 1 |
| 1.1 | General | 1 |
| 1.2 | Gravitation between two masses | 2 |
| 1.3 | The potential of a point mass | 5 |
| 1.4 | Potential of a spherical shell | 6 |
| 1.5 | Computing the attraction from the potential | 9 |
| 1.6 | Potential of a solid body | 11 |
| 1.7 | Example: The potential of a line of mass | 14 |
| 1.8 | Laplace and Poisson equations | 16 |
| 1.9 | Gauge invariance | 17 |
| 1.10 | Single mass-density layer | 18 |
| 1.11 | Double mass-density layer | 20 |
| 1.12 | The Gauss integral theorem | 22 |
| 1.13 | Green's theorems | 28 |
| 1.14 | The Chasles theorem | 33 |
| 1.15 | Boundary-value problems | 35 |
| | Self-test questions | 36 |



| | |
|--|-----------|
| Exercise 1 – 1: Core of the Earth | 37 |
| Exercise 1 – 2: Atmosphere | 38 |
| Exercise 1 – 3: The Gauss theorem | 38 |
| 2. The Laplace equation and its solutions | 41 |
| 2.1 The nature of the Laplace equation | 41 |
| 2.2 The Laplace equation in rectangular co-ordinates . . . | 43 |
| 2.3 The Laplace equation in polar co-ordinates | 48 |
| 2.4 Spherical, geodetic, ellipsoidal co-ordinates | 50 |
| 2.5 The Laplace equation in spherical co-ordinates | 52 |
| 2.6 Dependence on height | 54 |
| 3. Legendre functions and spherical harmonics | 55 |
| 3.1 Legendre functions | 55 |
| 3.2 Symmetry properties of spherical harmonics | 62 |
| 3.3 Orthogonality of Legendre functions | 64 |
| 3.4 Low-degree spherical harmonics | 66 |
| 3.5 Splitting a function into degree constituents | 68 |
| 3.6 Spectral representations of various quantities | 70 |
| 3.7 Often-used spherical-harmonic expansions | 73 |
| 3.8 Ellipsoidal harmonics | 75 |
| Self-test questions | 79 |
| Exercise 3 – 1: Attenuation with height of a spherical-harmonic expansion | 80 |
| Exercise 3 – 2: Symmetries of spherical harmonics | 81 |
| Exercise 3 – 3: Algebraic-sign domains of spherical harmonics | 83 |
| Exercise 3 – 4: Escape velocity | 83 |



| | |
|--|------------|
| 4. The normal gravity field | 85 |
| 4.1 The basic idea of a normal field | 85 |
| 4.2 The centrifugal force and its potential | 87 |
| 4.3 Level surfaces and plumb lines | 89 |
| 4.4 Natural co-ordinates | 94 |
| 4.5 The normal potential in ellipsoidal co-ordinates | 95 |
| 4.6 Normal gravity on the reference ellipsoid | 97 |
| 4.7 Numerical values and calculation formulas | 98 |
| 4.8 The normal potential as a spherical-harmonic expansion | 102 |
| 4.9 The disturbing potential | 103 |
| Self-test questions | 105 |
| Exercise 4–1: The Somigliana–Pizzetti equation | 106 |
| Exercise 4–2: Centrifugal force | 107 |
| 5. Anomalous quantities of the gravity field | 109 |
| 5.1 Disturbing potential, geoid height, deflections of the plumb line | 109 |
| 5.2 Gravity disturbances | 113 |
| 5.3 Gravity anomalies | 115 |
| 5.4 Units used for gravity anomalies | 117 |
| 5.5 The boundary-value problem of physical geodesy | 118 |
| 5.6 The telluroid mapping and the “quasi-geoid” | 121 |
| 5.7 Free-air anomalies | 122 |
| Self-test questions | 125 |
| Exercise 5–1: The spectrum of gravity anomalies | 125 |
| Exercise 5–2: Deflections of the plumb line and geoid tilt | 125 |
| Exercise 5–3: Gravity anomaly, geoid height | 126 |



| | |
|--|------------|
| 6. Geophysical reductions | 127 |
| 6.1 General | 127 |
| 6.2 Bouguer anomalies | 128 |
| 6.3 Terrain effect and terrain correction | 132 |
| 6.4 Spherical Bouguer anomalies | 138 |
| 6.5 Helmert condensation | 140 |
| 6.6 Isostasy | 142 |
| 6.7 Isostatic reductions | 150 |
| 6.8 The “isostatic geoid” | 152 |
| Self-test questions | 157 |
| Exercise 6 – 1: Gravity anomaly | 157 |
| Exercise 6 – 2: Bouguer reduction | 158 |
| Exercise 6 – 3: Terrain correction and Bouguer reduction . . . | 158 |
| Exercise 6 – 4: Isostasy | 159 |
| 7. Vertical reference systems | 161 |
| 7.1 Levelling, orthometric heights and the geoid | 161 |
| 7.2 Orthometric heights | 163 |
| 7.3 Normal heights | 166 |
| 7.4 Difference between geoid height and height anomaly . | 173 |
| 7.5 Difference between orthometric and normal heights . . | 176 |
| 7.6 Calculating orthometric heights precisely | 176 |
| 7.7 Calculating normal heights precisely | 179 |
| 7.8 Calculation example for heights | 180 |
| 7.9 Orthometric and normal corrections | 181 |
| 7.10 A vision for the future: relativistic levelling | 184 |
| Self-test questions | 186 |
| Exercise 7 – 1: Calculating orthometric heights | 187 |



| | |
|--|------------|
| Exercise 7–2: Calculating normal heights | 187 |
| Exercise 7–3: Difference between orthometric and normal height | 187 |
| 8. The Stokes equation and other integral equations | 189 |
| 8.1 The Stokes equation and the Stokes integral kernel . . . | 189 |
| 8.2 Example: The Stokes equation in polar co-ordinates . . | 193 |
| 8.3 Plumb-line deflections and Vening Meinesz equations . | 198 |
| 8.4 The Poisson integral equation | 199 |
| 8.5 Gravity anomalies in the exterior space | 202 |
| 8.6 The vertical gradient of the gravity anomaly | 204 |
| 8.7 Gravity reductions in geoid determination | 209 |
| 8.8 The remove–restore method | 215 |
| 8.9 Kernel modification | 216 |
| 8.10 Advanced kernel modifications | 220 |
| 8.11 Block integration | 222 |
| 8.12 Effect of the local zone | 223 |
| Self-test questions | 225 |
| Exercise 8–1: The Stokes equation | 226 |
| 9. Spectral techniques, FFT | 229 |
| 9.1 The Stokes theorem as a convolution | 229 |
| 9.2 Integration by FFT | 232 |
| 9.3 Solution in latitude and longitude | 234 |
| 9.4 Bordering and tapering of the data area | 241 |
| 9.5 Computing a geoid model with FFT | 244 |
| 9.6 Use of FFT in other contexts | 245 |
| 9.7 Computing terrain corrections with FFT | 247 |
| Self-test questions | 250 |



| | |
|--|------------|
| 10. Statistical methods | 251 |
| 10.1 The role of uncertainty in geophysics | 251 |
| 10.2 Linear functionals | 252 |
| 10.3 Statistics on the Earth's surface | 253 |
| 10.4 The covariance function of the gravity field | 256 |
| 10.5 Least-squares collocation | 258 |
| 10.6 Prediction of gravity anomalies | 270 |
| 10.7 Covariance function and degree variances | 273 |
| 10.8 Propagation of covariances | 276 |
| 10.9 Global covariance functions | 282 |
| 10.10 Collocation and the spectral viewpoint | 283 |
| Self-test questions | 287 |
| Exercise 10–1: Variance of prediction | 288 |
| Exercise 10–2: Hirvonen's covariance equation and prediction | 289 |
| Exercise 10–3: Predicting gravity anomalies | 290 |
| Exercise 10–4: Predicting gravity anomalies (2) | 291 |
| Exercise 10–5: Propagation of covariances | 291 |
| Exercise 10–6: Kaula's rule for gravity gradients | 292 |
| Exercise 10–7: Underground mass points | 293 |
| 11. Gravimetric measurement devices | 295 |
| 11.1 History | 295 |
| 11.2 The relative or spring gravimeter | 297 |
| 11.3 The absolute or ballistic gravimeter | 304 |
| 11.4 Network hierarchy in gravimetry | 309 |
| 11.5 The superconducting gravimeter | 310 |
| 11.6 Atmospheric influence on gravity measurement | 312 |
| 11.7 Airborne gravimetry and GNSS | 314 |



| | | |
|------------|--|------------|
| 11.8 | Measuring the gravity gradient | 317 |
| | Self-test questions | 319 |
| | Exercise 11 – 1: Absolute gravimeter | 320 |
| | Exercise 11 – 2: Spring gravimeter | 321 |
| | Exercise 11 – 3: Air pressure and gravity | 322 |
| 12. | The geoid, mean sea level, and sea-surface topography | 323 |
| 12.1 | Basic concepts | 323 |
| 12.2 | Geoids and national height datums | 325 |
| 12.3 | The geoid and post-glacial land uplift | 327 |
| 12.4 | Methods for determining the sea-surface topography . | 331 |
| 12.5 | Global sea-surface topography and heat transport . . . | 331 |
| 12.6 | The global behaviour of the sea level | 334 |
| 12.7 | The sea-level equation | 336 |
| | Self-test questions | 341 |
| | Exercise 12 – 1: Coriolis force, ocean current | 342 |
| | Exercise 12 – 2: Land subsidence and the mechanism of land uplift | 342 |
| 13. | Satellite altimetry and satellite gravity missions | 343 |
| 13.1 | Satellite altimetry | 343 |
| 13.2 | Crossover adjustment | 348 |
| 13.3 | Choice of satellite orbit | 357 |
| 13.4 | In-flight calibration | 364 |
| 13.5 | Retracking | 365 |
| 13.6 | Oceanographic research using satellite altimetry | 367 |
| 13.7 | Satellite gravity missions | 369 |
| | Self-test questions | 374 |
| | Exercise 13 – 1: Altimetry, crossover adjustment | 375 |



| | |
|---|------------|
| Exercise 13–2: Satellite orbit | 376 |
| Exercise 13–3: Kepler’s third law | 376 |
| 14. Tides, the atmosphere, and Earth crustal movements | 377 |
| 14.1 The theoretical tide | 377 |
| 14.2 Deformation caused by the tidal force | 382 |
| 14.3 The permanent part of the tide | 385 |
| 14.4 Tidal corrections between height systems | 387 |
| 14.5 Loading of the Earth’s crust by sea and atmosphere | 388 |
| Self-test questions | 389 |
| Exercise 14–1: Tide | 390 |
| 15. Earth gravity field research | 391 |
| 15.1 Internationally | 391 |
| 15.2 Europe | 392 |
| 15.3 The Nordic countries | 393 |
| 15.4 Finland | 393 |
| 15.5 Textbooks | 394 |
| A. Field theory and vector calculus — core knowledge | 395 |
| A.1 Vector calculus | 395 |
| A.2 Scalar and vector fields | 399 |
| A.3 Integrals | 406 |
| A.4 The continuity of matter | 411 |
| B. Function spaces | 413 |
| B.1 An abstract vector space | 413 |
| B.2 The Fourier function space | 414 |
| B.3 Sturm–Liouville differential equations | 418 |
| B.4 Legendre polynomials | 424 |



| | | |
|-----------|---|------------|
| B.5 | Spherical harmonics | 424 |
| | Self-test questions | 427 |
| | Exercise B–1: Orthonormality of the Fourier basis functions . | 427 |
| C. | Why does FFT work? | 429 |
| D. | Helmert condensation | 433 |
| D.1 | The exterior potential of the topography | 434 |
| D.2 | The interior potential of the topography | 435 |
| D.3 | The exterior potential of the condensation layer | 436 |
| D.4 | Total potential of Helmert condensation | 437 |
| D.5 | The dipole method | 440 |
| E. | The Laplace equation in spherical co-ordinates | 443 |
| E.1 | Derivation | 443 |
| E.2 | Solution | 446 |
| | Bibliography | 451 |
| | Index | 469 |

List of Tables

| | | |
|-----|---|----|
| 3.1 | Legendre polynomials | 56 |
| 3.2 | Associated Legendre functions | 58 |
| 3.3 | Semi-wavelengths for different degrees and orders | 61 |
| 3.4 | Plotting a surface spherical-harmonic map | 64 |
| 3.5 | EGM96 coefficients and mean errors | 75 |



| | | |
|------|---|-----|
| 3.6 | Legendre functions of the second kind | 78 |
| 4.1 | GRS80 normal potential spherical-harmonic coefficients . | 103 |
| 5.1 | Orders of magnitude of gravity variations | 119 |
| 8.1 | Stokes equation in two dimensions, octave code | 197 |
| 8.2 | Derivation of the kernel for the vertical gradient of gravity anomaly | 206 |
| 13.1 | Altimetric satellites through the ages | 344 |
| 13.2 | Calculating the height of a satellite from its period | 364 |
| 14.1 | The various periods in the theoretical tide | 381 |

List of Figures

| | | |
|------|--|----|
| 1.1 | Gravitation is universal | 3 |
| 1.2 | A thin spherical shell consists of rings | 7 |
| 1.3 | Dependence of potential and attraction on distance. | 9 |
| 1.4 | A double mass-density layer | 20 |
| 1.5 | A graphical explanation of the Gauss integral theorem . . | 23 |
| 1.6 | A little rectangular box | 25 |
| 1.7 | Eight-unit cube | 27 |
| 1.8 | Green's third theorem for an exterior point | 30 |
| 1.9 | Green's third theorem for an interior point | 31 |
| 1.10 | Green's third theorem for the space external to a body . . | 32 |
| 1.11 | Iron ore body | 39 |
| 2.1 | Attenuation of the gravitational field with height | 47 |
| 2.2 | Vertically shifting the potential field | 47 |



| | | |
|-----|---|-----|
| 2.3 | Definition of spherical co-ordinates | 51 |
| 2.4 | Definition of geodetic co-ordinates | 52 |
| 3.1 | Some Legendre polynomials | 56 |
| 3.2 | Associated Legendre functions | 58 |
| 3.3 | The algebraic signs of spherical harmonics | 60 |
| 3.4 | Surface spherical harmonics as maps | 60 |
| 3.5 | Monopole, dipole, and quadrupole | 68 |
| 3.6 | Radially shifting the potential field | 71 |
| 4.1 | The normal gravity field of the Earth | 86 |
| 4.2 | Gravitation and centrifugal force | 87 |
| 4.3 | The curvature of level surfaces | 91 |
| 4.4 | The curvature of the plumb line | 92 |
| 4.5 | Natural co-ordinates | 94 |
| 4.6 | Meridian ellipse and latitude types | 98 |
| 4.7 | The normal field's potential over the equator | 101 |
| 5.1 | Geoid undulations and deflections of the plumb line | 110 |
| 5.2 | A Finnish geoid model | 112 |
| 5.3 | Equipotential surfaces of gravity and normal gravity fields | 114 |
| 5.4 | Various reference surfaces | 118 |
| 5.5 | Free-air gravity anomalies for Southern Finland. | 124 |
| 6.1 | The attraction of a Bouguer plate | 129 |
| 6.2 | The Bouguer plate as an approximation to the topography | 131 |
| 6.3 | Behaviour of different anomaly types in the mountains | 133 |
| 6.4 | Terrain-corrected Bouguer anomalies for Southern Finland | 134 |
| 6.5 | Calculating the terrain correction using the prism method | 135 |
| 6.6 | The steps in computing the Bouguer anomaly | 136 |



| | | |
|------|---|-----|
| 6.7 | A special terrain shape | 137 |
| 6.8 | Helmert condensation and the gravity field | 141 |
| 6.9 | Friedrich Robert Helmert | 142 |
| 6.10 | Isostasy and the bending of plumb lines | 143 |
| 6.11 | Pratt–Hayford isostatic hypothesis | 144 |
| 6.12 | Airy–Heiskanen isostatic hypothesis | 145 |
| 6.13 | Quantities in isostatic compensation | 145 |
| 6.14 | The modern understanding of isostasy | 149 |
| 6.15 | Isostatic gravity anomalies for Southern Finland. | 151 |
| 6.16 | Isostatic reduction as a pair of surface density layers | 155 |
| 6.17 | Terrain shape. | 158 |
| 7.1 | The principle of levelling | 162 |
| 7.2 | Height reference pillar in Kaivopuisto, Helsinki | 164 |
| 7.3 | Levelled heights and geopotential numbers. | 165 |
| 7.4 | Lake Päijänne: water flows “uphill” | 167 |
| 7.5 | Mikhail Sergeevich Molodensky | 168 |
| 7.6 | A graphic cartoon of the proof of Molodensky’s find | 172 |
| 7.7 | Geoid, quasi-geoid, telluroid and topography | 172 |
| 7.8 | An optical lattice clock | 185 |
| 8.1 | The principle of gravimetric geoid determination | 190 |
| 8.2 | Integrating the Stokes equation geometrically | 191 |
| 8.3 | The Stokes kernel function | 192 |
| 8.4 | The Stokes kernel function on the circle | 196 |
| 8.5 | Simulation of gravity anomalies and geoid undulations | 198 |
| 8.6 | The geometry of the generating function of the Legendre polynomials | 200 |
| 8.7 | The Poisson kernel for gravity anomalies | 205 |



| | | |
|------|---|-----|
| 8.8 | Residual terrain modelling (RTM) | 212 |
| 8.9 | The remove–restore method as a commutative diagram . | 216 |
| 8.10 | Modified Stokes kernel functions | 219 |
| 8.11 | Simpson integration nodal weights in two dimensions . . | 224 |
| 9.1 | Map projection co-ordinates in the local tangent plane . . | 230 |
| 9.2 | Commutative diagram for FFT. | 234 |
| 9.3 | “Tapering” 25 % | 243 |
| 9.4 | Example images for FFT transform | 243 |
| 9.5 | The Finnish FIN2000 geoid | 246 |
| 10.1 | Geocentric angular distance and azimuth | 257 |
| 10.2 | Hirvonen’s covariance function in two dimensions | 264 |
| 10.3 | An example of least-squares collocation | 265 |
| 10.4 | Collocation example | 267 |
| 10.5 | Global covariance functions as degree variances | 284 |
| 10.6 | Circular geometry | 286 |
| 11.1 | Jean Richer’s report | 296 |
| 11.2 | Autograv CG5 spring gravimeter | 297 |
| 11.3 | Operating principle of spring gravimeter | 300 |
| 11.4 | The idea of astatism | 303 |
| 11.5 | Operating principle of a ballistic absolute gravimeter . . . | 305 |
| 11.6 | absolute gravimeter of type FG5 | 306 |
| 11.7 | Principle of operation of an atomic gravimeter | 309 |
| 11.8 | International intercomparison of absolute gravimeters . . | 310 |
| 11.9 | Principle of operation of a superconducting gravimeter . | 311 |
| 12.1 | The mechanism of post-glacial land uplift | 329 |
| 12.2 | The Fennoscandian gravity line on the 63 rd parallel north | 330 |



| | | |
|-------|--|-----|
| 12.3 | Connection between sea-surface topography and ocean currents | 334 |
| 12.4 | Sea-surface topography map produced by GOCE | 335 |
| 12.5 | The sea-level equation | 337 |
| 12.6 | Sea-level rise after the last ice age | 339 |
| 13.1 | Results from the TOPEX/Poseidon and Jason satellites | 346 |
| 13.2 | Satellite altimetry as a measurement method | 347 |
| 13.3 | Simple crossover geometry | 350 |
| 13.4 | Track geometry of satellite altimetry | 355 |
| 13.5 | Kepler's orbital elements | 358 |
| 13.6 | The mechanism of a Sun-stationary orbit | 360 |
| 13.7 | Geometry of a "no-shadow" orbit | 361 |
| 13.8 | A satellite orbit example | 362 |
| 13.9 | Analysing the altimeter return pulse | 365 |
| 13.10 | Ice volume on the Arctic Ocean | 367 |
| 13.11 | Gravity field determination from GPS orbital tracking | 370 |
| 13.12 | The principle of the GRACE satellites | 371 |
| 13.13 | GRACE mission results | 372 |
| 13.14 | Gravity field determination with GOCE | 373 |
| 13.15 | Satellite altimetric track geometry | 375 |
| 14.1 | Theoretical tide | 378 |
| 14.2 | The main components of the theoretical tide | 382 |
| 14.3 | Constituents of the permanent tide | 386 |
| A.1 | Exterior or vectorial product | 398 |
| A.2 | Kepler's second law | 399 |
| A.3 | The gradient | 402 |
| A.4 | The divergence | 403 |



| | | |
|-----|---|-----|
| A.5 | The curl | 405 |
| A.6 | The Stokes curl theorem | 408 |
| A.7 | The Gauss integral theorem | 410 |
| B.1 | Fourier analysis on a step function | 417 |
| E.1 | Gauss integral theorem applied to a co-ordinate aligned volume element | 444 |



Acronyms

- ACS** Advanced Camera for Surveys, instrument on the Hubble Space Telescope
3
- AGU** American Geophysical Union 392
- AR** autoregressive process 265
- BGI** *Bureau Gravimétrique International*, International Gravity Bureau 122, 132,
149, 391, 392
- BVP** boundary-value problem 34
- CHAMP** Challenging Minisatellite Payload for Geophysical Research and
Applications 74, 244, 369, 370
- DMA** Defense Mapping Agency (USA) 73
- DORIS** Doppler Orbitography and Radiopositioning Integrated by Satellite, a
French satellite positioning system 344, 345
- DTM** digital terrain model 131
- EGM2008** Earth Gravity Model 2008 61, 74, 115, 122, 132
- EGM96** Earth Gravity Model 1996 73–75
- EGU** European Geosciences Union 392
- ENSO** El Niño Southern Oscillation 323, 346
- ESA** European Space Agency 3, 344, 345, 371
- FAS** member of the French Academy of Sciences (*Académie des sciences*) 424
- FFT** Fast Fourier Transform 150, 195, 196, 212, 214, 230, 232, 234, 235, 237,
239–242, 244, 245, 248, 249, 284, 286, 326, 429, 430

- FGI** Finnish Geospatial Research Institute, formerly Finnish Geodetic Institute
394
- FIN2000** geoid model (Finland) 243, 244, 326
- FIN2005N00** geoid model (Finland) 244, 393
- FRAS** Fellow of the Royal Astronomical Society 296
- FRS** Fellow of the Royal Society (of London) 4, 17, 221, 296, 381, 383, 424
- FRSE** Fellow of the Royal Society of Edinburgh 17, 381, 424
- GDR** geophysical data record 348, 365
- GFZ** *Geoforschungszentrum* (Potsdam, Germany), German Research Centre for Geosciences 369
- GIA** glacial isostatic adjustment 327, 339, 340
- GNSS** Global Navigation Satellite Systems, which comprise, besides American GPS, the satellite positioning systems of other countries, such as the Russian GLONASS and the European Galileo 113, 126, 184, 242, 244, 315, 326, 327, 330, 344, 348, 364, 368, 372, 384, 385, 389, 393
- GOCE** Geopotential and Steady-state Ocean Circulation Explorer 74, 244, 283, 316, 317, 333, 334, 368, 371–374
- GPS** Global Positioning System 68, 99, 169, 314, 319, 344, 369, 370
- GRACE** Gravity Recovery And Climate Experiment 74, 244, 369–372
- GRAVSOF**T Geopotential determination software, mainly developed in Denmark 242
- GRS80** Geodetic Reference System 1980 6, 99, 102, 106, 108, 115, 244, 313, 326
- GWR20** superconducting gravimeter built by GWR Instruments 310
- HUT** Helsinki University of Technology, today part of Aalto University 394
- IAG** International Association of Geodesy 242, 310, 391, 392
- IB** inverted barometer 323
- ICET** International Center for Earth Tides 392
- ICGEM** International Center for Global Earth Models 392
- IDEMS** International Digital Elevation Model Service 392
- IGeC** International Geoid Commission (obsolete) 392
- IGeS** International Geoid Service (obsolete) 392
- IGETS** International Geodynamics and Earth Tide Service 310
- IGFS** International Gravity Field Service 391, 392



- IMGC-02** transportable absolute rise-and-fall gravimeter, built by the *Istituto di Metrologia «G. Colonnetti»*, formerly the *Istituto Nazionale di Ricerca Metrologica* in Torino, Italy. 307
- ISG** International Service for the Geoid 391, 392
- J₂** second dynamic form factor, “gravitational flattening” 74, 99, 102, 359, 360, 374
- Jason** American-French-European radar altimetry satellite series, successors of **TOPEX/Poseidon** 344–346, 361, 374
- JHU** Johns Hopkins University 3
- KCB** Knight Commander of the Bath, British order of chivalry 381
- KKJ** National Grid Co-ordinate System (Finland) 121
- LAGEOS** LAser GEOdynamic Satellite 358
- Lego™** “*Leg Godt*”, Engl. “*Play Well*”, Danish toy brand 26
- LLR** Lunar laser ranging 304
- LSC** least-squares collocation 150
- M_f** Moon, fortnightly tide 381
- N2000** height system (Finland) 161, 164, 244, 325
- N60** height system (Finland) 160, 161, 244, 325, 326
- NAP** *Normaal Amsterdams Peil*, height system (Western Europe) 161
- NASA** National Aeronautics and Space Administration (USA) 3
- NAVD88** North American Vertical Datum 1988 161
- NC** normal correction 181
- NGA** National Geospatial-Intelligence Agency (USA, formerly NIMA) 73, 391
- NIMA** National Imagery and Mapping Agency (USA, formerly DMA) 73
- NKG** *Nordiska Kommissionen för Geodesi*, Nordic Geodetic Commission 393
- NKG2004** geoid model (Nordic area) 393
- NKG2015** geoid model (Nordic area) 393
- NOAA** National Oceanic and Atmospheric Administration (USA) 334
- OC** orthometric correction 179
- OSU** Ohio State University, Columbus, Ohio, USA 74
- ppb** parts per billion 116



- ppm** parts per million 116
- PRARE** Precise Range And Range-Rate Equipment, not operational 344
- PRS** President of the Royal Society 2, 118, 142
- RTM** residual terrain modelling 208–210, 224
- SI** *Système international d'unités*, International System of Units 11, 37, 99, 116, 117, 123
- SK-42** Reference system of the Soviet Union, also known as the Krasovsky 1940 reference ellipsoid 100
- SLR** satellite laser ranging 344, 358
- SRAL** Synthetic Aperture Radar Altimeter 345
- Ssa** Sun, semi-annual tide 381
- SST** satellite-to-satellite tracking 371
- STScI** Space Telescope Science Institute 3
- SWH** significant wave height 347, 348
- TC** terrain correction 130, 131, 133, 135, 136, 248
- TOPEX/Poseidon** Topography Experiment / Poseidon, American-French radar altimetry satellite xxi, 325, 344–346, 361, 374
- UCO** University of California Observatories 3
- WGS84** World Geodetic System 1984 68, 99





Fundamentals of the theory of gravitation

1



1.1 General

In this chapter we present the foundations of Newton's theory of gravitation. Intuitively, the theory of gravitation is easiest to understand as "action at a distance," Latin *actio ad distans*, where the force between two masses is proportional to the masses themselves, and inversely proportional to the square of the distance between them. This is the form of Newton's general law of gravitation familiar to all.

There exists an alternative but equivalent presentation, *field theory*, which portrays gravitation as a phenomenon propagating through space, a *field*. The propagation is expressed in *field equations*. The field approach is not quite as intuitive, but is a powerful theoretical tool¹.

In this chapter we acquaint ourselves with the central concept of field theory, the *gravitational potential*. We also get to know the potential fields of the theoretically interesting single and double *mass-density layers*. Practical and theoretical applications of these include isostasy

¹There is also a philosophical side to this. To many, for example to Leibniz, the idea of a force that jumps from object to object was an abomination. Many tried to explain gravitation — and also electromagnetism, etc. — by a "world aether". It was not until the advent of relativity theory that the understanding gained ground that a physical theory does not have to satisfy our preconceptions about what constitutes a "sensible explanation" — as long as it presents the physical phenomena correctly.

and Helmholtz condensation, the properties of which we will study in later chapters.

We will learn about important *integral theorems* like the theorems of Gauss and Green, with the aid of which we may infer the whole potential field in space from field values given only for a certain surface. Other similar examples are the Chasles theorem and the solution to Dirichlet's problem.

In chapter 3, we apply these fundamentals of potential theory to derive a spectral representation of the Earth's gravitational field, a *spherical-harmonic expansion*.

Here, at the beginning of the text, we derive an extensive set of mathematical equations, such as well-known integral equations. This is unfortunately necessary preliminary work. These equations, however, are not an end in themselves and are not worth committing to memory. Try rather to understand their logic, and how these various results have been arrived at historically. Try as well to acquire an intuition, a fingertip feeling, about the nature of this theory.



1.2 Gravitation between two masses

We start the investigation of the Earth's gravity field suitably with Isaac Newton's² general law of gravitation:

$$F = G \frac{m_1 m_2}{\ell^2}. \quad (1.1)$$

F is the attractive force between bodies 1 and 2, m_1 and m_2 are the masses of the bodies, and ℓ is the distance between them. We assume the masses to be points. The constant G , the *universal gravitational constant*, has the value

$$G = 6.674 \cdot 10^{-11} \text{ m}^3/\text{kg s}^2.$$

²Sir Isaac Newton **PRS** (1642–1727) was an English universal genius who derived the mathematical underpinning of astronomy, and much of geophysics, in his major work, *Philosophiæ Naturalis Principia Mathematica* (Mathematical Foundations of Physics).



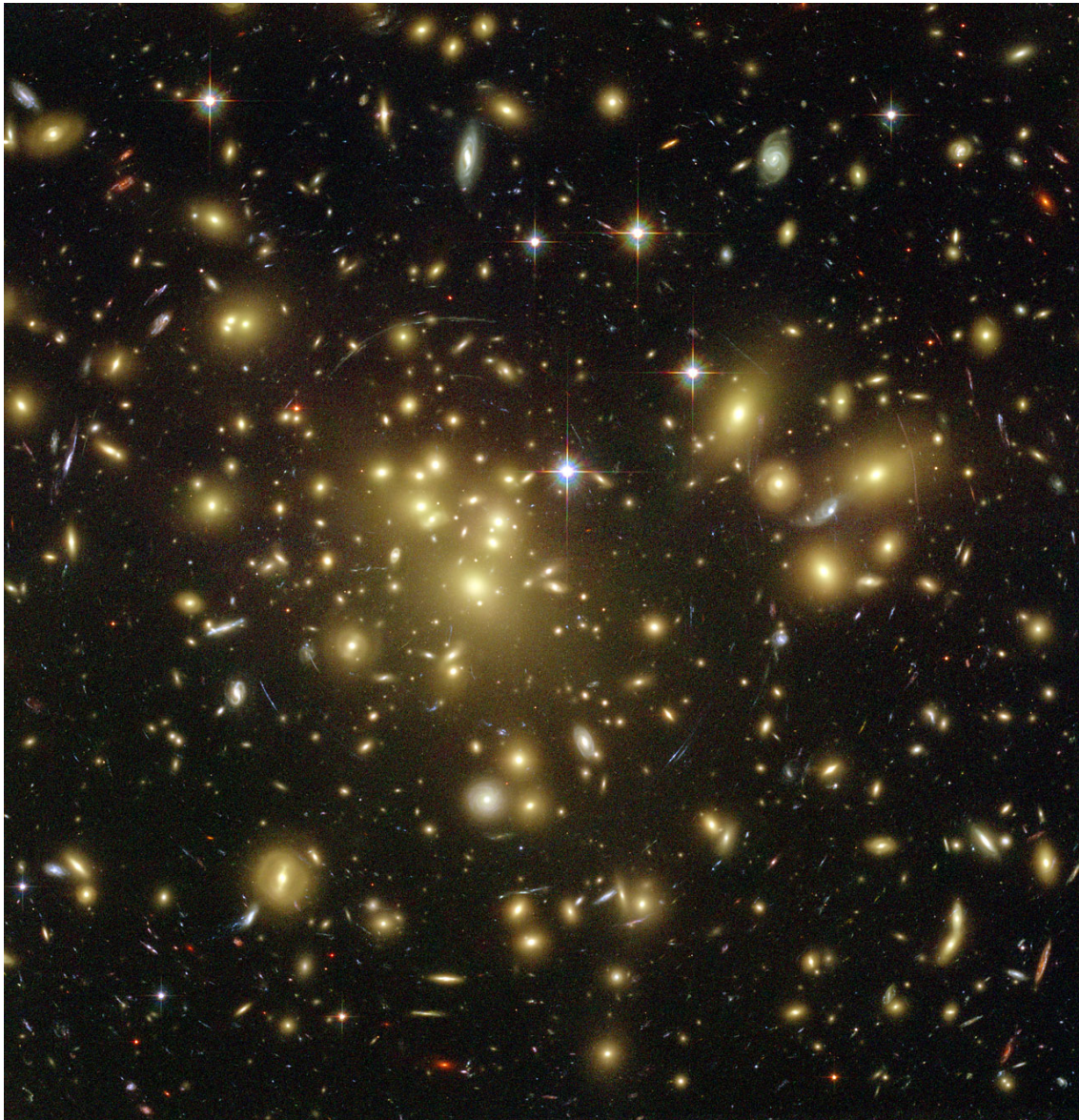


FIGURE 1.1. Gravitation is universal. A gravitational lens imaged by the Hubble Space Telescope, the Abell 1689 cluster of galaxies at a distance of 2.2 billion light years. [Benitez et al. \(2003\)](#).

Credits: [NASA](#), [N. Benitez \(JHU\)](#), [T. Broadhurst \(The Hebrew University\)](#), [H. Ford \(JHU\)](#), [M. Clampin \(STScI\)](#), [G. Hartig \(STScI\)](#), [G. Illingworth \(UCO / Lick Observatory\)](#), the [ACS Science Team](#) and the [ESA](#).



The value of G was determined for the first time by Henry Cavendish³ using a sensitive torsion balance (Cavendish, 1798).
 torsiovaaka,
 kiertoheiluri

Let us call the small body or test mass, for example a satellite, m , and the large mass, the planet or the Sun, M . Then, $m_1 = M$ may be called the *attracting* mass, and $m_2 = m$ the *attracted* mass, and we obtain

$$F = G \frac{mM}{\ell^2}.$$

According to Newton's law of motion

$$F = ma,$$

in which a is the gravitational acceleration of the body m . From this follows

$$a = G \frac{M}{\ell^2}.$$

From this equation, the quantity $m = m_2$ has vanished. This is the famous observation by Galileo that *all bodies fall equally fast*,⁴ irrespective of their mass. This is also known as Einstein's principle of equivalence.⁵

Both the force F and the acceleration a have the same direction as the line connecting the bodies. For this reason one often writes equation 1.1 as a *vector equation*, which is more expressive:

$$\mathbf{a} = -GM \frac{\mathbf{r} - \mathbf{R}}{\ell^3}, \quad (1.2)$$

³Henry Cavendish FRS (1731–1810) was a British natural scientist from a wealthy, noble background. He did also pioneering work in chemistry. He was extremely shy, and the renowned neurologist Oliver Sacks retrodiagnosed him as living with Asperger syndrome (Sacks, 2001).

⁴At least in a vacuum. The Apollo astronauts showed impressively how on the Moon a feather and a hammer fall equally fast! YouTube, Hammer vs. Feather.

⁵Albert Einstein (1879–1955) was a theoretical physicist of Jewish German descent, who created both the special and general theories of relativity, applying the latter to cosmology, and did fundamental work in quantum theory.



The potential of a point mass

in which the three-dimensional vectors of place of both the attracting and attracted masses are defined as follows in rectangular co-ordinates:⁶

$$\begin{aligned}\mathbf{r} &= x\mathbf{i} + y\mathbf{j} + z\mathbf{k}, \\ \mathbf{R} &= X\mathbf{i} + Y\mathbf{j} + Z\mathbf{k},\end{aligned}$$

where the triad of unit vectors $\{\mathbf{i}, \mathbf{j}, \mathbf{k}\}$ is an *orthonormal basis*⁷ in Euclidean space and

$$\ell = \|\mathbf{r} - \mathbf{R}\| = \sqrt{(x - X)^2 + (y - Y)^2 + (z - Z)^2} \quad (1.3)$$

is the distance between the masses computed by the Pythagoras theorem.

Vector equation 1.2 contains a minus sign, which tells us that the direction of the force is opposite to that of the vector $\mathbf{r} - \mathbf{R}$. This vector is the location of the attracted mass m reckoned from the location of the attracting mass M . In other words, this tells us that we are dealing with an *attraction* and not a repulsion.



1.3 The potential of a point mass

The gravitational field is a special field: if it is stationary, that is, not time-dependent, it is *conservative*. This means that a body moving inside the field along a closed path will, at the end of the journey, not have lost or gained energy. Because of this, one may attach to each point in the field a “label” onto which is written the amount of energy gained or lost by a unit or test mass when travelling from an agreed-upon *starting point* to the point under discussion. The value written on the label is called the *potential*.

⁶As vector notation, one uses either \vec{v} (an arrow above the letter) or \mathbf{v} (bolding the letter). Here we use the bold notation, except for vectors designated by Greek letters, which cannot be bolded.

⁷This means that $\|\mathbf{i}\| = \|\mathbf{j}\| = \|\mathbf{k}\| = 1$ and $\langle \mathbf{i} \cdot \mathbf{j} \rangle = \langle \mathbf{i} \cdot \mathbf{k} \rangle = \langle \mathbf{j} \cdot \mathbf{k} \rangle = 0$, where the norm of vector \mathbf{a} is defined as $\|\mathbf{a}\| \stackrel{\text{def}}{=} \sqrt{\langle \mathbf{a} \cdot \mathbf{a} \rangle}$, and $\langle \mathbf{a} \cdot \mathbf{b} \rangle$ is the *inner* or *scalar product* of vectors \mathbf{a}, \mathbf{b} defined in the space.



Note that the choice of starting point is *arbitrary*. We shall return to this significant matter.

The *potential function* defined in this way for a point-like body M is

$$V = GM/\ell, \quad (1.4)$$

where ℓ is again, as above, the length of the vector $\mathbf{r} - \mathbf{R}$, $\ell = \|\mathbf{r} - \mathbf{R}\|$.

The constant GM has in the case of the Earth (according to the **GRS80** system, conventionally) the value

$$GM_{\oplus} = 3.986\,005 \cdot 10^{14} \text{ m}^3/\text{s}^2.$$

The currently best available physical value is slightly more precise:

$$GM_{\oplus} = 3.986\,004\,4 \cdot 10^{14} \text{ m}^3/\text{s}^2.$$



1.4 Potential of a spherical shell

We may write, based on equation 1.4, the potential of an extended body M into the following form:

$$V(\mathbf{r}) = G \int_M \frac{dm(\mathbf{R})}{\ell} = G \int_M \frac{dm(\mathbf{R})}{\|\mathbf{r} - \mathbf{R}\|}. \quad (1.5)$$

This is an integral over the mass elements dm of the body, where every such mass element is located at its own place \mathbf{R} . The potential V is evaluated at location \mathbf{r} , and the distance $\ell = \|\mathbf{r} - \mathbf{R}\|$.

We now derive the equation for the potential of a thin spherical shell, see figure 1.2, where we have placed the centre of the sphere at the origin O .

Because the circumference of a narrow ring, width $b \cdot d\theta$, is $2\pi b \sin \theta$, its surface area is

$$(2\pi b \sin \theta) (b \cdot d\theta).$$

Let the thickness of the shell be p (small) and its density ρ . We obtain for the total mass of the ring

$$2\pi\rho pb^2 \sin \theta d\theta.$$



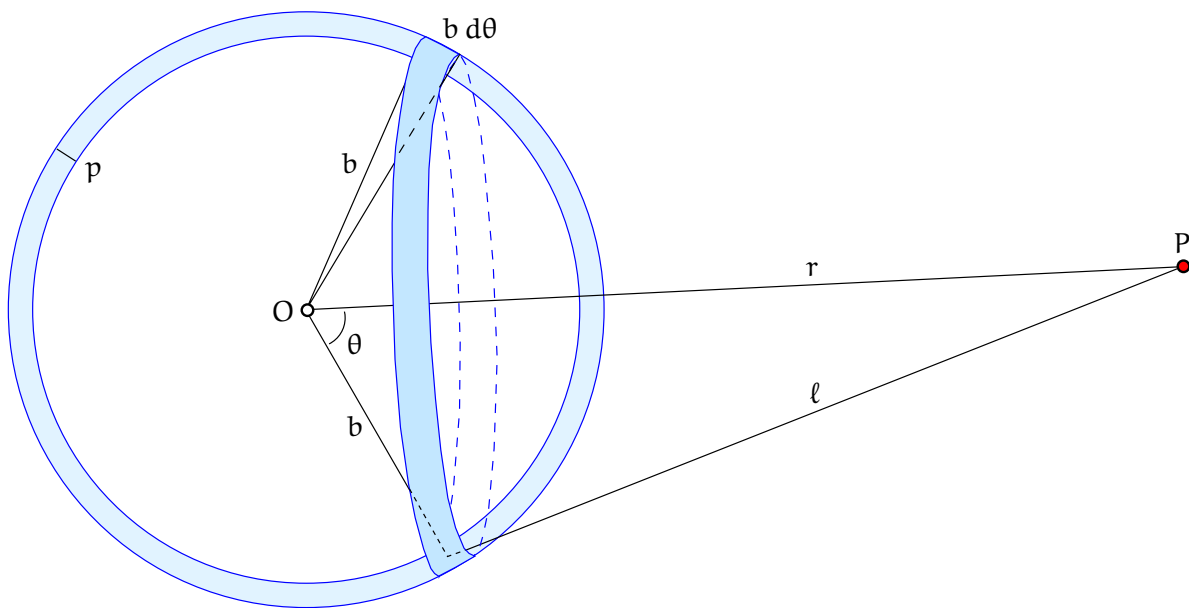


FIGURE 1.2. A thin spherical shell consists of rings.

Because every point of the ring is at the same distance ℓ from point P, we may write for the potential of the ring at point P:

$$V_P = \frac{2\pi G \rho p b^2 \sin \theta d\theta}{\ell}.$$

With the cosine rule

$$\ell^2 = r^2 + b^2 - 2rb \cos \theta \tag{1.6}$$

we obtain, using equation 1.5, for the potential of the whole shell

$$V_P = 2\pi G \rho p b^2 \int \frac{\sin \theta d\theta}{\sqrt{r^2 + b^2 - 2rb \cos \theta}}.$$

In order to evaluate this integral, we must replace the integration variable θ by ℓ . Differentiating equation 1.6 yields

$$\ell d\ell = br \sin \theta d\theta,$$

and remembering that $\ell = \sqrt{r^2 + b^2 - 2rb \cos \theta}$ we obtain

$$V_P = 2\pi G \rho p b^2 \int_{\ell_1}^{\ell_2} \frac{d\ell}{br}.$$



In the case that point P is outside the shell, the integration bounds of ℓ are $\ell_1 = r - b$ and $\ell_2 = r + b$, and we obtain for the potential of point P

$$V_P = 2\pi G \rho p b^2 \left[\frac{\ell}{br} \right]_{\ell=r-b}^{\ell=r+b} = \frac{4\pi G \rho p b^2}{r}.$$

Because the mass of the whole shell is $M_b = 4\pi b^2 \rho p$, it follows that the potential of the shell is *the same as that of an equal-sized mass in its centre* O:

$$V_P = \frac{GM_b}{r},$$

where r is now the distance of computation point P from the centre of the sphere O. We see that this is identical to equation 1.4.

In the same way, the attraction, or rather, *acceleration*, caused by the spherical shell is⁸

$$\mathbf{a}_P = \nabla V|_P = -4\pi G \rho p b^2 \frac{\mathbf{r}_P - \mathbf{r}_O}{r^3} = -GM_b \frac{\mathbf{r}_P - \mathbf{r}_O}{r^3},$$

in which $r = \|\mathbf{r}_P - \mathbf{r}_O\|$. This result is identical to the acceleration caused by an equal-sized point mass located in point O, equation 1.2.

In the case that point P is inside the shell, $\ell_1 = b - r$ and $\ell_2 = b + r$ and the above integral changes to the following:

$$V_P = 2\pi G \rho p b^2 \left[\frac{\ell}{br} \right]_{\ell=b-r}^{\ell=b+r} = 4\pi G \rho p b.$$

As we see, this is a *constant* and not dependent upon the location of point P. Therefore $\nabla V_P = 0$ and the attraction, being the gradient of the potential, vanishes.

The end result is that the attraction of a spherical shell is, outside the shell,

$$\mathbf{a} = \|\mathbf{a}\| = \frac{GM}{r^2},$$

where M is the total mass of the shell and $r = \|\mathbf{r}_P - \mathbf{r}_O\|$ the distance of the observation point from the shell's centre; and 0 inside the shell.

In figure 1.3 we have drawn the curves of potential and attraction — or rather, acceleration, attractive force per unit of mass. If a body

⁸Here, the ∇ (nabla) operator is used, to be explained in section 1.5.



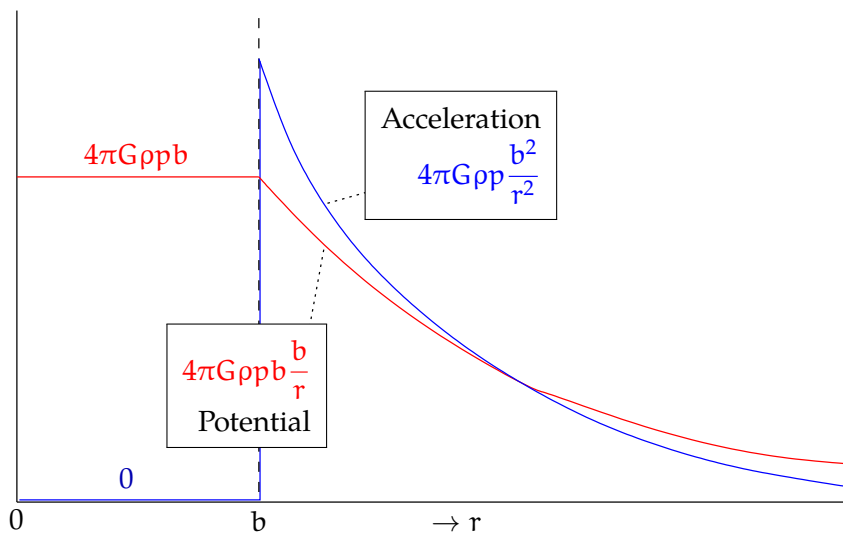


FIGURE 1.3. Dependence of potential and attraction on distance r from the centre of a spherical shell.

consists of many concentric spherical shells (like rather precisely the Earth and many celestial bodies), then inside the body only those layers of mass “internal” to — i.e., closer to the centre than — the observation point participate in causing attraction, and this attraction is the same as it would be if the mass of all these layers was concentrated in the centre of the body. This case, where the distribution of mass density inside a body only depends on the distance from its centre, is called an *isotropic density distribution*.

1.5 Computing the attraction from the potential

As we argued earlier, the potential V is a *path integral*. Conversely we can compute, from the potential, the components of the gravitational acceleration vector by *differentiating* $V(x, y, z)$ with respect to *place*, by applying the *gradient operator*, which is a vector operator:

$$\mathbf{a} = \nabla V = \text{grad } V = \frac{\partial V}{\partial x} \mathbf{i} + \frac{\partial V}{\partial y} \mathbf{j} + \frac{\partial V}{\partial z} \mathbf{k}. \quad (1.7)$$



Here, the symbol ∇ (nabla), is a frequently used *partial differential operator*

$$\nabla = \mathbf{i} \frac{\partial}{\partial x} + \mathbf{j} \frac{\partial}{\partial y} + \mathbf{k} \frac{\partial}{\partial z}.$$

Here, $\{\mathbf{i}, \mathbf{j}, \mathbf{k}\}$ is again a *basis* of mutually orthogonal unit vectors in Euclidean space parallel to the (x, y, z) axes.

Let us try this differentiation in the case of the potential field of the point mass M . Substitute the above equations for V 1.4 and ℓ 1.3:⁹

$$\frac{\partial V}{\partial x} = \frac{\partial V}{\partial \ell} \frac{\partial \ell}{\partial x} = GM \cdot -\frac{1}{\ell^2} \cdot \frac{x - X}{\ell} = -GM \frac{x - X}{\ell^3}.$$

Similarly we compute the y and z components:

$$\frac{\partial V}{\partial y} = -GM \frac{y - Y}{\ell^3}, \quad \frac{\partial V}{\partial z} = -GM \frac{z - Z}{\ell^3}.$$

These are the components of gravitational acceleration when the *source* of the field is one point mass M . So, in this concrete case, the vector equation given above applies:

$$\mathbf{a} = \text{grad } V = \nabla V.$$

Remark In physical geodesy — unlike in physics — the potential is reckoned to be always positive if the attracting mass M is positive (as it is known to always be). However, the *potential energy* of

⁹From the equation

$$\ell = \sqrt{(x - X)^2 + (y - Y)^2 + (z - Z)^2} = \left((x - X)^2 + (y - Y)^2 + (z - Z)^2 \right)^{1/2}$$

it follows with the chain rule that

$$\begin{aligned} \frac{\partial \ell}{\partial x} &= \frac{\partial \left((x - X)^2 + (y - Y)^2 + (z - Z)^2 \right)^{1/2}}{\partial \left((x - X)^2 + (y - Y)^2 + (z - Z)^2 \right)} \cdot \frac{\partial (x - X)^2}{\partial x} = \\ &= \frac{1}{2} \left((x - X)^2 + (y - Y)^2 + (z - Z)^2 \right)^{-1/2} \cdot 2(x - X) = \frac{x - X}{\ell}. \end{aligned}$$



body m inside the field V of mass M is negative! More precisely, the potential energy of body m is

$$E_{\text{pot}} = -Vm.$$

One calls the vector of gravitational acceleration in brief the “gravitational vector”.



1.6 Potential of a solid body

In the following we study a *solid body*, the mass of which is distributed throughout space and thus not concentrated in a single point. For example, the mass distribution of the Earth in space may be described by a matter *density function* ρ :

$$\rho(x, y, z) = \frac{dm(x, y, z)}{dV(x, y, z)},$$

in which dm is a mass element and dV is the corresponding element of spatial volume. The dimension of ρ is density, its unit in the SI system, kg/m^3 .

Because the gravitational acceleration 1.7 is a linear expression in the potential V , and both the force and acceleration vectors may be summed linearly, it follows that the total potential of the body can also be obtained by summing together the potentials of all its parts. For example, the potential of a set of n mass points is

$$V(\mathbf{r}) = G \sum_{i=1}^n \frac{m_i}{l_i} = G \sum_{i=1}^n \frac{m_i(\mathbf{R}_i)}{\|\mathbf{r} - \mathbf{R}_i\|},$$

from which we obtain the gravitational acceleration by simply using gradient theorem 1.7.

The potential of a solid body is obtained similarly by replacing the



sum by an integral, in the following way:¹⁰

$$V = G \iiint_{\text{body}} \frac{dm}{\ell} = G \iiint_{\text{body}} \frac{\rho}{\ell} d\mathcal{V}. \quad (1.8)$$

The symbol ρ inside the integral designates the matter's density at the location of $d\mathcal{V}$. The quantity $\ell = \|\mathbf{r} - \mathbf{R}\| = \sqrt{(x - X)^2 + (y - Y)^2 + (z - Z)^2}$ is the distance between the point of measurement and the attracting mass element. More clearly:

$$V(x, y, z) = G \iiint_{\text{body}} \frac{\rho(X, Y, Z)}{\sqrt{(x - X)^2 + (y - Y)^2 + (z - Z)^2}} dX dY dZ.$$

As we showed already above for mass points, the first derivative with respect to place or *gradient* of the potential V of a solid body,

$$\text{grad } V = \nabla V = \mathbf{a}, \quad (1.9)$$

is also the acceleration vector caused by the attraction of the body. This applies generally.

1.6.1 Behaviour at infinity

If a body is of finite extent — in other words, it lies completely within a sphere of size ϵ around the origin — and its density is also bounded everywhere, it follows that

$$\|\mathbf{r}\| \rightarrow \infty \implies V(\mathbf{r}) \rightarrow 0,$$

because, according to the triangle inequality,

$$\ell = \|\mathbf{r} - \mathbf{R}\| \geq \|\mathbf{r}\| - \|\mathbf{R}\| \geq \|\mathbf{r}\| - \epsilon$$

and thus

$$\|\mathbf{r}\| \rightarrow \infty \implies 1/\ell \rightarrow 0.$$

¹⁰Unfortunately almost the same symbols V and \mathcal{V} are used here for the potential and volume, respectively.



For the acceleration of gravitation, the same applies for all three components, and thus also for the length of this vectorial quantity:

$$\|\mathbf{r}\| \rightarrow \infty \implies \|\nabla V\| \rightarrow 0.$$

This result can still be sharpened: if $\|\mathbf{r}\| \rightarrow \infty$, then, again by the triangle inequality,

$$\ell = \|\mathbf{r} - \mathbf{R}\| \leq \|\mathbf{r}\| + \|\mathbf{R}\| \leq \|\mathbf{r}\| + \epsilon,$$

and thus

$$\frac{1}{\|\mathbf{r}\| + \epsilon} \leq \frac{1}{\ell} \leq \frac{1}{\|\mathbf{r}\| - \epsilon} \implies \frac{1}{\|\mathbf{r}\|} \frac{1}{1 + \epsilon/\|\mathbf{r}\|} \leq \frac{1}{\ell} \leq \frac{1}{\|\mathbf{r}\|} \frac{1}{1 - \epsilon/\|\mathbf{r}\|}.$$

It is seen, again with the notation $r = \|\mathbf{r}\|$, that

$$r \rightarrow \infty \implies 1/\ell \rightarrow 1/r.$$

When we substitute this into integral 1.8, it follows that for large distances $r \rightarrow \infty$:

$$V = G \iiint_{\text{body}} \frac{\rho}{\ell} d\mathcal{V} \approx \frac{G}{r} \iiint_{\text{body}} \rho d\mathcal{V} = \frac{GM}{r},$$

in which M , the integral of density over the volume of the body, is precisely its *total mass*. From this we see that, at great distance, the field of a finite-sized body M is *nearly identical* with the field generated by a point mass the mass of which is equal to the *total mass* of the body. This important observation was already made by Newton. Thanks to this phenomenon, we may treat, in the celestial mechanics of the solar system, the Sun and planets¹¹ as mass points, although we know that they are not.

¹¹The only important exception is formed by the forces between a planet and its moons, due both to the flattening of the planet and tidal effects.





1.7 Example: The potential of a line of mass

The potential of a vertical line of mass having a linear mass density of unity is

$$V(x, y, z) = G \int_0^H \frac{1}{\sqrt{(X-x)^2 + (Y-y)^2 + (Z-z)^2}} dZ, \quad (1.10)$$

in which (X, Y) is the location in the plane of the mass line, (x, y, z) is the location of the point at which the potential is being evaluated, and the mass line extends from sea level $Z = 0$ to height $Z = H$.

Firstly we write $\Delta x = X - x$, $\Delta y = Y - y$, $\Delta z = Z - z$, and the potential becomes

$$V(\Delta x, \Delta y, \Delta z) = G \int_{-z}^{H-z} \frac{1}{\sqrt{\Delta x^2 + \Delta y^2 + \Delta z^2}} d(\Delta z).$$

The indefinite integral is

$$\ln\left(\Delta z + \sqrt{\Delta x^2 + \Delta y^2 + \Delta z^2}\right)$$

and substituting the integration bounds yields

$$V = G \ln \frac{H - z + \sqrt{\Delta x^2 + \Delta y^2 + (H - z)^2}}{-z + \sqrt{\Delta x^2 + \Delta y^2 + z^2}}.$$

Now we can expand this into a Taylor series in H around the point $H = 0$: the first derivative of equation 1.10 is

$$\frac{\partial V}{\partial H} = \frac{G}{\sqrt{(X-x)^2 + (Y-y)^2 + (H-z)^2}} = \frac{G}{\ell}$$

in which $\ell(H) = \sqrt{(X-x)^2 + (Y-y)^2 + (H-z)^2}$. The second derivative is, using the chain rule,

$$\begin{aligned} \frac{\partial^2 V}{\partial H^2} &= \frac{\partial}{\partial H} \left(\frac{G}{\ell} \right) = G \cdot \frac{\partial \ell^{-1}}{\partial \ell} \cdot \frac{\partial \ell}{\partial H} = G \cdot -\ell^{-2} \cdot \frac{1}{2} \ell^{-1} \cdot 2(H-z) = \\ &= -G \frac{H-z}{\ell^3}. \end{aligned}$$



Example: The potential of a line of mass

The third derivative, obtained in the same way:

$$\frac{\partial^3 V}{\partial H^3} = -G \frac{\partial}{\partial H} \left(\frac{H-z}{\ell^3} \right) = G \left(\frac{3(H-z)^2}{\ell^5} - \frac{1}{\ell^3} \right) = G \frac{3(H-z)^2 - \ell^2}{\ell^5},$$

and so on. The Taylor expansion is

$$V = \underbrace{V|_{H=0}}_0 + G \underbrace{\frac{1}{\ell_0}}_{\frac{\partial_H V|_{H=0}}{\ell_0}} H + \frac{1}{2} G \underbrace{\frac{z}{\ell_0^3}}_{\frac{\partial_H^2 V|_{H=0}}{\ell_0^3}} H^2 + \frac{1}{6} G \underbrace{\frac{3z^2 - \ell_0^2}{\ell_0^5}}_{\frac{\partial_H^3 V|_{H=0}}{\ell_0^5}} H^3 + \dots \quad (1.11)$$

in which $\ell_0 = \sqrt{(X-x)^2 + (Y-y)^2 + z^2}$, so the values of the derivatives used in this expansion are obtained by substituting $H = 0$.

Question How can we exploit this result for computing the gravitational potential of a complete, realistic topography?

Answer In this expansion, the coefficients $1/\ell_0, \frac{1}{2}z/\ell_0^3, \dots$, like ℓ_0 , depend only on the *differences* $\Delta x = X - x$ and $\Delta y = Y - y$ between the co-ordinates of the location of the mass line (X, Y) and those of the evaluation location (x, y) — and of the height z of the evaluation point. If the topography is given in the form of a grid, we may evaluate the above expansion 1.11 term-wise for the given z value and for all possible value pairs $(\Delta x, \Delta y)$.

Then, if the grid is, say, $N \times N$ in size, we need only N^2 operations to calculate every coefficient. The brute-force evaluation of the Taylor expansion itself *for the whole topography*, for every point of the terrain grid and every point of the evaluation grid, requires after that $N^2 \cdot N^2 = N^4$ operations, but those are much simpler: the coefficients themselves have been precomputed. And brute force is not even the best approach: as we shall see, the above *convolution* can be computed much faster using the Fast Fourier Transform.

We shall return to this subject more extensively in connection with terrain-effect evaluation, in sections 6.3 and 9.7.





1.8 Laplace and Poisson equations

The *second derivative* with respect to the place of the geopotential, the first derivative with respect to the place of the gravitational acceleration vector called its *divergence*, is also of geophysical interest. We may write:

$$\begin{aligned} \operatorname{div} \mathbf{a} &\stackrel{\text{def}}{=} \langle \nabla \cdot \mathbf{a} \rangle = \langle \nabla \cdot (\nabla V) \rangle = \langle \nabla \cdot \nabla \rangle V = \\ &= \Delta V = \frac{\partial^2}{\partial x^2} V + \frac{\partial^2}{\partial y^2} V + \frac{\partial^2}{\partial z^2} V, \end{aligned} \quad (1.12)$$

in which

$$\Delta \stackrel{\text{def}}{=} \langle \nabla \cdot \nabla \rangle = \frac{\partial^2}{\partial x^2} + \frac{\partial^2}{\partial y^2} + \frac{\partial^2}{\partial z^2}$$

is a well-known symbol called the *Laplace operator*.¹²

In equation 1.4 for the potential of a point mass we may show, by performing all partial derivations 1.12, that

$$\Delta V = 0, \quad (1.13)$$

the well-known *Laplace equation*. This equation applies outside a point mass, and more generally everywhere in empty space: all masses can in the limit be considered to consist of point-like mass elements. Or, in equation 1.8 we may directly differentiate inside the triple integral sign, exploiting the circumstance that it is permitted to interchange integration and partial differentiation, if both exist.

A potential field for which Laplace equation 1.13 applies, is called a *harmonic* field or function.

In the case where the mass density does not vanish everywhere, we have a different equation, with ρ the mass density:

$$\Delta V = -4\pi G\rho. \quad (1.14)$$

¹²Pierre-Simon, marquis de Laplace (1749–1827) was a French universal genius who contributed to mathematics and the natural sciences. He is one of the 72 French scientists, engineers and mathematicians whose names were inscribed on the Eiffel Tower, [Eiffel Tower, 72 names](#).



This equation is called the Poisson equation.¹³

The pair of equations

$$\text{grad } V = \mathbf{a}, \quad \text{div } \mathbf{a} = -4\pi G\rho$$

are known as the *field equations* of the gravitational field. They play the same role as Maxwell's¹⁴ field equations in electromagnetism. Unlike in Maxwell's equations, however, in the above there is no time coordinate. Because of this, it is not possible to derive an equation describing the propagation in space of gravitational waves, like the one for electromagnetic waves in Maxwell's theory.

We know today that these "Newton field equations" are only approximate, and that Einstein's general theory of relativity is a more precise theory. Nevertheless, in physical geodesy Newton's theory is generally precise enough and we shall use it exclusively.



1.9 Gauge invariance

An important property of the potential is that if we add a *constant* C to it, nothing related to gravitation that can actually be measured, changes. This is called *gauge invariance*.

mittainvarianssi

Gravitation itself is obtained by differentiation of the potential, an operation that eliminates the constant term. Therefore the definition of potential is ambiguous: all potential fields V obtained by different choices of C are equally valid.

Observations only give us potential *differences*, as spirit levellers know all too well.

¹³Siméon Denis Poisson (1781–1840) was a French mathematician, physicist and geodesist, one of the 72 names inscribed on the Eiffel Tower, [Eiffel Tower, 72 names](#).

¹⁴James Clerk Maxwell **FRS FRSE** (1831–1879) was a Scottish physicist, the discoverer of the field equations of electromagnetism. He found a wave-like solution to the equations, and, based on propagation speed, identified *light* as such.



An often-chosen definition of potential is based on requiring that, if $r \stackrel{\text{def}}{=} \|\mathbf{r}\| \rightarrow \infty$, then also $V \rightarrow 0$, which makes physical sense and yields simple equations. However, in work on the Earth's surface, a more practical alternative may be $V = 0$ at the mean sea surface — although that is not free of problems, either.

For example, for the mass of the Earth M_{\oplus} a physically sensible form of the potential is, in spherical approximation,

$$V = \frac{GM_{\oplus}}{r},$$

which vanishes at infinity $r \rightarrow \infty$, when again a geodetically sensible definition would be

$$V = \frac{GM_{\oplus}}{r} - \frac{GM_{\oplus}}{R},$$

in which $R = \|\mathbf{R}\|$ is the radius of the Earth sphere. The latter potential vanishes where $r = R$, on the surface of a spherical Earth. In the limit $r \rightarrow \infty$ its value is $-GM_{\oplus}/R$, not zero.



1.10 Single mass-density layer

If we apply to the surface S of a body a mass “coating”, of mass-density value

$$\kappa = \frac{dm}{dS},$$

we obtain for the potential an integral equation otherwise similar to equation 1.8, but a *surface integral*:

$$V = G \iint_{\text{surface}} \frac{dm}{\ell} = G \iint_{\text{surface}} \frac{\kappa}{\ell} dS. \quad (1.15)$$

Here again ℓ is the distance between the point at which the potential is to be calculated, and the moving mass element in integration dm — or surface element dS . The dimension of the mass surface density κ is kg/m^2 , different from the dimension of ordinary or volume mass density, which is kg/m^3 .



This case is theoretically interesting, although physically unrealistic. The function V is everywhere continuous, also at the surface S , however its first derivatives with place are already discontinuous. The discontinuity appears in the direction perpendicular to the surface, in the *normal derivative*.

Let us look at the simple case where a sphere of radius R has been coated with a layer of constant surface density κ . By computing the above integral 1.15 we may prove — in a complicated way, see section 1.4 — that the exterior potential is the same as it would be if all of the mass of the body were concentrated in the sphere's centre. Also in section 1.4 we proved that the potential interior to the sphere is *constant*.

Thus, the exterior attraction ($r > R$), with r the distance of the point of computation from the centre of the sphere, is

$$a_{\text{ext}}(r) = G \frac{M}{r^2} = G \frac{\kappa \cdot 4\pi R^2}{r^2} = 4\pi G \kappa \left(\frac{R}{r}\right)^2.$$

The interior attraction ($r < R$) is

$$a_{\text{int}}(r) = 0.$$

This means that on the surface of the sphere, $\ell = R$, the attraction is *discontinuous*:

$$a_{\text{ext}}(R) - a_{\text{int}}(R) = 4\pi G \kappa.$$

In this symmetric case we see that

$$a = \|\mathbf{a}\| = \frac{\partial V}{\partial n}, \quad (1.16)$$

in which the differentiation variable n represents the *normal direction*, the direction perpendicular to the surface S . If the surface S is an *equipotential surface* of the potential V , equation 1.16 applies generally. Then, the attraction vector — more precisely, the acceleration vector — is perpendicular to the surface S , and its magnitude is equal to that of the normal derivative of the potential.



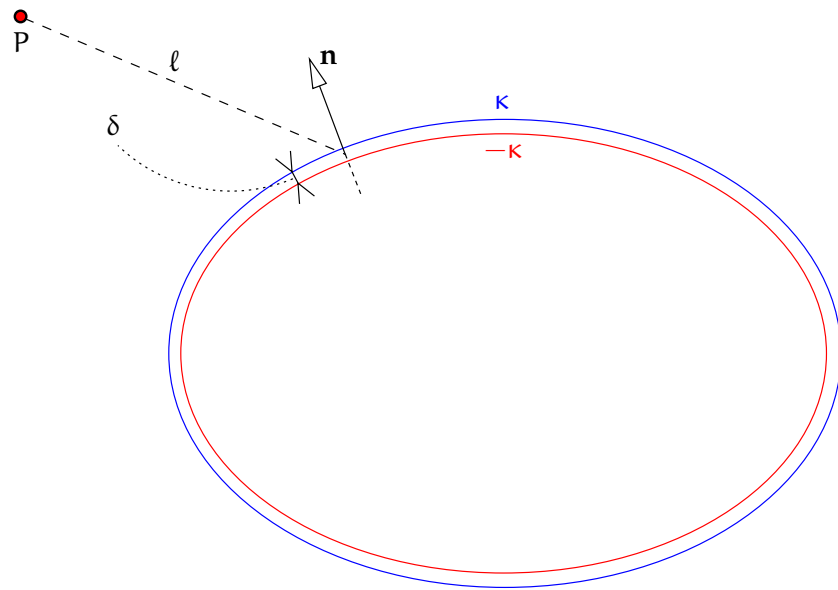


FIGURE 1.4. A double mass-density layer.



1.11 Double mass-density layer

A double mass-density layer may be interpreted as a *dipole-density layer*. The dipoles are oriented in the direction of the surface's normal.

If the dipole consists of two “charges” m and $-m$ in locations \mathbf{r}_1 and \mathbf{r}_2 , in such a way that the vectorial separation between them is $\Delta\mathbf{r} = \mathbf{r}_1 - \mathbf{r}_2$, then the dipole *moment* is $\mathbf{d} = m\Delta\mathbf{r}$, a vectorial quantity. See figure 1.4.

Let the dipole surface density be

$$\mu = \frac{d\mathcal{D}}{dS},$$

in which $d\mathcal{D}$ is a “dipole-layer element”. This layer may be seen as being made up of two single layers. If we have a positive layer at density κ and a negative layer at density $-\kappa$, and the distance between them is δ , we get for small values of δ an approximate correspondence:

$$\mu \approx \delta\kappa. \quad (1.17)$$



The combined potential of the two single mass-density layers computed as explained in the previous section, equation 1.15, is

$$V = G \iint_{\text{surface}} \kappa \left(\frac{1}{\ell_1} - \frac{1}{\ell_2} \right) dS.$$

The following relationship exists between the quantities ℓ_1 , ℓ_2 and δ (Taylor expansion of the function $1/\ell$):

$$\frac{1}{\ell_1} = \frac{1}{\ell_2} + \delta \cdot \frac{\partial}{\partial n} \left(\frac{1}{\ell} \right) + \dots,$$

in which $\frac{\partial}{\partial n}$ is again the derivative of the quantity in the normal direction of the surface.

Substitution into the equation yields

$$V \approx G \iint_{\text{surface}} \kappa \delta \frac{\partial}{\partial n} \left(\frac{1}{\ell} \right) dS = G \iint_{\text{surface}} \mu \frac{\partial}{\partial n} \left(\frac{1}{\ell} \right) dS. \quad (1.18)$$

In the limit in which δ is arbitrarily small and κ correspondingly large, this equation, like equation 1.17, holds exactly.

One can easily show that the above potential is not even continuous. The discontinuity happens at the surface S . Let us look again, for the sake of simplicity, at a sphere of radius R , coated with a double layer of constant dipole density μ .

The exterior potential ($r > R$, r the distance from the centre of the sphere) is

$$V_{\text{ext}} = G\mu \iint_{\text{surface}} \frac{\partial}{\partial n} \left(\frac{1}{\ell} \right) dS = 0,$$

because the potential equals the difference between the potentials of two concentric spherical shells of the same mass.

The interior potential ($r < R$) is

$$V_{\text{int}} = G\mu \iint_{\text{surface}} \frac{\partial}{\partial n} \left(\frac{1}{\ell} \right) dS = G\mu \cdot 4\pi R^2 \left(-\frac{1}{R^2} \right) = -4\pi G\mu,$$

by computing the surface integral using the sphere's centre as the evaluation point, and using the earlier established circumstance that



inside a sphere covered by a *single* constant-density mass-density layer the potential is constant.

Now in the limit $r \rightarrow R$ the result is different for the exterior and interior potentials. The difference is

$$V_{\text{ext}}(R) - V_{\text{int}}(R) = 4\pi G\mu.$$



1.12 The Gauss integral theorem



1.12.1 Presentation

The Gauss integral theorem,¹⁵ famous from physics, looks in vector form like this:

$$\iiint_{\mathcal{V}} \operatorname{div} \mathbf{a} \, d\mathcal{V} = \iint_{\partial\mathcal{V}} \langle \mathbf{a} \cdot \mathbf{n} \rangle \, dS, \quad (1.19)$$

in which \mathbf{n} is the exterior normal to surface S , now as a vector: the length of the vector is assumed $\|\mathbf{n}\| = 1$. $\partial\mathcal{V}$ is the total surface of body \mathcal{V} .

This theorem applies to all differentiable vector fields \mathbf{a} and all “well-behaved” bodies \mathcal{V} on whose surface $\partial\mathcal{V}$, a normal direction \mathbf{n} exists everywhere. In other words, this is not a special property of the gravitational acceleration vector, though it also applies to this vector field.



1.12.2 Intuitive description

Let us note, that¹⁶

$$\operatorname{div} \mathbf{a} = \Delta V = -4\pi G\rho$$

lähteet, nielut

is a *source function*. It stands for the amount, in the part of space inside surface $\partial\mathcal{V}$, of positive and negative “sources” and “sinks” of the gravitational field.

¹⁵Johann Carl Friedrich Gauss (1777–1855) was a German mathematician and universal genius. *Princeps mathematicorum*.

¹⁶Assuming that the potential V exists.



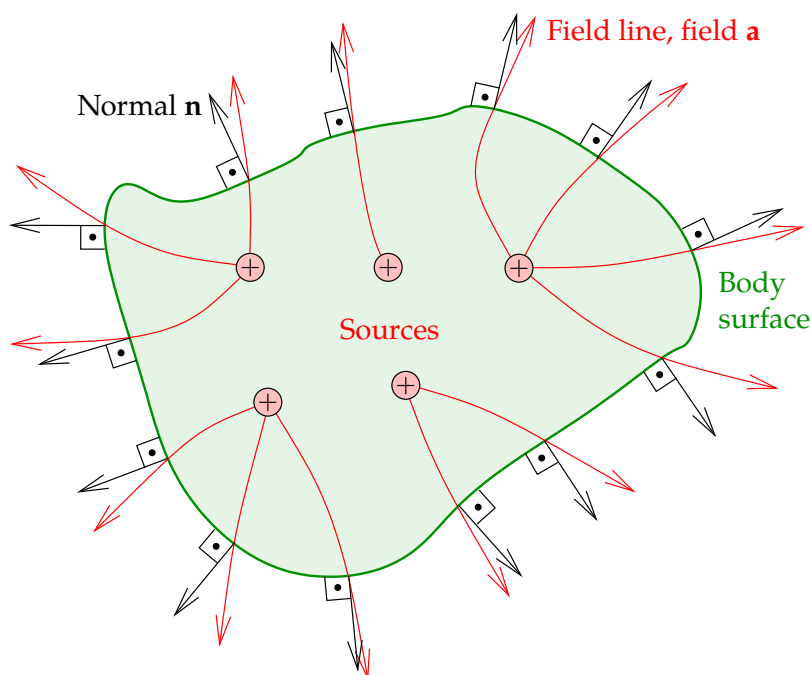


FIGURE 1.5. A graphical explanation of the Gauss integral theorem. The concept of the *field line* was Michael Faraday's invention. The *flux* is the scalar product $\langle \mathbf{a} \cdot \mathbf{n} \rangle$.

The situation is analogous to the flow pattern of a liquid: positive charges correspond to points where liquid is added to the flow, negative charges¹⁷ correspond to “sinks” through which liquid disappears. The vector \mathbf{a} is in this metaphor the velocity of flow; in the absence of “sources” and “sinks” it satisfies the condition $\text{div } \mathbf{a} = 0$, which expresses the conservation and incompressibility of matter.

On the other hand, the function

$$\langle \mathbf{a} \cdot \mathbf{n} \rangle = \frac{\partial V}{\partial n}$$

is often called the *flux*, in other words, how much field stuff “flows out” — just like a liquid flow — from the space inside the surface ∂V through the surface to the outside. vuo

¹⁷But the “charges” for gravitation, the masses, are always positive.



The Gauss integral theorem states the two amounts to be equal: it is in a way a *book-keeping statement* demanding that everything which is produced inside a surface — $\text{div } \mathbf{a}$ — also has to come out through the surface — $\langle \mathbf{a} \cdot \mathbf{n} \rangle$.

In figure 1.5 it is graphically explained that the sum of “sources” over the inner space of the body, $\sum (+ + + \dots)$, has to be the same as the sum of “flux” $\sum (\uparrow\uparrow\uparrow \dots)$ through the whole boundary surface delimiting this inner space.



1.12.3 The potential version of the Gauss theorem

Let us write the Gauss integral theorem a little differently, using the *potential* V instead of the gravitational vector:

$$\iiint_{\mathcal{V}} \Delta V \, d\mathcal{V} = \iint_{\partial\mathcal{V}} \frac{\partial V}{\partial n} \, dS, \quad (1.20)$$

in which we have made the above substitutions. We also here see the popular notation $\partial\mathcal{V}$ for the surface of the body \mathcal{V} . The presentational forms 1.20 and 1.19 are connected by the equations 1.12 and 1.9, connecting V and \mathbf{a} .



1.12.4 Example 1: A little box

Let us look at a little rectangular box with sides Δx , Δy and Δz . The box is so little that the field $\mathbf{a}(x, y, z)$ inside it is an almost linear function of place. Let us write the vector \mathbf{a} into components:

$$\mathbf{a} = a_1 \mathbf{i} + a_2 \mathbf{j} + a_3 \mathbf{k}.$$

Now the volume integral

$$\iiint_{\mathcal{V}} \text{div } \mathbf{a} \, d\mathcal{V} = \left(\frac{\partial a_1}{\partial x} + \frac{\partial a_2}{\partial y} + \frac{\partial a_3}{\partial z} \right) \Delta x \Delta y \Delta z \quad (1.21)$$

while the surface integral

$$\begin{aligned} \iint_{\partial\mathcal{V}} \langle \mathbf{a} \cdot \mathbf{n} \rangle \, dS &= \\ &= (a_1^+ - a_1^-) \Delta y \Delta z + (a_2^+ - a_2^-) \Delta x \Delta z + (a_3^+ - a_3^-) \Delta x \Delta y. \end{aligned}$$



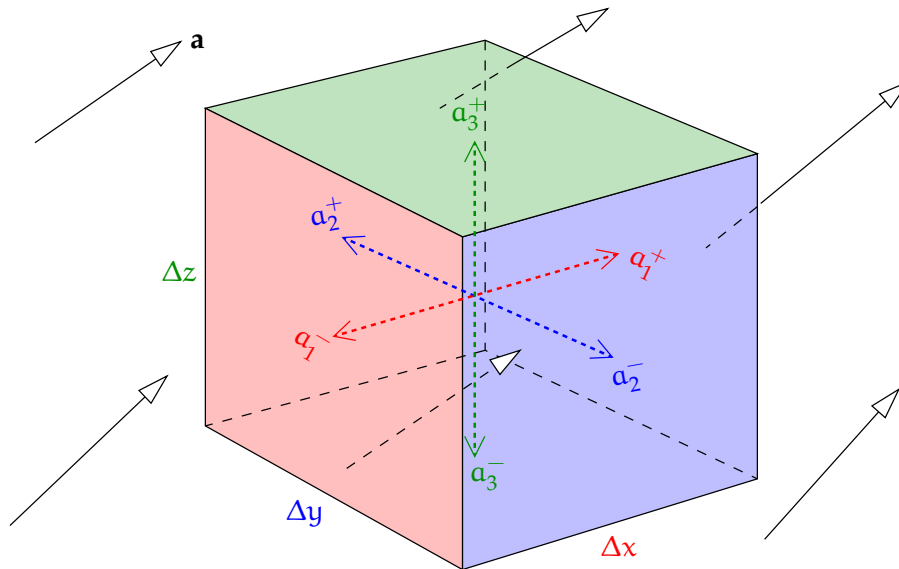


FIGURE 1.6. A little rectangular box.

Here, a_1^+ is the value of component a_1 on the one face in the x direction, and a_1^- its value on the other face, and so on. For example, a_3^+ is the value of a_3 on the box's upper and a_3^- on its lower face. A box has of course six faces, in each of three co-ordinate directions both "up- and downstream".

Then

$$a_1^+ - a_1^- \approx \frac{\partial a_1}{\partial x} \Delta x, \quad a_2^+ - a_2^- \approx \frac{\partial a_2}{\partial y} \Delta y, \quad a_3^+ - a_3^- \approx \frac{\partial a_3}{\partial z} \Delta z,$$

and by substitution we see that

$$\begin{aligned} \iint_{\partial V} \langle \mathbf{a} \cdot \mathbf{n} \rangle dS &\approx \\ &\approx \frac{\partial a_1}{\partial x} \Delta x \cdot \Delta y \Delta z + \frac{\partial a_2}{\partial y} \Delta y \cdot \Delta x \Delta z + \frac{\partial a_3}{\partial z} \Delta z \cdot \Delta x \Delta y = \\ &= \left(\frac{\partial a_1}{\partial x} + \frac{\partial a_2}{\partial y} + \frac{\partial a_3}{\partial z} \right) \Delta x \Delta y \Delta z, \end{aligned}$$

the same equation as 1.21. So, in this simple case, the Gauss equation applies.



Obviously the equation also works, if we build out of these “Lego™ bricks” a larger body, because the faces of the bricks touching each other are oppositely oriented and cancel from the surface integral of the whole body. It is a little harder to prove that the equation also applies to bodies having inclined surfaces.

1.12.5 Example 2: The Poisson equation for a sphere

According to Poisson equation 1.14 we have

$$\Delta V = -4\pi G\rho.$$

Assume a sphere of radius R , within which the mass density ρ is constant. The volume integral over the sphere gives

$$\iiint_{\mathcal{V}} \Delta V \, d\mathcal{V} = -4\pi G\rho \iiint_{\mathcal{V}} d\mathcal{V} = -4\pi G\rho\mathcal{V} = -4\pi GM, \quad (1.22)$$

in which $M = \rho\mathcal{V}$ is the total mass of the sphere.

On the surface of the sphere, the normal derivative is

$$\frac{\partial V}{\partial n} = \left. \frac{\partial}{\partial r} \frac{GM}{r} \right|_{r=R} = -\frac{GM}{R^2},$$

a constant, and its integral over the surface of the sphere is

$$\iint_{\partial\mathcal{V}} \frac{\partial V}{\partial n} \, dS = -\frac{GM}{R^2} \cdot S = -\frac{GM}{R^2} \cdot 4\pi R^2 = -4\pi GM. \quad (1.23)$$

Results 1.23 and 1.22 are identical, as Gauss theorem 1.20 requires.

1.12.6 Example 3: A point mass in an eight-unit cube

See figure 1.7.

Let us assume that we have a point mass of size GM in the centre of a cube bounded by the co-ordinate planes $x = \pm 1$, $y = \pm 1$, and $z = \pm 1$. In that case, the volume integral is

$$\iiint_{\mathcal{V}} \Delta V \, d\mathcal{V} = -4\pi GM \iiint_{\mathcal{V}} \delta(\mathbf{r}) \, d\mathcal{V} = -4\pi GM,$$



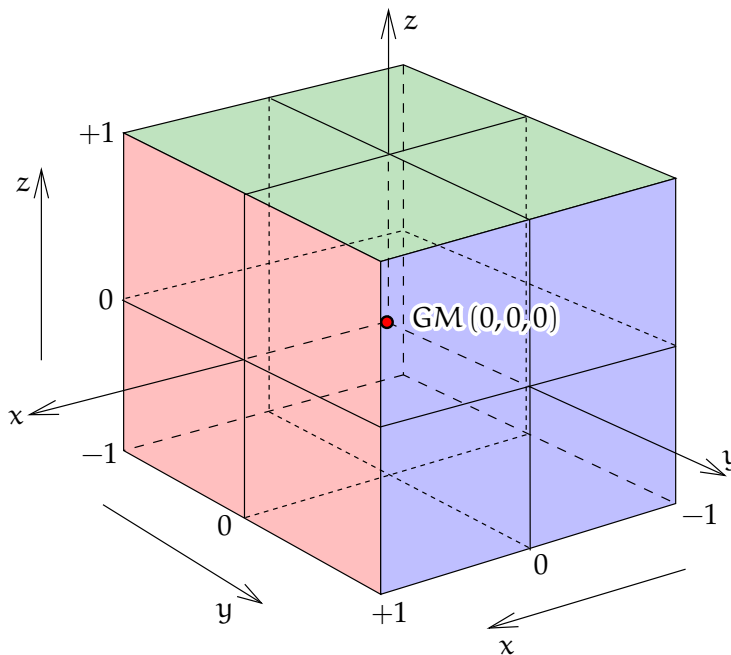


FIGURE 1.7. Eight-unit cube.

in which $\delta(\mathbf{r})$ is Dirac's¹⁸ delta function in space, having an infinite spike at the origin, being zero elsewhere, and producing a value of 1 upon volume integration. The surface integral is six times that over the top face

$$-GM \int_{-1}^{+1} \left(\int_{-1}^{+1} \frac{1}{(x^2 + y^2 + 1)^{3/2}} dx \right) dy.$$

Integrating with respect to x (expression in large brackets) yields

$$\int_{-1}^{+1} \frac{1}{(x^2 + y^2 + 1)^{3/2}} dx = \left[\frac{x}{(y^2 + 1) \sqrt{x^2 + y^2 + 1}} \right]_{-1}^{+1} = \frac{2}{(y^2 + 1) \sqrt{y^2 + 2}}.$$

¹⁸Paul Adrien Maurice Dirac (1902–1984) was an English quantum physicist who found the relativistic wave equation for the electron, and theoretically predicted the existence of antimatter. He was a physics Nobel laureate 1933, shared with Erwin Schrödinger. He is also believed to have been on the autism spectrum (Farmelo, 2011).



Integrating this with respect to y yields

$$\begin{aligned} \int_{-1}^{+1} \frac{2}{(y^2 + 1)\sqrt{y^2 + 2}} dy &= \left[2 \arctan \frac{y}{\sqrt{y^2 + 2}} \right]_{-1}^{+1} = \\ &= 4 \arctan \frac{1}{\sqrt{3}} = 4 \cdot \frac{\pi}{6} = \frac{2}{3}\pi. \end{aligned}$$

Adding the six faces together yields

$$\begin{aligned} -6 \cdot GM \int_{-1}^{+1} \left(\int_{-1}^{+1} \frac{1}{(x^2 + y^2 + 1)^{3/2}} dx \right) dy &= -6 \cdot GM \cdot \frac{2}{3}\pi = \\ &= -4\pi GM, \end{aligned}$$

agreeing with the volume result above.



1.13 Green's theorems

Apply the Gauss integral theorem to the vector field

$$\mathbf{F} = U \nabla V.$$

Here, U and V are two different scalar fields. We obtain

$$\begin{aligned} \iiint_{\mathcal{V}} \operatorname{div} \mathbf{F} d\mathcal{V} &= \iiint_{\mathcal{V}} \langle \nabla \cdot (U \nabla V) \rangle d\mathcal{V} = \\ &= \iiint_{\mathcal{V}} U \langle \nabla \cdot \nabla \rangle V d\mathcal{V} + \iiint_{\mathcal{V}} \langle \nabla U \cdot \nabla V \rangle d\mathcal{V} = \\ &= \iiint_{\mathcal{V}} U \Delta V d\mathcal{V} + \iiint_{\mathcal{V}} \left(\frac{\partial U}{\partial x} \frac{\partial V}{\partial x} + \frac{\partial U}{\partial y} \frac{\partial V}{\partial y} + \frac{\partial U}{\partial z} \frac{\partial V}{\partial z} \right) d\mathcal{V} \end{aligned}$$

and

$$\begin{aligned} \iint_{\partial \mathcal{V}} \langle \mathbf{F} \cdot \mathbf{n} \rangle dS &= \iint_{\partial \mathcal{V}} \langle U \nabla V \cdot \mathbf{n} \rangle dS = \iint_{\partial \mathcal{V}} U \langle \nabla V \cdot \mathbf{n} \rangle dS = \\ &= \iint_{\partial \mathcal{V}} U \frac{\partial V}{\partial n} dS. \end{aligned}$$



The result is *Green's¹⁹ first theorem*:

$$\begin{aligned} \iiint_{\mathcal{V}} u \Delta v \, d\mathcal{V} + \iiint_{\mathcal{V}} \left(\frac{\partial u}{\partial x} \frac{\partial v}{\partial x} + \frac{\partial u}{\partial y} \frac{\partial v}{\partial y} + \frac{\partial u}{\partial z} \frac{\partial v}{\partial z} \right) d\mathcal{V} = \\ = \iint_{\partial \mathcal{V}} u \frac{\partial v}{\partial n} \, dS. \end{aligned}$$

This may be cleaned up, because the second term on the left is *symmetric* for the interchange of the scalar fields u and v . Let us therefore interchange u and v , and subtract the equations obtained from each other. The result is *Green's second theorem*:

$$\iiint_{\mathcal{V}} (u \Delta v - v \Delta u) \, d\mathcal{V} = \iint_{\partial \mathcal{V}} \left(u \frac{\partial v}{\partial n} - v \frac{\partial u}{\partial n} \right) dS.$$

We assume in all operations that the functions u and v are “well-behaved”: for example, all required derivatives exist everywhere in body \mathcal{V} .

A useful special case arises by choosing for the function u :

$$u = 1/\ell,$$

in which ℓ is the distance from the given point of evaluation P . This function u is well-behaved everywhere *except* precisely at point P , where it is not defined.

In the case when point P is outside the surface $\partial \mathcal{V}$, the result, *Green's third theorem*, is now obtained by substitution:

$$\iiint_{\mathcal{V}} \frac{1}{\ell} \Delta v \, d\mathcal{V} = \iint_{\partial \mathcal{V}} \left(\frac{1}{\ell} \frac{\partial v}{\partial n} - v \frac{\partial}{\partial n} \left(\frac{1}{\ell} \right) \right) dS.$$

This case is depicted in figure 1.8.

In the case that point P is inside surface $\partial \mathcal{V}$, the computation becomes a little more complicated. Let us learn about a clever technique that — in this case as in others — comes to the rescue.

¹⁹George Green (1793–1841) was a British mathematical physicist, an autodidact, working as a miller near Nottingham. He also invented the word “potential”. [Green \(1828\)](#); [O'Connor and Robertson \(1998\)](#); [Green's Windmill](#).



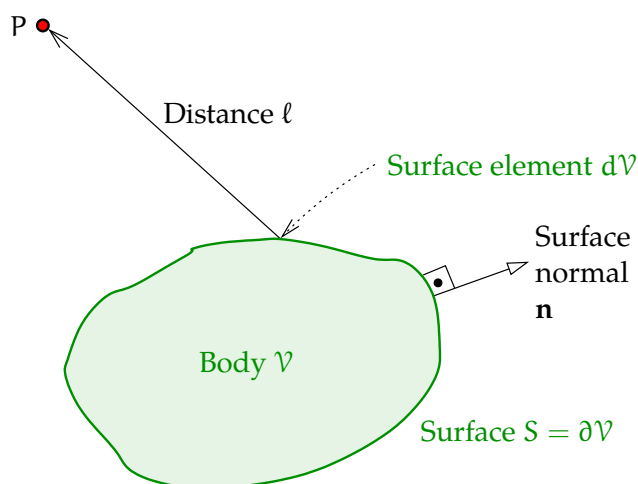


FIGURE 1.8. Geometry for deriving Green's third theorem if point P is outside surface $\partial\mathcal{V}$.

We form a small sphere of radius ϵ called \mathcal{V}_2 around point P; now we can formally define the body (containing a hole) $\mathcal{V} \stackrel{\text{def}}{=} \mathcal{V}_1 - \mathcal{V}_2$, and also its surface $\partial\mathcal{V}$ which consists of two parts, $\partial\mathcal{V} = \partial\mathcal{V}_1 - \partial\mathcal{V}_2$.

Now we may write the volume integral into two parts:

$$\iiint_{\mathcal{V}} \frac{1}{\ell} \Delta V \, d\mathcal{V} = \iiint_{\mathcal{V}_1} \frac{1}{\ell} \Delta V \, d\mathcal{V} - \iiint_{\mathcal{V}_2} \frac{1}{\ell} \Delta V \, d\mathcal{V},$$

where the second term can be integrated in spherical co-ordinates:

$$\iiint_{\mathcal{V}_2} \frac{1}{\ell} \Delta V \, d\mathcal{V} \approx \Delta V_P \int_0^\epsilon 4\pi\ell^2 \frac{1}{\ell} \, d\ell = 2\pi\Delta V_P \epsilon^2,$$

which will go to zero in the limit $\epsilon \rightarrow 0$.

For the first surface integral we obtain using Gauss integral theorem

1.20 :

$$\iint_{\partial\mathcal{V}_2} \frac{1}{\ell} \frac{\partial V}{\partial n} \, dS = \frac{1}{\epsilon} \iint_{\partial\mathcal{V}_2} \frac{\partial V}{\partial n} \, dS = \frac{1}{\epsilon} \iiint_{\mathcal{V}_2} \Delta V \, d\mathcal{V} \approx \frac{1}{\epsilon} \Delta V_P \cdot \frac{4}{3}\pi\epsilon^3,$$

which also goes to zero for $\epsilon \rightarrow 0$.

The second surface integral (the normal is pointing away from P):

$$-\iint_{\partial\mathcal{V}_2} V \frac{\partial}{\partial n} \left(\frac{1}{\ell} \right) \, dS = -\iint_{\partial\mathcal{V}_2} V \cdot -\frac{1}{\epsilon^2} \, dS \approx 4\pi\epsilon^2 \cdot \frac{1}{\epsilon^2} V_P = 4\pi V_P.$$



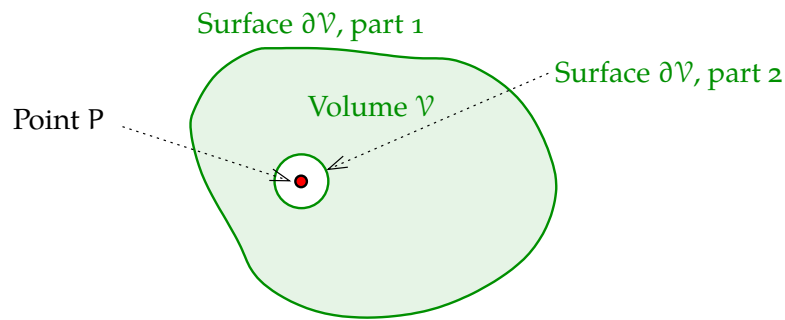


FIGURE 1.9. Geometry for deriving Green's third theorem if point P is inside surface $\partial\mathcal{V}$.

By combining all results with their correct algebraic signs we obtain for the case where P is inside surface $\partial\mathcal{V}_1 \sim \partial\mathcal{V}$:

$$\iiint_{\mathcal{V}} \frac{1}{\ell} \Delta V \, d\mathcal{V} = -4\pi V_P + \iint_{\partial\mathcal{V}} \left(\frac{1}{\ell} \frac{\partial V}{\partial n} - V \frac{\partial}{\partial n} \left(\frac{1}{\ell} \right) \right) dS. \quad (1.24)$$

After this it must be intuitively clear, and we present without formal proof, that

$$\iiint_{\mathcal{V}} \frac{1}{\ell} \Delta V \, d\mathcal{V} = -2\pi V_P + \iint_{\partial\mathcal{V}} \left(\frac{1}{\ell} \frac{\partial V}{\partial n} - V \frac{\partial}{\partial n} \left(\frac{1}{\ell} \right) \right) dS$$

if point P is precisely *on* the boundary surface $\partial\mathcal{V}$ of body \mathcal{V} . This however presupposes that the normal derivative, and especially the *normal direction*, actually exist at precisely point P!

In geodesy, the typical situation is that where the body \mathcal{V} over the volume of which one wants to evaluate the volume integral, is *the whole space outside the Earth*. In this case, we conveniently have $\Delta V = 0$ and the whole volume integral appearing above vanishes.

Result 1.24 may be generalised to this case, where \mathcal{V} is the whole space outside surface $\partial\mathcal{V}$. This generalisation is made by now choosing as the surface $\partial\mathcal{V}$ the three-part surface $\partial\mathcal{V} = \partial\mathcal{V}_1 + \partial\mathcal{V}_2 + \partial\mathcal{V}_3$, in which $\partial\mathcal{V}_3$ is a sphere of large radius centred on P. Its radius is then allowed to *grow* in the limit *to infinity*, and it can be shown that both integrals over the



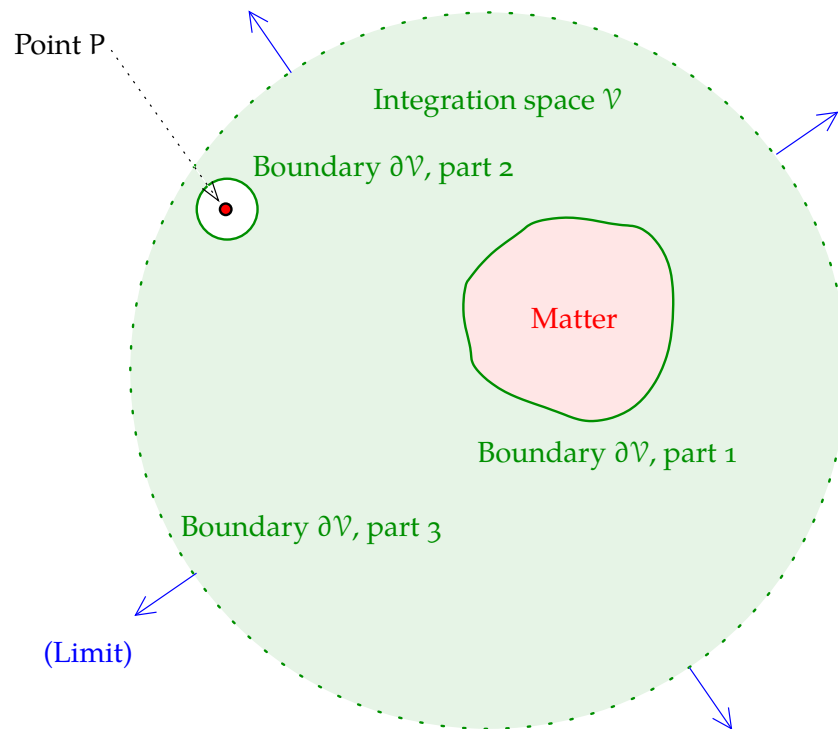


FIGURE 1.10. Green's third theorem for the space external to a body.

surface $\partial\mathcal{V}_3$ vanish. The volume integral over the part of space outside this surface also vanishes, being over empty space where $\Delta V = 0$.

The end result is — note that \mathbf{n} is now the exterior normal of the Earth's surface:

$$\iiint_{\mathcal{V}} \frac{1}{\ell} \Delta V \, d\mathcal{V} = -4\pi V_P - \iint_{\partial\mathcal{V}} \left(\frac{1}{\ell} \frac{\partial V}{\partial \mathbf{n}} - V \frac{\partial}{\partial \mathbf{n}} \left(\frac{1}{\ell} \right) \right) dS, \quad (1.25)$$

Because in this case, in which \mathcal{V} is the empty space exterior to the Earth, the left-hand side volume integral vanishes, we may express the potential V_P at point P suitably as a two-term surface integral over surface $\partial\mathcal{V}$.



1.14 The Chasles theorem

We study the above-described case where the “body” is the space outside the surface $\partial\mathcal{V}$ — in practice: the space outside the Earth.

From Green’s theorem 1.25 derived above, we may derive for a *harmonic function* V (so, $\Delta V = 0$) in the exterior space:

$$V_P = -\frac{1}{4\pi} \iint_{\partial\mathcal{V}} \frac{1}{\ell} \frac{\partial}{\partial n} V \, dS + \frac{1}{4\pi} \iint_{\partial\mathcal{V}} V \frac{\partial}{\partial n} \left(\frac{1}{\ell} \right) \, dS. \quad (1.26)$$

Interpretation The exterior, harmonic potential of an arbitrarily shaped body can be represented as the sum of a single and a double mass-density layer on the body’s surface.

Explanation We obtain the surface density of a single mass layer using equation 1.15,

$$\kappa = -\frac{1}{4\pi G} \frac{\partial}{\partial n} V, \quad (1.27)$$

and the surface density of a double mass layer using equation 1.18,

$$\mu = \frac{V}{4\pi G}.$$

If we plug these into equation 1.26, we obtain

$$V_P = G \iint_{\partial\mathcal{V}} \left(\frac{\kappa}{\ell} + \mu \frac{\partial}{\partial n} \left(\frac{1}{\ell} \right) \right) \, dS.$$

In the case that the surface $\partial\mathcal{V}$ is an equipotential surface of the potential V , so $V = V_0$, it follows that a single mass-density layer suffices, because in that case

$$\iint_{\partial\mathcal{V}} V \frac{\partial}{\partial n} \left(\frac{1}{\ell} \right) \, dS = V_0 \iint_{\partial\mathcal{V}} \frac{\partial}{\partial n} \left(\frac{1}{\ell} \right) \, dS = 0.$$

The right-hand side integral vanishes based on the Gauss integral theorem. This is because the function $1/\ell$, with ℓ the distance from point P , is *harmonic inside* the Earth’s body. The surface of the Earth is



∂V . This is the Chasles²⁰ theorem, also called the Green equivalent-layer theorem.

The theorem is used in Molodensky's²¹ theory. The representation of the Earth's gravity field by underground point-mass layers, for example Vermeer (1984), could also be justified with this theorem.

The case where ∂V is an equipotential surface is realised if the body is fluid and seeks by itself an external form equal to an equipotential surface. For planet Earth, this applies for the ocean surface. In electrostatic theory, for a conductor in which the electrons can move freely, the physical surface will also become an equipotential surface. And the electric charges of a conductor are always on its outer surface.²²

Equation 1.26, with substitution 1.27, simplifies in this case as follows:

$$V_P = -\frac{1}{4\pi} \iint_{\partial V} \frac{1}{\ell} \frac{\partial}{\partial n} V \, dS = G \iint_{\partial V} \frac{\kappa}{\ell} \, dS. \quad (1.28)$$

The equation tells us that we can compute the whole potential exterior to the Earth, if only on the surface of the Earth — the shape of which we also assume given in order to compute $1/\ell$! — is given the gradient of the potential in the normal or vertical direction $\frac{\partial}{\partial n} V$. This gradient is precisely the gravitational acceleration, a quantity obtainable from gravimetric measurements. All of gravimetric geopotential determination ("geoid determination"), ever since G. G. Stokes, has been based on this.

²⁰Michel Chasles (1793–1880) was a French mathematician and geometrician, one of the 72 whose names are inscribed on the Eiffel Tower, [Eiffel Tower, 72 names](#).

²¹Mikhail Sergeevich Molodensky (1909–1991) was an illustrious Russian physical geodesist.

²²This is because the electrostatic potential inside a conductor must also be constant. Even a single electron inside the body would make this impossible.





1.15 Boundary-value problems

The boundary-value problem (BVP) is the problem of computing the potential V throughout space (or throughout a body's exterior or interior part of space) from given values relating to V on the boundary surface of the body, for example on the surface of the Earth. The simplest boundary-value problem is Dirichlet's²³ problem: the potential V itself is given on the boundary surface. More complicated boundary-value problems are based on *linear functionals* of the potential: on the boundary, some linear expression in V is given, for example a derivative or linear combination of derivatives, generally

reuna-
arvotehtävä

$$L\{V\},$$

with $L\{\cdot\}$ being a linear operator.

The Dirichlet boundary-value problem *in the form popular in geodesy* is: determine the potential field V if its values are given on a closed surface S , and furthermore it is given that V is *harmonic* ($\Delta V = 0$) outside surface S . In the vacuum of space, the potential is always harmonic, as already earlier noted: the potential of a point mass m_P , $V = Gm_P/\ell$, is a harmonic function everywhere except at point P — and an extended body consists, in the limit, of many point masses or mass elements.

In the general case, this is a theoretically challenging problem. The existence and uniqueness of the solution has been proven very generally, see [Heiskanen and Moritz \(1967, page 18\)](#).

Based on the values of the potential function V on the surface S we may thus compute the harmonic function $V(x, y, z)$ throughout space outside the surface. The boundary-value problem is a powerful general method also applied in physical geodesy. One must however note that from potential values given on the surface it is not possible to

²³Peter Gustav Lejeune Dirichlet (1805–1859) was a German mathematician also known for his contributions to number theory.



uniquely resolve *the mass distribution inside the Earth*, which generates this potential.

This is clear already in the simple case of a constant potential on the surface of a sphere. If additionally it is given that the mass distribution is spherically symmetric, then nevertheless the density profile along the radius remains indeterminate. All mass may be concentrated in the centre, or it may form a thin layer just below the sphere's surface, or any alternative between these two extremes. Without additional information — for example from seismic studies or geophysical density models — we cannot resolve this issue.

The Chasles theorem mentioned above, equation 1.26, and its special case, equation 1.28, are also examples of this: the theorem shows how one may describe the exterior potential as generated by a mass distribution on the surface of a body, although *we know* that the field's source is a mass distribution extending throughout the body!

This is a fundamental limitation of all methods that try to obtain information on the situation inside the Earth based only on *gravimetric* measurements on or outside the Earth.



Self-test questions

1. Which instrument was used to determine the constant G ? Why is it difficult to obtain a precise value for this constant?
2. Why do all objects, irrespective of their mass, undergo the same acceleration of free fall, although the gravitational attraction on a more massive body is obviously stronger?
3. What is a *conservative* force field?
 - (a) A force field for which the force can be written as the gradient of a unique potential.
 - (b) A force field in which an object carried along a closed loop will not gain and not lose energy.



- (c) An attractive force field from which no object can escape.
- (d) A force field the curl of which vanishes everywhere.
4. On the surface of a homogeneous, spherical asteroid the acceleration of free fall is 1 cm/s^2 . What is the acceleration of free fall on another asteroid that is otherwise similar, but has twice the diameter?
- (a) 0.25 cm/s^2
- (b) 1 cm/s^2
- (c) 2 cm/s^2
- (d) 4 cm/s^2
5. What is a *harmonic* potential?
6. What is the *order* of the Laplace differential equation?
7. Is a linear potential, $V(x, y, z) = a + bx + cy + dz$ (a, b, c, d constants), harmonic?
8. If the potential in the previous question is a gravitational potential, calculate its *acceleration vector*.
9. Under what condition is it possible to describe the external gravitational field emanating from a body as produced by a single mass-density layer on the surface of that body?
10. The dipole-layer density μ is mentioned in section 1.11. What is the SI unit of this quantity?



Exercise 1 – 1: Core of the Earth

- Derive the equation giving the acceleration of gravity g on the surface of a homogeneous-density sphere, if the density ρ and radius R_{core} are given.
- The Earth's iron-nickel core has a mean density of 11 g/cm^3 and its radius is 3500 km. Compute the acceleration of gravitation on its surface g_{core} .



3. What is the attraction g at the centre of the core? What can you say *in general* about the geopotential in this point (*do not try to calculate it*)?
4. Derive the equation for the radial gravitational gradient $\frac{\partial}{\partial r}g$ on the surface of a homogeneous-density sphere of density ρ .



Exercise 1 – 2: Atmosphere

1. The mean pressure of the atmosphere at sea level is 1013.25 hPa (the unit for pressure, the Pascal, is defined as $\text{Pa} = \text{N}/\text{m}^2$.) On the Earth's surface gravity is $9.81 \text{ m}/\text{s}^2$. Calculate the mean surface density as a thin layer κ in units of kg/m^2 .
2. Calculate the total mass of the atmosphere using the spherical shell approximation. You may take as its radius 6378 km.
3. Calculate the attraction generated by the atmosphere outside it, both as acceleration and as a fraction of the total Earth attraction.
4. How much is the attraction from the atmosphere inside the atmosphere?



Exercise 1 – 3: The Gauss theorem

There is a deposit (body) of iron ore inside the Earth, which generates (in the flat Earth approximation!) an attraction on the Earth's surface, which has been drawn as the a curve. See figure 1.11.

The true attraction curve is *approximated* by a simple function

$$a = \begin{cases} a_0 & \text{if } r \leq d \\ 0 & \text{if } r > d \end{cases}$$

(red dashed line), where r is the distance from the point on the Earth's surface straight above the ore deposit. So, the area where $a \neq 0$ is a *disk* of radius d on the surface of the Earth.



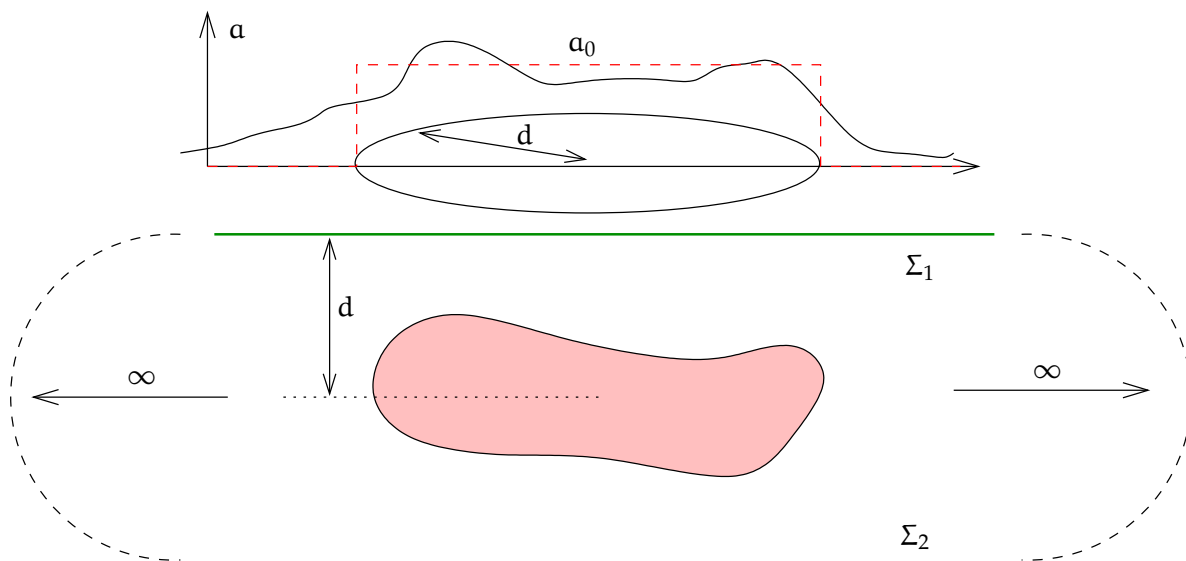


FIGURE 1.11. Iron ore body.

1. Compute, using the above approximation for \mathbf{a} , the surface integral

$$\iint_{\Sigma_1} \mathbf{a} \, dS,$$

where Σ_1 is the surface of the Earth, see figure 1.11.

2. According to the Gauss integral theorem

$$\begin{aligned} \iint_{\Sigma_1} \langle \mathbf{a}_1 \cdot \mathbf{n}_1 \rangle \, dS + \iint_{\Sigma_2} \langle \mathbf{a}_2 \cdot \mathbf{n}_2 \rangle \, dS &= \iiint_{\text{volume}} \Delta V \, dV = \\ &= \iiint_{\text{volume}} -4\pi G \rho_{\text{iron}} \, dV = -4\pi G M_{\text{body}}, \end{aligned}$$

in which $\Sigma_1 + \Sigma_2$ is the (two part) closed surface around the body. The parts meet at infinity. \mathbf{a}_1 and \mathbf{a}_2 are the attraction vectors on the surface of the Earth and on the surface Σ_2 , and \mathbf{n}_1 and \mathbf{n}_2 are the exterior normals to the surfaces.

Assuming that

$$\iint_{\Sigma_1} \langle \mathbf{a}_1 \cdot \mathbf{n}_1 \rangle \, dS = \iint_{\Sigma_2} \langle \mathbf{a}_2 \cdot \mathbf{n}_2 \rangle \, dS = - \iint_{\Sigma_1} \mathbf{a} \, dS,$$

calculate GM_{body} . Be careful with the algebraic signs!



3. Assuming that the deposit is a sphere at depth d , calculate GM using Newton's law of gravitation from the value a_0 straight above the deposit at the Earth's surface.
4. Compare results 2 and 3 and draw conclusions. Is the function a given above a good approximation?





The Laplace equation and its solutions

2



2.1 The nature of the Laplace equation

The Laplace equation is central to the study of the Earth's gravitational field:

$$\Delta V = \left(\frac{\partial^2}{\partial x^2} + \frac{\partial^2}{\partial y^2} + \frac{\partial^2}{\partial z^2} \right) V = 0.$$

We call the symbol Δ the *Laplace operator*. Often, the alternative notation ∇^2 is used.

If we study gravitation as a field, the Laplace equation is more natural than Newton's formalism. Newton's equation is used when the mass distribution is known: it yields directly the gravitational force caused by the masses.

The Laplace equation, on the other hand, is a *partial differential equation*. Its solution gives the *potential* $V(x, y, z)$ of the gravitational field throughout space or a part of space. From this potential one may then calculate the effect of the field on a body moving in space at the location where the body is. This is a two-phase process. It is conceptually new here that a certain property, a *field*, is attributed to empty space, and we no longer talk about action at a distance directly between two bodies.

Solving the Laplace equation in the general case may be difficult. The approach generally taken is that we choose some co-ordinate frame

— a rectangular frame (as above), spherical co-ordinates, cylindrical co-ordinates, toroidal co-ordinates, or whatever — which agrees best with the geometry of the problem at hand. Then, we *transform* the Laplace equation to those co-ordinates, we find special solutions of a certain form, and finally we compose a general — or not-so-general — solution as a linear combination of those special solutions, i.e., a *series expansion*.

Fortunately, the theory of linear partial differential equations is well-developed. Similar theoretical problems are encountered in the theories of electromagnetic fields (Maxwell theory) and quantum mechanics (Schrödinger¹ equation), not to mention fluid and heat flow.

It is important to note that the Laplace equation is *linear*. This means that, if two solutions are given

$$\Delta V_1 = 0, \quad \Delta V_2 = 0,$$

then their linear combinations

$$V = \alpha V_1 + \beta V_2, \quad \alpha, \beta \in \mathbb{R}$$

are also good solutions: $\Delta V = 0$. This property of linearity makes it possible to seek general solutions as linear combinations or series expansions of basic solutions.

A peculiarity that also distinguishes the Laplace equation from Newton's equation is that it is a *local* equation. It characterises the behaviour of the potential field in a small neighbourhood of one point. However, the solution is sought for a whole area. The solution approach commonly used is the *boundary-value problem*. This means that the field

raja-arvotehtävä

¹Erwin Rudolf Josef Alexander Schrödinger (1887–1961) was a German physicist and quantum theorist, the inventor of the wave equation of matter named after him, which earned him the 1933 physics Nobel (shared with Paul Dirac), and of the eponymous unobserved cat, which finds itself in a superposition state of being both alive and dead.



values (“boundary values”) have to be given only on the boundary of a certain part of space, for example on the Earth’s surface. From this, one calculates the values of the field in outer space — the behaviour of the field inside the Earth remains outside the scope of our interest. From the perspective of the exterior gravitational field, one does not even need to know the precise mass distribution inside the Earth — and one cannot even determine it using only measurement values obtained on and above the Earth’s surface!



2.2 The Laplace equation in rectangular co-ordinates

It is a learning experience to write and solve the Laplace equation in rectangular co-ordinates. The case is analogous to that of spherical co-ordinates but the maths is much simpler.

Assume that the Earth’s surface, or sea level, is the level surface for z co-ordinates $z = 0$. Then

$$\Delta V = \left(\frac{\partial^2}{\partial x^2} + \frac{\partial^2}{\partial y^2} + \frac{\partial^2}{\partial z^2} \right) V = \Delta(X(x) \cdot Y(y) \cdot Z(z)),$$

in which we have “experimentally” written

$$V(x, y, z) = X(x) \cdot Y(y) \cdot Z(z).$$

In other words, we write experimentally V as the product of three factor functions, with each factor function depending only on one co-ordinate — the “separation of variables”. A realistic potential function V will of course usually not be in this form. We may however hope to write it as a linear combination of terms that *are* in the above form, thanks to the linearity of the Laplace equation.

muuttujen
erottaminen

By taking all the partial derivatives, we obtain

$$YZ \frac{\partial^2}{\partial x^2} X + XZ \frac{\partial^2}{\partial y^2} Y + XY \frac{\partial^2}{\partial z^2} Z = 0.$$

Dividing by the expression XYZ yields

$$\frac{1}{X(x)} \frac{\partial^2}{\partial x^2} X(x) + \frac{1}{Y(y)} \frac{\partial^2}{\partial y^2} Y(y) + \frac{1}{Z(z)} \frac{\partial^2}{\partial z^2} Z(z) = 0.$$



Because this has to be true in the whole space, i.e., for *all* combinations of values x, y, z , it follows that *each term must be a constant*. If we take for the first and second constants $-\omega_x^2$ and $-\omega_y^2$, we get in conclusion for the third constant $\omega_x^2 + \omega_y^2$. By writing this definition and result out and moving the denominator to the other side, we obtain

$$\frac{\partial^2}{\partial x^2} X(x) = -\omega_x^2 X(x),$$

(why the minus sign? We shall presently see. . .)

$$\frac{\partial^2}{\partial y^2} Y(y) = -\omega_y^2 Y(y),$$

and

$$\frac{\partial^2}{\partial z^2} Z(z) = (\omega_x^2 + \omega_y^2) Z(z).$$

Now, the solution is readily found at least to the first two equations: they are *harmonic oscillators*, and their basis solutions² are

harmoninen
värehtelijä

$$X(x) = \exp(\pm i\omega_x x),$$

$$Y(y) = \exp(\pm i\omega_y y).$$

The solution of the Z equation, on the other hand, is exponential:

$$Z(z) = \exp\left(\pm z\sqrt{\omega_x^2 + \omega_y^2}\right).$$

We can now form basis solutions in space:

$$V_{\omega_x\omega_y}(x, y, z) = \exp\left(i(\pm\omega_x x \pm \omega_y y) \pm z\sqrt{\omega_x^2 + \omega_y^2}\right).$$

The general solution is obtained by summing the terms $V_{\omega_x\omega_y}$ for different values of ω_x and ω_y with varying coefficients.

We cannot choose the value pair (ω_x, ω_y) entirely freely. The values which are allowed will depend on the *boundary conditions* given.

Let us assume that in both the x and y directions the size of our world is L ("shoebox world"³). Let us make things a little simpler by

²Alternative basis solutions are $X(x) = \sin \omega_x x$, $X(x) = \cos \omega_x x$ etc. They are equivalent to those presented because $\exp(i\omega_x x) = \cos \omega_x x + i \sin \omega_x x$, $\exp(-i\omega_x x) = \cos \omega_x x - i \sin \omega_x x$.

³. . . although real-world shoeboxes are rarely square.



The Laplace equation in rectangular co-ordinates

assuming that on the boundary surfaces of our shoebox world we have the *boundary conditions*

$$V(0, y, z) = V(L, y, z) = V(x, 0, z) = V(x, L, z) = 0.$$

It then follows that the only pairs (ω_x, ω_y) that yield a solution that fits the box are

$$\omega_x = \frac{\pi j}{L}, \omega_y = \frac{\pi k}{L}, j, k \in \mathbb{Z},$$

and the only suitable functions are sine functions. Thus we obtain as a solution:

$$V_{jk}(x, y, z) = \sin\left(\pi j \frac{x}{L}\right) \sin\left(\pi k \frac{y}{L}\right) \exp\left(\pm \pi \sqrt{(j^2 + k^2)} \frac{z}{L}\right).$$

This particular solution may now be generalised by multiplying it by suitable coefficients, and summing it over different index values $j = 0, \pm 1, \pm 2, \dots$ and $k = 0, \pm 1, \pm 2, \dots$. We may however remark that the terms for which $j = 0$ or $k = 0$ will always vanish, and the terms that contain $j = +n$ and $j = -n$, or $k = +n$ and $k = -n$, $n \in \mathbb{N}$, are (apart from their algebraic signs) identical. Therefore in practice we sum over the values $j = 1, 2, \dots$ and $k = 1, 2, \dots$.

Different boundary conditions will give slightly different general solutions. Their general form is, however, always similar.

The zero-level $z = 0$ expansion resulting from the general solution is the familiar Fourier⁴ sine expansion:

$$V(x, y, 0) = \sum_{j=1}^{\infty} \sum_{k=1}^{\infty} v_{jk} \overbrace{\sin\left(\pi \frac{jx}{L}\right) \sin\left(\pi \frac{ky}{L}\right)}^{V_{jk}(x,y)}, \quad (2.1)$$

in which v_{jk} are Fourier coefficients, and the expressions

$$V_{jk}(x, y) \stackrel{\text{def}}{=} \sin\left(\pi \frac{jx}{L}\right) \sin\left(\pi \frac{ky}{L}\right)$$

⁴Joseph Fourier (1768–1830) was a French mathematician and physicist — and some would say, climatologist — one of the Eiffel Tower's 72 names, [Eiffel Tower, 72 names](#).



are two-dimensional basis functions on the Earth's surface, more precisely, on level $z = 0$.

We refer to section **B.2.2** in appendix **B** for a description with illustration of how a Fourier analysis and synthesis on a simple function is done, and how the Fourier expansion approximates the original function as terms are added.

A complete three-dimensional expansion again is

$$V(x, y, z) = \sum_{j=1}^{\infty} \sum_{k=1}^{\infty} \overbrace{v_{jk} \sin\left(\pi \frac{jx}{L}\right) \sin\left(\pi \frac{ky}{L}\right)}^{V_{jk}(x,y)} \exp\left(\pm \pi \sqrt{j^2 + k^2} \frac{z}{L}\right). \quad (2.2)$$

The z expression may have a positive as well as a negative algebraic sign! Of course the solution with a positive sign goes to $\rightarrow \infty$ when $z \rightarrow \infty$, which is not physically realistic in the exterior space.

Note also that $V(x, y, 0)$ and v_{jk} represent *the same gravitational field* in two essentially different ways: in the space domain, and in the — spatial — frequency, or wave-number, domain. The information content in the two is the same. They can be transformed into each other by the forward and inverse Fourier transforms \mathcal{F} and \mathcal{F}^{-1} .

In fact, the information content in $V(x, y, 0)$ is in principle the same as that in $V(x, y, z)$ for *any* level z : knowing the potential on one surface means — with the Laplace equation — knowing the potential throughout space.

kommutoiva
kaavio

We summarise equations **2.1** and **2.2** still in commutative diagram **2.2**.

The takeaway from this is that the operation of vertically shifting the potential field V from zero level to the level z , which is not straightforward in the space domain, becomes simple — as in a straightforward multiplication — in the frequency domain.⁵ The same applies in

⁵The reason for this, as we shall later discuss more generally, is that the vertical shift operation is a *convolution*.



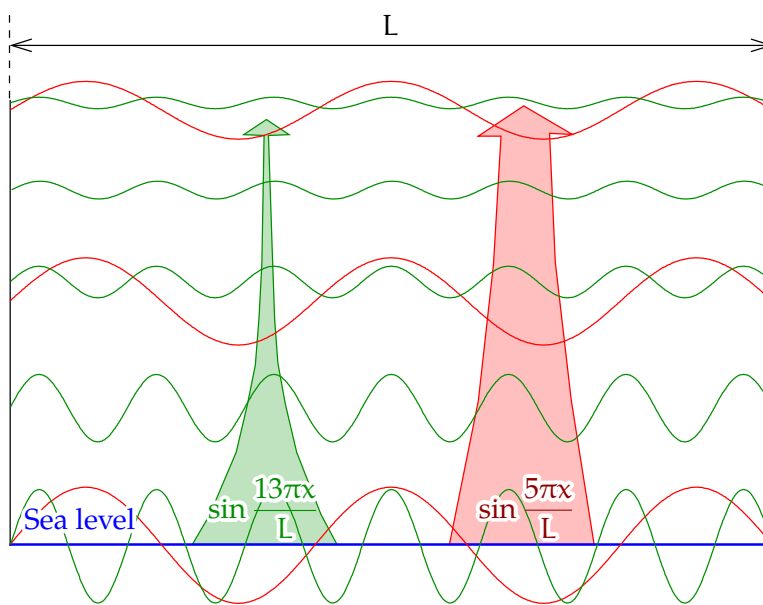


FIGURE 2.1. The exponential attenuation of gravitational field Fourier waviness with height. Rectangular geometry, one dimension. Long waves (small wave numbers, red) attenuate more slowly with height than short waves (green), meaning that height acts as a low-pass filter.

spherical co-ordinates, where the frequency domain means spherical-harmonic coefficients, as we shall see.

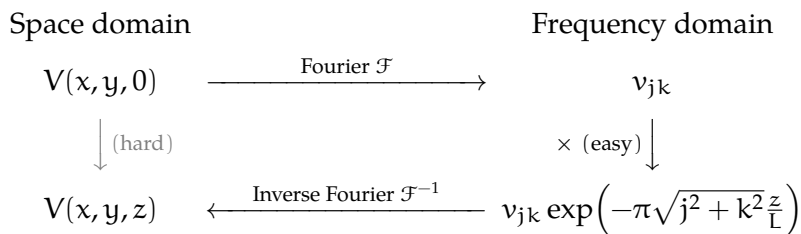


FIGURE 2.2. Vertically shifting the potential field V in the space and frequency domains. Rectangular geometry.





2.3 The Laplace equation in polar co-ordinates

In polar co-ordinates, two-dimensionally, the Laplace equation is

$$\Delta V = \frac{\partial^2 V}{\partial r^2} + \frac{1}{r} \frac{\partial V}{\partial r} + \frac{1}{r^2} \frac{\partial^2 V}{\partial \alpha^2} = 0.$$

We perform on this the same kind of separation of variables as in section 2.2. Write first

$$V(\alpha, r) = A(\alpha)R(r)$$

and then split the above equation into two equations, one for the right-hand side function $R(r)$ and one for the function $A(\alpha)$. Substitution yields

$$A(\alpha) \frac{\partial^2 R(r)}{\partial r^2} + \frac{A(\alpha)}{r} \frac{\partial R(r)}{\partial r} + \frac{R(r)}{r^2} \frac{\partial^2 A(\alpha)}{\partial \alpha^2} = 0.$$

Multiply by the expression $r^2/A(\alpha)R(r)$:

$$\left(\frac{r^2}{R(r)} \frac{\partial^2 R(r)}{\partial r^2} + \frac{r}{R(r)} \frac{\partial R(r)}{\partial r} \right) + \frac{1}{A(\alpha)} \frac{\partial^2 A(\alpha)}{\partial \alpha^2} = 0.$$

Both terms must be constant:

$$\begin{aligned} r \left(r \frac{\partial^2 R(r)}{\partial r^2} + \frac{\partial R(r)}{\partial r} \right) - k^2 R(r) &= 0, \\ \frac{\partial^2 A(\alpha)}{\partial \alpha^2} + k^2 A(\alpha) &= 0. \end{aligned}$$

Here, the algebraic sign of the constant k^2 has been chosen so that $A(\alpha)$ gets a periodic solution. Such a general solution would be

$$A_k(\alpha) = a_k \cos k\alpha + b_k \sin k\alpha,$$

in which, because angle α has a period of 2π , k has to be a non-negative integer: $k = 0, 1, 2, \dots$. Negative k does not give different solutions, because

$$\begin{aligned} a_k \cos k\alpha &= a_k \cos(-k\alpha), \\ b_k \sin k\alpha &= -b_k \sin(-k\alpha). \end{aligned}$$



The other equation, in the function $R(r)$, is harder to solve. A test solution is a power law:

$$R(r) = r^q.$$

Substitution yields

$$\begin{aligned} r(rq(q-1)r^{q-2} + qr^{q-1}) - k^2r^q &= 0 \\ \implies q^2 - k^2 &= 0 \\ \implies q^2 &= k^2. \end{aligned}$$

This works for positive $q = 2, 3, \dots$ and negative $q = -1, -2, \dots$. For $q = 1$ we find

$$r - k^2r = 0 \implies k^2 = 1 = q^2.$$

For $q = 0$, besides the trivial constant solution, the non-trivial solution $R(r) = \ln r$ is found:

$$r\left(r \cdot -\frac{1}{r^2} + \frac{1}{r}\right) - k^2 \ln r = 0 \implies k = 0.$$

Thus we obtain the general solution

$$R_k(r) = \begin{cases} 1 \text{ or } \ln r & \text{if } k = 0, \\ r^k \text{ or } r^{-k} & \text{if } k = 1, 2, \dots \end{cases}$$

We see that, if we require the solution to exist at the origin $r = 0$, we need the *first* solutions, obtaining

$$V_1(\alpha, r) = a_0 + \sum_{k=1}^{\infty} r^k (a_k \cos k\alpha + b_k \sin k\alpha),$$

but if we require existence — or, at least, good behaviour — at infinity⁶ $r \rightarrow \infty$, we need the *second* solutions,

$$V_2(\alpha, r) = a_0 + b_0 \ln r + \sum_{k=1}^{\infty} r^{-k} (a_k \cos k\alpha + b_k \sin k\alpha). \quad (2.3)$$

There is a clear similarity here to the three-dimensional, i.e., spherical co-ordinates, case.

⁶In fact, $\lim_{r \rightarrow \infty} V_2 \rightarrow \infty$ but $\lim_{r \rightarrow \infty} \frac{\partial}{\partial r} V_2 = 0$.





2.4 Spherical, geodetic, ellipsoidal co-ordinates

In physical geodesy we use geometrical and physical concepts side by side. For example, the co-ordinates of a point can be given in the form (X, Y, Z) , which are in principle geometric — except for the physical assumption that the origin of the co-ordinate system is in the centre of mass of the Earth.

As the Earth is not precisely a sphere but rather an oblate ellipsoid of revolution, one cannot use geographical co-ordinates as if they were spherical co-ordinates. Because the flattening of the Earth — some 0.3% — cannot be ignored, this difference is significant. The connection between spherical co-ordinates (ϕ, λ, r) and rectangular ones (X, Y, Z) is the following:

$$\begin{aligned} X &= r \cos \phi \cos \lambda, \\ Y &= r \cos \phi \sin \lambda, \\ Z &= r \sin \phi. \end{aligned} \quad (2.4)$$

Here ϕ is the geocentric latitude and λ is the (ordinary — geocentric, geodetic or geographical, all three are the same) longitude, while r is the distance from the Earth's centre. The X axis points in the direction of the Greenwich meridian. See figure 2.3.

On the Earth's surface, these spherical co-ordinates are not very useful because of the Earth's flattening, but in space, spherical co-ordinates are much-used. On the Earth's surface most often *geodetic* — also called geographical — co-ordinates (φ, λ, h) are used:

$$\begin{aligned} X &= (N + h) \cos \varphi \cos \lambda, \\ Y &= (N + h) \cos \varphi \sin \lambda, \\ Z &= (N + h - e^2 N) \sin \varphi, \end{aligned} \quad (2.5)$$

in which

$$N(\varphi) = \frac{a}{\sqrt{1 - e^2 \sin^2 \varphi}} = \frac{a^2}{\sqrt{a^2 \cos^2 \varphi + b^2 \sin^2 \varphi}}. \quad (2.6)$$



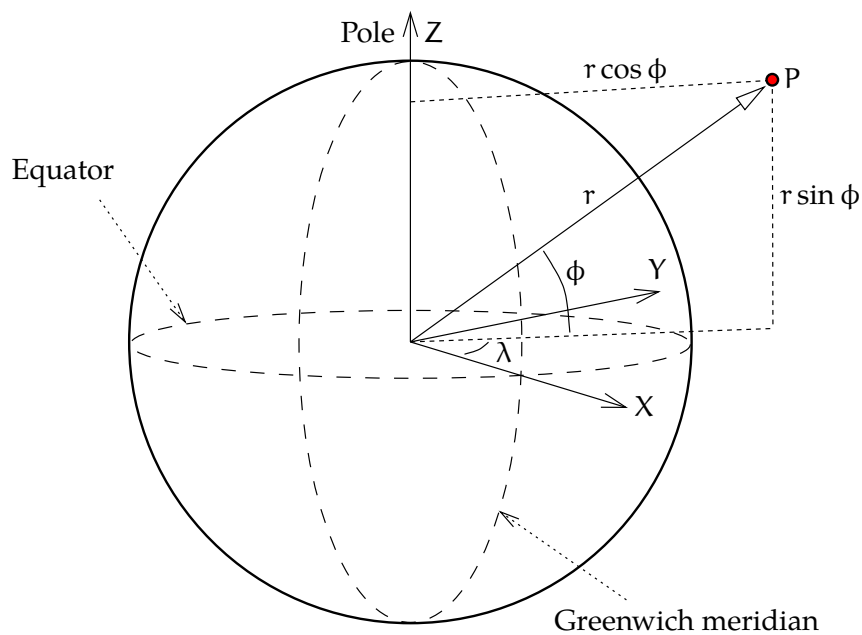


FIGURE 2.3. Definition of spherical co-ordinates.

The quantity N defined in equation 2.6 is the west-east direction, or *transversal*, radius of curvature of the reference ellipsoid. In the equation, a is the equatorial radius of the reference ellipsoid used,

$$e^2 \stackrel{\text{def}}{=} \frac{a^2 - b^2}{a^2}$$

is the square of the *first eccentricity*,⁷ and in equations 2.5, h is the height of the point above the reference ellipsoid, see figure 2.4.

Converting rectangular co-ordinates into geodetic ones is easiest to do iteratively, although the literature also offers closed formulas.

Spherical co-ordinates and geodetic, also called geographical, co-ordinates are considerably different. In latitude, the difference is up to 11 minutes of arc, or almost 20 kilometres. This maximum is attained for latitudes $\pm 45^\circ$.

⁷The parameter is connected to the Earth's flattening f through the equation $e^2 = 2f - f^2$.



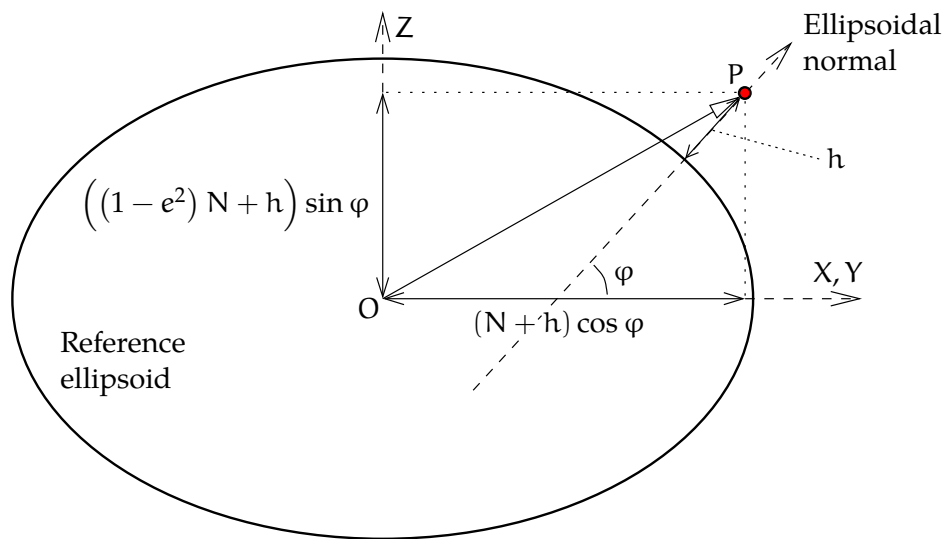


FIGURE 2.4. Definition of geodetic co-ordinates.

redukoitu
leveysaste

In theoretical work one also uses *ellipsoidal co-ordinates* (β, λ, u) . The co-ordinate β is called the *reduced latitude*. The relationship with rectangular co-ordinates is

$$\begin{aligned} X &= \sqrt{u^2 + E^2} \cos \beta \cos \lambda, \\ Y &= \sqrt{u^2 + E^2} \cos \beta \sin \lambda, \\ Z &= u \sin \beta. \end{aligned} \quad (2.7)$$

If the semimajor axis of the Earth ellipsoid is a and its semiminor axis b , it follows that $E^2 = a^2 - b^2$.



2.5 The Laplace equation in spherical co-ordinates

The Laplace equation transformed to spherical co-ordinates reads (see appendix E for a simple geometric proof):

$$\Delta V = \frac{\partial^2 V}{\partial r^2} + \frac{2}{r} \frac{\partial V}{\partial r} + \frac{1}{r^2} \frac{\partial^2 V}{\partial \phi^2} - \frac{\tan \phi}{r^2} \frac{\partial V}{\partial \phi} + \frac{1}{r^2 \sin^2 \phi} \frac{\partial^2 V}{\partial \lambda^2} = 0, \quad (2.8)$$

in which ϕ is the (geocentric) latitude, λ is the longitude, and r is the distance from the origin or centre of the Earth.



Here we shall not derive the solution of this equation by separation of variables, as it is pretty complicated. It can be found in section E.2 and in the literature (Heiskanen and Moritz, 1967, section 1-9). What is significant is that the solution looks somewhat similar to the solution in rectangular co-ordinates presented earlier, section 2.2. The basis solutions of the Laplace equation are

$$\tilde{V}_{n,1}(\phi, \lambda, r) = r^n Y_n(\phi, \lambda), \quad \tilde{V}_{n,2}(\phi, \lambda, r) = \frac{Y_n(\phi, \lambda)}{r^{n+1}}, \quad n = 0, 1, \dots \quad (2.9)$$

of which the first is again *nonphysical* in outer space, because, unlike the true geopotential, these expressions grow to infinity for $r \rightarrow \infty$.

In the above equations, the functions $Y_n(\phi, \lambda)$ are called *surface spherical harmonics*, whereas the functions $\tilde{V}_n(\phi, \lambda, r)$ are *solid spherical harmonics*. The latter are *harmonic* functions everywhere in space except at the origin (2.9, rightmost equation) or at infinity (leftmost, physically unrealistic equation).

pintapallofunktiot

avaruus-pallofunktiot

The functions Y_n are

$$Y_n(\phi, \lambda) = \sum_{m=0}^n P_{nm}(\sin \phi) (a_{nm} \cos m\lambda + b_{nm} \sin m\lambda). \quad (2.10)$$

The functions P_{nm} are *Legendre functions*, on which more later on. With the help of expression 2.10, we obtain, by using the second, physically realistic alternative from equations 2.9, the following solution or *series expansion* for the potential V in space:

$$V(\phi, \lambda, r) = \sum_{n=0}^{\infty} \frac{1}{r^{n+1}} \sum_{m=0}^n P_{nm}(\sin \phi) (a_{nm} \cos m\lambda + b_{nm} \sin m\lambda). \quad (2.11)$$

pallofunktio-kehitemä

The coefficients a_{nm} and b_{nm} are called the coefficients of the spherical-harmonic expansion, in short, *spectral coefficients*. Together they represent the function V , in somewhat the same way that the Fourier coefficients v_{jk} do in rectangular co-ordinates in equation 2.2. The subscripts n and m are called *degree* and *order*.

asteluku, järjestysluku



Often we will be using a somewhat freer notation for the scaled functions Y_n/R^{n+1} . For example, if we expand the disturbing potential T into spherical harmonics, we shall use the notation $T_n(\phi, \lambda)$ for its surface harmonics. Similarly, $\Delta g_n(\phi, \lambda)$ is the surface harmonic of the gravity anomaly Δg for degree n , and so on. Then, it holds on the Earth's surface $r = R$ (*degree constituent expansion*) that

$$T(\phi, \lambda, R) = \sum_{n=0}^{\infty} T_n(\phi, \lambda), \quad \Delta g(\phi, \lambda, R) = \sum_{n=0}^{\infty} \Delta g_n(\phi, \lambda),$$

and so on.



2.6 Dependence on height

From the above equations 2.9 one sees that for different values of the degree n the function $\tilde{V}_n(\phi, \lambda, r)$ has a different dependence on the distance r from the Earth's centre, or equivalently, on the height $H = r - R$, if by R we denote the radius of the Earth sphere, i.e., sea level. The dependence is

$$\tilde{V}_n(\phi, \lambda, r) = \frac{Y_n(\phi, \lambda)}{r^{n+1}}.$$

At sea level

$$\tilde{V}_n(\phi, \lambda, R) = \frac{Y_n(\phi, \lambda)}{R^{n+1}} \stackrel{\text{def}}{=} V_n(\phi, \lambda).$$

Therefore, we may write

$$\begin{aligned} \tilde{V}_n(\phi, \lambda, r) &= \left(\frac{R}{r}\right)^{n+1} V_n(\phi, \lambda) = \left(\frac{R+H}{R}\right)^{-(n+1)} V_n(\phi, \lambda) = \\ &= \left(1 + \frac{H}{R}\right)^{-(n+1)} V_n(\phi, \lambda) \approx \exp\left(-\frac{H}{R}(n+1)\right) V_n(\phi, \lambda). \end{aligned}$$

We see that the attenuation of the potential with height is *again exponential*, and the harmonic degree number n appears in the exponent, as also did the wave number in rectangular geometry, see equation 2.2 and figure 2.1. The analogy works.





Legendre functions and spherical harmonics

3



3.1 Legendre functions

In equations 2.10 and 2.11, the functions P are *Legendre¹ functions* that pop up whenever we solve a Laplace-like equation in spherical co-ordinates. There exist various effective, so-called recursive algorithms, for example the following algorithm only for ordinary Legendre polynomials $P_n = P_{n0}$:

$$nP_n(t) = -(n-1)P_{n-2}(t) + (2n-1)tP_{n-1}(t). \quad (3.1)$$

Similar equations also exist for the functions P_{nm} , $m > 0$. There are even alternatives to choose from, although most equations are complicated. One should be careful that, in their computation, the factorials do not go overboard. Already $30!$ (factorial of 30) is a larger number than computers can handle even as 64-bit integers — not to mention $360!$, the factorial of 360. Heiskanen and Moritz's (1967) equation 1-62, contrary to what is stated there, is *not* directly suitable for computer use!

The first Legendre polynomials are listed in table 3.1. Higher polynomials than this are rarely needed in manual computation.

¹Adrien-Marie Legendre (1752–1833) was a French mathematician known for his work on number theory, statistics — he invented the method of least-squares independently from Gauss — and elliptical functions. His name is inscribed on the Eiffel Tower, [Eiffel Tower, 72 names](#).

TABLE 3.1. Legendre polynomials. $t = \sin \phi$.

| Function of t | Expressed in sines and cosines |
|--|--|
| $P_0(t) = 1$ | $P_0(\sin \phi) = 1$ |
| $P_1(t) = t$ | $P_1(\sin \phi) = \sin \phi$ |
| $P_2(t) = \frac{3}{2}t^2 - \frac{1}{2}$ | $P_2(\sin \phi) = -\frac{3}{4} \cos 2\phi + \frac{1}{4}$ |
| $P_3(t) = \frac{5}{2}t^3 - \frac{3}{2}t$ | $P_3(\sin \phi) = -\frac{5}{8} \sin 3\phi + \frac{3}{8} \sin \phi$ |
| $P_4(t) = \frac{1}{8} (35t^4 - 30t^2 + 3)$ | |
| $P_5(t) = \frac{1}{8} (63t^5 - 70t^3 + 15t)$ | |
| $P_6(t) = \frac{1}{16} (231t^6 - 315t^4 + 105t^2 - 5)$ | |

For comparison, the Fourier *basis functions* (like, in a more complicated way, sines and cosines as well!)

$$F_j(x) = \exp\left(2\pi i j \frac{x}{L}\right),$$

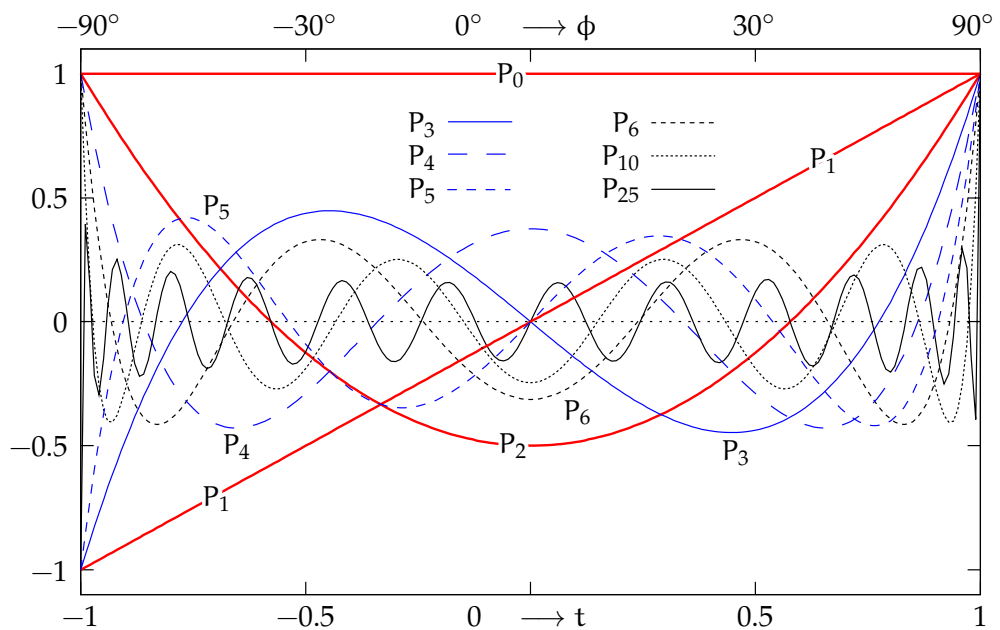


FIGURE 3.1. A number of Legendre polynomials $P_0(t), \dots, P_{25}(t)$ as functions of the argument $t = \sin \phi$.



in which $i^2 = -1$, can also be computed recursively:

$$F_{j+1}(x) = F_j(x) \cdot F_1(x).$$

3.1.1 Properties of Legendre polynomials

- The even polynomials — those polynomials of which the harmonic degree number n is even — are mirror symmetric through the origin $\phi = t = 0$, i.e., the equatorial plane: $P_n(-t) = P_n(t)$, or equivalently $P_n(\sin(-\phi)) = P_n(\sin \phi)$. This means that their values at the same latitude north and south of the equator are identical. The odd polynomials are again antisymmetric: $P_n(-t) = -P_n(t)$ or $P_n(\sin(-\phi)) = -P_n(\sin \phi)$, meaning that their values at the same latitude north and south of the equator are of opposite signs.
- From figure 3.1, we see that the polynomials $P_n(t)$ go, on the whole interval $t \in [-1, 1]$, or $\phi \in [-90^\circ, 90^\circ]$, precisely n times through zero.
- As the values in the end points $t = \pm 1$, $\phi = \pm 90^\circ$ are ± 1 , it follows that there are precisely $n + 1$ “algebraic-sign intervals”, meaning intervals of t or ϕ on which the polynomial assumes only positive or only negative values.

3.1.2 Properties of associated Legendre functions

We give several of the associated Legendre functions P_{nm} , $m \neq 0$ in table 3.2 for illustration.

Legendren
liitännäisfunktiot

One defining equation for these is

$$P_{nm}(t) = (1 - t^2)^{m/2} \frac{d^m P_n(t)}{dt^m}. \quad (3.2)$$

- The associated Legendre functions are also either mirror symmetric through the origin or equatorial plane, $P_{nm}(-t) = P_{nm}(t)$, or equivalently, $P_{nm}(\sin(-\phi)) = P_{nm}(\sin \phi)$, or antisymmetric, $P_{nm}(-t) = -P_{nm}(t)$ or $P_{nm}(\sin(-\phi)) = -P_{nm}(\sin \phi)$, depending on the values of order number m and degree number n .



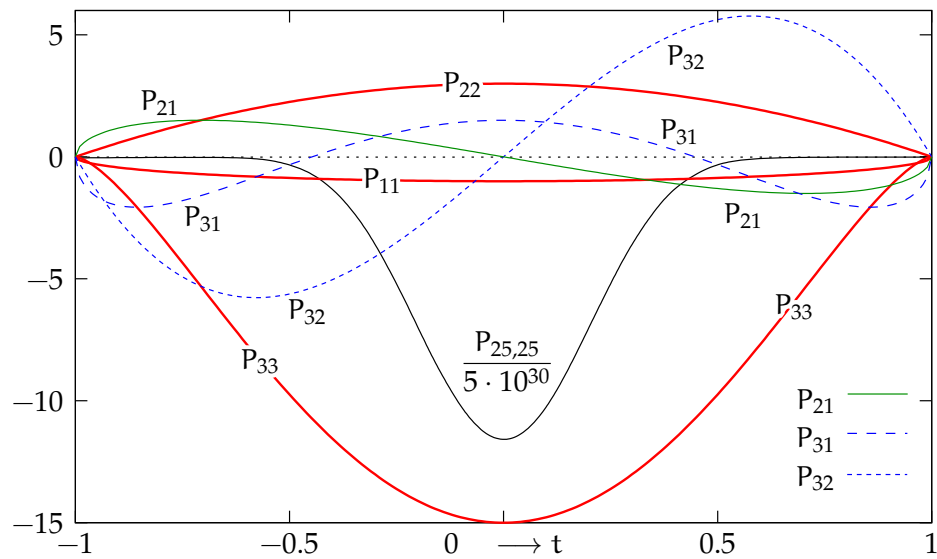


FIGURE 3.2. Associated Legendre functions. Note the extremely different scale used for the function $P_{25,25}$, see equation 3.7.

- o Figure 3.2 suggests that the polynomials $P_{nm}(t)$ go on $t \in [-1, 1]$, or $\phi \in [-90^\circ, 90^\circ]$, precisely $n - m$ times through zero. This is indeed the case.
- o As the values in the end points $t = \pm 1$, $\phi = \pm 90^\circ$ are also zero, it follows that there are precisely $n - m + 1$ “algebraic-sign intervals”.

TABLE 3.2. Associated Legendre functions.

| Function of t | Trigonometric function |
|---|--|
| $P_{11}(t) = \sqrt{1 - t^2}$ | $P_{11}(\sin \phi) = \cos \phi$ |
| $P_{21}(t) = 3t\sqrt{1 - t^2}$ | $P_{21}(\sin \phi) = 3 \sin \phi \cos \phi$ |
| $P_{22}(t) = 3(1 - t^2)$ | $P_{22}(\sin \phi) = 3 \cos^2 \phi$ |
| $P_{31}(t) = \frac{3}{2}(5t^2 - 1)\sqrt{1 - t^2}$ | $P_{31}(\sin \phi) = \frac{3}{2}(5 \sin^2 \phi - 1) \cos \phi$ |
| $P_{32}(t) = 15t(1 - t^2)$ | $P_{32}(\sin \phi) = 15 \sin \phi \cos^2 \phi$ |
| $P_{33}(t) = 15(1 - t^2)^{3/2}$ | $P_{33}(\sin \phi) = 15 \cos^3 \phi$ |



3.1.3 Surface spherical harmonics

Starting from equation 2.10, we may write

$$\begin{aligned}
 Y_n(\phi, \lambda) &= \\
 &= \sum_{m=0}^n (a_{nm} P_{nm}(\sin \phi) \cos m\lambda + b_{nm} P_{nm}(\sin \phi) \sin m\lambda) = \\
 &= \sum_{m=-n}^n v_{nm} Y_{nm}(\phi, \lambda),
 \end{aligned}$$

in which m now runs from $-n$ to $+n$. Here

$$Y_{nm}(\phi, \lambda) = \begin{cases} P_{nm}(\sin \phi) \cos m\lambda & \text{if } m \geq 0, \\ P_{n|m|}(\sin \phi) \sin |m|\lambda & \text{if } m < 0. \end{cases} \quad (3.3)$$

These are the *surface spherical harmonics of degree n and order m* .

pintapallofunktioit

Surface spherical harmonics come in three kinds:

Zonal harmonics $m = 0$. These functions depend only on latitude.

vyöhykefunktioit

Sectorial harmonics $m = n$. the *algebraic signs* of these functions depend only on longitude and not on latitude. The functions themselves however *do* depend on both latitude and longitude!

sektorifunktioit

Tesseral harmonics $0 < m < n$. These functions, the algebraic sign of which changes with both latitude and longitude, form a checkerboard pattern on the surface of the sphere, if the positive values are painted white and the negative ones grey (Latin *tessera* = a tile, as used in a mosaic).

ruutufunktioit

Every function will, on the interval $\sin \phi \in [-1, +1]$, go precisely $n - m$ times through zero. Every function is either symmetric or antisymmetric through the origin as a function of ϕ or of $t = \sin \phi$.

Spherical harmonics thus represent a wave phenomenon of sorts. They are however not wave functions (sines or cosines): the connection to those is complicated at least. It nevertheless makes sense to speak of their *wavelength*.



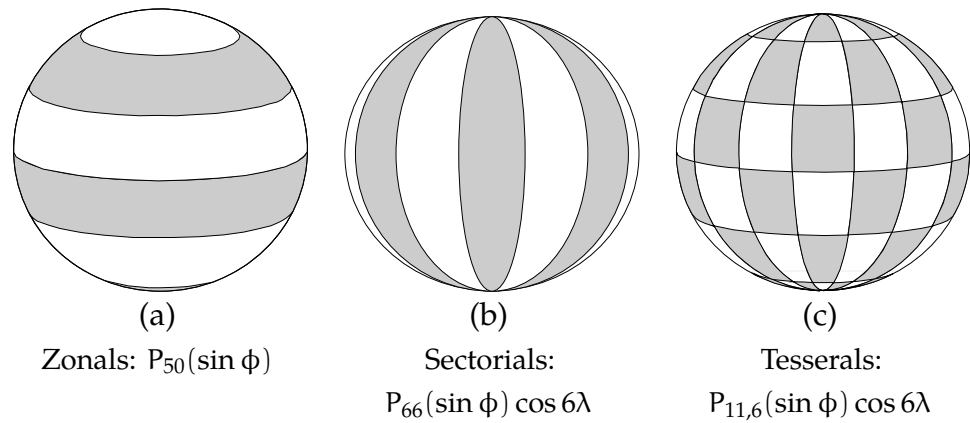


FIGURE 3.3. The algebraic signs of spherical harmonics on the Earth's surface. White means positive, grey negative. The functions "wave" in a sine or cosine function-like fashion.



etumerkit Figure 3.3 depicts how the algebraic signs of the different spherical harmonics behave on the Earth's surface — and above. This is a perspective sketch and not all white and grey areas are visible!

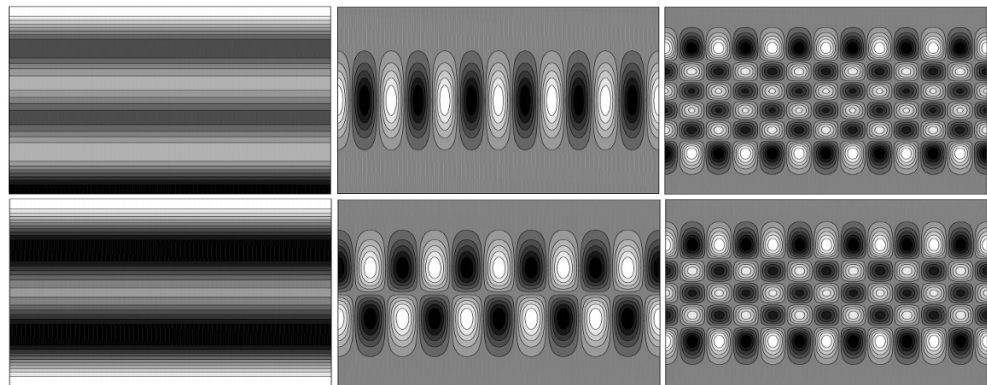



FIGURE 3.4. Surface spherical harmonics as maps. Horizontal axis $\lambda \in [0, 360^\circ)$, vertical axis $\phi \in [-90^\circ, 90^\circ]$. Functions depicted are

$$\begin{array}{lll} P_{50}(\sin \phi) & P_{66}(\sin \phi) \cos 6\lambda & P_{11,6}(\sin \phi) \cos 6\lambda \\ P_{40}(\sin \phi) & P_{65}(\sin \phi) \cos 5\lambda & P_{10,6}(\sin \phi) \cos 6\lambda \end{array}$$



 TABLE 3.3. Semi-wavelengths for different degrees and orders of spherical harmonics.

| m or n – m | Semi-wavelength (km) | In degrees |
|------------|----------------------|------------|
| 10 | 2000 | 18 |
| 40 | 500 | 4°5 |
| 180 | 111 | 1 |
| 360 | 55 | 30' = 0°5 |
| 1800 | 11 | 6' = 0°1 |
| 10 800 | 1.85 | 1' = 0°017 |

In equation 2.10, the expressions $\cos m\lambda$ and $\sin m\lambda$ go around a full circle, the equator, $0^\circ \leq \lambda < 360^\circ$, or $0 \leq \lambda < 2\pi$, precisely $2m$ times through zero. The “semi-wavelength” is thus

$$\frac{2\pi R}{2m} = \pi \frac{R}{m'}$$

in which R is again the radius of the Earth.

A similar formula also applies for the functions $P_{nm}(\sin \phi)$: as the function passes through zero $n - m$ times on the interval — from pole to pole — $-90^\circ < \phi < 90^\circ$ or $-\pi/2 < \phi < \pi/2$, it follows that also in this case, the semi-wavelength is

$$\frac{\pi R}{n - m'}$$

If we plug various values for m and $n - m$ into this, we obtain table 3.3. This table also gives the *resolution* that can be achieved with a spherical-harmonic expansion, or in how detailed a fashion the expansion can describe the Earth’s gravity field. The expansions available today, like the model EGM2008, go to harmonic degree $n = 2159$; the “sharpness” of a geopotential image based on them is thus 9 km. Models based on satellite orbit perturbations often extend only to degree 20, meaning that only details the size of continents — order of magnitude 1000 km — will be visible. On the other hand, experimental spherical-harmonic

puoliaallonpituus



expansions of the topography go even up to degree 10 800 (Balmino et al., 2012).



3.2 Symmetry properties of the spherical-harmonic expansion

We recapitulate the spherical-harmonic expansion given at the beginning, equation 2.11:

$$V(\phi, \lambda, r) = \sum_{n=0}^{\infty} \frac{1}{r^{n+1}} \sum_{m=0}^n P_{nm}(\sin \phi) (a_{nm} \cos m\lambda + b_{nm} \sin m\lambda).$$



3.2.1 Dependence on latitude ϕ

It is seen that the dependence on ϕ only works through the Legendre function $P_{nm}(\sin \phi)$. This function can, in terms of mirror symmetry between the northern and southern hemispheres, be either *symmetric* in ϕ or *antisymmetric* in ϕ . This means that either (symmetric case)

$$P_{nm}(\sin \phi) = P_{nm}(\sin(-\phi))$$

or (antisymmetric case)

$$P_{nm}(\sin \phi) = -P_{nm}(\sin(-\phi)).$$

Equivalently, it means, with $t = \sin \phi$, that either (symmetric case)

$$P_{nm}(t) = P_{nm}(-t)$$

or (antisymmetric case)

$$P_{nm}(t) = -P_{nm}(-t).$$

Which case applies depends on the values of both n and m . To work it out, one can look at, say, equation 3.2:

$$P_{nm}(t) = (1 - t^2)^{m/2} \frac{d^m P_n(t)}{dt^m}.$$

We need to answer two questions:



1. For which values n is the polynomial $P_n(t)$ symmetric, for which is it antisymmetric in t ? For this, you may look at the recursive algorithm for computation of the polynomials, eq. 3.1. We already know that $P_0(t) = 1$ is symmetric, and that $P_1(t) = t$ is antisymmetric. The rule for other n values follows recursively (or you could cheat by looking at table 3.1).
2. What does *differentiation* $\frac{d}{dt}$ do to the symmetry or antisymmetry of the function?

Multiplication by $\sqrt{1-t^2} = \cos \phi$ changes nothing, as this factor is symmetric in t or ϕ .

So, in order to make expansion 2.11 *mirror symmetric* between northern and southern hemispheres, one has to set the coefficients a_{nm}, b_{nm} for which the corresponding P_{nm} is antisymmetric, to zero. Then, those terms vanish from the expansion. The coefficients, and terms, remaining are those for which the corresponding P_{nm} is symmetric.

In tableau 3.4 we give a code fragment in the octave rapid-prototyping language to plot an arbitrary surface spherical harmonic, in order to visually judge its symmetry properties. Do not believe, test.

3.2.2 Dependence on longitude λ

This dependence works through the “Fourier basis functions” $\cos m\lambda$ and $\sin m\lambda$. The interesting property here is *rotational symmetry*: does the spherical-harmonic expansion 2.11 change when we change the longitude λ ?

We see immediately that, for $m \neq 0$, there will be dependence on λ if any coefficient a_{nm}, b_{nm} is non-zero. So, in order to obtain rotational symmetry, all coefficients a_{nm}, b_{nm} for values $m > 0$ must be suppressed: $a_{11} = b_{11} = a_{21} = b_{21} = a_{22} = b_{22} = \dots = 0$.

Of the remaining coefficients, we can say that for $m = 0$, $\sin m\lambda = 0$ identically, so the coefficients $b_{00}, b_{10}, b_{20}, \dots$ simply do not matter. They may be any value, including zero. The coefficients $a_{00}, a_{10}, a_{20}, \dots$





TABLEAU 3.4. Plotting a surface spherical-harmonic map.

```

% Plotting surface spherical harmonics
phi=linspace(-90,90,72);
lab=linspace(0,360,144);
[f,l]=meshgrid(phi,lab);
n=5; m=-3;
leg=legendre(n,sin(phi.*pi./180));
if m >= 0
cs=cos(m.*lab.*pi./180);
else
cs=sin(abs(m).*lab.*pi./180);
end
v=leg(abs(m)+1,:)'*cs;
contourf(l,f,v')
xlabel('Longitude', 'FontSize', 16)
ylabel('Latitude', 'FontSize', 16)
str=sprintf('Surface spherical harmonic n=%d, m=%d', n, m)%
title(str, 'FontSize', 20)
axis ([0 360 -90 90])
colorbar()
print('legendre2D.jpg', '-djpg')

```

however *do* matter, as for $m = 0$, $\cos m\lambda = 1$ identically. So we obtain as the *rotationally symmetric expansion*

$$V(\phi, \lambda, r) = V(\phi, r) = \sum_{n=0}^{\infty} \frac{1}{r^{n+1}} a_n P_n(\sin \phi),$$

in which $P_n = P_{n0}$ are the familiar Legendre polynomials, and $a_n = a_{n0}$.



3.3 Orthogonality of Legendre functions

Legendre's *polynomials* are *orthogonal*: the integral — formally, a scalar product of vectors — is

$$\int_{-1}^{+1} P_n(t)P_{n'}(t) dt = \begin{cases} \frac{2}{2n+1} & \text{if } n = n', \\ 0 & \text{if } n \neq n'. \end{cases} \quad (3.4)$$



This orthogonality is just one example of a more general way to look at functions and integrals over functions. There exists a useful analogy with vector spaces, see appendix B.

Alternatively we may write, on the surface of a *unit sphere* σ , using a parametrisation² (ψ, α) by angular distance and azimuth, see figure 10.1:

$$\begin{aligned} \iint_{\sigma} P_n(\cos \psi) P_{n'}(\cos \psi) d\sigma &= \\ &= \int_0^{2\pi} \int_0^{\pi} P_n(\cos \psi) P_{n'}(\cos \psi) \sin \psi d\psi d\alpha = \\ &= -2\pi \int_{+1}^{-1} P_n(t) P_{n'}(t) dt = 2\pi \int_{-1}^{+1} P_n(t) P_{n'}(t) dt, \end{aligned}$$

in which $t = \cos \psi$ and the surface element of the unit sphere $d\sigma = \sin \psi d\psi d\alpha$, in which again $\sin \psi$ is the *determinant of Jacobi*³ of the co-ordinates (ψ, α) . So, we have

$$\iint_{\sigma} P_n(\cos \psi) P_{n'}(\cos \psi) d\sigma = \begin{cases} \frac{4\pi}{2n+1} & \text{if } n = n', \\ 0 & \text{if } n \neq n', \end{cases} \quad (3.5)$$

in which ψ is the angular distance from some point on the surface of the sphere. Equation 3.5 tells us that Legendre polynomials are mutually *orthogonal* if the vectorial product is defined as an integral over the surface of the unit sphere σ .

Alternatively, we may also define *fully normalised* Legendre polynomials

$$\bar{P}_n(\cos \psi) \stackrel{\text{def}}{=} \sqrt{2n+1} P_n(\cos \psi). \quad (3.6)$$

Now the modified scalar product — the mean product over the unit

²This parametrisation may be regarded as a latitude, longitude co-ordinate system: the latitude is $90^\circ - \psi = \frac{1}{2}\pi - \psi$, the longitude is α .

³Carl Gustav Jacob Jacobi (1804–1851) was a German mathematician.



sphere — is

$$\frac{1}{4\pi} \iint_{\sigma} \bar{P}_n(\cos \psi) \bar{P}_{n'}(\cos \psi) d\sigma = \begin{cases} 1 & \text{if } n = n', \\ 0 & \text{if } n \neq n', \end{cases}$$

showing the polynomials now to be *orthonormal*.⁴ Similarly fully normalised *associated* Legendre functions also exist, see [Heiskanen and Moritz 1967](#), page 31:

$$\bar{P}_{nm}(\cos \psi) \stackrel{\text{def}}{=} \sqrt{2(2n+1) \frac{(n-m)!}{(n+m)!}} P_{nm}(\cos \psi). \quad (3.7)$$

In this case, the orthonormal functions are those of equation 3.3, but normalized:

$$\bar{Y}_{nm}(\psi, \alpha) = \begin{cases} \bar{P}_{nm}(\cos \psi) \cos m\alpha & \text{if } m \geq 0, \\ \bar{P}_{n|m|}(\cos \psi) \sin |m|\alpha & \text{if } m < 0. \end{cases}$$

The scalar product that applies is

$$\frac{1}{4\pi} \iint_{\sigma} \bar{Y}_{nm}(\psi, \alpha) \bar{Y}_{n'm'}(\psi, \alpha) d\sigma = \begin{cases} 1 & \text{if } n = n' \text{ and } m = m', \\ 0 & \text{otherwise.} \end{cases}$$



3.4 Low-degree spherical harmonics

The potential field of a point mass is (equation 1.4):

$$V = \frac{GM}{r}.$$

The corresponding term in the potential expansion 2.11 for degree $n = 0$ is

$$\tilde{V}_0(\phi, \lambda, r) = \frac{1}{r} a_{00} P_0(\sin \phi) = \frac{a_{00}}{r},$$

⁴And also

$$\frac{1}{2} \int_{-1}^{+1} \bar{P}_n(t) \bar{P}_{n'}(t) dt = \begin{cases} 1 & \text{if } n = n', \\ 0 & \text{if } n \neq n', \end{cases}$$

again, the mean product over the domain of integration.



from which

$$a_{00} = GM.$$

So, a_{00} represents the force field of a point mass or spherically symmetric mass distribution centred at the origin. The higher spherical-harmonic coefficients are “perturbations” on top of this.

The expansion for the degree-one coefficients looks as follows:

$$\tilde{V}_1(\phi, \lambda, r) = \frac{1}{r^2} (a_{11} \cos \phi \cos \lambda + b_{11} \cos \phi \sin \lambda + a_{10} \sin \phi).$$

Write this in vector form using the expression for the location vector

$$\mathbf{r} = (r \cos \phi \cos \lambda) \mathbf{i} + (r \cos \phi \sin \lambda) \mathbf{j} + (r \sin \phi) \mathbf{k}$$

— in which $\{\mathbf{i}, \mathbf{j}, \mathbf{k}\}$ is an orthonormal basis of the Euclidean space — yielding

$$\tilde{V}_1(\mathbf{r}) = \frac{1}{r^3} \langle (a_{11} \mathbf{i} + b_{11} \mathbf{j} + a_{10} \mathbf{k}) \cdot \mathbf{r} \rangle.$$

The potential field of a *dipole* is

$$V(\mathbf{r}) = \frac{G}{r^3} \langle \mathbf{d} \cdot \mathbf{r} \rangle,$$

in which \mathbf{d} is the dipole moment. Comparison yields

$$a_{11} \mathbf{i} + b_{11} \mathbf{j} + a_{10} \mathbf{k} = G \mathbf{d},$$

so the first-degree $n = 1$ spherical-harmonic coefficients represent the Earth’s gravitational field’s *dipole moment*.

Every mass element dm of our Earth may be taken to consist of

- a *monopole* at the origin of the co-ordinate system, magnitude dm
- a *dipole*, magnitude $\mathbf{r} \cdot dm$, in which \mathbf{r} is the location vector of the mass element.

In that case we may compute the dipole moment of the whole Earth by integration:

$$\mathbf{d}_{\oplus} = \iiint_{\text{Earth}} \mathbf{r} dm = \iiint_{\text{Earth}} \rho \mathbf{r} dV = M_{\oplus} \cdot \mathbf{r}_{\text{com}},$$



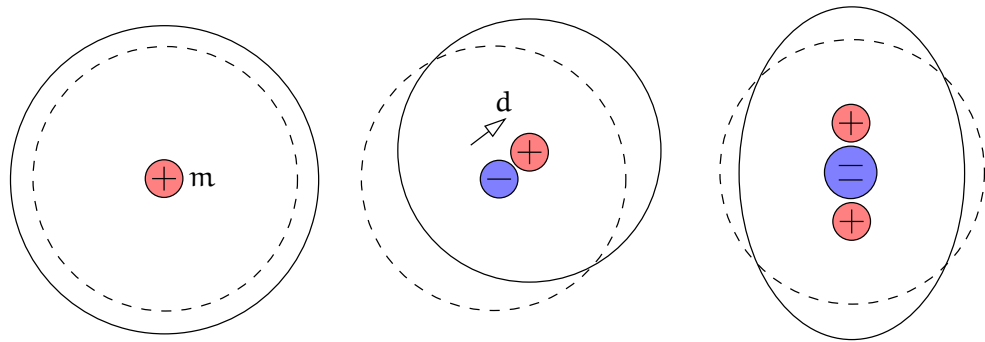


FIGURE 3.5. Monopole, dipole, and quadrupole at the Earth's centre and their effects on the geoid.

in which, by definition, \mathbf{r}_{com} is the location of the *centre of mass* of the Earth. From this follows that, if we choose our co-ordinate system so that the origin is in the centre of mass of the Earth, the spherical-harmonic coefficients a_{11} , b_{11} , a_{10} *vanish*. If the equations of motion of satellites are formulated in a certain co-ordinate system, like in the case of GPS satellites the WGS84 system, then the origin of the system is automatically in the centre of mass of the Earth, and the degree-one spherical-harmonic coefficients are really zero.

The same logic applies to higher degrees of spherical harmonics. The degree-two coefficients represent the *quadrupole moment* of the Earth — corresponding to her inertial tensor — and so on.

3.5 Splitting a function into degree constituents

There exists a useful integral equation for surface spherical harmonics, if the function itself f on the surface of the sphere has been given. The equation is Heiskanen and Moritz (1967) equation 1-71, using our notation $Y_n \rightarrow f_n$:

$$f_n(\phi, \lambda) = \frac{2n+1}{4\pi} \iint_{\sigma} f(\phi', \lambda') P_n(\cos \psi) d\sigma', \quad (3.8)$$



in which ψ is the geocentric angular distance between evaluation point (ϕ, λ) and moving data or integration point (ϕ', λ') , see figure 8.2. In this *degree constituent equation* 3.8 there is a certain similarity with the projection or coefficient computation formula B.11. Nevertheless, here we do not have a computation of spectral coefficients, but of “spectral constituent functions” f_n .

asteosuusyhtälö

We bring to mind the core property of the functions f_n ,

$$f(\phi, \lambda) = \sum_{n=0}^{\infty} f_n(\phi, \lambda)$$

on the surface of the sphere.

For the proof, we choose without loss of generality as the “north pole” of the co-ordinate system the evaluation point (ϕ, λ) , so $\phi = 90^\circ$. Then, $\phi' = 90^\circ - \psi$. By writing (see equation 2.11):

$$f(\phi', \lambda') = \sum_{n=0}^{\infty} \sum_{m=0}^n P_{nm}(\cos \psi) (a_{nm} \cos m\lambda' + b_{nm} \sin m\lambda'),$$

substituting this into the degree constituent equation 3.8, and exploiting the orthogonality of the Legendre functions, we obtain on the right-hand side:

$$\begin{aligned} I_R &= \frac{2n+1}{4\pi} \iint_{\sigma} f(\phi', \lambda') P_n(\cos \psi) d\sigma' = \\ &= \frac{2n+1}{4\pi} a_{n0} \iint_{\sigma} P_n^2(\cos \psi) d\sigma' \end{aligned}$$

Then, using equation 3.5:

$$I_R = \frac{2n+1}{4\pi} a_{n0} \frac{4\pi}{2n+1} = a_{n0} \stackrel{\text{def}}{=} a_n.$$

On the left-hand side of the degree constituent equation we obtain, because on the assumed north pole $\phi = 90^\circ$ and thus $\sin \phi = 1$:

$$\begin{aligned} I_L &= f_n(\phi, \lambda) = f_n(90^\circ, \lambda) = \\ &= \sum_{m=0}^n P_{nm}(1) (a_{nm} \cos m\lambda + b_{nm} \sin m\lambda) = P_{n0}(1) a_{n0} = a_n, \end{aligned}$$



by using equation 2.10 and

$$P_{n0}(1) = 1, \quad P_{nm}(1) = 0 \text{ if } m \neq 0.$$

As this applies for every point (ϕ, λ) , it follows that the degree constituent equation 3.8 is generally true. Note that the values a_n depend on the point choice!

3.6 Spectral representations of various quantities

3.6.1 Potential

Starting from equation 2.9, we write the *spectral expansion* of the geopotential V in space:

$$V(\phi, \lambda, r) = \sum_{n=0}^{\infty} \left(\frac{R}{r}\right)^{n+1} V_n(\phi, \lambda), \quad (3.9)$$

in which the degree constituents V_n are

$$\begin{aligned} V_n(\phi, \lambda) &= \frac{Y_n(\phi, \lambda)}{R^{n+1}} = \\ &= \frac{1}{R^{n+1}} \sum_{m=0}^n P_{nm}(\sin \phi) (a_{nm} \cos m\lambda + b_{nm} \sin m\lambda) = \\ &= \frac{1}{R^{n+1}} \sum_{m=-n}^n v_{nm} Y_{nm}(\phi, \lambda). \end{aligned}$$

Here, the basis functions Y_{nm} are given by equation 3.3:

$$Y_{nm}(\phi, \lambda) = \begin{cases} P_{nm}(\sin \phi) \cos m\lambda & \text{if } m \geq 0, \\ P_{n|m|}(\sin \phi) \sin |m|\lambda & \text{if } m < 0, \end{cases}$$

and the coefficients are

$$v_{nm} = \begin{cases} a_{nm} & \text{if } m \geq 0, \\ b_{n|m|} & \text{if } m < 0. \end{cases}$$



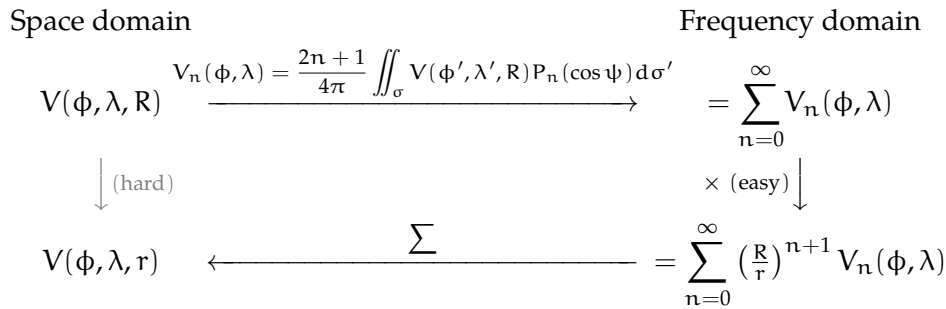


FIGURE 3.6. Radially shifting the potential field V , in the space and frequency domains. Spherical geometry.

On the Earth's surface ($r = R$) we obtain

$$V(\phi, \lambda, R) = \sum_{n=0}^{\infty} V_n(\phi, \lambda) = \sum_{n=0}^{\infty} \frac{1}{R^{n+1}} \sum_{m=-n}^n v_{nm} Y_{nm}(\phi, \lambda). \quad (3.10)$$

We may summarise the relationships found in *commutative diagram 3.6*. Again, as in section 2.2 for rectangular geometry, it is seen that the shift of the potential function V from the spherical level R to the level $r = R + H$ is essentially easier in the frequency domain — the degree constituents $V_n(\phi, \lambda)$ — than it is in the space domain.

kommutoiva
kaavio

3.6.2 Gravitation

In the *Neumann*⁵ boundary-value problem we solve a function V of which the normal derivative, $\frac{\partial}{\partial n} V$, is given on the surface of a body or a closed surface in space.

In the case of a spherical body, we may assume $\frac{\partial}{\partial n} V = \frac{\partial}{\partial r} V$ and work with spherical-harmonic expansions. By differentiating equation 3.9 we obtain

$$\frac{\partial V}{\partial r} = - \sum_{n=0}^{\infty} \frac{n+1}{r} \left(\frac{R}{r} \right)^{n+1} V_n(\phi, \lambda) = - \sum_{n=0}^{\infty} \frac{n+1}{R} \left(\frac{R}{r} \right)^{n+2} V_n(\phi, \lambda).$$

⁵Carl Gottfried Neumann (1832–1925) was a German mathematician.



At sea level this means

$$\left. \frac{\partial V}{\partial r} \right|_{r=R} = - \sum_{n=0}^{\infty} \frac{n+1}{R} V_n(\phi, \lambda).$$

If we also write at sea level for the *gravitation*

$$g(\phi, \lambda, R) \stackrel{\text{def}}{=} \left. \frac{\partial V}{\partial r} \right|_{r=R} \stackrel{\text{def}}{=} \sum_{n=0}^{\infty} g_n(\phi, \lambda),$$

it follows by analogy that

$$g_n(\phi, \lambda) = - \frac{n+1}{R} V_n(\phi, \lambda),$$

and conversely that

$$V_n(\phi, \lambda) = - \frac{R}{n+1} g_n(\phi, \lambda).$$

As a result of this, we obtain the *spectral representation of the solution* to a certain Neumann problem:

$$V(\phi, \lambda, r) = \sum_{n=0}^{\infty} \left(\frac{R}{r} \right)^{n+1} V_n(\phi, \lambda) = -R \sum_{n=0}^{\infty} \left(\frac{R}{r} \right)^{n+1} \frac{g_n(\phi, \lambda)}{n+1}. \quad (3.11)$$

We may write equivalently to expression 3.10 for the potential:

$$g(\phi, \lambda, R) = \sum_{n=0}^{\infty} g_n(\phi, \lambda) \stackrel{\text{def}}{=} \sum_{n=0}^{\infty} \frac{1}{R^{n+1}} \sum_{m=-n}^n g_{nm} Y_{nm}(\phi, \lambda),$$

and comparison yields

$$g_{nm} = - \frac{n+1}{R} v_{nm}. \quad (3.12)$$

This is an interesting result worth thinking about:

1. Firstly, note how simple the connection 3.12 between potential v_{nm} and gravitation g_{nm} is in the frequency domain!



2. Secondly, if measurement values of gravitational acceleration $g(\phi, \lambda)$ are available over the whole surface area of the Earth, we may derive from these the degree constituent functions $g_n(\phi, \lambda)$ using the method explained earlier. In this way we can then obtain the solution by means of equation 3.11 for the whole exterior geopotential field! This is the basic idea of geopotential — or geoid — determination, from the spectral perspective.

3.7 Often-used spherical-harmonic expansions

Of the existing global spherical-harmonic expansions we must mention the already outdated EGM96. It was developed by researchers from Ohio State University using very extensive, mostly gravimetric, data collected by the American NIMA (*National Imagery and Mapping Agency*, the former *Defense Mapping Agency DMA*, the current *National Geospatial-Intelligence Agency NGA*). This expansion goes up to harmonic degree 360. Its standard presentation⁶ is

$$V = \frac{GM_{\oplus}}{r} \left(1 + \sum_{n=2}^{360} \left(\frac{a}{r} \right)^n \sum_{m=0}^n \bar{P}_{n,m}(\sin \phi) (\bar{C}_{n,m} \cos m\lambda + \bar{S}_{n,m} \sin m\lambda) \right). \quad (3.13)$$

This form of presentation — the algebraic sign in front of the expansion, which starts from degree number $n = 2$, the number one inside the parentheses which represents the point mass in the origin equal in magnitude to the total mass of the Earth, and the dimensionless and “fully normalised” coefficients \bar{C} and \bar{S} — is an industry standard in the global research community in the field of computing spherical-harmonic expansions as models of the Earth’s gravitational field. Professor

täysin
normalisoidut
kertoimet

⁶Here $a = a_{\oplus}$ is used to signify the equatorial radius of the Earth’s reference ellipsoid, not R , and ϕ , signifying *geocentric* latitude. The co-ordinates (ϕ, λ, r) form a spherical co-ordinate system.



Richard H. Rapp at Ohio State University has been a pioneer, which is why the models are often called **OSU** models.

Generally in these models the lower terms — $2 \leq n \leq 20$ — are derived primarily from analysis of satellite orbit perturbations. Because of this, the models are in a co-ordinate system with the origin in the Earth's centre of mass. This explains the absence of the degree-one coefficients, as explained earlier.

The higher coefficients again — $20 < n \leq 360$ — were before the year 2000 mostly the result of the analysis of gravimetric data (over land) and satellite radar altimetric data (over the ocean). After the launches of the gravimetric satellite missions **CHAMP**, **GRACE**, and **GOCE**, and as a result of their measurements, nowadays at least the degree number interval $20 < n \leq 200$ is the product of space geodesy. Only the still higher-degree coefficients continue to come from terrestrial data. The newer model **EGM2008** (Pavlis et al., 2008, 2012) goes up to degree 2159.

In tableau 3.5 we give the first and last coefficients of the **EGM96** model, the newest and best spherical-harmonics model from the time just before the satellite gravity missions. The values tabulated are n , m , \bar{C}_{nm} , \bar{S}_{nm} and the mean errors (standard deviations) of both coefficients from their computation. Note that all \bar{S}_{n0} vanish!

Sometimes non-normalised coefficients are also used, and we write

$$V = \frac{GM_{\oplus}}{r} \left(1 - \sum_{n=2}^{\infty} \left(\frac{a}{r} \right)^n \sum_{m=0}^n P_{nm}(\sin \phi) (J_{nm} \cos m\lambda + K_{nm} \sin m\lambda) \right). \quad (3.14)$$

Then we use the notation $J_n = J_{n0}$. The coefficient J_2 is the most important spherical-harmonic coefficient of the Earth's gravity field, expressing the flattening of the Earth. Based on equations 3.6 and 3.7, the relationship with the parameters \bar{C} , \bar{S} is

$$\begin{aligned} \begin{Bmatrix} J_{n0} \\ K_{n0} \end{Bmatrix} &= -\sqrt{2n+1} \begin{Bmatrix} \bar{C}_{n0} \\ \bar{S}_{n0} \end{Bmatrix}, \\ \begin{Bmatrix} J_{nm} \\ K_{nm} \end{Bmatrix} &= -\sqrt{2(2n+1) \frac{(n-m)!}{(n+m)!}} \begin{Bmatrix} \bar{C}_{nm} \\ \bar{S}_{nm} \end{Bmatrix} \text{ if } m \neq 0. \end{aligned} \quad (3.15)$$



TABLEAU 3.5. Coefficients and mean errors of the EGM96 spherical-harmonic expansion.

| n | m | \bar{C}_{nm} | \bar{S}_{nm} | \bar{C}_{nm} mean error | \bar{S}_{nm} mean error |
|-----|-----|---------------------|---------------------|---------------------------|---------------------------|
| 2 | 0 | -0.484165371736E-03 | 0.000000000000E+00 | 0.35610635E-10 | 0.00000000E+00 |
| 2 | 1 | -0.186987635955E-09 | 0.119528012031E-08 | 0.10000000E-29 | 0.10000000E-29 |
| 2 | 2 | 0.243914352398E-05 | -0.140016683654E-05 | 0.53739154E-10 | 0.54353269E-10 |
| 3 | 0 | 0.957254173792E-06 | 0.000000000000E+00 | 0.18094237E-10 | 0.00000000E+00 |
| 3 | 1 | 0.904627768605E-06 | 0.248513158716E-06 | 0.13965165E-09 | 0.13645882E-09 |
| 3 | 2 | 0.904627768605E-06 | -0.619025944205E-06 | 0.10962329E-09 | 0.11182866E-09 |
| 3 | 3 | 0.721072657057E-06 | 0.141435626958E-05 | 0.95156281E-10 | 0.93285090E-10 |
| 4 | 0 | 0.539873863789E-06 | 0.000000000000E+00 | 0.10423678E-09 | 0.00000000E+00 |
| 4 | 1 | -0.536321616971E-06 | -0.473440265853E-06 | 0.85674404E-10 | 0.82408489E-10 |
| 4 | 2 | 0.350694105785E-06 | 0.662671572540E-06 | 0.16000186E-09 | 0.16390576E-09 |
| 4 | 3 | 0.990771803829E-06 | -0.200928369177E-06 | 0.84657802E-10 | 0.82662506E-10 |
| 4 | 4 | -0.188560802735E-06 | 0.308853169333E-06 | 0.87315359E-10 | 0.87852819E-10 |
| 5 | 0 | 0.685323475630E-07 | 0.000000000000E+00 | 0.54383090E-10 | 0.00000000E+00 |
| 5 | 1 | -0.621012128528E-07 | -0.944226127525E-07 | 0.27996887E-09 | 0.28082882E-09 |
| 5 | 2 | 0.652438297612E-06 | -0.323349612668E-06 | 0.23747375E-09 | 0.24356998E-09 |
| 5 | 3 | -0.451955406071E-06 | -0.214847190624E-06 | 0.17111636E-09 | 0.16810647E-09 |
| 5 | 4 | -0.295301647654E-06 | 0.496658876769E-07 | 0.11981266E-09 | 0.11849793E-09 |
| 5 | 5 | 0.174971983203E-06 | -0.669384278219E-06 | 0.11642563E-09 | 0.11590031E-09 |
| 6 | 0 | -0.149957994714E-06 | 0.000000000000E+00 | 0.14497863E-09 | 0.00000000E+00 |
| 6 | 1 | -0.760879384947E-07 | 0.262890545501E-07 | 0.22415138E-09 | 0.21957296E-09 |
| 6 | 2 | 0.481732442832E-07 | -0.373728201347E-06 | 0.27697363E-09 | 0.28105811E-09 |
| 6 | 3 | 0.571730990516E-07 | 0.902694517163E-08 | 0.19432407E-09 | 0.18682712E-09 |
| 6 | 4 | -0.862142660109E-07 | -0.471408154267E-06 | 0.15229150E-09 | 0.15328004E-09 |
| 6 | 5 | -0.267133325490E-06 | -0.536488432483E-06 | 0.89838470E-10 | 0.87820905E-10 |
| 6 | 6 | 0.967616121092E-08 | -0.237192006935E-06 | 0.11332010E-09 | 0.11518036E-09 |
| ⋮ | ⋮ | | | | |
| 360 | 358 | 0.709604781531E-10 | 0.691761006753E-10 | 0.50033977E-10 | 0.50033977E-10 |
| 360 | 359 | 0.183971631467E-10 | -0.310123632209E-10 | 0.50033977E-10 | 0.50033977E-10 |
| 360 | 360 | -0.447516389678E-24 | -0.830224945525E-10 | 0.50033977E-10 | 0.50033977E-10 |

3.8 Ellipsoidal harmonics

Laplace differential equation 1.13 may be written and solved in ellipsoidal co-ordinates instead of spherical co-ordinates. The result



is known as an *ellipsoidal-harmonic expansion*.⁷ They are little-used, because the maths needed is more complicated. Moreover, ellipsoidal co-ordinates are mostly only theoretically interesting and not in any broad use within geodesy.

The form of presentation is

$$V(\beta, \lambda, \mathbf{u}) = \sum_{n=0}^{\infty} \sum_{m=0}^n \frac{Q_{nm}\left(i\frac{u}{E}\right)}{Q_{nm}\left(i\frac{b}{E}\right)} P_{nm}(\sin \beta) (A_{nm}^e \cos m\lambda + B_{nm}^e \sin m\lambda), \quad (3.16)$$

in which $Q_{nm}(\mathbf{z})$ are the *Legendre functions of the second kind*, sampled in table 3.6. Although the general argument \mathbf{z} is complex, equation 3.16 gives a real result for real-valued coefficients A_{nm}^e, B_{nm}^e .

Those interested in the derivation of the above equation can find it in [Heiskanen and Moritz \(1967\)](#) or other textbooks on potential theory.

3.8.1 The scaling to standard form of the expansion

Assume $A_{10}^e = A_{11}^e = B_{11}^e = 0$, meaning the vanishing of the dipole moment.

We can also show that in expansion 3.16 the first coefficient is

$$A_{00}^e = A_0^e = \frac{GM_{\oplus}}{E} \arctan \frac{E}{b}$$

and the expansion specialised for a rotationally symmetric field becomes

$$\Psi(\beta, \mathbf{u}) = \sum_{n=0}^{\infty} \tilde{\Psi}_n(\beta, \mathbf{u}) = \sum_{n=0}^{\infty} \frac{Q_n\left(i\frac{u}{E}\right)}{Q_n\left(i\frac{b}{E}\right)} A_{n0}^e P_n(\sin \beta). \quad (3.17)$$

Also

$$\tilde{V}_0(\mathbf{u}) = \tilde{\Psi}_0(\mathbf{u}) = \frac{Q_0\left(i\frac{u}{E}\right)}{Q_0\left(i\frac{b}{E}\right)} \frac{GM_{\oplus}}{E} \arctan \frac{E}{b},$$

⁷This expansion for the ellipsoid of revolution differs from the expansion into Lamé functions found for the triaxial ellipsoid.



the gravitational potential of the field constituent of ellipsoidal degree zero.

With the substitutions (Heiskanen and Moritz, 1967, page 66)

$$Q_0\left(i\frac{u}{E}\right) = -i \arctan \frac{E}{u}, \quad Q_0\left(i\frac{b}{E}\right) = -i \arctan \frac{E}{b} \quad (3.18)$$

we obtain

$$\tilde{V}_0(u) = \tilde{\Psi}_0(u) = \frac{GM_{\oplus}}{E} \arctan \frac{E}{u}. \quad (3.19)$$

This corresponds to the “central field” of a spherical harmonic expansion GM_{\oplus}/r . Using this, we may “scale” equation 3.16 by substituting the above identities 3.18. The coefficients need to be divided by the constant expression

$$\frac{GM_{\oplus}}{E} \arctan \frac{E}{b},$$

as the central field, expression 3.19, is moved outside the expansion. The result is

$$V(\beta, \lambda, u) = \frac{GM_{\oplus}}{E} \arctan \frac{E}{u} \cdot \left(1 + \sum_{n=2}^{\infty} \sum_{m=0}^n \frac{\arctan \frac{E}{b}}{\arctan \frac{E}{u}} \frac{Q_{nm}\left(i\frac{u}{E}\right)}{Q_{nm}\left(i\frac{b}{E}\right)} \bar{P}_{nm}(\sin \beta) \left(\bar{C}_{nm}^e \cos m\lambda + \bar{S}_{nm}^e \sin m\lambda \right) \right),$$

in which we have also introduced fully normalized coefficients $\bar{C}_{nm}^e, \bar{S}_{nm}^e$ and Legendre functions $\bar{P}_{nm}(\sin \beta)$.

This is an ellipsoidal-harmonic expansion that agrees with the spherical-harmonic expansion 3.13, with the total mass of the Earth outside the parentheses and the coefficients dimensionless. This equation has apparently not been used for any geopotential determination.

3.8.2 Equivalence of the Rapp and ellipsoidal expansions

We can demonstrate the equivalence of spherical expansions 3.13 or 3.14 and ellipsoidal expansion 3.16, if the flattening of the Earth $\rightarrow 0$, and thus also $b \rightarrow a$, $\beta \rightarrow \phi$, and $u \rightarrow r$. We assume that Heiskanen





TABLE 3.6. Legendre functions of the second kind.

| | |
|---|---|
| $Q_0(z) = \frac{1}{2} \ln \frac{z+1}{z-1}$ | $(n+1) Q_{n+1}(z) - (2n+1) z Q_n(z) + n Q_{n-1}(z) = 0$ |
| $Q_1(z) = \frac{1}{2} z \ln \frac{z+1}{z-1} - 1$ | |
| $Q_2(z) = \left(\frac{3}{4} z^2 - \frac{1}{4}\right) \ln \frac{z+1}{z-1} - \frac{3}{2} z$ | $Q_{nm}(z) = (1-z^2)^{m/2} \frac{d^m}{dz^m} Q_n(z)$ |
| $Q_3(z) = \left(\frac{5}{4} z^3 - \frac{3}{4} z\right) \ln \frac{z+1}{z-1} - \frac{5}{2} z^2 + \frac{2}{3}$ | |

and Moritz (1967) equation 1-112,

$$\lim_{E \rightarrow 0} \frac{Q_{nm}\left(i \frac{u}{E}\right)}{Q_{nm}\left(i \frac{b}{E}\right)} = \left(\frac{a}{r}\right)^{n+1}$$

is valid. Substitution into equation 3.16 yields

$$\begin{aligned} V(u, \beta, \lambda) &= V(r, \phi, \lambda) = \\ &= \sum_{n=0}^{\infty} \sum_{m=0}^n \left(\frac{a}{r}\right)^{n+1} P_{nm}(\sin \phi) (A_{nm}^e \cos m\lambda + B_{nm}^e \sin m\lambda), \quad (3.20) \end{aligned}$$

which, with the identifications $A_{00}^e = GM_{\oplus}/a$, $A_{10}^e = A_{11}^e = B_{11}^e = 0$ and relations 3.15, suggests

$$\begin{aligned} \begin{Bmatrix} A_{n0}^e \\ B_{n0}^e \end{Bmatrix} &= -\frac{GM_{\oplus}}{a} \begin{Bmatrix} J_{n0} \\ K_{n0} \end{Bmatrix} = \frac{GM_{\oplus}}{a} \sqrt{(2n+1)} \begin{Bmatrix} \bar{C}_{n0} \\ \bar{S}_{n0} \end{Bmatrix}, \\ \begin{Bmatrix} A_{nm}^e \\ B_{nm}^e \end{Bmatrix} &= -\frac{GM_{\oplus}}{a} \begin{Bmatrix} J_{nm} \\ K_{nm} \end{Bmatrix} = \\ &= \frac{GM_{\oplus}}{a} \sqrt{2(2n+1) \frac{(n-m)!}{(n+m)!}} \begin{Bmatrix} \bar{C}_{nm} \\ \bar{S}_{nm} \end{Bmatrix} \quad \text{if } m \neq 0. \end{aligned}$$

Substituting these into equation 3.20 affirms its equivalence with equations 3.13 and 3.14 for spherical harmonics.



3.8.3 Advantages of using ellipsoidal harmonics

- The expression for the normal gravitational potential is simple in this form of presentation, see Heiskanen and Moritz (1967)



equation 2-56. A spherical-harmonic expansion of the same field would instead require theoretically an infinite number of coefficients. In practice, this number is only 3 to 4, so an expansion up to J_6 or J_8 will suffice.

- The convergence will be more rapid, as less terms are needed. suppeneminen
This is because, due to the Earth's flattening, the equator is some 23 km further from the Earth's centre than the poles. Therefore, high-degree spherical harmonics in particular will have difficulty converging efficiently both at the poles and in the equatorial region. This problem is worst for very high-degree expansions (for example [Wenzel, 1998](#)). Already for a degree number of 360, the semi-wavelength of a spherical harmonic will be only 55 km!

3.8.4 Disadvantage of using ellipsoidal harmonics

Evaluation of an ellipsoidal-harmonic expansion is clearly more laborious and expensive than that of a spherical-harmonic one, in terms of computer resources.

Self-test questions

1. How does separation of variables work?
2. Why does solving the Laplace equation require *boundary conditions*?
3. What are the harmonic degree and harmonic order in a spherical-harmonic expansion? How do they relate to the *resolution* of the expansion on the Earth's surface?
4. What types of spherical harmonics are there? Explain their dependence on latitude and longitude.
5. How many times does a surface spherical harmonic $Y_{nm}(\phi, \lambda)$ change its algebraic sign travelling along a meridian from the



south pole to the north pole? How many times when travelling around the Earth along the equator?

6. What does it mean if it is said that two functions are mutually orthogonal? Give a possible definition of the *scalar product* of two functions.
7. How does the *attenuation* of spherical harmonics with height behave? Why does a gravimetric satellite that is trying to map the gravity field of the Earth at a high resolution fly in as low an orbit as possible?
8. What does the *degree constituent equation* express?
9. Which spherical-harmonic coefficients are associated with the *dipole moment* of the Earth's mass distribution? Why are they missing from tableau 3.5?



Exercise 3 – 1: Attenuation with height of a spherical-harmonic expansion

If

$$V(\phi, \lambda, r) = \sum_{n=0}^{\infty} \tilde{V}_n(\phi, \lambda, r) = \sum_{n=0}^{\infty} \left(\frac{R}{r}\right)^{n+1} V_n(\phi, \lambda),$$

we may call

$$\frac{\tilde{V}_n(\phi, \lambda, r)}{V_n(\phi, \lambda)} = \left(\frac{R}{r}\right)^{n+1}$$

the *attenuation factor* of the potential with height.

Differentiation with respect to r yields

$$\frac{\partial \tilde{V}_n(\phi, \lambda, r)}{\partial r} = -\frac{n+1}{R} \left(\frac{R}{r}\right)^{n+2} V_n(\phi, \lambda), \quad (3.21)$$

or, because, at sea level, similarly

$$\left. \frac{\partial \tilde{V}_n(\phi, \lambda, r)}{\partial r} \right|_{r=R} = -\frac{n+1}{R} V_n(\phi, \lambda), \quad (3.22)$$



it follows that the attenuation factor for the *attraction* is the ratio of expressions 3.21 and 3.22:

$$\left(\frac{R}{r}\right)^{n+2}.$$

1. Draw a *log-linear graph* of the attenuation factors of both the potential and the attraction for values $n = 0, 1, 2, \dots, 100$, by hand or by machine. Choose $R = 6378$ km, $r = 7378$ km — a height 1000 km above the Earth's surface.
2. Based on this, if the satellite is 1000 km above the Earth's surface, for what degree number n will the accelerations $\frac{\partial}{\partial r} \tilde{V}_n(\phi, \lambda, r)$ caused by the attraction at the satellite's level be less than 1 % of what they are on the Earth's surface?
3. For what degree number n will they be less than $10^{-4} \times$ of what they are on the Earth's surface?



Exercise 3 – 2: Symmetries of spherical harmonics

See equation 2.11. In it, $P_{n,m}(\sin \phi) = P_{n,m}(t)$, $t = \sin \phi$ is only a function of latitude ϕ . When ϕ runs from the south pole through the equator to the north pole, $-90^\circ \leq \phi \leq +90^\circ$, parameter t will run through the values $-1 \leq t \leq +1$ on the interval $[-1, 1]$.

For the Legendre functions exists the closed expression 3.2:

$$P_{n,m}(t) = (1 - t^2)^{m/2} \frac{d^m}{dt^m} P_n(t),$$

in which the $P_n(t)$ are ordinary Legendre polynomials:

$$P_n(t) = \frac{1}{2^n n!} \frac{d^n}{dt^n} \left((t^2 - 1)^n \right).$$

We can observe the following properties:

1. Differentiating a symmetric function of t will produce an antisymmetric function, and vice versa.
2. The function $(t^2 - 1)$ and its powers are symmetric.



3. Thus: for even n values, $P_n(t) = +P_n(-t)$: P_n is *symmetric* between the northern and southern hemispheres, and for odd n values $P_n(t) = -P_n(-t)$: P_n is *antisymmetric* between hemispheres.
4. Similarly, for even n , $P_n(\sin \phi) = +P_n(\sin(-\phi))$, and for odd n , $P_n(\sin \phi) = -P_n(\sin(-\phi))$.

Questions

1. What is the corresponding rule for the functions P_{nm} , in other words, for which (n, m) values is it symmetric and for which values antisymmetric?
2. Fill in the diagram ($n = 0, \dots, 5$, $m = 0, \dots, n$) with either 'S' or 'A' in each framed cell:

| | $n = 0$ | 1 | 2 | 3 | 4 | 5 |
|---------|---------|---|---|---|---|---|
| $m = 0$ | | | | | | |
| 1 | | | | | | |
| 2 | | | | | | |
| 3 | | | | | | |
| 4 | | | | | | |
| 5 | | | | | | |

3. What is the logic of symmetry?
4. If the field is *mirror symmetric* between the northern and southern hemispheres, i.e., $V(\phi, \lambda, r) = V(-\phi, \lambda, r)$, which of the spherical-harmonic coefficients a_{nm} , b_{nm} drop out of the series expansion? *Why?*
(Hint: see the example formulas and graphs for $P_{nm}(\sin \phi)$ in this chapter and try to guess a general rule. Then, verify.)
5. The same question if the potential is *rotationally symmetric* about the Earth's rotation axis: $V(\phi, \lambda, r) = V(\phi, r)$.



Exercise 3 – 3: Algebraic-sign domains of spherical harmonics

We have seen in section 3.1 that the associated Legendre functions $P_{nm}(t)$ have precisely $n - m + 1$ algebraic-sign intervals on their interval of definition $\phi \in [-90^\circ, 90^\circ]$. We can show that the functions $\cos m\lambda$ and $\sin m\lambda$ each have $2m$ zero crossings and $2m$ algebraic-sign intervals on their domain of definition $\lambda \in [0, 360^\circ)$, assumed to form a closed circle. How many *algebraic-sign domains* — grey or white areas, visible or occluded — are there in figure 3.3 for each surface spherical harmonic

$$Y_{nm}(\phi, \lambda) = \begin{cases} P_{nm}(\sin \phi) \cos m\lambda & \text{if } m \geq 0, \\ P_{n|m|}(\sin \phi) \sin |m|\lambda & \text{if } m < 0 \end{cases}$$

?

Exercise 3 – 4: Escape velocity

1. Given a spherically symmetric planet, mass GM , radius R , from the surface of which a cannon shoots projectiles at flight velocity v . What is the minimum value for v — the *escape velocity* — if it is desired that the projectile can travel to arbitrarily large distances from the planet and never fall back? The kinetic energy of the projectile is $E_{\text{kin}} = \frac{1}{2}mv^2$, in which m is the projectile's mass.
2. Given, in *two-dimensional geometry*, a circularly symmetric planet, mass GM , radius R , with the gravitational field of the planet represented by potential V as given in section 2.3, what does V look like in terms of those parameters? Make an educated guess.
3. There is again a cannon on the edge of the circle planet. What can you now say about the escape velocity v (do *not* try to compute it!)?





The normal gravity field

4



4.1 The basic idea of a normal field

Just as the figure of the Earth can be approximated by an ellipsoid of revolution, the gravity field of the Earth can also be approximated by a field of which one equipotential surface, or *level surface*, is precisely this ellipsoid of revolution, the *reference ellipsoid*. tasopinta

This brings a logical idea to mind: why not define intercompatibly a *reference ellipsoid* and a geopotential or *normal potential*, one of the equipotential surfaces of which is the reference ellipsoid? After that, a *gravity formula* is obtained by taking the gradient of this normal potential.

After this we may define *anomalous* quantities, such as the disturbing potential and the gravity anomaly, which then again will be intercompatible, while being numerically much smaller.

Let the normal potential be $U(x, y, z)$. Then, normal gravity will be

$$\gamma(x, y, z) = \|\vec{\gamma}\| = \|\nabla U\| = -\langle \vec{\gamma} \cdot \mathbf{n} \rangle = -\frac{\partial U}{\partial n},$$

in which $\frac{\partial}{\partial n}$ denotes differentiation in the direction of the exterior surface normal \mathbf{n} to a level surface of the normal field, itself an ellipsoid as well, see figure 4.1. This direction will differ from the direction of the normal to the level surfaces of the gravity field, or *plumb line*, by luotiviiva

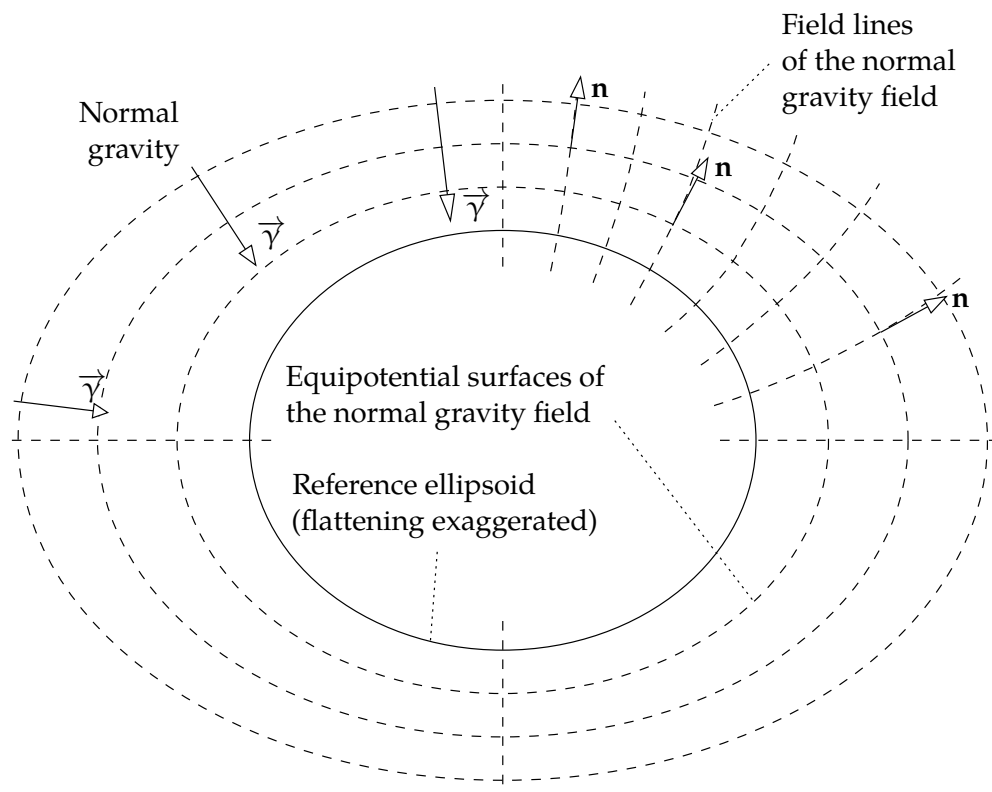


FIGURE 4.1. The normal gravity field of the Earth.

luotiviivan
poikkeama

precisely the plumb-line deflection. The deflection of the plumb line is also typically a very small angle.

We shall see in the next section that the pseudo-force generated by the Earth's rotation may, in a system rotating along with the Earth, be described by a *rotational potential* Φ — also called centrifugal potential. The normal potential U is also defined in such a way that the rotational potential Φ is included in it: the normal potential is the reference potential of the *gravity field*, not the *gravitational field*. If we denote the normal *gravitational* potential using Ψ — a quantity rarely used in geodesy — then the normal *gravity* potential or *normal potential* U is

$$U = \Psi + \Phi,$$

in which Φ is the centrifugal potential. In other words: Ψ , like V , is



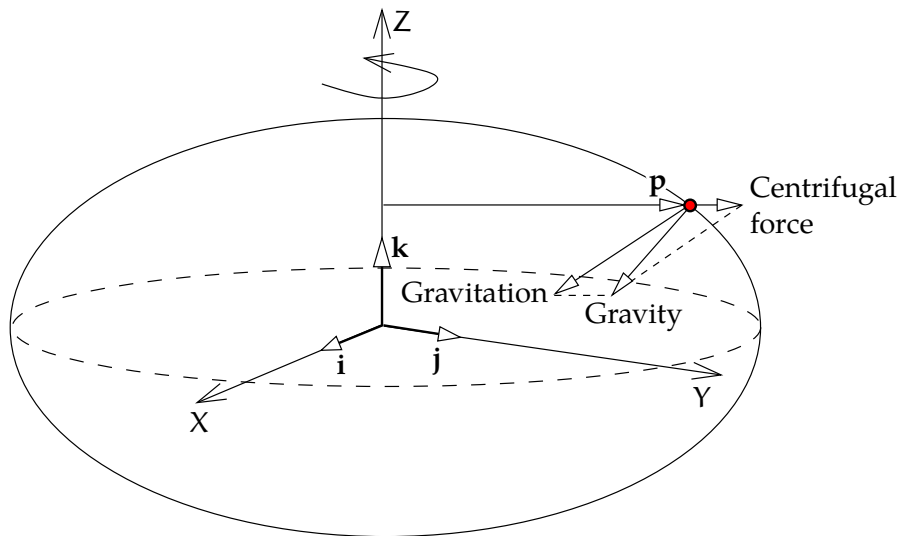


FIGURE 4.2. Gravitation and centrifugal force.

defined in a non-rotating (inertial) system, whereas U , like W , is defined in a system that co-rotates with the Earth and is non-inertial. The word *gravity* refers to a force acting in a co-rotating system, whereas in an inertial system we use the word *gravitation*.

painovoima
vetovoima

4.2 The centrifugal force and its potential

The rotation of the Earth affects the gravity field. In an inertial reference system one speaks of gravitation and gravitational potential V . On the Earth's surface, however, in a non-inertial or *co-rotating* system, we talk of *gravity* and *gravity potential* W . They are different things, and the rotational motion and its centrifugal force are the cause of the difference. See figure 4.2.

mukana pyörivä

To derive the equation for centrifugal force, write first

$$\mathbf{p} = X\mathbf{i} + Y\mathbf{j}.$$

The vectors $\{\mathbf{i}, \mathbf{j}, \mathbf{k}\}$ form an orthonormal basis along the (X, Y, Z) axes. It follows that

$$p = \|\mathbf{p}\| = \sqrt{\langle \mathbf{p} \cdot \mathbf{p} \rangle} = \sqrt{X^2 + Y^2}.$$



Now the centrifugal force — or rather, acceleration — is, in metres per second squared,

$$\mathbf{f} = \omega_{\oplus}^2 \mathbf{p} = \omega_{\oplus}^2 (X\mathbf{i} + Y\mathbf{j}),$$

with ω_{\oplus} the rotation rate of the Earth in radians per second.

Here on Earth, gravity measurements are generally made using an instrument that is *at rest* with respect to the Earth's surface: it follows the rotation of the Earth. If the instrument moves, one must, in addition to the centrifugal force, take into account another pseudo-force: the Coriolis¹ force. Fluids — water, air — on the Earth's surface, if they are at rest, only sense the centrifugal force. Currents in addition also sense the Coriolis force, which deflects them sideways and causes the well-known eddy phenomena in the oceans and atmosphere.

We may describe centrifugal force as *the gradient of a potential*. If we write for this *centrifugal potential*

$$\Phi = \frac{1}{2} \omega_{\oplus}^2 (X^2 + Y^2),$$

we may directly calculate the gradient

$$\begin{aligned} \mathbf{f} = \nabla\Phi &= \frac{\partial\Phi}{\partial X}\mathbf{i} + \frac{\partial\Phi}{\partial Y}\mathbf{j} + \frac{\partial\Phi}{\partial Z}\mathbf{k} = \\ &= \frac{1}{2}\omega_{\oplus}^2 \cdot 2X \cdot \mathbf{i} + \frac{1}{2}\omega_{\oplus}^2 \cdot 2Y \cdot \mathbf{j} + 0 = \omega_{\oplus}^2 (X\mathbf{i} + Y\mathbf{j}), \end{aligned}$$

which corresponds to the above centrifugal-force equation.

If we add to the gravitational potential V the centrifugal potential Φ , we obtain the *gravity potential* W :

$$W = V + \Phi.$$

We may also derive from the centrifugal potential Φ the following equation by differentiating it twice:

$$\Delta\Phi = \nabla^2\Phi = \langle \nabla \cdot \mathbf{f} \rangle = \frac{\partial}{\partial X} \omega_{\oplus}^2 X + \frac{\partial}{\partial Y} \omega_{\oplus}^2 Y + \frac{\partial}{\partial Z} 0 = 2\omega_{\oplus}^2, \quad (4.1)$$

¹Gaspard-Gustave Coriolis (1792–1843) was a French mathematician, physicist and mechanical engineer. His name is inscribed on the Eiffel Tower, [Eiffel Tower, 72 names](#).



from which follows, with Poisson equation 1.14,

$$\Delta W = -4\pi G\rho + 2\omega_{\oplus}^2, \quad (4.2)$$

the Poisson equation for the gravity potential.

The difference between gravitation and gravity is essential. The force, or acceleration, of gravitation $\tilde{\mathbf{g}} = \nabla V$ is just an attractive force, whereas the acceleration of gravity $\mathbf{g} = \nabla W$ is the vector sum of gravitation and centrifugal force. Attraction and centrifugal force act in the same fashion: the force is proportional to the mass of the test object. In other words, the acceleration is always the same independently of the mass of the test object. This is the famous *equivalence principle* (Galileo, Einstein), which has been proven to hold to very great precision. We may mention in particular the clever tests by the Hungarian baron Loránd Eötvös.²

Water masses on the Earth's surface, as also the atmosphere — and on a vastly longer time-scale also the “solid” Earth rock forming mountain ranges and ocean depths — react to gravity without distinguishing between attraction and centrifugal force. For this reason, the sea surface coincides within a metre or so with an equipotential or *level surface* of the W function or *geopotential*. Moreover, on dry land, we measure heights from this surface, the *geoid* (according to Gauss, the “mathematical figure of the Earth”).

4.3 Level surfaces and plumb lines

Surfaces of constant gravity potential or *geopotential*, equipotential surfaces or *level surfaces*, are the following surfaces:

tasopinnat

$$W(x, y, z) = \text{constant.}$$

²Loránd baron Eötvös de Vásárosnamény (1848–1919) was a Hungarian physicist and student of gravitation.

Let $\{\mathbf{i}, \mathbf{j}, \mathbf{k}\}$ again be an orthonormal basis along the (x, y, z) axes. Then, in the direction of the unit vector

$$\mathbf{e} = e_1\mathbf{i} + e_2\mathbf{j} + e_3\mathbf{k}$$

the potential changes as follows:

$$\frac{\partial W}{\partial e} = e_1 \frac{\partial W}{\partial x} + e_2 \frac{\partial W}{\partial y} + e_3 \frac{\partial W}{\partial z},$$

which vanishes if and only if

$$\langle \mathbf{e} \cdot \nabla W \rangle = 0,$$

in other words, the potential is stationary only in directions that are perpendicular to the Earth's gravity vector

$$\nabla W = \mathbf{g}.$$

Level surfaces and gravity vectors, or plumb lines, are always perpendicular to each other.

4.3.1 Curvature of level surfaces

Let there be given a plane that at P has the same direction as the level surface: its *tangent plane*, figure 4.3. If the local curvature of the level surface in the x direction is ρ_x and the x co-ordinate of point P is x_0 , we may develop the distance between the surfaces in a Taylor series:

$$\epsilon \approx \frac{1}{2\rho_x} (x - x_0)^2.$$

From this we obtain the difference in W values between the surfaces ($g = \|\mathbf{g}\| = \|\nabla W\|$):

$$\delta W \approx -\epsilon g \approx -(x - x_0)^2 \frac{g}{2\rho_x}.$$



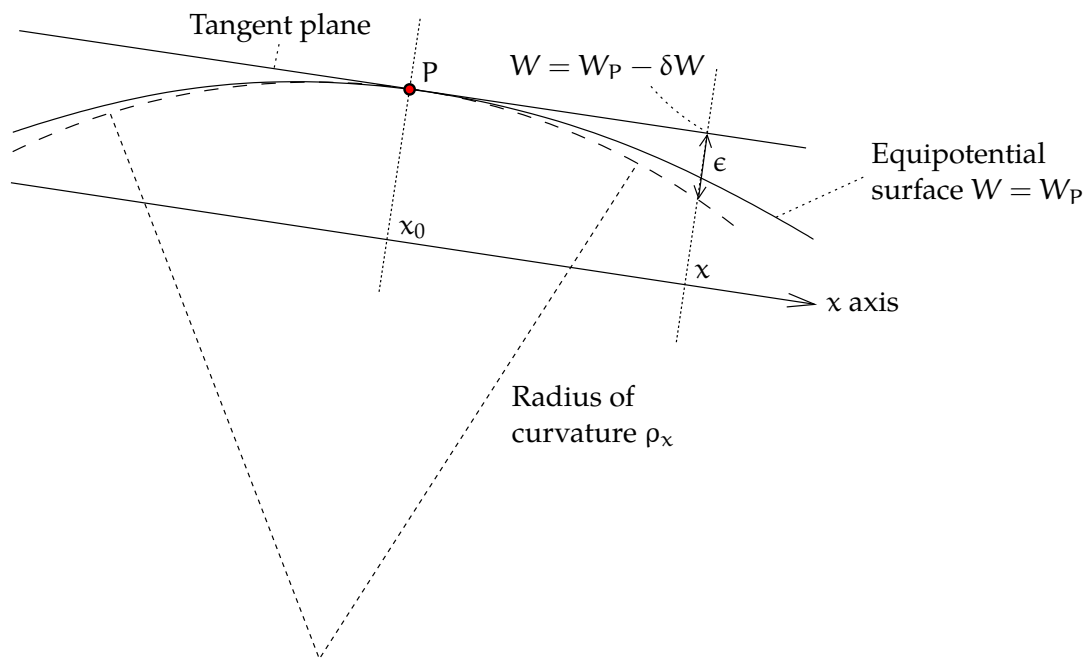


FIGURE 4.3. The curvature of level surfaces.

By differentiating (note that W here is now the geopotential *on the tangent or horizontal plane*), we obtain

$$\frac{\partial^2}{\partial x^2} \delta W = \frac{\partial^2}{\partial x^2} W = \partial_{xx} W = -\frac{g}{\rho_x},$$

from which

$$\rho_x = -\frac{g}{\partial_{xx} W}.$$

By determining the curvature in the x and y directions,

$$K_x \stackrel{\text{def}}{=} \frac{1}{\rho_x} = -\frac{\partial_{xx} W}{g}, \quad K_y \stackrel{\text{def}}{=} \frac{1}{\rho_y} = -\frac{\partial_{yy} W}{g}, \quad (4.3)$$

we obtain the mean or Germain³ curvature, in most locations a positive number:

$$J = \frac{K_x + K_y}{2} = -\frac{\partial_{xx} W + \partial_{yy} W}{2g},$$

and by using Poisson equation 4.2,

$$\Delta W = \partial_{xx} W + \partial_{yy} W + \partial_{zz} W = -4\pi G\rho + 2\omega_{\oplus}^2,$$



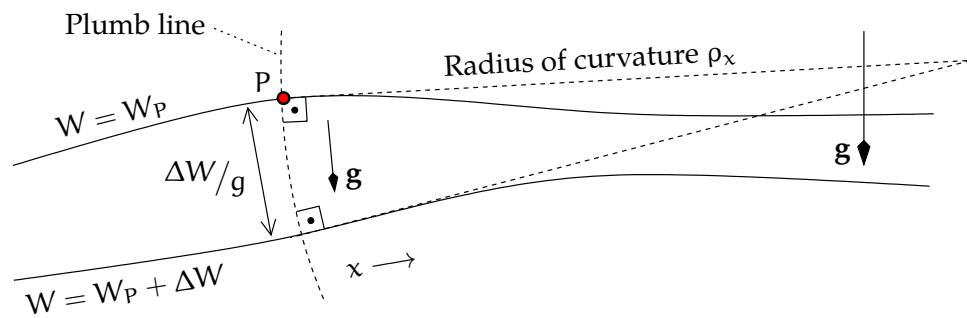


FIGURE 4.4. The curvature of the plumb line.

we obtain

$$-2gJ + \partial_{zz}W = -4\pi G\rho + 2\omega_{\oplus}^2.$$

By using

$$\partial_{zz}W = -\frac{\partial g}{\partial z} = -\frac{\partial g}{\partial H},$$

in which H is the height co-ordinate, we obtain for the vertical gradient of gravity (Heiskanen and Moritz, 1967, equation 2-20):

$$\frac{\partial g}{\partial H} = -2gJ + 4\pi G\rho - 2\omega_{\oplus}^2,$$

an equation found by Ernst Heinrich Bruns (Bruns, 1878, page 13).

We also showed the compact *Euler notation* for partial derivatives, $\partial_{xx}, \partial_{yy}, \partial_{zz}$, which is often convenient.



4.3.2 Curvature of plumb lines

Plumb lines are curved because gravity is not constant in the horizontal direction. If gravity increases in a horizontal direction, then the equipotential surfaces will come closer together too, and they will not be parallel. This means that the plumb lines, being perpendicular to all equipotential surfaces, must be curved in that direction.

³Marie-Sophie Germain (1776–1831) was a brilliant French mathematician, number theorist and student of elasticity. She corresponded with Gauss on number theory (Friedelmeyer, 2014) and did foundational work towards a proof of Fermat's last theorem. Her name is missing from the Eiffel Tower.



Consider two equipotential surfaces, one for potential W_p and one for potential $W_p + \Delta W$. The distance separating them will be $\Delta H = \Delta W/g$. In the direction of co-ordinate x the relative tilt between the two surfaces will be

$$\frac{\partial}{\partial x} \Delta H(x) = \frac{\partial}{\partial x} \left(\frac{\Delta W}{g(x)} \right) = -\frac{\Delta W}{g^2} \frac{\partial g}{\partial x}.$$

If the starting distance between the surfaces is ΔH , it will take a distance of

$$\rho_x = -\Delta H / \frac{\partial}{\partial x} \Delta H = -\left(\frac{\Delta W}{g} \right) / \left(-\frac{\Delta W}{g^2} \frac{\partial g}{\partial x} \right) = g / \frac{\partial g}{\partial x}$$

to bring the tangents together, see figure 4.4. The curvature of the plumb line is the inverse of this, in both the x and the y co-ordinate directions:

$$\kappa_x = \frac{1}{\rho_x} = \frac{1}{g} \frac{\partial g}{\partial x}, \quad \kappa_y = \frac{1}{\rho_y} = \frac{1}{g} \frac{\partial g}{\partial y}.$$

We can derive the curvature of the field lines of the *normal gravity field* in the same way. The difference is, however, that we can find a simple mathematical expression for gravity on the surface of the reference ellipsoid, for example equation 4.5. A good approximation is

$$\gamma(\varphi) \approx \gamma_a \cos^2 \varphi + \gamma_b \sin^2 \varphi.$$

With the chain rule

$$\begin{aligned} \frac{\partial \gamma}{\partial x} &= \frac{\partial \gamma}{\partial \varphi} \frac{\partial \varphi}{\partial x} = \frac{1}{R} \frac{\partial \gamma}{\partial \varphi} = \frac{1}{R} (-2\gamma_a \cos \varphi \sin \varphi + 2\gamma_b \sin \varphi \cos \varphi) = \\ &= \frac{\gamma_b - \gamma_a}{R} \sin 2\varphi. \end{aligned}$$

This means in the x or south-north and y or west-east direction:

$$\kappa_x^* = \frac{1}{\gamma} \frac{\partial \gamma}{\partial x} \approx \frac{1}{R} \frac{\gamma_b - \gamma_a}{\gamma_a} \sin 2\varphi, \quad \kappa_y^* = \frac{1}{\gamma} \frac{\partial \gamma}{\partial y} = 0.$$



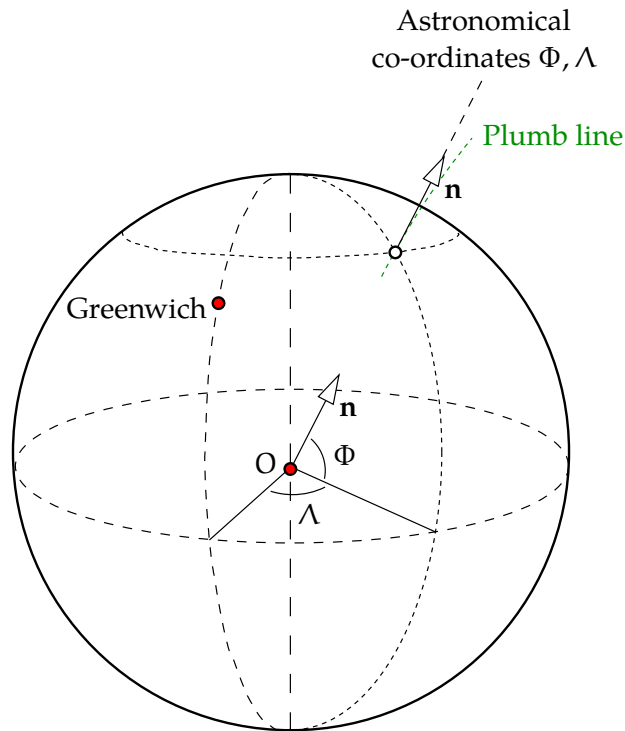


FIGURE 4.5. Natural co-ordinates Φ and Λ . In addition, a natural height co-ordinate, for example the geopotential W , is needed.

4.4 Natural co-ordinates

Before the satellite era it was impossible to directly measure the geocentric co-ordinates X, Y and Z . Today this is possible, and we obtain at the same time the height from the reference ellipsoid h , a purely geometric quantity.

In earlier times, one could measure only the direction of the plumb line as shown in figure 4.5, as well as the potential difference between an observation point and sea level by levelling. The direction of the plumb line \mathbf{n} was measured astronomically: astronomical latitude Φ (not to be confused with the centrifugal potential) and astronomical longitude Λ . The third co-ordinate, the gravity potential difference $W(x, y, z) - W_0$ from the potential W_0 of sea level, was determined by



levelling. Co-ordinates Φ, Λ and W are called *natural co-ordinates*.

Often, instead of the potential, *orthometric height* H is used. Its definition is easy to understand if one writes

$$\frac{\partial W}{\partial H} = -g \implies dH = -\frac{1}{g}dW \implies H_P = -\int_{W_0}^{W_P} \frac{1}{g(W)}dW, \quad (4.4)$$

in which the integral is taken along the plumb line of point P . $\frac{\partial}{\partial H}$ is the derivative in the direction of the plumb line, the local normal to the level surfaces. g is the acceleration of gravity along the plumb line as a function of place — or of geopotential level. In this case of orthometric heights, g is the *true* gravity inside the rock, which is a non-linear function of place and will also depend on the rock density. This trickiness of their determination is a problem specific to orthometric heights. We will return to this later (Heiskanen and Moritz, 1967, chapter 4).

The co-ordinates Φ, Λ and H also form a natural co-ordinate system.



4.5 The normal potential in ellipsoidal co-ordinates

We have already presented equation 3.16 for the expansion of the geopotential into ellipsoidal harmonics. It is required of the normal potential U that it is constant on the reference ellipsoid $u = b$. We expand the centrifugal potential Φ into ellipsoidal harmonics, obtaining

$$\begin{aligned} \Phi(\beta, u) &= \frac{1}{2}\omega_{\oplus}^2 (x^2 + y^2) = \frac{1}{2}\omega_{\oplus}^2 (u^2 + E^2) \cos^2 \beta = \\ &= \frac{1}{2}\omega_{\oplus}^2 (u^2 + E^2) (1 - \sin^2 \beta) = \\ &= \frac{1}{2}\omega_{\oplus}^2 (u^2 + E^2) \left(-\frac{2}{3}P_2(\sin \beta) + \frac{2}{3}P_0(\sin \beta)\right) = \\ &= -\frac{1}{3}\omega_{\oplus}^2 (u^2 + E^2) (P_2(\sin \beta) - P_0(\sin \beta)). \end{aligned}$$

In addition, based on equation 3.17 we have for the rotationally symmetric normal gravitational potential Ψ :

$$\Psi(\beta, u) = \sum_{n=0}^{\infty} \tilde{\Psi}_n(\beta, u) = \sum_{n=0}^{\infty} \frac{Q_n\left(i\frac{u}{E}\right)}{Q_n\left(i\frac{b}{E}\right)} A_n^e P_n(\sin \beta).$$



Now

$$U(\beta, u) = \Psi(\beta, u) + \Phi(\beta, u).$$

On the reference ellipsoid $u = b$ we have as a requirement $U(\beta, b) = U_0$, which is possible only if

$$\begin{aligned} U_0 &= A_0^e + \frac{1}{3}\omega_{\oplus}^2 (b^2 + E^2) = A_0^e + \frac{1}{3}\omega_{\oplus}^2 a^2, \\ 0 &= A_1^e, \\ 0 &= A_2^e - \frac{1}{3}\omega_{\oplus}^2 (b^2 + E^2) = A_2^e - \frac{1}{3}\omega_{\oplus}^2 a^2, \\ 0 &= A_n^e, n = 3, 4, 5, \dots \end{aligned}$$

The quantity U_0 can be computed uniquely, if the Earth's mass GM_{\oplus} and the measures of the reference ellipsoid a, b are known. The result, given in [Heiskanen and Moritz \(1967\)](#) as equation 2-61, is

$$U_0 = \frac{GM_{\oplus}}{E} \arctan \frac{E}{b} + \frac{1}{3}\omega_{\oplus}^2 a^2.$$

From this follows

$$A_0^e = U_0 - \frac{1}{3}\omega_{\oplus}^2 a^2 = \frac{GM_{\oplus}}{E} \arctan \frac{E}{b}.$$

The normal *gravity* potential U is obtained as follows (remember the identities [3.18](#)):

$$\begin{aligned} U(\beta, u) &= \Psi(\beta, u) + \Phi(\beta, u) = \overbrace{\frac{GM_{\oplus}}{E} \arctan \frac{E}{u}}^{\tilde{\Psi}_0(u)} + \\ &+ \overbrace{\frac{1}{3}\omega_{\oplus}^2 a^2}^{A_2^e} \frac{Q_2(i\frac{u}{E})}{Q_2(i\frac{b}{E})} \overbrace{\left(\frac{3}{2}\sin^2 \beta - \frac{1}{2}\right)}^{P_2(\sin \beta)} + \overbrace{\frac{1}{2}\omega_{\oplus}^2 (u^2 + E^2) \cos^2 \beta}^{\Phi(\beta, u)} = \\ &= C_0(u) + C_1(u) \sin^2 \beta + C_2(u) \cos^2 \beta, \end{aligned}$$

in which $C_0, C_1,$ and C_2 are suitable functions of u . The function $\tilde{\Psi}_0$ is the term for $n = 0$ in expansion [3.17](#).



On the surface of the reference ellipsoid ($u = b$), using $a^2 = b^2 + E^2$:

$$\begin{aligned}
 U(\beta, b) &= \\
 &= \overbrace{\frac{GM_{\oplus}}{E} \arctan \frac{E}{b}}^{\tilde{\Psi}_0(b)} + \overbrace{\frac{1}{2}\omega_{\oplus}^2 a^2 \sin^2 \beta - \frac{1}{6}\omega_{\oplus}^2 a^2}^{A_2^s P_2(\sin \beta)} + \overbrace{\frac{1}{2}\omega_{\oplus}^2 a^2 \cos^2 \beta}^{\Phi(\beta, b)} = \\
 &= \frac{GM_{\oplus}}{E} \arctan \frac{E}{b} + \frac{1}{3}\omega_{\oplus}^2 a^2,
 \end{aligned}$$

the constant U_0 , as it had better be!

4.6 Normal gravity on the reference ellipsoid

Without proof, we mention that for *normal gravity* (the quantity $\gamma = \frac{\partial}{\partial h} U$) the following equation applies on the reference ellipsoid:

$$\gamma(\beta) = \frac{a\gamma_b \sin^2 \beta + b\gamma_a \cos^2 \beta}{\sqrt{a^2 \sin^2 \beta + b^2 \cos^2 \beta}}.$$

By substitution we find immediately that γ_a is normal gravity on the equator ($\beta = 0$) and γ_b normal gravity on the poles ($\beta = \pm 90^\circ$).

Equations 2.5 and 2.7 yield

$$\tan \beta = \frac{\sin \beta}{\cos \beta} = \frac{Z/b}{\sqrt{X^2 + Y^2}/a} = \frac{a}{b} \frac{Z}{\sqrt{X^2 + Y^2}} = \frac{a}{b} \tan \phi$$

and

$$\tan \phi = \frac{\sin \phi}{\cos \phi} = \frac{Z/(1-e^2)N}{\sqrt{X^2 + Y^2}/N} = \frac{1}{1-e^2} \frac{Z}{\sqrt{X^2 + Y^2}} = \frac{a^2}{b^2} \tan \beta,$$

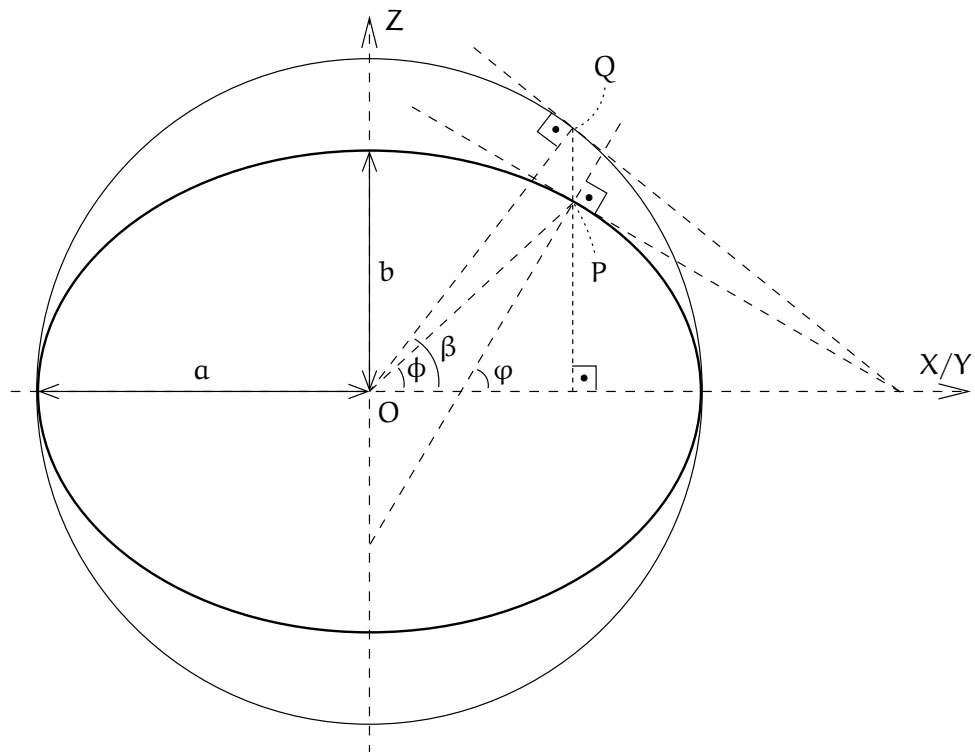
in which ϕ is the *geocentric* latitude, see equations 2.4. From this follows directly


$$\tan \beta = \frac{b}{a} \tan \phi,$$

in which the latitude angle ϕ is the geodetic or geographic latitude. β is still the *reduced latitude*. Now it can be shown (exercise!) that

$$\gamma(\phi) = \frac{a\gamma_a \cos^2 \phi + b\gamma_b \sin^2 \phi}{\sqrt{a^2 \cos^2 \phi + b^2 \sin^2 \phi}}. \quad (4.5)$$





 FIGURE 4.6. Geometry of the meridian ellipse and various types of latitude.

This is the famous *Somigliana–Pizzetti*⁴ equation. These geodesists demonstrated for the first time that an “ellipsoidal” normal gravity field which has the reference ellipsoid as one of its equipotential or level surfaces exists exactly, and that the gravity formula is also a closed expression in geographic latitude.

4.7 Numerical values and calculation formulas

When the reference ellipsoid has been chosen, we may calculate the normal potential and normal gravity corresponding to it. The fundamental quantities are

⁴Carlo Somigliana (1860–1955) was an Italian mathematician and physicist. Paolo Pizzetti (1860–1918) was an Italian geodesist.



a the equatorial radius of the ellipsoid of revolution, its semimajor axis

f the flattening

$$f \stackrel{\text{def}}{=} \frac{a - b}{a},$$

in which b is the polar radius or semiminor axis

ω_{\oplus} the rotation rate of the Earth

GM_{\oplus} the total mass of the Earth, including the atmosphere.

Nowadays the most commonly used reference ellipsoid *cum* normal potential is the **GRS80**, the Geodetic Reference System 1980:

$$\begin{aligned} a &= 6\,378\,137 \text{ m}, & \omega_{\oplus} &= 7\,292\,115 \cdot 10^{-11} \text{ s}^{-1}, \\ \frac{1}{f} &= 298.257\,222\,101, & GM_{\oplus} &= 3\,986\,005 \cdot 10^8 \text{ m}^3/\text{s}^2. \end{aligned}$$

In reality, f is not a defining constant of **GRS80**, but the constant J_2 is used instead, which is a defining quantity for the gravitational field, see equation 3.14.

The **WGS84** (World Geodetic System 1984) used by the **GPS** system has a reference ellipsoid that is *almost* identical to that of the **GRS80**.

The normal potential is (Heikkinen, 1981), in SI units:

$$\begin{aligned} U &= 62\,636\,860.8500 + \\ &+ \left(\begin{array}{l} -9.780\,326\,77 - 0.051\,630\,75 \sin^2 \varphi - \\ -0.000\,227\,61 \sin^4 \varphi - 0.000\,001\,23 \sin^6 \varphi \end{array} \right) h + \\ &+ \left(\begin{array}{l} +0.015\,438\,99 \cdot 10^{-4} - 0.000\,021\,95 \cdot 10^{-4} \sin^2 \varphi - \\ -0.000\,000\,10 \cdot 10^{-4} \sin^4 \varphi \end{array} \right) h^2 + \\ &+ \left(-0.000\,024\,22 \cdot 10^{-8} + 0.000\,000\,07 \cdot 10^{-8} \sin^2 \varphi \right) h^3, \end{aligned}$$

and normal gravity (note the minus sign, U is positive and diminishes



going upwards):

$$\begin{aligned} \gamma = -\frac{\partial U}{\partial h} = & + 9.780\,326\,77 + 0.051\,630\,75 \sin^2 \varphi + \\ & + 0.000\,227\,61 \sin^4 \varphi + 0.000\,001\,23 \sin^6 \varphi + \\ & - \left(+ 0.030\,877\,98 \cdot 10^{-4} - 0.000\,043\,90 \cdot 10^{-4} \sin^2 \varphi - \right. \\ & \quad \left. - 0.000\,000\,20 \cdot 10^{-4} \sin^4 \varphi \right) h + \\ & - \left(- 0.000\,072\,65 \cdot 10^{-8} + 0.000\,000\,21 \cdot 10^{-8} \sin^2 \varphi \right) h^2. \quad (4.6) \end{aligned}$$

Here, the unit of potential is m^2/s^2 , and the unit of gravity, m/s^2 . φ is geodetic latitude; h (in metres) is the height above the reference ellipsoid. More precise equations can be found from [Heikkinen \(1981\)](#). In these equations, the coefficient $9.780\,32\dots \text{m}/\text{s}^2$ is equatorial gravity, and the value $-0.030\,87\dots \text{s}^{-2}$ is the vertical gradient of gravity on the equator.

Other gravity formulas and reference ellipsoids still in legacy use (and slowly vanishing) are Helmert's 1906 ellipsoid, the Krasovsky ellipsoid or [SK-42](#) in Eastern Europe, the International or Hayford ellipsoid (1924) and its gravity formula, and the Geodetic Reference System 1967.

4.7.1 Numerical example

According to the above equation, the normal potential over the equator is

$$\begin{aligned} U = 62\,636\,860.8500 - 9.780\,326\,77 h + 0.015\,438\,99 \cdot 10^{-4} h^2 - \\ - 0.000\,024\,22 \cdot 10^{-8} h^3. \end{aligned}$$

- Draw this function for values of h in the range 0–7000 km.
- Draw for comparison the quadratic version, from which the last term is left off.

Questions

1. What is the minimum of the quadratic function?
2. How physically realistic is this?



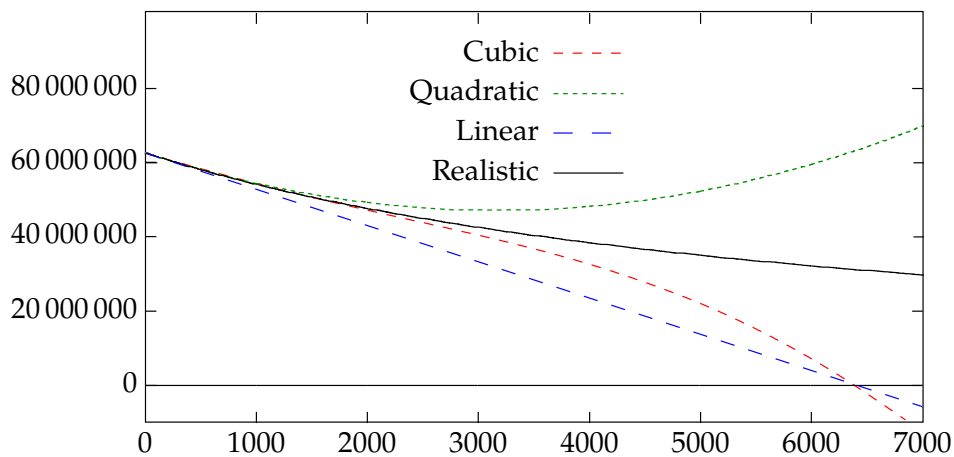


FIGURE 4.7. The normal field's potential over the equator. Heights in kilometres, potential in m^2/s^2 .



Answers

1. See figure 4.7. The minimum of the quadratic function is at height 3000 km. The cubic function does not have a minimum.
2. Not very physical: the stationary point for potential U (the normal potential in a co-rotating reference system) should be located at approximately 36 000 km height, at the geostationary orbit.

This tells us that polynomial approximation cannot be extrapolated very far. In this case, the interval of extrapolation is of the same order as the radius of the Earth, and that will no longer work.



4.8 The normal potential as a spherical-harmonic expansion

The spherical-harmonic expansion of an ellipsoidal gravitational field also contains, besides the second-degree harmonic, higher-degree harmonics. If we write, as is customary, the potential outside the Earth in the following form ([Heiskanen and Moritz, 1967](#) equation 2-39, also equation 3.14):

$$V(\phi, \lambda, r) = \frac{GM_{\oplus}}{r} \left(1 - \sum_{n=2}^{\infty} \left(\frac{a}{r} \right)^n \sum_{m=0}^n P_{nm}(\sin \phi) (J_{nm} \cos m\lambda + K_{nm} \sin m\lambda) \right),$$

then we may also write the normal gravitational potential, Ψ , into the form

$$\Psi(\phi, r) = \frac{GM_{\oplus}}{r} \left(1 - \sum_{\substack{n=2 \\ \text{even}}}^{\infty} J_n \left(\frac{a}{r} \right)^n P_n(\sin \phi) \right),$$

which contains only even coefficients $J_n = J_{n0}$, because the normal field is *symmetric* about the equatorial plane.

The coefficients for the [GRS80](#) normal gravitational potential are found⁵ in table 4.1. Higher terms are usually not needed. The relationship between fully normalised and non-normalised coefficients is $J_n = \bar{J}_n \sqrt{2n+1}$.


For comparison: in section 4.5 it was shown that in the expansion of the same field into *ellipsoidal* harmonics, only the degree-zero and degree-two coefficients are non-zero! This is one reason why these functions are used at all.

⁵They can also be calculated from equation (2-92) given in [Heiskanen and Moritz \(1967\)](#):

$$J_{2n} = (-1)^{n+1} \frac{3(e^2)^n}{(2n+1)(2n+3)} \left(1 - n + 5n \frac{J_2}{e^2} \right),$$

starting from the values J_2 and e^2 . The results are the same as in the table's left column.



 TABLE 4.1. GRS80 normal potential spherical-harmonic coefficients (Heikkinen, 1981; Heiskanen and Moritz, 1967).

| Non-normalised | Fully normalised |
|---|--|
| $J_2 = J_{2,0} = 1082.63 \cdot 10^{-6}$ | $\bar{J}_2 = -\bar{C}_{2,0} = 484.166\,854\,896 \cdot 10^{-6}$ |
| $J_4 = J_{4,0} = -2.370\,912\,22 \cdot 10^{-6}$ | $\bar{J}_4 = -\bar{C}_{4,0} = -0.790\,304\,073 \cdot 10^{-6}$ |
| $J_6 = J_{6,0} = +0.006\,083\,47 \cdot 10^{-6}$ | $\bar{J}_6 = -\bar{C}_{6,0} = +0.001\,687\,251 \cdot 10^{-6}$ |
| $J_8 = J_{8,0} = -0.000\,014\,27 \cdot 10^{-6}$ | $\bar{J}_8 = -\bar{C}_{8,0} = -0.000\,003\,461 \cdot 10^{-6}$ |

Instead of using an ellipsoidal model, we may also use as a normal gravity potential formula the first two or three terms of the spherical-harmonic expansion of the real geopotential. Then we obtain, taking the centrifugal potential along:

$$U = \frac{Y_0}{r} + \frac{Y_2(\phi, \lambda)}{r^3} + \frac{1}{2}\omega_{\oplus}^2 (X^2 + Y^2),$$

with the corresponding equipotential surface $U = U_0$ being the “Bruns spheroid”, or

$$U = \frac{Y_0}{r} + \frac{Y_2(\phi, \lambda)}{r^3} + \frac{Y_4(\phi, \lambda)}{r^5} + \frac{1}{2}\omega_{\oplus}^2 (X^2 + Y^2),$$

the “Helmert spheroid”. Here, $Y_0 \stackrel{\text{def}}{=} GM_{\oplus}$ while $Y_2(\phi, \lambda)$ and $Y_4(\phi, \lambda)$ are taken from the true geopotential.

These equations are easy to compute, but their equipotential or level surfaces are not ellipsoids of revolution, and in fact not even rotationally symmetric. They are quite complicated surfaces (Heiskanen and Moritz, 1967, section 2-12)!

However, in geometric geodesy we always use a reference ellipsoid, so this is also a wise thing to do in physical geodesy.

4.9 The disturbing potential

Write the gravity potential

$$W = V + \Phi,$$



in which Φ is the centrifugal potential (see above), and the normal potential

$$U = \Psi + \Phi.$$

häiriöpotentiaali The difference between them is the *disturbing potential*.

$$T \stackrel{\text{def}}{=} W - U = V - \Psi.$$

Both V and Ψ can be expanded into spherical harmonics. If we write the gravity potential

$$W = V + \Phi = \Phi + \frac{GM_{\oplus}}{r} \cdot \left(1 - \sum_{n=2}^{\infty} \left(\frac{a}{r} \right)^n \sum_{m=0}^n P_{nm}(\sin \phi) (J_{nm} \cos m\lambda + K_{nm} \sin m\lambda) \right),$$

and the normal potential

$$U = \Phi + \frac{GM_{\oplus}}{r} \left(1 - \sum_{\substack{n=2 \\ \text{even}}}^{\infty} \left(\frac{a}{r} \right)^n J_n^* P_n(\sin \phi) \right),$$

we obtain by subtraction for the disturbing potential

$$T = W - U = -\frac{GM_{\oplus}}{r} \cdot \left(\sum_{n=2}^{\infty} \left(\frac{a}{r} \right)^n \sum_{m=0}^n P_{nm}(\sin \phi) (\delta J_{nm} \cos m\lambda + K_{nm} \sin m\lambda) \right),$$

in which

$$\begin{cases} \delta J_{n0} = J_{n0} - J_n^* & \text{if } n \text{ even,} \\ \delta J_{nm} = J_{nm} & \text{otherwise.} \end{cases}$$

The above equation for the disturbing potential T is shortened as follows (Heiskanen and Moritz, 1967, equation 2-152):

$$T(\phi, \lambda, r) = \sum_{n=2}^{\infty} \left(\frac{a}{r} \right)^{n+1} T_n(\phi, \lambda), \quad (4.7)$$



where, in every term, the degree constituent T_n has the same dimension as T , and

$$T_n(\phi, \lambda) = -\frac{GM_{\oplus}}{a} \sum_{m=0}^n P_{nm}(\sin \phi) (\delta J_{nm} \cos m\lambda + K_{nm} \sin m\lambda).$$

On the surface of the reference sphere of radius a :⁶

$$T(\phi, \lambda) = \sum_{n=2}^{\infty} T_n(\phi, \lambda),$$

from which we see that on the reference level, the terms $T_n(\phi, \lambda)$ are really the *degree constituents* of the disturbing potential T for a certain degree number n .

The above expansions are all missing the terms $n = 0, 1$. Of these, $T_0(\phi, \lambda) = T_0$ is a constant — the global average of the disturbing potential — and $T_1(\phi, \lambda)$ has the form of a dipole field. Its value is proportional to the cosine of the angle between the geocentric location vector of the point of calculation and that of the dipole vector. Both vanish because it is assumed that

- the total mass of the Earth GM_{\oplus} assumed by the normal field is realistic
- the origin of the co-ordinate reference system is assumed to be at the centre of mass of the Earth.

See section 3.4 for more.



Self-test questions

1. What is the basic idea behind using a normal gravity field?
2. What is the difference between gravity and gravitation?

⁶Earlier we also used for this reference radius (in spherical approximation) the symbol R .



3. Given the centrifugal potential

$$\Phi = \frac{1}{2}\omega^2 (X^2 + Y^2),$$

derive the centrifugal acceleration as a vector. X, Y, Z are rectangular co-ordinates of a frame rotating at angular rate ω around the Z axis.

4. Explain the idea of natural co-ordinates.
5. What was the relationship between M. Le Blanc and C. F. Gauss? Use Google.
6. What makes Somigliana–Pizzetti equation 4.5 valuable?
7. What are the defining parameters of the Geodetic Reference System 1980?
8. Why does the spherical-harmonic expansion of the normal potential contain only a small number of terms and coefficients?
9. Why does the spherical-harmonic expansion of the normal potential not contain any terms of order $m \neq 0$?
10. Why does the spherical-harmonic expansion of the normal potential contain only terms with even degree numbers n ?



Exercise 4 – 1: The Somigliana–Pizzetti equation

1. Given gravity on the equator γ_a and on the poles γ_b , what is the gravity on geodetic latitude $\varphi = 45^\circ$? Derive an expression that may also contain a and b .
2. And what is the gravity on the reduced latitude $\beta = 45^\circ$? Compare with the previous.
3. Given are the semimajor axis a and semiminor axis b . What are the differences, for the same point, between the different latitudes (geodetic φ , geocentric ϕ , and reduced β) at most, in minutes of arc? Assume that the maximum happens at latitudes $\pm 45^\circ$.



4. Compute for both a geodetic and a reduced latitude of 45° numerical values of gravity for the case of the **GRS80** reference ellipsoid. By how much do they differ?



Exercise 4 – 2: Centrifugal force

Given is the rotation rate of the Earth in radians per second: $\omega_{\oplus} = 7292\,115 \cdot 10^{-11} \text{ s}^{-1}$.

1. Compute (roughly) the *centrifugal force* caused by the Earth's rotation at Southern Finland ($\varphi = 60^\circ$, $R = 6378 \text{ km}$, spherical Earth). In what direction does the force point (sketch!)?
2. How much does the centrifugal force contribute to local gravity, i.e., by how much does it change gravity, both as an acceleration and as a percentage?
3. Compute from the ω_{\oplus} value given above, the rotation time of the Earth in hours. Why is it not precisely 24^{h} ?





Anomalous quantities of the gravity field

5



5.1 Disturbing potential, geoid height, deflections of the plumb line

The first *anomalous quantity*, which we already discussed above, is the difference between the true gravity potential W and the normal gravity potential U , the *disturbing potential*:

$$T \stackrel{\text{def}}{=} W - U.$$

All other anomalous quantities are various functions of the disturbing potential, such as the geoid height N and the plumb-line deflections ξ, η . They are generally obtained by subtracting from each other

- a natural quantity related to the Earth's real gravity field, and
- a corresponding quantity related to the normal gravity field of the reference ellipsoid of the Earth.

For example, *deflections of the plumb line*

$$\begin{aligned}\xi &\stackrel{\text{def}}{=} \Phi - \varphi, \\ \eta &\stackrel{\text{def}}{=} (\Lambda - \lambda) \cos \varphi,\end{aligned}$$

in which (Φ, Λ) are astronomical latitude and longitude, that together make up the direction of the local plumb line, and the geodetic latitude

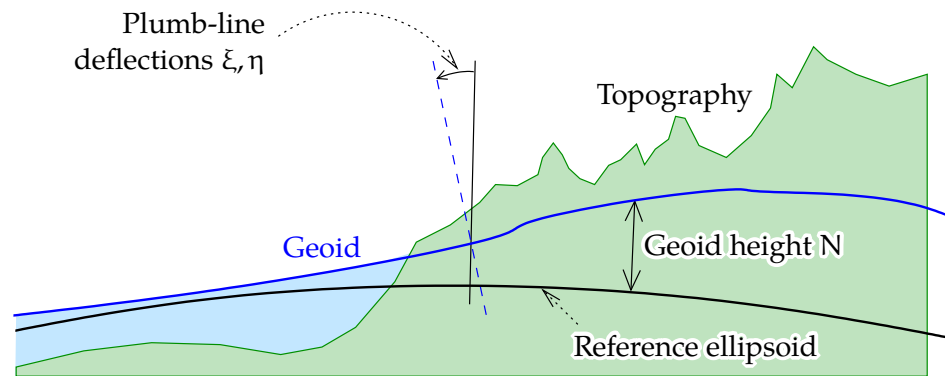


FIGURE 5.1. Geoid undulations and deflections of the plumb line.

and longitude (φ, λ) , that similarly make up the direction of the normal gravity vector or “normal plumb line”.¹ See figure 5.1.

The geoid height or *geoid undulation* is

$$N \stackrel{\text{def}}{=} H - h,$$

in which H is the orthometric height — reckoned from mean sea level — and h the height above the reference ellipsoid.

Deflections of the plumb line in Finland are a few seconds of arc (") in magnitude. Geoid undulations range from 15 to 32 m (for comparison, globally the range of variation is -107 m to $+85$ m), relative to the **GRS80** ellipsoid as is today customary. At sea level, the plumb-line deflections — expressed in radians! — equal the horizontal gradients of the geoid undulation. See figures 5.1 and 5.2.

For any reference ellipsoid, for example the **GRS80** ellipsoid, there exists its own mathematically exact standard or *normal gravity field*, of which one equipotential or level surface is precisely that reference

¹This holds exactly only on the reference ellipsoid. Elsewhere one should add to φ a correction for the curvature of the field lines of the normal gravity field or “normal plumb lines”, see figure 4.1. The correction is $\delta\varphi_n = 0.171'' \text{ km}^{-1} \cdot h \sin 2\varphi$, with h the height in kilometres from the reference ellipsoid (Heiskanen and Moritz, 1967, equation 5-34). See also section 4.3.2.



ellipsoid. Using this field, we may calculate for each gravity field quantity the corresponding normal quantity. By subtracting the normal quantity from the original one, we obtain the corresponding *anomalous* quantity.

For heights above the reference ellipsoid there exists an expression analogous to expression 4.4 for orthometric heights. In the expression, U is the normal potential and γ normal gravity:²

$$h_p = - \int_{U_0}^{U_p} \frac{1}{\gamma(U)} dU.$$

The geoid height in point P is now

$$\begin{aligned} N_p &= h_p - H_p = \int_{W_0}^{W_p} \frac{1}{g(W)} dW - \int_{U_0}^{U_p} \frac{1}{\gamma(U)} dU = \\ &= \int_{W_0}^{W_p} \frac{1}{g(W)} dW - \int_{W_0}^{W_p} \frac{1}{\gamma(U)} dU - \int_{W_p}^{U_p} \frac{1}{\gamma(U)} dU + \int_{W_0}^{U_0} \frac{1}{\gamma(U)} dU \\ &= \int_{W_0}^{W_p} \frac{\gamma(W') - g(W')}{g(W')\gamma(W')} dW' - \int_{W_p}^{U_p} \frac{1}{\gamma(U)} dU + \int_{W_0}^{U_0} \frac{1}{\gamma(U)} dU \\ &= \int_0^{H_p} \frac{\gamma(z) - g(z)}{\gamma(z)} dz - \int_{W_p}^{U_p} \frac{1}{\gamma(U)} dU + \int_{W_0}^{U_0} \frac{1}{\gamma(U)} dU, \quad (5.1) \end{aligned}$$

by re-naming the integration variables $W, U \rightarrow W'$ and changing it to a length: $dW' = -g dz$.

In equation 5.1 the last term vanishes if we assume³ $U_0 = W_0$. The first and second terms both depend on the height of point P, but their sum N_p does not. Therefore we place point P at mean sea level — the zero point of the height system used. It follows that the first term also

²This is not exactly true, due to the “normal plumb line” not being the same as the normal on the reference ellipsoid. The error made is tiny.

³This is not self-evident! In a local vertical datum the potential of the zero point could well differ by as much as the equivalent of a metre from the normal potential of a global reference ellipsoid.



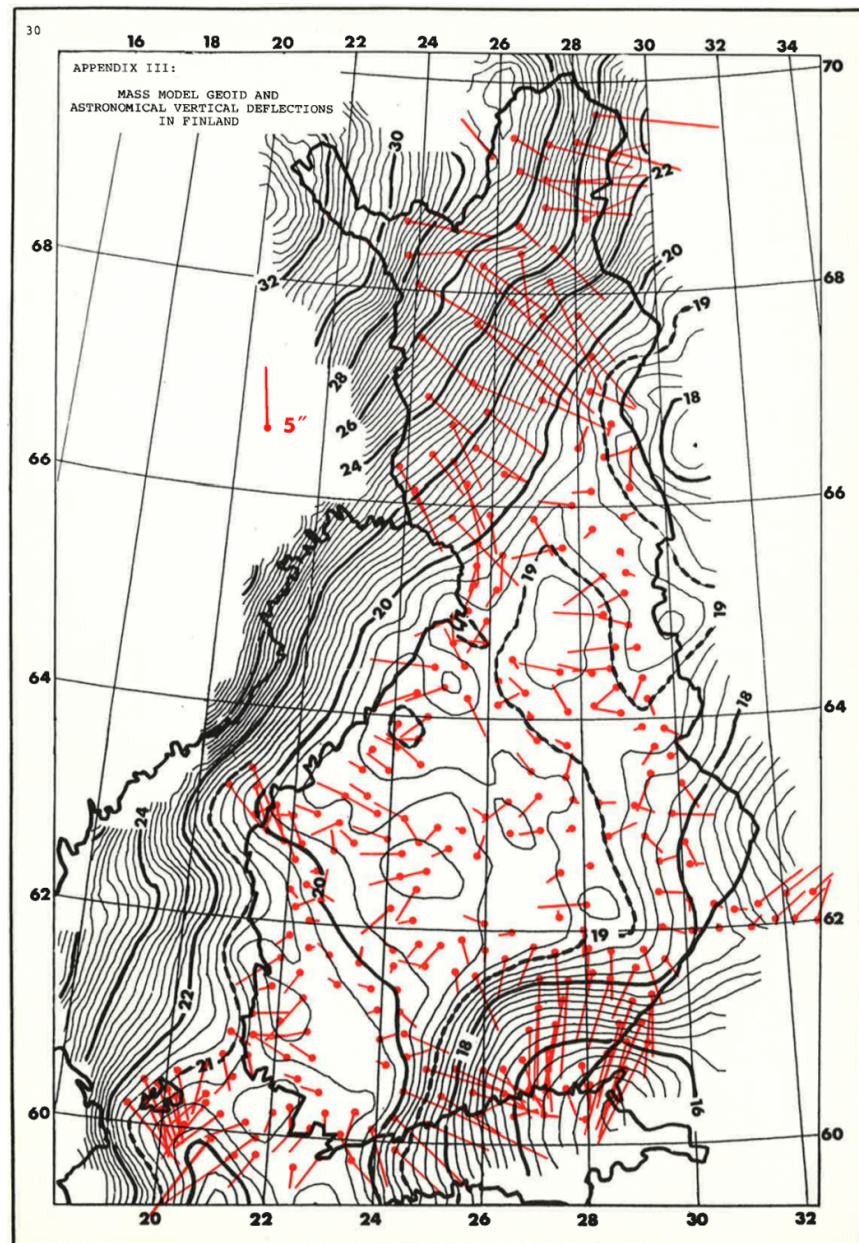


FIGURE 5.2. A geoid model for Finland from 1984. Deflections of the plumb line from observations in red (Vermeer, 1984).

vanishes: $H_P = 0$. So

$$N_P = - \int_{W_P}^{U_P} \frac{1}{\gamma(U)} dU \approx \frac{1}{\gamma_P} (W_P - U_P) = \frac{T_P}{\gamma_P},$$



where we have substituted $T = W - U$, the disturbing potential. All quantities are assumed to be at sea level. More compactly:

$$N = T/\gamma. \quad (5.2)$$

This is the famous *Brunns*⁴ equation (Heiskanen and Moritz, 1967, equation 2-144).

Figure 5.3 depicts the situation still better. In this figure, the normal gravity vector $\vec{\gamma} = \text{grad } U$ has a length of $\frac{\partial}{\partial h} U$, from which it follows, with equation $T = W - U$, that the separation between “matching” surfaces $W = W_P$ and $U = U_Q$, when $W_P = U_Q$, is

$$N \approx \frac{U_Q - U_P}{\gamma} = \frac{W_P - U_P}{\gamma} = \frac{T}{\gamma}.$$

5.2 Gravity disturbances

The difference between the true and normal gravity accelerations is called the *gravity disturbance*,

$$\delta g \stackrel{\text{def}}{=} g - \gamma = \|\mathbf{g}\| - \|\vec{\gamma}\| \approx -\left(\frac{\partial W}{\partial H} - \frac{\partial U}{\partial h}\right),$$

in which the differentiation is done along the plumb line for W and — slightly imprecisely — along the normal on the reference ellipsoid for U . The directions of the plumb line and surface normal on the ellipsoid are actually very close to each other. Therefore, to good approximation

$$\delta g \approx -\left(\frac{\partial W}{\partial H} - \frac{\partial U}{\partial H}\right) = -\frac{\partial T}{\partial H}.$$

In spherical approximation we have

$$\delta g \approx -\frac{\partial T}{\partial r}. \quad (5.3)$$

⁴Ernst Heinrich Bruns (1848–1919) was an eminent German mathematician and mathematical geodesist.



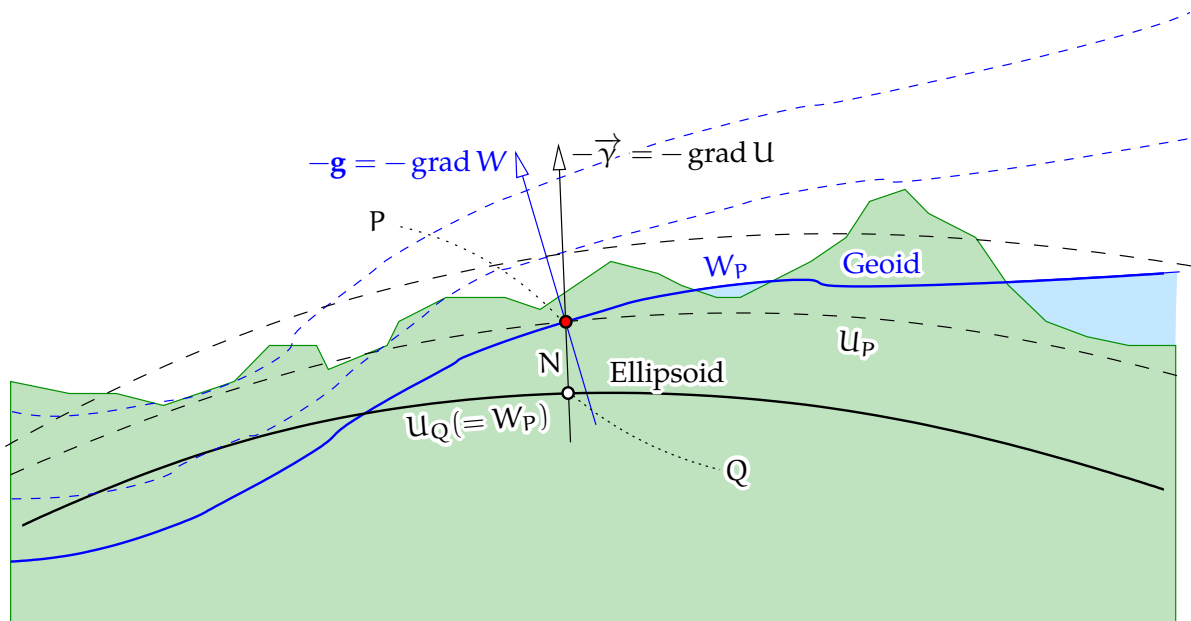


FIGURE 5.3. Equipotential surfaces of the gravity field (W) and the normal gravity field (U).

We already expanded the disturbing potential T into constituents for different spherical-harmonic degree numbers, equation 4.7, and now we obtain by differentiating with respect to r :

$$\begin{aligned} \delta g(\phi, \lambda, r) &= -\frac{\partial T(\phi, \lambda, r)}{\partial r} = -\frac{\partial}{\partial r} \left(\sum_{n=2}^{\infty} \left(\frac{R}{r} \right)^{n+1} T_n(\phi, \lambda) \right) = \\ &= \sum_{n=2}^{\infty} \frac{n+1}{r} \left(\frac{R}{r} \right)^{n+1} T_n(\phi, \lambda), \quad (5.4) \end{aligned}$$

and at sea level ($r = R$):

$$\delta g(\phi, \lambda, R) = \sum_{n=2}^{\infty} \frac{n+1}{R} T_n(\phi, \lambda).$$

This is the *spectral representation* of the gravity disturbance at sea level, i.e., on an Earth sphere of radius R . As a suitable value for the reference radius R one may take the equatorial radius a_{\oplus} of a reference ellipsoid for the Earth.



We can observe gravity disturbances only if, in addition to measuring the acceleration of gravity $g_P (= \frac{\partial}{\partial H} W|_P)$ at a point P , we have a way to measure P 's *location* in space, relative to the geocentre, so one may calculate normal gravity $\gamma_P = \frac{\partial}{\partial h} U|_P$ at the same point. Nowadays this is even easy using **GNSS**, but traditionally it has been impossible. For this reason, gravity disturbances are little-used. One rather uses gravity *anomalies*, about which more below.



5.3 Gravity anomalies

Normal gravity is calculated as a function of location expressed in *geodetic* co-ordinates (φ, λ, h) . However, in traditional gravimetric field work, before the satellite positioning era, one only had access to the geodetic co-ordinates φ and λ , but not to any accurate height h above the reference ellipsoid. One only had access to the height H above sea level (the geoid), determined, for example, through a national levelling network — or, in the worst case, barometrically.

This means that, although the true gravity g is measured at point P , the height of which above sea level is H_P , the normal gravity γ must of necessity be calculated *at another point* Q , the height of which *above the reference ellipsoid* is $h_Q = H_P$. See figure 5.4.

In other words, the measured height of point P *above mean sea level* is substituted, brute-force style, into the normal gravity formula, which, however, expects a height *above the reference ellipsoid*! This special trait of the definition of gravity anomalies may be called a “free boundary-value problem”.

According to this, we calculate gravity anomalies as follows:

$$\begin{aligned} \Delta g_P &= g_P - \gamma_Q = (g_P - \gamma_P) + (\gamma_P - \gamma_Q) = \\ &= - \left(\frac{\partial W}{\partial H} \Big|_P - \frac{\partial U}{\partial h} \Big|_P \right) + (\gamma_P - \gamma_Q) \\ &\approx - \frac{\partial (W - U)}{\partial H} \Big|_P + (h_P - h_Q) \frac{\partial \gamma}{\partial H} \Big|_P = \end{aligned}$$



$$\begin{aligned}
&= -\frac{\partial T}{\partial H}\Big|_p + (h_p - H_p) \frac{\partial \gamma}{\partial H}\Big|_p = \\
&= -\frac{\partial T}{\partial H}\Big|_p + N_p \frac{\partial \gamma}{\partial H}\Big|_p = \left(-\frac{\partial T}{\partial H} + \frac{T}{\gamma} \frac{\partial \gamma}{\partial H}\right)\Big|_p,
\end{aligned}$$

using almost all the equations above. This equation,

$$\Delta g = -\frac{\partial T}{\partial H} + \frac{1}{\gamma} \frac{\partial \gamma}{\partial H} T, \quad (5.5)$$

is known as the *fundamental equation of physical geodesy*. It is the boundary condition of the *third boundary-value problem* (Heiskanen and Moritz, 1967, section 1-17). It enables the solution of T in the exterior space, if Δg is given everywhere on the Earth's surface.

If we assume that the Earth is a sphere of radius R and that the normal gravity field is spherically symmetric, we may approximate:

$$\Delta g = -\frac{\partial T}{\partial r} - \frac{2}{r} T, \quad (5.6)$$

in which $r = R + H$ is the distance from the Earth's centre.

By substituting into this equation 5.3 for δg we obtain

$$\Delta g = \delta g - \frac{2}{r} T.$$

From this we obtain by substituting the above spectral representations 4.7 and 5.4 for T and δg :

$$\Delta g(\phi, \lambda, r) = \sum_{n=2}^{\infty} \left(\frac{n+1}{r} - \frac{2}{r} \right) T_n(\phi, \lambda) = \sum_{n=2}^{\infty} \frac{n-1}{r} T_n(\phi, \lambda).$$

Choose the following notation:

$$\Delta g_n(\phi, \lambda) \stackrel{\text{def}}{=} \frac{n-1}{R} T_n(\phi, \lambda). \quad (5.7)$$

The presence of the factor $n - 1$ shows that gravity anomalies cannot contain constituents of degree $n = 1$, even if T would contain them. It



is always wise to place the origin of the co-ordinate system in the centre of mass of the Earth, but if the origin is not located there, at least gravity anomalies do not change.

We obtain by substitution

$$\begin{aligned}\Delta g(\phi, \lambda, r) &= \sum_{n=2}^{\infty} \frac{n-1}{r} \left(\frac{R}{r}\right)^{n+1} T_n(\phi, \lambda) = \\ &= \sum_{n=2}^{\infty} \frac{n-1}{R} \left(\frac{R}{r}\right)^{n+2} T_n(\phi, \lambda) = \sum_{n=2}^{\infty} \left(\frac{R}{r}\right)^{n+2} \Delta g_n(\phi, \lambda). \quad (5.8)\end{aligned}$$

At sea level $r = R$ we find

$$\Delta g(\phi, \lambda, R) = \sum_{n=2}^{\infty} \Delta g_n(\phi, \lambda),$$

showing the Δg_n to be the *degree constituents* of gravity anomaly Δg .

Observe that the term $n = 1$ is missing: $\Delta g_1 = 0$. It is also assumed that $\Delta g_0 = -T_0/R = 0$, meaning that the true exterior potential is on global average the same as the normal potential. Also the total mass GM_{\oplus} and geoid volume⁵ of the Earth are assumed to be the same as the total mass and volume of the reference ellipsoid. The assumption is largely justified because GM_{\oplus} can be, and has been, determined very precisely by satellites, and modern models for the normal potential, like **GRS80**, are based on these determinations.⁶

5.4 Units used for gravity anomalies

A common unit of measurement for gravity variations is the *milligal*. The connection with the SI system is $1 \text{ mGal} = 10^{-5} \text{ m/s}^2$. The unit μGal or 10^{-8} m/s^2 is also used. The units $\mu\text{m/s}^2$ and nm/s^2 , which formally belong

⁵In fact, the atmosphere complicates this matter.

⁶However, **GRS80** has an equatorial radius of 6 378 137.0 m, while the newer models like **EGM2008** give a smaller value of 6 378 136.3 m as the location of global mean sea level. Uncertainty continues to be of decimetre order.



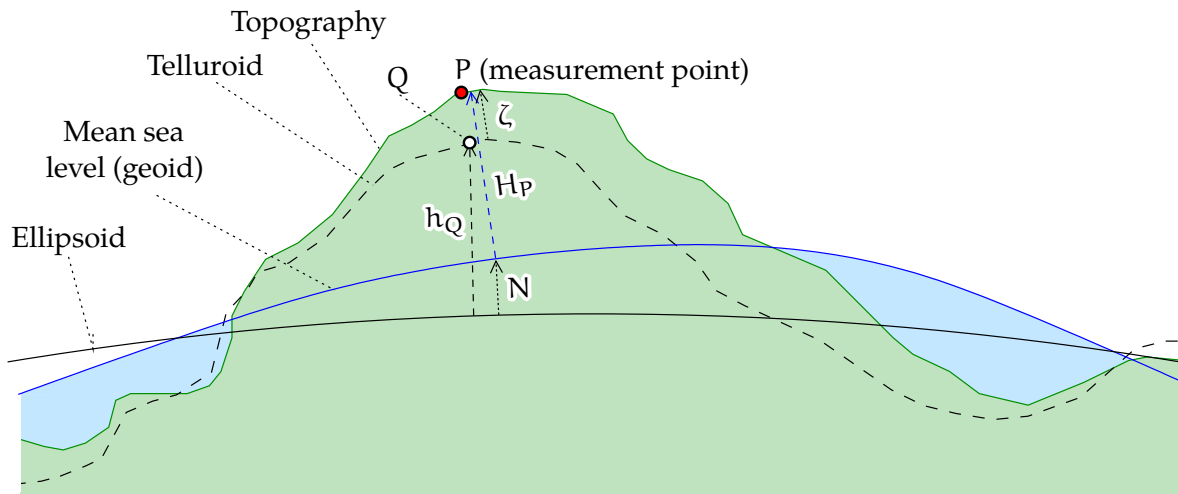


FIGURE 5.4. Reference ellipsoid, mean sea level (geoid), and gravity measurement.

to the **SI** system, are also used in modern books. Nevertheless, milligals and microgals are more familiar still, and correspond to 1 **ppm** (part per million) and 1 **ppb** (part per billion) of ambient gravity close to the Earth's surface.

In table 5.1 we give a few values in order to get an idea of the orders of magnitude of phenomena.

A popular unit for measuring gravity *gradients* is the Eötvös, symbol E. In **SI** units it is 10^{-9} s^{-2} , corresponding to 10^{-4} mGal/m . On the Earth's surface the vertical gradient $\frac{\partial}{\partial H} g$ is on average some $-0.3 \text{ mGal/m} = -3000 \text{ E}$.

5.5 The boundary-value problem of physical geodesy

As we explained in the above section, gravimetric measurement is more complicated than just measuring the quantity $\frac{\partial}{\partial H} W \approx \frac{\partial}{\partial r} W$. When we measure the vertical derivative of the geopotential, we do it *in a place we do not precisely know*. Even if we know the height of the measurement location above sea level, that still does not give us the measurement





TABLE 5.1. Orders of magnitude of gravity variations.

| Phenomenon | Fraction of gravity | SI units | mGal |
|-------------------------------------|---------------------------|---------------------------|--------------------|
| Ambient gravity | 1 | 9.81 | 981 000 |
| Variation with location | $\pm 10^{-4}$ | $\pm 10^{-3}$ | ± 100 |
| Difference equator – poles | 0.5 % | 0.05 | 5000 |
| Difference sea surface – 10 km high | 0.3 % | 0.03 | 3000 |
| Gravimeter accuracy | $\pm 10^{-8}$ – 10^{-7} | $\pm 10^{-7}$ – 10^{-6} | ± 0.01 – 0.1 |

point's location in space. This location depends additionally on the location of sea level, i.e., the *geoid*, in space; more precisely its height above or below the reference ellipsoid.

This is how we arrive at the third boundary-value problem.⁷ The *boundary-value problem of physical geodesy* is to determine the potential V outside a body if given on its surface is the *linear combination*

$$c_1 V + c_2 \frac{\partial V}{\partial n},$$

with c_1, c_2 suitable coefficients. The variable n represents here differentiation in the direction of the normal to the boundary surface, in practice the same as H or r .

In physical geodesy, the following linear combination is given as a boundary condition:

$$\Delta g = -\frac{\partial T}{\partial H} + \frac{1}{\gamma} \frac{\partial \gamma}{\partial H} T.$$

We see that $c_1 = -1$ and $c_2 = \frac{\partial}{\partial H} \gamma / \gamma$. This equation, the *definition 5.5* of gravity anomalies, is known as the *fundamental equation of physical geodesy*.

⁷The third or mixed boundary-value problem is associated with Victor Gustave Robin (1855–1897), a French mathematician. Then, the Dirichlet problem could be called the first and the Neumann problem the second boundary-value problem.



In spherical approximation we have equations 5.6 and 5.8:

$$\Delta g = -\frac{\partial T}{\partial r} - \frac{2}{r}T,$$

$$\Delta g(\phi, \lambda, r) = \sum_{n=2}^{\infty} \frac{n-1}{r} \left(\frac{R}{r}\right)^{n+1} T_n(\phi, \lambda) = \sum_{n=2}^{\infty} \left(\frac{R}{r}\right)^{n+2} \Delta g_n(\phi, \lambda),$$

or at sea level ($r = R$):

$$\Delta g = \sum_{n=2}^{\infty} \frac{n-1}{R} T_n(\phi, \lambda) = \sum_{n=2}^{\infty} \Delta g_n(\phi, \lambda),$$

in which the degree constituents $\Delta g_n(\phi, \lambda)$ are defined in equation 5.7. Remember that these functions are computable with the help of the degree constituent equation 3.8 when $\Delta g(\phi, \lambda)$ is known all over the Earth.

Thus we also obtain the solution of this boundary-value problem in spectral representation (which is thus valid in the *whole* exterior space) by using degree constituent equation 3.8:

$$\begin{aligned} T(\phi, \lambda, r) &= R \sum_{n=2}^{\infty} \left(\frac{R}{r}\right)^{n+1} \frac{\Delta g_n(\phi, \lambda)}{n-1} = \\ &= \frac{R}{4\pi} \sum_{n=2}^{\infty} \frac{2n+1}{n-1} \left(\frac{R}{r}\right)^{n+1} \iint_{\sigma} \Delta g(\phi', \lambda', R) P_n(\cos \psi) d\sigma'. \end{aligned} \quad (5.9)$$

This is precisely the boundary-value problem that is created if surface gravity anomalies are given everywhere on the Earth, land and sea.

The integral equation corresponding to the above spectral equation 5.9 is known as the Stokes⁸ equation:

$$T(\phi, \lambda, r) = \frac{R}{4\pi} \iint_{\sigma} S(\psi, r) \Delta g(\phi', \lambda', R) d\sigma',$$

in which the *Stokes kernel* is

$$S(\psi, r, R) = \sum_{n=2}^{\infty} \frac{2n+1}{n-1} \left(\frac{R}{r}\right)^{n+1} P_n(\cos \psi). \quad (5.10)$$

⁸Sir George Gabriel Stokes PRS (1819–1903) was an Irish-born, gifted mathematician and physicist who made his career in Cambridge.



In section 8.1 we will give closed expression 8.2 for this function, for the case $r = R$, and a graph.

5.6 The telluroid mapping and the “quasi-geoid”

If we measure the astronomical latitude and longitude (Φ, Λ) and *interpret* them as geodetic (geographical) co-ordinates (φ, λ) , and also *interpret* the potential difference $-(W - W_0)$ as a measure for the height above the reference ellipsoid h , we perform, as it were, a *mapping*. This mapping adds to every point P a corresponding point Q , the *geodetic* co-ordinates of which are the same as the *natural* co-ordinates of point P .

This approach is called *telluroid mapping*. The telluroid is the surface that follows the shapes of the Earth’s topography, but is everywhere below the topography by an amount ζ if positive, or above it by an amount $-\zeta$ otherwise. The quantity ζ is called a *height anomaly*.

Telluroid mapping is an important tool in Molodensky’s gravity field theory. It is, however, a pretty abstract concept. One may say that the telluroid is a *model* of the Earth’s surface, obtained by assuming that

- the true potential field of the Earth is the normal potential
- the mathematical mean sea surface or *geoid*, the reference surface for height measurement, coincides with the reference ellipsoid.

In other words, the telluroid is a model for the Earth’s topographic surface that is obtained by taking *levelled* heights — more precisely, geopotential numbers obtained from levelling — as if they represented differences of the *normal* potential from that of the reference ellipsoid.

In practice, a map of values ζ is often called a “quasi-geoid” model. The quasi-geoid is usually close to the geoid, except in the mountains, where the differences can exceed a metre.

One should however remember that the height anomaly ζ is defined *on the topographic surface*; a surface that is quite rough in many places.



This also means that all variations in topographic height will also be reflected as variations in this quasi-geoid, in such a way that the quasi-geoid *correlates* strongly with the small details in the topography. One can thus not say that the shape of the quasi-geoid only expresses the figure of the Earth's potential field. In it, variations in geopotential and in topographic height are hopelessly mixed up.

This is why the quasi-geoid is an unfortunate compromise, a concession to “reference-surface thinking”, which only really works within the classical geoid concept. Better stick — within Molodensky's theory — to the concept of *height anomaly*, which is a three-dimensional function or field

$$\zeta(X, Y, Z) = \zeta(\varphi, \lambda, h).$$



5.7 Free-air anomalies

If we measure gravity g at point P, the height of which over sea level is H and the latitude Φ , we may calculate the gravity anomaly Δg at the point as follows:

$$\Delta g \stackrel{\text{def}}{=} g - \gamma(\Phi, H),$$

in which $\gamma(\Phi, H)$ is normal gravity calculated according to its definition at height H and latitude Φ .

ilma-anomalia

This is how we define free-air anomalies.

We *linearise* this as follows:

$$\begin{aligned} \Delta g = g - \gamma(\Phi, H) &\approx g - \left(\gamma(\varphi, h) + (\Phi - \varphi) \frac{\partial \gamma}{\partial \varphi} + (H - h) \frac{\partial \gamma}{\partial h} \right) \approx \\ &\approx g - \left(\gamma(\varphi, 0) + h \frac{\partial \gamma}{\partial h} + (H - h) \frac{\partial \gamma}{\partial h} \right) = g - \gamma(\varphi, 0) - H \frac{\partial \gamma}{\partial h}, \end{aligned}$$

making the approximation that the vertical gradient $\frac{\partial}{\partial h} \gamma$ of normal gravity is constant.⁹

⁹For the greatest precision, one should consider that the latitude Φ may also not



Thus, free-air anomalies can be calculated in a simpler way. The gravity formula of the normal field 4.6 gives for latitude 60° :

$$\gamma = 981\,919.178 - 0.308\,449\,4 H + \dots \text{ mGal.}$$

So, in linear approximation (close to the Earth's surface) gravity attenuates some 0.3 mGal for every metre in height. This value is worth committing to memory.

An approximate equation for calculating free-air anomalies then is

$$\Delta g_P = g_P - \gamma_0(\varphi) + 0.3084 \text{ mGal/m } H, \quad (5.11)$$

in which $\gamma_0(\varphi) \stackrel{\text{def}}{=} \gamma(\varphi, 0)$, normal gravity at sea level, is only a function of latitude. In a country like Finland, equation 5.11 is often sufficiently precise, although the evaluation of the original equation 4.6 is also easy.

Free-air anomalies are widely used. Generally, when one discusses gravity anomalies, one means just this, free-air anomalies. They express the Earth's exterior gravity field, including mountains, valleys and everything.

Questions

1. If gravity at sea level is 9.81 m/s^2 , at what height will gravity disappear, as computed according to the above-mentioned vertical gravity gradient -0.3 mGal/m ?
2. How physically realistic is this?

Answers

1. At -0.3 mGal/m , it takes $\left(9.81 \cdot 10^5 / 0.3\right) \text{ m} = 3270 \text{ km}$ to go to zero.

be a latitude on a geocentric reference ellipsoid. It could be astronomical latitude, or latitude in some old national co-ordinate system computed on a non-geocentric ellipsoid, like in Finland **KKJ**, the National Map Grid Co-ordinate System, which was computed on the Hayford ellipsoid. The error caused by this is however two, three orders of magnitude smaller than the effect caused by $H - h$.



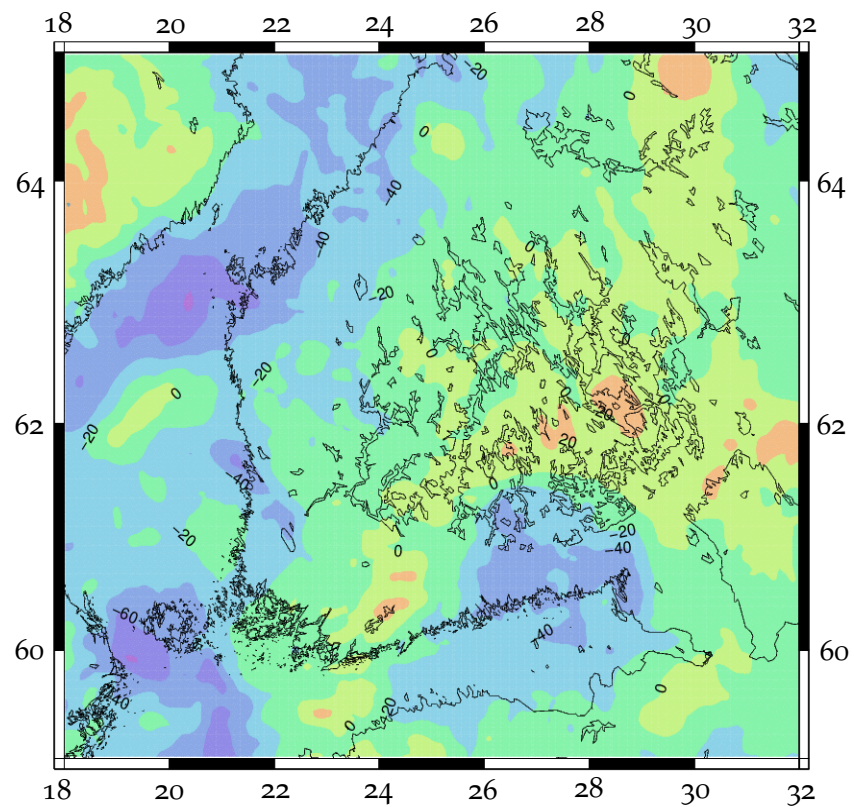


FIGURE 5.5. Free-air gravity anomalies for Southern Finland, computed from the **EGM2008** spherical-harmonic expansion. Data © Bureau Gravimétrique International (BGI) / International Association of Geodesy. Web service **BGI, EGM2008**.

2. Not very. The gravity gradient itself drops quickly from the value of -0.3 mGal/m going up, so this linear extrapolation is simply wrong.



**Self-test questions**

1. How do deflections of the plumb line and geoid heights relate to each other?
2. What is the fundamental equation of physical geodesy in spherical approximation?
3. In what way is a gravity disturbance different from a gravity anomaly?
4. What units are used for measuring gravity anomalies and gravity gradients? How are they related to the SI system?
5. How does the geoid height and the disturbing potential relate to each other?
6. Explain telluroid mapping and height anomalies.

**Exercise 5 – 1: The spectrum of gravity anomalies**

Use equation 5.7. If we assume that the quadratic mean of the degree constituents Δg_n of gravity anomalies,

$$\overline{\Delta g_n} \stackrel{\text{def}}{=} \sqrt{\frac{1}{4\pi} \iint_{\sigma} \Delta g_n^2(\phi, \lambda) d\sigma},$$

does not depend on the chosen degree number n , how then does the similarly defined \overline{T}_n depend on n ?

In other words: which degree numbers of the gravity field are relatively strongest in the disturbing potential, and which in the gravity anomalies?

**Exercise 5 – 2: Deflections of the plumb line and geoid tilt**

If, in the south-north components of plumb-line deflections in a country, there is a systematic error of one arc second, what error does this cause



in the difference $N_2 - N_1$ between the geoid heights in points 1 and 2 of which the inter-point distance is approximately 1000 km in the south-north direction? See figures 5.1 and 5.2.



Exercise 5 – 3: Gravity anomaly, geoid height

In Finland there is a place where the (free-air) gravity anomaly is $\Delta g = 100 \text{ mGal} = 10^{-3} \text{ m/s}^2$. In the same place the disturbing potential T is $200 \text{ m}^2/\text{s}^2$.

1. Using the fundamental equation of physical geodesy 5.6:

$$\Delta g = -\frac{\partial T}{\partial r} - \frac{2}{r}T,$$

calculate $\frac{\partial}{\partial r}T$ and compare it with the quantity $2T/r$. Assume $r \approx R$. Which of the two, $\frac{\partial}{\partial r}T$ or $2T/r$, dominates?

2. Assume that the point is close to sea level. Using the Bruns equation

$$N = T/\gamma,$$

where γ is average gravity 9.81 m/s^2 , compute the geoid height N of the point.





Geophysical reductions

6



6.1 General

We see that integral equations, like Green's third theorem 1.25, offer a possibility to calculate the whole exterior potential of the Earth — as well as all the quantities that may be calculated from the potential, such as, for example, the gravitational acceleration — using values of V or $\frac{\partial}{\partial n}V$ observed on the boundary surface only. Green's third theorem is but one example of many: every integral theorem is the solution of some *boundary-value problem*.

reuna-
arvotehtävä

There are three alternatives for choosing a boundary surface:

1. Choose the topographic surface of the Earth.
2. Choose mean sea level, more precisely, an equipotential surface close to mean sea level called the *geoid*.
3. Choose the reference ellipsoid.
 - Alternative 1 has been developed mostly by the Molodensky school (Molodensky et al., 1962) in the former Soviet Union. The advantage of the method is that *we need no gravity reduction*, as all masses are already inside the boundary surface. Its disadvantage is that the, often complex, shape of the topography must be taken into account when the boundary-value problem is formulated and solved.

epäsuora
vaikutus

- Alternative 2 is classical geoid or geopotential determination. In this case *geophysical reductions* are needed to the input gravity data: some masses are outside the computation boundary and need to be computationally removed or moved to the inside.

A further complication of the method then is that the geopotential or geoid solution obtained is not that of the original mass distribution, but of the *reduced* one. This surface is called the *co-geoid*. We need a “restoration step” where this influence of the reduction step on the geopotential and geoid is determined and reversed. This influence is called the “indirect effect”.

In the literature, this method is also referred to as the *remove–restore* method.

- Alternative 3 has been used rarely, because it has not been traditionally possible to make gravity measurements in a location known in the absolute sense, relative to the geocentre or the reference ellipsoid. Nowadays this is possible using **GNSS**, for example in Antarctica and Greenland’s interior, where there is no sea-level-bound height system.

We may expect this approach to gain more traction as heights of gravimetric stations are more and more determined directly using **GNSS**. See for example [Märdla \(2017\)](#).



6.2 Bouguer anomalies

Free-air anomalies depend on the topography, because gravity itself contains the attractive effect of topographic masses. A map of free-air anomalies shows the same small details as seen in the topography. One way of removing the effect of the topography is the so-called *Bouguer*¹

¹Pierre Bouguer (1698–1758) was a French professor in hydrography, who participated in the public discussion on the figure of the Earth, and in 1735–1743 led an expedition of the French Academy of Sciences doing a grade measurement in Peru, South America, at the same time as De Maupertuis was carrying out a similar grade measurement in



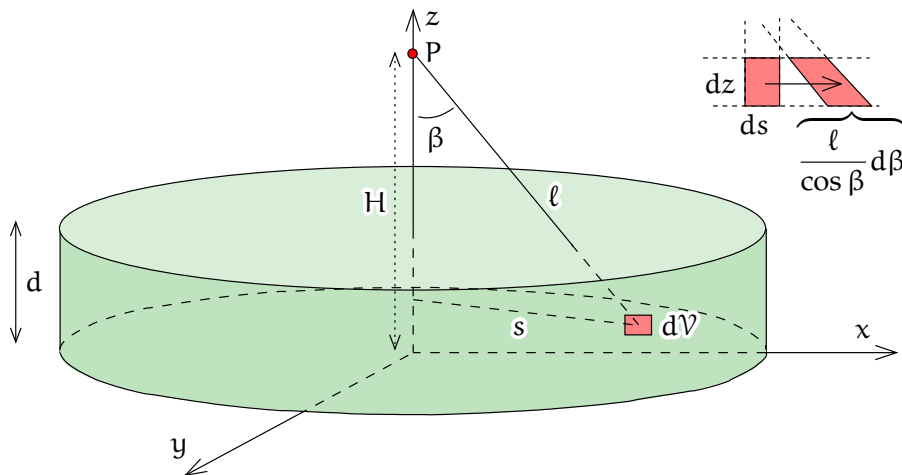


FIGURE 6.1. The attraction of a Bouguer plate.

reduction.

6.2.1 Calculation

We calculate the effect of a homogeneous plate on gravity. Assume that the plate is infinite in size; thickness d , matter density ρ , and height of point P above the lower surface of the plate H . See figure 6.1. The attraction at point P (which is directed straight downwards for reasons of symmetry) is obtained by integrating. The volume integral to be computed has a volume element

$$dV = ds \cdot dz \cdot s \, d\alpha$$

in the cylindrical co-ordinates (s, z, α) . We transform this to the co-ordinates (β, z, α) . We forget about α and study the surface element (figure 6.1, top right)

$$ds \, dz = \frac{\ell}{\cos \beta} d\beta \, dz,$$

in which the determinant of Jacobi needed, $\ell/\cos \beta$, is seen.

Lapland. In addition to geodesy, he was also active in astronomy.



We carry out the integration:

$$\begin{aligned} \alpha \stackrel{\text{def}}{=} \|\mathbf{a}\| &= G \iiint \frac{\cos \beta}{\ell^2} \rho \, dV = G\rho \int_0^{2\pi} \int_0^d \int_0^\infty \frac{\cos \beta}{\ell^2} \cdot ds \, dz \cdot s \, d\alpha = \\ &= G\rho \int_0^{2\pi} \int_0^d \int_0^{\pi/2} \frac{\cos \beta}{\ell^2} \cdot \frac{\ell}{\cos \beta} \, d\beta \, dz \cdot s \, d\alpha = \\ &= 2\pi G\rho \int_0^d \int_0^{\pi/2} \frac{s}{\ell} \, d\beta \, dz = 2\pi G\rho \int_0^d \left(\int_0^{\pi/2} \sin \beta \, d\beta \right) dz. \end{aligned}$$

Here, the integral

$$\int_0^{\pi/2} \sin \beta \, d\beta = [-\cos \beta]_0^{\pi/2} = 1,$$

and the end result is

$$\alpha = 2\pi G\rho d. \quad (6.1)$$

This is the formula for the attraction of a Bouguer plate. As a side result, we obtain the attraction of a circular disk of radius r :

$$\int_0^{\beta_0(z)} \sin \beta \, d\beta = [-\cos \beta]_0^{\beta_0(z)} = 1 - \cos(\beta_0(z)),$$

and the whole integral

$$\alpha = 2\pi G\rho \int_0^d \left(1 - \frac{H-z}{\sqrt{(H-z)^2 + r^2}} \right) dz.$$

The indefinite integral is

$$\int \frac{H-z}{\sqrt{(H-z)^2 + r^2}} dz = -\sqrt{(H-z)^2 + r^2}.$$

Substituting the bounds yields

$$\int_0^d \left(1 - \frac{H-z}{\sqrt{(H-z)^2 + r^2}} \right) dz = d + \sqrt{(H-d)^2 + r^2} - \sqrt{H^2 + r^2}.$$



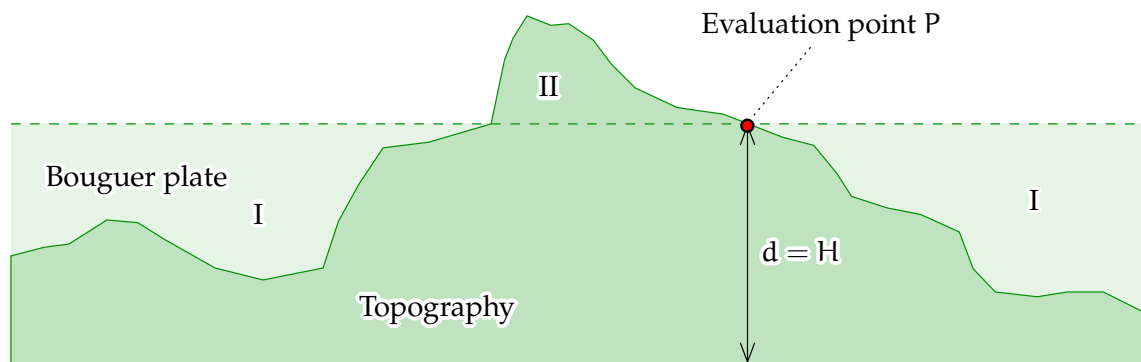


FIGURE 6.2. The Bouguer plate as an approximation to the topography.

We obtain for the whole integral

$$a = 2\pi G\rho \left(d + \sqrt{(H-d)^2 + r^2} - \sqrt{H^2 + r^2} \right).$$

In the limit $r \rightarrow \infty$, and thus

$$\sqrt{(H-d)^2 + r^2} - \sqrt{H^2 + r^2} \rightarrow 0,$$

this is identical to equation 6.1.

Bouguer anomalies are computed in order to remove the attraction of masses of the Earth's crust above sea level, i.e., above the *geoid*. The true topography is *approximated* by a Bouguer plate, see figure 6.2.

There is no standard way to treat sea-covered areas:

- Some maps show Bouguer anomalies over land and free-air anomalies over the sea. This is an option if no good quality depth data is available.
- A more correct way is to replace sea water by a rocky Bouguer plate, the thickness of which equals the local sea depth or *bathymetry*.

The calculation goes as follows:

$$\Delta g_B = \Delta g_{FA} - 2\pi G\rho H = \Delta g_{FA} - 0.1119 H, \quad (6.2)$$

where we assume for the density ρ of the plate an often-used value for the average density of the Earth's crust, $\rho = 2670 \text{ kg/m}^3$. By substituting



into this equation 5.11, we obtain

$$\Delta g_B = g_P - \gamma_0(\varphi) + (0.3084 - 0.1119)H = g_P - \gamma_0(\varphi) + 0.1965 H. \quad (6.3)$$

The quantity Δg_B is called a (simple) *Bouguer anomaly*.

The difference between the attraction of a Bouguer plate and that of the true topography is called the *terrain correction TC* (volumes I and II in figure 6.2). We shall return to its computation later.



6.2.2 Properties

systematiikka

Unlike free-air anomalies which vary on both sides of zero, Bouguer anomalies are *strongly negative*, especially in the mountains. For example, if the mean elevation of a mountain range is $\bar{H} = 1000$ m, the Bouguer anomalies will, as a consequence of this, contain a *bias* of $1000 \times (-0.1119 \text{ mGal}) = -112 \text{ mGal}$, about -100 mGal for every kilometre of elevation.

The *advantage* of Bouguer anomalies is their smaller variation with place. For this reason they are suited especially for the *interpolation* and *prediction* of gravity anomalies, in situations where the available gravimetric material is geographically sparse. However, one then has to have access to topographic heights of a better spatial density.

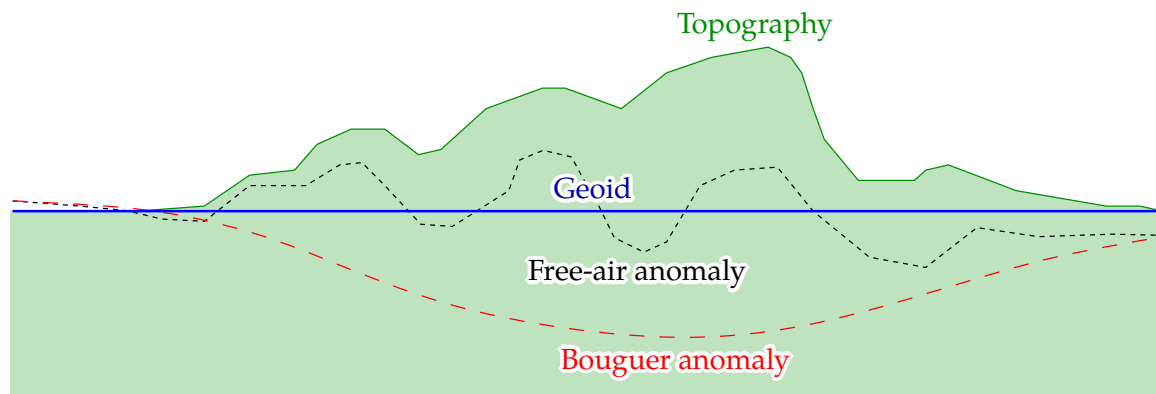



6.3 Terrain effect and terrain correction

Using the simple Bouguer reduction does not remove precisely from gravity anomalies the attractive effect of the whole topography. Figure 6.2 shows that we make *two types of error*:

- The attraction of volumes I is taken along, although there is nothing there.
- The attraction of volumes II, where there actually is something, is ignored.





 FIGURE 6.3. Behaviour of different anomaly types in mountainous terrain.

Both errors work in the same direction! Because volumes I are below the point of evaluation, their attraction — which the simple Bouguer reduction considers present, and removes — would act downwards. And because volumes II are above the point of evaluation, their attraction — which in the simple Bouguer reduction is not corrected for — acts upwards. The error made is in the same direction as in the previous case.

The terrain correction is always positive.

We write

$$\Delta g'_B = \Delta g_B + TC,$$

where *TC* — the “terrain correction” — is positive. $\Delta g'_B$ is called the *terrain-corrected Bouguer anomaly*.

The terrain correction is calculated by numerical integration. Figure 6.5 shows the *prism integration method*, and how both prisms, I and II, lead to a positive correction, because prism I is computationally added and prism II removed when applying the terrain correction. One needs a digital terrain model, *DTM*, which must be, especially around the evaluation point, extremely dense: according to experience, 500 m is the maximum inter-point separation in a country like Finland, in the



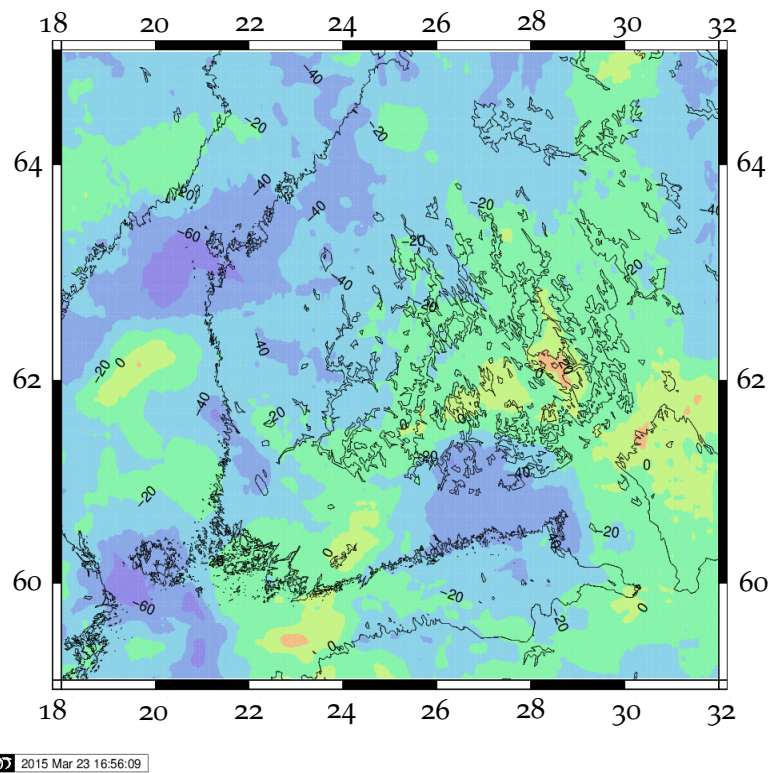


FIGURE 6.4. Terrain-corrected Bouguer anomalies for Southern Finland, computed from the spherical-harmonic expansion **EGM2008**. Data © Bureau Gravimétrique International (**BGI**) / International Association of Geodesy. Web service **BGI**, **EGM2008**. In comparison to figure 5.5 on page 124, there is a strong negative bias of Bouguer anomalies — although part of this is due to post-glacial isostatic unbalance and also visible in the free-air map. Bouguer anomalies are also smoother, but that is harder to see here, as Southern Finland is already a smooth area.

mountains one needs even 50 m. The systematic nature of the terrain correction makes a too-sparse terrain model cause, possibly serious, *biases* in the insufficiently corrected gravity anomalies.

To compute the terrain correction with the prism method, we use the following equation, assuming a constant crustal density ρ and a flat



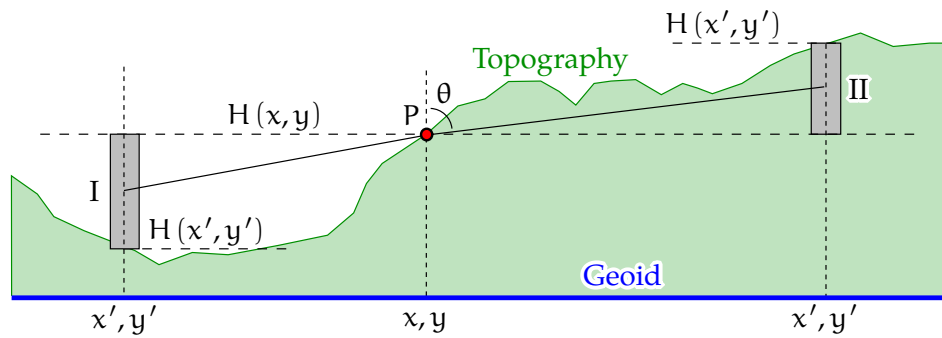


FIGURE 6.5. Calculating the classical terrain correction using the prism method.

Earth, in rectangular map co-ordinates x, y :

$$TC(x, y) = \frac{1}{2} G \rho \int_{-D}^{+D} \int_{-D}^{+D} \frac{1}{\ell^3} \left(H(x', y') - H(x, y) \right)^2 dx' dy',$$

in which

$$\ell = \sqrt{(x - x')^2 + (y - y')^2 + \left(\frac{1}{2} (H(x', y') - H(x, y)) \right)^2}$$

is the distance between the evaluation point

$$\begin{bmatrix} x & y & H(x, y) \end{bmatrix}^T$$

and the centre point on the central axis of the prism

$$\begin{bmatrix} x' & y' & \frac{1}{2} (H(x', y') + H(x, y)) \end{bmatrix}^T.$$

Of course, this is only an approximation, but it works well enough in terrain where slopes generally do not exceed 45° . In the integral above, the limit D is typically tens or hundreds of kilometres. In the latter case, the curvature of the Earth already starts having an effect, which the formula does not consider.

The values of the terrain correction TC vary from fractions of a milligal (Southern Finland) to hundreds of milligals (high mountain ranges). In the “arm” of Finland — the north-western, somewhat mountainous



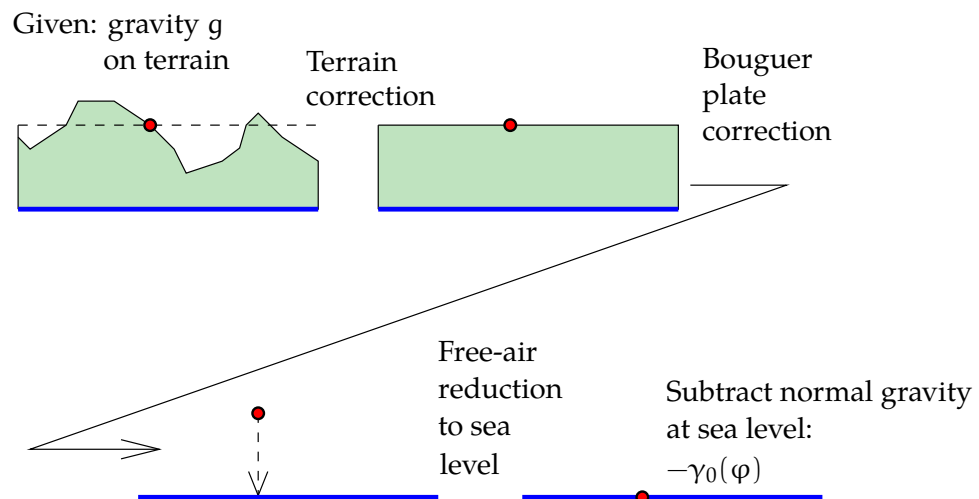


FIGURE 6.6. The steps in calculating the Bouguer anomaly. The reduction to sea level uses the standard free-air vertical gravity gradient, -0.3084 mGal/m , the vertical gradient of normal gravity.

border area with Sweden and Norway — the terrain correction may be tens of milligals.

Figure 6.6 shows the stages of calculating Bouguer anomalies from gravity observations through terrain correction, Bouguer-plate correction and free-air reduction.

6.3.1 Example: applying the terrain correction in a special case

The special terrain shape rendered in quasi-3D in figure 6.7 is given. Here, the height differences are $PQ' = 300 \text{ m}$ and $QQ' = 200 \text{ m}$. The rock density is the standard crustal density, 2670 kg/m^3 .

Questions

1. Calculate the terrain correction at point P (hint: use the attraction formula for the Bouguer plate). *Algebraic sign?*
2. Calculate the terrain correction at point Q. *Algebraic sign?*
3. If at point P it is given that the free-air anomaly is 50 mGal , how much is the Bouguer anomaly at the point?



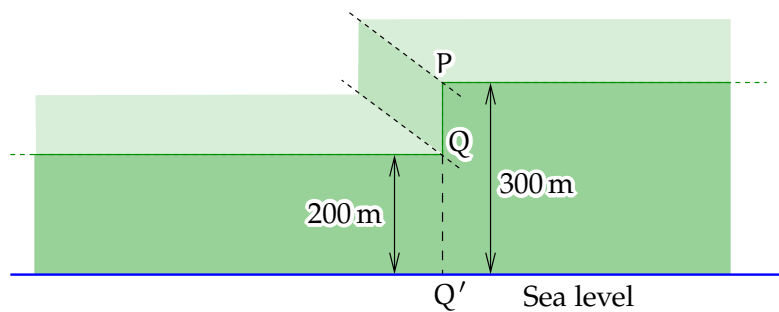


FIGURE 6.7. A special terrain shape. The vertical rock wall at PQ is also straight on a map and extends to infinity in both directions.

4. If at point Q it is given that the Bouguer anomaly is 22 mGal, how much is the free-air anomaly at the point?

Answers

1. The terrain correction at point P is the change in gravity if the terrain is filled up on the left side up to a level of 300 m. This means *adding half a Bouguer plate*, thickness 100 m, below the level of P . The effect (projected onto the vertical direction) is

$$\begin{aligned} TC &= \frac{1}{2} \cdot 2\pi G\rho \cdot H = \frac{1}{2} \cdot 0.1119 \text{ mGal/m} \cdot 100 \text{ m} = \\ &= 5.595 \text{ mGal.} \end{aligned}$$

2. The terrain correction at point Q is the change in gravity if we remove *the half Bouguer plate* to the right of and above the point, which is 100 m thick. Its vertical gravity effect is, as calculated above,

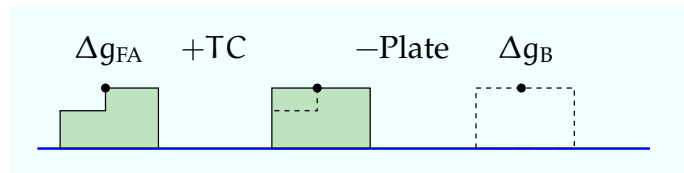
$$TC = 5.595 \text{ mGal,}$$

and, because a semi-plate is *removed* that is *above* the level of point Q , the algebraic sign of TC is again positive.

3. Free air to Bouguer:

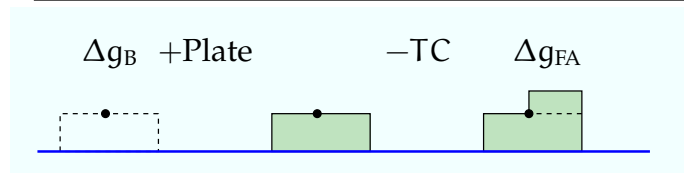


| | |
|------------------------------|--------------|
| $\Delta g_{FA}(P)$ | 50.000 mGal |
| <i>TC</i> | +5.595 mGal |
| Bouguer plate removal, 300 m | -33.570 mGal |
| $\Delta g_B(P)$ | 22.025 mGal |



4. Bouguer to free air:

| | |
|-------------------------------|--------------|
| $\Delta g_B(Q)$ | 22.000 mGal |
| Bouguer plate addition, 200 m | +22.380 mGal |
| <i>TC</i> "uncorrection" | -5.595 mGal |
| $\Delta g_{FA}(Q)$ | 38.785 mGal |



6.4 Spherical Bouguer anomalies

More recently, *spherical Bouguer anomalies* have also been calculated, for example [Balmino et al. \(2012\)](#); [Kuhn et al. \(2009\)](#); [Hirt and Kuhn \(2014\)](#). In this calculation, the topography and bathymetry of the whole Earth is taken into account, in spherical geometry (the error caused by neglecting the Earth's flattening is in this calculation negligible). Spherical Bouguer anomalies differ from Bouguer-plate anomalies in four ways:

1. the attraction of a Bouguer shell of thickness H is $4\pi G\rho H$, twice as much as the corresponding Bouguer-plate attraction. The remote part of the shell contributes as much attraction as the neighbourhood of the evaluation point!



2. The bathymetry of the oceans is accounted for² by replacing the water with standard-density crustal rock. This contribution to the anomalies is *positive*.
3. The topography and bathymetry of remote parts of the globe are also taken into account realistically. As most of the Earth is covered by deep ocean, this causes a strong *positive general bias*, which in moderately elevated areas like Southern Finland more than cancels the negative one caused by the local topography!
4. As the terrain correction is now calculated over the whole globe, in spherical geometry, it is no longer a small number and may be strongly negative as well as positive (Abrehdary et al., 2016).

There is a large systematic difference between the planar and spherical Bouguer anomalies, which however is very long-wavelength in nature, and even in an area the size of Australia almost a constant, -18.6 mGal within a variation interval of a few milligals. The details in the Bouguer maps look the same (Kuhn et al., 2009).

Just for fun, we compute the net mass effect of doing the complete spherical Bouguer reduction globally. The mean height of the land topography is 800 m, land occupying 29 % of the globe. The mean ocean depth is 3700 m, corresponding to an equivalent rock depth to be “filled in” of

$$3700 \times \frac{2670 - 1030}{2670} \text{ m} = 2272 \text{ m},$$

assuming a density for crustal rock of 2670 kg/m^3 , a sea-water density of 1030 kg/m^3 , and ocean occupying 71 % of the globe. The sum weighted by area is thus

$$(0.29 \times 800 - 0.71 \times 2272) \text{ m} = -1381 \text{ m}.$$

Interpretation There is not enough topography to fill all of the oceans, even if we are allowed to compress sea water into standard crustal

²One can also do so, and often does, in connection with the Bouguer-plate correction.



rock. If we try this bulldozing experiment, we will end up 1381 m short, i.e., below the current sea level.

If, instead, we add standard crustal rock to end up at current sea level — the definition of spherical Bouguer reduction! — we will add to the Earth's attraction as sensed from space an amount of $4\pi G\rho \times 1381 \text{ m} = 309 \text{ mGal}$.

The global mean planar Bouguer reduction, as well as the difference between planar and spherical Bouguer reductions, on average over the globe, will be half of this, $\approx +155 \text{ mGal}$. Coastal plains and seas, both close to sea level, will have similarly positive spherical Bouguer anomalies.

6.5 Helmert condensation

An often-used method, proposed by Friedrich Robert Helmert,³ for removing the effect of the masses exterior to the geoid is *condensation*. In this method, we shift mathematically all the continental masses vertically downwards to mean sea level into a simple mass-density layer

$$\kappa = \rho H,$$

where H is the height of the topography above sea level and ρ its mean matter density. This mass surface density can be interpreted as a column mass integral:

$$\kappa = \rho \int_R^{R+H} dz.$$

For a spherical Earth, the corresponding integral is

$$\kappa = \rho \int_R^{R+H} \left(\frac{r}{R}\right)^2 dr = \rho \frac{1}{R^2} \left[\frac{1}{3}r^3\right]_R^{R+H} = \rho H \left(1 + \frac{H}{R} + \frac{1}{3}\frac{H^2}{R^2}\right), \quad (6.4)$$

where it is understood that mass is moved from a column cross-section of r^2/R^2 to sea level, where the cross-section is 1.

³Friedrich Robert Helmert (1843–1917) was an eminent German geodesist known for his work on mathematical and statistical geodesy.



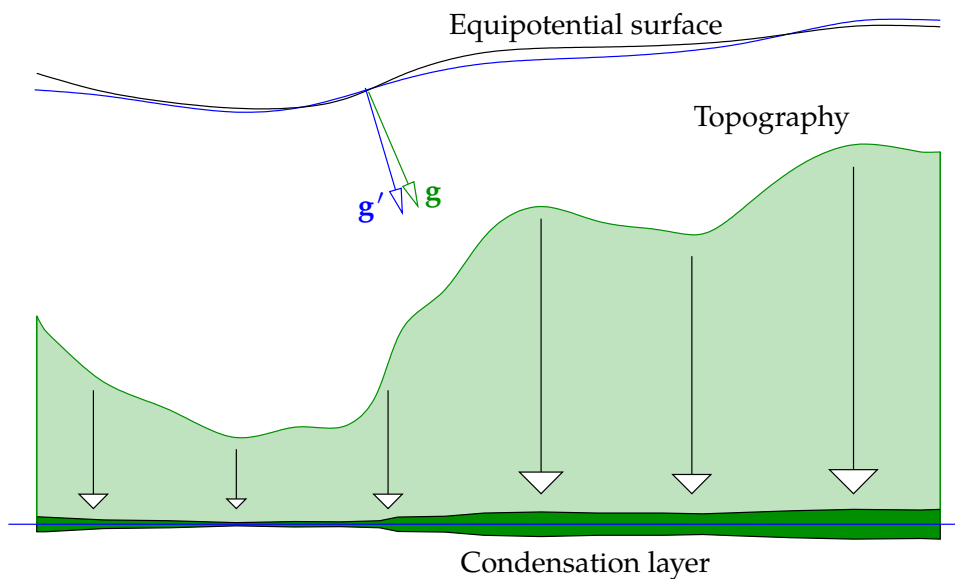


FIGURE 6.8. Helmert condensation and the changes it causes in the gravity field.

The advantage of Helmert condensation over Bouguer reduction is that *no mass is being removed*. The Bouguer reduction amounts to the computational removal of topographic masses on a large scale. Therefore, unlike with Bouguer reduction, in Helmert condensation gravity anomalies will not change systematically.

In appendix D we derive series expansions in spherical geometry which express both the external and the internal potential as functions of the “degree constituents” of the various powers of the topography $H(\phi, \lambda)$. The extensively presented derivation in the appendix is much-used in gravity field theory to model the gravity effect of the topography. In this theory, issues of convergence are difficult, although we gloss over those here.



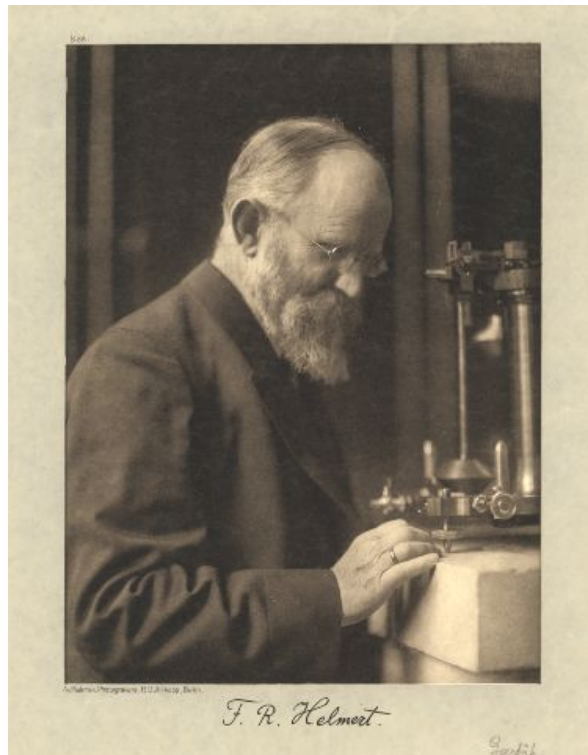


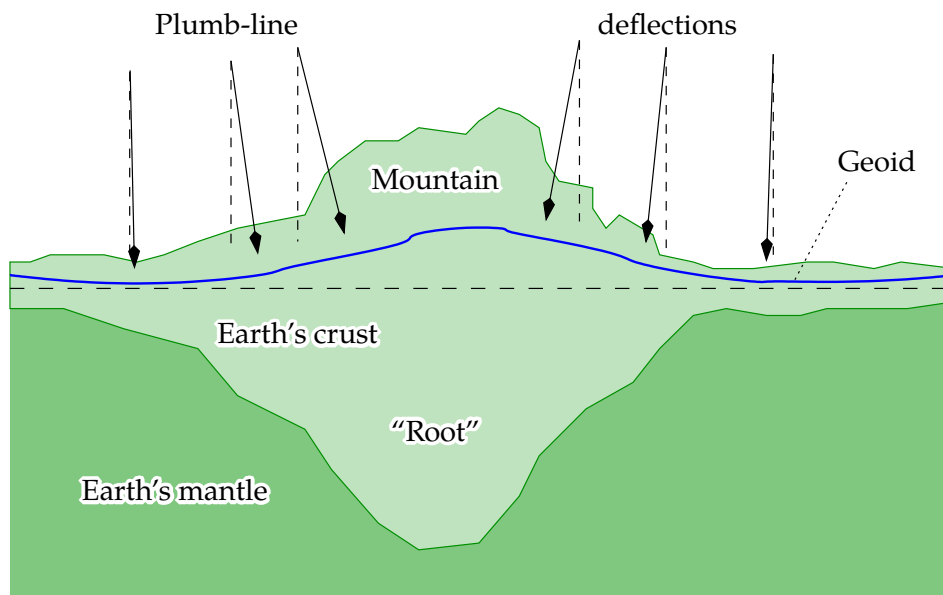
 FIGURE 6.9. Friedrich Robert Helmert. [Humboldt University Berlin \(2017\)](#).


6.6 Isostasy

6.6.1 Classical hypotheses

As early as in the 18th and 19th centuries, also thanks to Bouguer's work in South America as well as that of British geodesists in the Indian Himalayas, it was understood that mountain ranges were not just piles of rock on top of the Earth's crust. The gravity field surrounding the mountains, specifically the deflections of the plumb line, could only be explained by assuming that under every mountain range there was also a "root" made from lighter rock species. The origin of this root was speculated to be the almost hydrostatic behaviour of the Earth's crust over geological time-scales. This assumption of hydrostatic equilibrium was called the *hypothesis of isostasy*, also *isostatic compensation*.





 FIGURE 6.10. Isostasy and the bending of plumb lines towards the mountain.

Back then, unlike now, it was not yet possible to get a precise or even correct picture using physical methods (seismology) of how these mountain roots are really shaped. That is why simplified working hypotheses were formulated.

One classic isostatic hypothesis is the Pratt–Hayford hypothesis. This was proposed by J. H. Pratt⁴ in the middle of the 19th century (Pratt, 1855, 1859, 1864), and J. F. Hayford⁵ developed the mathematical tools needed for computation. According to this hypothesis, the density of the “root” under a mountain would vary with the height of the mountain, so that under the highest mountains would be the lightest material, and the boundary between this light root material and the denser material of the Earth’s mantle would be at a fixed depth. This

⁴John Henry Pratt (1809–1871) was a British clergyman and mathematician who worked as the archdeacon of Kolkata, India. [Wikipedia, John Pratt](#).

⁵John Fillmore Hayford (1868–1925) was a United States geodesist who studied isostasy and the figure of the Earth.



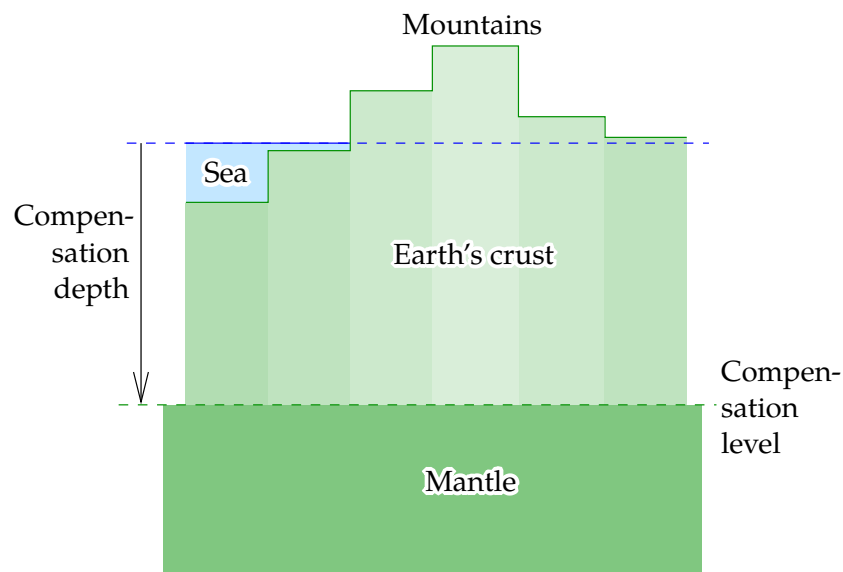


FIGURE 6.11. Pratt–Hayford isostatic hypothesis.

model, which nowadays finds little acceptance, is illustrated in figure 6.11.

Another classical isostatic hypothesis is due to G. B. Airy.⁶ Because V. A. Heiskanen⁷ used it extensively and developed its mathematical form, it is called the Airy–Heiskanen model. In this model, it is assumed that the mass density of the “root” is fixed, and that the isostatic compensation is realised by varying the depth to which the root extends down into the Earth’s mantle. In our current understanding, this corresponds better to what is really happening inside the Earth. This hypothesis is illustrated in figure 6.12.

⁶George Biddell Airy [PRS](#) (1801–1892) was an English mathematician and astronomer, “Astronomer Royal” 1835–1881.

⁷Veikko Aleksanteri Heiskanen (1895–1971), “the great Heiskanen” ([Hermans, 2007](#)) was an eminent Finnish geodesist who also worked in Ohio, USA. He is known for his work on isostasy and global geoid modelling, the “Columbus geoid”. See [Kakkuri \(2008\)](#).



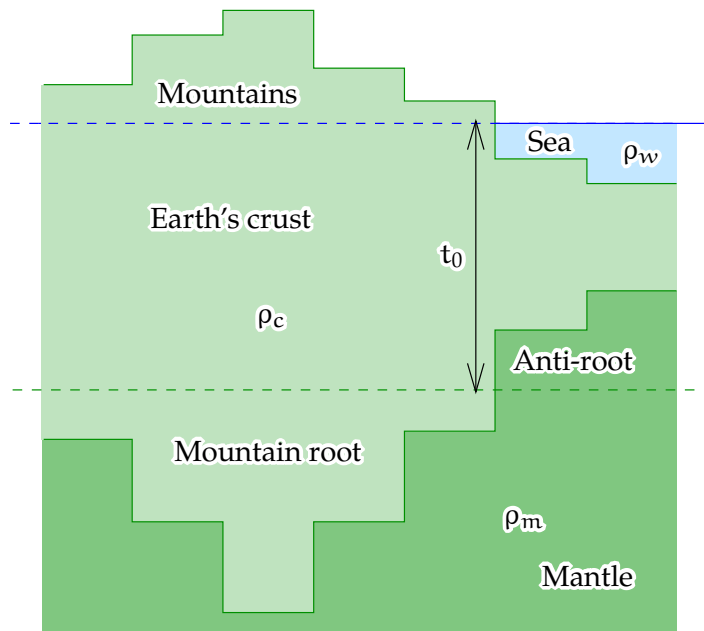


FIGURE 6.12. Airy-Heiskanen isostatic hypothesis.



6.6.2 Calculation formulas



Airy's isostatic hypothesis assumes that in every place the total mass of a column of matter is the same. So, let the density of the Earth's crust be

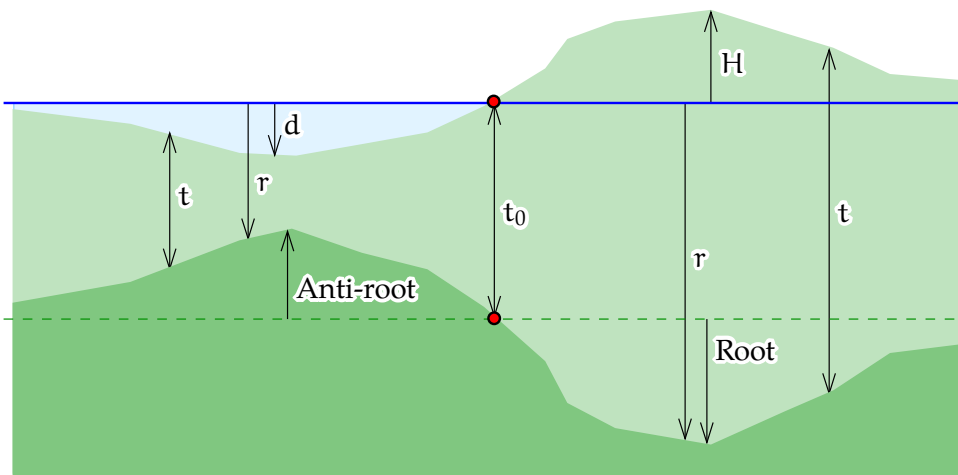


FIGURE 6.13. Quantities in isostatic compensation.



ρ_c , the density of the mantle ρ_m , the density of sea water ρ_w , sea depth d , crustal thickness t , and topographic height H . We obtain

$$t\rho_c + d\rho_w - (t + d)\rho_m = c \implies t = -\frac{d(\rho_m - \rho_w) + c}{\rho_m - \rho_c}$$

on the sea, and

$$t\rho_c - (t - H)\rho_m = c \implies t = \frac{H\rho_m - c}{\rho_m - \rho_c}$$

on land. c is a suitable constant.⁸ Here we have conveniently forgotten about the curvature of the Earth: we use the “flat Earth model”.

Under land, the depth of a mountain root is

$$r = t - H = \frac{H\rho_m - c}{\rho_m - \rho_c} - \frac{H\rho_m - H\rho_c}{\rho_m - \rho_c} = \frac{H\rho_c - c}{\rho_m - \rho_c}.$$

Similarly under the sea

$$r = t + d = -\frac{d(\rho_m - \rho_w) + c}{\rho_m - \rho_c} + \frac{d\rho_m - d\rho_c}{\rho_m - \rho_c} = -\frac{d(\rho_c - \rho_w) + c}{\rho_m - \rho_c}.$$

In the equations, the constant c is arbitrary and expresses the fact that the level from which one computes the depth of the root — less precisely, the “average thickness of the crust” — can be chosen arbitrarily.

Another approach: instead of c , use the “zero topography compensation level” t_0 , to be computed from the above equations by setting $H = d = 0$:

$$t_0(\rho_c - \rho_m) = c.$$

This yields under the land the root depth

$$r = \frac{H\rho_c - t_0(\rho_c - \rho_m)}{\rho_m - \rho_c} = t_0 + H\frac{\rho_c}{\rho_m - \rho_c}, \quad (6.5)$$

and under the sea

$$r = -\frac{d(\rho_c - \rho_w) + t_0(\rho_c - \rho_m)}{\rho_m - \rho_c} = t_0 - d\frac{\rho_c - \rho_w}{\rho_m - \rho_c}, \quad (6.6)$$

⁸Its dimension, after multiplication with ambient gravity g , is *pressure*: according to Archimedes’ law, the pressure of the crustal (plus sea-water) column minus the pressure of the column of displaced mantle material.



somewhat simpler equations that are also more intuitive.

Still a third form:

$$H\rho_c + (-r)(\rho_m - \rho_c) = c,$$

$$(-d)(\rho_c - \rho_w) + (-r)(\rho_m - \rho_c) = c.$$

In other words,

$$\sum_{\text{interfaces}} (\text{deviation} \times \text{density contrast}) = \text{constant}.$$

The effect of the different isostatic hypotheses on gravity is pretty much the same: the hypotheses cannot be distinguished based on gravity measurements alone. The effect of the choice of hypothesis on the geoid is stronger.

6.6.3 Example: Norway

The southern Norwegian *Hardanger plateau* (*Hardangervidda*) is a highland at, on average, 1100 m above sea level. It is the largest peneplain in Europe, a national park, and a popular tourist attraction, being traversed by the *Bergensbanen*, the highest regular railway in Northern Europe.

puolitasanko

The *Norwegian Sea* is the part of the Atlantic Ocean adjoining Norway, and does not belong to the continental shelf. It is on average 2 km deep.

mannerjalusta

Questions

1. What is the depth of the root under the Hardanger plateau, relative to the compensation depth t_0 ?
2. What is the negative depth of the anti-root under the Norwegian Sea, relative to the same compensation depth?
3. What is the *relative* depth of the root of the Hardanger plateau, compared to the nearby Norwegian Sea?

Answers



1. We use equation 6.5, finding

$$\begin{aligned} r - t_0 &= H \frac{\rho_c}{\rho_m - \rho_c} = \\ &= 1100 \text{ m} \times \frac{2670 \text{ kg/m}^3}{(3370 - 2670) \text{ kg/m}^3} = 4196 \text{ m}. \end{aligned}$$

Here we have used standard densities for crustal and mantle rock, respectively.

2. We use equation 6.6, finding

$$\begin{aligned} r - t_0 &= -d \frac{\rho_c - \rho_w}{\rho_m - \rho_c} = \\ &= -2000 \text{ m} \times \frac{(2670 - 1030) \text{ kg/m}^3}{(3370 - 2670) \text{ kg/m}^3} = -4686 \text{ m}, \end{aligned}$$

using the standard density value for sea water.

3. The depth contrast between root and anti-root is $4196 - (-4686) \text{ m} = 8882 \text{ m}$. For perspective, Mount Everest is 8848 m above sea level.



6.6.4 The modern understanding of isostasy

Nowadays we have a much better understanding of the internal situation in the Earth. However, isostasy continues to be a valid concept. A more realistic understanding of the internal structure of the Earth is given in figure 6.14.

mannerjäätiköt

An important subject for current research is the effect on vertical motion of the Earth's crust of the growing and melting of the ice masses of the Earth, like the continental ice sheets. This includes both the direct effect of the varying ice masses and the effect of the changes caused in the water masses of the ocean. *Paleo-research* concentrates on the changes over the glacial cycle, while modern retreats of glaciers, as in Alaska and on Spitsbergen, cause their own, observable local uplift of the Earth's crust. More in chapter 12.



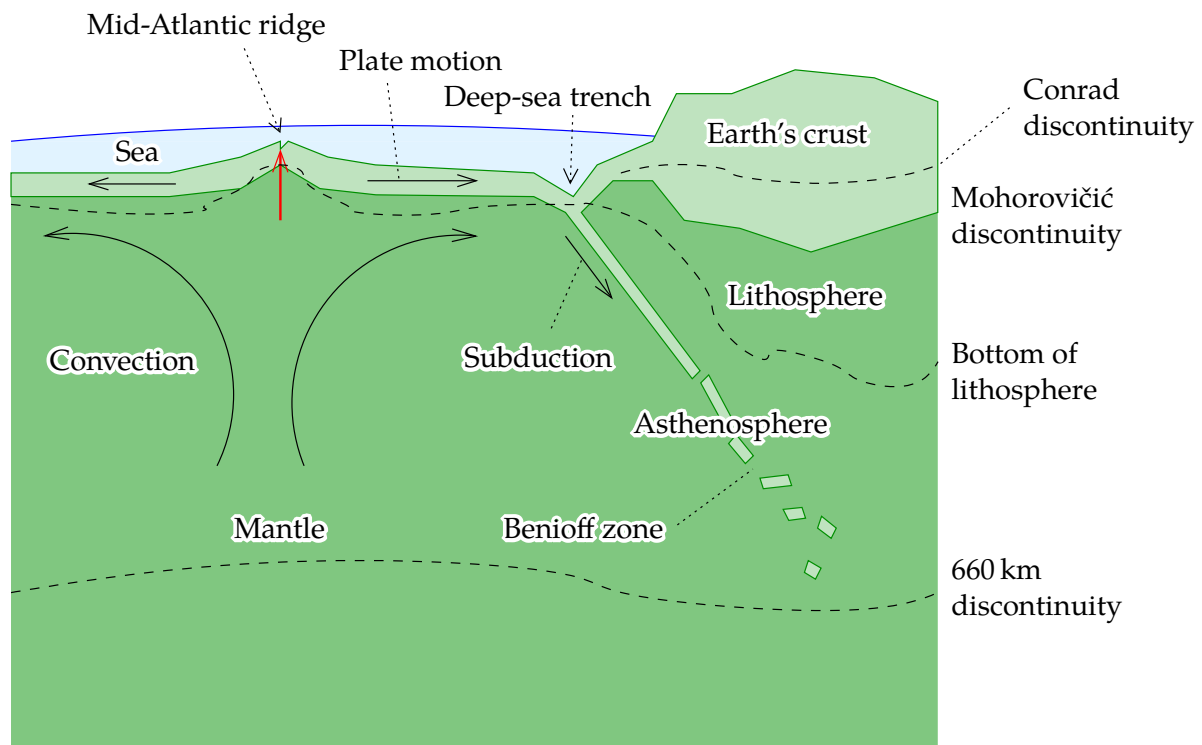


FIGURE 6.14. The modern understanding of isostasy and plate tectonics. Deep-sea trenches are known to be in isostatic disequilibrium.



6.6.5 Example: Fennoscandian land uplift

During the last glacial maximum, some 20 000 years ago, Fennoscandia was covered by a continental ice sheet of thickness up to 3 km.

Questions

1. How much was the Earth's surface depressed by this load, assuming isostatic equilibrium?
2. Currently the land is rising in central Fennoscandia, where the ice thickness was maximal, at a rate of 10 mm/a . How long would it take at this rate for the depression to vanish?

Answers

1. We assume for the ice density a value of 920 kg/m^3 . With an



upper mantle density of 3370 kg/m^3 — note that it is Earth's mantle material that is being displaced by the ice, the Earth's crust just transmits the load! See figure 12.1a — we find for the depression

$$\Delta H = 3000 \text{ m} \times \frac{920 \text{ kg/m}^3}{3370 \text{ kg/m}^3} = 819 \text{ m}.$$

2. At the rate of 10 mm/a it will take $819 \text{ m}/0.01 \text{ m/a} = 81\,900$ years total for the depression to vanish. Part of this uplift has already taken place since the last deglaciation.

In reality, of course, the rate has decreased substantially, and will continue to decrease, over time.

6.7 Isostatic reductions

The computational removal of both the topography and its isostatic compensation from the measured quantities of the gravity field is called *isostatic reduction*. It serves two purposes:

- By removing as many as possible “superficial” effects from the gravity field, we are left with a field where only the effect of the Earth's deep layers remains. This is useful for geophysical studies.
- These “superficial” effects are also generally very local: in spectral language, very *short-wavelength*. By removing those, we are left with a residual field that is much smoother, and that can be interpolated or *predicted* better. This is important especially in areas where there is a paucity of real measurement data, like the oceans, deserts, polar areas, etc.

Isostatic anomalies, free-air anomalies to which isostatic reduction has been applied, are very smooth (like Bouguer anomalies), and their *predictive properties* are good. However, unlike Bouguer anomalies, isostatic anomalies are on average zero. They lack the large bias that makes Bouguer anomalies strongly negative especially in mountainous



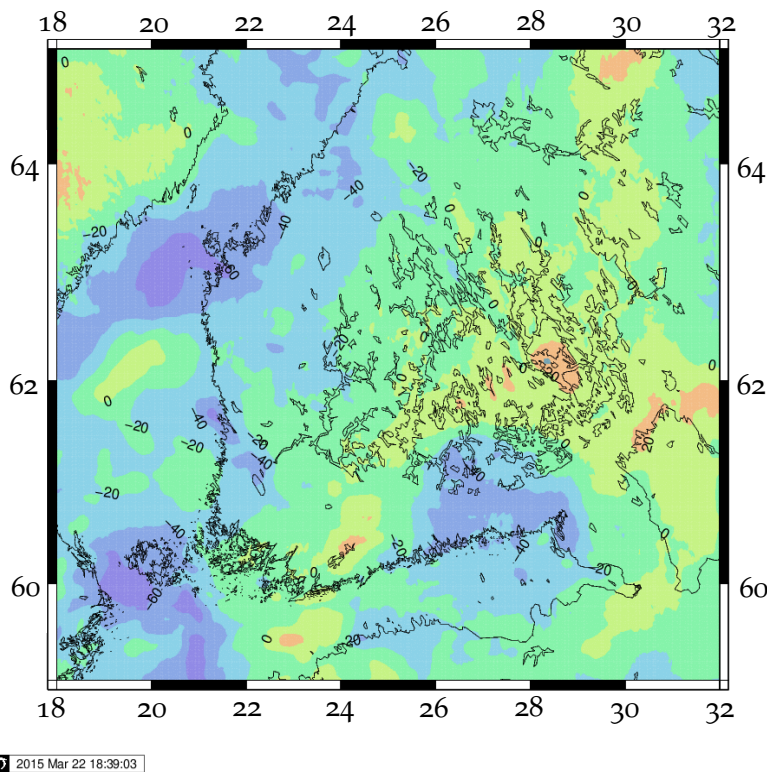


FIGURE 6.15. Isostatic gravity anomalies for Southern Finland. Airy–Heiskanen hypothesis, compensation depth 30 km. Data © Bureau Gravimétrique International (BGI) / International Association of Geodesy, World Gravity Map project. Web service BGI, WGM2012. Here, on the thick, rigid Fennoscandian Shield, the local features of the topography are not isostatically compensated and the map looks rather similar to the free-air anomaly map 5.5 on page 124.

areas, section 6.2. This of course is because isostatic reduction is only the *shifting* of masses from one place to another — from mountains to roots beneath the same mountains, the mass deficit of which is pretty precisely the same as the mass of the mountains themselves sticking out above sea level — rather than *removal* of masses, which is what Bouguer reduction does.

The reduction methods used in isostatic calculations are the same as



in other reductions. We will discuss them later: numerical integration in the space domain — grid integration, spherical-cap integration, least-squares collocation (LSC), finite elements, etc. — or in the spectral domain, for example FFT and “Fast Collocation”.

The question of the hypothesis assumed to apply is a more interesting one. Traditionally, the Pratt or Airy hypotheses have been used, developed into quantitative methodologies by Hayford or Heiskanen or Vening Meinesz.⁹ A newer approach has been to use real measurement data from *seismic tomography* in order to model the interior structure of the Earth. With real measurement data, if reliable, one should get better results.



6.8 The “isostatic geoid”

Let us look at how the “isostatic geoid”, more precisely the *co-geoid of isostatic reduction*, is computed. Isostatic reduction is one possible method for computationally removing the masses outside the geoid, in order to formulate a boundary-value problem on the geoid.

We can show (Heiskanen and Moritz, 1967, page 142), that under the continents, the isostatic co-geoid is as much as several metres below the geoid. In other words, the indirect effect (the “restore” step) is of this order. Under the oceans, similarly the isostatic co-geoid is somewhat above the geoid.

As one of the requirements for geoid determination methods is a small indirect effect, it follows that isostatic methods are not perhaps the best possible if the intent is to calculate a model of the geoid or quasi-geoid representing the exterior potential.¹⁰ Heiskanen and Moritz

⁹Felix Andries Vening Meinesz (1887–1966) was a Dutch geophysicist, geodesist and gravimetrist. He wrote with V. A. Heiskanen the textbook *The Earth and its Gravity Field* (1958).

¹⁰Of course Bouguer reduction is even worse! The indirect effect can be hundreds of metres.



(1967, page 152) call the indirect effect “moderate”.

However, isostatic methods are very suitable for elucidating the interior structure of the Earth, because both the topography and the “impression” it makes on the Earth’s mantle, the isostatic compensation, are computationally removed.

Research has shown that the great topographic features of the Earth are some 85–90% isostatically compensated (Heiskanen, 1960). This is valuable information if no other knowledge is available.

This is the second reason why the isostatic geoid is of interest: the gravity field of an Earth from which the effect of mountains has been removed completely — mountain roots and all — can uncover physical unbalances existing in deeper layers, and processes causing these. Such processes include especially convection currents in the Earth’s mantle as well as the possible effect of the liquid outer core of the Earth on these currents. Interesting correlations have been found between mantle convection patterns, the global map of the geoid, and the electric current patterns in the core causing the Earth’s magnetic field (Wen and Anderson, 1997; Prutkin, 2008; Kogan et al., 1985).

Isostatic reduction consists of two parts:

- computational removal of the topography
- computational removal of the isostatic compensation of the topography.

It is possible to calculate both parts exactly using prism integration, see section 6.3. Here however we shall gain understanding by a qualitative approach. We *approximate* both parts with a single mass-density layer, with density for example $\kappa = \rho H$ for the topography. We place the first layer at level $H = 0$, and the second, density $-\kappa$, at *compensation depth* $H = -D$. The situation is depicted in figure 6.16.

In the following we use the “generating function” equation 8.6,

$$\frac{1}{\ell} = \frac{1}{R} \sum_{n=0}^{\infty} \left(\frac{R}{r}\right)^{n+1} P_n(\cos \psi),$$



together with the single mass-density layer equation 1.15:

$$V = G \iint_{\text{surface}} \frac{\kappa}{\ell} dS = GR^2 \iint_{\text{surface}} \frac{\kappa}{\ell} d\sigma.$$

We obtain for the potential field of the mass-density layer at sea level, when the evaluation point is also placed at sea level, $H = 0 \implies r = R$:

$$V_{\text{top}} = GR \iint_{\sigma} \kappa \sum_{n=0}^{\infty} P_n(\cos \psi) d\sigma$$

and with the density layer at compensation depth (source level $R - D$, evaluation level R):

$$\begin{aligned} V_{\text{comp}} &= \frac{GR^2}{R-D} \iint_{\sigma} (-\kappa) \sum_{n=0}^{\infty} \left(\frac{R-D}{R}\right)^{n+1} P_n(\cos \psi) d\sigma = \\ &= -GR \iint_{\sigma} \kappa \sum_{n=0}^{\infty} \left(\frac{R-D}{R}\right)^n P_n(\cos \psi) d\sigma, \end{aligned}$$

from which the combined effect ($n = 0$ drops out):

$$\begin{aligned} \delta V_{\text{iso}} &= -(V_{\text{top}} + V_{\text{comp}}) = \\ &= -GR \iint_{\sigma} \kappa \sum_{n=1}^{\infty} \left(1 - \left(\frac{R-D}{R}\right)^n\right) P_n(\cos \psi) d\sigma. \quad (6.7) \end{aligned}$$

Here, the mass density per unit of surface area κ is

$$\kappa = \begin{cases} \rho_c H & \text{if } H \geq 0, \\ (\rho_c - \rho_w) H & \text{if } H < 0, \end{cases}$$

so we replace ocean depths with equivalent “dry” depths.¹¹ Now we use again the degree constituent equation, [Heiskanen and Moritz \(1967\)](#) equation 1-71, or our equation 3.8, in the following form:

$$\kappa_n(\phi, \lambda) \stackrel{\text{def}}{=} \frac{2n+1}{4\pi} \iint_{\sigma} \kappa(\phi', \lambda') P_n(\cos \psi) d\sigma'.$$

¹¹This works on dry land and on the ocean. Lakes, glaciers and areas like the Dead Sea are more complicated.



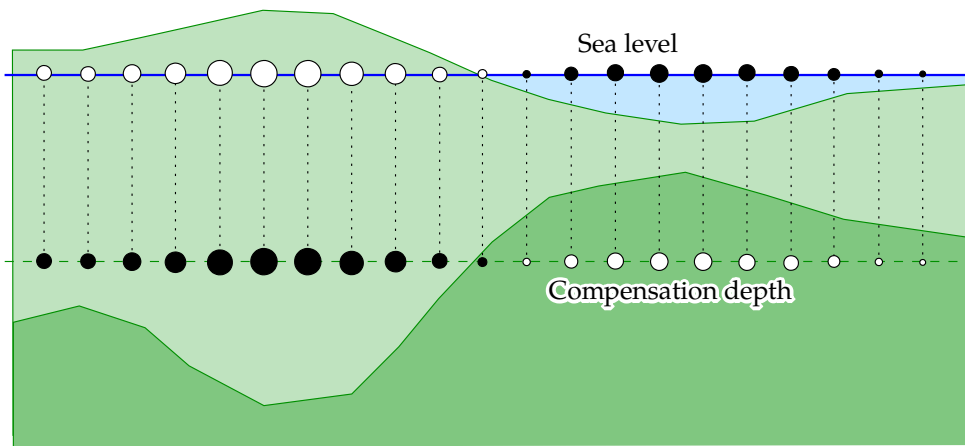


FIGURE 6.16. Isostatic reduction as a pair of surface density layers.

Multiplying both sides by the factor

$$-\frac{4\pi GR}{2n+1} \left(1 - \left(\frac{R-D}{R}\right)^n\right)$$

and moving it inside the integral, we obtain

$$\begin{aligned} -\frac{4\pi GR}{2n+1} \left(1 - \left(\frac{R-D}{R}\right)^n\right) \kappa_n(\phi, \lambda) &= \\ &= -GR \iint_{\sigma} \kappa(\phi', \lambda') \left(1 - \left(\frac{R-D}{R}\right)^n\right) P_n(\cos \psi) d\sigma'. \end{aligned}$$

Summation yields expression 6.7 above:

$$\begin{aligned} -\sum_{n=1}^{\infty} \frac{4\pi GR}{2n+1} \left(1 - \left(\frac{R-D}{R}\right)^n\right) \kappa_n(\phi, \lambda) &= \\ &= -GR \iint_{\sigma} \kappa(\phi', \lambda') \sum_{n=1}^{\infty} \left(1 - \left(\frac{R-D}{R}\right)^n\right) P_n(\cos \psi) d\sigma'. \end{aligned}$$

It follows using equation 6.7 that

$$\begin{aligned} \delta V_{\text{iso}} &= -\sum_{n=1}^{\infty} \frac{2}{2n+1} R \left(1 - \left(\frac{R-D}{R}\right)^n\right) 2\pi G \kappa_n = \\ &= -\sum_{n=1}^{\infty} \frac{2}{2n+1} R \left(1 - \left(\frac{R-D}{R}\right)^n\right) (A_B)_n. \end{aligned}$$



Here we have used the notation $A_B = 2\pi G\kappa$. This represents the equivalent Bouguer-plate attraction of a mass-density layer κ , and its degree constituents are $(A_B)_n = 2\pi G\kappa_n$.

Let us first look at the contribution from¹² $0 < n \leq N = R/D$. Then, as

$$\left(\frac{R-D}{R}\right)^n \approx 1 - \frac{nD}{R},$$

the following approximation holds:

$$\delta V_{\text{iso}} \approx - \sum_{n=1}^N \frac{2nD}{2n+1} (A_B)_n \approx - \sum_{n=1}^N D (A_B)_n \approx -DA_B,$$

and

$$\delta N_{\text{iso}} = \frac{\delta T_{\text{iso}}}{\gamma} \approx -\frac{DA_B}{\gamma}. \quad (6.8)$$

This is the *indirect effect of isostatic reduction*.

Let us substitute realistic values. Let the depth of the Mohorovičić¹³ discontinuity be on average ~ 20 km.¹⁴

On land $H \approx 0.8$ km, the Earth's mean topographic height, and we obtain $\delta N_{\text{iso}} \approx -1.8$ m.

On the ocean $H \approx -3.7$ km on average. We must still multiply by the ratio

$$\frac{\rho_c - \rho_w}{\rho_c} = \frac{2670 - 1030}{2670},$$

¹²The contribution from degree numbers $n > R/D$ is

$$\delta V_{\text{iso}} \approx - \sum_{n=N+1}^{\infty} \frac{2R}{2n+1} (A_B)_n,$$

where the terms are small and rapidly falling to zero. In this degree range, the mass-density layer approximation for the topography and its compensation breaks down, but it hardly matters as these short wavelengths aren't even isostatically compensated.

¹³Andrija Mohorovičić (1857–1936) was a Croatian meteorologist and a pioneer of modern seismology.

¹⁴Under the continents, the depth is 35 km, under the oceans 7 km below the sea floor, according to *Encyclopædia Britannica* ([Encyclopaedia Britannica, Moho](#)). Using these values, we find $\delta N_{\text{iso}} = -3.2$ m on land, +2.8 m on the ocean.



_____ in order to take the water into account. We obtain $\delta N_{\text{iso}} \approx +5.2 \text{ m}$.

In other words, this effect can be sizeable.

Equation 6.8 is *linear* in the height H . This means that, under the continents, the isostatic co-geoid will run on the order of a few metres below the classical geoid, when on the oceans again it must be a few metres above the geoid (mean sea level). We may also conclude that in the isostatic reduction's effect on the geoid – at least for longer wavelengths $2\pi R/n$, longer than the compensation depth D — all wavelengths are represented in the spectrum in approximately in the same proportions as in the topography itself, and the effect is in fact proportional to the topography.



Self-test questions

1. Which effects are computationally removed in
 - (a) the simple Bouguer reduction?
 - (b) the terrain-corrected Bouguer reduction?
 - (c) the isostatic reduction?
2. Why is the terrain correction always positive?
3. Why do Bouguer anomalies have good interpolation properties, and on what condition — in other words, which additional information must be available at the interpolation stage?
4. How was it discovered that mountains have roots?
5. Explain the isostatic hypotheses of Pratt–Hayford and Airy–Heiskanen.



Exercise 6 – 1: Gravity anomaly

Given point P , height above sea level $H = 500 \text{ m}$, local gravity $g_P = 9.82 \text{ m/s}^2$. Normal gravity at sea level for local latitude φ is $\gamma_0(\varphi) =$



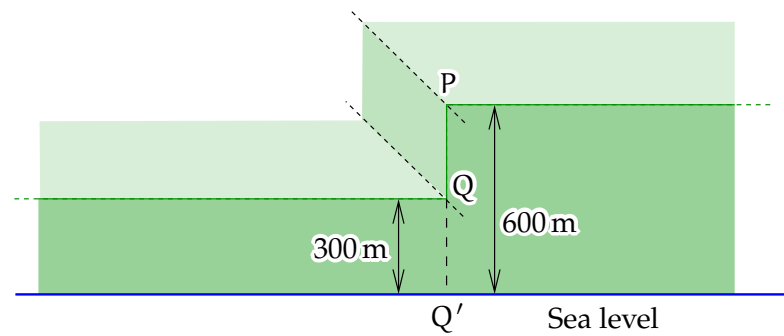


FIGURE 6.17. Terrain shape.

9.820 192 m/s².

1. Compute point P's free-air anomaly Δg .
2. Compute point P's Bouguer anomaly (without terrain correction) Δg_B .



Exercise 6 – 2: Bouguer reduction

1. Point P is 500 m above sea level. Its free-air anomaly is $\Delta g_{FA} = 25$ mGal. Calculate the Bouguer anomaly Δg_B of the point. Forget about the terrain correction.
2. See section 6.2: Bouguer anomalies. Derive equations 6.2 and 6.3 anew, assuming that the mean density of the Earth's crust is $\rho = 3370$ kg/m³.



Exercise 6 – 3: Terrain correction and Bouguer reduction

Given the terrain shape, figure 6.17.

The vertical rock wall PQ is also straight on a map and extends in both directions (“into” and “out of” the paper) to infinity.

Height differences: $PQ' = 600$ m, $QQ' = 300$ m.



1. Compute the *terrain correction* at point P (hint: use the formula for the attraction of a Bouguer plate. We have here a *half* Bouguer plate, with only half the attraction of a full one.)
2. Compute the terrain correction at point Q. Algebraic sign?
3. If at point P it is given that the free-air anomaly is 60 mGal, how much is the Bouguer anomaly at the point? (Use the complete Bouguer reduction.)
4. If it is given at point Q that the Bouguer anomaly is 10 mGal, how much is the point's free-air anomaly?



Exercise 6 – 4: Isostasy

Assume Airy–Heiskanen isostatic compensation (figure 6.12). The density of the Earth's crust $\rho_c = 2670 \text{ kg/m}^3$, density of the mantle $\rho_m = 3370 \text{ kg/m}^3$, so the density contrast at the crust-mantle interface is 700 kg/m^3 . Let the *reference level* for the interface corresponding to zero topography be -25 km , so $t_0 = 25 \text{ km}$.

1. Calculate the depth of the “root” of an 8 km high mountain below the reference level -25 km , assuming it is isostatically compensated.
2. Mauna Kea is 4 km above sea level, however the surrounding sea is 5 km deep. How deep is the root of Mauna Kea below the reference level?
3. How much is the “anti-root” of the surrounding sea *above* the reference level? Let the density of sea water be 1030 kg/m^3 .
4. So, how deep is the root of Mauna Kea *relative to its surroundings*?





Vertical reference systems

7



7.1 Levelling, orthometric heights and the geoid

Heights have traditionally been determined by *levelling*. Levelling is a technique for determining height differences using a level (levelling instrument) and two rods or staffs. The level comprises a telescope and a spirit level, and in the measurement situation the telescope's optical axis, the sight axis, is pointing along the local horizon. Levelling staffs are placed on two measurement points, and through the measuring telescope, measurement values are read off them. The difference between the two values gives the height difference between the two points in metres.

The distance between level and staffs is 40–70 m, as longer distances would cause too large errors due to atmospheric refraction. Longer distances are measured by repeat measurements using several instrument stations and intermediate points.

The height differences ΔH thus obtained are not, however, directly useable. The "height difference" between two points P and Q, obtained by directly summing the height differences ΔH , depends namely also on the path chosen when levelling from P to Q. Also the sum of height differences $\sum_{\circ} \Delta H$ around a closed path is (generally) *not zero*.

Geometric height is not a conservative field.

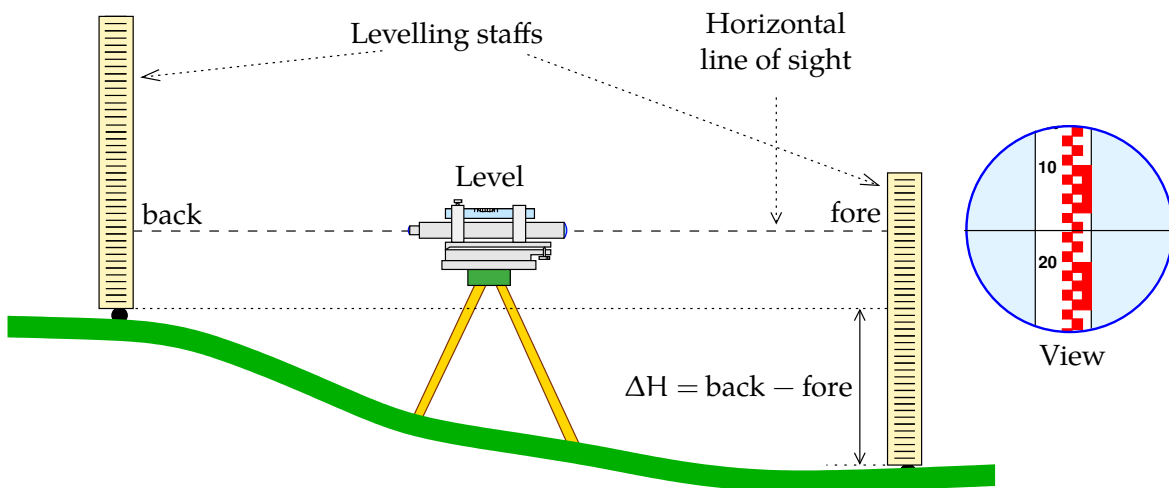


FIGURE 7.1. The principle of levelling.

This is why, in precise levelling, the height differences are always converted to *potential differences*: $\Delta W = -\Delta H \cdot g$, in which g is the local gravity, which is either measured or — like in Finland — interpolated from an existing gravity survey data base. The sum of potential differences around a closed loop is *always zero*: $\sum_{\bigcirc} \Delta W = 0$.

For the potential at an arbitrary terrain point P we find

$$W_P = W_0 - \sum_{\text{sea level}}^P (\Delta H \cdot g),$$

the summation being done directly from sea level (potential W_0) up to point P. The quantity

$$C_P = -(W_P - W_0) = \sum_{\text{sea level}}^P (\Delta H \cdot g),$$

geopotentialiluku which is positive above sea level, is called the *geopotential number* of point P.

W_0 is the potential of the national height reference level. In Finland, the reference level of the old N60 system is in principle the mean sea level in Helsinki harbour at the beginning of 1960, which is why the



system is called **N60**. However, the precise realisation is a special pillar in the garden of the Helsinki astronomical observatory in Kaivopuisto.¹ The new Finnish height system is called **N2000**, and the realisation of its reference level is a pillar at the Metsähovi research station. In practice **N2000** heights are, at the decimetric precision level, heights over the Amsterdam **NAP** datum.

Other countries have their own, similar height reference or datum points: Russia has Kronstadt, Western Europe the widely used Amsterdam datum **NAP**, southern Europe has the old Austro-Hungarian harbour city of Trieste, North America the North American Vertical Datum 1988 (**NAVD88**) with the datum point Father Point (Pointe-au-Père)² in Rimouski, Quebec, Canada, etc.



7.2 Orthometric heights

To create a vertical reference, it would be simplest to use the original geopotential differences from sea level, the geopotential numbers defined above, $C = -(W - W_0)$, directly as height values. However, this is psychologically and practically difficult: people want their heights to be in metres.

Geopotential numbers have clear advantages: they represent the *amount of energy* that is needed (for a unit test mass) to move to the point from the reference level. Fluids — sea water, but also air, or, on geological time-scales, even bedrock! — always flow downwards and seek the state of minimum energy.

¹However, the value engraved on the pillar is the reference height of the still older NN system, not **N60**. The correct reference value for **N60** for this pillar, 30.513 76 m, is given in the publication **Kääriäinen (1966, page 49)**.

²The district Pointe-au-Père of the city of Rimouski was named after the Jesuit priest Father Henri Nouvel (1621?–1701?), who served forty years with the native population of New France, today's Quebec. Pointe-au-Père is also notorious as the location of the RMS *Empress of Ireland* shipwreck in 1914, in which over a thousand passengers perished.





FIGURE 7.2. Height reference pillar in the garden of the Helsinki astronomical observatory in Kaivopuisto, [Kääriäinen \(1966\)](#). Text:

*Suomen
tarkka-
vaakituksen
pääkiintopiste
30,4652 m yli nollan*

*Utgångspunkt för
precisionsnivellemetet
i Finland
30,4652 m öfver noll*

(Reference bench mark of the precise levelling of Finland, 30.4652 m above zero).



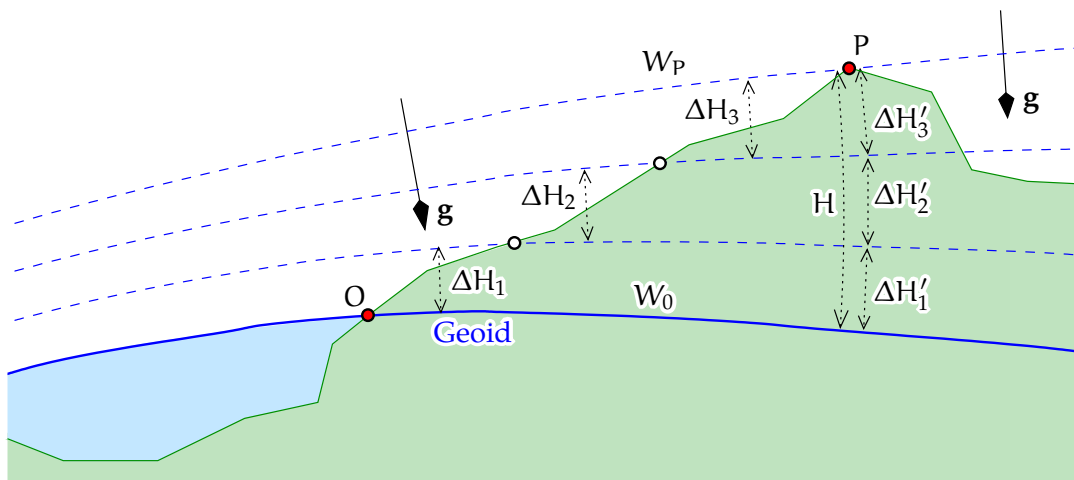


FIGURE 7.3. Levelled heights and geopotential numbers. The height obtained by summing the levelled height differences, $\sum_{i=1}^3 \Delta H_i$, is not the “correct” height above the geoid, i.e., $\sum_{i=1}^3 \Delta H'_i$ computed along the plumb line.

The equipotential or *level surfaces* of the geopotential are not at all parallel: because of this, a journey along the Earth’s surface may well go “upwards”, to increasing heights above the geoid, although the geopotential number decreases. Thus, water may flow “upwards”.

The gravity vector \mathbf{g} is everywhere perpendicular to the level surfaces, and its length is inversely proportional to the distance separating the surfaces.



In Finland, as in many other countries, *orthometric heights* have been long in use. They are physically defined heights above “mean sea level” or the *geoid*. See figure 7.3.

The classical *geoid* is defined as

“The level surface of the Earth’s gravity field that fits on average best to the mean sea level.”

The orthometric height H of point P is defined as the height obtained by measuring the *distance of P from the geoid along the plumb line*.



This is a very physical definition, however not a very operational one, because we (generally) do not get to measure along a plumb line inside the Earth, and the geoid is not visible there. This is why orthometric heights are calculated from geopotential numbers: if the geopotential number of point P is C_P , we calculate the orthometric height using the formula

$$H = C_P / \bar{g},$$

where \bar{g} , the average gravity along the plumb line, is

$$\bar{g} = \frac{1}{H} \int_0^H g(z) dz,$$

and z is the measured distance from the geoid along the plumb line. Because the formula for \bar{g} already itself contains H , we obtain the solution iteratively, starting from a crude initial estimate for H . The iteration converges fast.

We shall see that determining precise orthometric heights is challenging, especially in the mountains.

7.3 Normal heights

In Finland, currently, with the **N2000** height system, *normal heights* are used. They are, like orthometric heights, heights *above mean sea level*. The mathematical representation of mean sea level in this case is the *quasi-geoid*. In sea areas, the quasi-geoid is identical to the geoid. Over land, it differs a little from the geoid, and in mountainous areas the difference may be substantial.

7.3.1 Molodensky's theory

The renowned theorist M. S. Molodensky (figure 7.5) developed a theory in which the height of a point from “mean sea level” is defined by the following equation:

$$H^* \stackrel{\text{def}}{=} C / \gamma_{0H},$$



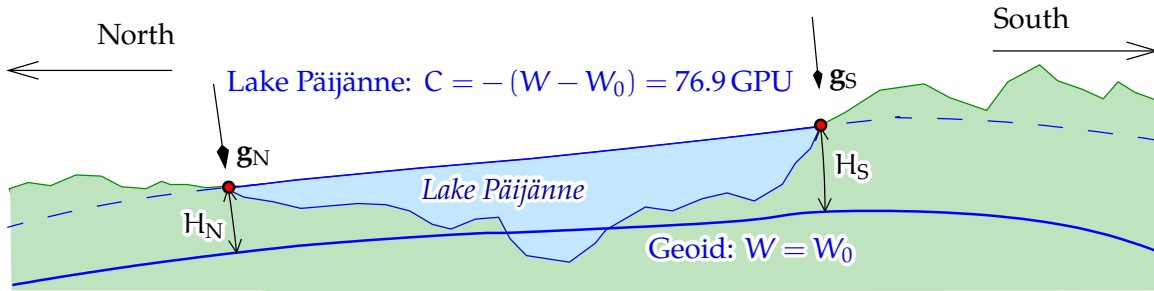


FIGURE 7.4. In terms of orthometric heights, water may sometimes flow “upwards”. Although the north and south ends of Lake Päijänne are on the same geopotential level — 76.9 geopotential units below that of mean sea level — the orthometric height of the south end H_S is greater than that of the north end H_N , because local gravity g is stronger in the north than in the south. The height difference in the case of Lake Päijänne is 8 mm (Jaakko Mäkinen, personal communication). Calculation using the normal gravity field yields 6 mm. The balance of 2 mm comes from the difference between the gravity anomalies at the northern and southern ends.



in which $\overline{\gamma_{0H}}$ is the average normal gravity computed between the zero level (reference ellipsoid) and H^* along the *ellipsoidal normal*. So, the method of computing is the same as in the case of orthometric heights, but using the *normal gravity field* instead of the true gravity field.

Heights “above sea level” are for practical reasons given *in metres*. For large, continental networks we want to give heights above a computational reference ellipsoid in metres, and thus heights above “sea level” also have to be in metres.

Molodensky also proposed that instead of the geoid, *height anomalies* would be used, the definition of which is

$$\zeta \stackrel{\text{def}}{=} T / \overline{\gamma_{Hh}}, \quad (7.1)$$

in which now $\overline{\gamma_{Hh}}$ is the average normal gravity at terrain level; more precisely: the average of normal gravity along the ellipsoidal normal over the interval $z \in [H^*, h]$, in which H^* is the normal height of the



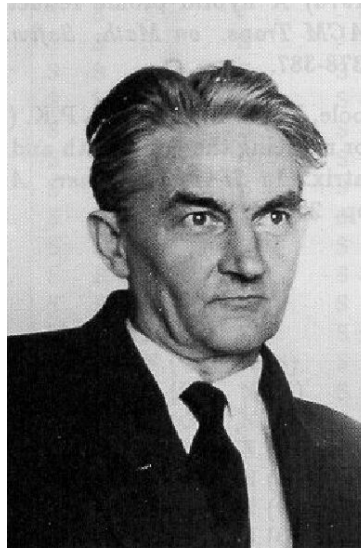


FIGURE 7.5. Mikhail Sergeevich Molodensky (1909–1991), source obscure. More photographs and background information in [Brovar et al. \(2000\)](#).

point and h its height from the reference ellipsoid. The parameter z is the distance from the reference ellipsoid reckoned along the ellipsoidal normal. T is the disturbing potential at the point.

Based on these assumptions, Molodensky showed that

$$H^* + \zeta = h.$$

This equation is very similar to the corresponding one for orthometric heights and geoid heights

$$H + N = h.$$

Also otherwise ζ , the *height anomaly*, also called “quasi-geoid height”, is very close to N , and correspondingly H^* is close to H .

7.3.2 Molodensky’s realisation

The Molodensky school realised that, because normal gravity along the plumb line is very close to a linear function of place, one could define a



height type that can be computed directly from geopotential numbers, and that also would be compatible with similarly defined, so-called height anomalies, and with geometric heights h reckoned from the reference ellipsoid.

The geometric height h from the reference ellipsoid may be connected to the potential U of the normal gravity field indirectly, though the following integral equation:

$$U = U_0 - \int_0^h \gamma(z) dz.$$

Here, U is the normal potential and γ normal gravity. One level surface of U , $U = U_0$, is also the reference ellipsoid. The variable z is the distance from the ellipsoid along its local normal.³

By defining

$$\overline{\gamma_{0h}} \stackrel{\text{def}}{=} \frac{1}{h} \int_0^h \gamma(z) dz \quad (7.2)$$

we obtain

$$h = -\frac{U - U_0}{\overline{\gamma_{0h}}}.$$

By using $W = U + T$ and dividing by $\overline{\gamma_{0h}}$ we obtain

$$\frac{W - W_0}{\overline{\gamma_{0h}}} = \frac{T}{\overline{\gamma_{0h}}} - h$$

assuming $W_0 = U_0$, the normal potential on the reference ellipsoid.

Next, one could define

$$H^+ \stackrel{?}{=} -\frac{W - W_0}{\overline{\gamma_{0h}}}$$

as a new height type, and

$$N^+ \stackrel{?}{=} h - H^+ = \frac{T}{\overline{\gamma_{0h}}}$$

³Here we ignore that the normal gravity vector $\vec{\gamma}(z)$ is for $z \neq 0$ not precisely parallel with the ellipsoidal normal: the curvature of the field lines of the normal gravity field or normal plumb lines, section 4.3.2.



as the corresponding new geoid height type. It has however the aesthetic flaw that we divide here by the average normal gravity computed between the levels 0 and h. This quantity is not operational without a means of determining the ellipsoidal height h.

This suggests the following improvement based on the circumstance that $\gamma(z)$ is a nearly linear function. This means that the vertical derivative $\frac{d}{dz}\gamma$ is nearly constant in the height interval considered.

We define in addition to equation 7.2:

$$\overline{\gamma_{0H}} \stackrel{\text{def}}{=} \frac{1}{H^+} \int_0^{H^+} \gamma(z) dz, \quad \overline{\gamma_{Hh}} \stackrel{\text{def}}{=} \frac{1}{N^+} \int_{H^+}^h \gamma(z) dz.$$

Now

$$\overline{\gamma_{0H}} \approx \overline{\gamma_{0h}} - \frac{1}{2}N^+ \frac{d\gamma}{dz} \approx \overline{\gamma_{0h}} \left(1 - \frac{N^+}{R}\right), \quad (7.3)$$

$$\overline{\gamma_{Hh}} \approx \overline{\gamma_{0h}} + \frac{1}{2}H^+ \frac{d\gamma}{dz} \approx \overline{\gamma_{0h}} \left(1 + \frac{H^+}{R}\right). \quad (7.4)$$

R is the Earth's radius in spherical approximation: $\frac{d}{dz}\gamma \approx \frac{d}{dr}\gamma \approx 2\gamma/R$.

Next, we also exploit that both N^+/R and H^+/R are $\ll 1$, so

$$\left(1 - \frac{N^+}{R}\right)^{-1} \approx \left(1 + \frac{N^+}{R}\right), \quad \left(1 + \frac{H^+}{R}\right)^{-1} \approx \left(1 - \frac{H^+}{R}\right),$$

and with equations 7.3, 7.4, and the definitions above of H^+ and N^+ ,

$$\begin{aligned} \zeta &\stackrel{\text{def}}{=} \frac{T}{\overline{\gamma_{Hh}}} = \frac{T}{\overline{\gamma_{0h}}} \cdot \frac{\overline{\gamma_{0h}}}{\overline{\gamma_{Hh}}} \approx N^+ \left(1 - \frac{H^+}{R}\right) = N^+ - \frac{N^+H^+}{R}, \\ H^* &\stackrel{\text{def}}{=} -\frac{W - W_0}{\overline{\gamma_{0H}}} = -\frac{W - W_0}{\overline{\gamma_{0h}}} \cdot \frac{\overline{\gamma_{0h}}}{\overline{\gamma_{0H}}} \approx H^+ \left(1 + \frac{N^+}{R}\right) = \\ &= H^+ + \frac{N^+H^+}{R}. \end{aligned}$$

Because the, already small, correction terms N^+H^+/R cancel, we finally obtain

$$H^* + \zeta = H^+ + N^+ = h. \quad (7.5)$$



The quantity $\overline{\gamma_{0H}}$, and thus also normal height H^* , can be, unlike $\overline{\gamma_{0h}}$, computed using *only information obtained by* (spirit or trigonometric) *levelling*, without having to know the height h above the reference ellipsoid, which would again require knowledge of the local geoid.

This was Molodensky's realisation (Molodensky et al., 1962) as early as in 1945, long before the Global Positioning System GPS, or a global, geocentric reference ellipsoid, existed. Back then, continental triangulation networks, like the one of the Soviet Union, were computed on their own, regionally defined reference ellipsoids.

The size of the correction term N^+H^+/R is, for heights of the global geoid up to 110 m, 17 mm for each kilometre of terrain height. The errors remaining after applying this term are microscopically small, because normal gravity is, unlike true gravity, *extremely linear along the plumb line* — as equations 7.3 and 7.4 already assumed.

Figure 7.6 attempts to visualise the derivation.

7.3.3 Normal height and height anomaly

Normal height

$$H^* = \frac{C}{\overline{\gamma}} = -\frac{W - W_0}{\overline{\gamma}}, \quad (7.6)$$

in which (recursive definition!)

$$\overline{\gamma} = \overline{\gamma_{0H}} = \frac{1}{H^*} \int_0^{H^*} \gamma(z) dz.$$

Height anomaly

$$\zeta = \frac{W - U}{\overline{\gamma_{Hh}}} = \frac{T}{\overline{\gamma_{Hh}}},$$

in which

$$\overline{\gamma_{Hh}} = \frac{1}{\zeta} \int_{H^*}^h \gamma(z) dz.$$

The height anomaly ζ , which otherwise is a quantity similar to the geoid height N , is however located at the level of the *topography*,



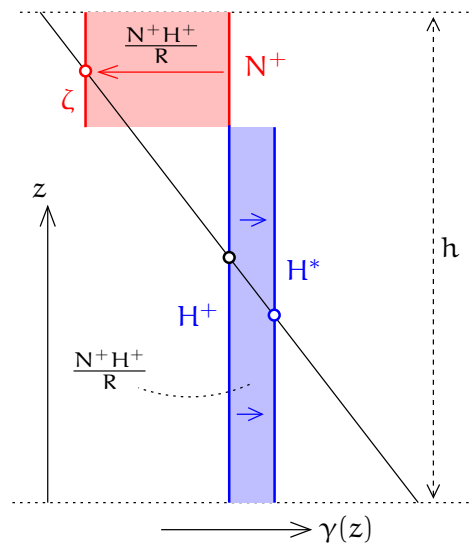


FIGURE 7.6. A graphic cartoon of the proof of Molodensky's realisation. The blue and red areas, which are equal, represent the correction terms which convert N^+ to ζ and H^+ to H^* , respectively. The red and blue arrows stand for the conversion process. The balls represent midpoints of averaging intervals for the function $\gamma(z)$.

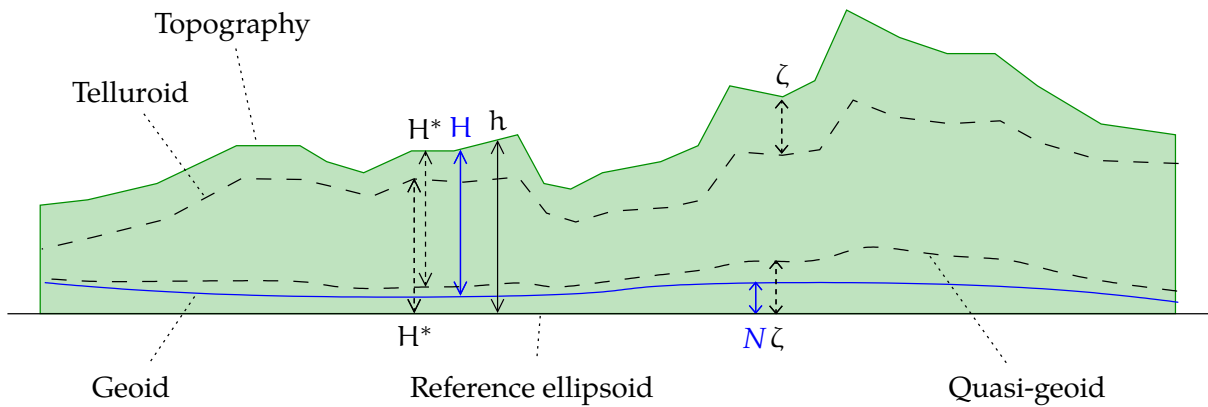


FIGURE 7.7. Geoid, quasi-geoid, telluroid and topography. Note the correlation between the quasi-geoid and topography. Depicted is the situation where $N > 0$.



not at sea level. The surface formed by points which are a distance H^* above the reference ellipsoid (and thus a distance ζ below or $-\zeta$ above the topography), is called the *telluroid*. It is a mapping of sorts of the topographic surface: the set of points Q whose *normal* potential U_Q is the same as the *true* potential W_P of the *true* topography's corresponding point P . See figure 5.4.

Often, as a concession to old habits, we construct a surface that is at a distance ζ above or a distance $-\zeta$ below the reference ellipsoid. This surface is called the *quasi-geoid*. It lacks physical meaning: it is not a level surface, although out at sea it coincides with the geoid. Its short-wave features, unlike those of the geoid, *correlate* with the short-wavelength features of the topography.

Height above the ellipsoid (assumed $U_0 = W_0$)

$$h = \frac{U - U_0}{\overline{\gamma}_{0h}},$$

where

$$\overline{\gamma}_{0h} = \frac{1}{h} \int_0^h \gamma(z) dz.$$

The *relationship* between the three quantities is

$$h = H^* + \zeta.$$

In all three cases, the quantity is defined by dividing the potential difference by some sort of “average normal gravity”, suitably computed along a segment of the local plumb line. In the case of the height anomaly ζ , a piece of plumb line is used high up, *close to the topographic surface*, between level H^* (telluroid) and level h (topography).



7.4 Difference between geoid height and height anomaly

Normal heights are very *operational*. They are always used together with “quasi-geoid” heights — more correctly: height anomalies — ζ .



Orthometric heights — for example Helmert heights — on the other hand are always used together with geoid heights N . For computing both, H and N , one needs the topographic mass density ρ , for which a standard constant value is often assumed (2670 kg/m^3), and the local vertical gradient of gravity, for which generally the vertical normal gravity gradient (-0.3084 mGal/m) is assumed.

The difference between height anomaly and geoid height is calculated as follows.

1. First, calculate the separation between the quasi-geoid and the “free-air geoid”. The free-air geoid is an equipotential surface of the harmonically downwards continued exterior potential. If T_{FA} is the disturbing potential of the exterior, harmonically downwards continued field, then its difference between topography level and sea level is:

$$T_{\text{FA}}(H) - T_{\text{FA}}(0) = \int_0^H \frac{\partial T_{\text{FA}}(z)}{\partial z} dz \approx -\Delta g_{\text{FA}} H, \quad (7.7)$$

and by using the Bruns equation twice, $\zeta = T(H)/\gamma = T_{\text{FA}}(H)/\gamma$ (height anomaly or quasi-geoid height) and $N_{\text{FA}} = T_{\text{FA}}(0)/\gamma$ (“free-air geoid height”, FA = Free Air), we obtain⁴

$$\zeta - N_{\text{FA}} \approx -\frac{\Delta g_{\text{FA}} H}{\gamma}. \quad (7.8)$$

2. Thus we have obtained the difference between the height anomalies and heights of the “free-air geoid”. It remains to determine the separation between the “free-air geoid” and geoid.

Let us approximate the topography by a Bouguer plate. Then

- In the case of the “free-air geoid” N_{FA} the thickness of the plate is the height H of point P . This is because the free-air geoid is based on the harmonically downwards continued

⁴Here we made the approximation that γ is the same on the topography level as at sea level.



exterior field, meaning that the Bouguer-plate attraction acting at P must also be continued downwards, i.e., taken fully into account.

Because the surface mass density of the plate is $H\rho$, its *assumed* attraction is *everywhere* on the plumb line of point P:

$$2\pi G\rho H. \quad (7.9)$$

- Now in the case of the *geoid height* $N = T(0)/\bar{\gamma}$, we have to be physically realistic: in an arbitrary location z on the plumb line of point P, the Bouguer plate is partly below the location, and partly above it. The attraction is then only

$$2\pi G\rho z - 2\pi G\rho (H - z) = 2\pi G\rho (2z - H). \quad (7.10)$$

By integrating the difference between equations 7.9 and 7.10, like we did for equation 7.7, we obtain

$$\begin{aligned} T(0) - T_{\text{FA}}(0) &= 2\pi G\rho \int_0^H ((2z - H) - H) dz = \\ &= 2\pi G\rho [z^2 - 2Hz]_{z=0}^{z=H} = -2\pi G\rho H^2 \approx -A_B H, \end{aligned}$$

in which A_B is the attraction of a Bouguer plate of thickness H . We obtain again by dividing the equation by normal gravity:

$$N - N_{\text{FA}} = -\frac{A_B H}{\gamma}.$$

By subtracting this latest result from equation 7.8, we find

$$\zeta - N = \frac{(-\Delta g_{\text{FA}} + A_B) H}{\gamma} = -\frac{\Delta g_B H}{\gamma}. \quad (7.11)$$

See also [Heiskanen and Moritz \(1967, pages 327–328\)](#). As the Bouguer anomaly Δg_B is strongly negative in the mountains, it follows that the quasi-geoid is there always *above* the geoid: approximately, using equation 6.2:

$$\zeta - N \approx \frac{0.1119 \text{ mGal/m}}{9.81 \text{ m/s}^2} H^2 \approx 10^{-7} \text{ m}^{-1} \cdot H^2.$$



Or, if H is in units of km and $\zeta - N$ in units of m:

$$\zeta - N \approx 0.1 \text{ m/km}^2 \cdot H^2.$$

7.5 Difference between orthometric and normal heights

The geoid is the level from which orthometric heights are measured. Therefore, we may write

$$h = H + N,$$

in which h is the height above the reference ellipsoid, and H is the orthometric height.

We may also bring back to memory equation 7.5:

$$h = H^* + \zeta,$$

in which ζ is the height anomaly, and H^* is the normal height.

We obtain simply

$$H - H^* = \zeta - N = -\frac{\Delta g_B H}{\gamma}, \quad (7.12)$$

using equation 7.11.

7.6 Calculating orthometric heights precisely

Orthometric heights are a traditional way of expressing height “above sea level”. Orthometric heights are heights above a real geoid, i.e., a level surface inside the Earth that is, in the mean, located at the same level as the mean sea level.

We may write

$$W = W_0 - \int_0^H g(z) dz,$$

in which g is the true gravity inside the topographic masses. From this we obtain

$$H = \frac{C}{g} = \frac{-(W - W_0)}{g},$$



in which the mean gravity along the plumb line is

$$\bar{g} = \frac{1}{H} \int_0^H g(z) dz.$$

The method is recursive: H appears on both the left and right sides. This is not a problem: both H and \bar{g} are obtained iteratively. Convergence is fast.

In practice one calculates orthometric height using an approximate formula. In Finland, *Helmert orthometric heights* have long been used, for which gravity measured on the Earth's surface, $g(H)$, is extrapolated downwards by using the estimated vertical gravity gradient interior to the rock. It is assumed that its standard value outside the rock, the value -0.3084 mGal/m (the free-air gradient), changes to a value that is 0.2238 mGal/m greater (twice the standard-density 2670 kg/m^3 Bouguer-plate effect⁵): the end result is the total inside-rock gravity gradient, -0.0846 mGal/m .

This is called the *Prey*⁶ *reduction*. As the end result we obtain the following equations (the coefficient is *half* the gravity gradient, so the mean gravity along the plumb line is the same as gravity at the midpoint of the plumb line):

$$\bar{g} = g(H) - 0.0846 \text{ mGal/m} \left(-\frac{1}{2}H\right) = g(H) + 0.0423 \text{ mGal/m} \cdot H,$$

thus

$$H = \frac{C}{\bar{g}} = \frac{C}{g(H) + 0.0423 \text{ mGal/m} \cdot H}, \quad (7.13)$$

in which C is the geopotential number (potential difference with mean sea level) and $g(H)$ is gravity at the Earth's surface. See also [Heiskanen and Moritz \(1967, pages 163–167\)](#). The term $0.0423 \text{ mGal/m} \cdot H$ is typically

⁵In Finland, however, density values read from a geological map were used.

⁶Adalbert Prey (1873–1949) was an Austrian astronomer and geodesist and an author of textbooks.



much smaller than $g(H)$, which is about $9.81 \text{ m/s}^2 = 981\,000 \text{ mGal}$! So, an iteration in which the denominator is first calculated using a crude H value, converges very fast.

The use of Helmert heights as an approximation to orthometric heights is imprecise for the following reasons:

- The assumption that gravity changes linearly along the plumb line. This is not the case, especially not because of the effect of the surrounding terrain. In the precise computation of orthometric heights, one ought to compute the terrain correction separately for every point on the plumb line.
- The assumption that the free-air vertical gravity gradient is a constant, -0.3084 mGal/m . This is not the case, the gradient can easily vary by $\pm 10\%$.
- The assumption that the rock density is $\rho = 2670 \text{ kg/m}^3$. The true density value may easily vary by $\pm 10\%$ or more around this assumed value.

The first approximation, neglecting the terrain effect, can be corrected by using Niethammer's⁷ method, see [Heiskanen and Moritz \(1967, page 167\)](#). It requires that, in geoid computation, too, the terrain is correspondingly taken into account.

The third approximation, the density, can be removed as a problem by conventionally agreeing to also use a *standard density* $\rho = 2670 \text{ kg/m}^3$ in the corresponding geoid computation. The surface thus obtained is not any more a true geoid then, but a "fake geoid", for which no suitable name comes to mind.

The second approximation could be eliminated by using the *true* free-air gravity gradient instead of a standard value. However, the true free-air gradient depends sensitively on local crustal density variations. Moreover, the value of the free-air gradient on the Earth's surface is not

⁷Theodor Niethammer (1876–1947) was a Swiss astronomer and geodesist who was the first to map the gravity field of the Swiss Alps.



precisely representative for the downwards continued free-air gradient along the whole plumb line. To compute the gradient, one can use the Poisson equation, on which more later.

The precise calculation of orthometric heights is thus laborious: just as laborious as the precise determination of the geoid, and for the same reasons. Fortunately in non-mountainous countries, Helmert heights are good enough. In Finland they were even computed using for the ρ values “true” crustal densities according to a geological map (Kääriäinen, 1966, page 32).

7.7 Calculating normal heights precisely

For this we use equation 7.6:

$$H^* = \frac{C}{\bar{\gamma}} = -\frac{W - W_0}{\bar{\gamma}},$$

where the average value of normal gravity along the plumb line is

$$\bar{\gamma} = \overline{\gamma_{0H}} = \frac{1}{H^*} \int_0^{H^*} \gamma(z) dz.$$

Because normal gravity is in good approximation a linear function of z , we may write

$$\bar{\gamma} = \gamma_0 + \frac{1}{2} H^* \frac{\partial \gamma}{\partial z},$$

in which $\frac{\partial}{\partial z} \gamma = -0.3084 \text{ mGal/m}$ and $\gamma_0(\varphi) \stackrel{\text{def}}{=} \gamma(\varphi, 0)$ is normal gravity computed at height zero. We obtain

$$\bar{\gamma} = \gamma_0 - 0.1542 \text{ mGal/m} \cdot H^*.$$

The solution is again obtained iteratively:

$$H^* = \frac{C}{\bar{\gamma}} = \frac{C}{\gamma_0 - 0.1542 \text{ mGal/m} \cdot H^*} \quad (7.14)$$

in which $\gamma_0(\varphi)$ can be calculated exactly when local latitude φ is known. H^* appears on both sides of the equation, but the iterative



solution converges fast due to the first term of the denominator γ_0 , some $9.81 \text{ m/s}^2 = 981\,000 \text{ mGal}$, being a lot larger than $0.1542 \text{ mGal/m} \cdot H^*$.

Calculation of normal heights, unlike calculation of orthometric heights, is not sensitive to Earth crustal density hypotheses. It depends, however, on the choice of normal gravity field, i.e., the reference ellipsoid.



7.8 Calculation example for heights

At point P the potential difference with the sea level is $C = 5000 \text{ m}^2/\text{s}^2$. Local gravity is $g = 9.820\,000 \text{ m/s}^2$.

Normal gravity calculated at level zero under point P equals $\gamma_0 = 9.821\,500 \text{ m/s}^2$.

Questions

1. Calculate the orthometric height of point P.
2. Calculate the free-air gravity anomaly Δg_{FA} of point P.
3. Calculate the Bouguer anomaly (without terrain correction) Δg_{B} of point P.
4. Calculate the normal height of point P.
5. If the geoid height at point P is $N = 25.000 \text{ m}$, how much is the *height anomaly* (“quasi-geoid height”) ζ ?

Answers

1. First attempt:

$$H^{(0)} = \frac{C}{g} = \frac{5000}{9.82} \text{ m} = 519.165 \text{ m}.$$

Second attempt (equation 7.13):

$$\begin{aligned} H^{(1)} &= \frac{5000 \text{ m}^2/\text{s}^2}{9.820\,000 \text{ m/s}^2 + 0.0423 \cdot 10^{-5} \text{ s}^{-2} \cdot 519.165 \text{ m}} = \\ &= 509.154 \text{ m}. \end{aligned}$$

After that, the millimetres no longer change.



2. The free-air anomaly is

$$\begin{aligned}\Delta g_{\text{FA}} &= 9.820\,000 \text{ m/s}^2 - \\ &\quad - (9.821\,500 - 0.3084 \cdot 10^{-5} \cdot 509.154) \text{ m/s}^2 = \\ &= 7.023 \text{ mGal.}\end{aligned}$$

3. The Bouguer anomaly is (equation 6.2):

$$\Delta g_{\text{B}} = \Delta g_{\text{FA}} - 0.1119 \text{ mGal/m} \cdot H = -49.951 \text{ mGal.}$$

4. The first attempt is again

$$H^{*(0)} = \frac{C}{\gamma_0} = 509.087 \text{ m.}$$

The second, equation 7.14:

$$\begin{aligned}H^{*(1)} &= \frac{5000 \text{ m}^2/\text{s}^2}{9.821\,500 \text{ m/s}^2 - 0.1542 \cdot 10^{-5} \text{ s}^{-2} \cdot 509.087 \text{ m}} = \\ &= 509.128 \text{ m,}\end{aligned}$$

also final on the millimetre level.

5. The difference equation 7.12 yields

$$\zeta - N = -\frac{\Delta g_{\text{B}} H}{\gamma} = 0.026 \text{ m.}$$

Also (check) $H - H^* = 0.026 \text{ m}$. So

$$\zeta = N + 0.026 \text{ m} = 25.026 \text{ m.}$$

7.9 Orthometric and normal corrections

In practical orthometric height calculations, one often starts by adding together the height differences ΔH measured by levelling (“staff-reading differences”) between points A and B as a *tentative* or crude height difference

$$\sum_A^B \Delta H,$$



after which the non-exactness of this method is accounted for by applying the “orthometric correction” (OC):

$$H_B = H_A + \sum_A^B \Delta H + OC_{AB}.$$

The fact that the difference in orthometric heights between two points A and B is not equal to the sum of the levelled height differences is due to gravity not being the same everywhere.

With C_A, C_B and ΔC the geopotential numbers at A and B, and the geopotential differences along the levelling line, we have $C_B - C_A - \sum_A^B \Delta C = 0$ because of the conservative nature of the geopotential. Dividing by a constant γ_0 yields

$$\frac{C_B}{\gamma_0} - \frac{C_A}{\gamma_0} - \sum_A^B \frac{\Delta C}{\gamma_0} = 0.$$

On the other hand, we have

$$OC_{AB} = H_B - H_A - \sum_A^B \Delta H = \frac{C_B}{\bar{g}_B} - \frac{C_A}{\bar{g}_A} - \sum_A^B \frac{\Delta C}{g},$$

with \bar{g}_A, \bar{g}_B average gravity values along the plumb lines of A and B and g gravity along the levelling line. In this expression, we compare $\sum_A^B \Delta H$, the naively calculated sum of levelled height differences, with the difference between the orthometric heights of the end points A and B, calculated according to the definition.

Subtraction yields

$$OC_{AB} - 0 = \left(\frac{C_B}{\bar{g}_B} - \frac{C_B}{\gamma_0} \right) - \left(\frac{C_A}{\bar{g}_A} - \frac{C_A}{\gamma_0} \right) - \sum_A^B \left(\frac{\Delta C}{g} - \frac{\Delta C}{\gamma_0} \right),$$

in which

$$\begin{aligned} \frac{C_B}{\bar{g}_B} - \frac{C_B}{\gamma_0} &= \left(\frac{\gamma_0 - \bar{g}_B}{\gamma_0} \right) \frac{C_B}{\bar{g}_B} = \left(\frac{\gamma_0 - \bar{g}_B}{\gamma_0} \right) H_B, \\ \frac{C_A}{\bar{g}_A} - \frac{C_A}{\gamma_0} &= \left(\frac{\gamma_0 - \bar{g}_A}{\gamma_0} \right) H_A, \\ \frac{\Delta C}{g} - \frac{\Delta C}{\gamma_0} &= \left(\frac{\gamma_0 - g}{\gamma_0} \right) \Delta H, \end{aligned}$$



yielding the *orthometric correction*

$$OC_{AB} = \sum_A^B \left(\frac{g - \gamma_0}{\gamma_0} \right) \Delta H + \left(\frac{\bar{g}_A - \gamma_0}{\gamma_0} \right) H_A - \left(\frac{\bar{g}_B - \gamma_0}{\gamma_0} \right) H_B, \quad (7.15)$$

which is identical to Heiskanen and Moritz's (1967) equation 4-33.

The choice of the constant γ_0 is arbitrary; it is wise to choose it close to the average gravity in the area of the levelling line AB, so as to keep the numerics small.

Similarly we may also calculate the *normal correction (NC)* in calculating normal heights. Start from the equation

$$NC_{AB} = H_B^* - H_A^* - \sum_A^B \Delta H = \frac{C_B}{\bar{\gamma}_B} - \frac{C_A}{\bar{\gamma}_A} - \sum_A^B \frac{\Delta C}{g}, \quad (7.16)$$

from which, as above, follows by subtraction:

$$NC_{AB} = \sum_A^B \left(\frac{g - \gamma_0}{\gamma_0} \right) \Delta H + \left(\frac{\bar{\gamma}_A - \gamma_0}{\gamma_0} \right) H_A^* - \left(\frac{\bar{\gamma}_B - \gamma_0}{\gamma_0} \right) H_B^*. \quad (7.17)$$

The identical first term in both equation 7.15 and equation 7.17 can be traced back to the term

$$\sum_A^B \frac{\Delta C}{g} = \sum_A^B \Delta H,$$

the naive summation of height differences ΔH in the case of both orthometric and normal correction, which is the generic basis of the concept of both corrections.

Equation 7.16 yields

$$H_B^* = H_A^* + \sum_A^B \Delta H + NC_{AB}.$$

What changes between the orthometric and normal corrections is the definition of heights: H^* instead of H , requiring division by the average of normal gravity along the plumb line $\bar{\gamma}$, not by that of true gravity \bar{g} .



Both the orthometric correction 7.15 and the normal correction 7.17 can be calculated one staff interval at a time: one must know, in addition to the levelled height difference ΔH , local gravity g along the levelling line. Furthermore one must know $g(H)$ or $\gamma(0)$ at both end points in order to calculate mean gravity \bar{g} or $\bar{\gamma}$ along the plumb lines of those end points. All this goes well with the equations given above. Remember that gravity g along the levelling line is needed in any case in order to reduce the individual levelled height differences ΔH to geopotential number differences ΔC . This reduction is part of the computation of both the orthometric and the normal correction.



7.10 A vision for the future: relativistic levelling

yleinen suhteellisuusteoria
metriikka

According to general relativity, the deeper a clock is inside the potential well of masses, the slower it ticks. This is most easily seen by looking at the Schwarzschild⁸ metric for a spherically symmetric field:

$$\begin{aligned} c^2 d\tau^2 &= \\ &= \left(1 - \frac{2GM}{c^2 r}\right) c^2 dt^2 - \left(1 - \frac{2GM}{c^2 r}\right)^{-1} dr^2 - r^2 (d\phi^2 + \cos^2 \phi d\lambda^2) = \\ &= \left(1 - \frac{2W}{c^2}\right) c^2 dt^2 - \left(1 - \frac{2W}{c^2}\right)^{-1} dr^2 - r^2 (d\phi^2 + \cos^2 \phi d\lambda^2), \end{aligned}$$

ominaisaika

in spherical co-ordinates plus time (ϕ, λ, r, t) . Here we see how the rate of proper time τ is slowed down compared to stationary co-ordinate time t (time at infinity $r \rightarrow \infty$), when the geopotential W increases closer to the mass. The slowing-down ratio is

$$\frac{\partial \tau}{\partial t} = \sqrt{1 - \frac{2W}{c^2}} \approx 1 - \frac{W}{c^2}.$$

⁸Karl Schwarzschild (1873–1916) was a German physicist who was the first to derive, in 1915 while serving on the Russian front, a closed spherically symmetric, non-rotating solution to the field equation of Albert Einstein's general theory of relativity, the *Schwarzschild metric*.



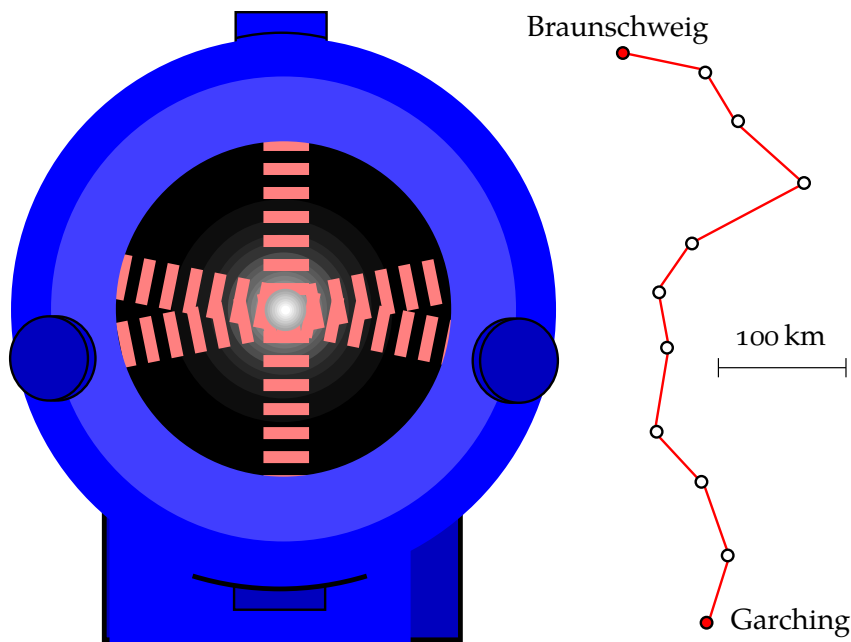


FIGURE 7.8. An optical lattice clock: the ultra-precise atomic clock of the future operates at optical wavelengths. To the right, the trajectory of the [Predehl et al. \(2012\)](#) experiment.

Now c^2 , the speed of light squared, is, in the units of daily life, a huge number: $10^{17} \text{ m}^2/\text{s}^2$. This means that measuring a potential difference of $1 \text{ m}^2/\text{s}^2$ — corresponding to a height difference of 10 cm — using this method, requires a precision of $1 : 10^{17}$. More traditional, microwave-based atomic clocks can do precisions of 10^{-12} – 10^{-14} ([Vermeer, 1983a](#)). With the new optical clocks, the objective should be achievable and relativistic levelling may become a reality.

The clock works in this way: an extremely cold, so-called Bose–Einstein condensate of atoms is trapped inside an optical lattice formed by six laser beams, an electromagnetic pattern of standing waves. The readout beam of the clock oscillation uses a different frequency. A Bose–Einstein condensate has the property that all atoms are in precisely the same quantum state — like the photons in an operating laser: their matter waves are *coherent*. In a way, all the atoms together act as one

valohila



virtual atom.

The condensate may consist of millions of atoms, and can actually be seen through the window of the vacuum chamber as a small plasma blob.

Unfortunately it is not enough that just one laboratory measures time to extreme precision. One has also to be able to *compare* the ticking rates of different clocks over geographical distances. For this, a solution has also been found: existing fibreoptic cables already in global use for Internet and telephony are useable for this with small modifications. The modifications concern the amplifiers in the cables at distances of some 100 km, which must be replaced by modified ones (Predehl et al., 2012). In this way, both the traditional precise levelling networks and the height systems based on GNSS technology and geoid determination may be replaced by this hi-tech (and hi-science!) solution.



Self-test questions

1. Why are heights calculated directly from levelled height differences not good enough as a height *system*?
2. What is a geopotential number?
3. What are orthometric heights?
4. What are normal heights?
5. What is the classical definition of the geoid?
6. What is a height anomaly?
7. What is the quasi-geoid?
8. Why might water sometimes flow in the “wrong” direction, to a greater height?
9. What is the telluroid?
10. What are the orthometric correction and the normal correction?



 **Exercise 7–1: Calculating orthometric heights**


The potential difference with sea level at point P, $-(W - W_0)$, equals $1000 \text{ m}^2/\text{s}^2$. Gravity at the point is $g_P = 9.820\,000 \text{ m}/\text{s}^2$. Calculate the orthometric height of the point. Aim for millimetre precision.

 **Exercise 7–2: Calculating normal heights**

At point P, the potential difference with sea level is

$$-(W - W_0) = 5000 \text{ m}^2/\text{s}^2.$$

Below the point at sea level, normal gravity is $\gamma_0 = 9.821\,500 \text{ m}/\text{s}^2$. Calculate the normal height of the point.

 **Exercise 7–3: Difference between orthometric and normal height**

At point P, the Bouguer anomaly is $\Delta g_B = -120 \text{ mGal}$. The orthometric height of the point is 1150 m.

1. Calculate the normal height of point P.
2. If the geoid height in point P is $N = 21.75 \text{ m}$, calculate the height anomaly ζ of the point.



The Stokes equation and other integral equations

8



8.1 The Stokes equation and the Stokes integral kernel

The following assumes a spherical Earth. By suitably combining the equations in section 5.3, one obtains at sea level

$$T = \sum_{n=2}^{\infty} T_n = R \sum_{n=2}^{\infty} \frac{\Delta g_n}{n-1},$$

with $T_n = T_n(\phi, \lambda)$ the degree constituents of the disturbing potential field $T = T(\phi, \lambda)$, and $\Delta g_n = \Delta g_n(\phi, \lambda)$ those of the gravity anomaly field. The summation starts from $n = 2$; for the degree numbers $n = 0, 1$, the Δg_n are assumed to vanish, as $\Delta g_0 \neq 0$ would mean a different total mass for the normal field than for the Earth, and $\Delta g_1 \neq 0$ an offset of the co-ordinate origin from the Earth's centre of mass, see section 3.4.

This is now the Stokes equation's *spectral form*.

Substituting into this degree constituent equation 3.8, one obtains the integral equation

$$\begin{aligned} T &= \frac{R}{4\pi} \sum_{n=2}^{\infty} \frac{2n+1}{n-1} \iint_{\sigma} \Delta g P_n(\cos \psi) d\sigma = \\ &= \frac{R}{4\pi} \iint_{\sigma} \left(\sum_{n=2}^{\infty} \frac{2n+1}{n-1} P_n(\cos \psi) \right) \Delta g d\sigma = \frac{R}{4\pi} \iint_{\sigma} S(\psi) \Delta g d\sigma, \end{aligned}$$

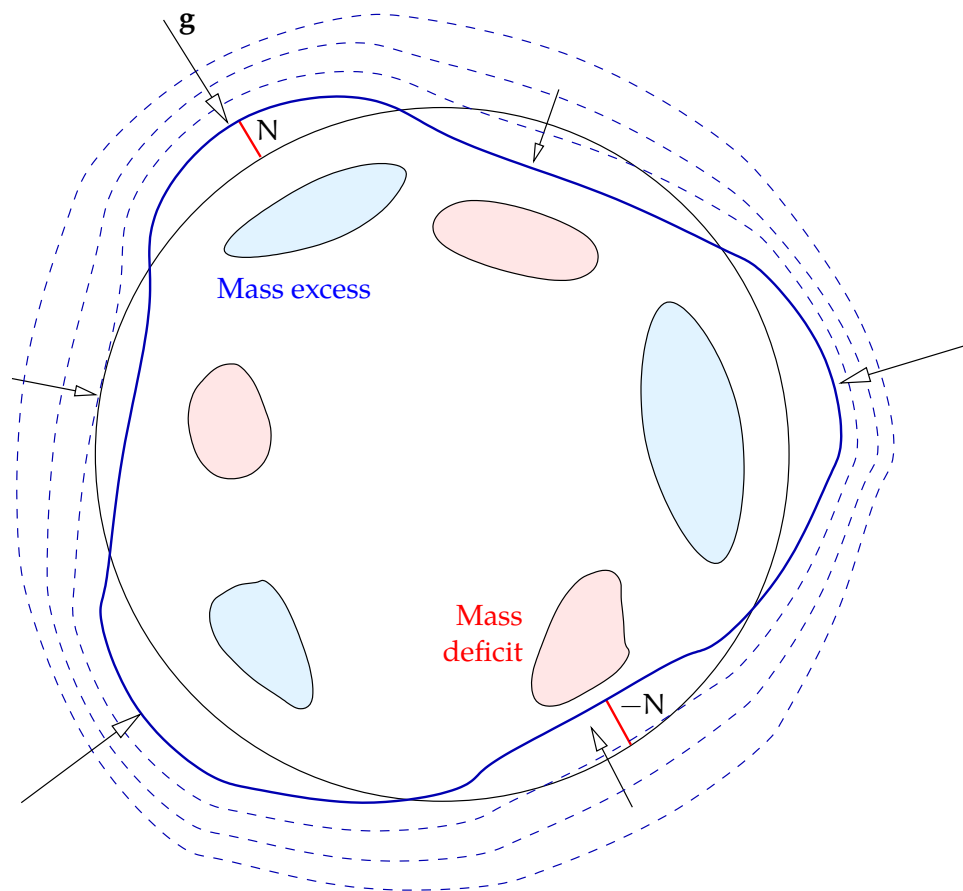


FIGURE 8.1. The principle of gravimetric geoid determination.

in which

$$S(\psi) = \sum_{n=2}^{\infty} \frac{2n+1}{n-1} P_n(\cos \psi),$$

the Stokes kernel function. The angle ψ is the geocentric angular distance between the evaluation point and moving observation point, see figure 8.2. The equation above allows the calculation, from global gravimetric data and for every point on the surface of the Earth sphere, of the disturbing potential T , and from that, the *geoid height* N using Bruns equation 5.2, $N = T/\gamma$. The result is



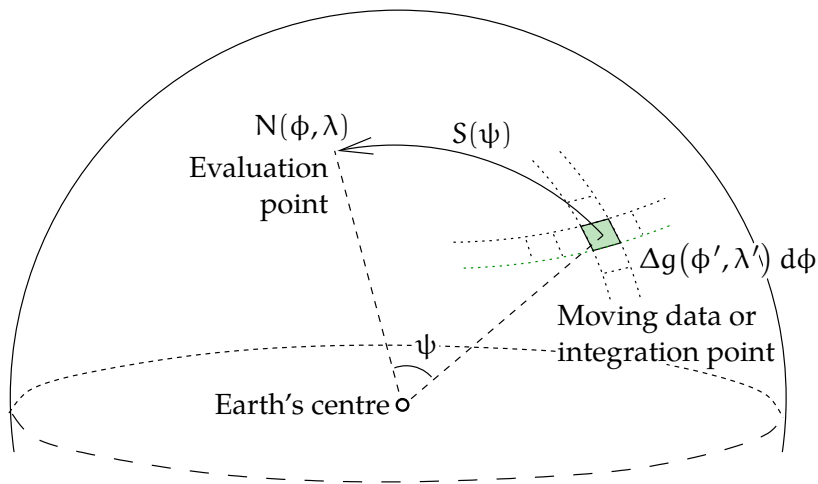


FIGURE 8.2. Integrating the Stokes equation geometrically.

$$N(\phi, \lambda) = \frac{T(\phi, \lambda)}{\gamma} = \frac{R}{4\pi\gamma} \iint_{\sigma} S(\psi) \Delta g(\phi', \lambda') d\sigma, \quad (8.1)$$

in which (ϕ, λ) and (ϕ', λ') are the evaluation point and the moving point (“data point”), respectively, and the angular distance between them is ψ . Equation 8.1 is the classical Stokes equation of gravimetric geoid determination.

The above illustrates the correspondence between integral equations and spectral expansions. There are other examples of this, like the spectral representation of the function $1/\ell$, equation 8.6, Heiskanen and Moritz’s (1967) equation 1-81. Of course $1/\ell$ is also the kernel function of an integral equation, the one yielding the potential V if the single-layer mass density κ is given.

A version of the Stokes equation for the *exterior space* also exists. We gave it earlier, equation 5.9. The spectral form of its kernel function is equation 5.10:

$$S(\psi, r, R) = \sum_{n=2}^{\infty} \left(\frac{R}{r}\right)^{n+1} \frac{2n+1}{n-1} P_n(\cos \psi).$$



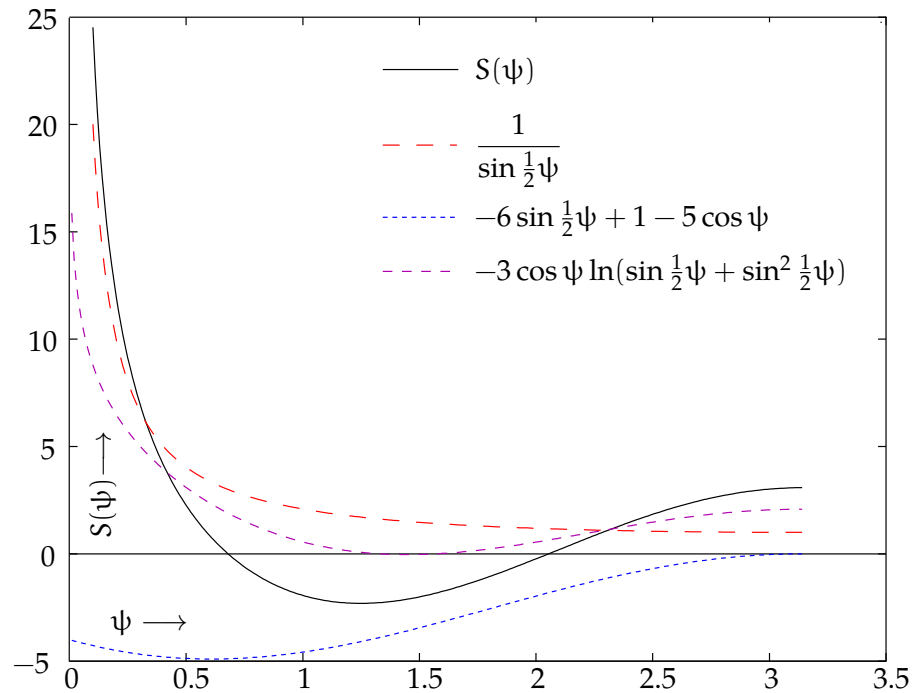


FIGURE 8.3. The Stokes kernel function $S(\psi)$. The argument ψ is in radians $[0, \pi)$. Also plotted are the three parts of analytical expression 8.2 with their different asymptotic behaviours.

The Stokes kernel function on the Earth's surface is depicted in figure 8.3, in which the angle ψ is in radians ($1 \text{ rad} \approx 57^\circ.29578$). The curve was calculated using the following closed expression (Heiskanen and Moritz, 1967, section 2-16, equation 2-164):

$$S(\psi) = \frac{1}{\sin \frac{1}{2}\psi} - 6 \sin \frac{1}{2}\psi + 1 - 5 \cos \psi - 3 \cos \psi \ln(\sin \frac{1}{2}\psi + \sin^2 \frac{1}{2}\psi). \quad (8.2)$$

This closed expression helps us to understand better how the function behaves close to the origin $\psi = 0$: the first term, $1/\sin \frac{1}{2}\psi$, goes to infinity when $\psi \rightarrow 0$. The next three terms, $-6 \sin \frac{1}{2}\psi + 1 - 5 \cos \psi$, are all bounded on the whole interval $[0, \pi)$ and the limit for $\psi \rightarrow 0$ is -4 . The last, complicated term $-3 \cos \psi \ln(\sin \frac{1}{2}\psi + \sin^2 \frac{1}{2}\psi)$ also goes to infinity — *positive* infinity! — for $\psi \rightarrow 0$, but much more slowly because



of the logarithm.

8.2 Example: The Stokes equation in polar co-ordinates

In section 2.3 we derived a general solution to the Laplace equation in two dimensions in polar co-ordinates. Below we develop a “toy” computational framework for gravimetric geoid determination in two dimensions, which allows us to do simple numerical simulations in order to get a feel for the behaviour of these things.

Firstly we derive the disturbing potential, gravity anomaly, and Stokes integral kernel for this solution, equation 2.3, assuming a normal potential $U(r) = a_0 + b_0 \ln r$.

- Disturbing potential:

$$\begin{aligned} T(\alpha, r) &= V_2(\alpha, r) - (a_0 + b_0 \ln r) = \\ &= \sum_{k=1}^{\infty} r^{-k} (a_k \cos k\alpha + b_k \sin k\alpha). \end{aligned}$$

- Normal gravity:

$$\gamma(r) = -\frac{\partial U}{\partial r} = -\frac{b_0}{r}.$$

- Normal gravity gradient:

$$\frac{\partial \gamma}{\partial r} = -\frac{\partial^2 U}{\partial r^2} = \frac{b_0}{r^2}.$$

- Gravity anomaly, equation 5.5:

$$\begin{aligned} \Delta g(\alpha, r) &= -\frac{\partial T}{\partial r} + \frac{T}{\gamma} \frac{\partial \gamma}{\partial r} = \\ &= \sum_{k=1}^{\infty} \frac{k}{r} r^{-k} (a_k \cos k\alpha + b_k \sin k\alpha) + \\ &\quad + \frac{1}{\gamma} \frac{\partial \gamma}{\partial r} \sum_{k=1}^{\infty} r^{-k} (a_k \cos k\alpha + b_k \sin k\alpha) = \end{aligned}$$



$$\begin{aligned}
&= \sum_{k=1}^{\infty} \left(\frac{k}{r} + \frac{1}{\gamma} \frac{\partial \gamma}{\partial r} \right) r^{-k} (a_k \cos k\alpha + b_k \sin k\alpha) = \\
&= \sum_{k=2}^{\infty} \frac{k-1}{r} r^{-k} (a_k \cos k\alpha + b_k \sin k\alpha).
\end{aligned}$$

We see that, if we write

$$T(\alpha, r) = \sum_{k=1}^{\infty} \left(\frac{R}{r} \right)^k T_k(\alpha), \quad T_k(\alpha) \stackrel{\text{def}}{=} R^{-k} (a_k \cos k\alpha + b_k \sin k\alpha),$$

it follows that

$$\begin{aligned}
\Delta g(\alpha, r) &= \sum_{k=2}^{\infty} \left(\frac{R}{r} \right)^{k+1} \Delta g_k(\alpha), \\
\Delta g_k(\alpha) &\stackrel{\text{def}}{=} (k-1) R^{-(k+1)} (a_k \cos k\alpha + b_k \sin k\alpha),
\end{aligned}$$

and, like in the case of spherical co-ordinates,

$$\Delta g_k(\alpha) = \frac{k-1}{R} T_k(\alpha). \quad (8.3)$$

According to Fourier theory, the basis functions $\cos k\alpha, \sin k\alpha$ are *orthonormal* on the circle $r = R$ when choosing the following integral as the scalar product:

$$\begin{aligned}
\frac{1}{\pi} \int_0^{2\pi} \cos k\alpha \cos m\alpha \, d\alpha &= \frac{1}{\pi} \int_0^{2\pi} \sin k\alpha \sin m\alpha \, d\alpha = \begin{cases} 0 & \text{if } k \neq m, \\ 1 & \text{if } k = m, \end{cases} \\
\frac{1}{\pi} \int_0^{2\pi} \cos k\alpha \sin m\alpha \, d\alpha &= 0 \text{ always.}
\end{aligned}$$

This means that, with

$$\Delta g(\alpha, R) = \sum_{k=2}^{\infty} \Delta g_k(\alpha),$$

we may decompose $\Delta g(\alpha)$ into its Fourier terms as follows:

$$\begin{aligned}
\Delta g_k(\alpha) &\stackrel{\text{def}}{=} (k-1) R^{-(k+1)} (a_k \cos k\alpha + b_k \sin k\alpha) = \\
&= \overbrace{(k-1) R^{-(k+1)} a_k}^{A_k} \cos k\alpha + \overbrace{(k-1) R^{-(k+1)} b_k}^{B_k} \sin k\alpha.
\end{aligned}$$



This yields the following Fourier coefficients:

$$\begin{Bmatrix} A_k \\ B_k \end{Bmatrix} = (k-1) R^{-(k+1)} \begin{Bmatrix} a_k \\ b_k \end{Bmatrix}, \quad k = 2, 3, \dots$$

and on the circle $r = R$ the expansion is

$$\Delta g(\alpha, R) = \sum_{k=2}^{\infty} \Delta g_k(\alpha) = \sum_{k=2}^{\infty} (A_k \cos k\alpha + B_k \sin k\alpha).$$

The substitutions

$$\begin{Bmatrix} a_k \\ b_k \end{Bmatrix} = \frac{R^{k+1}}{k-1} \begin{Bmatrix} A_k \\ B_k \end{Bmatrix}$$

yield

$$\begin{aligned} T(\alpha, R) &= \sum_{k=2}^{\infty} T_k(\alpha) = \sum_{k=2}^{\infty} R^{-k} (a_k \cos k\alpha + b_k \sin k\alpha) = \\ &= \sum_{k=2}^{\infty} R^{-k} \left(\frac{R^{k+1}}{k-1} A_k \cos k\alpha + \frac{R^{k+1}}{k-1} B_k \sin k\alpha \right) = \\ &= \sum_{k=2}^{\infty} \frac{R}{k-1} (A_k \cos k\alpha + B_k \sin k\alpha). \end{aligned}$$

Using the equations for the Fourier coefficients,

$$\begin{Bmatrix} A_k \\ B_k \end{Bmatrix} = \frac{1}{\pi} \int_0^{2\pi} \Delta g(\alpha, R) \begin{Bmatrix} \cos k\alpha \\ \sin k\alpha \end{Bmatrix} d\alpha,$$

and the cosine difference equation ([Wolfram Demonstrations, Difference formula for cosine](#)), we obtain

$$\begin{aligned} T(\alpha, R) &= \frac{1}{\pi} \cdot \\ &\cdot \sum_{k=2}^{\infty} \frac{R}{k-1} \left(\cos k\alpha \int_0^{2\pi} \Delta g(\alpha', R) \cos k\alpha' d\alpha' + \sin k\alpha \int_0^{2\pi} \Delta g(\alpha', R) \sin k\alpha' d\alpha' \right) = \\ &= \frac{1}{\pi} \sum_{k=2}^{\infty} \frac{R}{k-1} \int_0^{2\pi} \Delta g(\alpha', R) \cdot \cos(k(\alpha - \alpha')) d\alpha'. \end{aligned}$$



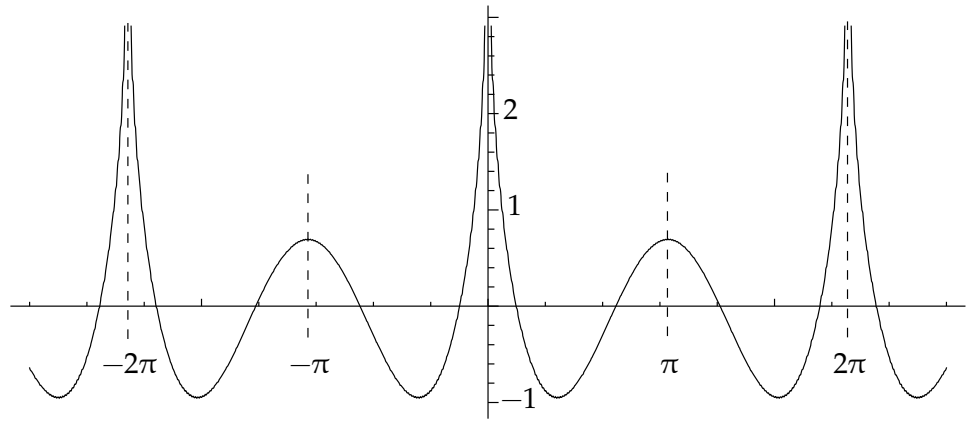


FIGURE 8.4. The Stokes kernel function on the circle $r = R$ in two-dimensional geometry. Note the symmetry and periodicity. Compare with the spherical Stokes kernel, figure 8.3.



Define the Stokes kernel for this two-dimensional situation:

$$N(\alpha) = \frac{T(\alpha, R)}{\gamma} = \frac{R}{\pi\gamma} \int_0^{2\pi} \Delta g(\alpha', R) S(\alpha - \alpha') d\alpha',$$

$$\text{with } S(\alpha - \alpha') \stackrel{\text{def}}{=} \sum_{k=2}^{\infty} \frac{\cos(k(\alpha - \alpha'))}{k-1}.$$

For small values of $\alpha - \alpha'$ we may approximate (Wolfram Functions, $\sum_{k=1}^{\infty} \frac{\cos kx}{k}$):

$$S(\alpha - \alpha') = \sum_{k'=1}^{\infty} \frac{\cos((k'+1)(\alpha - \alpha'))}{k'} \approx \sum_{k'=1}^{\infty} \frac{\cos(k'(\alpha - \alpha'))}{k'} =$$

$$= \frac{1}{2} \ln\left(\frac{1}{2(1 - \cos(\alpha - \alpha'))}\right) \approx -\ln(\alpha - \alpha').$$

More abstractly, we may also write relationship 8.3 in terms of the discrete Fourier transform and its inverse, as

$$\mathcal{F}\{\Delta g\} = \frac{k-1}{R} \mathcal{F}\{T\} \implies T = \mathcal{F}^{-1}\left\{\frac{R}{k-1} \mathcal{F}\{\Delta g\}\right\}.$$

Here, $\mathcal{F}\{f\}$ represents the Fourier transform of a function $f(\alpha)$ of spatial co-ordinate α on the circle, as a function of the spatial wave number (number of waves around the circle) k .





TABLEAU 8.1. Stokes equation in two dimensions, octave code.

```

% Stokes equation simulator in two dimensions
R = 6378137;
g = 9.8;
ak(1:180) = 0;
bk(1:180) = 0;
dg(1:360) = 0.0;
T(1:360) = 0.0;
for i=1:359
% Gauss-Markov
    dg(i+1) = 0.8*dg(i) + 50*(rand()-0.5);
end
dgsum = 0.0;
for i=1:360
    % Enforce circularity
    dg(i) = dg(i) - (dg(360) - dg(1)) * (i/359);
    dgsum = dgsum + dg(i);
end
for i = 1:360
    % Enforce zero expectation
    dg(i) = dg(i) - dgsum/360;
    for k = 2:180
        ak(k) = ak(k) + dg(i) * cos(k*i*pi/180)/180;
        bk(k) = bk(k) + dg(i) * sin(k*i*pi/180)/180;
    end
end
for i=1:360
    for k = 2:180
        T(i) = T(i) +(ak(k)*cos(k*i*pi/180)+bk(k)*sin(k*i*pi/180))*R/(k-1);
    end
end
hold on
plot(1:360, dg, 'b') plot(1:360, 0.00001*T/g, 'm')
print -dpdf stokes2D-out.pdf

```

This formulation has the merit of being able to use any standard **FFT** software library offering compatible versions of both the forward Fourier transform $\mathcal{F}\{\cdot\}$ and the inverse transform $\mathcal{F}^{-1}\{\cdot\}$.



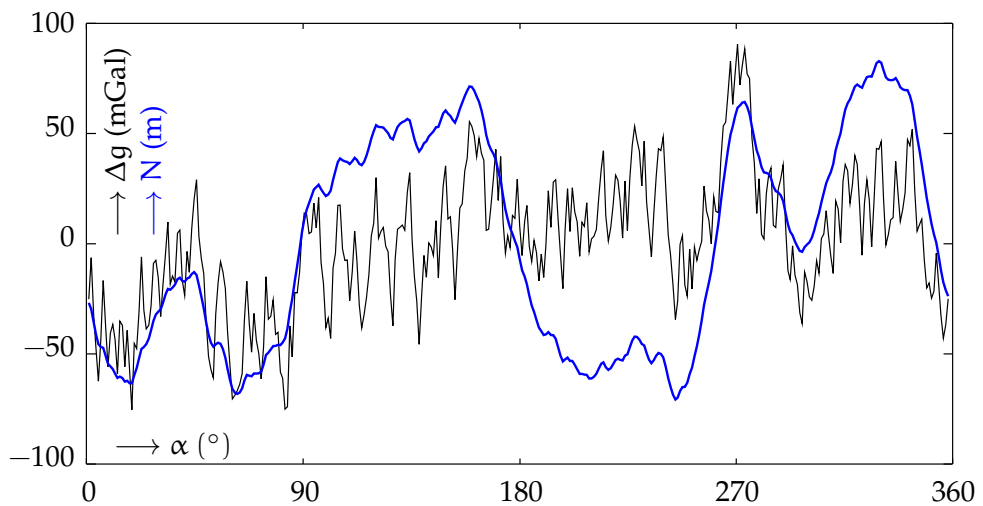


FIGURE 8.5. Simulation of gravity anomalies (Gauss–Markov process) and geoid undulations (blue) in two-dimensional geometry on the circle. Note the spectral behaviour of both.



For more about **FFT**, see appendix **C**.

In figure 8.5 we show a simulation result in which a randomly generated set of gravity anomalies on the circle $r = R$ has been used to calculate geoid undulations on the same circle. Both curves display fairly realistic statistical behaviour. The code used is given in tableau 8.1.



8.3 Plumb-line deflections and Vening Meinesz equations

By differentiating the Stokes equation with respect to place, we obtain integral equations for the components of the deflection of the plumb line (Heiskanen and Moritz, 1967, equation 2-210’):

$$\begin{Bmatrix} \xi \\ \eta \end{Bmatrix} = \frac{1}{4\pi\gamma} \iint_{\sigma} \Delta g \frac{dS(\psi)}{d\psi} \begin{Bmatrix} \cos \alpha \\ \sin \alpha \end{Bmatrix} d\sigma =$$



$$= \frac{1}{4\pi\gamma} \iint_{\sigma} \Delta g \frac{dS(\psi)}{d\psi} \begin{Bmatrix} \cos \alpha \\ \sin \alpha \end{Bmatrix} \cdot \sin \psi \, d\alpha \, d\psi, \quad (8.4)$$

in which ξ and η are the south-north and west-east direction deflections of the plumb line, and the unit-sphere surface element is $d\sigma = \sin \psi \, d\alpha \, d\psi$, in which $\sin \psi$ is Jacobi's determinant of the (ψ, α) co-ordinates.

These equations were derived for the first time by the Dutch geophysicist Vening Meinesz. The angle α is the azimuth or direction angle between the calculation or evaluation point (ϕ, λ) and the moving integration or observation point (ϕ', λ') . These equations are much harder to write in spectral form, as the kernel functions are now also functions of the azimuth direction α ; in other words, they are *anisotropic*.

The disturbing potential, the gravity disturbance, and the gravity anomaly, are all so-called *isotropic* quantities: they do not depend on the azimuth and therefore, in the spectral representation the transformations between them are functions of harmonic degree n only.

8.4 The Poisson integral equation

Look at figure 8.6. The point Q of the body is located at \mathbf{R} , and the observation point P at \mathbf{r} . The geocentric angular distance between the two location vectors, i.e., the angular distance as seen from the origin, is ψ . The distance between points P and Q is ℓ .

With the definitions $R \stackrel{\text{def}}{=} \|\mathbf{R}\|$ and $r \stackrel{\text{def}}{=} \|\mathbf{r}\|$, we may write (cosine rule):

$$\ell = \sqrt{r^2 + R^2 - 2rR \cos \psi}. \quad (8.5)$$

We may also write the function $1/\ell$ as the following expansion (Heiskanen and Moritz, 1967, equation 1-81):

$$\frac{1}{\ell} = \frac{1}{\sqrt{r^2 + R^2 - 2rR \cos \psi}} = \frac{1}{R} \sum_{n=0}^{\infty} \left(\frac{R}{r}\right)^{n+1} P_n(\cos \psi), \quad (8.6)$$



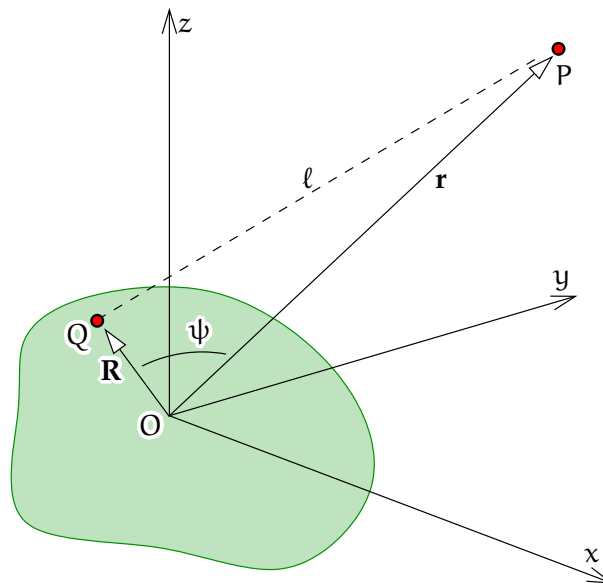


FIGURE 8.6. The geometry of the generating function of the Legendre polynomials.

in which r and R are the distances of points P and Q from the origin, the centre of the Earth. Function 8.6 is called the *generating function* of the Legendre polynomials.

Differentiating equation 8.6 with respect to r yields

$$-\frac{r - R \cos \psi}{\ell^3} = -\frac{1}{R} \sum_{n=0}^{\infty} \frac{n+1}{r} \left(\frac{R}{r}\right)^{n+1} P_n(\cos \psi).$$

This we multiply by $2r$:

$$-\frac{2r^2 - 2rR \cos \psi}{\ell^3} = -\frac{1}{R} \sum_{n=0}^{\infty} (2n+2) \left(\frac{R}{r}\right)^{n+1} P_n(\cos \psi).$$

Now we add together this equation and equation 8.6:

$$\frac{-2r^2 + 2rR \cos \psi + \ell^2}{\ell^3} = -\frac{1}{R} \sum_{n=0}^{\infty} (2n+1) \left(\frac{R}{r}\right)^{n+1} P_n(\cos \psi).$$

Substitute ℓ^2 from equation 8.5:

$$\frac{-2r^2 + 2rR \cos \psi + \ell^2}{\ell^3} = \frac{R^2 - r^2}{\ell^3},$$



and the result is, after multiplying with $-R$,

$$\frac{R(r^2 - R^2)}{\ell^3} = \sum_{n=0}^{\infty} (2n + 1) \left(\frac{R}{r}\right)^{n+1} P_n(\cos \psi). \quad (8.7)$$

Applying degree constituent equation 3.8 to the harmonic potential field V on the spherical Earth's surface, radius R :

$$V_n(\phi, \lambda) = \frac{2n + 1}{4\pi} \iint_{\sigma} V(\phi', \lambda', R) P_n(\cos \psi) d\sigma',$$

as well as the spectral expansion of the field in space 3.9:

$$V(\phi, \lambda, r) = \sum_{n=0}^{\infty} \left(\frac{R}{r}\right)^{n+1} V_n(\phi, \lambda),$$

we obtain

$$\begin{aligned} V(\phi, \lambda, r) &= \\ &= \frac{1}{4\pi} \sum_{n=0}^{\infty} \left(\frac{R}{r}\right)^{n+1} (2n + 1) \iint_{\sigma} V(\phi', \lambda', R) P_n(\cos \psi) d\sigma' = \\ &= \frac{1}{4\pi} \iint_{\sigma} V(\phi', \lambda', R) \left[\sum_{n=0}^{\infty} (2n + 1) \left(\frac{R}{r}\right)^{n+1} P_n(\cos \psi) \right] d\sigma' = \\ &= \frac{1}{4\pi} \iint_{\sigma} \frac{R(r^2 - R^2)}{\ell^3} V(\phi', \lambda', R) d\sigma' \end{aligned}$$

by replacing the expression in square brackets by equation 8.7.

Thus we have obtained the Poisson equation for computing a harmonic field V from values given on the Earth's surface:

$$V_P = \frac{1}{4\pi} \iint_{\sigma} \frac{R(r^2 - R^2)}{\ell^3} V_Q d\sigma_Q, \quad (8.8)$$

in which ℓ is again the straight-line distance between evaluation point P (where V_P is being computed) and moving data point Q (on the surface of the sphere, V_Q under the integral sign). In this equation we have



given the points symbolic names: the co-ordinates of evaluation point P are (ϕ, λ, r) , the co-ordinates of data point Q are (ϕ', λ', R) .

Still a third way to write the same equation, useful when the function or field V is not actually defined between the topographic Earth's surface and sea level, is

$$V = \frac{1}{4\pi} \iint_{\sigma} \frac{R (r^2 - R^2)}{\ell^3} V^* d\sigma.$$

Here, V^* denotes the value of a *harmonically downwards continued* function V — downwards continued into the topography, all the way down to sea level, or, in spherical approximation, to the surface of the sphere $r = R$. This is a function that above the topography is identical to V, is harmonic, and exists also between the topography and sea level. The question of the existence of such a function has been a classical theoretical nut to crack. . .

Equation 8.8 solves for this special case the so-called *Dirichlet boundary-value problem*, finding a harmonic function in an area of space when the value of the function on the boundary of the area has been given.



8.5 Gravity anomalies in the exterior space

The equation derived in section 8.4, equation 8.8, applies for an arbitrary *harmonic* field V, i.e., any field for which $\Delta V = 0$. The equation applies conveniently to the expression $r\Delta g$, the gravity anomaly multiplied by the geocentric radius, which is also a harmonic field. This is how we can express the gravity anomaly in the external space $\Delta g(\phi, \lambda, r)$ as a function of gravity anomalies $\Delta g(\phi', \lambda', R)$ on a reference sphere of radius R. The function $r\Delta g$ is harmonic, because according to equation 5.8

$$\Delta g = \frac{1}{r} \sum_{n=2}^{\infty} (n-1) \left(\frac{R}{r}\right)^{n+1} T_n,$$

so

$$r\Delta g = \sum_{n=2}^{\infty} \left(\frac{R}{r}\right)^{n+1} (n-1) T_n = \sum_{n=2}^{\infty} \left(\frac{R}{r}\right)^{n+1} T'_n,$$



in which $T'_n(\phi, \lambda) = (n - 1) T_n(\phi, \lambda)$ is a perfectly legal surface spherical harmonic just like $T_n(\phi, \lambda)$ itself. Also, the dependence on the radius r , the factor $(R/r)^{n+1}$, is the same as for the (harmonic) potential. So, Poisson's integral equation 8.8 applies to function $r\Delta g$:

$$[r\Delta g(\phi, \lambda, r)] = \frac{1}{4\pi} \iint_{\sigma} \frac{R (r^2 - R^2)}{\ell^3} [R\Delta g(\phi', \lambda', R)] d\sigma'$$

or

$$\Delta g(\phi, \lambda, r) = \frac{1}{4\pi} \iint_{\sigma} \frac{R R (r^2 - R^2)}{r \ell^3} \Delta g(\phi', \lambda', R) d\sigma'. \quad (8.9)$$

An alternative notation is

$$\Delta g = \frac{1}{4\pi} \iint_{\sigma} \frac{R R (r^2 - R^2)}{r \ell^3} \Delta g^* d\sigma,$$

in which Δg^* denotes the gravity anomaly at sea level, again calculated by *harmonic downwards continuation* of the exterior field, in this case the expression $r\Delta g$.

From equation 8.9 we may lift the closed form of the kernel:

$$K(\ell, r, R) = \frac{R R (r^2 - R^2)}{r \ell^3},$$

with which

$$\Delta g(\phi, \lambda, r) = \frac{1}{4\pi} \iint_{\sigma} K(r, \psi, R) \Delta g(\phi', \lambda', R) d\sigma'.$$

Using the approximation $r + R \approx 2r$ still yields

$$\Delta g(\phi, \lambda, r) \approx \frac{1}{2\pi} \iint_{\sigma} R^2 \frac{r - R}{\ell^3} \Delta g(\phi', \lambda', R) d\sigma'.$$

Alternatively, we derive the *spectral form*:

$$\Delta g = \frac{1}{r} \sum_{n=2}^{\infty} \left(\frac{R}{r}\right)^{n+1} (n - 1) T_n(\phi, \lambda) = \sum_{n=2}^{\infty} \left(\frac{R}{r}\right)^{n+2} \Delta g_n(\phi, \lambda).$$



Degree constituent equation 3.8 gives the functions Δg_n :

$$\Delta g_n(\phi, \lambda) = \frac{2n+1}{4\pi} \iint_{\sigma} \Delta g(\phi', \lambda', R) P_n(\cos \psi) d\sigma',$$

with the aid of which

$$\begin{aligned} \Delta g &= \frac{1}{4\pi} \sum_{n=2}^{\infty} \left(\frac{R}{r}\right)^{n+2} (2n+1) \iint_{\sigma} \Delta g(\phi', \lambda', R) P_n(\cos \psi) d\sigma' = \\ &= \frac{1}{4\pi} \iint_{\sigma} \left(\sum_{n=2}^{\infty} \left(\frac{R}{r}\right)^{n+2} (2n+1) P_n(\cos \psi) \right) \Delta g(\phi', \lambda', R) d\sigma' = \\ &= \frac{1}{4\pi} \iint_{\sigma} K_{\text{mod}} \Delta g(\phi', \lambda', R) d\sigma', \end{aligned}$$

in which

$$K_{\text{mod}}(\psi, r, R) \stackrel{\text{def}}{=} \sum_{n=2}^{\infty} \left(\frac{R}{r}\right)^{n+2} (2n+1) P_n(\cos \psi)$$

is the modified spectral version of the Poisson kernel for gravity anomalies. From this kernel, the constituents of degree number 0 and 1 have been removed, see Heiskanen and Moritz (1967, equation 2-159).

Compared to the Stokes kernel, the Poisson kernel drops off fast to zero for growing values of ℓ . In other words, the evaluation of the kalotti integral equation may be restricted to a very local area, like a cap of radius 1° . See figure 8.7. The main use of Poisson's kernel is the *harmonic continuation*, upwards or downwards, of gravity anomalies measured and computed at various levels, shifting them to the same reference level.

In the limit $r \rightarrow R$ (sea level becomes the level of evaluation), this kernel function goes asymptotically to the Dirac δ function.

8.6 The vertical gradient of the gravity anomaly

Differentiate an equation obtained from equations 5.7 and 5.8:

$$\Delta g = \sum_{n=2}^{\infty} \left(\frac{R}{r}\right)^{n+2} \Delta g_n \implies \frac{\partial \Delta g}{\partial r} = -\frac{1}{R} \sum_{n=2}^{\infty} \left(\frac{R}{r}\right)^{n+3} (n+2) \Delta g_n.$$



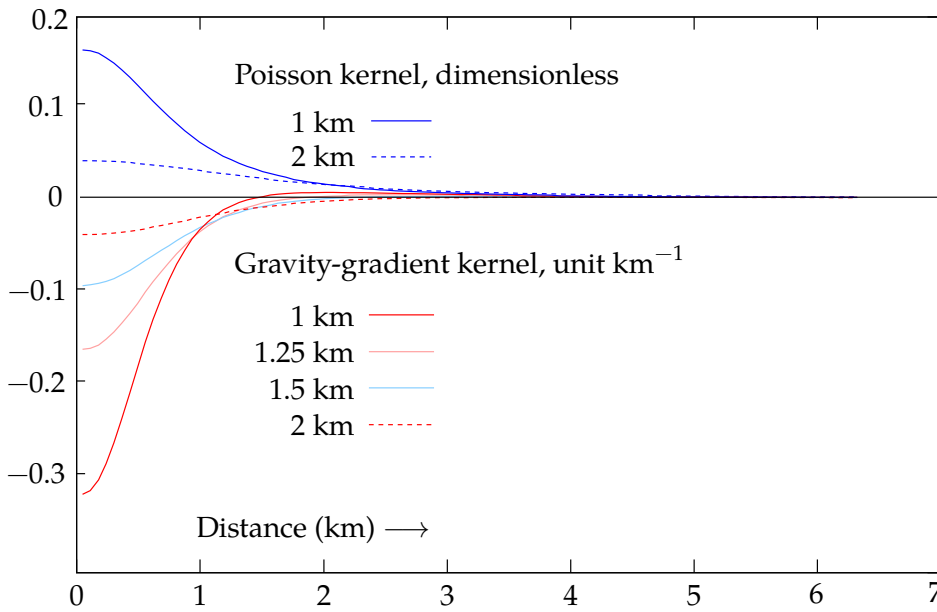


FIGURE 8.7. The Poisson kernel function for gravity anomalies as well as the kernel for the anomalous vertical gravity gradient, both at various height levels. These kernels are used when evaluating the surface integral in map co-ordinates x, y in kilometres.

This equation is exact in spherical approximation. Its kernel function is well *localised*, in other words, it drops off to zero very fast. For calculation, a small “cap” also suffices here.

Δg_n is expressed, using degree constituent equation 3.8, as an integral over the anomaly field at sea level:


$$\Delta g_n(\phi, \lambda) = \frac{2n+1}{4\pi} \iint_{\sigma} \Delta g(\phi', \lambda', R) P_n(\cos \psi) d\sigma',$$

so

$$\left| \frac{\partial \Delta g(\phi, \lambda, r)}{\partial r} = -\frac{1}{4\pi R} \sum_{n=2}^{\infty} \left(\frac{R}{r}\right)^{n+3} (2n+1)(n+2) \iint_{\sigma} \Delta g(\phi', \lambda', R) P_n(\cos \psi) d\sigma' = \right.$$

$$\left. = \frac{1}{4\pi R} \iint_{\sigma} K'(\psi, r, R) \Delta g(\phi', \lambda', R) d\sigma', \quad (8.10) \right.$$



 TABLEAU 8.2. Derivation of the kernel for the vertical gradient of gravity anomaly.

$$\begin{aligned}
\frac{\partial \Delta g(\phi, \lambda, r)}{\partial r} &= \frac{R^2}{4\pi} \frac{\partial}{\partial r} \left(\iint_{\sigma} \frac{1}{r} \frac{r^2 - R^2}{(r^2 + R^2 - 2rR \cos \psi)^{3/2}} \Delta g(\phi', \lambda', R) \, d\sigma' \right) = \\
&= \frac{R^2}{4\pi} \iint_{\sigma} \frac{1}{\ell^3} \left(2 - \frac{r^2 - R^2}{r^2} - \frac{3(2r - 2R \cos \psi)(r^2 - R^2)}{2r\ell^2} \right) \Delta g(\phi', \lambda', R) \, d\sigma' = \\
&= \frac{R^2}{4\pi} \iint_{\sigma} \frac{1}{\ell^3} \left(2 - \frac{3(\ell^2 + r^2 - R^2)(r^2 - R^2)}{2r^2\ell^2} \right) \Delta g(\phi', \lambda', R) \, d\sigma' - \\
&\quad - \frac{1}{r} \cdot \frac{1}{4\pi} \iint_{\sigma} \frac{R}{r} \frac{R(r^2 - R^2)}{\ell^3} \Delta g(\phi', \lambda', R) \, d\sigma' = \\
&= \frac{R^2}{4\pi} \iint_{\sigma} \frac{1}{\ell^3} \left(2 - \frac{3(r^2 - R^2)}{2r^2} - \frac{3(r^2 - R^2)(r^2 - R^2)}{2r^2\ell^2} \right) \Delta g(\phi', \lambda', R) \, d\sigma' - \frac{1}{r} \Delta g(\phi, \lambda, r) = \\
&= \frac{R^2}{4\pi} \iint_{\sigma} \frac{1}{\ell^3} \left(2 - \frac{3(r^2 - R^2)^2}{2r^2\ell^2} \right) \Delta g(\phi', \lambda', R) \, d\sigma' - \left(\frac{1}{r} + \frac{3}{2r} \right) \Delta g(\phi, \lambda, r), \\
&= \frac{R^2}{4\pi} \iint_{\sigma} \frac{1}{\ell^3} \left[2 - \frac{3(r^2 - R^2)^2}{2r^2\ell^2} \right] \Delta g(\phi', \lambda', R) \, d\sigma' - \frac{5}{2r} \Delta g(\phi, \lambda, r). \quad (8.11)
\end{aligned}$$

in which the kernel function is now

$$K'(\psi, r, R) = - \sum_{n=2}^{\infty} \left(\frac{R}{r} \right)^{n+3} (2n+1)(n+2) P_n(\cos \psi).$$

Alternatively, we derive a closed expression. We start from Poisson equation 8.9 for gravity anomalies, and differentiate¹ with respect to r . See tableau 8.2.

In the result, the last term is small, of an order of less than one part in a thousand, compared to the preceding term.

The terms inside the square brackets require their own consideration. In the local zone $\ell \approx r - R$ the terms are of the same order of magnitude;

¹Hint: use symbolic algebra software.



the second term goes however rapidly to zero for $\ell \gg r - R$. This means that the contribution of the second term to the integral will be only of order $(r - R)^2 / R^2$ times, or less than a millionth part of, that of the first term. We may thus write

$$\frac{\partial \Delta g(\phi, \lambda, r)}{\partial r} \approx \frac{R^2}{2\pi} \iint_{\sigma} \frac{\Delta g(\phi', \lambda', R)}{\ell^3} d\sigma' - \frac{5}{2r} \Delta g(\phi, \lambda, r). \quad (8.12)$$

This equation will only behave well for $r > R$: for $r \rightarrow R$ the kernel function $1/\ell^3$ will go to infinity for $\psi \rightarrow 0$. Regularisation can be done by observing that a globally constant gravity anomaly field

$$\widetilde{\Delta g}_0(\phi, \lambda, r) = \widetilde{\Delta g}_0(r) = \left(\frac{R}{r}\right)^2 \Delta g_0$$

has a gradient of

$$\frac{\partial \widetilde{\Delta g}_0(\phi, \lambda, r)}{\partial r} = -\frac{2}{r} \widetilde{\Delta g}_0(\phi, \lambda, r), \quad (8.13)$$

but also, like equation 8.12:

$$\frac{\partial \widetilde{\Delta g}_0(\phi, \lambda, r)}{\partial r} \approx \frac{R^2}{2\pi} \iint_{\sigma} \frac{\widetilde{\Delta g}_0(\phi, \lambda, r)}{\ell^3} d\sigma' - \frac{5}{2r} \widetilde{\Delta g}_0(\phi, \lambda, r). \quad (8.14)$$

Subtract equation 8.14 from equation 8.12 and substitute equation 8.13, yielding

$$\begin{aligned} \frac{\partial \Delta g(\phi, \lambda, r)}{\partial r} &= \frac{\partial (\Delta g(\phi, \lambda, r) - \widetilde{\Delta g}_0(\phi, \lambda, r))}{\partial r} + \frac{\partial \widetilde{\Delta g}_0(\phi, \lambda, r)}{\partial r} = \\ &= \frac{R^2}{2\pi} \iint_{\sigma} \frac{\Delta g(\phi', \lambda', R) - \widetilde{\Delta g}_0(\phi', \lambda', R)}{\ell^3} d\sigma' - \\ &\quad - \frac{5}{2r} (\Delta g(\phi, \lambda, r) - \widetilde{\Delta g}_0(\phi, \lambda, r)) - \frac{2}{r} \widetilde{\Delta g}_0(\phi, \lambda, r) = \\ &= \frac{R^2}{2\pi} \iint_{\sigma} \frac{\Delta g(\phi', \lambda', R) - \Delta g_0}{\ell^3} d\sigma' - \\ &\quad - \frac{5}{2r} \left(\Delta g(\phi, \lambda, r) - \left(\frac{R}{r}\right)^2 \Delta g_0 \right) - \frac{2}{r} \left(\frac{R}{r}\right)^2 \Delta g_0. \end{aligned}$$



Choose the constant $\Delta g_0 \stackrel{\text{def}}{=} \Delta g(\phi, \lambda, r)$, the anomaly in the evaluation point:

$$\begin{aligned} \frac{\partial \Delta g(\phi, \lambda, r)}{\partial r} &= \frac{R^2}{2\pi} \iint_{\sigma} \frac{\Delta g(\phi', \lambda', R) - \Delta g(\phi, \lambda, r)}{\ell^3} d\sigma' - \\ &\quad - \frac{5}{2r} \left(1 - \left(\frac{R}{r}\right)^2\right) \Delta g(\phi, \lambda, r) - \frac{2}{r} \left(\frac{R}{r}\right)^2 \Delta g(\phi, \lambda, r) \approx \\ &\approx \frac{R^2}{2\pi} \iint_{\sigma} \frac{\Delta g(\phi', \lambda', R) - \Delta g(\phi, \lambda, r)}{\ell^3} d\sigma' - \frac{2}{r} \left(\frac{R}{r}\right)^2 \Delta g(\phi, \lambda, r). \end{aligned} \quad (8.15)$$

This corresponds to [Heiskanen and Moritz \(1967, equation 2-217\)](#). For well-behaved gravity anomalies, the integrand will now be well-behaved also when $r \rightarrow R$.

If we are integrating over the surface of a spherical Earth of radius R rather than the unit sphere σ of radius 1, the factor R^2 drops out from equations [8.9](#), [8.11](#), [8.12](#) and [8.15](#).

In Molodensky's method this or similar equations can be rapidly evaluated from very local gravimetric data.

The closed expression given in [Heiskanen and Moritz \(1967, expression 2-217\)](#), is the anomalous vertical gravity gradient evaluated at sea level (on the reference sphere). In our equations [8.15](#) and [8.10](#) we also need gravity anomalies at sea level. However, anomalies at the *topographic surface* level are available. In practice, we may proceed iteratively, by initially assuming that the anomaly values observed at topography level *are* at sea level:

$$\Delta g^{(0)}(\phi', \lambda', R) \approx \Delta g(\phi', \lambda', r) = \Delta g(\phi', \lambda', R + H),$$

in which $H = H(\phi', \lambda')$ is the topographic height at point (ϕ', λ') . When a crude anomalous gradient has been calculated, for example using equation [8.15](#), we may perform a real *reduction to sea level*, in linear approximation:

$$\Delta g^{(1)}(\phi', \lambda', R) \approx \Delta g(\phi', \lambda', r) - \left. \frac{\partial \Delta g^{(0)}}{\partial z} \right|_{z=r} H.$$

This may be iterated.



8.7 Gravity reductions in geoid determination

8.7.1 Classical methods

Use of the Stokes equation for gravimetric geoid determination presupposes that all masses are *inside the geoid* — and that the exterior field is thus harmonic. For this reason we move the topographic masses computationally to inside the geoid, in a way that needs to be specified. The classical methods for this are

- Helmert's (second) condensation method, section 6.5: the masses are shifted vertically down to the geoid into a surface density layer. After this, shifting gravity down from the topographic surface to sea level is easy. The indirect effect (the effect of the mass shifts on the geoid, the “restore” step) is small.
- Isostatic reduction, in which the effects of both the topography and its compensation, the “roots” of mountains below sea level, are computationally removed. The indirect effect of this method is larger. See section 6.7 and equation 6.8.
- Bouguer reduction, section 6.2: the effect of the topographic masses is brutally removed from the observed gravity data, and, after geoid calculation, it is equally brutally restored to the result. Bouguer anomalies contain large negative biases in the mountains and therefore, the indirect effect of Bouguer reduction is excessive and extends over a large area. This is why Bouguer reduction is used more rarely.

8.7.2 The residual terrain modelling method

Imagine that, conceptually, the topographic masses are shifted to below the geoid in a way that *does not change the exterior field*. This is materially the same as determining the geoid associated with the *harmonically downwards continued exterior field*.

The problem here is that such a mass distribution below sea level



which produces the harmonically downwards continued external potential in the space between topographic surface and geoid does not always precisely exist. Or that a suitable mass distribution exists but contains extremely large positive and negative masses close to each other, which is physically unrealistic.

huonosti asetettu One expresses this by saying that the problem is “*ill-posed*”. In such cases, one uses *regularisation*: one changes the exterior field a little — as little as possible, so that it becomes a sensible field that *can* be harmonically continued below the topographic surface. Then, some sensible mass distribution interior to the geoid producing this field will also exist.

One can start, for example, by filtering out the short-wave parts caused by the topography using a high-resolution digital terrain model. This is called the **RTM** (residual terrain modelling) method.

puskutraktori In this method, we do not actually move all topographic masses to below the geoid. Instead, we use a bulldozer technique, figure 8.8: only masses close to the topographic surface are either removed or filled in, in a way that creates a smooth replacement topography that is long-wavelength only. The exterior field of this smoothed topography, unlike that of the original topography, lacks the shortest wavelengths. It may thus be downwards continued to the geoid with sufficient precision.

First, we computationally remove from the topography *only* the short wavelengths (under 30 km) by moving the masses of the peaks into the valleys: a low-pass filtering. The effect of this on the free-air gravity anomalies Δg calculated from measurements is evaluated and taken into account: the “remove” step.

In detail:

1. At each point P we apply the *terrain correction* to the gravity anomalies as described in section 6.3.
2. Next, we remove the attraction of a Bouguer plate of thickness $H - H_{\text{RTM}}$, in which H stands for the terrain height of point P , and



H_{RTM} for the height of the smoothed, or low-pass filtered, terrain at the location of point P. This effect is, according to equation 6.1, equal to

$$2\pi G\rho (H - H_{\text{RTM}}),$$

in which ρ is the rock density assumed in the calculation.

3. After this, the *location* of the gravity anomaly is moved down (or up!) — “downwards continuation” — from the original terrain level H to the surface of the new, smoothed terrain, H_{RTM} . Equation 8.15 for the vertical gradient of the free-air gravity anomaly may be used for this.

If this anomalous vertical gradient is small, meaning that the vertical gravity gradient of the terrain-reduced external field equals the vertical gradient of normal gravity — according to section 5.4, -0.3 mGal/m — this operation will leave the anomaly unchanged. Typically, there will be a change: one may show — exercise 1-1 item 4 — that on the surface of a buried sphere of anomalous density $\Delta\rho$, there will be a radial anomalous gravity gradient of $\frac{8}{3}\pi G\Delta\rho$. For $\Delta\rho \ll \rho$, this will be negligible compared to the Bouguer-plate coefficient in item 2.

4. Rigorously speaking, an inverse terrain correction for the shapes of the smoothed terrain should be applied, to arrive at gravity anomalies realistic for this new replacement topography. Often this step is left out as the effect is small.
5. After that, harmonic downwards continuation of the exterior field succeeds: almost only long wavelengths are left in the exterior field.

Because the mass shifts in the **RTM** method are so small, take place over such small distances, and are of such a short wavelength in nature, the *indirect effect* or “restore” step — the change in geopotential due to the mass shifts that has to be applied in reverse to arrive at the final geopotential or geoid solution — is so small as to often be negligible.



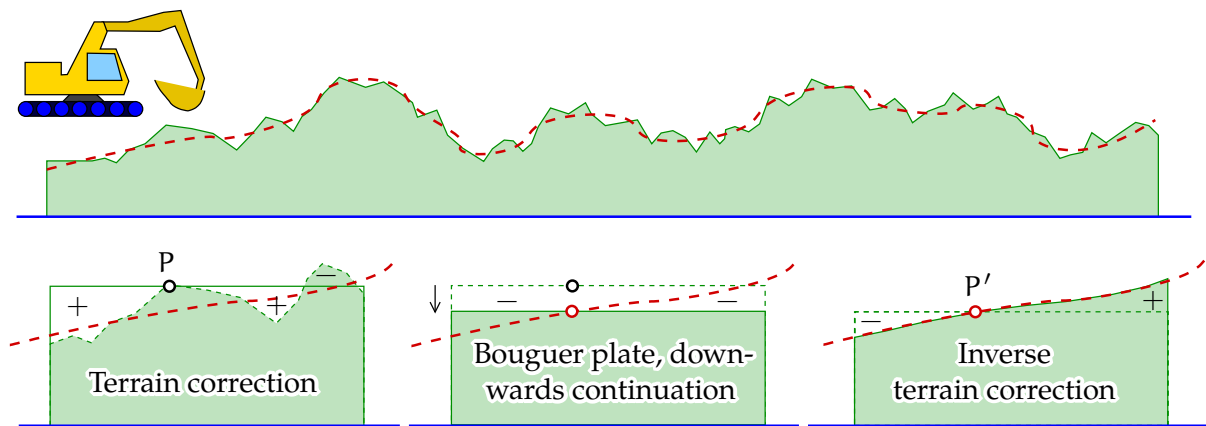


FIGURE 8.8. Residual terrain modelling (RTM). One removes the short wavelengths, i.e., the differences from the red dashed line, from the terrain computationally: the masses rising above it are removed, the valleys below it are filled. After reduction, the red line, smoother than the original terrain, is the new terrain surface. The exterior potential of the new mass distribution will differ only little from the original one, but may be harmonically downwards continued to sea level.

Left, terrain correction for point P, middle, Bouguer-plate and gradient reduction to the level of smoothed terrain point P', and right, the inverse terrain correction for point P'.



For the same reason, the effect of unknown topographic density will also remain small.

Finally we note that, because the RTM method removes the effect of the short-wavelength topography, it is also a suitable method for *interpolating* gravity anomalies. See Märdla (2017).



8.7.3 Downwards continuation in linear approximation

The approach described above can, following Molodensky, be *linearised*:

$$T(\phi, \lambda, H) = \frac{R}{4\pi} \iint_{\sigma} \left(\Delta g(\phi', \lambda', H') - \frac{\partial \Delta g}{\partial z} \Big|_{z=H'} \right) S(\psi) d\sigma' +$$



$$+ \left. \frac{\partial T}{\partial z} \right|_{z=H} H. \quad (8.16)$$

So, first we reduce the Δg measured and calculated at the topographic surface to sea level using the gradient of the anomalies and the terrain height H' of the measurement point, with the result

$$\Delta g^* = \Delta g - \left. \frac{\partial \Delta g}{\partial z} \right|_{z=H'} H'.$$

After this, we apply, at sea level, the Stokes equation, and obtain the disturbing potential at sea level T^* . After this, the disturbing potential is “unreduced” back to terrain level, to the evaluation point, with the equation

$$T = T^* + \left. \frac{\partial T}{\partial z} \right|_{z=H} H.$$

In these equations T , its vertical derivative $\frac{\partial}{\partial H} T$, Δg , and *its* vertical derivative $\frac{\partial}{\partial H} \Delta g$ always belong to the *exterior* harmonic gravity field. The connection between them is the fundamental equation of physical geodesy, equation 5.6, in spherical geometry

$$\Delta g = -\frac{\partial T}{\partial r} - \frac{2}{r} T,$$

in which $r = R + H$. Here, we need firstly the vertical derivative of the disturbing potential. This is easy: we have

$$\frac{\partial T}{\partial H} = \frac{\partial T}{\partial r} = -\Delta g - \frac{2}{r} T,$$

where the first term on the right is directly measured, and the second term’s T is obtained iteratively from the main product of the solution process.

Calculating the vertical gradient of gravity anomalies, i.e., the *anomalous vertical gradient of gravity*, is harder. For this task, section 8.6 offers calculation options. Luckily for practical calculations, the kernels of the integral equations are very localised and one does not need gravity anomalies from a very large area.



8.7.4 The evaluation point as the reference level

In the above equation 8.16 we used as the *reference level* the sea surface. This is arbitrary: we may use whatever reference level, for example H_0 , in which case

$$\begin{aligned} T(\phi, \lambda, H) &= \\ &= \frac{R + H_0}{4\pi} \iint_{\sigma} \left(\Delta g(\phi', \lambda', H') - \frac{\partial \Delta g}{\partial z} \Big|_{z=H'} (H' - H_0) \right) S(\psi) d\sigma' + \\ &\quad + \frac{\partial T}{\partial z} \Big|_{z=H} (H - H_0). \end{aligned}$$

If we now choose $H_0 = H$, the last term drops off, and we obtain

$$\begin{aligned} T(\phi, \lambda, H) &= \\ &= \frac{R + H}{4\pi} \iint_{\sigma} \left(\Delta g(\phi', \lambda', H') - \frac{\partial \Delta g}{\partial z} \Big|_{z=H'} (H' - H) \right) S(\psi) d\sigma'. \end{aligned}$$

In this case, the reduction takes place from the height of the Δg measurement point to the height of the T evaluation point. This is likely to be a shorter distance than from sea level to evaluation height, especially in the immediate surroundings of the evaluation point. This means that the *linearisation error will remain smaller*.² What is bad, on the other hand, is that the expression in parentheses is now different for each evaluation point. This complicates the use of FFT-based computation techniques, on which more later.

Here, we were all the time discussing the determination of the *disturbing potential* $T(\phi, \lambda, H)$; this is in practice the same as determining the *height anomaly*

$$\zeta(\phi, \lambda, H) = \frac{T(\phi, \lambda, H)}{\overline{\gamma_{Hh}}} \approx \frac{T(\phi, \lambda, H)}{\gamma(\phi, \frac{1}{2}(H + h))}'$$

equation 7.1. Here, γ is normal gravity calculated for point latitude³ ϕ and topographic height $\frac{1}{2}(H + h) = H + \frac{1}{2}\zeta = h - \frac{1}{2}\zeta$.

²The linearisation error could be even further tuned down by choosing as the evaluation level for the vertical gradient $z = \frac{1}{2}(H' + H)$.

³In an actual calculation one would calculate $\overline{\gamma_{Hh}}$ using the true geodetic latitude φ





8.8 The remove–restore method

All current geoid determination methods are in one way or another “remove–restore” methods, even in several different ways.

1. From the observed gravity values, first the effect of a global gravity field model is removed. This model is generally given in the form of a *spherical-harmonic expansion*. Thus, a *residual gravity field* is obtained
 - that has numerically smaller values which are easier to work with
 - that is *more local*: the long “wavelengths”, the patterns extending over large areas, have been removed from the residual field, only the local details remain.
2. From the observed gravity, the effects are removed of all masses that are *outside the geoid* — in practice, the topography. The purpose of this is to obtain a residual gravity field
 - to which the Stokes equation may be applied, because no masses are left outside the boundary surface
 - from which especially the very small “wavelengths” — details the size of which is of the order of a few kilometres — caused by the topography, are gone. After this, *prediction* of gravity values from sparse measurement values will work better.

Some gravity reduction methods — methods which computationally remove the gravity effect of the exterior masses — with good prediction properties were already presented in subsection 8.7.1: Bouguer reduction and isostatic reduction. Also Helmert condensation may be mentioned, although its prediction properties are poor.

We may illustrate the remove–restore method by *commutative diagram*

kommutoiva
kaavio

and equation 4.6. The height $\frac{1}{2}(H + h)$ has to be correct within a few metres in order to attain millimetre precision in ζ .



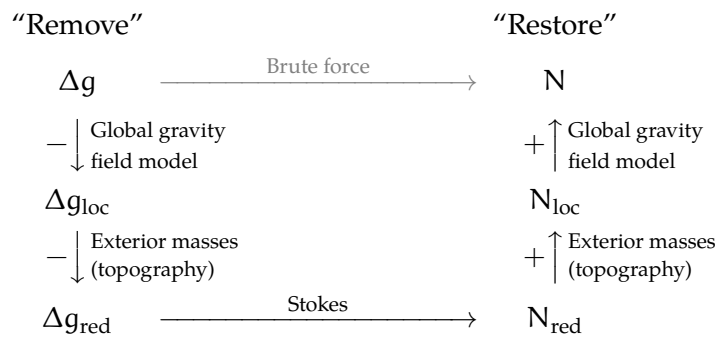


FIGURE 8.9. The remove–restore method as a commutative diagram.

8.9. In this diagram, the black arrows with text denote calculations that are recommended, because they are easy and accurate. The grey arrow with text refers to direct computation, which again is troublesome and computing intensive.



8.9 Kernel modification

In the remove–restore method described above, the handling of reduced gravity anomalies Δg_{red} and geoid heights N_{red} happens ordinarily within a small area. For example, when using the **FFT** method, the area of computation is often a rectangular area in the map projection plane, drawn generously around the country or area for which a geoid model is being computed.

Furthermore, if we compute a geoid model directly by integrating the Stokes equation, we will evaluate this integral, after removing the effect of the global model from the given gravity data, only over a limited

kalotti area or *cap*: evaluate the equation

$$N_{\text{red}} = \frac{R}{4\pi\gamma} \iint_{\sigma_0} S(\psi) \Delta g_{\text{red}}(\phi', \lambda') d\sigma', \quad (8.17)$$

in which σ_0 is a cap on the unit sphere the radius of which is, say, ψ_0 .

The (possibly dangerous) assumption behind this is that, outside the



cap, Δg_{red} is both small and rapidly varying, because the longer wavelengths have been removed from it with the global-model reduction.

Write, in the above equation 8.17,

$$S(\psi) = \sum_{n=2}^{\infty} \frac{2n+1}{n-1} P_n(\cos \psi)$$

and

$$\Delta g_{\text{red}}(\phi', \lambda') = \sum_{n=L+1}^{\infty} \Delta g_n(\phi', \lambda'),$$

assuming that L is the largest degree number that is still along in the global spherical-harmonic expansion, or gravity model, that was subtracted from the data — and that the model is accurate up to that degree number.

Now, because Δg_n is a certain linear combination of the surface spherical harmonics

$$Y_{nm}(\psi, \alpha) = \begin{cases} P_{nm}(\cos \psi) \cos m\alpha & \text{if } m = 0, \dots, n, \\ P_{n|m|}(\cos \psi) \sin |m|\alpha & \text{if } m = -n, \dots, -1, \end{cases}$$

for example like this:

$$\Delta g_n(\phi', \lambda') \Delta g_n(\psi, \alpha) = \frac{1}{R^{n+1}} \sum_{m=-n}^n \Delta g_{nm} Y_{nm}(\psi, \alpha),$$

and also

$$P_n(\cos \psi) = P_{n0}(\cos \psi) \cos(0 \cdot \alpha) = Y_{n0}(\psi, \alpha),$$

it follows from the orthogonality of the Y functions that

$$\iint_{\sigma} P_n(\cos \psi) \Delta g_{n'}(\phi', \lambda') d\sigma' = 0 \quad \text{if } n \neq n'.$$



Now we may write — the terms $n \leq L$ drop away:

$$\begin{aligned} \iint_{\sigma} S(\psi) \Delta g_{\text{red}}(\phi', \lambda') d\sigma' &= \\ &= \iint_{\sigma} \left(\sum_{n=2}^{\infty} \frac{2n+1}{n-1} P_n(\cos \psi) \right) \left(\sum_{n=L+1}^{\infty} \Delta g_n(\phi', \lambda') \right) d\sigma' = \\ &= \iint_{\sigma} \left(\sum_{n=L+1}^{\infty} \frac{2n+1}{n-1} P_n(\cos \psi) \right) \left(\sum_{n=L+1}^{\infty} \Delta g_n(\phi', \lambda') \right) d\sigma' = \\ &= \iint_{\sigma} S^L(\psi) \Delta g_{\text{red}}(\phi', \lambda') d\sigma', \end{aligned}$$

in which

$$S^L(\psi) = \sum_{n=L+1}^{\infty} \frac{2n+1}{n-1} P_n(\cos \psi)$$

is a so-called *modified Stokes kernel function*. The harmonic degree number L is called the *modification degree*. The size of the evaluation area σ_0 is chosen to be compatible with this.

The modification method described here, restricting the Legendre expansion of the S function to higher degree numbers, is called the *Wong–Gore*⁴ modification (Wong and Gore, 1969). A desirable property of the new kernel function S^L is that it would be — at least compared to the original function S — *small* outside the cap area σ_0 . In that case, restricting the integral to the cap instead of the whole unit sphere (equation 8.17) does not do much damage. It is clear that S^L is much narrower than S , as only the higher harmonic degrees are represented in it. This can be verified by plotting a graph of both curves (figure 8.10). The graph does not however go totally to zero outside the cap but oscillates somewhat.

The reason for the oscillation is that in the frequency, i.e., degree-number, domain the modified kernel's cut-off is quite sharp. Transforming such a sharp edge between the space and frequency domains

⁴L. Wong and R. C. Gore worked at the Aerospace Corporation, a space technology research institution in California. [Wikipedia, The Aerospace Corporation.](#)



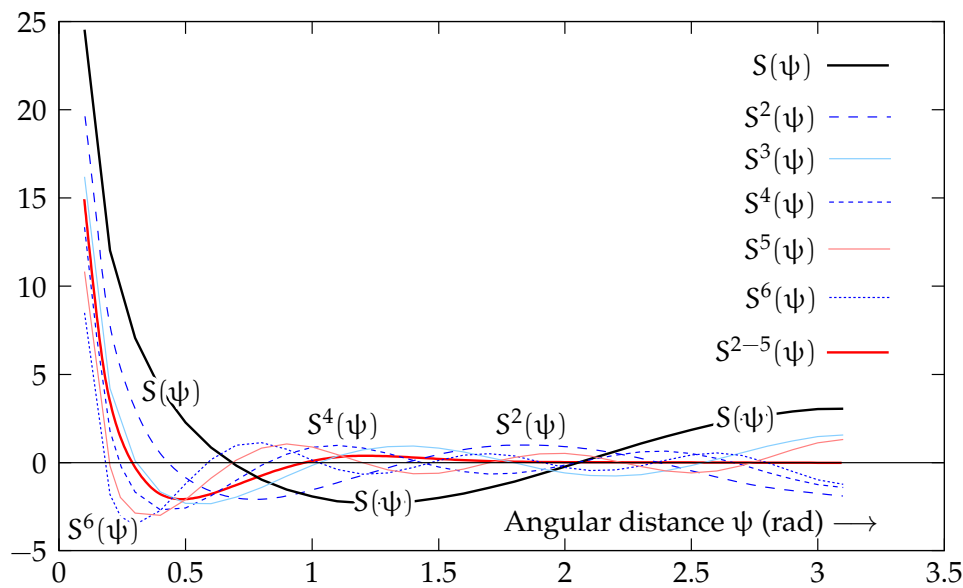


FIGURE 8.10. Modified Stokes kernel functions. Note how the kernel values for higher modification degree numbers L approach zero outside the local area. The red curve has been "soft modified" over a modification degree range of 2–5.



will invariably produce an oscillation, which is related to the so-called *Gibbs⁵ phenomenon*.

Gibbsin ilmiö

In figure 8.10 we have drawn in red a Stokes kernel that was modified or tapered "softly", by instead of removing the lower-degree terms altogether, forcing them gradually to zero going from degree number 5 down to 2. The curve is seen to go even better to zero than the "sharply" modified kernels.

⁵Josiah Willard Gibbs (1839–1903) was an American physicist, chemist, thermodynamicist, mathematician and engineer.





8.10 Advanced kernel modifications

Other kernel modification methods are found in the literature. Their general form is

$$\begin{aligned} S^L(\psi) &= \sum_{n=L+1}^{\infty} \frac{2n+1}{n-1} P_n(\cos \psi) + \sum_{n=2}^L (1-s_n) \frac{2n+1}{n-1} P_n(\cos \psi) = \\ &= S(\psi) - \sum_{n=2}^L s_n \frac{2n+1}{n-1} P_n(\cos \psi), \quad (8.18) \end{aligned}$$

in which the modification coefficients s_n , $n = 2, \dots, L$ can be chosen.⁶ They are chosen so as to minimise the values of the kernel S^L in the area outside the cap, $\sigma - \sigma_0$. In this way one may eliminate the truncation error of equation 8.17 and the oscillation of the Wong–Gore modification almost entirely. Molodensky et al. (1962) had already developed such a method earlier. See also Bucha et al. (2019).

In the above equation 8.18 we want to minimise the function

$$S^L(\psi) = S(\psi) - \sum_{n=2}^L s_n \frac{2n+1}{n-1} P_n(\cos \psi)$$

over the area outside a local cap, $\sigma - \sigma_0$. Let us multiply this expression with each of the Legendre polynomials $P_n(\cos \psi)$, $n = 2, \dots, L$ in turn, and integrate over the area $\sigma - \sigma_0$ outside the local cap:

$$\begin{aligned} &\int_{\sigma-\sigma_0} S(\psi) P_n(\cos \psi) d\sigma - \\ &- \sum_{n'=2}^L s_{n'} \frac{2n'+1}{n'-1} \int_{\sigma-\sigma_0} P_{n'}(\cos \psi) P_n(\cos \psi) d\sigma = 0, \quad n = 2, \dots, L, \end{aligned}$$

a system of $L - 1$ equations in the $L - 1$ unknowns $s_{n'}$:

$$\sum_{n'=2}^L \frac{2n'+1}{n'-1} e_{nn'} s_{n'} = Q_n,$$

⁶The choice $s_n = 1$ again gives the simply (Wong–Gore) modified Stokes kernel from which the low degrees have been completely removed.



with

$$Q_n = \frac{1}{2\pi} \int_{\sigma-\sigma_0} S(\psi) P_n(\cos \psi) d\sigma = \int_{\psi_0}^{\pi} S(\psi) P_n(\cos \psi) \sin \psi d\psi,$$

and similarly

$$\begin{aligned} e_{nn'} &= \frac{1}{2\pi} \int_{\sigma-\sigma_0} P_n(\cos \psi) P_{n'}(\cos \psi) d\sigma = \\ &= \int_{\psi_0}^{\pi} P_n(\cos \psi) P_{n'}(\cos \psi) \sin \psi d\psi. \end{aligned}$$

The coefficients Q_n are known as Molodensky's truncation coefficients, $e_{nn'}$ as Paul's (1973) coefficients.

From this, we can solve the s_n for every degree number n from 2 to L .

This solution also sets to zero the expressions

$$\int_{\sigma-\sigma_0} S^L(\psi) P_n(\cos \psi) d\sigma, \quad (8.19)$$

for all values n from 2 to L .

Expressions 8.19 can be understood as *inner or scalar products*, between functions S^L and P_n . Similarly, the elements of $e_{nn'}$ contain the scalar products between functions P_n and $P_{n'}$. These scalar products do not vanish: when integrating over $\sigma - \sigma_0$, unlike over the whole sphere σ , the Legendre polynomials are *not* mutually orthogonal. Therefore, e is a full matrix, not a diagonal matrix like when integrating over the full unit sphere σ .

The Legendre polynomials *are*, however, independent of each other on the domain $\sigma - \sigma_0$, and together span an $L - 1$ -dimensional linear vector space.

Now, outside the cap σ_0 of radius ψ_0 , the Stokes kernel $S(\psi)$, by visual inspection, is "*smooth*". Depending of course on the values of cap radius ψ_0 and modification degree L , it may be so smooth that it does not contain any significant contribution from degree numbers higher than L . If this applies for S , it will also apply for S^L . This means that S^L will



be a linear combination of the Legendre polynomials, i.e., an element of the vector space spanned by the polynomials P_n , $n = 2, \dots, L$. But if this is so, and the scalar products 8.19 with each of the basis vectors vanish, then S^L must be the zero function on $\sigma - \sigma_0$.

See also Featherstone (2003).

Appendix A.1 explains more about linear vector spaces and the scalar product of vectors.



8.11 Block integration

In numerical gravimetric geoid determination one uses *averages* of anomalies computed over standard-sized cells or *blocks*, generally $5' \times 5'$, $10' \times 10'$, $30' \times 30'$ etcetera. At European latitudes, often sizes like $3' \times 5'$, $5' \times 10'$, $6' \times 10'$ are used, which are approximately square.

The following equation applies when evaluating an integral using block averages:

$$N(\phi, \lambda) = \frac{R}{4\pi\gamma} \sum_i S_i(\phi, \lambda) \overline{\Delta g}_i, \quad (8.20)$$

in which $\overline{\Delta g}_i$ is the mean of block i

$$\overline{\Delta g}_i = \frac{1}{\omega(\sigma_i)} \iint_{\sigma_i} \Delta g(\phi, \lambda) d\sigma = \frac{1}{\omega(\sigma_i)} \iint_{\sigma_i} \Delta g(\phi, \lambda) \cos \phi d\phi d\lambda,$$

and the block value of the Stokes kernel similarly

$$S_i(\phi, \lambda) = \frac{1}{\omega(\sigma_i)} \iint_{\sigma_i} S(\psi(\phi, \lambda; \phi', \lambda')) \cos \phi' d\phi' d\lambda',$$

in which σ_i is the area of block i and its size on the unit sphere is

$$\omega(\sigma_i) = \iint_{\sigma_i} d\sigma = \iint_{\sigma_i} \cos \phi d\phi d\lambda.$$



Numerical evaluation of such an integral, or *quadrature*, is done conveniently using Simpson's rule:⁷

$$\begin{aligned} S_i(\phi, \lambda) &= \\ &= \frac{1}{\omega(\sigma_i)} \int_{\lambda_i - \Delta\lambda/2}^{\lambda_i + \Delta\lambda/2} \int_{\phi_i - \Delta\phi/2}^{\phi_i + \Delta\phi/2} S(\psi(\phi, \lambda; \phi', \lambda')) \cos \phi' d\phi' d\lambda' \approx \\ &\approx \frac{\Delta\phi \Delta\lambda}{\omega(\sigma_i)} \sum_{j=-1}^1 w_j \sum_{k=-1}^1 w_k S_{i,jk}, \end{aligned}$$

in which $\Delta\lambda$ and $\Delta\phi$ are the block sizes in the latitude and longitude directions, and $w_{-1} = w_1 = \frac{1}{6}$, $w_0 = \frac{4}{6}$ are the weights.

$$S_{i,jk}(\phi, \lambda) = S\left(\psi(\phi, \lambda; \phi_i + \frac{1}{2}j\Delta\phi, \lambda_i + \frac{1}{2}k\Delta\lambda)\right) \cos(\phi_i + \frac{1}{2}j\Delta\phi),$$

$j, k = -1, 0, 1$

are the values of expression $S(\psi(\phi, \lambda; \phi', \lambda')) \cos \phi'$ at the nodal points used in the evaluation, 3×3 of them. See figure 8.11. More complicated formulas (repeated Simpson or Romberg) can also be employed.

8.12 Effect of the local zone

One can show that the effect of the local (inner) zone on the geoid at the evaluation point (ϕ, λ) is proportional to the gravity anomaly in the point itself, $\Delta g(\phi, \lambda)$. Starting from Stokes equation 8.1 with $S(\psi) \approx 1/\sin \frac{\psi}{2} \approx 2/\psi$, we find, for a circular inner zone of radius ψ_0 :

$$\begin{aligned} \delta N_0 &= \frac{R}{4\pi\gamma} \int_0^{2\pi} \int_0^{\psi_0} \frac{2}{\psi} \Delta g(\psi, \alpha) \sin \psi d\psi d\alpha \approx \\ &\approx \frac{R}{4\pi\gamma} \cdot 2\pi \cdot \overline{\Delta g_0} \cdot 2\psi_0 = \frac{s_0}{\gamma} \overline{\Delta g_0}. \end{aligned}$$

⁷Thomas Simpson FRS (1710–1761) was an English mathematician and textbook writer. Actually Simpson's rule was already being used a century earlier by Johannes Kepler.



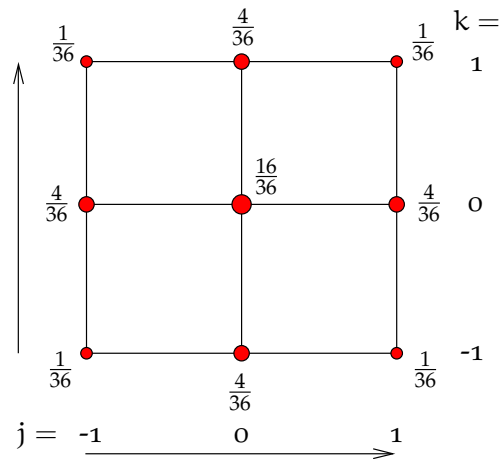


FIGURE 8.11. Simpson integration nodal weights in two dimensions.

Here $s_0 = R\psi_0$ is the radius of the local block or cap in units of length. The quantity

$$\overline{\Delta g}_0 \stackrel{\text{def}}{=} \frac{1}{s_0} \int_0^{s_0} \left(\frac{1}{2\pi} \int_0^{2\pi} \Delta g \, d\alpha \right) ds$$

is a special average of the gravity anomaly, the average of “ring averages” for radii s between zero and s_0 . If s_0 is small, one may take for this the anomaly value $\Delta g(\phi, \lambda)$ at the centre without incurring much error.

The local contributions to the deflections of the plumb line are again proportional to the *horizontal gradients* of gravity anomalies. We start from Vening Meinesz equations 8.4, with the above approximations for a local cap:

$$\begin{Bmatrix} \delta \xi_0 \\ \delta \eta_0 \end{Bmatrix} \approx \frac{1}{4\pi\gamma} \int_0^{\psi_0} \int_0^{2\pi} \left(-\frac{2}{\psi^2} \right) \Delta g \begin{Bmatrix} \cos \alpha \\ \sin \alpha \end{Bmatrix} \cdot \sin \psi \, d\alpha \, d\psi.$$

We expand Δg into local linear rectangular co-ordinates x, y :

$$\begin{aligned} \Delta g &\approx \Delta g_0 + x \frac{\partial \Delta g}{\partial x} + y \frac{\partial \Delta g}{\partial y} \approx \\ &\approx \Delta g_0 + R \sin \psi \left(\cos \alpha \frac{\partial \Delta g}{\partial x} + \sin \alpha \frac{\partial \Delta g}{\partial y} \right), \end{aligned}$$

and substitute:



$$\left\{ \begin{array}{l} \delta\xi_0 \\ \delta\eta_0 \end{array} \right\} \approx \frac{1}{4\pi\gamma} \cdot \int_0^{\psi_0} \int_0^{2\pi} -\frac{2}{\psi^2} \left(\Delta g_0 + R \sin \psi \left(\cos \alpha \frac{\partial \Delta g}{\partial x} + \sin \alpha \frac{\partial \Delta g}{\partial y} \right) \right) \left\{ \begin{array}{l} \cos \alpha \\ \sin \alpha \end{array} \right\} \sin \psi \, d\alpha \, d\psi.$$

Here, the terms in Δg_0 drop out in α integration (because $\int_0^{2\pi} \sin \alpha \, d\alpha = \int_0^{2\pi} \cos \alpha \, d\alpha = 0$). So do the mixed terms in $\sin \alpha \cos \alpha$. What remains is

$$\begin{aligned} \delta\xi_0 &\approx -\frac{1}{4\pi\gamma} \int_0^{\psi_0} \int_0^{2\pi} \frac{2}{\psi^2} R \sin \psi \cos \alpha \frac{\partial \Delta g}{\partial x} \cos \alpha \cdot \sin \psi \, d\alpha \, d\psi \approx \\ &\approx -\frac{R}{2\pi\gamma} \int_0^{\psi_0} \int_0^{2\pi} \frac{\partial \Delta g}{\partial x} \cos^2 \alpha \cdot d\alpha \, d\psi \approx -\frac{R\psi_0}{2\gamma} \frac{\partial \Delta g}{\partial x}, \\ \delta\eta_0 &\approx -\frac{1}{4\pi\gamma} \int_0^{\psi_0} \int_0^{2\pi} \frac{2}{\psi^2} R \sin \psi \sin \alpha \frac{\partial \Delta g}{\partial y} \sin \alpha \cdot \sin \psi \, d\alpha \, d\psi \approx \\ &\approx -\frac{R}{2\pi\gamma} \int_0^{\psi_0} \int_0^{2\pi} \frac{\partial \Delta g}{\partial y} \sin^2 \alpha \cdot d\alpha \, d\psi \approx -\frac{R\psi_0}{2\gamma} \frac{\partial \Delta g}{\partial y}. \end{aligned}$$

Evaluating these integrals assumed the partial derivatives to be constant within the cap. Using $R\psi_0 = s_0$ yields now

$$\delta\xi_0 \approx -\frac{s_0}{2\gamma} \frac{\partial \Delta g}{\partial x}, \quad \delta\eta_0 \approx -\frac{s_0}{2\gamma} \frac{\partial \Delta g}{\partial y}.$$

These equations might be useful as standard block integration, equation 8.20, behaves numerically poorly in the immediate surroundings of the evaluation point if the kernel function is singular in the origin $\psi = 0$. Both the Stokes 8.1 and Vening Meinesz 8.4 kernels are of this kind.



Self-test questions

1. What do the Stokes equation and its spectral form look like?
2. What does the Stokes kernel function $S(\psi)$ look like when expanded in Legendre polynomials?



3. What is a suitable approximation of the Stokes kernel when ψ is small?
4. What is an isotropic, what an anisotropic quantity on the Earth's surface? Give an example of the latter.
5. What does the Poisson integral equation describe?
6. Why are gravity reductions necessary when using the Stokes equation for computing a geoid model?
7. Which gravity reduction methods are available?
8. Explain the residual terrain modelling (RTM) method.
9. Explain the remove–restore method.
10. Why, in geoid determination, is the Stokes kernel function often modified? What does such a modification look like?
11. What is the Gibbs phenomenon?



Exercise 8 – 1: The Stokes equation

1. Derive a simpler form of the Stokes function $S(\psi)$ which is valid when the angular distance ψ is *small*. This simpler form really consists of only one term!
2. Using this form, write the integral equation

$$N = \frac{R}{4\pi\gamma} \iint_{\sigma} S(\psi) \Delta g \, d\sigma$$

into polar co-ordinates, as an integral of the form

$$\int_0^{2\pi} \int_0^{\infty} \dots \, ds \, d\alpha,$$

in which $s = \psi R$ is the linear distance from the evaluation point, and α the azimuth angle (direction angle) from the evaluation point for the geoid height N to the moving integration point for the gravity anomaly Δg .



Hint: you need to consider *Jacobi's determinant* for the polar coordinates (s, α) .

3. Compute N (as a formula) if $\Delta g = \Delta g_0$ only within a circular area $s \leq s_0$, and outside it $\Delta g = 0$. Assume that s_0 is small.





Spectral techniques, FFT

9



9.1 The Stokes theorem as a convolution

We start from the Stokes equation

$$T(\phi, \lambda) = \frac{R}{4\pi} \iint_{\sigma} S(\psi) \Delta g(\phi', \lambda') d\sigma',$$

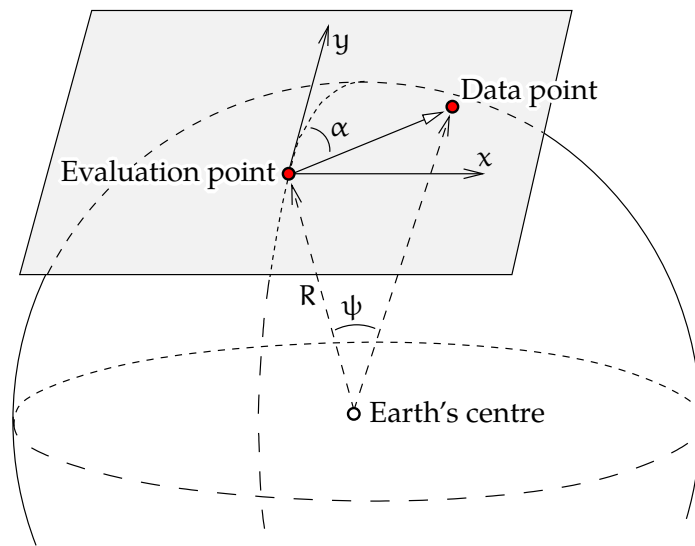
in which (ϕ', λ') is the location of the moving integration or observation point, and (ϕ, λ) is the location of the evaluation point, both at sea level, that is on the surface of a spherical Earth. So, the locations of both points are given in spherical co-ordinates (ϕ, λ) . The integration is carried out over the surface of the unit sphere σ : a surface element is $d\sigma = \cos \phi d\phi d\lambda$, in which $\cos \phi$ represents the determinant of Jacobi, for the spherical co-ordinates (ϕ, λ) .


However *locally*, in a sufficiently small area, one may also write the point co-ordinates in rectangular form and express the integral in rectangular co-ordinates. Suitable rectangular co-ordinates are, for example, *map projection co-ordinates*, see figure 9.1.

A simple example of rectangular co-ordinates in the tangent plane would be

$$x = \psi R \sin \alpha, \quad y = \psi R \cos \alpha, \quad (9.1)$$

in which α is the azimuth of the line connecting evaluation point and moving data point. The centre of this projection is the point where the



 FIGURE 9.1. Map projection co-ordinates x, y in the local tangent plane.

tangent plane touches the sphere. The locations of other points are measured by the angle ψ at the Earth's centre, i.e., the *geocentric angular distance*, and by the direction angle in the tangent plane or *azimuth* α .

A more realistic example uses a popular conformal map projection called the *stereographic projection*:

$$x = 2 \tan\left(\frac{\psi}{2}\right) R \sin \alpha, \quad y = 2 \tan\left(\frac{\psi}{2}\right) R \cos \alpha.$$

In the limit for small values of ψ this agrees with equations 9.1.

Taking the squares of equations 9.1, summing them, and dividing the result by R^2 yields

$$\psi^2 \approx \frac{x^2 + y^2}{R^2}.$$

More generally ψ is the angular distance between the points (x, y) (evaluation point) and (x', y') (data, integration or moving point) seen from the Earth's centre, approximately

$$\psi^2 \approx \left(\frac{x - x'}{R}\right)^2 + \left(\frac{y - y'}{R}\right)^2.$$



Furthermore, we must account for Jacobi's determinant R^2 of the projection:

$$d\sigma = R^{-2} dx dy \iff dx dy = R^2 d\sigma,$$

and the Stokes equation now becomes

$$T(x, y) \approx \frac{1}{4\pi R} \iint_{-\infty}^{\infty} S(x - x', y - y') \Delta g(x', y') dx' dy', \quad (9.2)$$

a two-dimensional *convolution*.¹

Convolutions have nice properties in Fourier theory. If we designate the Fourier transform with the symbol \mathcal{F} , and convolution with the symbol \otimes , we may abbreviate the above equation as follows:

$$T = \frac{1}{4\pi R} S \otimes \Delta g,$$

and according to the *convolution theorem* ("Fourier transforms a convolution into a multiplication"):

$$\mathcal{F}\{T\} = \frac{1}{4\pi R} \mathcal{F}\{S\} \cdot \mathcal{F}\{\Delta g\}.$$

This approximation in the (x, y) plane works only *if integration can be restricted to a local area*, where the curvature of the Earth's surface may be neglected. This is possible thanks to the use of global spherical-harmonic expansions, because these represent the long-wavelength part of the spatial variability of the Earth's gravity field. After we have removed the effect of the global spherical-harmonic model from the observed gravity anomalies Δg (the "remove" step) we may safely forget the effect of areas far removed from the evaluation point: after this removal, the anomaly field Δg_{loc} will contain only the remaining short-wavelength parts, the effect of which cancels out at greater distances.

pallofunktio-
kehitemä

¹The integration extends from minus to plus infinity in both co-ordinates x and y . This can only be realistic on a curved Earth if it is assumed that the kernel S is of *bounded support*: it differs from zero only in a bounded area. This is the case for the modified kernels discussed in section 8.9.



Of course, once the integral has been computed and the local disturbing potential T_{loc} , and the corresponding geoid undulation N_{loc} , have been obtained, we must remember to add to it again the effect of the global spherical-harmonic expansion on the disturbing potential T and geoid undulation N to be calculated separately. This is the “restore” step of the computation; see the commutative diagram 8.9.



9.2 Integration by FFT

The Fourier transform needed for applying the convolution theorem is calculated as a *discrete Fourier transform*. The highly efficient Fast Fourier Transform, **FFT**, exists for this purpose, for example [Vermeer \(1992a\)](#). There are several slightly differing formulations of the discrete Fourier transform to be found in the literature. It does not really matter which is chosen, as long as it is a compatible pair of a forward Fourier transform \mathcal{F} and a reverse Fourier transform \mathcal{F}^{-1} .

hilaesitys In preparation for this, we first compute a discrete *grid representation* of the function $\Delta g(x, y)$, a rectangular table of Δg values on an equidistant (x, y) grid of points. The values may be, say, the function values themselves at the grid points:²

$$\Delta g_{ij} = \Delta g(x_i, y_j),$$

in which the co-ordinates of the grid points are

$$x_i = i \delta x, \quad y_j = j \delta y, \quad i, j = 0, 1, \dots, N - 1,$$

for suitably chosen grid spacings $(\delta x, \delta y)$. The integer N is the grid size, assumed for simplicity to be the same in both directions.

Next, we do the same for the kernel function

$$S(\psi) = S(x - x', y - y') = S(\Delta x, \Delta y),$$

²There exist alternatives to this. For example, one could calculate for every grid point the average over a square cell surrounding the point.



so we write

$$S_{ij} = S(\Delta x_i, \Delta y_j),$$

where again

$$\Delta x_i = i \delta x, \quad \Delta y_j = j \delta y, \quad i, j = 0, 1, \dots, N - 1.$$

Note that the central peak at the origin of the symmetric function S — $S(\Delta x, \Delta y) \rightarrow \infty$ when $(\Delta x, \Delta y) \rightarrow (0, 0)$ — is placed at the origin $i = j = 0$ of the grid of function values S_{ij} . The peak of the function is thus split into four “quadrants”, one in each corner of the grid.

Next:

1. The grid representations S_{ij} and Δg_{ij} thus obtained of the functions S and Δg are transformed to the *frequency domain* — they become functions \mathcal{S}_{uv} and \mathcal{G}_{uv} of the two “frequencies”, the wave indices u and v in the x and y directions. The spatial frequencies or wave numbers³ $\tilde{\nu}$ and spatial wavelengths λ are $\tilde{\nu}_x = \lambda_x^{-1} = u/L$, $\tilde{\nu}_y = \lambda_y^{-1} = v/L$, in which $L = N\delta x = N\delta y$ is the size of the area, assumed to be square.
2. They are multiplied with each other “one frequency pair at a time”: we calculate

$$\mathcal{T}_{uv} = \frac{1}{4\pi R} \mathcal{S}_{uv} \cdot \mathcal{G}_{uv}, \quad u, v = 0, \dots, N - 1. \quad (9.3)$$

3. We transform the result, $\mathcal{T}_{uv} = \mathcal{F}\{T_{ij}\}$, back to the space domain: $T_{ij} = \mathcal{F}^{-1}\{\mathcal{T}_{uv}\}$, a point grid $T_{ij} = T(x_i, y_j)$ of the disturbing potential T . The disturbing potential of an arbitrary point can be obtained from this grid by interpolation. The co-ordinates x_i, y_j run as functions of i, j in the same way as described above for Δg .

The method described is good for computing the disturbing potential T — and similarly the geoid height $N = T/\gamma$ — from gravity anomalies

³This is the so-called linear frequency, whole waves per unit of length. The angular frequency is $\omega \stackrel{\text{def}}{=} 2\pi\tilde{\nu}$, radians of phase angle per unit of length.



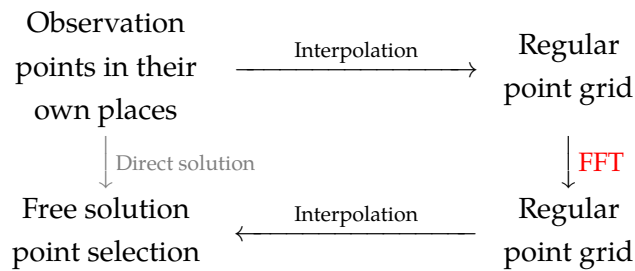


FIGURE 9.2. Commutative diagram for **FFT**.

using the Stokes equation. It is just as good for evaluating other quantities, like for example the vertical gradient of the gravity anomaly using equation 8.12. The only requirement is that the equation can be expressed as a *convolution*.

The *inversion calculation* is also easy, as we shall see: in the frequency domain it is just a simple division.

Using the discrete Fourier transform requires the input data in a field to be integrated — in the example, gravity anomalies — is given on a regular grid covering the area of computation, or can be converted into one. The result — in the example, the disturbing potential — is obtained on a regular grid in the same geometry. Values can then be *interpolated* to chosen locations.

kommutoiva
kaavio

The **FFT** method may be depicted as a *commutative diagram*, figure 9.2.

Appendix C offers a short explanation of why **FFT** works and what makes it as efficient as it is.



9.3 Solution in latitude and longitude

In the above equation 9.2, the grid co-ordinates x and y are rectangular. For practical reasons, we would rather use latitude and longitude (φ, λ) as grid co-ordinates. In that way, the need to generate a new (x, y) point grid by interpolating from the given (φ, λ) one through a map projection calculation is avoided. However, working in geographical co-ordinates causes errors due to *meridian convergence* — as a latitude and longitude



co-ordinate system is not actually rectangular. The co-ordinate pair $(\phi, \lambda \cos \phi)$ would be slightly more suitable.

The problem has also been addressed on a more conceptual level.

9.3.1 The Strang van Hees method

The Stokes kernel function $S(\psi)$ depends only on the geocentric angular distance ψ between evaluation point (ϕ, λ) and observation point (ϕ', λ') . The angular distance may be written as follows (cosine rule on the sphere):

$$\cos \psi = \sin \phi \sin \phi' + \cos \phi \cos \phi' \cos(\lambda - \lambda').$$

Substitute

$$\begin{aligned} \cos(\lambda - \lambda') &= 1 - 2 \sin^2 \frac{1}{2}(\lambda - \lambda'), \\ \cos \psi &= 1 - 2 \sin^2 \frac{1}{2}\psi, \\ \cos(\phi - \phi') &= 1 - 2 \sin^2 \frac{1}{2}(\phi - \phi'), \end{aligned}$$

and obtain the *half-angle cosine rule*:

$$\begin{aligned} \cos \psi &= \cos(\phi - \phi') - 2 \cos \phi \cos \phi' \sin^2 \frac{1}{2}(\lambda - \lambda') \\ \implies \sin^2 \frac{1}{2}\psi &= \sin^2 \frac{1}{2}(\phi - \phi') + \cos \phi \cos \phi' \sin^2 \frac{1}{2}(\lambda - \lambda'). \end{aligned}$$

Here we may use the following approximation:

$$\cos \phi' \approx \cos \phi \stackrel{\text{def}}{=} \cos \phi_0,$$

in which ϕ_0 is a reference latitude in the middle of the calculation area.

Now the above equation becomes

$$\sin^2 \frac{1}{2}\psi \approx \sin^2 \frac{1}{2}(\phi - \phi') + \cos^2 \phi_0 \sin^2 \frac{1}{2}(\lambda - \lambda'), \quad (9.4)$$

which depends *only* on the differences $\Delta\phi \stackrel{\text{def}}{=} \phi - \phi'$ and $\Delta\lambda \stackrel{\text{def}}{=} \lambda - \lambda'$, a requirement for convolution.



After this, the **FFT** method may be applied by using co-ordinates (ϕ, λ) ⁴ and the re-written Stokes kernel

$$S(\Delta\phi, \Delta\lambda) \stackrel{\text{def}}{=} S\left(2 \arcsin \sqrt{\sin^2 \frac{1}{2}\Delta\phi + \cos^2 \phi_0 \sin^2 \frac{1}{2}\Delta\lambda}\right).$$

This clever way of using **FFT** in geographical co-ordinates was invented by the Dutchman G. Strang van Hees⁵ in 1990.

9.3.2 “Spherical FFT”, multi-band model

We divide the area into several narrow latitude bands. In each band we apply the Strang van Hees method using its own optimal central latitude.

Write the Stokes equation as follows:

$$N(\phi, \lambda) = \frac{R}{4\pi\gamma} \iint S(\phi - \phi', \lambda - \lambda'; \phi) [\Delta g(\phi', \lambda') \cos \phi'] d\phi' d\lambda', \quad (9.5)$$

where we have expressed $S(\cdot)$ as a function of latitude difference, longitude difference and *evaluation latitude*. Now, choose two support latitudes, ϕ_i and ϕ_{i+1} . Assume furthermore that between these S is a linear function of ϕ . In that case we may write

$$S(\Delta\phi, \Delta\lambda; \phi) = \frac{(\phi - \phi_i) S_{i+1}(\Delta\phi, \Delta\lambda) + (\phi_{i+1} - \phi) S_i(\Delta\phi, \Delta\lambda)}{\phi_{i+1} - \phi_i},$$

where $\Delta\phi = \phi - \phi'$, $\Delta\lambda = \lambda - \lambda'$, and

$$\begin{aligned} S_i(\Delta\phi, \Delta\lambda) &= S(\phi - \phi', \lambda - \lambda'; \phi_i), \\ S_{i+1}(\Delta\phi, \Delta\lambda) &= S(\phi - \phi', \lambda - \lambda'; \phi_{i+1}). \end{aligned}$$

We obtain by substitution into integral equation 9.5:

⁴In practice one uses the geodetic or geographical latitude φ instead of ϕ without significant error.

⁵Govert L. Strang van Hees (1932–2012) was a Dutch gravimetric geodesist.



$$N(\phi, \lambda) = \frac{R}{4\pi\gamma} \left(\frac{\phi_{i+1} - \phi}{\phi_{i+1} - \phi_i} I_i + \frac{\phi - \phi_i}{\phi_{i+1} - \phi_i} I_{i+1} \right), \quad (9.6)$$

with

$$I_i = \iint S_i(\Delta\phi, \Delta\lambda) [\Delta g(\phi', \lambda') \cos \phi'] d\phi' d\lambda',$$

$$I_{i+1} = \iint S_{i+1}(\Delta\phi, \Delta\lambda) [\Delta g(\phi', \lambda') \cos \phi'] d\phi' d\lambda'.$$

This equation is the *linear combination of two convolutions*. Both are evaluated by **FFT**. One forms the weighted mean from the solutions obtained according to equation 9.6.

In this method we use, instead of approximative equation 9.4, an exact equation in which ϕ' is expressed into ϕ and $\Delta\phi$:

$$\begin{aligned} \sin^2 \frac{1}{2} \psi &= \sin^2 \frac{1}{2} (\phi - \phi') + \cos \phi \cos \phi' \sin^2 \frac{1}{2} (\lambda - \lambda') = \\ &= \sin^2 \frac{1}{2} \Delta\phi + \cos \phi \cos (\phi - \Delta\phi) \sin^2 \frac{1}{2} \Delta\lambda. \end{aligned}$$

Here again, we calculate S_i and S_{i+1} for the support latitude values ϕ_i and ϕ_{i+1} , we evaluate the integrals with the aid of the convolution theorem, and interpolate $N(\phi, \lambda)$ according to equation 9.6 when $\phi_i \leq \phi < \phi_{i+1}$. After this, the solution is not entirely exact, because inside every band we still use linear interpolation. However by making the bands narrower, we can keep the error arbitrarily small.

9.3.3 “Spherical FFT”, Taylor expansion model

This somewhat more complicated but also more versatile approach expands the Stokes kernel into a Taylor expansion with respect to latitude about a *reference latitude* located in the middle of the computation area.⁶ Each term in the expansion depends only on the *difference* in latitude.

⁶In the literature the method has been generalised by also expanding the kernel with respect to height.



The integral to be calculated similarly expands into terms, of which each contains a pure convolution.

Let us write the *general* problem as follows:

$$\ell(\phi, \lambda) = \int_0^{2\pi} \int_{-\pi/2}^{+\pi/2} C(\phi, \phi', \Delta\lambda) [m(\phi', \lambda') \cos \phi'] d\phi' d\lambda',$$

in which ℓ contains values to be computed, m values given, and C is the coefficient or kernel function. Here only *rotational symmetry* around the Earth's axis is assumed for the geometry: the kernel function depends only on the difference between longitudes $\Delta\lambda$ rather than the absolute longitudes λ, λ' .

In a concrete case, m contains for example gravity anomaly values Δg in various points (ϕ', λ') , ℓ contains geoid heights N in various points (ϕ, λ) , and C contains coefficients calculated using the Stokes kernel function.

We first change the dependence upon ϕ, ϕ' into a dependence upon $\phi, \Delta\phi$:

$$C = C(\phi, \phi', \Delta\lambda) = C(\Delta\phi, \Delta\lambda; \phi).$$

Linearise:

$$C = C_0(\Delta\phi, \Delta\lambda) + (\phi - \phi_0) C_\phi(\Delta\phi, \Delta\lambda) + \dots$$

where we define for a suitable *reference latitude* ϕ_0 :

$$C_0(\Delta\phi, \Delta\lambda) \stackrel{\text{def}}{=} C(\Delta\phi, \Delta\lambda; \phi_0), \quad C_\phi(\Delta\phi, \Delta\lambda) \stackrel{\text{def}}{=} \left. \frac{\partial}{\partial \phi} C(\Delta\phi, \Delta\lambda; \phi) \right|_{\phi=\phi_0}.$$

This expansion into two terms will work only for a limited range in $\Delta\phi$, and the kernel function C is assumed to be of bounded support. In this case, the integrals may be calculated within a limited area instead of over the whole Earth.



Substitution yields

$$\begin{aligned} \ell(\phi, \lambda) &= \iint C(\Delta\phi, \Delta\lambda; \phi) \cdot m(\phi', \lambda') \cos \phi' \, d\phi' \, d\lambda' = \\ &= \iint \left(C_0 + (\phi - \phi_0) C_\phi \right) \cdot m \cos \phi' \, d\phi' \, d\lambda' = \\ &= \iint C_0 \cdot m \cos \phi' \, d\phi' \, d\lambda' + (\phi - \phi_0) \iint C_\phi \cdot m \cos \phi' \, d\phi' \, d\lambda'. \end{aligned} \quad (9.7)$$

It is important here now that the integrals in the first and second terms,

$$\begin{aligned} \iint C_0(\Delta\phi, \Delta\lambda) [m(\phi', \lambda') \cos \phi'] \, d\phi' \, d\lambda' &= C_0 \circledast [m \cos \phi], \\ \iint C_\phi(\Delta\phi, \Delta\lambda) [m(\phi', \lambda') \cos \phi'] \, d\phi' \, d\lambda' &= C_\phi \circledast [m \cos \phi], \end{aligned}$$

are both convolutions: both C functions depend only on $\Delta\phi$ and $\Delta\lambda$. Both integrals can be calculated if both the data grid $m \cos \phi$ and the coefficient grids C_0 and C_ϕ are calculated first in preparation. After this — in principle expensive, but, thanks to **FFT** and the convolution theorem, a lot cheaper — integration, computing compound 9.7 is fast: one multiplication and one addition for each evaluation point (ϕ, λ) .

Example Let the evaluation area at latitude 60° be $10^\circ \times 20^\circ$ in size. If the grid mesh size is $5' \times 10'$, the number of cells is 120×120 . Let us choose, say, a 256×256 grid (so $N = 256$) and fill the missing values with extrapolated values.

The values of the kernel functions C_0 and C_ϕ are calculated on a 256×256 grid $(\Delta\phi, \Delta\lambda)$ as well. The number of these is thus also 65 536. Calculating the convolutions $C_0 \circledast [m \cos \phi]$ and $C_\phi \circledast [m \cos \phi]$ by means of **FFT** — i.e.,⁷

$$\iint C_0(\Delta\phi, \Delta\lambda) m(\phi', \lambda') \cos \phi' \, d\phi' \, d\lambda' =$$

⁷Fourier transforms are multiplied by multiplying the corresponding elements, see section 9.2 equation 9.3.



$$\begin{aligned}
&= C_0 \circledast [m \cos \phi] = \mathcal{F}^{-1} \{ \mathcal{F}\{C_0\} \cdot \mathcal{F}\{m \cos \phi\} \}, \\
\iint C_\phi(\Delta\phi, \Delta\lambda) m(\phi', \lambda') \cos \phi' d\phi' d\lambda' &= \\
&= C_\phi \circledast [m \cos \phi] = \mathcal{F}^{-1} \{ \mathcal{F}\{C_\phi\} \cdot \mathcal{F}\{m \cos \phi\} \},
\end{aligned}$$

requires $N^2 \times {}^2\log(N^2) = 65\,536 \times 16 =$ more than a million operations, multiplication with $(\phi - \phi_0)$ and adding together, each again 65 536 operations.

The grid matrices corresponding to functions C_0 and C_ϕ are obtained as follows: for three reference latitudes $\phi_{-1}, \phi_0, \phi_{+1}$ we compute numerically the grids

$$\begin{aligned}
C_{-1} &= C(\Delta\phi, \Delta\lambda; \phi_{-1}), \\
C_0 &= C(\Delta\phi, \Delta\lambda; \phi_0), \\
C_{+1} &= C(\Delta\phi, \Delta\lambda; \phi_{+1}),
\end{aligned}$$

in which C_0 is directly available, and

$$C_\phi \approx \frac{C_{+1} - C_{-1}}{\phi_{+1} - \phi_{-1}}.$$

Inversion calculation is thus also directly feasible. Let ℓ be given in suitable point grid form. We compute the first approximation to m as follows:⁸

$$\mathcal{F}\{C_0\} \cdot \mathcal{F}\{m \cos \phi\} = \mathcal{F}\{\ell\} \implies [m \cos \phi]^{(0)} = \mathcal{F}^{-1} \left\{ \frac{\mathcal{F}\{\ell\}}{\mathcal{F}\{C_0\}} \right\}.$$

The second approximation is obtained by first calculating

$$\ell^{(0)} = C_0 \circledast [m \cos \phi]^{(0)} + (\phi - \phi_0) \cdot C_\phi \circledast [m \cos \phi]^{(0)},$$

after which we make the improvement:

$$[m \cos \phi]^{(1)} = [m \cos \phi]^{(0)} + \mathcal{F}^{-1} \left\{ \frac{\mathcal{F}\{\ell - \ell^{(0)}\}}{\mathcal{F}\{C_0\}} \right\},$$

⁸A Fourier transform is divided by another one by dividing the corresponding elements, see section 9.2.



and so on, iteratively. Two, three iterations are usually enough. This method has been used to compute underground mass points from gravity anomalies to represent the exterior gravity field of the Earth.⁹ More is explained in [Forsberg and Vermeer \(1992\)](#); [Vermeer \(1992b\)](#).

9.3.4 “1D-FFT”

This is a limiting case of the previous ones, in which **FFT** is used only in the longitude direction. In other words, this is a zones method in which the zones have a width of only a single grid row. This method is exact if all longitudes $0^\circ \leq \lambda < 360^\circ$ are along in the calculation. It requires somewhat more computing time compared to the previous methods. In fact, it is identical to a Fourier transform in variable λ , longitude. Details are found in [Haagmans et al. \(1993\)](#).

9.4 Bordering and tapering of the data area

The discrete Fourier transform presupposes the data to be *periodically continuous*. In other words, it is assumed that when connecting the eastern edge of the data area to the western edge, and the northern edge to the southern edge, the data has to be continuous across these edges.¹⁰ In practice, this is not the case. We are faced with two different requirements:

- The data on the other side of an edge must be so far away as to have no noticeable influence across the edge on the result of the calculation.
- The data must be continuous across the edges.

⁹Because the relationship between the mass points and the observed gravity anomalies on the Earth’s surface can be described exactly in geodetic co-ordinates, the method may be used with geodetic latitude φ instead of geocentric latitude ϕ . Thus, errors caused by ignoring the Earth’s flattening are avoided.

¹⁰Topologically the area with the edges thus connected is equivalent to a *torus*, and the data is presupposed to be continuous on the surface of the torus.

Therefore, always when using FFT with the convolution theorem, two measures need to be taken.

1. We continue the data by adding a border area to the data area, so-called *bordering*. Often, the width of the border area is 25 % of the size of the data area, making the surface area of the whole calculation area four times that of the data area itself. The border is filled with measured values where those exist, otherwise with predicted (inter- or extrapolated) values.

The calculation area for the *kernel function* is also made similarly four times larger. In this case the border area is filled with real (computed) values. If the function is symmetric, it will automatically be periodically continuous.

2. Because the discrete Fourier transform assumes periodicity, one must make sure that the data is continuous across the edges. If the values at the edges are not zero, they may be forced to zero by multiplying the whole data area by a so-called *tapering* function, which goes smoothly to zero towards the edges. Such a function can easily be built: examples are a cubic spline polynomial or a Tukey or cosine taper. See figure 9.3, showing a 25 % tapering function, as well as example images 9.4, which show how non-continuity — sharply differing left and right, and upper and lower, edges — causes horizontal and vertical artefacts in the Fourier transform. These artefacts are related to the *Gibbs phenomenon*, already mentioned in section 8.9: a sharp cut-off or edge in the space domain will generate signal on all frequencies, up to the highest ones.

Many journal articles have appeared on these technicalities. Groups that were already involved in early development of FFT geoid determination in the 1980s include Forsberg's group in Copenhagen, Schwarz and Sideris' group in Calgary, Canada, the Delft group (Strang van Hees, Haagmans, De Min, Van Gelderen), the Milanese group (Sansò, Barza-



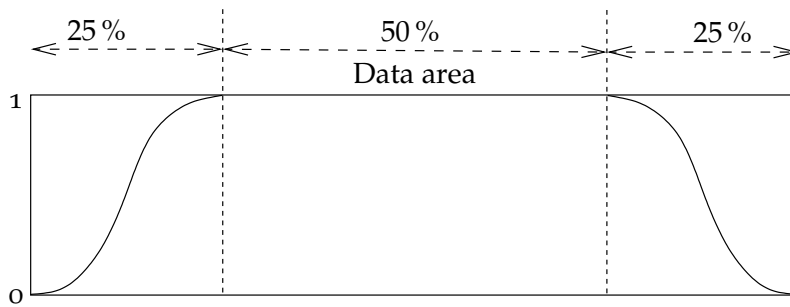


FIGURE 9.3. "Tapering" 25%.



FIGURE 9.4. Example images for FFT transform without (above) and with (below) tapering. The online FFT service from Watts (2004) was used. The images are amplitude spectra $|F_{uv}|$ plotted with the origin $u = v = 0$ in the centre, see appendix C.



ghi, Brovelli), Heiner Denker at the Hannover “*Institut für Erdmessung*”, and many others.

9.5 Computing a geoid model with FFT

Nowadays computing a geoid or quasi-geoid model is easy thanks to increased computing power, especially using **FFT**. On the other hand, the spread of precise geodetic satellite positioning has made the availability of precise geoid models an important issue, so that one can use **GNSS** technology for rapid and affordable height determination.

9.5.1 GRAVSOFTE software

The **GRAVSOFTE** geoid determination software has been mainly produced in Denmark. Authors include Carl Christian Tscherning,¹¹ René Forsberg, Per Knudsen, the Norwegian Dag Solheim, and the Greek Dimitris Arabelos. The manual for the software is [Forsberg and Tscherning \(2008\)](#).

This package is in widespread use and also offers, in addition to variants of **FFT** geoid determination, for example least-squares collocation, as well as routines for evaluating various terrain effects. Its popularity can be partly explained by it being free for scientific use, and being distributed as source code. It is also well-documented. Therefore it has also found commercial use, for example in the petroleum extraction industry.

GRAVSOFTE has also been used a great deal for teaching, for example at many research schools organised by the **IAG** (International Association of Geodesy) in various countries. [ISG, Geoid Schools](#).

¹¹Carl Christian Tscherning (1942–2014) was a Danish physical geodesist well-known for his research into the gravity field of the Earth. He did ground-breaking work on statistical computation methods for modelling the Earth’s gravity field from many different measurement types.



9.5.2 The Finnish FIN2000 geoid

Currently two geoid models are in use in Finland: **FIN2000** (figure 9.5) and **FIN2005N00** (Bilker-Koivula and Ollikainen, 2009). The first model is a reference surface for the **N60** height system: using it together with **GNSS** positioning allows determination of the **N60** heights of points. The model gives geoid heights above the **GRS80** reference ellipsoid. The second model is similarly a reference surface for the new **N2000** height system. It, too, gives heights from the **GRS80** reference ellipsoid.

The precisions (mean errors) of **FIN2000** and **FIN2005N00** are on the level of $\pm 2\text{--}3$ cm.

9.6 Use of FFT computation in other contexts

9.6.1 Satellite altimetry

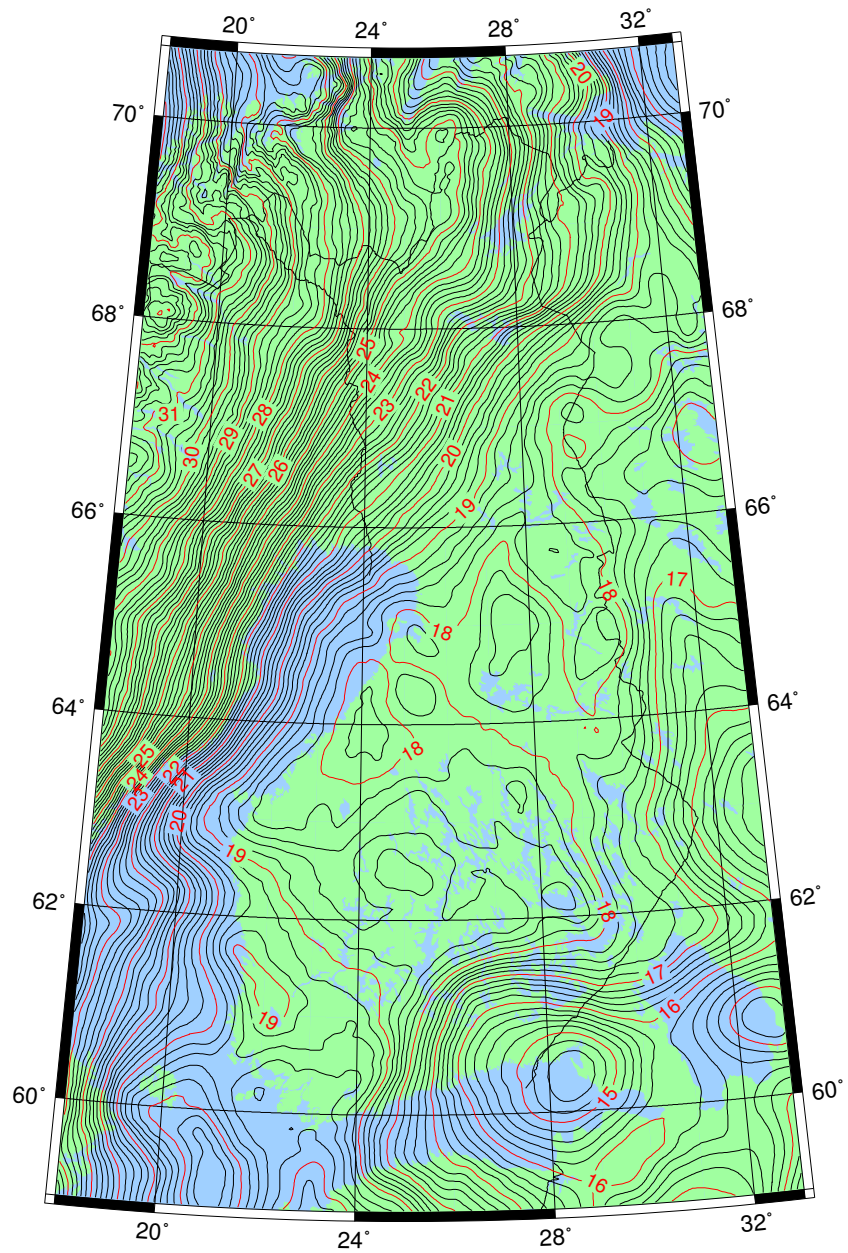
The Danish researchers Per Knudsen and Ole Balthasar Andersen have computed a gravity map of the world ocean by starting from satellite altimetry derived “geoid heights” and inverting them to gravity anomalies (Andersen et al., 2010). A pioneer of this method has been David Sandwell from the Scripps Institute of Oceanography in California (e.g., Garcia et al., 2014). The short-wavelength features in the map can tell us about the sea-floor topography.

9.6.2 Satellite gravity missions and airborne gravimetry

The data from satellite gravity missions (like **CHAMP**, **GRACE** and **GOCE**) can also be regionally processed using the **FFT** method: in the case of **GOCE**, the inversion of gradiometric measurements yields geoid heights on the Earth’s surface from measurements made at satellite level. Airborne gravity measurements are also processed in this way using **FFT**. The problem is called “harmonic downwards continuation” and is in principle unstable.

Airborne gravimetry is a practical method for the gravimetric mapping of large areas. In the pioneering days, the gravity field over





GM 2010 Oct 20 13:27:28

FIGURE 9.5. The Finnish FIN2000 geoid. Data © Finnish Geodetic Institute.



Greenland was mapped, as well as many areas around the Arctic and Antarctic. Later, areas were measured like the Brazilian Amazonas, Mongolia, and Ethiopia (Bedada, 2010), for which no full-coverage terrestrial gravimetric data existed. The advantage of this method is that one measures rapidly large areas in a homogeneous way.



9.7 Computing terrain corrections with FFT

Terrain correction is a very localised phenomenon, the calculation of which requires high-resolution terrain data from a relatively small area surrounding the computation point. Thus, calculating the terrain correction is ideally suited for the FFT method.

We show how, with FFT, we can simply and efficiently evaluate the terrain correction. We make the following simplifying *assumptions*:

- Terrain slopes are relatively gentle.
- The density ρ of the Earth's crust is constant.
- The Earth is flat — the “shoebox world”.

These assumptions are not mandatory. The general case, however, leads us into a jungle of equations without aiding the conceptual picture.

The *terrain correction*, the removal of the joint effect of all the topographic masses, or lacking topographic masses, above and below the height level H of the evaluation point, can be calculated under these assumptions using the following rectangular equation, which gives the attraction of rock columns projected onto the vertical (figure 6.5):

$$\begin{aligned} \text{TC}(x, y) &= \iint_{-\infty}^{+\infty} \frac{G\rho (H'(x', y') - H(x, y))}{\ell^2} \cos \theta \, dx' \, dy' = \\ &= \iint_{-\infty}^{+\infty} \frac{G\rho (H' - H)}{\ell^2} \cdot \frac{1}{2} \frac{H' - H}{\ell} \, dx' \, dy' = \\ &= \frac{1}{2} G\rho \iint_{-\infty}^{+\infty} \frac{(H' - H)^2}{\ell^3} \, dx' \, dy'. \quad (9.8) \end{aligned}$$



Here, $G\rho(H' - H)/\ell^2$ is the attraction of the column and $\frac{1}{2}(H' - H)/\ell$ is the cosine of the angle θ between the force vector — assumed coming from the midpoint of the rock column — and the vertical direction. This is the so-called *prism method*.

We will make a linear approximation, wherein ℓ , the slant distance between the evaluation point (x, y) and the moving data point (x', y') , is the *horizontal distance* as well:

$$\ell^2 \approx (x - x')^2 + (y - y')^2.$$

Equation 9.8 is easy to check straight from Newton's law of gravitation. When it is assumed that the terrain is relatively free of steep slopes, then ℓ is large compared to $H' - H$.

From equation 9.8 we obtain by expansion into terms:

$$\begin{aligned} \text{TC}(x, y) = \frac{1}{2}G\rho H^2 \iint_{-\infty}^{+\infty} \frac{1}{\ell^3} dx' dy' - G\rho H \iint_{-\infty}^{+\infty} \frac{H'}{\ell^3} dx' dy' + \\ + \frac{1}{2}G\rho \iint_{-\infty}^{+\infty} \frac{(H')^2}{\ell^3} dx' dy', \quad (9.9) \end{aligned}$$

in which every integral is a *convolution* with kernel ℓ^{-3} , and the functions to be integrated are 1, H' , and $(H')^2$.

Unfortunately the function ℓ^{-3} as implicitly defined above has no Fourier transform. Therefore, we change the above definition a tiny bit by adding a small term:

$$\ell^2 = (x - x')^2 + (y - y')^2 + \delta^2. \quad (9.10)$$

The terms in the above equation 9.9 are large numbers that almost cancel each other, giving a nearly correct result. Numerically this is however an unpleasant situation. There is a solution for this which we describe next.

If ℓ is defined according to equation 9.10, then the Fourier transform of kernel ℓ^{-3} is (Harrison and Dickinson, 1989; Forsberg, 1984):

$$\mathcal{F}\{\ell^{-3}\} = \frac{2\pi}{\delta} \exp(-2\pi\delta q) = \frac{2\pi}{\delta} \left(1 - 2\pi\delta q + \frac{4\pi^2\delta^2 q^2}{1 \cdot 2} - \dots \right),$$



in which $q \stackrel{\text{def}}{=} \sqrt{\tilde{v}_x^2 + \tilde{v}_y^2} = \sqrt{u^2 + v^2}/L$, u and v are wave indices, and $\tilde{v}_x = u/L$ and $\tilde{v}_y = v/L$ (linear) “spatial frequencies” or wave numbers in the x and y directions in the (x, y) plane. If we substitute this into equation 9.9, we notice that the terms containing $1/\delta$ sum to zero, and of course the terms containing positive powers of δ vanish as well when $\delta \rightarrow 0$. We obtain (Harrison and Dickinson, 1989):

$$\begin{aligned} \mathcal{F}\{\text{TC}\} &\approx \frac{1}{2}G\rho H^2 \mathcal{F}\{1\} \cdot \left(\frac{2\pi}{\delta} (1 - 2\pi\delta q)\right) - \\ &- G\rho H \mathcal{F}\{H'\} \cdot \left(\frac{2\pi}{\delta} (1 - 2\pi\delta q)\right) + \frac{1}{2}G\rho \mathcal{F}\{(H')^2\} \cdot \left(\frac{2\pi}{\delta} (1 - 2\pi\delta q)\right) \end{aligned}$$

where we left off all terms in higher powers of δ .

Re-order the terms:

$$\begin{aligned} \mathcal{F}\{\text{TC}\} &= \frac{\pi}{\delta}G\rho \left(H^2\mathcal{F}\{1\} - 2H\mathcal{F}\{H'\} + \mathcal{F}\{(H')^2\} \right) + \\ &+ 2\pi G\rho \cdot 2\pi q \cdot \left(-\frac{1}{2}H^2\mathcal{F}\{1\} + H\mathcal{F}\{H'\} - \frac{1}{2}\mathcal{F}\{(H')^2\} \right). \end{aligned}$$

Because $\mathcal{F}\{1\} = 0$ if $q \neq 0$, the first term inside the second term will always vanish. We obtain (remember that H is a constant, the height of the evaluation point):

$$\begin{aligned} \mathcal{F}\{\text{TC}\} &= \frac{\pi}{\delta}G\rho \left(\mathcal{F}\{H^2 - 2HH' + (H')^2\} \right) + \\ &+ 2\pi G\rho \cdot 2\pi q \cdot \left(H\mathcal{F}\{H'\} - \frac{1}{2}\mathcal{F}\{(H')^2\} \right) \end{aligned}$$

and the reverse Fourier transform yields

$$\begin{aligned} \text{TC} &= \frac{\pi}{\delta}G\rho \left(H^2 - 2H'H + (H')^2 \right) + \\ &+ 2\pi G\rho \mathcal{F}^{-1} \left\{ 2\pi q \cdot \left(H\mathcal{F}\{H'\} - \frac{1}{2}\mathcal{F}\{(H')^2\} \right) \right\}. \end{aligned}$$

In the first term

$$H^2 - 2H'H + (H')^2 = (H - H')^2 = 0$$

in point (x, y) in which $H' = H$, and we obtain

$$\text{TC} = 2\pi G\rho \mathcal{F}^{-1} \left\{ 2\pi q \cdot \left(H\mathcal{F}\{H'\} - \frac{1}{2}\mathcal{F}\{(H')^2\} \right) \right\},$$



from which the troublesome $1/\delta$ has now vanished.

A *condition* for this “regularisation” or “renormalisation” is that $H' = H$ at point (x, y) , i.e., the evaluation happens at the Earth’s surface. The convolutions above are evaluated by the **FFT** method.

For calculating the terrain correction **TC** in the *exterior space* — examples are airborne gravimetry, the effect of the sea floor at the sea surface, and the effect of the Mohorovičić discontinuity at the Earth’s surface — there are techniques that express **TC** as a sum of convolutions, a Taylor series expansion. An early paper on this is **Parker (1972)**.



Self-test questions

1. What is the definition of a convolution?
2. Explain the convolution theorem.
3. Check that the dimensions of the quantities on both sides of equation 9.2 match.
4. What is spatial frequency? What is the difference between linear and angular spatial frequency?
5. Explain the basic idea of the Strang van Hees method.
6. What other approaches are there to applying the **FFT** method on a curved (spherical or ellipsoidal) surface?
7. Why are bordering of the data area and tapering of the data necessary?
8. In addition to geoid determination, where in physical geodesy is the **FFT** method also used?
9. When computing the terrain correction on the Earth’s surface, explain the “ δ trick” used in the derivation. Why is it necessary, and how does one make the δ vanish again?





Statistical methods

10



10.1 The role of uncertainty in geophysics

In geophysics, we often obtain results based on uncertain, incomplete, or otherwise deficient observational data. This also applies in the study of the Earth's gravity field: the density of gravity observations on the Earth's surface, for example, varies greatly, and large areas of the oceans and polar regions are covered only by a very sparse network of measurements. We speak of *spatial undersampling*.

Measurement technologies that work from space, on the other hand, usually provide coverage of the whole globe, oceans, poles and all. They, however, do not measure at a very high *resolution*. Either the resolution of the method is limited — this holds for example for the gravity-field parameters calculated from satellite orbit perturbations — or the instruments measure only directly underneath the satellite's path, like satellite altimetry.

Another often relevant uncertainty factor is that one can do precise measurements on the Earth's surface, but inside the Earth the uncertainty is much larger and the data is obtained much more indirectly.

In previous chapters we described techniques by which we could calculate desired values or parameters for the Earth's gravity field, assuming that, for example, gravity anomalies are available everywhere on the Earth's surface, and with arbitrarily high resolution. In this

chapter we look at mathematical means to handle real-world situations where this is not the case.



10.2 Linear functionals

In mathematics, a mapping that associates with every function in a given function space a certain numerical value is called a *functional*. One such is, for example, a (partial) derivative at a certain point x_0 :

$$f \mapsto \left. \frac{\partial}{\partial x} f(x) \right|_{x=x_0}.$$

A trivial functional is also the *evaluation functional*, the function value itself (i.e., the “zeroth derivative”) for a certain argument value,

$$f \mapsto f(x_0).$$

Other functionals are for example the integral over a given area σ :

$$f \mapsto \int_{\sigma} f(x) \, dx,$$

and so on.

We may write symbolically

$$L = \left. \frac{\partial}{\partial x} \right|_{x=x_0}, \quad \text{meaning} \quad L\{f\} = \left. \frac{\partial}{\partial x} f(x) \right|_{x=x_0}.$$

lineariset
funktionaalit

A functional or operator is *linear* if

$$L\{\alpha f + \beta g\} = \alpha L\{f\} + \beta L\{g\}, \quad \alpha, \beta \in \mathbb{R}.$$

Remember that all partial derivatives, as also the *Laplace operator* Δ , are linear.

In physical geodesy, all interesting functionals are functionals of the function $T(\phi, \lambda, R) = T(\phi, \lambda, r)|_{r=R}$, i.e., of the disturbing potential at the surface of a spherical Earth. The theory thus uses the spherical approximation,¹ and the surface of the sphere of radius R corresponds

¹This is not mandatory, but the error of approximation is usually small.



to mean sea level. For example, the disturbing potential $T_P \stackrel{\text{def}}{=} T(\phi, \lambda, R)$ at a point P at sea-level location (ϕ, λ) is such a functional:

$$T(\cdot, \cdot, R) \mapsto T(\phi, \lambda, R).$$

If point P is not at sea level, a suitable functional also exists:

$$T(\cdot, \cdot, R) \mapsto T(\phi, \lambda, r).$$

If the quantity is not the disturbing potential, but, say, the gravity anomaly or the deflection of the plumb line:

$$T(\cdot, \cdot, R) \mapsto \Delta g(\phi, \lambda, r),$$

$$T(\cdot, \cdot, R) \mapsto \xi(\phi, \lambda, r),$$

$$T(\cdot, \cdot, R) \mapsto \eta(\phi, \lambda, r).$$

All these are also *linear* functionals. In fact, if we write

$$T(\phi, \lambda, r) = \sum_{n=2}^{\infty} \frac{1}{r^{n+1}} \sum_{m=0}^n P_{nm}(\sin \phi) (a_{nm} \cos m\lambda + b_{nm} \sin m\lambda),$$

even the spherical-harmonic coefficients a_{nm}, b_{nm} are all linear functionals of the disturbing potential T:

$$T(\cdot, \cdot, R) \mapsto a_{nm},$$

$$T(\cdot, \cdot, R) \mapsto b_{nm}.$$

Here, $T(\cdot, \cdot, R)$ is shorthand for the whole function

$$T(\phi, \lambda, R), \phi \in [-\pi/2, +\pi/2], \lambda \in [0, 2\pi).$$

10.3 Statistics on the Earth's surface

In statistics, we define a *stochastic process* as a stochastic quantity, or random variable, the *domain* of which is a function space. In other words, määrittelyjoukko it is a random variable, the realisation values of which are *functions*. A



stochastic process may be a quantity developing over time, the precise behaviour of which is uncertain, for example a satellite orbit. In the same way as for a (real-valued) stochastic quantity \underline{x} we may calculate an expected value or *expectancy* $E\{\underline{x}\}$ and a *variance*

$$C_{xx} = \text{Var}\{\underline{x}\} = E\{(\underline{x} - E\{\underline{x}\})^2\},$$

we may also do so for a stochastic process. The only difference is that by doing so we obtain *functions*.

Let, for example, the stochastic process $\underline{x}(t)$ be a function of time. Then we may compute its variance function as follows:

$$C_{xx}(t) = \text{Var}\{\underline{x}(t)\}.$$

However, much more can be computed for a stochastic process, for example the covariance of values of the same process taken at different points in time, the *autocovariance*:

$$\begin{aligned} A_{xx}(t_1, t_2) &= \text{Cov}\{\underline{x}(t_1), \underline{x}(t_2)\} = \\ &= E\{(\underline{x}(t_1) - E\{\underline{x}(t_1)\})(\underline{x}(t_2) - E\{\underline{x}(t_2)\})\}. \end{aligned}$$

Similarly if we have two different processes, we may compute the *cross covariance* between them.

The argument of a stochastic process is commonly *time* t . However in geophysics we study stochastic processes the arguments of which are locations on the Earth's surface, i.e., we talk of processes of the form $\underline{x}(\phi, \lambda)$. The definitions of auto- and cross-covariances work otherwise in the same way, but in the case of the Earth we have a special problem. A stochastic quantity is generally defined as a quantity \underline{x} from which *realisations* x_1, x_2, x_3, \dots are obtained, which together have certain statistical properties.

The classical example is the *dice* throw. A die can be thrown again and again, and one can practise the art of statistics on the results of the throws. Another classic example is *measurement*. Measurement of the



same quantity can be repeated, and is repeated, in order to improve precision.

For a stochastic process defined on the Earth's surface, the situation is different.

We have only one Earth.

For this reason, statistics must be done in a somewhat different fashion.

Given a stochastic process on the surface of the Earth, $\underline{x}(\phi, \lambda)$, we define a quantity similar to the statistical expectancy $E\{\cdot\}$, the *geographic mean*

$$M\{x\} \stackrel{\text{def}}{=} \frac{1}{4\pi} \iint_{\sigma} x(\phi, \lambda) d\sigma = \frac{1}{4\pi} \int_0^{2\pi} \int_{-\pi/2}^{+\pi/2} x(\phi, \lambda) \cos \phi \, d\phi \, d\lambda. \quad (10.1)$$

Here $x(\phi, \lambda)$ is the one and only realisation of process \underline{x} that is available on this Earth.

Clearly this definition makes sense only in the case where the statistical behaviour of the process $\underline{x}(\phi, \lambda)$ is the same everywhere on Earth, independently of location (ϕ, λ) . This is called the *assumption of homogeneity*. It is in fact the assumption that the spherical symmetry of the Earth extends to the statistical behaviour of her gravity field.

homogeenisuus

Similarly to the statistical variance based on expectancy, we may define the *geographic variance*:

$$C_{xx}(\phi, \lambda) \stackrel{\text{def}}{=} \text{Var}\{\underline{x}(\phi, \lambda)\} \stackrel{\text{def}}{=} M\left\{ (x - M\{x\})^2 \right\}. \quad (10.2)$$

The global average of gravity anomalies $\Delta g(\phi, \lambda)$ *vanishes*² based on their definition:

$$M\{\Delta g\} = 0.$$

²This is not exactly valid if, for example, the normal gravity field used in calculating the anomalies contains the mass of the atmosphere, but gravity values measured close to sea level do not contain the attraction of the atmosphere. There are other small effects due to the non-realism of the normal field.



In that case, equation 10.2 is simplified as follows:

$$C_{\Delta g \Delta g}(\phi, \lambda) = \text{Var}\{\underline{\Delta g}(\phi, \lambda)\} = M\{\Delta g^2\} = \frac{1}{4\pi} \iint_{\sigma} (\Delta g(\phi, \lambda))^2 d\sigma.$$

The definition given here of the geographic mean $M\{\cdot\}$ is based on *integration* of the one and only realisation over the surface of the Earth. As has been seen, in statistics the mean is defined slightly differently, as the *expectancy* of a stochastic process. For gravity anomalies it is $E\{\underline{\Delta g}\}$, in which $\underline{\Delta g}$ is the anomaly *considered as a stochastic process*, the series of values of Δg that results if we look at an endless series of randomly formed Earths. Not very practical!

ergodisuus If the expectancy of a stochastic process is the same as the mean of one realisation computed by integration — and other statistical properties are similarly the same — we speak of an *ergodic process*. Establishing empirically in geophysics that a process is ergodic is typically difficult to impossible.



10.4 The covariance function of the gravity field

Defining a *covariance function* between points P and Q is more complicated. Something like equations 10.1 and 10.2 cannot be used directly, because *both* Δg_P and Δg_Q can move independently over the whole Earth's surface. We have

$$\begin{aligned}\Delta g_P &= \Delta g(\phi_P, \lambda_P), \\ \Delta g_Q &= \Delta g(\phi_Q, \lambda_Q).\end{aligned}$$

In the following we assume that the covariance to be calculated will only depend on the *relative* location of points P and Q. In a homogeneous gravity field, the covariance function will not depend on the absolute location of the points, but only on the *difference* in location between points P and Q.

Write

$$\phi_Q = \phi_Q(\phi_P, \lambda_P, \psi_{PQ}, \alpha_{PQ}), \quad \lambda_Q = \lambda_Q(\phi_P, \lambda_P, \psi_{PQ}, \alpha_{PQ}).$$



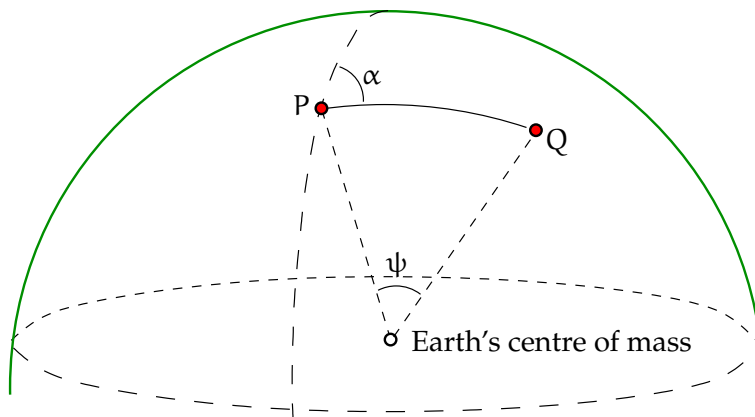


FIGURE 10.1. Definition of geocentric angular distance and azimuth.

ϕ_Q and λ_Q can be computed³ if we know ϕ_P and λ_P as well as both the *geocentric angular distance* ψ_{PQ} and the *azimuth angle* α_{PQ} . See figure 10.1.

Now we may write

$$\begin{aligned} \Delta g_Q &= \Delta g_Q \left(\phi_Q(\phi_P, \lambda_P, \psi_{PQ}, \alpha_{PQ}), \lambda_Q(\phi_P, \lambda_P, \psi_{PQ}, \alpha_{PQ}) \right) = \\ &= \Delta g_Q(\phi_P, \lambda_P, \psi_{PQ}, \alpha_{PQ}), \end{aligned}$$

and we may define as the *covariance function*

$$\begin{aligned} C_{\Delta g \Delta g}(\psi_{PQ}, \alpha_{PQ}) &\stackrel{\text{def}}{=} M_P \{ \Delta g_P(\phi_P, \lambda_P) \Delta g_Q(\phi_P, \lambda_P, \psi_{PQ}, \alpha_{PQ}) \} = \\ &= \frac{1}{4\pi} \iint_{\sigma} \Delta g_P(\phi_P, \lambda_P) \Delta g_Q(\phi_P, \lambda_P, \psi_{PQ}, \alpha_{PQ}) \, d\sigma_P. \end{aligned}$$

Also here, M_P is a geographic-mean operator. First we fix point Q in relation to point P : both azimuth α_{PQ} and distance ψ_{PQ} are held fixed. Point P , and with it, point Q , is moved over the whole of the Earth's surface. We compute the corresponding integral over the unit sphere

³This is called the *geodetic forward problem* on the sphere.



σ_P , and divide by 4π :

$$\begin{aligned} C_{\Delta g \Delta g}(\psi_{PQ}, \alpha_{PQ}) &= M_P \{ \Delta g_P \Delta g_{Q(P)} \} = \frac{1}{4\pi} \iint_{\sigma} \Delta g_P \Delta g_{Q(P)} d\sigma = \\ &= \frac{1}{4\pi} \int_{-\pi/2}^{+\pi/2} \int_0^{2\pi} \Delta g_P \Delta g_{Q(P)} d\lambda_P \cos \phi_P d\phi_P, \end{aligned}$$

in which $d\sigma = \cos \phi d\lambda d\phi$ was used, $\cos \phi$ being *Jacobi's determinant* for the co-ordinates (ϕ, λ) on the unit sphere.

In addition to the assumption of homogeneity, we may make still the *assumption of isotropy*: the covariance function — or more generally, the statistical behaviour of the gravity field — does *not* depend on the relative direction or *azimuth* α_{PQ} of point pair (P, Q) , but only on the *angular distance* ψ_{PQ} between them. (This, too, is, like homogeneity, one of the forms in which the Earth's spherical symmetry is expressed.) In this case we may compute the geographic mean in a slightly different way, by also averaging over all azimuth angles $\alpha_{PQ} \in [0, 2\pi)$:

$$\begin{aligned} C_{\Delta g \Delta g}(\psi_{PQ}) &\stackrel{\text{def}}{=} \\ &\stackrel{\text{def}}{=} M'_P \{ \Delta g_P \Delta g_{Q(P)} \} = \frac{1}{2\pi} \int_0^{2\pi} M_P \{ \Delta g_P \Delta g_{Q(P)} \} d\alpha_{PQ} = \\ &= \frac{1}{8\pi^2} \int_0^{2\pi} \int_{-\pi/2}^{+\pi/2} \int_0^{2\pi} \Delta g_P \Delta g_{Q(P)} d\lambda_P \cos \phi_P d\phi_P d\alpha_{PQ}. \quad (10.3) \end{aligned}$$

Remark The true gravity field of the Earth is not terribly homogeneous or isotropic, but in spite of this, both hypotheses are widely used.



10.5 Least-squares collocation



10.5.1 Stochastic processes in one dimension

pienimmän
neliösumman
kollokaatio

Collocation is a statistical estimation technique used to estimate the values of a *stochastic process* and calculate the uncertainties (like mean errors) of the estimates.



Let $\underline{s}(t)$ be a stochastic process, the autocovariance function of which is $C(t_i, t_j)$. Let the process furthermore be *stationary*, in other words, for any two moments in time t_i, t_j it holds that $C(t_i, t_j) = C(t_j - t_i) = C(\Delta t)$. The argument t is generally time, but could be any parameter, for example the distance of a journey.

Of this process, we have *observations* made at times t_1, t_2, \dots, t_N , when the corresponding process values for those times are $\underline{s}(t_1), \underline{s}(t_2), \dots, \underline{s}(t_N)$. Let us assume, for the moment, that these values are *error-free* observations. Then the observations are function values of process \underline{s} , stochastic quantities, the variance matrix of which we may write as follows:

$$\text{Var}\{\underline{s}_i\} = \begin{bmatrix} C(t_1, t_1) & C(t_2, t_1) & \cdots & C(t_1, t_N) \\ C(t_1, t_2) & C(t_2, t_2) & \cdots & \vdots \\ \vdots & \vdots & \ddots & \vdots \\ C(t_1, t_N) & C(t_2, t_N) & \cdots & C(t_N, t_N) \end{bmatrix}.$$

We also call this autocovariance matrix the *signal variance matrix* of \underline{s} . We use the symbol C_{ij} for this, both for one element $C_{ij} = C(t_i, t_j)$ of the matrix and for the whole matrix: $C_{ij} = \begin{bmatrix} C(t_i, t_j), & i, j = 1, \dots, N \end{bmatrix}$. The symbol \underline{s}_i again denotes a vector $\begin{bmatrix} \underline{s}(t_i), & i = 1, \dots, N \end{bmatrix}$ consisting of process values — or one of its elements $\underline{s}(t_i)$.

Note that, if the function $C(t_i, t_j)$, or $C(\Delta t)$, is known, then the whole matrix and all of its elements can be calculated, provided all argument values (observation times) t_i are known.

Let the shape of the problem now be that one should *estimate*, i.e., *predict*, the value of process \underline{s} at the moment in time T , i.e., $\underline{s}(T)$, based on our knowledge of the above-described *observations* $\underline{s}(t_i)$, $i = 1, \dots, N$.

In the same way as we calculated above the covariances between $\underline{s}(t_i)$ and $\underline{s}(t_j)$ (elements of the signal variance matrix C_{ij}), we also compute the covariances between $\underline{s}(T)$ and all $\underline{s}(t_i)$, $i = 1, \dots, N$. We obtain

$$\text{Cov}\{\underline{s}(T), \underline{s}(t_i)\} = \begin{bmatrix} C(T, t_1) & C(T, t_2) & \cdots & C(T, t_N) \end{bmatrix}.$$



For this we may use the notation C_{Tj} . It is assumed here that there is only one point in time T for which estimation is done. Generalisation to the case where there are several T_p , $p = 1, \dots, M$, is straightforward. In that case, the signal covariance matrix will be of size $M \times N$:

$$\text{Cov}\{\underline{s}(T_p), \underline{s}(t_i)\} = \begin{bmatrix} C(T_1, t_1) & C(T_1, t_2) & \cdots & C(T_1, t_N) \\ C(T_2, t_1) & C(T_2, t_2) & \cdots & C(T_2, t_N) \\ \vdots & \vdots & & \vdots \\ C(T_M, t_1) & C(T_M, t_2) & \cdots & C(T_M, t_N) \end{bmatrix}.$$

For this we may use the more general notation C_{pj} .

10.5.2 Signal and noise

The process $\underline{s}(t)$ is called the *signal*. It is a *physical phenomenon* that we are *interested* in. There also exist physical phenomena that are otherwise similar, but that we are *not* interested in: on the contrary, we wish to *remove* their influence. Such stochastic processes are called *noise*.

When we make an observation, the purpose of which is to obtain a value for the quantity $\underline{s}(t_i)$, we obtain *in reality* a value that is not absolutely precise. The real observation thus is

$$\underline{\ell}_i = \underline{s}(t_i) + \underline{n}_i. \quad (10.4)$$

Here, \underline{n}_i is a stochastic quantity: *observational error* or *noise*. Let its variance — or more precisely, the joint noise variance matrix of multiple observations — be D_{ij} . This is a very similar matrix to the above C_{ij} , and also symmetric and positive definite. The only difference is that D_{ij} designates *noise*, which we are *not* interested in. Often it may be assumed that the errors $\underline{n}_i, \underline{n}_j$ of two different observations $\underline{\ell}_i, \underline{\ell}_j$ do not correlate, in which case D_{ij} is a diagonal matrix.

10.5.3 Estimator and variance of prediction

Now we construct an *estimator*

$$\hat{\underline{s}}(T_p) \stackrel{\text{def}}{=} \sum_i \Lambda_{pi} \underline{\ell}_i,$$



as a linear combination of the observations at our disposal $\underline{\ell}_i$. The purpose in life of this estimator is to get as close as possible to $\underline{s}(T_p)$. So, the quantity to be minimised is the difference

$$\widehat{s}(T_p) - \underline{s}(T_p) = \Lambda_{pi} \underline{\ell}_i - \underline{s}(T_p) = \Lambda_{pi} (\underline{s}(t_i) + \underline{n}_i) - \underline{s}(T_p).$$

Here, for the sake of writing convenience, we left the summation sign \sum off (Einstein summation convention): We always sum over adjacent, identical indices, in this case i .

Study the variance of this difference, the so-called *variance of prediction*:

$$\Sigma_{pp} \stackrel{\text{def}}{=} \text{Var}\{\widehat{s}(T_p) - \underline{s}(T_p)\}.$$

We exploit *propagation of variances*, the notations introduced above, and our knowledge that surely there is no physical relationship, or *correlation*, between observation process noise \underline{n} and signal \underline{s} :

varianssien
kasautuminen

$$\begin{aligned} \text{Cov}\left\{(\underline{s}(t_i) + \underline{n}_i), (\underline{s}(t_j) + \underline{n}_j)\right\} &= \\ &= \text{Cov}\{\underline{s}(t_i), \underline{s}(t_j)\} + \text{Cov}\{\underline{n}_i, \underline{n}_j\} = C_{ij} + D_{ij}, \end{aligned}$$

and⁴

$$\begin{aligned} \Sigma_{pq} &= \text{Cov}\left\{\left(\widehat{s}(T_p) - \underline{s}(T_p)\right), \left(\widehat{s}(T_q) - \underline{s}(T_q)\right)\right\} = \\ &= \Lambda_{pi} \text{Cov}\left\{(\underline{s}(t_i) + \underline{n}_i), (\underline{s}(t_j) + \underline{n}_j)\right\} \Lambda_{jq} + \text{Cov}\left\{\underline{s}(T_p), \underline{s}(T_q)\right\} - \\ &\quad - \Lambda_{pi} \text{Cov}\left\{\underline{s}(t_i), \underline{s}(T_q)\right\} - \text{Cov}\left\{\underline{s}(T_p), \underline{s}(t_j)\right\} \Lambda_{jq} = \\ &= \Lambda_{pi} (C_{ij} + D_{ij}) \Lambda_{jq} + C_{pq} - \Lambda_{pi} C_{iq} - C_{pj} \Lambda_{jq}. \quad (10.5) \end{aligned}$$

The variances, or diagonal elements, Σ_{pp} of the matrix are now obtained by setting $q = p$.

10.5.4 Showing optimality

Here we show that the optimal estimator is indeed the one producing the minimum possible variances.

⁴The matrix C_{iq} is the transpose of C_{pj} , the matrix Λ_{jq} the transpose of Λ_{pi} .



Choose

$$\Lambda_{pj} \stackrel{\text{def}}{=} C_{pi} (C_{ij} + D_{ij})^{-1}.$$

Then, from equation 10.5 and exploiting the symmetry of the C and D matrices, we obtain

$$\begin{aligned} \Sigma_{pp} &= C_{pi} (C_{ij} + D_{ij})^{-1} C_{jp} + C_{pp} - \\ &\quad - C_{pi} (C_{ij} + D_{ij})^{-1} C_{jp} - C_{pi} (C_{ij} + D_{ij})^{-1} C_{jp} = \\ &= C_{pp} - C_{pi} (C_{ij} + D_{ij})^{-1} C_{jp}. \end{aligned} \quad (10.6)$$

Let us study next the *alternative choice*

$$\Lambda_{pj} = C_{pi} (C_{ij} + D_{ij})^{-1} + \delta\Lambda_{pj}.$$

In this case we obtain by substitution

$$\begin{aligned} \Sigma'_{pp} &= \overbrace{\Lambda_{pi} (C_{ij} + D_{ij}) \Lambda_{jp}}^{\text{I}} + C_{pp} \overbrace{-\Lambda_{pj} C_{jp}}^{\text{II}} \overbrace{-C_{pi} \Lambda_{ip}}^{\text{III}} = \\ &= \overbrace{\left[C_{pi} (C_{ij} + D_{ij})^{-1} + \delta\Lambda_{pj} \right] (C_{ij} + D_{ij}) \left[(C_{jk} + D_{jk})^{-1} C_{kp} + \delta\Lambda_{kp} \right]}^{\text{I}} + \\ &\quad + C_{pp} \overbrace{-\left[C_{pi} (C_{ij} + D_{ij})^{-1} + \delta\Lambda_{pj} \right] C_{jp}}^{\text{II}} \overbrace{-C_{pi} \left[(C_{ij} + D_{ij})^{-1} C_{jp} + \delta\Lambda_{ip} \right]}^{\text{III}} = \\ &= \overbrace{\cancel{C_{pi} (C_{ij} + D_{ij})^{-1} C_{jp}} + \cancel{C_{pi} \delta\Lambda_{ip}} + \delta\Lambda_{pi} C_{ip} + \delta\Lambda_{pi} (C_{ij} + D_{ij}) \delta\Lambda_{jp}}^{\text{I}} + \\ &\quad + C_{pp} \overbrace{-\cancel{C_{pi} (C_{ij} + D_{ij})^{-1} C_{jp}} - \delta\Lambda_{pi} C_{ip}}^{\text{II}} \overbrace{-\cancel{C_{pi} (C_{ij} + D_{ij})^{-1} C_{jp}} - \cancel{C_{pi} \delta\Lambda_{ip}}}_{\text{III}} = \\ &= C_{pp} - C_{pi} (C_{ij} + D_{ij})^{-1} C_{jp} + \delta\Lambda_{pi} (C_{ij} + D_{ij}) \delta\Lambda_{jp}. \end{aligned}$$

Here, the last term — the only difference from result 10.6 — is positive, because the matrices C_{ij} and D_{ij} are positive definite: $\Sigma'_{pp} > \Sigma_{pp}$, except when $\delta\Lambda_{pi} = 0$. In other words, the solution given above,

$$\Lambda_{pj} = C_{pi} (C_{ij} + D_{ij})^{-1} \implies \hat{s}(T_p) = C_{pi} (C_{ij} + D_{ij})^{-1} \ell_j,$$

is *optimal* in the sense of least-squares — more precisely, in the sense of minimising the variance of prediction Σ_{pp} .



10.5.5 The covariance function of gravity anomalies

Least-squares collocation is used extensively to optimally estimate gravity values and other functionals of the gravity field on the Earth's surface.

If we have two points, P and Q, with measured gravity anomalies $\underline{\Delta g}_P = \underline{\Delta g}(\phi_P, \lambda_P)$ and $\underline{\Delta g}_Q = \underline{\Delta g}(\phi_Q, \lambda_Q)$, we would like to have the covariance between these two anomalies,

$$\text{Cov}\{\underline{\Delta g}_P, \underline{\Delta g}_Q\}.$$

As argued in section 10.4, we can only empirically derive such a covariance by looking at all point pairs (P, Q) that are in the same relative position around the globe, and averaging over them using the M or M' operator.

Normally the covariance is assumed to depend *only* on the geocentric angular distance ψ between points P and Q. Then, we speak of an *isotropic process* $\underline{\Delta g}(\phi, \lambda)$. Then, the covariance will also be

$$\text{Cov}\{\underline{\Delta g}_P, \underline{\Delta g}_Q\} = M'_P\{\Delta g_P \Delta g_{Q(P)}\} = C(\psi_{PQ}).$$

A popular covariance function for gravity anomalies is Hirvonen's⁵ equation:

$$C(\psi) = \frac{C_0}{1 + (\psi/\psi_0)^2}, \quad (10.7)$$

in which $C_0 = C(0)$ and ψ_0 are parameters describing the behaviour of the gravity field. $C_0 = \text{Var}\{\underline{\Delta g}(\phi, \lambda)\} = M\{\Delta g^2\}$ is called the *signal variance*, ψ_0 the *correlation length*. ψ_0 gives the distance at which the correlation between the gravity anomalies in two points is still 50%.⁶

In local applications, instead of the angular distance ψ one uses the linear distance

$$s = \psi R,$$

⁵Reino Antero Hirvonen (1908–1989) was a Finnish physical and mathematical geodesist.

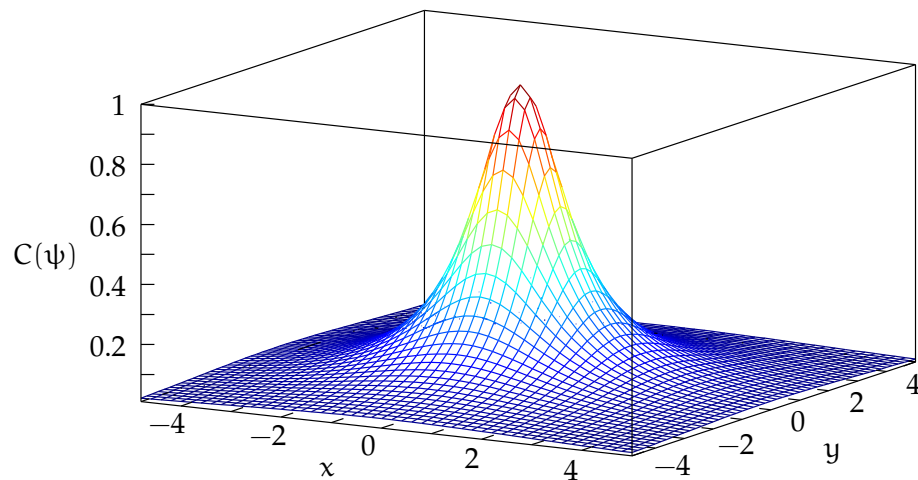


FIGURE 10.2. Hirvonen's covariance function in two dimensions. $C_0 = \psi_0 = 1$ is assumed.

where R is the radius of the Earth. Then

$$C(s) = \frac{C_0}{1 + (s/d)^2}.$$

This equation was derived from gravimetric data for Ohio state, USA, but it has broader validity. $C(0) = C_0$, the signal variance when $s = 0$. The variable $d = R\psi_0$ is also called the correlation length. It is the distance d for which $C(d) = \frac{1}{2}C_0$, as seen from the equation.

The quantity C_0 varies considerably between areas, from hundreds to thousands of mGal^2 , and tends to be largest in mountainous areas. The quantity d is generally of the order of magnitude of tens of kilometres.

Alternative functions that are also often used in local applications are the covariance functions of first- and second-order autoregressive

⁶The correlation is

$$\text{Corr}\{\underline{\Delta g}_P, \underline{\Delta g}_Q\} = \frac{\text{Cov}\{\underline{\Delta g}_P, \underline{\Delta g}_Q\}}{\sqrt{\text{Var}\{\underline{\Delta g}_P\} \text{Var}\{\underline{\Delta g}_Q\}}} = \frac{\frac{C_0}{1 + (\psi/\psi_0)^2}}{\sqrt{C_0 C_0}} = \frac{1}{1 + (\psi/\psi_0)^2},$$

which is 0.5 if $\psi = \psi_0$.



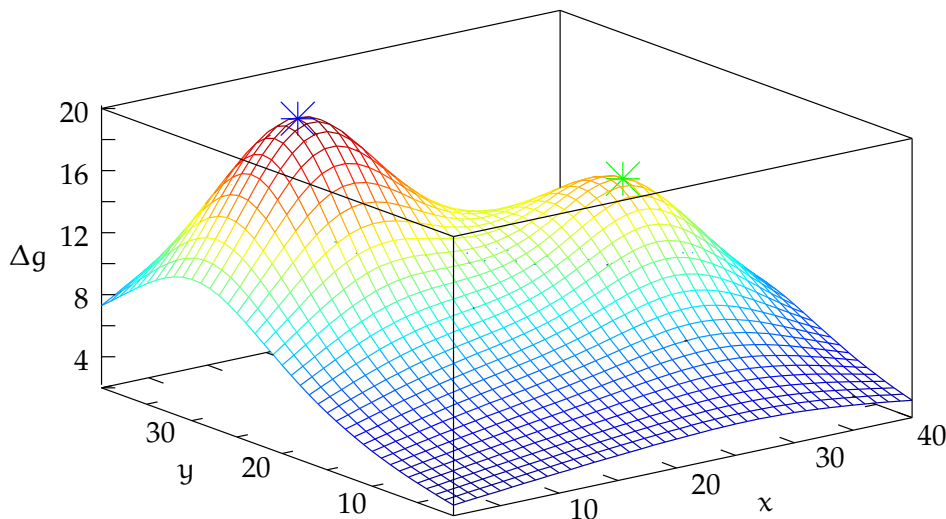


FIGURE 10.3. An example of least-squares collocation. Here are given two data points (stars); the surface plotted gives the estimated value $\widehat{\Delta g}_P$ for each point P in the area. We use least-squares collocation for inter- and extrapolating gravimetric data.



processes, or AR(1) or AR(2) processes:

$$C(\psi) = C_0 \exp(-\psi/\psi_0) \quad \text{or} \quad C(\psi) = C_0 \exp\left(-(\psi/\psi_0)^2\right).$$

An AR(1) process is also called a Gauss–Markov process.



10.5.6 Least-squares collocation for gravity anomalies

If N points P_i , $i = 1, \dots, N$ are given, where were measured gravity values — more precisely, anomalies — $\underline{\Delta g}_i = \underline{\Delta g}(\phi_i, \lambda_i)$, we may, as above, construct a *signal variance matrix*

$$C_{ij} \stackrel{\text{def}}{=} \text{Var}\{\underline{\Delta g}_i\} = \begin{bmatrix} C_0 & C(\psi_{21}) & \cdots & C(\psi_{N1}) \\ C(\psi_{12}) & C_0 & \cdots & C(\psi_{N2}) \\ \vdots & \vdots & \ddots & \vdots \\ C(\psi_{1N}) & C(\psi_{2N}) & \cdots & C_0 \end{bmatrix} = \begin{bmatrix} C_0 & C_{21} & \cdots & C_{N1} \\ C_{12} & C_0 & \cdots & C_{N2} \\ \vdots & \vdots & \ddots & \vdots \\ C_{1N} & C_{2N} & \cdots & C_0 \end{bmatrix},$$



in which all elements $C(\psi_{ij})$ are calculated using covariance function 10.7 given above.

If we also compute for the point P at which gravity is unknown:

$$\text{Cov}\{\underline{\Delta g}_p, \underline{\Delta g}_i\} = \begin{bmatrix} C(\psi_{P1}) & C(\psi_{P2}) & \cdots & C(\psi_{PN}) \end{bmatrix} \stackrel{\text{def}}{=} C_{Pi},$$

we obtain, in the same way as before, for the *least-squares collocation* solution

$$\widehat{\Delta g}_p = C_{Pi} (C_{ij} + D_{ij})^{-1} \underline{\ell}_j \approx C_{Pi} C_{ij}^{-1} \underline{\ell}_j,$$

in which the $\underline{\ell}_j = \underline{\Delta g}_j + \underline{n}_j$ are gravity anomaly observations made in points $j = 1, \dots, N$. The matrix D_{ij} , which we leave out of consideration here, again describes the random observation error, observation uncertainty, or *noise* \underline{n}_i associated with making those observations. Often D_{ij} is a diagonal matrix, meaning that the observations are statistically independent and do not correlate with each other.

We may also compute a precision assessment of this solution, the *variance of prediction*, equation 10.10:

$$\Sigma_{PP} = C_0 - C_{Pi} (C_{ij} + D_{ij})^{-1} C_{jP} \approx C_0 - C_{Pi} C_{ij}^{-1} C_{jP}$$

in the case of one unknown prediction point P. Its square root

$$\sigma_{\Delta g_p} = \sqrt{\Sigma_{PP}}$$

is the *mean error* of estimator $\widehat{\Delta g}_p$.

10.5.7 Calculation example

See figure 10.4. Two points are given where gravity has been measured and gravity anomalies calculated: $\underline{\Delta g}_1 = 15 \text{ mGal}$, $\underline{\Delta g}_2 = 20 \text{ mGal}$. The co-ordinates in the x and y directions are in kilometres. It is assumed that between the gravity anomalies of different points, Hirvonen's covariance function,

$$C(s) = \frac{C_0}{1 + (s/d)^2},$$



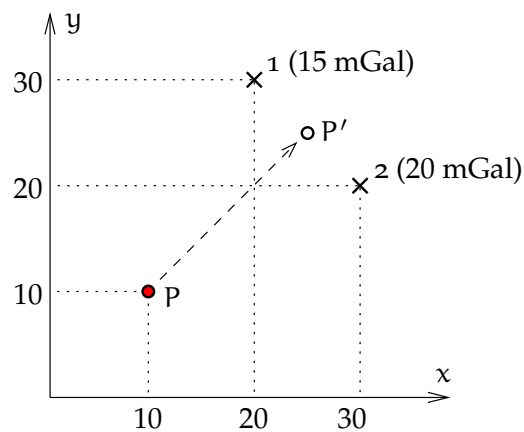


FIGURE 10.4. Collocation example.

applies, in which $d = 20$ km and $C_0 = \pm 1000$ mGal². In addition, it is assumed that the gravity measurements done — including height determination of the gravity points! — were *errorless*. So, $D_{ij} = 0$, $i, j = 1, 2$.

Calculate an estimate of the gravity anomaly $\widehat{\Delta g}_P$ at point P and its mean error $\sigma_{PP} = \sqrt{\Sigma_{PP}}$.

Calculate first the distances s and the corresponding covariances C .

$$s_{12}^2 = \left((30 - 20)^2 + (20 - 30)^2 \right) \text{ km}^2 = 200 \text{ km}^2,$$

$$C_{12} = C_{21} = \frac{1000 \text{ mGal}^2}{1 + 200/400} = 666.66 \dots \text{ mGal}^2,$$

$$s_{1P}^2 = \left((30 - 10)^2 + (20 - 10)^2 \right) \text{ km}^2 = 500 \text{ km}^2,$$

$$C_{1P} = \frac{1000 \text{ mGal}^2}{1 + 500/400} = 444.44 \dots \text{ mGal}^2,$$

$$s_{2P}^2 = \left((20 - 10)^2 + (30 - 10)^2 \right) \text{ km}^2 = 500 \text{ km}^2,$$

$$C_{2P} = \frac{1000 \text{ mGal}^2}{1 + 500/400} = 444.44 \dots \text{ mGal}^2.$$

From this follows

$$C_{ij} + D_{ij} = C_{ij} = \begin{bmatrix} C_{11} & C_{12} \\ C_{21} & C_{22} \end{bmatrix} = \begin{bmatrix} 1000 & 666.66 \\ 666.66 & 1000 \end{bmatrix} \text{ mGal}^2,$$



and its inverse matrix

$$(C_{ij} + D_{ij})^{-1} = \begin{bmatrix} 0.0018 & -0.0012 \\ -0.0012 & 0.0018 \end{bmatrix} \text{mGal}^{-2}.$$

Furthermore

$$C_{Pi} = \begin{bmatrix} C_{P1} & C_{P2} \end{bmatrix} = \begin{bmatrix} 444.44 & 444.44 \end{bmatrix} \text{mGal}^2.$$

As the vector of observations is

$$\underline{\Delta g}_j = \begin{bmatrix} \underline{\Delta g}_1 \\ \underline{\Delta g}_2 \end{bmatrix} = \begin{bmatrix} 15 \\ 20 \end{bmatrix} \text{mGal},$$

we obtain the result

$$\begin{aligned} \widehat{\Delta g}_p &= \begin{bmatrix} 444.44 & 444.44 \end{bmatrix} \begin{bmatrix} 0.0018 & -0.0012 \\ -0.0012 & 0.0018 \end{bmatrix} \begin{bmatrix} 15 \\ 20 \end{bmatrix} \text{mGal} = \\ &= 9.333 \text{mGal}. \end{aligned}$$

The precision, the *variance of prediction*, equation 10.10:

$$\begin{aligned} \Sigma_{PP} &= C_{PP} - C_{Pi} (C_{ij} + D_{ij})^{-1} C_{jP} = C_0 - \\ &- \begin{bmatrix} 444.44 & 444.44 \end{bmatrix} \begin{bmatrix} 0.0018 & -0.0012 \\ -0.0012 & 0.0018 \end{bmatrix} \begin{bmatrix} 444.44 \\ 444.44 \end{bmatrix} \text{mGal}^2 = \\ &= 762.96 \text{mGal}^2, \end{aligned}$$

so

$$\sigma_{\Delta g_p} = \sqrt{\Sigma_{PP}} = \pm 27.622 \text{mGal}.$$

Summarising the result:

$$\widehat{\Delta g}_p = 9.333 \pm 27.622 \text{mGal}.$$

Observe that the gravity anomaly estimate found is much smaller than its own uncertainty, and thus *does not differ significantly from zero*. In fact, not using the observational data at all would leave us with the *a priori* estimate

$$\widehat{\Delta g}_p = 0 \pm \sqrt{1000} \text{mGal} = 0 \pm 31.623 \text{mGal},$$



almost as good.

If, instead, we had used point P' *in between* points 1 and 2, at location (25 km, 25 km), then

$$C_{P'1} = C_{P'2} = 1000 \text{ mGal}^2 / (1 + 50/400) = 888.89 \text{ mGal}^2$$

and $\widehat{\Delta g}_{P'} = 18.667 \pm 7.201 \text{ mGal}$, which is clearly better than the *a priori* estimate of zero.

And if we had chosen instead the Gauss–Markov covariance function

$$C = C_0 \exp(-s/d)$$

we would have obtained the results $\widehat{\Delta g}_p = 7.663 \pm 29.272 \text{ mGal}$ for the original point location, and $\widehat{\Delta g}_{p'} = 16.460 \pm 18.426 \text{ mGal}$ for the shifted point location.

10.5.8 Theory of least-squares collocation

Above we presented one popular application of least-squares collocation. Here we look at the method more generally. The basic equation is

$$\widehat{\mathbf{f}} = C_{fg} (C_{gg} + D_{gg})^{-1} (\mathbf{g} + \mathbf{n}). \quad (10.8)$$

The vector \mathbf{g} contains *observed quantities* g_i , the vector \mathbf{n} contains the observational *noise*, and $\widehat{\mathbf{f}}$ is a vector of quantities \widehat{f}_p to be *predicted*. The hat is a commonly used symbol for an estimator.

Both vectors \mathbf{g} and $\widehat{\mathbf{f}}$ can, for example, be gravity anomalies, in which case we have *homogeneous prediction*, a type of inter- or extrapolation. More generally $\widehat{\mathbf{f}}$ and \mathbf{g} are of different types: for example $\widehat{\mathbf{f}}$ consists of geoid heights \mathbf{N}_p and \mathbf{g} of gravity anomalies Δg_i . In the latter case, the Stokes equation is “covertly” along in the structure of the C matrices.

These matrices are built from covariance functions. Their elements



can be expressed as follows:⁷

$$\left[C_{fg} \right]_{pi} = M\{f_p g_i\}, \quad \left[C_{gg} \right]_{ij} = M\{g_i g_j\}, \quad \left[D_{gg} \right]_{ij} = E\{\underline{n}_i \underline{n}_j\},$$

in which \underline{n}_i , an element of vector \underline{n} , represents the *uncertainty* of the observation process appearing in observation equation 10.4:

$$\underline{\ell}_i = g_i + \underline{n}_i, \quad \text{or equivalently} \quad \underline{\ell} = \underline{g} + \underline{n}.$$

$\underline{\ell}$ is the vector of the observation values themselves, including observation uncertainty \underline{n} .

The D matrix is the variance matrix of observational uncertainty, the *noise variance matrix* describing a property of the observational process, not of the gravity field. While the values of $M\{\Delta g_i \Delta g_j\}$ can be as large as 1200 mGal^2 , the values of $E\{\underline{n}_i \underline{n}_j\}$ can be much smaller, depending on the measurement technique used, for example as small as 0.01 mGal^2 .

This does not apply however in the case of block averages — for example averages over blocks of size $1^\circ \times 1^\circ$, computed from scattered measurements — which are often very imprecise.

The great advantage of least-squares collocation is its *flexibility*. Different observation types may be handled with a single unified theory and method, the locations of observation points are free, and the result is obtained directly as freely choosable quantities in locations where one wants them.



10.6 Prediction of gravity anomalies

If the quantity to be calculated or estimated, \hat{f} , is of the same type as the observed quantity, \underline{g} , we often speak of *homogeneous prediction*. For example, the prediction equation for gravity anomalies already presented

⁷Here, we use the *geographic mean* $M\{\cdot\}$ for evaluating the signal covariances. In doing so, f and g are no longer considered stochastic. It is assumed that their global geographic mean vanishes: $M\{f\} = M\{g\} = 0$.



in subsection 10.5.6 is obtained from equation 10.8 by substitution:

$$\widehat{\Delta g}_P = C_{Pi} (C_{ij} + D_{ij})^{-1} \ell_j. \quad (10.9)$$

Here are several points j where gravity is given: let us say, N observations $\ell_j = \underline{\Delta g}_j + \underline{n}_j$, $j = 1, \dots, N$. The number of points to be predicted may be one, i.e., point P , or many. The matrices C_{ij} and D_{ij} are square, and the inverse of their sum exists. C_{Pi} is a rectangular matrix. If there is only one point P , it is a size $1 \times N$ row matrix.

The *prediction error* is now the difference quantity⁸ $\widehat{\Delta g}_P - \underline{\Delta g}_P$, and its variance (“variance of prediction”) is

ennustusvarianssi

$$\begin{aligned} \Sigma_{PP} &\stackrel{\text{def}}{=} \text{Var}\{\widehat{\Delta g}_P - \underline{\Delta g}_P\} = \\ &= \text{Var}\{\widehat{\Delta g}_P\} + \text{Var}\{\underline{\Delta g}_P\} - \text{Cov}\{\widehat{\Delta g}_P, \underline{\Delta g}_P\} - \text{Cov}\{\underline{\Delta g}_P, \widehat{\Delta g}_P\}. \end{aligned}$$

Here (propagation of variances applied to equation 10.9):

$$\begin{aligned} \text{Var}\{\widehat{\Delta g}_P\} &= C_{Pi} (C_{ij} + D_{ij})^{-1} (C_{jk} + D_{jk}) (C_{kl} + D_{kl})^{-1} C_{lP} = \\ &= C_{Pi} (C_{ij} + D_{ij})^{-1} C_{jP} \end{aligned}$$

and

$$\begin{aligned} \text{Cov}\{\widehat{\Delta g}_P, \underline{\Delta g}_P\} &= \text{Cov}\left\{C_{Pi} (C_{ij} + D_{ij})^{-1} (\underline{\Delta g}_j + \underline{n}_j), \underline{\Delta g}_P\right\} = \\ &= C_{Pi} (C_{ij} + D_{ij})^{-1} \left(\text{Cov}\{\underline{\Delta g}_j, \underline{\Delta g}_P\} + 0\right) = \\ &= C_{Pi} (C_{ij} + D_{ij})^{-1} C_{jP}, \end{aligned}$$

and also

$$\text{Cov}\{\underline{\Delta g}_P, \widehat{\Delta g}_P\} = C_{Pi} (C_{ij} + D_{ij})^{-1} C_{jP}$$

and finally, the signal variance $\text{Var}\{\underline{\Delta g}_P\} = C_{PP}$.

⁸Be aware that here, $\underline{\Delta g}_P$ is the *true value* of the gravity anomaly at point P , which we do not know empirically. The *measured value* would be $\ell_P = \underline{\Delta g}_P + \underline{n}_P$, in which \underline{n}_P is the random error or “noise” of the gravimetric observation.



Here, C_{iP} (also called C_{jP} , or even $C_{\ell P}$) is the transpose of C_{Pi} . The matrix $(C_{ij} + D_{ij})^{-1}$ is symmetric and its own transpose.

The end result is

$$\begin{aligned}\Sigma_{PP} &= C_{Pi}(C_{ij} + D_{ij})^{-1}C_{jP} + C_{PP} - \\ &\quad - C_{Pi}(C_{ij} + D_{ij})^{-1}C_{jP} - C_{Pi}(C_{ij} + D_{ij})^{-1}C_{jP} = \\ &= C_{PP} - C_{Pi}(C_{ij} + D_{ij})^{-1}C_{jP}.\end{aligned}$$

In case $D_{ij} \ll C_{ij}$, we obtain a simpler, often-used result:

$$\Sigma_{PP} \approx C_{PP} - C_{Pi}C_{ij}^{-1}C_{jP}. \quad (10.10)$$

Borderline cases

- Point P is far from all points i. Then $C_{Pi} \approx 0$ and $\Sigma_{PP} \approx C_{PP}$, so prediction is impossible in practice, and the prediction equation 10.9 will yield the value zero. The *mean error of prediction* $\sigma_{\Delta g_P} = \sqrt{\Sigma_{PP}}$ is the same as the variability $\sqrt{C_{PP}}$ of the gravity anomaly signal, the square root of the signal variance.
- Point P is identical with one of the points i. Then, if we use only that point i, we obtain

$$\Sigma_{PP} = C_{PP} - C_{PP}C_{PP}^{-1}C_{PP} = 0,$$

no prediction error whatsoever — as the value at the prediction point was already known!.

However, if $D_{PP} \neq 0$ (but small), the result is $\Sigma_{PP} \approx D_{PP}$.



10.7 Covariance function and degree variances

10.7.1 The covariance function of the disturbing potential

In theoretical work we use, instead of gravity anomalies, the covariance function of the *disturbing potential* T on the Earth's surface:

$$K(P, Q) = K(\psi_{PQ}, \alpha_{PQ}) \stackrel{\text{def}}{=} M_P \{T_P T_{Q(P)}\},$$

or alternatively using equation 10.3:

$$\begin{aligned} K(P, Q) &= K(\psi_{PQ}) \stackrel{\text{def}}{=} M'_P \{T_P T_{Q(P)}\} = \\ &= \frac{1}{8\pi^2} \int_0^{2\pi} \int_{-\pi/2}^{+\pi/2} \int_0^{2\pi} T_P T_{Q(P)} d\lambda_P \cos \phi_P d\phi_P d\alpha_{PQ}. \quad (10.11) \end{aligned}$$

Here it is assumed that the disturbing potential is *isotropic*: K does not depend on α but only on ψ .

We choose on the unit sphere a co-ordinate system where point P is a "pole". In this system, the parameters α_{PQ} and ψ_{PQ} are the spherical co-ordinates of point Q . The covariance function is expanded into the following sum:

$$K(\psi) = \sum_{n=2}^{\infty} \sum_{m=-n}^n k_{nm} Y_{nm}(\psi, \alpha)$$

with Y_{nm} defined as in equation 3.3:

$$Y_{nm}(\psi, \alpha) = \begin{cases} P_{nm}(\cos \psi) \cos m\alpha & \text{if } m \geq 0, \\ P_{n|m|}(\cos \psi) \sin |m| \alpha & \text{if } m < 0. \end{cases} \quad (10.12)$$

Based on isotropy, all coefficients for which the order $m \neq 0$, vanish: the expressions on the right-hand side of equation 10.12 can only be independent of α if $m = 0$. So

$$K(\psi) = \sum_{n=2}^{\infty} k_{n0} Y_{n0}(\psi) = \sum_{n=2}^{\infty} k_n P_n(\cos \psi). \quad (10.13)$$



astevarianssit The coefficients k_n are called the *degree variances* (of the disturbing potential). For isotropic covariance functions $K(\psi)$, the information content of the degree variances k_n , $n = 2, 3, \dots$ is the same as that of the function itself, and is in fact its *spectral representation*.

10.7.2 Degree variances and spherical-harmonic coefficients

Multiply equation 10.13 with $P_{n'}(\cos \psi) \sin \psi$ and integrate:

$$\begin{aligned} \int_0^\pi K(\psi) P_{n'}(\cos \psi) \sin \psi \, d\psi &= \\ &= \sum_{n=2}^{\infty} k_n \int_0^\pi P_n(\cos \psi) P_{n'}(\cos \psi) \sin \psi \, d\psi = \\ &= \sum_{n=2}^{\infty} k_n \int_{-1}^1 P_n(t) P_{n'}(t) \, dt = k_{n'} \frac{2}{2n+1} \end{aligned}$$

using orthogonality condition 3.4. It follows that

$$k_n = \frac{2n+1}{2} \int_0^\pi K(\psi) P_n(\cos \psi) \sin \psi \, d\psi, \quad (10.14)$$

meaning that, if $K(\psi)$ is given, we can calculate all k_n .

Substituting $K(\psi_{PQ})$ from equation 10.11 yields, with abbreviations $\phi = \phi_P, \lambda = \lambda_P, \psi = \psi_{PQ}, \alpha = \alpha_{PQ}$:

$$\begin{aligned} k_n &= \frac{2n+1}{2} \int_0^\pi \overbrace{\frac{1}{8\pi^2} \int_0^{2\pi} \int_{-\pi/2}^{+\pi/2} \int_0^{2\pi} T_P T_{Q(P)} \, d\lambda \cos \phi \, d\phi \, d\alpha}^{K(\psi)} P_n(\cos \psi) \sin \psi \, d\psi = \\ &= \frac{2n+1}{16\pi^2} \int_{-\pi/2}^{+\pi/2} \int_0^{2\pi} T_P \overbrace{\int_0^{2\pi} \int_0^\pi T_{Q(P)} P_n(\cos \psi) \sin \psi \, d\psi \, d\alpha \, d\lambda}^I \cos \phi \, d\phi. \end{aligned}$$

Here we have interchanged the order of the integrals, as is allowed, and moved T_P to another place.



The expression I is a surface integral over the unit sphere:

$$\begin{aligned} I &= \int_0^{2\pi} \int_0^\pi T_{Q(P)} P_n(\cos \psi_{PQ}) \sin \psi_{PQ} \, d\psi_{PQ} \, d\alpha_{PQ} = \\ &= \iint_\sigma T_{Q(P)} P_n(\cos \psi_{PQ}) \, d\sigma_Q = \frac{4\pi}{2n+1} T_{n,P}, \end{aligned}$$

in which $T_{n,P} = T_n(\phi_P, \lambda_P)$. T_n is the constituent of the disturbing potential T for the harmonic degree number n , compare the degree constituent equation 3.8. Substitution yields

$$\begin{aligned} k_n &= \frac{1}{4\pi} \int_{-\pi/2}^{+\pi/2} \int_0^{2\pi} T_P T_{n,P} \, d\lambda_P \cos \phi_P \, d\phi_P = \\ &= \frac{1}{4\pi} \iint_\sigma T T_n \, d\sigma = M\{T T_n\} = \frac{1}{4\pi} \iint_\sigma T_n^2 \, d\sigma = M\{T_n^2\}, \end{aligned}$$

according to the definition of operator M and considering the mutual orthogonality of the functions T_n .

The degree variances are the geographic variance of the degree constituents of the disturbing potential.

We write based on equation 3.13 :

$$\begin{aligned} T(\phi, \lambda, r) &= \\ &= \frac{GM_\oplus}{R} \sum_{n=2}^{\infty} \left(\frac{R}{r}\right)^{n+1} \sum_{m=0}^n \bar{P}_{nm}(\sin \phi) (\delta \bar{C}_{nm} \cos m\lambda + \bar{S}_{nm} \sin m\lambda), \end{aligned}$$

in which the normal field, coefficients \bar{C}_n^* , has been subtracted out:

$$\begin{cases} \delta \bar{C}_{n0} = \bar{C}_{n0} - \bar{C}_n^* & \text{if } n \text{ even,} \\ \delta \bar{C}_{nm} = \bar{C}_{nm} & \text{otherwise.} \end{cases}$$

We see that

$$T_n(\phi, \lambda) = \frac{GM_\oplus}{R} \sum_{m=0}^n \bar{P}_{nm}(\sin \phi) (\delta \bar{C}_{nm} \cos m\lambda + \bar{S}_{nm} \sin m\lambda).$$



We obtain

$$k_n = \frac{1}{4\pi} \iint_{\sigma} T_n^2 d\sigma = \left(\frac{GM_{\oplus}}{R} \right)^2 \sum_{m=0}^n \left(\overline{\delta C}_{nm}^2 + \overline{S}_{nm}^2 \right).$$

Here, we have exploited the *orthonormality* of the fully normalised basis functions $\overline{P}_{nm}(\sin \phi) \cos m\lambda$ and $\overline{P}_{nm}(\sin \phi) \sin m\lambda$ on the surface of unit sphere σ . So

The degree variances k_n of the disturbing potential can be calculated directly from the spherical-harmonic coefficients.

The literature offers many alternative notations, such as

$$k_n = \sigma_n^2 = \sigma_i^{\text{TT}}.$$



10.8 Propagation of covariances

The covariance function K of the disturbing potential derived above can also be used to derive the covariance functions of other quantities. This works in principle for quantities that can be expressed as linear functionals of the disturbing potential $T(\cdot, \cdot, R)$ on the surface of the spherical Earth, as explained in section 10.2.



10.8.1 Example: *upwards continuation of the potential*

ylöspäin
jatkaminen

Let us write the disturbing potential in space $T(\phi, \lambda, r)$ as a functional of the surface disturbing potential $T(\phi, \lambda, R) = T(\cdot, \cdot, R)$. With the definition of the degree constituents T_n ,

$$T(\phi, \lambda, R) \stackrel{\text{def}}{=} \sum_{n=2}^{\infty} T_n(\phi, \lambda),$$

it holds that

$$T(\phi, \lambda, r) = \sum_{n=2}^{\infty} \left(\frac{R}{r} \right)^{n+1} T_n(\phi, \lambda).$$



Symbolically

$$T(\phi, \lambda, r) = L\{T(\cdot, \cdot, R)\}.$$

Here, L is the linear functional

$$L\{f\} = \sum_{n=2}^{\infty} \left(\frac{R}{r}\right)^{n+1} f_n,$$

in which the f_n are defined according to degree constituent equation 3.8, so that on the sea level of a spherical Earth

$$f = \sum_{n=2}^{\infty} f_n.$$

Symbolically

$$L\{f\} = \sum_{n=2}^{\infty} L^n f_n,$$

in which

$$L^n = \left(\frac{R}{r}\right)^{n+1}$$

is the *spectral representation* of the functional L .

We may write *at a certain point* P , location (ϕ_P, λ_P, r_P) in space:

$$L_P\{f\} = \sum_{n=2}^{\infty} L_P^n f_{n,P},$$

in which

$$L_P^n = \left(\frac{R}{r_P}\right)^{n+1}.$$

Concretely, for the disturbing potential $T(\phi_P, \lambda_P, r_P)$ in point P , this means

$$T(\phi_P, \lambda_P, r_P) = L_P\{T(\cdot, \cdot, R)\} = \sum_{n=2}^{\infty} L_P^n T_{n,P} = \sum_{n=2}^{\infty} \left(\frac{R}{r_P}\right)^{n+1} T_n(\phi_P, \lambda_P).$$



Now, the covariance function *in space* of T is obtained:

$$\begin{aligned} K(r_P, r_Q, \psi_{PQ}) &= M'_P \left\{ T(\phi_P, \lambda_P, r_P) T(\phi_{Q(P)}, \lambda_{Q(P)}, r_Q) \right\} = \\ &= M'_P \left\{ L_P \{ T(\cdot, \cdot, R) \} L_{Q(P)} \{ T(\cdot, \cdot, R) \} \right\} = \\ &= M'_P \left\{ \sum_{n=2}^{\infty} (L_P^n T_{n,P}) \sum_{n'=2}^{\infty} (L_Q^{n'} T_{n',Q(P)}) \right\} = \\ &= \sum_{n=2}^{\infty} \sum_{n'=2}^{\infty} L_P^n L_Q^{n'} M'_P \{ T_{n,P} T_{n',Q(P)} \}. \end{aligned}$$

According to equation 10.11:

$$\begin{aligned} M'_P \{ T_{n,P}, T_{n',Q(P)} \} &= \\ &= \frac{1}{8\pi^2} \int_0^{2\pi} \int_{-\pi/2}^{+\pi/2} \int_0^{2\pi} T_{n,P} T_{n',Q(P)} d\lambda_P \cos \phi_P d\phi_P d\alpha_{PQ}. \end{aligned}$$

A trial expansion is

$$M'_P \{ T_{n,P}, T_{n',Q(P)} \} = \tilde{k}_n P_n(\sin \psi_{PQ}),$$

the coefficients of which are according to equation 10.14:

$$\tilde{k}_n = \frac{2n+1}{2} \int_0^\pi M'_P \{ T_{n,P}, T_{n',Q(P)} \} P_n(\cos \psi_{PQ}) \sin \psi_{PQ} d\psi_{PQ}.$$

Substitution yields, with the abbreviations $\phi = \phi_P, \lambda = \lambda_P, \psi = \psi_{PQ}, \alpha = \alpha_{PQ}$:

$$\begin{aligned} \tilde{k}_n &= \frac{2n+1}{2} \frac{1}{8\pi^2} \int_0^\pi \int_0^{2\pi} \int_{-\pi/2}^{+\pi/2} \int_0^{2\pi} \overbrace{T_{n,P} T_{n',Q(P)} d\lambda \cos \phi d\phi d\alpha}^{M'_P \{ T_{n,P}, T_{n',Q(P)} \}} P_n(\cos \psi) \sin \psi d\psi = \\ &= \frac{2n+1}{16\pi^2} \int_{-\pi/2}^{+\pi/2} \int_0^{2\pi} T_{n,P} \overbrace{\int_0^{2\pi} \int_0^\pi T_{n',Q(P)} P_n(\cos \psi) \sin \psi d\psi d\alpha}^I d\lambda \cos \phi d\phi. \end{aligned}$$



The integral, using degree constituent equation 3.8:

$$\begin{aligned} I &= \int_0^{2\pi} \int_0^\pi T_{n',Q(P)} P_n(\cos \psi_{PQ}) \sin \psi_{PQ} \, d\psi_{PQ} \, d\alpha_{PQ} = \\ &= \int_\sigma T_{n',Q(P)} P_n(\cos \psi_{PQ}) \, d\sigma_Q = \frac{4\pi}{2n'+1} T_{n',P}, \end{aligned}$$

so

$$\begin{aligned} \tilde{k}_n &= \frac{2n+1}{16\pi^2} \frac{4\pi}{2n'+1} \int_{-\pi/2}^{+\pi/2} \int_0^{2\pi} T_{n,P} T_{n',P} \, d\lambda_P \cos \phi_P \, d\phi_P = \\ &= \frac{2n+1}{2n'+1} \cdot \frac{1}{4\pi} \int_\sigma T_n T_{n'} \, d\sigma = \frac{2n+1}{2n'+1} M\{T_n T_{n'}\}. \end{aligned}$$

Using orthogonality yields

$$M'_P\{T_{n,P} T_{n',Q(P)}\} = \begin{cases} M\{T_n^2\} = k_n P_n(\cos \psi_{PQ}) & \text{if } n = n', \\ 0 & \text{if } n \neq n', \end{cases}$$

the harmonic components of the surface covariance function, equation 10.13.

This should not surprise us: if the spatial covariance function is isotropic, it must have the general form

$$K(r_P, r_Q, \psi_{PQ}) = \sum_{n=2}^{\infty} K_n^r(r_P, r_Q) K_n^\psi(\psi_{PQ}),$$

and $K_n^\psi(\psi_{PQ})$ must have the same form as in equation 10.13:

$$K_n^\psi(\psi_{PQ}) = k_n P_n(\cos \psi_{PQ}).$$

When $K_n^r(r_P, r_Q) = 1$, i.e., at sea level, the coefficients k_n are those given by equation 10.14.



Thus we obtain⁹

$$\begin{aligned} K(r_P, r_Q, \psi_{PQ}) &= \sum_{n=2}^{\infty} L_P^n L_Q^n k_n P_n(\cos \psi_{PQ}) = \\ &= \sum_{n=2}^{\infty} \left(\frac{R}{r_P}\right)^{n+1} \left(\frac{R}{r_Q}\right)^{n+1} k_n P_n(\cos \psi_{PQ}) = \\ &= \sum_{n=2}^{\infty} \left(\frac{R^2}{r_P r_Q}\right)^{n+1} k_n P_n(\cos \psi_{PQ}). \quad (10.15) \end{aligned}$$

Here we have expressed the covariance function of the disturbing potential in space $T(\phi, \lambda, r)$ into an expansion into the degree variances k_n of the corresponding sea-level disturbing potential $T(\phi, \lambda, R)$, by applying *propagation of covariances* on expansion 10.13 of function K . Thus we have obtained the *three-dimensional covariance function* for the disturbing potential, needed for example in mountainous countries and in air and space applications.

10.8.2 Example: the covariance function of gravity anomalies

We know from equation 5.8 that there exists the following relationship between gravity anomalies and the disturbing potential:

$$\Delta g = \sum_{n=2}^{\infty} \frac{n-1}{r} \left(\frac{R}{r}\right)^{n+1} T_n,$$

symbolically: $\Delta g = L_{\Delta g}\{T\}$ for a suitable operator L_g :

$$L_{\Delta g}\{f\} = \sum_{n=2}^{\infty} L_{\Delta g}^n f_n, \quad L_{\Delta g}^n = \frac{n-1}{r} \left(\frac{R}{r}\right)^{n+1}.$$

Again, at a concrete point P ,

$$\begin{aligned} \Delta g(\phi_P, \lambda_P, r_P) &= L_{\Delta g, P}\{T(\cdot, \cdot, R)\} = \\ &= \sum_{n=2}^{\infty} L_{\Delta g, P}^n T_{n, P} = \sum_{n=2}^{\infty} \frac{n-1}{r_P} \left(\frac{R}{r_P}\right)^{n+1} T_{n, P}. \end{aligned}$$

⁹This only works this cleanly because in this case, the operator L^n is of multiplier type, $(R/r)^{n+1}$.



We can show in the same way as above that

$$\begin{aligned} \text{Cov}\{\underline{\Delta g}_P, \underline{\Delta g}_Q\} &= M'_P\{\Delta g_P \Delta g_{Q(P)}\} = \\ &= \sum_{n=2}^{\infty} L_{\Delta g, P}^n L_{\Delta g, Q}^n M'_P\{T_{n, P} T_{n, Q(P)}\} = \\ &= \sum_{n=2}^{\infty} \frac{n-1}{r_P} \left(\frac{R}{r_P}\right)^{n+1} \frac{n-1}{r_Q} \left(\frac{R}{r_Q}\right)^{n+1} k_n P_n(\cos \psi_{PQ}) = \\ &= \sum_{n=2}^{\infty} \left(\frac{R^2}{r_P r_Q}\right)^{n+2} \left(\frac{n-1}{R}\right)^2 k_n P_n(\cos \psi_{PQ}). \end{aligned}$$

Often, we write

$$C(\psi_{PQ}, r_P, r_Q) \stackrel{\text{def}}{=} M'_P\{\Delta g_P \Delta g_{Q(P)}\} = \sum_{n=2}^{\infty} \left(\frac{R^2}{r_P r_Q}\right)^{n+2} c_n P_n(\cos \psi_{PQ}),$$

in which the *degree variances of gravity anomalies* are

$$c_n = \left(\frac{n-1}{R}\right)^2 k_n.$$

Similarly we also calculate the “mixed covariances” between disturbing potential and gravity anomaly:

$$\begin{aligned} \text{Cov}\{T_P, \underline{\Delta g}_Q\} &= \\ &= M'_P\{T_P \Delta g_{Q(P)}\} = \sum_{n=2}^{\infty} L_P^n L_{\Delta g, Q}^n M'_P\{T_{n, P} T_{n, Q(P)}\} = \\ &= \sum_{n=2}^{\infty} \left(\frac{R}{r_P}\right)^{n+1} \frac{n-1}{r_Q} \left(\frac{R}{r_Q}\right)^{n+1} k_n P_n(\cos \psi_{PQ}) = \\ &= \sum_{n=2}^{\infty} \frac{n-1}{r_Q} \left(\frac{R^2}{r_P r_Q}\right)^{n+1} k_n P_n(\cos \psi_{PQ}). \end{aligned}$$

All these are examples of *propagation of covariances*, when applied to a series expansion:

kovarianssien kulkeutuminen

$$\begin{aligned} \text{Cov}\{L_1\{T_P\}, L_2\{T_Q\}\} &= \sum_n L_{1, P}^n L_{2, Q}^n M'_P\{T_{n, P} T_{n, Q(P)}\} = \\ &= \sum_n L_{1, P}^n L_{2, Q}^n k_n P_n(\cos \psi_{PQ}), \end{aligned}$$



for *arbitrary* linear functionals

$$L_1\{T_P\} = \sum_n L_{1,P}^n T_{n,P}, \quad L_2\{T_Q\} = \sum_n L_{2,Q}^n T_{n,Q},$$

in which $T_{n,P} = T_n(\phi_P, \lambda_P)$ and $T_{n,Q} = T_n(\phi_Q, \lambda_Q)$ are the degree constituents of the disturbing potential on the Earth's surface. The problem, in each case, is identifying the spectral form of this linear functional. This is done by expanding the quantity concerned into T_n , and lifting the coefficient found from the equation. These coefficients are indicated above by red and blue colouring.



10.9 Global covariance functions

Empirical covariance functions have been calculated often. There have been only a few empirical covariance functions for the whole Earth. They are commonly given in the form of a *degree variance formula*. The best known is the rule observed by William Kaula (Rapp, 1989):¹⁰

$$k_n = \alpha \frac{2n+1}{n^4}.$$

By writing

$$c_n = \left(\frac{n-1}{R}\right)^2 k_n,$$

in which c_n are the degree variances of *gravity anomalies*, we obtain

$$c_n = \alpha \frac{2n+1}{n^4} \left(\frac{n-1}{R}\right)^2 \approx \frac{2\alpha}{nR^2}.$$

Here, α is a planet specific constant, according to Kaula's estimate $\alpha = 10^{-10} (GM_{\oplus}/a_{\oplus})^2$.

The Kaula rule does not hold very precisely. It applies, by the way, fairly well for the gravity field of Mars, of course with a different constant (Yuan et al., 2001).

¹⁰William M. Kaula (1926–2000) was an American geophysicist and space geodesist who studied the determination of the Earth's gravity field by means of satellite geodesy.



Another well-known rule is the Tscherning–Rapp equation (Tscherning and Rapp, 1974):

$$c_n = \frac{A(n-1)}{(n-2)(n+B)} = \left(\frac{n-1}{R}\right)^2 k_n.$$

The constants are, according to the authors, $A = 425.28 \text{ mGal}^2$ and $B = 24$ (exactly). As a technical detail, one usually chooses $R = R_B = 0.999\bar{R}$, the radius of a *Bjerhammar*¹¹ sphere inside the Earth (\bar{R} is the Earth's mean radius). The form of the equation is chosen so the covariance functions of various quantities will be closed expressions.

10.10 Collocation and the spectral viewpoint

The calculations in least-squares collocation can also be executed efficiently by way of FFT. For this one should study the symmetries present in the geometry, especially the *rotational symmetry*, which exists, for example, in the direction of longitude on the whole Earth: nothing changes when we turn the whole Earth by a certain angle θ around her axis of rotation: for all longitudes, what happens is $\lambda \mapsto \lambda + \theta$.

In the following we discuss a simplified example in one dimension. Let observations $\underline{\ell}_i = \underline{g}_i + \underline{n}_i$ of a field $\underline{g}(\psi)$, $\psi \in [0, 2\pi)$ be given on the edge of a circle, in points $\psi_i \stackrel{\text{def}}{=} 2\pi i/N$, $i = 0, 1, 2, \dots, N-1$. Let us assume that also the results of the calculation, estimates \hat{f}_i of the result function $f(\psi)$, are desired at the same points. Then we have equation 10.8:

$$\hat{\mathbf{f}} = \mathbf{C}_{fg} [\mathbf{C}_{gg} + \mathbf{D}_{gg}]^{-1} (\underline{\mathbf{g}} + \underline{\mathbf{n}}),$$

with

$$\begin{aligned} \left[\mathbf{C}_{fg} \right]_{ij} &= \mathbf{C}_{fg}(f(\psi_i), g(\psi_j)) = \mathbf{C}_{fg}(\psi_i, \psi_j), \\ \left[\mathbf{C}_{gg} \right]_{ij} &= \mathbf{C}_{gg}(g(\psi_i), g(\psi_j)) = \mathbf{C}_{gg}(\psi_i, \psi_j), \end{aligned}$$

¹¹Arne Bjerhammar (1917–2011) was an eminent Swedish geodesist.

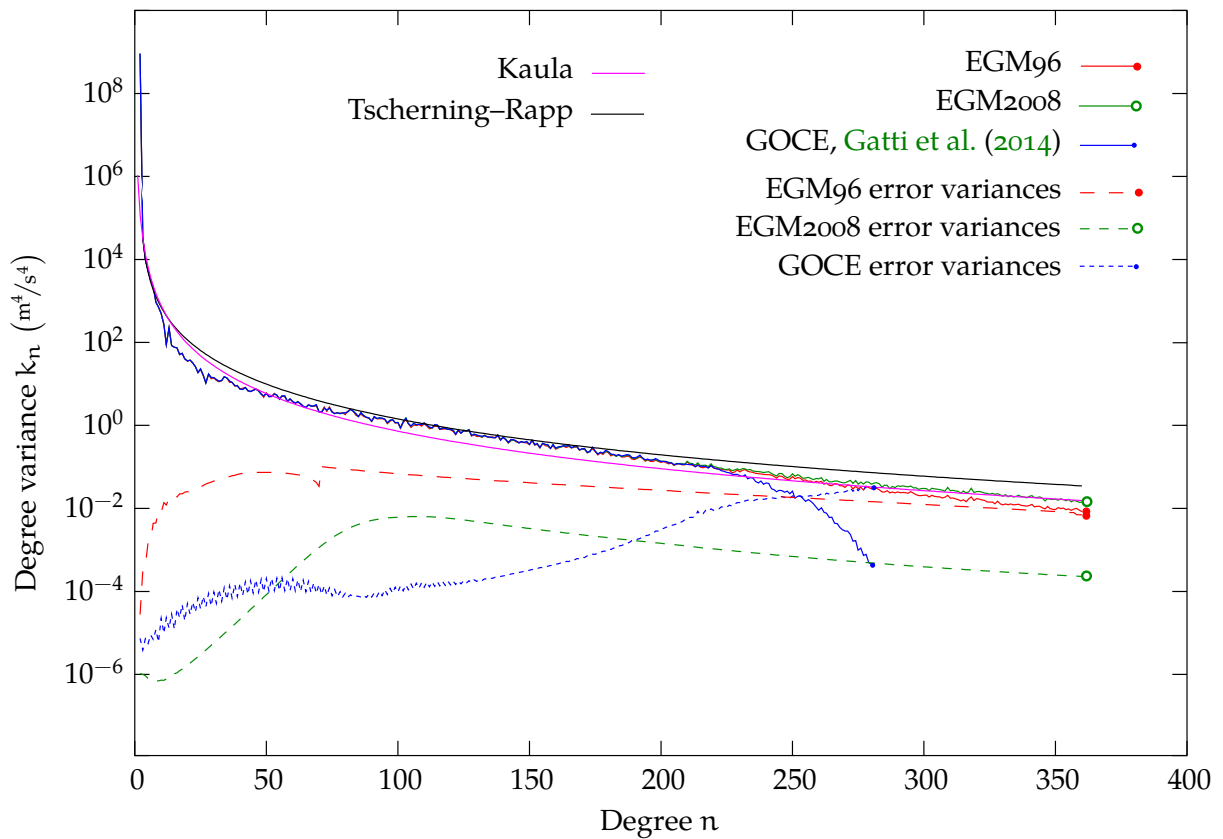


FIGURE 10.5. Global covariance functions as degree variances. The **GOCE** model cuts off at degree 280.

$$\left[D_{gg} \right]_{ij} = D_{gg} (g(\psi_i), g(\psi_j)) = D_{gg}(\psi_i, \psi_j).$$

If the *physics* of the whole situation, including the physics of the measurement process, is rotationally symmetric, we must have

$$\begin{aligned} \left[C_{fg} \right]_{i,j(i)} &= M_{\circ} \{ f(\psi_n)g(\psi_{j(n)}) \} = \\ &= \frac{1}{N} \sum_{n=0}^{N-1} f(\psi_n)g(\psi_{j(n)}) \stackrel{\text{def}}{=} \left[C_{fg} \right]_k, \end{aligned}$$

with $j(i) = (i + k) \bmod N$. Here, the operator M_{\circ} is the “circle average”



of a function,

$$M_{\circ}\{h\} \stackrel{\text{def}}{=} \frac{1}{N} \sum_{n=0}^{N-1} h(\psi_n),$$

which, like the geographic average in section 10.4, replaces the statistical average.

In the same way we obtain

$$\begin{aligned} \left[C_{gg} \right]_{i,j(i)} &= M_{\circ}\{g(\psi_n)g(\psi_{j(n)})\} = \\ &= \frac{1}{N} \sum_{n=0}^{N-1} g(\psi_n)g(\psi_{j(n)}) \stackrel{\text{def}}{=} \left[C_{gg} \right]_k. \end{aligned}$$

Now C_{fg} , C_{gg} are functions of only k , and we may write them

$$\begin{aligned} \left[C_{fg} \right]_{ij} &= C_{fg}(\psi_i, \psi_j) = C_{fg}(\Delta\psi_k) = \left[C_{fg} \right]_k, \\ \left[C_{gg} \right]_{ij} &= C_{gg}(\psi_i, \psi_j) = C_{gg}(\Delta\psi_k) = \left[C_{gg} \right]_k, \end{aligned}$$

in which $\Delta\psi_k \stackrel{\text{def}}{=} (\psi_j - \psi_i) \bmod 2\pi$ and $k = (j - i) \bmod N$.

Furthermore

$$\left[D_{gg} \right]_{ij} = D_{gg}(\psi_i, \psi_j) = D_{gg}(\Delta\psi_k) = \left[D_{gg} \right]_k = E\{\underline{n}_i \underline{n}_{j(i)}\},$$

the traditional statistical variance of the observation noise. Also because generally the observations do not correlate with each other, we have¹²

$$D_{gg} = \sigma^2 I_N,$$

σ^2 (the variance of observations, assumed equal for all) times the $N \times N$ sized unit matrix.

Matrices of this form are called *Toeplitz circulant matrices*.¹³ Thanks

Toeplitz-
sirkulantti
matriisi

¹²In fact, the unit or identity matrix is also known as the Kronecker delta, and as a Toeplitz matrix may be interpreted as a discrete version of the Dirac delta function. Its discrete Fourier transform is “white”:

$$\mathcal{F}\{I_N\} = \frac{1}{N},$$

with the same power for all frequencies.



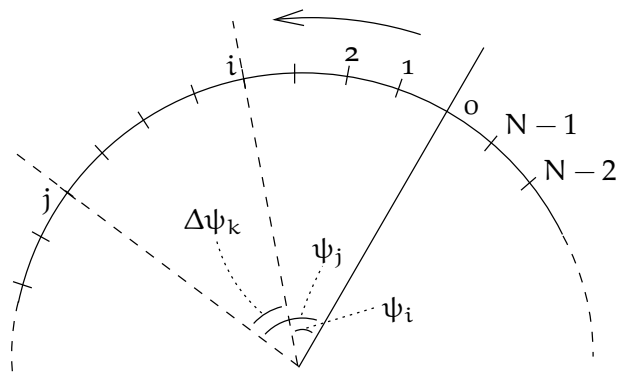


FIGURE 10.6. Circular geometry.

to this property, equation 10.8 is a string of *convolutions*.

Without proof we present that the spectral version of equation 10.8 looks like this:

$$\mathcal{F}\{\hat{f}\} = \frac{\mathcal{F}\{C_{fg}\}}{\mathcal{F}\{C_{gg}\} + \mathcal{F}\{D_{gg}\}} \cdot \mathcal{F}\{\underline{g} + \underline{n}\} = \frac{\mathcal{F}\{C_{fg}\}}{\mathcal{F}\{C_{gg}\} + \sigma^2/N} \cdot \mathcal{F}\{\underline{g} + \underline{n}\}.$$

This is an easy and rapid way to calculate the solution using FFT. If for a suitable operator L we have $f = L\{g\}$, the equation simplifies as follows:

$$\mathcal{F}\{\hat{f}\} = \frac{\mathcal{F}\{L\} \cdot \mathcal{F}\{C_{gg}\}}{\mathcal{F}\{C_{gg}\} + \sigma^2/N} \cdot \mathcal{F}\{\underline{g} + \underline{n}\}.$$

In the limit in which the observations are exact, $\sigma^2 = 0$ and thus $\underline{n} = 0$, it holds that

$$\mathcal{F}\{\hat{f}\} = \mathcal{F}\{L\} \cdot \mathcal{F}\{\underline{g}\} \iff \hat{f} = L\{g\}.$$

For example, if g are gravity anomalies and f are values of the disturbing potential, then¹⁴

$$\mathcal{F}\{L\} = \frac{R}{n - 1}.$$

¹³Otto Toeplitz (1881–1940) was a German Jewish mathematician who contributed to functional analysis.

¹⁴In real computation it is not so simple. . . the harmonic degree number n, which refers to global spherical geometry, must first be converted to the Fourier wave number expressed on the computational grid used.



The approach is called *Fast Collocation*, for example [Bottoni and Barzaghi \(1993\)](#). Of course it is used in two dimensions on the Earth's surface, although our example is one-dimensional. As always, it requires that the observations are given on a *grid*, and in this case also that the precision of the material is *homogeneous* — the same everywhere — over the area. This requirement is hardly ever precisely fulfilled.



Self-test questions

1. What is the difference between *signal* and *noise*?
 - (a) Signal is not a random stochastic process, whereas noise is.
 - (b) Signal is a stochastic process that we are interested in and wish to estimate, while noise is a stochastic process that we are not interested in and that we would like to filter out.
 - (c) Signal is a stochastic process with a greater variance and is therefore more easily detectable than noise.
 - (d) Signal is a property of a real-world system, while noise is a property of an observation instrument or method.
2. What is a functional?
 - (a) A mapping from a function space to a set of numbers, for example the real numbers.
 - (b) A random-valued function.
 - (c) A functional associates with every (well-behaved) function defined on some domain, a number.
 - (d) A function of a vectorial argument.
3. What is a linear functional?
 - (a) A linear functional associates a number $L\{f\}$ with any linear function $f(x) = a + bx$ defined on some domain



(b) If, for any functions f and g it holds for a functional L that

$$L\{af + bg\} = aL\{f\} + bL\{g\}$$

for any real values a, b , then L is a linear functional.

(c) A linear functional associates with any (well-behaved) function defined on some domain, a linear expression $L\{f\} = a + bx$.

4. The statistical behaviour of a stochastic process defined on the Earth's surface is the same independently of where on Earth you are. This property is called isotropy | ergodicity | homogeneity | stationarity.
5. The statistical behaviour of a stochastic process of time is the same independently of where on the time axis you are. This property is called isotropy | ergodicity | homogeneity | stationarity.
6. Why, in the study of the Earth's gravity field, does one use as the average of quantities the geographical average rather than the statistical average?
7. Which two different kinds of covariance functions are used for gravity anomalies on the Earth's surface? Give the formulas and name the free parameters.
8. Explain *degree variances*. What is the difference between degree variances k_n and c_n ?
9. What does Kaula's rule express?
10. What is a Toeplitz circulant matrix?



Exercise 10 – 1: Variance of prediction

The equation for the variance of prediction at a point P is

$$\Sigma_{PP} = C_{PP} - C_{Pi}(C_{ij} + D_{ij})^{-1}C_{jP},$$



in which the observation points are $i = 1, \dots, N$. Assume there is only one observation point, point P. Then

$$\Sigma_{PP} = C_{PP} - C_{PP}(C_{PP} + D_{PP})^{-1}C_{PP}.$$

Show that, if $D_{ij} \neq 0$ but however $D_{ij} \ll C_{ij}$,

$$\Sigma_{PP} \approx D_{PP}.$$



Exercise 10 – 2: Hirvonen’s covariance equation and prediction

Hirvonen’s covariance equation is

$$C(s) = \frac{C_0}{1 + (s/d)^2},$$

with the Ohio parameters $C_0 = 337 \text{ mGal}^2$ and $d = 40 \text{ km}$ (Heiskanen and Moritz, 1967, equation 7-9). The equation gives the covariance between the gravity anomalies at two points P and Q

$$C(s_{PQ}) = \text{Cov}\{\underline{\Delta g}_P, \underline{\Delta g}_Q\}.$$

s_{PQ} is the linear distance between the points.

1. Calculate $\text{Var}\{\underline{\Delta g}_P\}$ and $\text{Var}\{\underline{\Delta g}_Q\}$. Remember that, according to the definition, $\text{Var}\{\underline{x}\} = \text{Cov}\{\underline{x}, \underline{x}\}$!
2. Calculate $\text{Cov}\{\underline{\Delta g}_P, \underline{\Delta g}_Q\}$ if $s_{PQ} = 20 \text{ km}$.
3. Calculate the *correlation*

$$\text{Corr}\{\underline{\Delta g}_P, \underline{\Delta g}_Q\} \stackrel{\text{def}}{=} \frac{\text{Cov}\{\underline{\Delta g}_P, \underline{\Delta g}_Q\}}{\sqrt{\text{Var}\{\underline{\Delta g}_P\} \text{Var}\{\underline{\Delta g}_Q\}}}.$$

4. Assume now that *we only have a measurement in point P*. What is the “variance of prediction” of the gravity anomaly in point Q which is at a distance $s_{PQ} = 10 \text{ km}$ from the (precisely!) given anomaly in point P? Apply equation 10.10 as follows:

$$\sigma_{QQ}^2 = C_{QQ} - C_{QP}C_{PP}^{-1}C_{PQ}.$$

5. And item 4 if the distance is $s_{PQ} = 80 \text{ km}$?





Exercise 10 – 3: Predicting gravity anomalies

Let the measured gravity anomalies $\ell_1 = \underline{\Delta g}_1 + \underline{n}_1$ and $\ell_2 = \underline{\Delta g}_2 + \underline{n}_2$ be given at two points 1 and 2. The distance between the points is 80 km and between them, at the same distance of 40 km from both, is located point P. Compute the gravity anomaly of point P, Δg_P by means of prediction. The prediction equation is

$$\widehat{\Delta g}_P = C_{Pi} (C_{ij} + D_{ij})^{-1} \ell_j,$$

where $\ell_j = \underline{\Delta g}_j + \underline{n}_j$ is the (abstract) vector of gravity anomaly observations,

$$C_{ij} = \begin{bmatrix} \text{Var}\{\underline{\Delta g}_i\} & \text{Cov}\{\underline{\Delta g}_i, \underline{\Delta g}_j\} \\ \text{Cov}\{\underline{\Delta g}_i, \underline{\Delta g}_j\} & \text{Var}\{\underline{\Delta g}_j\} \end{bmatrix}$$

is the signal variance matrix of the vector $\underline{\Delta g}_i$, and

$$C_{Pi} = \begin{bmatrix} \text{Cov}\{\underline{\Delta g}_P, \underline{\Delta g}_1\} & \text{Cov}\{\underline{\Delta g}_P, \underline{\Delta g}_2\} \end{bmatrix}$$

is the signal covariance matrix between $\underline{\Delta g}_P$ and $\underline{\Delta g}_i$. D_{ij} is the variance matrix of the observation random uncertainty or *noise* \underline{n}_i , $i = 1, 2$:

$$D_{ij} = \begin{bmatrix} \text{Var}\{\underline{n}_i\} & \text{Cov}\{\underline{n}_i, \underline{n}_j\} \\ \text{Cov}\{\underline{n}_i, \underline{n}_j\} & \text{Var}\{\underline{n}_j\} \end{bmatrix}.$$

1. Compute the matrix C_{ij} , assuming again Hirvonen's covariance formula (previous exercise) and a parameter value of $d = 40$ km.
2. Compute C_{Pi} .
3. Compute $\widehat{\Delta g}_P$ expressed in the observed values ℓ_1 and ℓ_2 . Assume $D_{ij} = 0$ (and thus $\underline{n}_i = 0$). Inverting the C_{ij} matrix is possible by hand, but just use Matlab or octave.
4. Compute the *variance of prediction* (note $C_{jP} = C_{Pi}^T$) using

$$\sigma_{PP}^2 = C_{PP} - C_{Pi} C_{ij}^{-1} C_{jP}.$$



**Exercise 10 – 4: Predicting gravity anomalies (2)**

Let us again have points 1 and 2 with measured gravity anomalies $\ell_1 = \underline{\Delta g}_1$ and $\ell_2 = \underline{\Delta g}_2$. Now however the points 1, 2 and P are in a *triangular configuration*, with a right angle at point P, and the distances from P to points 1 and 2 still 40 km. The distance between points 1 and 2 is now only $40\sqrt{2}$ km.

1. Compute C_{ij} , C_{Pi} , $\widehat{\Delta g}_P$ and σ_{PP}^2 .
2. Compare the result with the previous one. Conclusion?

**Exercise 10 – 5: Propagation of covariances**

Given the covariance function 10.15 of the disturbing potential

$$\text{Cov}\{\underline{I}_P, \underline{I}_Q\} = \sum_{n=2}^{\infty} \left(\frac{R^2}{r_P r_Q} \right)^{n+1} k_n P_n(\cos \psi_{PQ}).$$

1. Calculate the covariance function of the gravity disturbance $\underline{\delta g}$ (equation 5.4). Hint: write first an expansion of the form

$$\delta g = \sum_{n=2}^{\infty} L_{\delta g}^n T_n$$

in order to find the expression for the coefficient $L_{\delta g}^n$. After this

$$\text{Cov}\{\underline{\delta g}_P, \underline{\delta g}_Q\} = \sum_{n=2}^{\infty} L_{\delta g, P}^n L_{\delta g, Q}^n k_n P_n(\cos \psi_{PQ}).$$

2. Compute the covariance function of the *gravity-gradient disturbance*

$$\frac{\partial^2}{\partial r^2} T = -\frac{\partial}{\partial r} \delta g,$$

i.e., the vertical gradient of the gravity *disturbance*.



Exercise 10 – 6: Kaula's rule for gravity gradients

For the disturbing potential

$$T(\phi, \lambda, r) = \sum_{n=2}^{\infty} \left(\frac{R}{r}\right)^{n+1} T_n(\phi, \lambda) \quad (10.16)$$

or on the Earth's surface ($r = R$)

$$T(\phi, \lambda, R) = \sum_{n=2}^{\infty} T_n(\phi, \lambda)$$

Kaula's rule applies, with the *degree variances*

$$k_n = \alpha \frac{2n + 1}{n^4}.$$

From these one can derive, using propagation of variances, the degree variances of *gravity anomalies*

$$\Delta g = \sum_{n=2}^{\infty} L_g^n T_n = \sum_{n=2}^{\infty} \left(\frac{n-1}{R}\right) T_n$$

as follows:

$$c_n = (L_{\Delta g}^n)^2 k_n = \left(\frac{n-1}{R}\right)^2 k_n \approx \frac{2\alpha}{nR^2}.$$

By differentiating the above expansion 10.16 for the disturbing potential

$$T(r, \phi, \lambda) = \sum_{n=2}^{\infty} \left(\frac{R}{r}\right)^{n+1} T_n(\phi, \lambda)$$

we obtain the second derivative

$$\frac{\partial^2 T}{\partial r^2} = \sum_{n=2}^{\infty} \frac{(n+1)(n+2)}{r^2} \left(\frac{R}{r}\right)^{n+1} T_n,$$

the connection between the disturbing potential and the *gravity gradient* in the spectral domain.

On the Earth's surface $r = R$, or



$$\left. \frac{\partial^2 T}{\partial r^2} \right|_{r=R} = \sum_{n=2}^{\infty} \frac{(n+1)(n+2)}{R^2} T_n \stackrel{\text{def}}{=} \sum_{n=2}^{\infty} L_{gg}^n T_n$$

with

$$L_{gg}^n = \frac{(n+1)(n+2)}{R^2}.$$

1. Derive an (approximate) equation for the degree variances for the *gravity gradient*. Designate them with the symbol gg_n , in an analogue fashion as above for the gravity anomaly degree variances c_n :

$$gg_n = \boxed{?} \cdot k_n \approx \boxed{?} \cdot n^{\boxed{?}}.$$

2. Conclusion?



Exercise 10 – 7: Underground mass points

1. If a mass point is placed inside the Earth at a depth D beneath an observation point P , what then is the *correlation length* s of the gravitational field it causes on the Earth's surface, for which $C(s) = \frac{1}{2}C_0$?
2. Thus, if we wish to construct a model made of mass points, where under each observation point Δg_P there is one mass point, how deep should we place them if the correlation length d is given?





Gravimetric measurement devices

11



11.1 History

The first measurement device ever built based on a *pendulum* was a clock. The pendulum equation,

$$P = 2\pi\sqrt{\frac{\ell}{g}},$$

tells that the swinging time or period P of a pendulum of a given length is a constant that depends only on the length ℓ and local gravity g , on condition that the swings are *small*. The Dutch Christiaan Huygens¹ built in 1657 the first useable pendulum clock based on this ([Wikipedia, Pendulum clock](#)).

When the young French researcher Jean Richer² visited French Guyana in 1671 with a pendulum clock, he noticed that the clock ran clearly slower. The matter was corrected simply by shortening the pendulum. The cause of the effect could not be the climatic conditions in the tropics, like the thermal expansion of the pendulum. The right

¹Christiaan Huygens (1629–1695) was a leading Dutch natural scientist and mathematician. Besides inventing the pendulum clock, he also was the first to realise (in 1655) that the planet Saturn has a ring.

²Jean Richer (1630–1696) was a French astronomer. He is really only remembered for his pendulum finding.

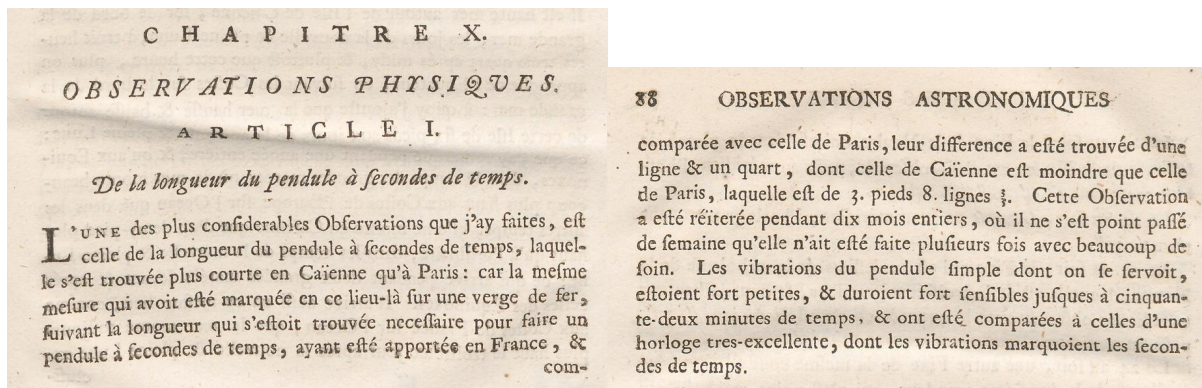


FIGURE 11.1. Jean Richer's report.

explanation was that in the tropics, gravity g is weaker than in Europe. After his return to France in 1673, Richer had to make his pendulum longer again. The observation is described in just one paragraph in his report *Observations astronomiques et physiques faites en l'isle de Caienne*, (Richer, 1731, pages 87–88).

This is how the *pendulum gravimeter* was invented. Later, much more precise special devices were built, for example Kater's³ reversion pendulum, and the four-pendulum Von Sterneck⁴ device, which was also used in Finland in the 1920s and 1930s (Pesonen, 1930; Hirvonen, 1937). We must also mention the submarine measurements, including in the Java Sea by the Dutch Vening Meinesz, in which it was observed that above the trenches in the ocean floor there is a notable shortage of gravity, and that they thus are in a state of strong isostatic disequilibrium (Vening Meinesz, 1928).

Pendulum gravimeters are however too hard to operate and too slow for high-productivity gravimetric observations. For that purpose, the *spring gravimeter* was developed, see section 11.2.


³Henry Kater FRS FRAS (1777–1835) was an English physicist.

⁴Robert Freiherr (baron) Daublebsky von Sterneck (1839–1910) was a major general in the Austro-Hungarian army and a geophysicist, astronomer and geodesist.

syvänmeren
hauta





 FIGURE 11.2. Autograv CG5 spring gravimeter. Image [Monniaux \(2011\)](#).

A pendulum gravimeter is in principle an absolute measurement device, as gravity is obtained directly as an acceleration. There are, however, systematic effects associated with the suspension, or *fulcrum*, of the pendulum, because of which one cannot trust in the absoluteness of the measurement after all. One attempted solution is the *very long wire pendulum*, for example [Hytönen \(1972\)](#). However, nowadays absolute measurements are made with ballistic gravimeters, see section 11.3. It has been observed that the older measurements made with pendulum apparatus in the so-called Potsdam system are systematically 14 mGal too large. . .

11.2 The relative or spring gravimeter

A spring gravimeter is at its simplest the same as a *spring balance*.

jousivaaka



In a linear spring balance the equation of motion of the test mass is

$$m \left(\frac{d^2 \ell}{dt^2} - g \right) = -k (\ell - \ell_0),$$

where m is the test mass, g the local (to be measured) gravity, and k the spring constant. The quantity ℓ_0 is the “rest length” of the spring; the length it would have if no external forces were acting on it. ℓ is the true, instantaneous length of the string.

The equilibrium between the spring force and gravity is

$$\frac{d^2 \ell}{dt^2} = 0 \implies mg = k (\ell - \ell_0) = k (\bar{\ell} - \ell_0), \quad (11.1)$$

in which $\bar{\ell}$ is the mean length of the spring during the oscillation, and also the *equilibrium length* in the absence of oscillations.

värähtely-yhtälö When the test mass is disturbed, it starts oscillating about its equilibrium position. The oscillation equation, obtained by summing the above two equations, is

$$\frac{d^2}{dt^2} (\ell - \bar{\ell}) = -\frac{k}{m} (\ell - \bar{\ell}).$$

The period is

$$P = 2\pi \sqrt{\frac{m}{k}} = 2\pi \sqrt{\frac{\bar{\ell} - \ell_0}{g}} = 2\pi \sqrt{\frac{\delta \ell}{g}}, \quad (11.2)$$

in which $\delta \ell = \bar{\ell} - \ell_0$ denotes the difference between the equilibrium length and the length in the state of rest: the *lengthening of the spring by gravity*.

The *sensitivity* of the instrument is obtained by differentiating equation 11.1 in the form

$$mg = k (\bar{\ell} - \ell_0) = k \delta \ell$$

with the result

$$\frac{d\bar{\ell}}{dg} = \frac{d(\delta \ell)}{dg} = \frac{m}{k} = \frac{P^2}{4\pi^2}. \quad (11.3)$$



Substitution of, for example, $\delta\ell = 5 \text{ cm}$ and $g = 10 \text{ m/s}^2$ into equation 11.2 yields $P = 0.44 \text{ s}$. One milligal of change in gravity g produces, according to equation 11.3, a lengthening of only $5 \cdot 10^{-8} \text{ m}$ (check). Clearly then, the sensor observing or compensating this displacement must be extremely sensitive!



11.2.1 Astatisation

An *astatised gravimeter* uses a different measurement geometry. The LaCoste-Romberg gravimeter, which long enjoyed great popularity, serves as an example. Inside it, the test mass is at the end of a lever beam, see figure 11.3. Two torques operate on the beam, which are in equilibrium. The torque caused by the spring is

$$\tau_s = k (\bar{\ell} - \ell_0) b \sin \beta,$$

in which $\bar{\ell}$ is the spring's true, stretched equilibrium length, and ℓ_0 the theoretical or state-of-rest length without loading.

According to the sine rule

$$\bar{\ell} \sin \beta = c \sin(90^\circ + \epsilon) = c \cos \epsilon,$$

substitution of which in the previous equation yields

$$\tau_s = k (\bar{\ell} - \ell_0) \frac{bc}{\bar{\ell}} \cos \epsilon.$$

The force of gravity pulling at the mass is mg , and the corresponding torque

$$\tau_g = mgp \cos \epsilon.$$

Between these there has to be *equilibrium*:

$$\tau_g - \tau_s = mgp \cos \epsilon - k (\bar{\ell} - \ell_0) \frac{bc}{\bar{\ell}} \cos \epsilon = 0$$

or

$$mgp\bar{\ell} - kbc (\bar{\ell} - \ell_0) = 0. \quad (11.4)$$



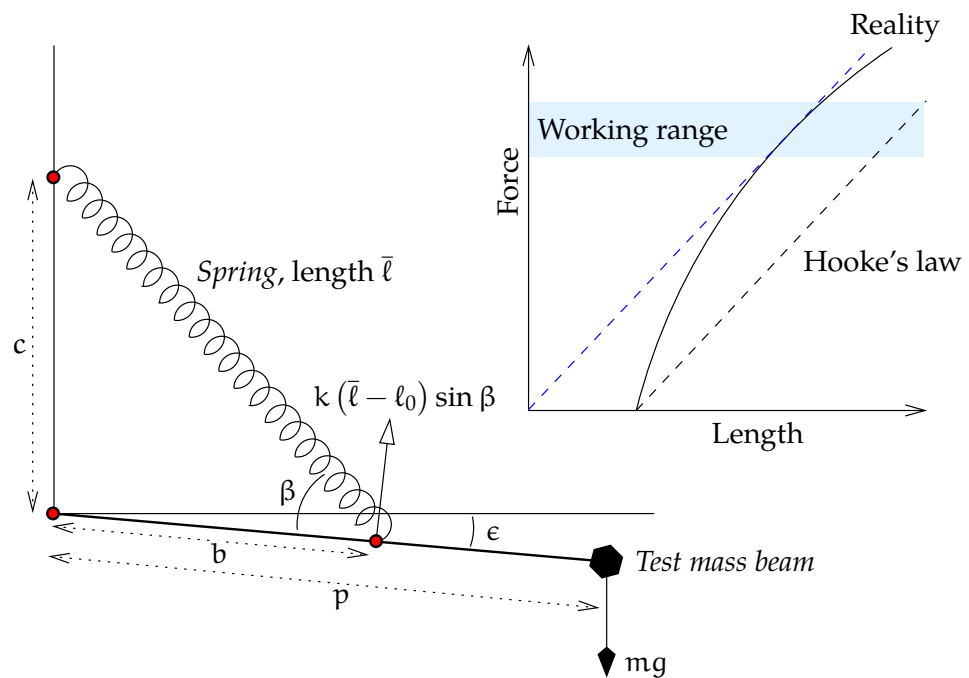


FIGURE 11.3. Operating principle of spring gravimeter. On the right, how to build a “zero-length spring”.



By differentiation

$$mp\bar{l} dg + mgp d\bar{l} - kbc d\bar{l} = 0,$$

from which we obtain, by substituting equation 11.4, a sensitivity equation:

$$\frac{d\bar{l}}{dg} = -\frac{mp\bar{l}}{mgp - kbc} = -\frac{mp\bar{l}}{mgp - mgp \bar{l} / (\bar{l} - l_0)} = \frac{\bar{l} \bar{l} - l_0}{g l_0}.$$

From this we see that the sensitivity can be driven up arbitrarily by choosing l_0 as short as possible, almost zero — a so-called zero-length spring solution (Wikipedia, Zero-length springs).

tasaus
rasiatasain

Of course, levelling the instrument, using its bull’s eye level and three footscrews, is critical.



For example, assuming $\bar{\ell} = 5 \text{ cm}$, $\ell_0 = 0.1 \text{ cm}$, $g = 10 \text{ m/s}^2$ gives

$$\frac{d\bar{\ell}}{dg} = 2.5 \cdot 10^{-6} \text{ m/mGal},$$

a 50 times⁵ better result than earlier! The improvement or *astatisation ratio* is precisely $(\bar{\ell} - \ell_0) / \ell_0$.

This is the operating principle of an *astatised* gravimeter, like the LaCoste-Romberg.⁶

11.2.2 Period of oscillation

There is another way to look at this: if the instrument is not in equilibrium, the lever beam will slowly oscillate about the equilibrium position. We start from equation 11.4:

$$m g p \bar{\ell} - k b c (\bar{\ell} - \ell_0) = 0, \quad (11.5)$$

but for a state of disequilibrium. Then, the test mass will be undergoing an acceleration a , positive downwards, and we have

$$m (g - a) p \ell - k b c (\ell - \ell_0) = 0,$$

where, instead of the equilibrium spring length $\bar{\ell}$, the instantaneous length ℓ appears. Subtracting the above two equations yields

$$m g p (\bar{\ell} - \ell) + m a p \ell - k b c (\bar{\ell} - \ell) = 0.$$

We use equation 11.5 again to eliminate $k b c$, yielding

$$m g p (\bar{\ell} - \ell) + m a p \ell - m g p \frac{\bar{\ell}}{\bar{\ell} - \ell_0} (\bar{\ell} - \ell) = 0.$$

⁵For comparability we should still multiply by $p/b \sin \beta$, if we measure the position of the test mass.

⁶Lucien LaCoste (1908–1995) was an American physicist and metrologist, who, as an undergraduate, together with his physics professor Arnold Romberg (1882–1974) discovered the principle of the astatised gravimeter and zero-length spring.



Rearranging terms gives

$$m a p l = m g p \frac{\ell_0}{\bar{\ell} - \ell_0} (\bar{\ell} - \ell)$$

or

$$a = -\frac{g}{\ell} \frac{\ell_0}{\bar{\ell} - \ell_0} (\ell - \bar{\ell}).$$

Here we see again the “astatisation ratio” $(\bar{\ell} - \ell_0)/\ell_0$ appear, which for a zero-length spring ($\ell_0 \approx 0$) is very large.

Now the string length disequilibrium $\ell - \bar{\ell}$ is connected with the vertical displacement z (reckoned downwards) of the test mass, as follows:

$$z = (\ell - \bar{\ell}) \frac{p}{b \sin \beta}.$$

With this, we obtain

$$a = \frac{d^2}{dt^2} z = -\frac{g}{\ell} \frac{\ell_0}{\bar{\ell} - \ell_0} \frac{b \sin \beta}{p} z.$$

This is again an oscillation equation in z . The oscillation period is

$$P = 2\pi \sqrt{\frac{\ell}{g} \frac{p}{b \sin \beta} \frac{\bar{\ell} - \ell_0}{\ell_0}}.$$

For the same values as above, $\ell_0 = 0.1 \text{ cm}$, $\bar{\ell} = 5 \text{ cm} \approx \ell$, $g = 10 \text{ m/s}^2$, and $p/b \sin \beta = 2$, we find

$$P = 4.4 \text{ s}.$$

What this long oscillation period also means is that the instrument is less sensitive to high-frequency vibrations, for example from passing traffic or microseismicity. This is a significant operational advantage.

11.2.3 Practicalities of measurement

An ordinary spring gravimeter is based on *elasticity*. Because there is no material that is perfectly elastic, but it is always plastic⁷ as well, the

⁷Plastic deformation in a metal crystal is mediated by crystal-lattice defects called *dislocations*. As dislocations travel through the crystal lattice under load, the properties



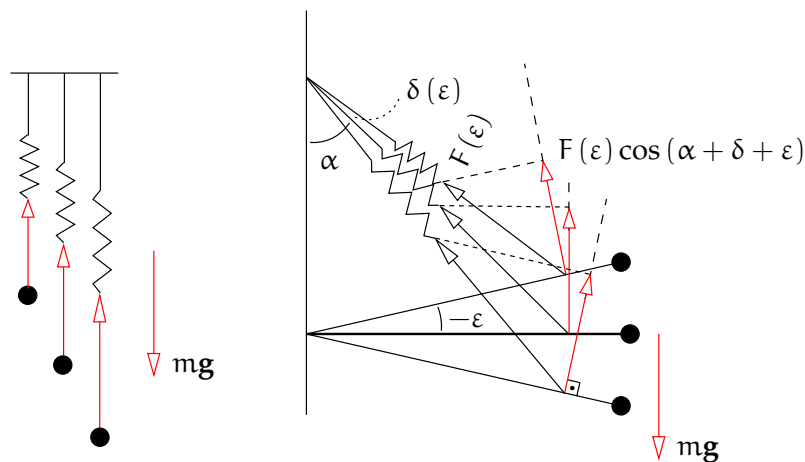


FIGURE 11.4. The idea of astatisation. The elastic force of an ordinary spring grows steeply with extension (left), whereas the weight of the test mass is constant. The lever beam and diagonal arrangement (right) causes the part of the force of the spring in the direction of motion of the lever (red) to *diminish* with extension, while the spring force itself *grows* similarly with extension. This near-cancellation boosts sensitivity. The spring used is a *zero-length spring*.



gravimeter itself *changes* during the measurement process. This change is called *drift*. The drift is managed in practical measurements by the following measures: käynti

- We measure along lines starting from a known point and ending on a known point, producing a *closing error*. A line is traversed as rapidly as possible. The closing error is eliminated by adjusting the values obtained from the measurement in proportion to their times of measurement.

of the metal change, which may eventually result in *metal fatigue*, a known problem for example in aviation. [Wikipedia, Dislocation](#). The art of making metals stronger by inhibiting the motion of dislocations, for example by adding carbon to iron to form steel, forms a large part of practical metallurgy. [Wikipedia, Strengthening mechanisms of materials](#).



- The gravimeter is transported carefully without bumping it.
- arretointi ○ We remember to always *arrest* (clamp down the lever beam) during transport!
- Because the elastic properties of the spring and the instrument geometry both depend on temperature, precision gravimeters are always *thermostated*.

vaimennus A sea gravimeter differs from an ordinary (land) gravimeter in having powerful *damping*. This applies also for an airborne gravimeter. Both types are mounted on a stabilised platform, keeping the axis of measurement along the local vertical in spite of vehicle motion.



11.3 The absolute or ballistic gravimeter

The ballistic or absolute gravimeter is a return to roots, the definition of gravity: it measures directly the *acceleration of free fall*. The instrument is made up of a vacuum tube, inside of which an object, a prism reflecting light, falls freely. See figure 11.5.

Here we describe briefly the JILA gravimeter, built at the University of Colorado at Boulder by Jim Faller,⁸ of which the Finnish Geodetic Institute has acquired two. Figure 11.6 shows the newer model, FG5, built by the same group. In Finland this instrument, serial number 221, has served as the national standard for the acceleration of free fall. It was upgraded to model FG5X in 2012.

During the fall of the prism, a “cage” with a window in the bottom moves along with the prism inside it without touching it. The purpose of the cage is to prevent the last remaining traces of air from affecting the motion of the prism. Approaching the bottom, the cage, which moves along a rail under computer control, decelerates, and the prism

⁸James E. Faller (born 1934) is an American physicist, metrologist, geodesist, and student of gravitation. He proposed the installation of laser retroreflectors on the lunar surface in the context of the Apollo project, in order to measure the distance to the Moon — LLR, lunar laser ranging.



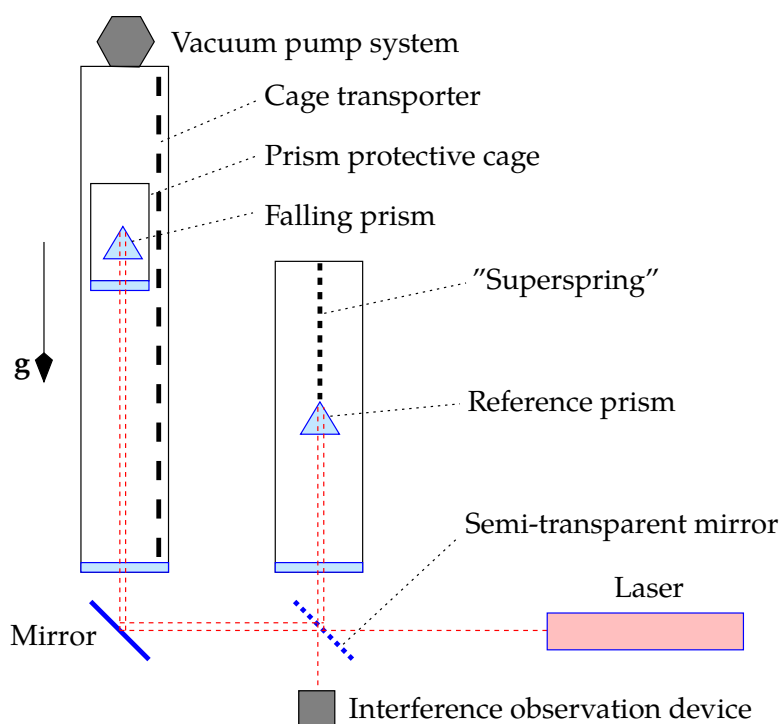


FIGURE 11.5. Operating principle of a ballistic absolute gravimeter.

lands relatively softly on its base. After that, the cage moves back to the top of the tube and a new measurement cycle starts.

A laser interferometer measures the locations of the prism during its fall. The measurements are repeated thousands of times to get good precision through averaging. Another prism, the reference prism, is suspended in another tube from a very soft spring (actually an electronically simulated "superspring") to protect it from microseismicity.

The instrument is designed to achieve the greatest precision possible; for example, the vibration caused by the drop is controlled by a well-designed mount. Precisions are of the order of several microgals, similar to what ordinary LaCoste-Romberg relative gravimeters are capable of.

The instrument is however large and, although transportable, cannot be called a field instrument. Of late, development has gone in the direction of smaller devices, which are essentially better portable.





FIGURE 11.6. Absolute gravimeter of type FG5. Figure United States National Oceanic and Atmospheric Administration.



The motion of a freely falling mass is given by the equation

$$\frac{d^2}{dt^2}z = g(z),$$

where it is assumed — realistically — that gravity g depends on the location z within the drop tube, reckoned downwards. If we nevertheless take g to be constant, we obtain by integration

$$\begin{aligned} \frac{d}{dt}z &= v_0 + gt, \\ z &= z_0 + v_0t + \frac{1}{2}gt^2, \end{aligned}$$

from which we obtain the *observation equations* of the measurement process

$$z_i = \begin{bmatrix} 1 & t_i & \frac{1}{2}t_i^2 \end{bmatrix} \cdot \begin{bmatrix} z_0 \\ v_0 \\ g \end{bmatrix} + \underline{n}_i.$$



Here, the unknowns⁹ to be estimated are z_0, v_0 and g . The quantities z_i are the interferometrically measured vertical locations of the falling prism, and \underline{n}_i are the measurement errors or “noise”. Determining precisely the corresponding measurement time or *epoch* t_i reckoned from the moment of release of the prism is of course essential. The volume of measurements obtained from each individual drop is substantial.

We write the observation equations in matrix form:

$$\underline{\ell} = \mathbf{A}\mathbf{x} + \underline{n},$$

in which

$$\underline{\ell} = \begin{bmatrix} z_1 \\ z_2 \\ \vdots \\ z_n \end{bmatrix}, \quad \underline{n} = \begin{bmatrix} \underline{n}_1 \\ \underline{n}_2 \\ \vdots \\ \underline{n}_n \end{bmatrix}, \quad \mathbf{A} = \begin{bmatrix} 1 & t_1 & t_1^2 \\ 1 & t_2 & t_2^2 \\ \vdots & \vdots & \vdots \\ 1 & t_n & t_n^2 \end{bmatrix}, \quad \mathbf{x} = \begin{bmatrix} z_0 \\ v_0 \\ g \end{bmatrix}.$$

The solution follows from this according to the method of least-squares adjustment, from the *normal equations*

$$\mathbf{A}^T \mathbf{A} \hat{\mathbf{x}} = \mathbf{A}^T \underline{\ell},$$

giving the solution (estimate)

$$\hat{\mathbf{x}} = (\mathbf{A}^T \mathbf{A})^{-1} \mathbf{A}^T \underline{\ell}.$$

The uncertainty of the estimates is given by the variance matrix

$$\text{Var}\{\hat{\mathbf{x}}\} = \sigma^2 (\mathbf{A}^T \mathbf{A})^{-1},$$

in which σ is the uncertainty (mean error) of a single observation z_i , also known as the mean error of unit weight.

An alternative type of absolute gravimeter *throws* the prism *up* (inside the tube), after which it moves along a symmetric parabolic path. An

painoyksikön
keskivirhe

⁹It would be easy (exercise!) to add an unknown representing the vertical gradient of gravity to this.



example of such a “rise-and-fall” instrument is the Italian **IMGC-02** (d’Agostino et al., 2008). Theoretically, this method would give more precise results; however, the technical challenges are larger than in the case of the dropping method. Intercomparisons between instruments of these two types have helped to identify error sources.

Recently so-called atomic or quantum gravimeters have also been built, in which the falling of individual atoms is measured interferometrically (de Angelis et al., 2009).

The idea of the device is that it measures the effect of gravity on the phase angle of the matter wave of falling atoms. Firstly a so-called Bose–Einstein condensate is prepared, which is extremely cold and consists of perhaps a million atoms in identical quantum states, with the same phase angle like marching soldiers. The condensate is dropped, and the first laser pulse splits it into two. Half of the atoms¹⁰ fall first slowly, then faster. The other half fall fast at first and then slower. In order to achieve this, a second laser pulse pair is used that acts like a mirror, or perhaps a tennis racket. The third and last laser pulse is for reading out interferometrically the phase difference between the two merging atomic beams. The interaction between light and atoms is based on the Raman effect.

As the atoms travel through space-time along two different paths on which the gravity potentials are different,¹¹ a phase difference is formed between these which can be measured. Without gravity (dashed lines) this phase difference would be zero, see figure 11.7, in which the horizontal axis is time.

¹⁰This is a quantum theoretically erroneous statement. The matter wave of *each individual atom* splits into two! [Wikipedia, Double-slit experiment](#).

¹¹In fact, the spinning of the atom’s phase angle acts like a clock, and the speed at which time elapses depends on the local geopotential (Vermeer, 1983a).



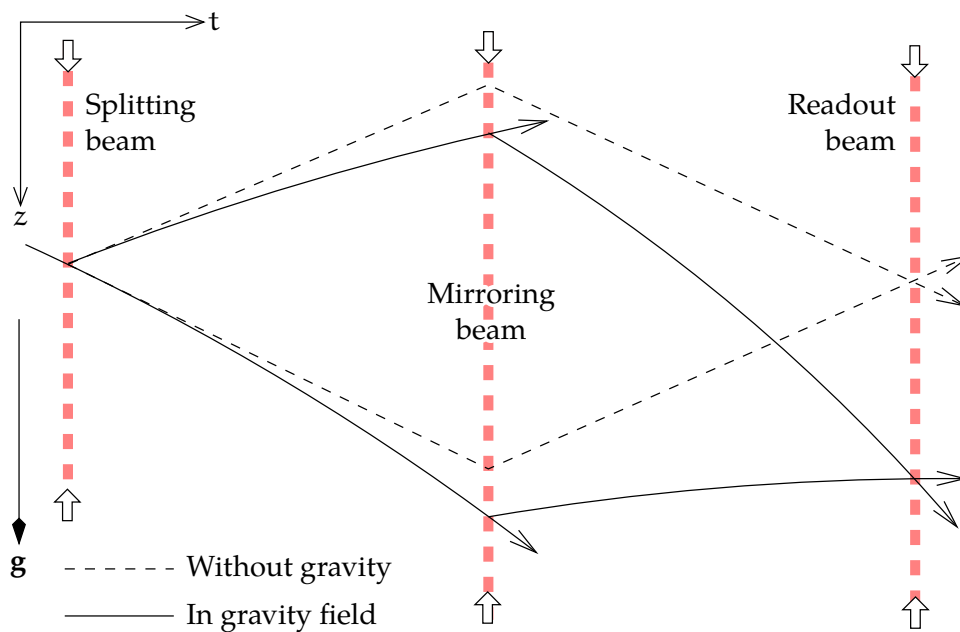


FIGURE 11.7. Principle of operation of an atomic gravimeter. The horizontal axis is time.



11.4 Network hierarchy in gravimetry

Network hierarchy is just as important in gravimetry as in measurements of location or height. The procedure has typically been that the highest measurement order consisted of points measured by absolute gravimeters — in the old days, this meant pendulum measurements. Stepwise densification of this network, i.e., measurement of the base network, was then done with relative or spring gravimeters, like the lowest-order measurements, gravity mapping surveys. In base network measurement, fast transportation was used, such as aircraft, and national or regional reference points were often located at airports.

Because pendulum instruments were not genuinely absolute, the old Potsdam system collected a 14 mGal systematic error: all values were that much too high. Nowadays we use ballistic free-fall gravimeters instead, the possible systematics of which are much smaller — but by





FIGURE 11.8. International intercomparison of absolute gravimeters in Walferdange, Luxembourg. Image courtesy © Olivier Francis.

no means non-existent, in the order of magnitude of microgals. As there are no better, i.e., more absolute, instruments than these, the issue cannot really be resolved. Nevertheless, international instrument intercomparisons, like the [International Intercomparison of Absolute Gravimeters](#), are regularly organised and are valuable.

In Finland, regular absolute gravimetric measurements have been made in Metsähovi, and also in Vaasa (two points), Joensuu (two points), Kuusamo, Sodankylä, Kevo, and Eurajoki.

11.5 The superconducting gravimeter

This gravimeter type is based on a superconducting metal sphere levitating on a magnetic field. The precise place of the sphere is measured electronically. Because a superconducting material is impenetrable by a magnetic field, the sphere will remain forever in the same spot inside the field: the Meissner effect. Of course the field itself must be constant.

käämit It is generated by superconducting solenoids inside a vessel made of mu-metal ([Wikipedia, Mu-metal](#)), which keeps out the Earth's magnetic field.



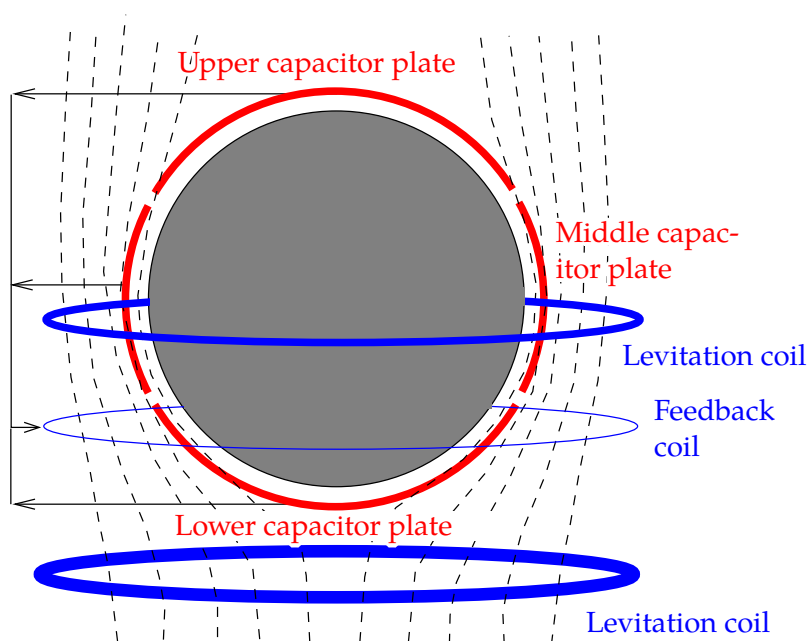


FIGURE 11.9. Principle of operation of a superconducting gravimeter. Reading out the sphere position is done capacitively.

Superconduction applied for this still demands working at the temperature of liquid helium (He). For this reason the device is not only expensive, but also requires an expensive laboratory in an environment where the societal infrastructure allows.

There are more than thirty superconducting gravimeters in the world. The work is co-ordinated by the IAG service IGETS, the International Geodynamics and Earth Tide Service. One GWR20-type instrument has been working since 1994 in Kirkkonummi at the Metsähovi research station of the then Finnish Geodetic Institute, now the National Land Survey, Virtanen and Kääriäinen (1995), Virtanen (1998). The instrument was upgraded in 2014.

The most important property of a superconducting gravimeter is, in addition to its superior precision,¹² its *stability*, i.e., its minimal drift. For

¹²Virtanen (2006) reports how the instrument at Metsähovi detected the change in



this reason, it is extremely suited to monitoring long-period phenomena, like the free oscillations of the solid Earth after large earthquakes,¹³ in which the whole Earth tolls like a church bell. Thus it is suitable for measurements that are unsuitable for an ordinary gravimeter because of its larger drift and poorer sensitivity, and measurements for which a seismometer is unsuited because the frequencies are too low.

A recent trend is the development of lightweight, “portable”, and remotely controllable superconducting gravimeters, for example the GWR *iGrav*, weighing 30 kg and not consuming any liquid helium at all. On the other hand it needs over a kilowatt in grid power for its refrigeration system (GWR Instruments, Inc., *iGRAV® Gravity Sensors*). Perhaps this will lead to improvement over the current situation where the bulk of the instruments are located in Europe and North America.



11.6 Atmospheric influence on gravity measurement

The atmosphere has the following effects on gravity:

- *Instrumental effects.* These are due to the way the gravimeter is constructed. Putting the instrument in a pressure chamber makes these effects go away. In practice it is easier to *calibrate* the instrument (in the laboratory) and calculate a correction term according to the calibration certificate to be applied to the field measurements.
- *Attraction of the atmosphere.* This is real gravitation. It contains irregular variations with place and time that we need to remove from the observed gravity values.

The effect of the atmosphere can be evaluated with the aid of the Bouguer-plate approximation: if air pressure is p , then the surface

gravity as workmen cleared snow from its laboratory roof, including a tea break! “Weighing” visitors to the lab by their gravitational attraction is also standard fare.

¹³Their periods are in the range of about 300–30 000 seconds — frequencies 0.03–3 mHz — and they are of considerable geophysical interest, [Wikipedia](#), [Earth normal modes](#).



mass density of the atmosphere is

$$\kappa = p/\gamma,$$

where γ is a representative gravity value inside the atmosphere. We do not make a large error by using the sea-level value $\gamma \approx 9.81 \text{ m/s}^2$. The standard value of air pressure at sea level is 1013.25 hPa, giving us on sea level¹⁴ $\kappa \approx 10329 \text{ kg/m}^2$. The effect of the Bouguer plate is

$$2\pi G\kappa = 0.43 \text{ mGal} \quad (11.6)$$

in the upwards direction.

It would however be wrong to apply this value as a correction! The standard atmosphere is in reality a spherical shell inside which the measurements are made, and inside the shell its attraction vanishes, see section 1.4.

Instead, *variations* in air pressure have a proportional effect. If the air pressure disturbance is $\Delta p = p - p_0$, in which p_0 is mean air pressure, the correction to be made to a gravity measurement will be

$$\delta g_A = 0.43 \frac{\Delta p}{p_0} \text{ mGal}.$$

During the passage of a storm or weather front, this beautiful theory collapses, and simple equations give misleading results. Then it is best to just not do any gravity measurements!

- *Including the atmosphere in the mass of the Earth.* This is not a correction to be applied to gravity measurements. It is a *reduction* which is applied in the calculation of gravity *anomalies*, if one wants anomalies in which the effect of the atmosphere does not produce a bias.

¹⁴So yes, the force acting on a standard 14-inch laptop screen is 540 kg. . . Fortunately it is not an old-fashioned vacuum cathode-ray tube.



Remember that the reference or normal gravity field of **GRS80** is defined in such a way that the parameter GM_{\oplus} contains the whole mass of the Earth, including the atmosphere, the Earth's attraction as satellites are feeling it (**Heikkinen, 1981**).

Therefore, if one wishes to calculate gravity anomalies that have a global mean of zero, one should also reduce measured gravity by computationally moving *the whole atmosphere above the point of measurement* to below the measurement point, for example to sea level.

The total mass of the atmosphere is

$$M_A = 4\pi\kappa R^2 = 4\pi\frac{p}{\gamma}R^2.$$

According to Newton its attraction is

$$\frac{GM_A}{R^2} = \frac{4\pi Gp}{\gamma},$$

twice the Bouguer-plate atmospheric reduction **11.6** calculated above. This is the value that should be added to the measured gravity values.

One may think of this value as the change in gravity if the local atmospheric Bouguer plate were *condensed*, Helmert condensation style, to below the measurement location, producing a double Bouguer correction.

At sea level, the correction is 0.87 mGal. At height, the correction is

$$0.87\frac{p(H)}{p_0}\text{mGal},$$

in which $p(H)$ and p_0 are the air pressures at height H and at sea level, respectively.



11.7 Airborne gravimetry and GNSS

In the early years of the 1990s **GPS**, the Global Positioning System, and more generally, satellite positioning, has changed *airborne gravimetry*



from a difficult technology to something completely operational. To understand this, one must know the principle of operation of airborne gravimetry.

An aircraft carries an airborne gravimeter, an instrument that, in the same way as a sea gravimeter, is strongly *damped*. The measurement is done automatically, generally using electrostatic compensation. The instrument is mounted on a stabilised platform that follows the local vertical.

During flight, the gravimeter measures *total gravity* on board the aircraft, consisting of two parts:

1. gravity proper — gravity as felt in a reference frame connected to the solid Earth and rotating with it
2. the pseudo-forces caused by the inevitable accelerations of the aircraft even in cruise flight.

Attached to the aircraft are a number of GNSS antennas. With these and a geodetic GNSS instrument, the motions of the aircraft can be monitored with centimetre accuracy. From these motions, we may then calculate the pseudo-forces mentioned above under item 2.

If we measure the position of the plane (or instrument) \mathbf{x}_i at moments t_i , $\Delta t = t_{i+1} - t_i$, we obtain estimated acceleration values as follows:

$$\mathbf{a}_i \approx \frac{\mathbf{x}_{i+1} + \mathbf{x}_{i-1} - 2\mathbf{x}_i}{(\Delta t)^2}. \quad (11.7)$$

When the acceleration measured by the gravimeter is Γ_i and the direction of the local plumb line (upwards) \mathbf{n}_i , local gravity g_i follows:

$$g_i = \Gamma_i - \langle \mathbf{a}_i \cdot \mathbf{n}_i \rangle.$$

The choice of the time constant Δt is critical in the whole method. It is best to choose it as long as possible, as then, the precision of the calculated GNSS accelerations \mathbf{a}_i is as good as possible. The damping of the gravimeter is also chosen in accordance with Δt , and the observations



are filtered digitally: all frequencies above the bound Δt^{-1} are removed, because they are almost entirely caused by the motions of the aircraft.

Often the high-frequency part removed from the signal is 10 000 times stronger than the gravity signal we are after! See for example [Lu et al. \(2017\)](#) figure 2.

If the uncertainty (mean error) of one GNSS vertical position *co-ordinate* measurement is σ_z (and the different co-ordinates do not correlate with each other!), then according to equation 11.7 the uncertainty of the vertical acceleration is

$$\sigma_a = \frac{\sigma_z \sqrt{6}}{(\Delta t)^2}.$$

Making the time interval Δt as long as possible without *resolution* suffering requires a low flight speed. Generally a propeller aircraft or even a helicopter is used. Of course the price of the measurement grows with the duration of the flight — a helicopter rotor hour is expensive!

For the flight height H we choose in accordance with resolution Δx :

$$H \sim \Delta x = v \Delta t,$$

where v is the flight speed. The separation between adjacent flight lines is chosen similarly.

The first major airborne gravimetry project was probably the *Greenland Aerogeophysics Project* ([Brozena, 1992](#)). In this ambitious American-Danish project in the summers of 1991 and 1992, over 200 000 km was flown, all the time measuring gravity and the magnetic field, and the height of the ice surface using altimetry.

After that, other large uninhabited areas in the Arctic and Antarctic regions were also mapped, see [Brozena et al. \(1996\)](#), [Brozena and Peters \(1994\)](#). Already in subsection 9.6.2 we made mention of other large surveys. Activity continues, see [Coakley et al. \(2013\)](#), [Kenyon et al. \(2012\)](#). The method is very suitable for large, uninhabited areas, but also, for example, for sea areas close to the coast where ship gravimeters would have difficulty navigating long straight tracks. In 1999, an airborne



gravimetry campaign was undertaken over the Baltic Sea, including the Gulf of Finland (Jussi Kääriäinen, personal communication).

In addition to the economic viewpoint, an important advantage of airborne gravimetry is that *homogeneous coverage* by gravimetric data is obtained from a large area. The homogeneity of surface gravimetric data collected over many decades is difficult to guarantee in the same way. Moreover, the effect of the very local terrain, which for surface measurements is a hard-to-remove systematic error source, especially in mountainous terrain (see section 6.3), does not come into play in the same way for airborne gravimetry.

The operating principle of *satellite gravimetry*, for example **GOCE** (Geopotential and Steady-state Ocean Circulation Explorer), is similar. An essential difference is, however, that the instrumentation on the satellite is in a state of weightlessness: $\Gamma = 0$ (in a high orbit, or when using an air drag compensation mechanism), or Γ is small and is measured using a sensitive accelerometer (in a low orbit, where air drag is significant).

ilmanvastus

The greatest challenge in planning a satellite mission is choosing the flight height. The lowest possible height is some 200 km. At that height, a tankload of propellant is already needed, or the flight will not last long. However, the resolution of the measurements on the Earth's surface is limited: for example, the smallest details in the Earth's gravity field "seen" by the **GOCE** satellite are 50–100 km in diameter.

ajoaine

erotuskyky

11.8 Measuring the gravity gradient

The acceleration of gravity \mathbf{g} is the gradient of the geopotential W . The acceleration of gravity varies itself with place, especially close to masses.



We speak of the *gravity-gradient tensor* or Eötvös tensor:

$$M \stackrel{\text{def}}{=} \begin{bmatrix} \frac{\partial^2}{\partial x^2} & \frac{\partial^2}{\partial x \partial y} & \frac{\partial^2}{\partial x \partial z} \\ \frac{\partial^2}{\partial y \partial x} & \frac{\partial^2}{\partial y^2} & \frac{\partial^2}{\partial y \partial z} \\ \frac{\partial^2}{\partial z \partial x} & \frac{\partial^2}{\partial z \partial y} & \frac{\partial^2}{\partial z^2} \end{bmatrix} W = \begin{bmatrix} \partial_{xx} & \partial_{xy} & \partial_{xz} \\ \partial_{yx} & \partial_{yy} & \partial_{yz} \\ \partial_{zx} & \partial_{zy} & \partial_{zz} \end{bmatrix} W.$$

We know that gravity increases going down, at least in free air. Going up, gravity diminishes, about 0.3 mGal for every metre of height.

In topocentric co-ordinates (x, y, z) , where z points to the zenith, this matrix is approximately

$$M \approx \begin{bmatrix} -0.15 & 0 & 0 \\ 0 & -0.15 & 0 \\ 0 & 0 & 0.3 \end{bmatrix} \text{ mGal/m},$$

in which $\partial_{zz} W = \partial_z g_z = -\partial_z g \approx 0.3 \text{ mGal/m}$ is the standard value for the free-air vertical gravity gradient: Newton's law gives for a spherical Earth

$$g_z = -\frac{GM}{(R+z)^2}.$$

The minus sign is because \mathbf{g} points downwards while the z co-ordinate increases going up. Derivation gives

$$\begin{aligned} \frac{\partial}{\partial z} g_z &= 2 \frac{GM}{(R+z)^3} \cdot \frac{\partial (R+z)}{\partial z} = -\frac{2g_z}{(R+z)} \approx \\ &\approx 3 \cdot 10^{-6} \text{ m/s}^2/\text{m} = 0.3 \text{ mGal/m}. \end{aligned}$$

The quantities $\partial_{xx} W$ and $\partial_{yy} W$ again represent the curvatures of the equipotential or level surfaces in the x and y directions, equations 4.3:

$$\partial_{xx} W = \frac{\partial^2 W}{\partial x^2} = -\frac{g}{\rho_x}, \quad \partial_{yy} W = \frac{\partial^2 W}{\partial y^2} = -\frac{g}{\rho_y},$$

in which ρ_x and ρ_y are the radii of curvature in the x and y directions. The substitution $\rho_x = \rho_y = R$ yields

$$\partial_{xx} W = \partial_{yy} W \approx -1.5 \cdot 10^{-6} \text{ m/s}^2/\text{m} = -0.15 \text{ mGal/m}.$$



The Hungarian researcher Loránd Eötvös did a number of clever experiments (Eötvös, 1998) in order to measure components of the gravity-gradient tensor with *torsion balances* built by him. The method continues to be in use in geophysical research, because the gravity gradient as a measured quantity is very sensitive to local variations in matter density in the Earth's crust.

torsiovaaka,
kiertoheiluri

In honour of Eötvös, we use as the unit of gravity gradient the Eötvös, symbol E:

$$1 \text{ E} = 10^{-9} \text{ m/s}^2/\text{m} = 10^{-4} \text{ mGal/m}.$$

The above tensor is now

$$M \approx \begin{bmatrix} -1500 & 0 & 0 \\ 0 & -1500 & 0 \\ 0 & 0 & 3000 \end{bmatrix} \text{ E}.$$

Note that

$$\frac{\partial^2 W}{\partial x^2} + \frac{\partial^2 W}{\partial y^2} + \frac{\partial^2 W}{\partial z^2} = \partial_{xx} W + \partial_{yy} W + \partial_{zz} W \approx 0,$$

the familiar Laplace differential equation. However, the equation is not exact here: in a co-ordinate system co-rotating with the Earth, the term for the centrifugal force divergence, $2\omega_{\oplus}^2$, must be added, equation 4.1.

The gravity-gradient field of Sun and Moon is known on the Earth's surface as the *tidal field*, see section 14.1.



Self-test questions

1. For the spring gravimeter described in section 11.2, one milligal of change in gravity g produces according to equation 11.3 a lengthening of $5 \cdot 10^{-8}$ m. Do a calculational check.
2. Why is a pendulum gravimeter, although theoretically absolute, not very accurate as an absolute gravimeter?



3. By which method choices do we, in practical measurements, take the drift of a relative gravimeter into account?
4. Why were the reference points of international fundamental gravimetric networks often on airports before the advent of absolute gravimeters?
5. In an absolute or ballistic gravimeter, what is the role of:
 - (a) the “cage” surrounding the falling prism
 - (b) the “superspring”?
6. According to Google
 - The Gulf War from 1990 to 1991 was the first conflict in which the military widely used **GPS**.
 - By December 1993, **GPS** achieved initial operational capability (IOC), indicating a full constellation (24 satellites) being available.
 - The Greenland Aerogeophysics Project, the first ever large-scale airborne gravimetric mission, mapped the gravity field of Greenland during the summers of 1991 and 1992.

Why are these three dates so close together?



Exercise 11 – 1: Absolute gravimeter

The observation process of absolute gravimetry is described by the equation

$$z = z_0 + v_0 t + \frac{1}{2} g t^2.$$

Let us assume that the distance of falling is 30 cm.

1. How long is the time of falling?
2. If we aim at an accuracy of $\pm 10 \mu\text{Gal}$, how precisely should the laser interferometer then measure the falling distance of the prism?
A crude order-of-magnitude guesstimate is enough!



3. The same question for the time registration of the falling time.



Exercise 11 – 2: Spring gravimeter

When we use a spring gravimeter in the field, we place the device at every measurement station on a solid base, for example bedrock, for measurement, and *level* it.

Furthermore we always take care that

- The device is *arrested* during transport: the beam is clamped to be motionless.
- The internal temperature of the device is kept constant by a *thermostat system*.

The reason for this is that the functioning of a spring gravimeter depends on the properties of the spring material, which may change as a result of careless handling or temperature variations.

Furthermore a gravimeter always has a *drift*: the relationship between measured value and true value changes slowly over time. In a non-factory-fresh gravimeter, this drift is however very regular and almost linear.

As a result of the drift, a spring gravimeter cannot be used for absolute gravity measurement and is therefore called a *relative gravimeter*.

Question How is the relative nature of a spring gravimeter and its drift taken into account

1. in planning the topology of the measurement network?
2. in planning the time order of the different measurements in a network?
3. in the choice of vehicles and point locations?





Exercise 11 – 3: Air pressure and gravity

1. How much does a low-pressure zone of 100 hPa (meaning that the pressure is 100 hPa *lower* than average air pressure 1013.25 hPa) affect gravity measured on the Earth's surface? You may assume the low-pressure zone to be very extended in area.
2. How much does sea water rise due to the “inverted barometer effect” under a low-pressure zone?
3. How much does the effect from point 2 amount to in local gravity measured *on a ship*? Assume that you are on the open sea, that the free-air gravity gradient is -0.3 mGal/m , and that the density of sea water is 1030 kg/m^3 . Analyse the situation carefully.¹⁵

¹⁵And I mean *really* carefully.





The geoid, mean sea level, and sea-surface topography

12



12.1 Basic concepts

On the ocean, the geoid is on average at the same level as the *mean sea level*, the surface obtained by removing all periodic and quasi-periodic variations from the instantaneous sea surface. These variations include

- tidal phenomena, caused by Sun and Moon, of an order of magnitude of ± 1 m, locally even more
- variations caused by air pressure variations (“inverted barometer effect”, **IB**). Typically of an order of decimetres, under tropical cyclones up to metres
- “wind pile-up”, water being pushed by winds
- in littoral seas, variation in the volume of fresh water flowing out from rivers into the sea
- eddies that are formed in the oceans in connection with, for example, the Gulf Stream and the Agulhas Stream (“mesoscale eddies”) that may live for months, and inside of which the sea surface may be even decimetres above or below that of the surroundings
- the continual shifting of ocean currents from one place to another
- the **ENSO**, El Niño Southern Oscillation, is a very long time-scale, quasi-periodic weather phenomenon happening in the waters of the Pacific Ocean and the air above it, but affecting weather

phenomena worldwide. The time-scale of variability ranges from two to seven years. See figure 13.1.

If we remove all these periodic and quasi-periodic variations, we are left with the *mean sea level*. If the water of the seas were in a state of equilibrium, this mean sea surface would be an equipotential or level surface of the Earth's gravity field, the *geoid*.

This is, however, not how things really are. Mean sea level differs from a level surface due to for example the following phenomena:

- Permanent ocean currents cause, through the Coriolis force, permanent differences in mean water level.
- Permanent differences in temperature and salinity also cause permanent differences in the mean water level, the latter for example in front of the mouths of rivers.

These physical phenomena, among other things, cause the so-called *sea-surface topography*, a permanent separation between the mean sea surface and the geoid.

The classical definition of the geoid is

"The level surface of the Earth's gravity field that fits on average best to the mean sea level."

The practical problem with this definition is that determining the correct level of the geoid requires knowledge of the mean sea level everywhere on the world ocean. This is why many "geoid" models in practice do not coincide with global mean sea level, but with some locally defined mean sea level — and often only approximately.

Mean sea level in its turn is also a problematic concept. It is sea level from which all periodic effects have been computationally removed — but who can know if a so-called secular effect in reality is perhaps long-period? The measure of permanency is the time series that are

mareografi



a century, when again modern satellite time series — **TOPEX/Poseidon** and its successors — are just about a quarter of a century long.

A sensible compromise may be the average sea level over 18 years, an important periodicity, *saros* ([Wikipedia, Saros](#)), in the orbital motion of the Moon.

The *sea-surface topography* is defined as the difference between the mean sea level and the geoid. See figure **12.4**. meritopografia

12.2 Geoids and national height datums

A locally determined geoid model is generally *relative*. Locally, at the current state of the art, we have no access to global mean sea level at an acceptable precision. This is likely to change with technology development.

In general, a local geoid model is tied to a *national height system*, and the difference from the classical definition is thus the same as the difference of the national height system from the global mean sea level.

In *Finland*, heights were determined for a long time in the **N60** height system, which is tied to the mean sea level in Helsinki harbour at the start of 1960. The difference between it and the global mean sea level is about 30 cm, due to the sea-surface topography in the Baltic Sea, see figure **12.4**. The *reference benchmark* of the system is located in nearby Kaivopuisto, figure **7.2**. Precise levelling disseminated heights from here all over Finland.

The modern Finnish height system is **N2000**, which is in principle tied to the mean sea level in Amsterdam, which is close to global mean sea level. The reference benchmark in Finland is similarly located at the Metsähovi research station in the Kirkkonummi municipality, west of Helsinki.

At the beginning of 1960, the reference surface of the Finnish height system **N60** was an equipotential or level surface of the Earth's gravity field. However, due to uplift, that is no longer the case: the *post-glacial*



land uplift varies from some four millimetres per year in the Helsinki area to ten millimetres per year in the area of maximum land uplift near Ostrobothnia. This is the main reason why in Fennoscandia height systems have a “best before” date and must be modernised a couple of times per century.

Generally, geoid maps for practical use, like **FIN2000**, the Finnish geoid model (figure 9.5), are constructed so that they transform heights in the national height system, for example **N60** heights (Helmert heights) above “mean sea level” to heights above the reference ellipsoid of the **GRS80** system.

As land uplift is an ongoing process, it must be tied to a certain epoch, a point in time at which the **GNSS** measurements were done to which the original gravimetric geoid solution has been fitted. In the case of **FIN2000** this was 1997.0 (Matti Ollikainen, personal communication; Bilker-Koivula and Ollikainen, 2009; Häkli et al., 2009).

Strictly speaking then, **FIN2000** is not a model of the geoid. A better name might be a “transformation surface”. This holds true, in fact, for *all* national or regional geoid models that are built primarily for the purpose of enabling the use of **GNSS** in height determination (“**GNSS** levelling”). These “geoid-like surfaces” are generally constructed in the following way:

1. We calculate a gravimetric geoid model by using the Stokes equation and remove–restore, for example using the **FFT** calculation technique.
2. We fit this geoid surface solution to a number of comparison points, in which both the height from levelling — “above sea level” — and from the **GNSS** method — above the reference ellipsoid — are known. The fit takes place for example by modelling the differences as a polynomial function:

$$\delta N = a + b(\lambda - \lambda_0) + c(\varphi - \varphi_0) + \dots$$

or something more complicated, and solving the coefficients



a, b, c, \dots from the differences between the two heights in these known comparison points by using the least-squares method.

12.3 The geoid and post-glacial land uplift

Global mean sea level is not constant. It rises slowly by an amount that, over the past century, has slowly grown. Over the whole 20th century, the rate has been 1.5–2.0 mm/a, for example 1.6 mm/a (Wöppelmann et al., 2009). Over the last several decades, the rate has accelerated and is now over 3 mm/a, see figure 13.1.

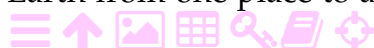
This value is called the *eustatic rise of mean sea level*. It is caused partly by the melting of glaciers, ice caps, and continental ice sheets, partly by the thermal expansion of sea water. A precise value for the eustatic rise is hard to determine: almost all tide gauges used for monitoring sea level have their own vertical motions, and distinguishing these from the rise in sea level requires a representative geographic distribution of measurement locations. The ongoing response of the solid Earth to the ending of the last ice age in particular, the latest deglaciation or termination, the so-called **GIA** (glacial isostatic adjustment), is a global phenomenon that it has only been possible to observe by satellite positioning in the most recent decades.

Because of eustatic sea-level rise, a distinction must be made between *absolute* and *relative* land uplift:

Absolute land uplift is the motion of the Earth's crust relative to the centre of mass of the Earth. This land uplift is measured when using satellites the orbits of which are determined in a co-ordinate reference system tied to the Earth's centre of mass, for example, positioning of tide gauges by means of **GNSS**.

Relative land uplift is the motion of the Earth's crust relative to the mean sea level. This motion is measured by tide gauges, also called *mareographs*.

Geoid rise As the post-glacial land uplift is the shifting of masses internal to the Earth from one place to another, it is clear that



the geoid must also change. The geoid rise is, however, small compared to the land uplift, only a few percent of it.

Equation (the point above a quantity denotes the time derivative with respect to time¹):

$$\dot{H} = \dot{h} - \dot{N} = \dot{H}_r + \dot{H}_e + \dot{H}_t,$$

in which

- \dot{H} absolute land uplift from the geoid
- \dot{h} absolute land uplift from the reference ellipsoid
- \dot{H}_r relative land uplift from the local mean sea level
- \dot{H}_e eustatic (global mean sea level) rise
- \dot{H}_t change over time of the sea-surface topography (likely small)
- \dot{N} geoid rise.

The rise of the geoid as a result of land uplift can be simply calculated with the Stokes equation:

$$\frac{dN}{dt} = \frac{R}{4\pi\gamma} \iint_{\sigma} S(\psi) \left(\frac{d}{dt} \Delta g \right) d\sigma.$$

Here, $\frac{d}{dt} \Delta g$ is the change of gravity anomalies over time due to land uplift. Unfortunately we do not precisely know the *mechanism* by which mass flows in the Earth's mantle to underneath the land-uplift area. We may posit

$$\frac{d}{dt} \Delta g = c \frac{dH}{dt} = c\dot{H},$$

in which the constant c may range from -0.16 to -0.31 mGal/m.

- The value -0.16 mGal/m is called the "Bouguer hypothesis": it corresponds to the situation in which upper mantle matter flows into the space freed up underneath the rising Earth's crust, in

¹This dot notation, fluxion, was introduced by Newton.



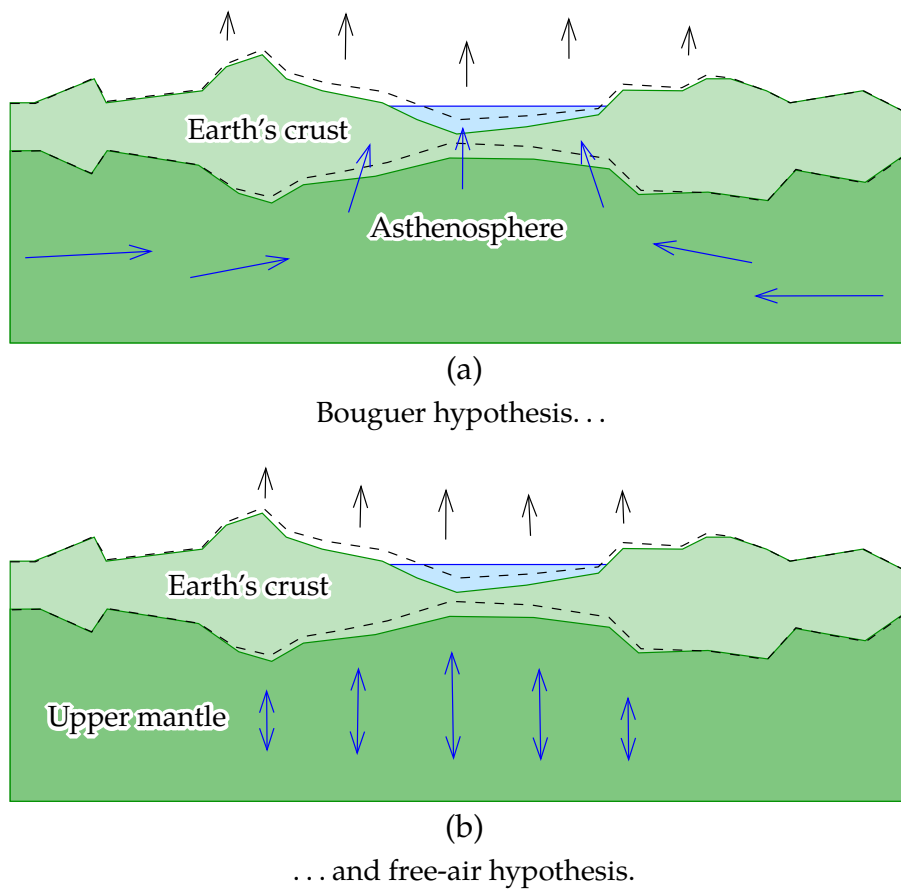


FIGURE 12.1. The two different hypotheses on the mechanism of post-glacial land uplift.

order to fill it. This matter may be roughly modelled as a Bouguer plate.

- The value -0.31 mGal/m is the opposite extreme, the “free-air hypothesis”. By this hypothesis, the ice load during the last ice age has only compressed the Earth’s mantle, and now it is slowly expanding again to its former volume (the “rising dough model”).

Up until fairly recently, the most likely value was about -0.2 mGal/m , with substantial uncertainty. The latest results (Mäkinen et al., 2010;



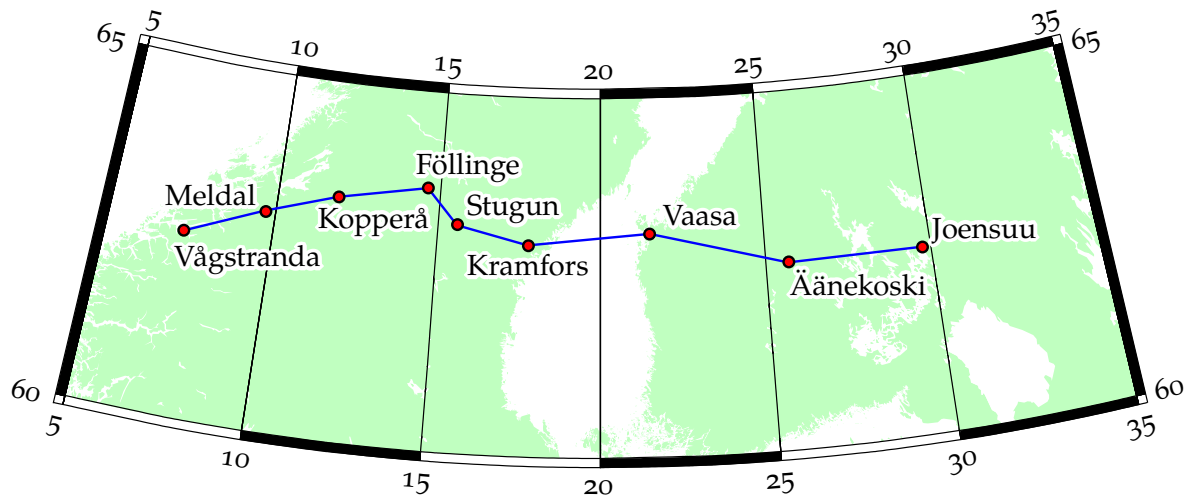


FIGURE 12.2. The Fennoscandian gravity line on the 63rd parallel north.

Olsson et al., 2019) may be summarized as -0.16 ± 0.02 mGal/m (one standard deviation), which would seem to settle the issue. It looks like the Bouguer hypothesis is closer to physical reality. The flow of mass probably happens within the *asthenosphere*.

This problem has been studied much in the Nordic countries. The method used has been gravimetric measurement along the 63rd parallel north (the “Blue Road Geotraverse” project). The measurement stations extend from the Norwegian coast to the Russian border, and have been chosen such that the gravity along them varies within a narrow range. In this way, the effect of the scale error of the gravimeters is avoided. Clearly, absolute gravity is of no interest here, only the *change* in gravity *differences* over time between the stations.

These measurements have been made over many years using high-precision spring or relative gravimeters. In recent years, there has been a shift to using absolute gravimeters, obviating the need for measurement *lines*.



12.4 Methods for determining the sea-surface topography

In principle three geodetic methods exist:

- satellite radar altimetry and gravimetric geoid determination
- positioning of tide gauges along the coast using **GNSS**, together with gravimetric geoid determination
- precise levelling along the coast connecting tide gauges.

In addition to this, we still have the oceanographic method, i.e., physical modelling. The method is termed *steric levelling* if temperature and salinity measurements along vertical profiles are used on the open ocean, and *geostrophic levelling* of ocean current measurements are used to determine the Coriolis effect, generally close to the coast.

All methods should give the same results. The Baltic Sea is a textbook example where all three geodetic methods have been used. It has been found that the whole Baltic Sea surface is tilted: relative to a level surface, the sea surface goes up from the Danish straits to the bottoms of the Gulf of Finland and the Bothnian Bay by 25–30 cm.

Oceanographic model calculations show that this tilt is mainly due to a *salinity gradient*: in the Atlantic Ocean, the salinity is 30–35 ‰, when in the Baltic it drops to 5–10 ‰, due to the massive production of fresh water by the rivers (**Ekman, 1992**). Of course on top of this come temporal variations, like oscillations such as those in a bathtub, the amplitude of which can be over a metre.

In **Ekman (1992)** more is said about the sea-surface topography of the Baltic and its determination.

12.5 Global sea-surface topography and heat transport

One important reason why researchers are interested in the global sea-surface topography is that it offers an opportunity to study more precisely the currents in the oceans and thus the transport of the



Sun's energy from the equator to higher latitudes. There are many matters whose study would be helped by more precise knowledge of ocean currents: carbon dioxide dissolved into the water, chlorophyll (phytoplankton), salinity, among many others.

The Coriolis force, or *acceleration*, caused by the Earth's rotation is

$$\mathbf{a} = 2 \langle \mathbf{v} \times \vec{\omega}_{\oplus} \rangle, \quad (12.1)$$

in which \mathbf{v} is the velocity vector in a system attached to the rotating Earth, and $\vec{\omega}_{\oplus}$ is the rotation vector of the Earth. This is an axial vector, pointing in the direction of the Earth's axis of rotation.

If a fluid flows on the Earth's surface, then, in the above equation 12.1, only the part of $\vec{\omega}_{\oplus}$ in the normal direction \mathbf{n} to the ocean surface will have an effect: this part has a length of $\langle \vec{\omega}_{\oplus} \cdot \mathbf{n} \rangle = \omega_{\oplus} \sin \varphi$, and the vector equation 12.1 may be replaced by the simpler scalar equation

$$a = 2v\omega_{\oplus} \sin \varphi,$$

in which $a \stackrel{\text{def}}{=} \|\mathbf{a} - \langle \mathbf{a} \cdot \mathbf{n} \rangle \mathbf{n}\|$, the length of the projection of \mathbf{a} onto the local horizon plane, and $v = \|\mathbf{v}\|$, $\omega_{\oplus} = \|\vec{\omega}_{\oplus}\|$ in the familiar way. The direction of the Coriolis acceleration is always perpendicular to the flow velocity: when watching along the flow direction, to the right in the northern hemisphere, to the left in the southern hemisphere.

As a result of the Coriolis force, the sea surface in the area of an ocean current is *tilted sideways* with respect to the current, at an angle

$$\frac{a}{\gamma} = 2v \frac{\omega_{\oplus}}{\gamma} \sin \varphi.$$

Here, γ is local gravity. This equilibrium between Coriolis force and the horizontal gradient of pressure is called the *geostrophic equilibrium*. On the equator, it can be seen from the equation that the tilt is zero, but everywhere else, ocean currents are tilted.

For example, in the case of the Gulf Stream, the height variation caused by this effect is several decimetres. If we define a local (x, y) coordinate system in which $x(\varphi, \lambda)$ is pointing north and $y(\varphi, \lambda)$ east, we



may write for the sea-surface topography H the geostrophic equations

$$\frac{\partial H}{\partial x} = -2v_y \frac{\omega_{\oplus}}{\gamma} \sin \varphi, \quad \frac{\partial H}{\partial y} = +2v_x \frac{\omega_{\oplus}}{\gamma} \sin \varphi. \quad (12.2)$$

As we will see in chapter 13, we can measure the location in space of the sea surface at a precision of a few centimetres using satellite radar altimetry. If we furthermore have a precise geoid map, we may calculate the sea-surface topography, and with the aid of equations 12.2 solve for the flow velocity vector field²

$$\begin{bmatrix} v_x(x, y) & v_y(x, y) \end{bmatrix}^T = \begin{bmatrix} v_x(\varphi, \lambda) & v_y(\varphi, \lambda) \end{bmatrix}^T.$$

An elegant property of these equations is that we do not even have to know the absolute level of the field $H(x, y) = H(\varphi, \lambda)$, because that vanishes in differentiation.

The method described, figure 12.3, requires a sufficiently precise geoid map of the oceans of the world. The **GOCE** satellite fits this need like a glove, see section 13.7. One objective of the mission was, as the name indicates, to get a full picture of ocean currents and especially their capacity for heat transport. This knowledge helps understand how the Earth's climate functions and how it is changing, also as a result of human activity. This is an important issue for Europe and Fennoscandia, and also Finland, as the heat energy brought by the Gulf Stream helps to keep these areas habitable (Caesar et al., 2018).

Even without a geoid model, we can study the *variations* of ocean currents using satellite altimetry. It has long been known that in the North Atlantic Ocean, *mesoscale eddies* have been moving alongside the Gulf Stream; eddies of size 10–100 km which show up in altimetric

²A popular, though unofficial, unit for ocean current is the sverdrup (Wikipedia, Sverdrup), a million cubic metres per second. All the rivers of the world together make about one sverdrup, while the Gulf Stream is 30–150 Sv. “There is a river in the ocean” – Matthew Fontaine Maury (1806–1873), American polymath and pioneer of oceanography.



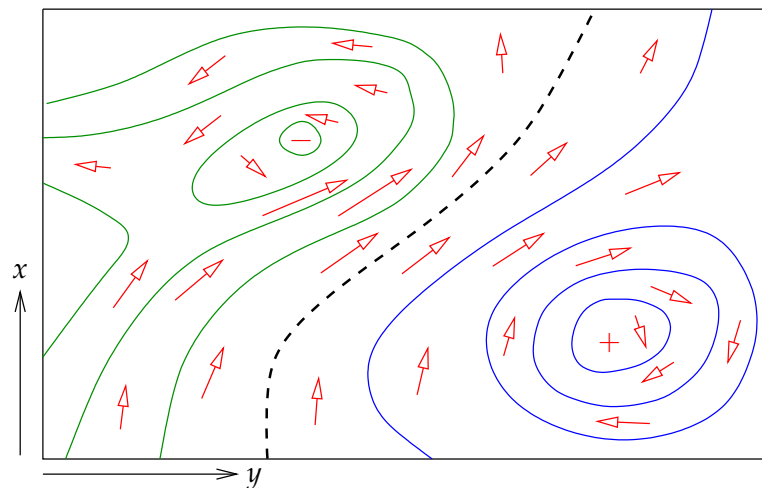


FIGURE 12.3. Connection between sea-surface topography and ocean currents. Red arrows depict ocean currents, curves, sea-surface topography.

imagery. It is interesting that the eddies also show up in maps of the ocean surface temperature, and biologists have observed that life inside the eddies differs from that outside them (Godø et al., 2012). The life span of the eddies can be weeks, even months.

A good, though somewhat dated, introduction to “geodetic oceanography” is given by Rummel and Sansó (1992).

12.6 The global behaviour of the sea level

Water exists on the Earth in three phases: liquid, ice, and vapour. During geological history, the ratio between liquid water and ice in particular has varied substantially. Also today, a large amount of ice is tied up in continental ice sheets, specifically in Antarctica and Greenland. Of these, the Eastern Antarctic ice sheet is overwhelmingly the largest. *mannerjäätikkö*

When the amount of water tied up in continental ice sheets varies, so does the sea level. The end of the last ice age has raised the sea level by as much as 120 m, a process that ran to completion some 7000 years



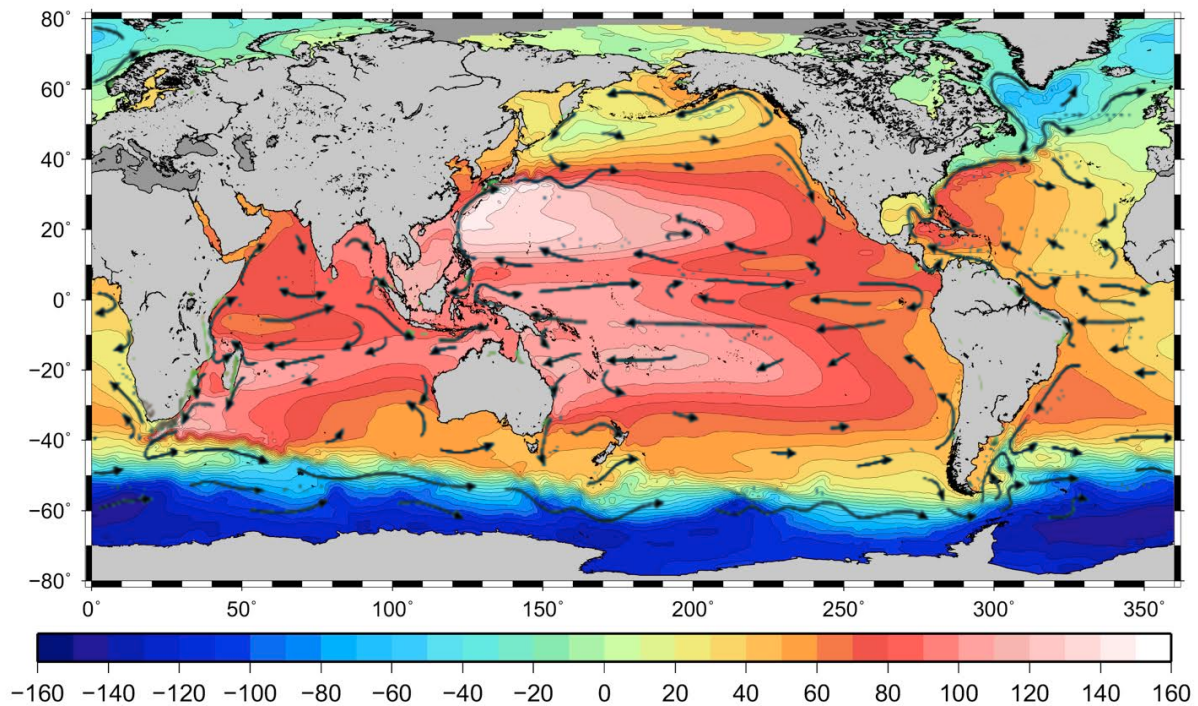


FIGURE 12.4. Sea-surface topography map produced by **GOCE**. Base map © European Space Agency. Unit: cm. Ocean currents superimposed: **NOAA** / Rick Lumpkin (**NOAA**, **Ocean currents**).

ago³ ([Wikipedia, Sea level rise](#)). Not until the last century or two has the sea level again started rising, and the rise accelerating, as a consequence of global warming.

We still live in the aftermath of the last glaciation. There were large continental ice sheets which have since melted away, like in Fennoscandia and in Canada (the Laurentide ice sheet): the land is still rising at an even pace, up to 10 and 14 millimetres per year, respectively. Around the land-uplift areas, in central Europe and the United States, a *subsidence* of the land is taking place at an annual rate of 0.5–1.7

mannerjäätikkö

maan vajoaminen

³7000 years “before present”, 7 ka BP. BP conventionally means: before 1950. Nowadays *b2k*, before the year 2000, is also used.



millimetres, for example [DeJong et al. \(2015\)](#). Directly underneath the hard crust of the Earth or lithosphere, in the upper mantle layer called *asthenosphere*, material is flowing slowly inwards under the rising Earth's crust.

In order to complicate the picture, the sea-level rise caused by the melting of continental ice sheets also presses the ocean floor down — by as much as 0.3 mm per year; the so-called Peltier effect ([Peltier, 2009](#)). Therefore, the measured sea-level rise — whether on the coast by tide gauges, or from space using satellite altimetry — *does not represent the whole change in total ocean water volume*. If the latter is what interests us, as it always does in climate research, this Peltier correction must still be added to the observation values.

vipuliike The subsidence of the sea floor has not even been globally uniform: at the edges of the continents a “lever motion” happens when the sea floor subsides but the dry land does not. And in the tropics in the Indian and Pacific Oceans, the sea level reached its maximum level, the *mid-Holocene highstand*, relative to the Earth's crust approximately 7000 years ago. After this, the local sea level subsided and the coral formations from that age remained, dead, some 2–3 m above the modern sea level. This is how, for example, Tuvalu and the Maldives were formed, which are now being threatened by the modern sea-level rise again.



12.7 The sea-level equation

Scientifically the variations in sea level are studied using the *sea-level equation*. A pioneer in this field has been the Canadian Peltier ([W. R. Peltier, FRSC, Home Page](#)), who has constructed physics-based models of how both the solid Earth and sea level respond when the total mass of the continental ice sheets changes.

The sea-level equation is ([Farrell and Clark, 1976](#); [Spada and Melini, 2015](#)):

$$S = S_E + \frac{G}{R} \left(\rho_i (G_s \circledast_i I - \overline{G_s \circledast_i I}) + \rho_w (G_s \circledast_o S - \overline{G_s \circledast_o S}) \right), \quad (12.3)$$



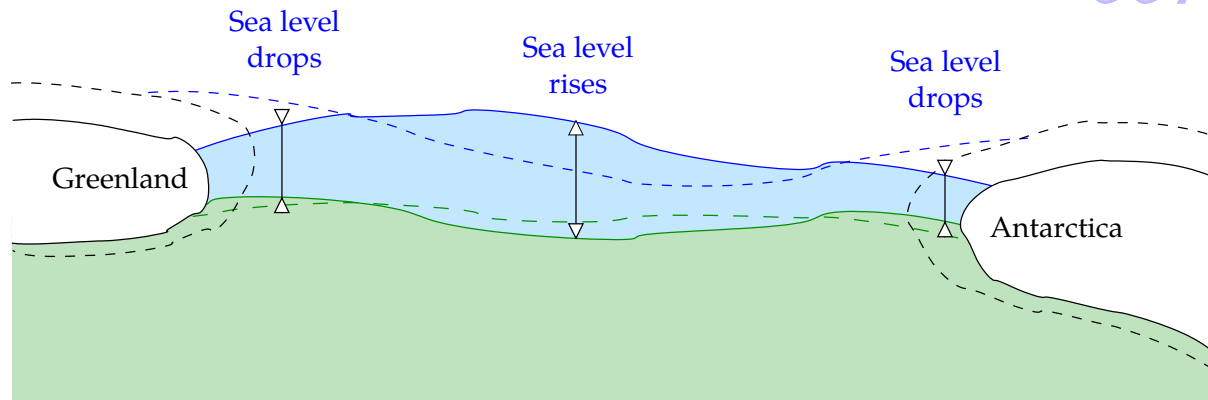


FIGURE 12.5. The sea-level equation. Sea level reacts in a complicated way when continental ice sheets melt.



in which

- $S = S(\omega, t) = S(\phi, \lambda, t)$ means the variations of sea level as a function of place $\omega = (\phi, \lambda)$ and time t . These variations are relative to the solid Earth's surface, i.e., changes in sea depth. S is also what tide gauges measure.
- $I = I(\omega, t)$ is similarly a function of place and time describing the variations in thickness of ice sheets and glaciers.
- S_E is the *eustatic term*, the variation in ice volume converted into "equivalent global sea-level variation", in an equation

$$S_E(t) = -\frac{m_i(t)}{\rho_w A_o},$$

in which $m_i(t)$ is the variation in total ice mass as a function of time, ρ_w the density of sea water, and A_o the total surface area of the oceans.

- R is the mean radius of the Earth, G Newton's universal gravitational constant, section 1.2.
- ρ is the density of matter: ρ_i that of ice, and ρ_w that of sea water.
- \otimes is the symbol of a convolution over the surface of the Earth and the time axis, \otimes_i over land ice, \otimes_o over the oceans: *Green's function*



is multiplied with the ice and sea functions and integrated over the domain in question. These integrals are, by the way, very similar to the ones discussed in section 8.1. For example

$$\begin{aligned} \{G_s \circledast_o S\}(\omega, t) &= \\ &= \int_{-\infty}^t \iint_{\text{ocean}} G_s(\psi(\omega, \omega'), (t - t')) S(\omega', t') d\omega' dt', \end{aligned}$$

in which $\psi(\omega, \omega')$ is the geocentric angular distance between evaluation point $\omega = (\phi, \lambda)$ and data point $\omega' = (\phi', \lambda')$. The measure of the surface integral is $d\omega = R^2 d\sigma = R^2 \cos \phi d\phi d\lambda$. As can be seen, we have here a convolution applied *both* over the Earth's surface ω *and* over the time axis t .

- The *overbar* designates *averaging* over the whole relevant surface area.
- G_s is the *Green's function of sea level*

$$G_s(\psi, \Delta t) = \frac{1}{\gamma} G_V(\psi, \Delta t) - G_r(\psi, \Delta t). \quad (12.4)$$

Here the *Green's function of the geopotential* is

$$G_V(\psi, \Delta t) = G_V^r(\psi, \Delta t) + G_V^e(\psi, \Delta t) + G_V^v(\psi, \Delta t),$$

where ψ is the angular distance of the evaluation point from the data point and $\Delta t = t - t' \geq 0$. The function $G_V^r(\psi, \Delta t) = \delta(\Delta t) / 2 \sin \frac{1}{2} \psi$ is the *rigid* partial Green's function, representing the change in potential caused by a mass of water or ice before any deformation takes place.

The functions G_V^e and G_V^v are the elastic and viscous partial Green's functions of deformation. These thus characterise the *rheological behaviour* of the Earth, and their theoretical calculation requires the internal density and viscosity distributions $\rho(r)$ and $\eta(r)$ of the Earth, assuming they are *isotropic*, only dependent upon r .

$$G_r(\psi, \Delta t) = G_r^e(\psi, \Delta t) + G_r^v(\psi, \Delta t)$$



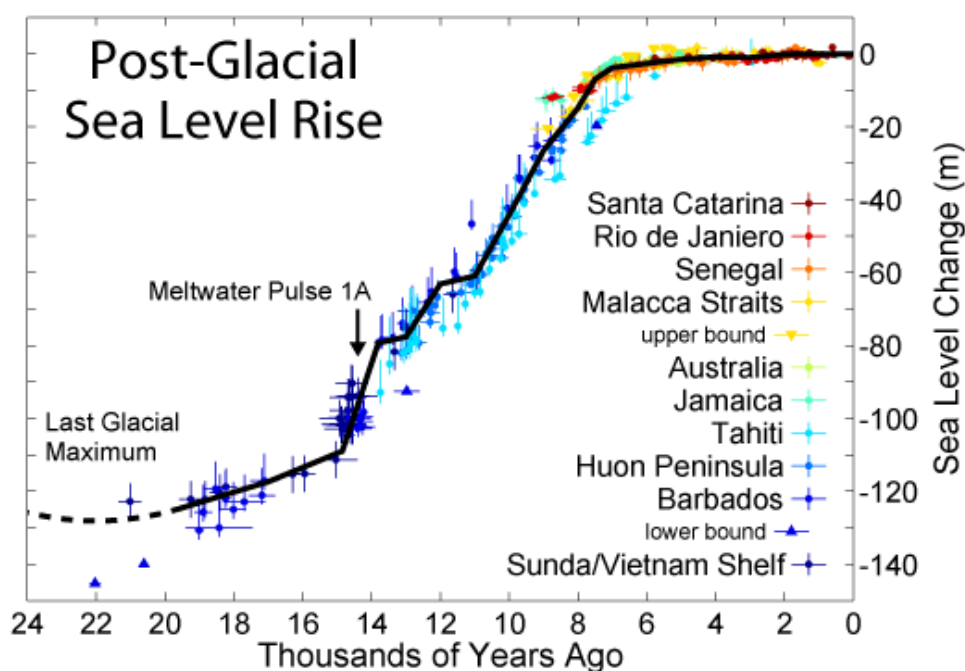


FIGURE 12.6. Sea-level rise after the last ice age (Rohde, 2005).

is similarly *Green's function of vertical or radial displacement* of the sea floor, in the same way split into elastic and viscous parts. There trivially is no “rigid” part.

The behaviour of the sea level can now be computed in this way where one first tries to construct an “ice-load history” $I(\omega, t)$. Then, from this one tries to calculate iteratively, using sea-level equation 12.3, $S(\omega, t)$. S signifies *relative* sea-level variation, changes in the relative positions of sea level and the Earth's solid body or Earth's crust. It is a *function of place*: one may not assume that it would be the same everywhere. Mitrovica et al. (2001) show how, for example, the meltwater from Greenland flees to the southern hemisphere, when the meltwater from Antarctica again comes similarly to the north. This is a consequence of the change in the *Earth's gravity field* and the geoid, when large volumes of ice melt. Another factor is also the fact that the physical shape of the Earth changes when the ice load changes: *glacial isostatic adjustment*,



GIA.

This also complicates the monitoring of the global mean sea level from local measurements: the problem is familiar in Fennoscandia, where the Earth's crust, for now, is rising faster than the global sea level. . .

Green's functions in the sea-level equation are functions of both ψ and time difference Δt . This tells us that **GIA** is a function of both place and time. On a spherically symmetric Earth, the functions may be written as *expansions*. See [Wiczerkowski et al. \(1999\)](#).

The *elastic* response of the Earth to loading is instantaneous on the geological time-scale. It is described by the same elastic Love numbers that appear in the theory of tidal deformation, see section 14.2. Like this:

$$G_s^e(\psi, \Delta t) = \frac{1}{\gamma} \cdot \delta(\Delta t) \sum_{n=0}^{\infty} \overbrace{k_n P_n(\cos \psi)}^{G_V^e(\psi, \Delta t)} - \frac{1}{\gamma} \cdot \delta(\Delta t) \sum_{n=0}^{\infty} \overbrace{h_n P_n(\cos \psi)}^{G_r^e(\psi, \Delta t)},$$

with k_n and h_n as defined in equations 14.4. $\delta(\Delta t)$ is Dirac's delta function.

GIA, however, is *viscous* deformation on a range of geological time-scales. Equation 12.4 yields

$$G_s^v(\psi, \Delta t) = \frac{1}{\gamma} \cdot \sum_{n=0}^{\infty} \overbrace{k_n^v(\Delta t) P_n(\cos \psi)}^{G_V^v(\psi, \Delta t)} - \frac{1}{\gamma} \sum_{n=0}^{\infty} \overbrace{h_n^v(\Delta t) P_n(\cos \psi)}^{G_r^v(\psi, \Delta t)},$$

with the *viscous Love numbers* for potential and vertical displacement:

$$k_n^v(\Delta t) = \sum_{i=1}^I r_{ni}^k \exp(-s_{ni} \Delta t), \quad h_n^v(\Delta t) = \sum_{i=1}^I r_{ni}^h \exp(-s_{ni} \Delta t).$$

Here, n is the degree number, and the index i counts the *viscous relaxation modes* for every degree number n . The ratios r_{ni}^k/s_{ni} and r_{ni}^h/s_{ni} are



called “modal strengths”, and the $\tau_{ni} = 1/s_{ni}$ are relaxation times in which the mode in question will decay over time.

Generally, the modes that are of large spatial extent — low degree numbers n — decay slower, when again the local modes — high degree numbers — tend to decay faster. The local modes of the last deglaciation have today already vanished: the geographic pattern of the Fennoscandian land uplift is already very smooth and the seismicity accompanying the deglaciation is pretty much over. Back then, during the retreat of the ice sheet at its edge, there were strong earthquakes, traces of which are visible in the landscape (Kuivamäki et al., 1998). The now-dominant viscous modes are many hundreds of kilometres in geographic extent and correspondingly of time-scales of thousands of years.



Self-test questions

1. List all the causes of sea-level variations that you are aware of.
2. What is the sea-surface topography?
3. What is eustatic sea-level rise?
4. What is the origin of the name “El Niño”?
5. What is absolute, and what is relative land uplift? What does the difference between the two consist of?
6. Which two main models are on offer for the mechanism of land uplift?
7. What three geodetic techniques are available for determining the sea-surface topography?
8. What is the shape of the sea-surface topography of the Baltic Sea, and what is its cause?
9. What is the Coriolis force, and how does it affect ocean currents?
10. What is the geostrophic balance?



11. In whose honour is the unit sverdrup named?
12. How can one invert a map of the sea-surface topography into a map of ocean currents? Where on Earth does this *not* work?
13. What is the Peltier effect? What is the mid-Holocene highstand?
14. What does the sea-level equation describe?
15. Why does the mean sea level in the Baltic Sea not rise when the Greenland continental ice sheet melts? What will happen in the Baltic Sea when the West Antarctic ice sheet melts?



Exercise 12 – 1: Coriolis force, ocean current

It is given that the velocity of flow of an ocean current is 0.1 m/s and its width 100 km.

1. How much is the height difference between its left and right edges? Assume that the current is at latitude 45° north.
2. If the same current was 200 km broad and the velocity of flow 0.05 m/s (so, assuming the same depth, the transport of water would also be the same), compute for that case the height difference between the left and the right edges.
3. [For fun] if the depth of the current is 1 km, what is the water transport in sverdrup?



Exercise 12 – 2: Land subsidence and the mechanism of land uplift

How does the post-glacial land subsidence observed in the United States and central Europe support a Bouguer type of land-uplift mechanism (figure 12.1a), rather than a free-air mechanism?





Satellite altimetry and satellite gravity missions

13



13.1 Satellite altimetry

Satellite altimetry is a measurement method in which the distance from a satellite straight down to the sea surface is measured using a microwave radar. Historically there have been many satellites carrying an altimetry radar: see table 13.1, which may not be complete.

- The GEOS-3 (1975-027A) and Seasat satellites were American testing satellites aimed at developing the altimetric technique. The measurement precision of GEOS-3 was still modest. Before that, satellite altimetry was also tested with a device, accuracy ± 1 m, on board the orbital laboratory Skylab (1973-027A).
- Seasat (1978-064A) broke down only three months after launch, probably due to a short-circuit.¹ However, the data from Seasat was the first large satellite altimetry data set used for determining the mean sea surface, and that of the Baltic Sea (Vermeer, 1983b).
- Geosat (1985-021A) was a satellite launched by the US Navy, intended to map the gravity field on the world's oceans; more precisely the deflections of the plumb line, which are needed to impart the correct departure direction to ballistic missiles launched from submarines. The 17-day repeat data from the

¹But read this: [Wikipedia, Seasat conspiracy theory](#).



TABLE 13.1. Altimetric satellites through the ages.

| Satellite | Launch year | Orbital inclination (°) | Orbital height (km) | Repeat periods (days) | Measurement precision (m) | Positioning technique |
|------------------|-------------|-------------------------|---------------------|-----------------------|---------------------------|-----------------------|
| GEOS-3 | 1975 | 115.0 | 843 | ~ 38 | 0.20 | |
| Seasat | 1978 | 108.0 | 780 | 3, 17 | 0.08 | |
| Geosat | 1985 | 108.0 | 780 | 3, 17 | 0.04 | |
| ERS-1 | 1991 | 98.5 | 780 | 3, 35, 168 | 0.03 | |
| TOPEX/Poseidon | 1992 | 66.0 | 1337 | 9.9156 | 0.033 | GPS, DORIS |
| ERS-2 | 1995 | 98.5 | 780 | 3, 35 | 0.03 | PRARE |
| Geosat follow-on | 1998 | 108.0 | 800 | 17 | 0.035 | |
| Envisat | 2001 | 98.5 | 784 | 35 | 0.045 | GPS, DORIS |
| Jason-1 | 2001 | 66.1 | 1336 | 9.9156 | 0.025 | GPS, DORIS |
| Jason-2 | 2008 | 66.04 | 1336 | 9.9156 | 0.025 | GPS, DORIS |
| Cryosat-2 | 2010 | 92.0 | 725 | 369 | | DORIS |
| HY-2A | 2011 | 99.3 | 970 | 14, 168 | 0.085 | DORIS, GPS |
| SARAL/AltiKa | 2013 | 98.5 | 781 | 35 | | DORIS |
| Jason-3 | 2016 | 66.04 | 1338 | 9.9927 | 0.025 | GPS, DORIS |
| Sentinel-3A | 2016 | 98.62 | 804 | 27 | 0.03 | DORIS, SLR, GNSS |

geodetic mission was initially classified. Later however, the data from the southern hemisphere was published for scientists to use, and still later, the whole data set was made public.

- The satellites ERS-1/2 (1991-050A, 1995-021A) and Envisat (2002-009A) were launched by the **ESA**, the European Space Agency. The altimeter was just one among many packages. A German positioning device called **PRARE** was on the ERS satellites, but it only functioned after launch on ERS-2.
- **TOPEX/Poseidon** (1992-052A) was an American-French collaboration, one goal of which was to precisely map the *sea-surface topography*. A special feature was the on-board precise **GPS** posi-



tioning device, which allowed the determination of the location of the sea surface *geocentrically*. Together with its successors *Jason-1*, 2 and 3 (2001-055A, 2008-032A, 2016-002A), this satellite mission has also produced, and continues to produce, valuable information on the global rise of the sea level over the last 25 years, of about 3 mm per year. See figure 13.1.

The famous oceanographer Walter Munk² characterised *TOPEX/Poseidon* in 2002 as “the most successful ocean experiment of all time” (Munk, 2002).

- HY-2A (2011-043A) is a Chinese satellite also launched by China.
- SARAL/AltiKa (2013-009A) is a satellite launched by India. The altimeter and *DORIS* are French contributions.
- Cryosat-2 (2010-013A) is a satellite launched by the *ESA* to study polar sea ice. Of special interest is the *freeboard*, the amount by which the ice sticks out of the water. From this, the thickness, and, with the surface area, the total volume may be calculated. In-orbit positioning is done using the French *DORIS* system.

The launch of Cryosat-1 failed.

- Sentinel-3A (2016-011A) is a versatile *ESA* remote-sensing satellite, the first of a planned constellation. It carries several instruments, among them the *SRAL*, or Synthetic Aperture Radar Altimeter.

The measurement method of satellite radar altimetry is presented in figure 13.2. The figure shows all the quantities playing a role in altimetry: the measured range s is the height h of the satellite above the reference ellipsoid corrected for the geoid height N , the sea-surface topography H , and variations of the sea surface, like tides, eddies, annual variation, and so on.

Furthermore, if the satellite does not contain a precise positioning device, the true orbit of the satellite will differ from the calculated orbit

²Walter Heinrich Munk (1917–2019) was a famous American physical oceanographer.



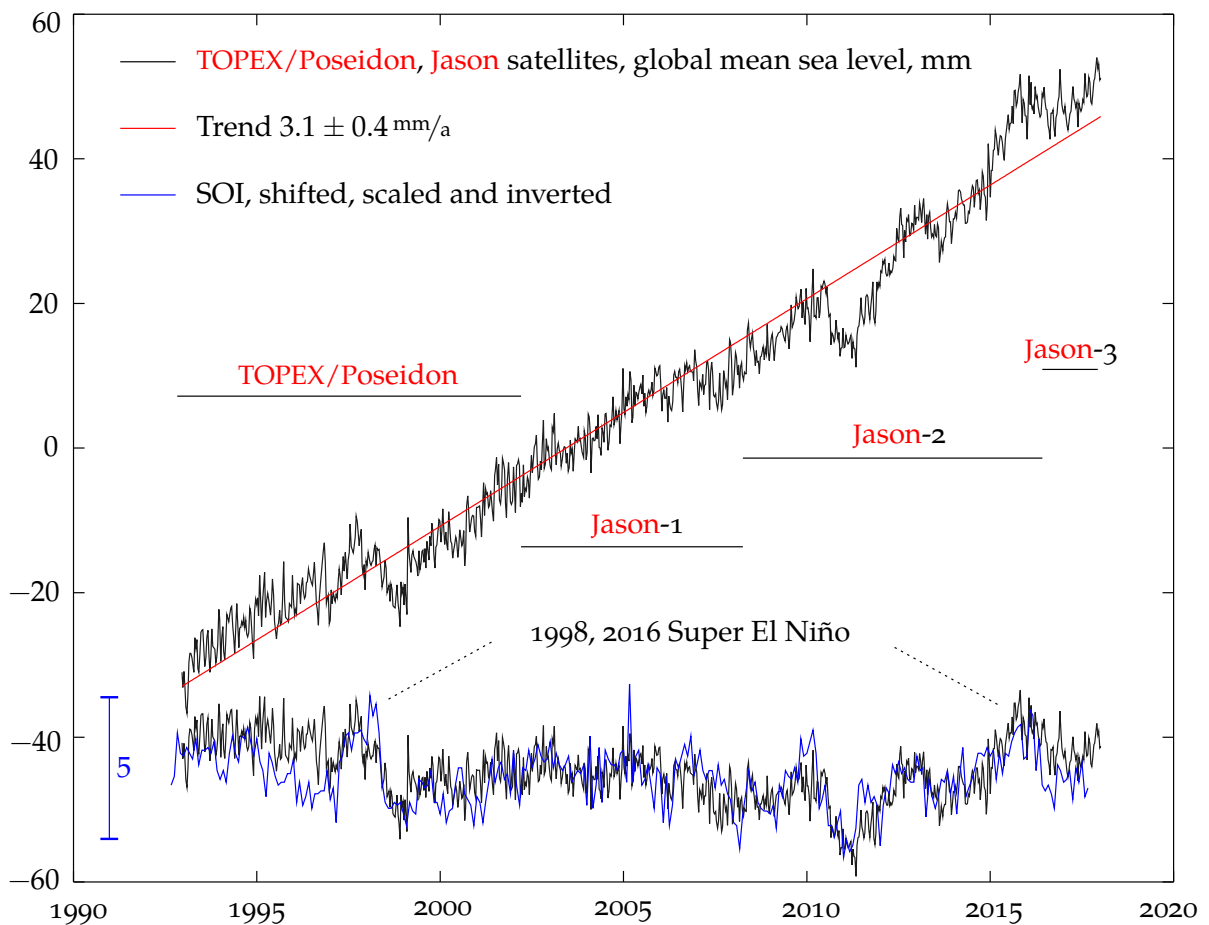


FIGURE 13.1. Results from the **TOPEX/Poseidon** and **Jason** satellites. Annual cycle removed. Comparison with **ENSO** (“El Niño”), SOI = Southern Oscillation Index. Data © Colorado University at Boulder’s **Sea Level Research Group**; **Nerem et al. (2010)**.

— even from the orbit calculated afterwards. Therefore,

$$h = h_0 + \Delta h,$$

in which h_0 is the calculated orbit, and Δh the orbit-error correction.

The measurements are performed by sending thousands of pulses down each second, measuring the travel times of the reflected return pulses on board the satellite, averaging them down to a measurement



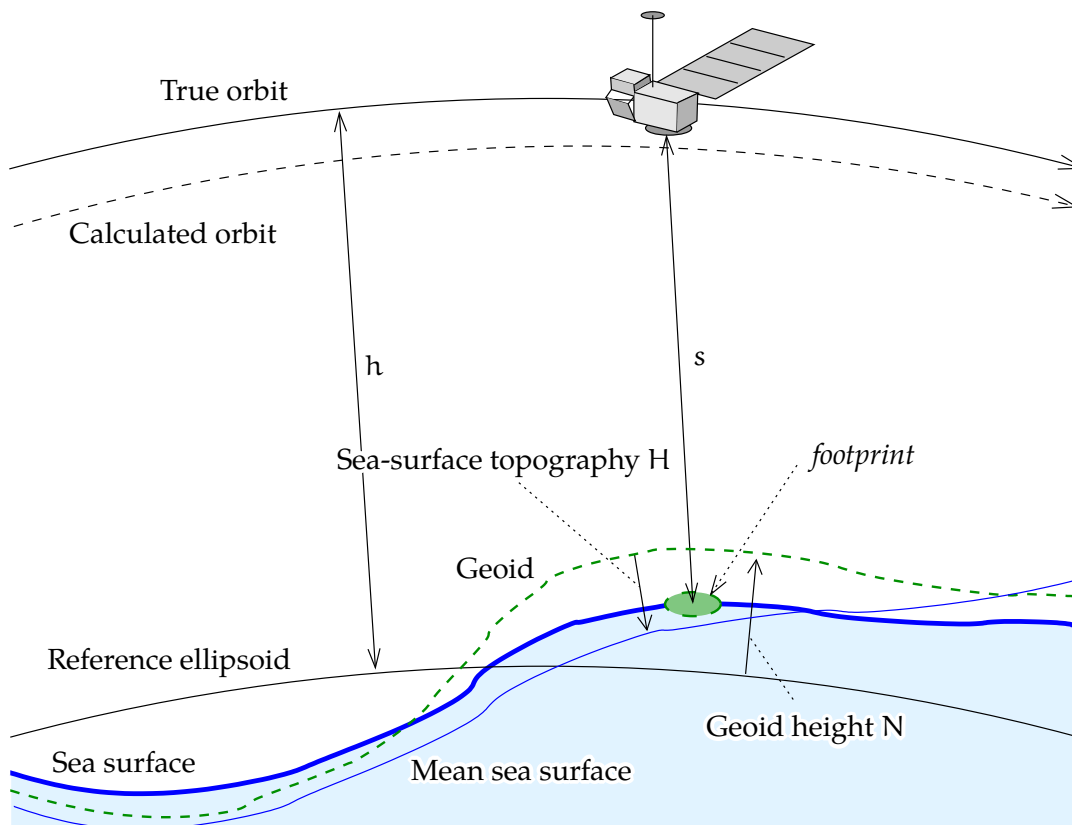


FIGURE 13.2. Satellite altimetry as a measurement method, concepts.

rate of 10–20 values per second, and transmitting these to Earth. Of these values, the largest and smallest are thrown away as possibly erroneous, and from the remainder, a mean value is calculated for the central epoch of the pulse train using linear regression. The value thus obtained from the regression line is the actual “measurement”: one every second, making the effective measurement frequency 1 Hz.

The details will vary from satellite to satellite. The pulse shape is never quite crisp, the place of the reflection on the ocean surface, or *footprint*, has a diameter of several kilometres. Especially if the ocean has wave motion (*significant wave height, SWH*), then, in the processing phase, one should make a careful correction so no bias is created: if the *SWH* is large, the altimeter footprint — the area on the sea from



which radio energy returns to the receiver — will also be larger, and the distance travelled by the radio waves will on average be a little longer.

The newest satellites use an interferometric technique that differs somewhat from the description above.

Of all the corrections related to instrumentation, atmosphere, ocean, and solid Earth, we mention

- the height of sea waves (SWH)
- solid-Earth tides
- ocean tides
- the “wet” tropospheric propagation delay, best derived from measurements with a water vapour radiometer on the satellite, otherwise from an atmospheric model
- the “dry” tropospheric propagation delay
- the ionospheric delay, only for the part of the ionosphere below the satellite, depending on flight height
- the altimeter’s own calibration correction — nowadays “in-flight” calibration is always strived for, using an ensemble of GNSS-positioned tide gauges.

The measurements and all corrections to be made to them are collected into a “geophysical data record” (GDR), one per observation epoch. The files built this way are distributed to researchers. This allows all kind of experimentation; for example, the replacement of a correction by one calculated from improved models.

13.2 Crossover adjustment

When a satellite orbits the Earth over months or years, thousands of points are formed where the tracks cross each other. If we assume that the sea level is the same for both satellite overflights, then this forms a *condition* that can be used to adjust away orbit errors.



The observation equation is

$$\underline{s} = h - N - H - \epsilon + \underline{n} = h_0 + \Delta h - N - H - \epsilon + \underline{n},$$

in which \underline{s} is the altimetric measurement of the height of the sea surface, h the actual, and h_0 the calculated height of the satellite above the reference ellipsoid. N is the geoid height, H is the *sea-surface topography*, i.e., the permanent deviation of the sea surface from an equipotential surface, Δh is the orbit-error correction, ϵ is the *residual variation* of the sea surface, the variation remaining after correcting for the tides and other effects that can be modelled, and \underline{n} is the random uncertainty, or noise, in the radar altimetry observations.

From this we obtain in the crossing point of tracks i and j :

$$\ell_k \stackrel{\text{def}}{=} (\underline{s}^i - h_0^i) - (\underline{s}^j - h_0^j) = (\Delta h_i - \Delta h_j) - (\epsilon_i - \epsilon_j) + (\underline{n}_i - \underline{n}_j).$$

This is the observation equation of crossover adjustment. Here we see the complication that in both, sea-surface residual variation and orbit corrections come along in the equation in the same way. They cannot be separately determined by crossover adjustment.

If we forget for now the sea-surface residual variation — or assume that it behaves randomly, in other words it is part of the noise \underline{n} — we may write more simply

$$\ell_k = \Delta h_i - \Delta h_j + \underline{n}_k, \quad \text{in which } \underline{n}_k \stackrel{\text{def}}{=} (\underline{n}_i - \underline{n}_j) - (\epsilon_i - \epsilon_j).$$

The index k counts crossover points, the indices i, j count tracks.

Next, we choose a suitable *model* for the satellite orbit error. The simplest choice, sufficient for a small area, is the assumption that the orbit correction is a constant for each track. See a simple example, figure 13.3.

13.2.1 A simple example

In the figure we have three tracks and two crossing points. The *observation equations*, which describe the discrepancies in the known



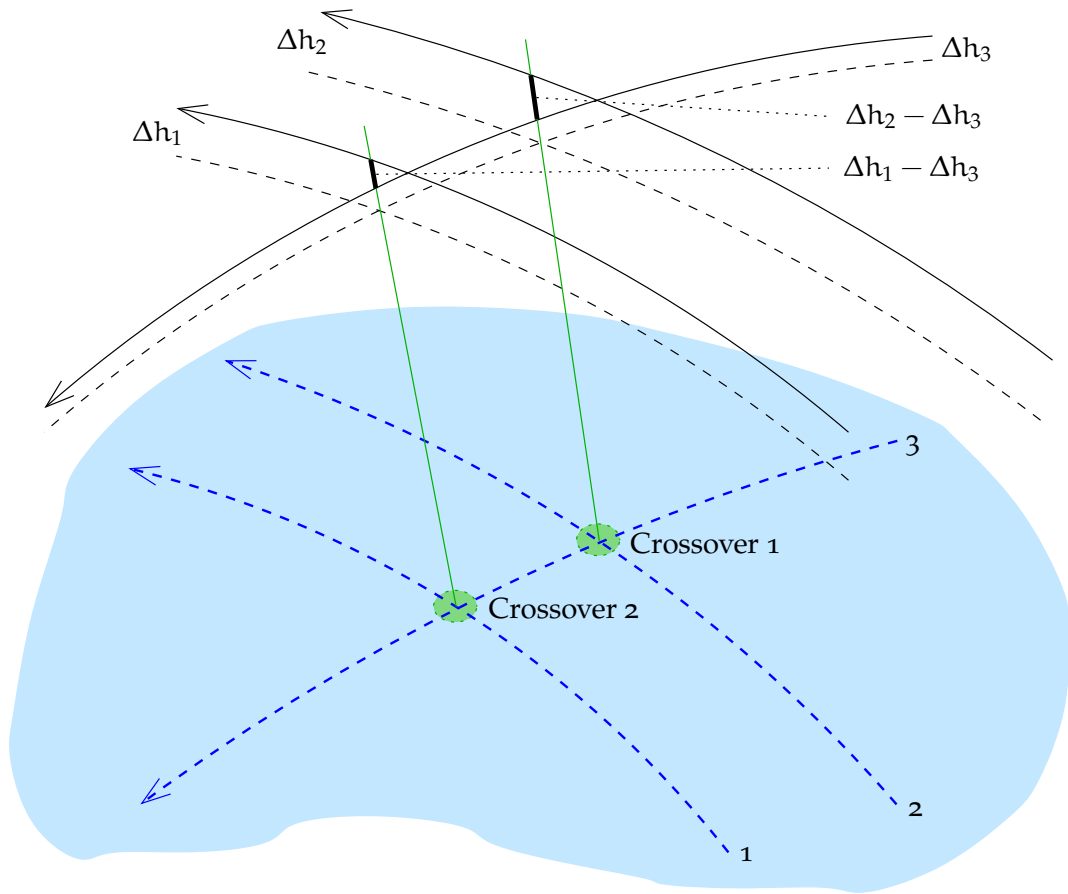


FIGURE 13.3. Simple crossover geometry.

crossover points as functions of the orbit corrections, are

$$\begin{aligned} \ell_1 &= \Delta h_2 - \Delta h_3 + \underline{n}_1, \\ \ell_2 &= \Delta h_1 - \Delta h_3 + \underline{n}_2, \end{aligned}$$

or in matrix form³

$$\begin{bmatrix} \ell_1 \\ \ell_2 \end{bmatrix} = \begin{bmatrix} 0 & 1 & -1 \\ 1 & 0 & -1 \end{bmatrix} \begin{bmatrix} \Delta h_1 \\ \Delta h_2 \\ \Delta h_3 \end{bmatrix} + \begin{bmatrix} \underline{n}_1 \\ \underline{n}_2 \end{bmatrix}, \quad (13.1)$$



symbolically

$$\underline{\ell} = A\mathbf{x} + \underline{n}.$$

If one now tries to calculate the solution using ordinary least-squares,

$$\hat{\mathbf{x}} = (A^T A)^{-1} A^T \underline{\ell},$$

this will not work. The *normal matrix* $A^T A$ is *singular* (check!). This makes sense, as one can move the whole track network up or down without the observations $\underline{\ell}_k$ changing. No unique solution can be found for such a system.

Finding a solution requires that *something* must be fixed: for example, one track — or, more democratically, the mean level of all tracks. This fixing is achieved by *adding* the following “observation equation”:

$$\ell_3 \stackrel{\text{def}}{=} 0 = \begin{bmatrix} c & c & c \end{bmatrix} \cdot \mathbf{x}, \quad (13.2)$$

in which c is some suitable constant. Then, matrix A becomes

$$A = \begin{bmatrix} 0 & 1 & -1 \\ 1 & 0 & -1 \\ c & c & c \end{bmatrix},$$

and the least-squares solution

$$\hat{\mathbf{x}} = \begin{bmatrix} \widehat{\Delta h}_1 \\ \widehat{\Delta h}_2 \\ \widehat{\Delta h}_3 \end{bmatrix} = (A^T A)^{-1} A^T \underline{\ell} = (A^T A)^{-1} A^T \begin{bmatrix} \underline{\ell}_1 \\ \underline{\ell}_2 \\ 0 \end{bmatrix},$$

where the matrix inversion is now possible. In this particular case, $\hat{\mathbf{x}} = A^{-1} \underline{\ell}$ will give the same solution, as A is square and invertible:

$$(A^T A)^{-1} A^T \underline{\ell} = A^{-1} (A^T)^{-1} A^T \underline{\ell} = A^{-1} \left((A^T)^{-1} A^T \right) \underline{\ell} = A^{-1} \underline{\ell}.$$

³Note the similarity with the observation equations for levelling! Instead of benchmarks, we have tracks, instead of levelling lines, crossover points.



Now the symbolic algebra system maxima ([SourceForge](#), [Maxima](#)) — or brute-force calculation — gives the readily verified inverse

$$\begin{aligned} A^{-1} &= \begin{bmatrix} 0 & 1 & -1 \\ 1 & 0 & -1 \\ c & c & c \end{bmatrix}^{-1} = \left(\begin{bmatrix} 1 & & \\ & 1 & \\ & & c \end{bmatrix} \begin{bmatrix} 0 & 1 & -1 \\ 1 & 0 & -1 \\ 1 & 1 & 1 \end{bmatrix} \right)^{-1} = \\ &= \begin{bmatrix} 0 & 1 & -1 \\ 1 & 0 & -1 \\ 1 & 1 & 1 \end{bmatrix}^{-1} \begin{bmatrix} 1 & & \\ & 1 & \\ & & c \end{bmatrix}^{-1} = \\ &= \frac{1}{3} \begin{bmatrix} -1 & 2 & 1 \\ 2 & -1 & 1 \\ -1 & -1 & 1 \end{bmatrix} \begin{bmatrix} 1 & & \\ & 1 & \\ & & \frac{1}{c} \end{bmatrix} = \frac{1}{3} \begin{bmatrix} -1 & 2 & \frac{1}{c} \\ 2 & -1 & \frac{1}{c} \\ -1 & -1 & \frac{1}{c} \end{bmatrix}, \end{aligned}$$

and the solution is

$$\begin{aligned} \begin{bmatrix} \widehat{\Delta h}_1 \\ \widehat{\Delta h}_2 \\ \widehat{\Delta h}_3 \end{bmatrix} &= A^{-1} \underline{\ell} = \frac{1}{3} \begin{bmatrix} -1 & 2 & \frac{1}{c} \\ 2 & -1 & \frac{1}{c} \\ -1 & -1 & \frac{1}{c} \end{bmatrix} \begin{bmatrix} \underline{\ell}_1 \\ \underline{\ell}_2 \\ 0 \end{bmatrix} = \\ &= \frac{1}{3} \begin{bmatrix} -1 & 2 \\ 2 & -1 \\ -1 & -1 \end{bmatrix} \begin{bmatrix} \underline{\ell}_1 \\ \underline{\ell}_2 \end{bmatrix}, \end{aligned}$$

from which c has vanished.

Another way to look at this is to first write the observation equations [13.1](#) and [13.2](#) together as

$$\begin{bmatrix} \underline{\ell}_1 \\ \underline{\ell}_2 \\ 0 \end{bmatrix} = \begin{bmatrix} 0 & 1 & -1 \\ 1 & 0 & -1 \\ c & c & c \end{bmatrix} \begin{bmatrix} \Delta h_1 \\ \Delta h_2 \\ \Delta h_3 \end{bmatrix} + \begin{bmatrix} \underline{n}_1 \\ \underline{n}_2 \\ 0 \end{bmatrix},$$

and then multiply the left-hand side and both terms on the right with the diagonal matrix

$$D \stackrel{\text{def}}{=} \begin{bmatrix} 1 & 0 & 0 \\ 0 & 1 & 0 \\ 0 & 0 & \frac{1}{c} \end{bmatrix}.$$



The result is

$$\overbrace{\begin{bmatrix} \underline{\ell}_1 \\ \underline{\ell}_2 \\ 0 \end{bmatrix}}^{D\ell} = \overbrace{\begin{bmatrix} 0 & 1 & -1 \\ 1 & 0 & -1 \\ 1 & 1 & 1 \end{bmatrix}}^{DA} \begin{bmatrix} \Delta h_1 \\ \Delta h_2 \\ \Delta h_3 \end{bmatrix} + \overbrace{\begin{bmatrix} \underline{n}_1 \\ \underline{n}_2 \\ 0 \end{bmatrix}}^{Dn},$$

from which c has also vanished.

The principle applies generally:

Minimal constraints added to observation equations with a datum defect do not essentially change the solution.

13.2.2 A more advanced orbit correction model

A more advanced representation of orbit corrections more suitable for use in a larger area, is a *linear function*:

$$\Delta h = a + b\tau,$$

where the parameter τ is the location along the track reckoned from its starting point. The dimension of this location can be time (seconds) or distance (degrees or kilometres). Now, the set of observation equations for the situation described above is

$$\overbrace{\begin{bmatrix} \underline{\ell}_1 \\ \underline{\ell}_2 \end{bmatrix}}^{\ell} = \overbrace{\begin{bmatrix} 0 & 0 & 1 & \tau_1^2 & -1 & -\tau_1^3 \\ 1 & \tau_2^1 & 0 & 0 & -1 & -\tau_2^3 \end{bmatrix}}^A \overbrace{\begin{bmatrix} a_1 \\ b_1 \\ a_2 \\ b_2 \\ a_3 \\ b_3 \end{bmatrix}}^x + \overbrace{\begin{bmatrix} \underline{n}_1 \\ \underline{n}_2 \end{bmatrix}}^n.$$

The design matrix A contains, besides the values 1 and -1 , also values $\pm\tau_k^i$, in which i is the number of the track and k that of the crossover



point. These values are computable when the geometry of the tracks is known.

Now there are *two* unknowns for every track, a and b , a constant and a trend. Of course also this system will prove to be singular. Removing the singularity can be done by fixing all three parameters b and one parameter a .⁴

The phenomenon that no solution can be found unless something is fixed is called a *datum defect*. Fixing something suitable will define a certain *datum*. Between two different datums exists a *transformation formula*: in the case of one orbit correction parameter per track, this transformation is a simple parallel shift or *translation* of all tracks up or down.

The situation is somewhat similar to when one is defining a height or vertical reference system for a country. One needs to fix one point, for example Helsinki harbour. If alternatively one fixes another point, for example Turku harbour, the result is another *datum*, in which all height values differ from the corresponding ones in the first datum by a certain fixed amount.

The argument continues to hold if there is a large number of tracks: say, ten north-going and ten south-going tracks, crossing at 10×10 crossover points. Here, for two parameters per track, we would have 40 unknowns and no less than 100 observations. Still, we must constrain the absolute level and the various trends and possible other deformations of the whole network of tracks. A simple approach is to attach *a priori* uncertainties to the unknowns a_i , b_i to be derived, for example, from the known uncertainties of the orbit prediction available. The least-squares

⁴In order to understand this, build, say, a three-track “wire-frame model” from pieces of iron wire, tied together by pieces of string at the crossover points. The crossover conditions do not in any way fix the values of the trends b , and the whole absolute level of the frame continues to be unconstrained.



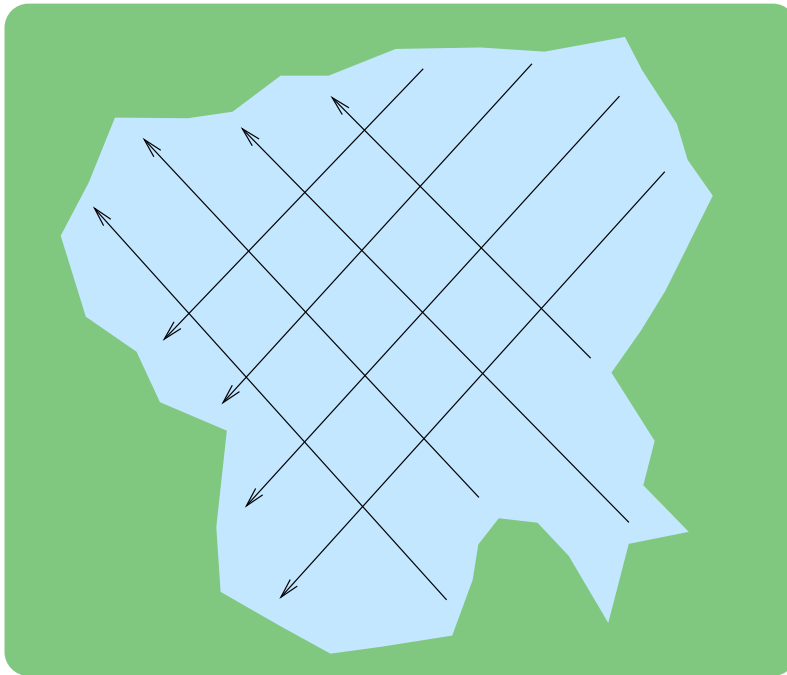


FIGURE 13.4. Example of track geometry of satellite altimetry.

adjustment equation then becomes

$$\hat{\mathbf{x}} = (\mathbf{A}^T \mathbf{A} + \sigma^2 \mathbf{\Sigma}^{-1})^{-1} \mathbf{A}^T \underline{\mathbf{l}}$$

in which $\mathbf{\Sigma}$ is the diagonal matrix containing the *a priori* variances⁵ $\sigma_{a,i}^2$ and $\sigma_{b,i}^2$ of the parameters of each track i . This is referred to as Tikhonov⁶ regularisation.



13.2.3 Another example

In diagram 13.4 describing a satellite altimetry geometry, there are 16 crossover points. We attempt a crossover adjustment.

⁵ σ is the mean error of unit weight, in this case the mean error of a crossover observation.

⁶Andrey Nikolayevich Tikhonov (1906–1993) was a Russian mathematician and geophysicist.



Questions

1. If the orbit correction Δh of each satellite track is described by a model with a single bias term, how many unknowns are there?
2. If we have available 16 “observations” or crossover differences, how many of them are redundant?
3. Is it geometrically possible to calculate this network?
4. If we fix one track in advance (*a priori* information), how many redundant observations are there? Can this network be calculated?
5. If every track has *two* unknowns, a bias as well as an error growing linearly with time or trend, what then needs to be fixed in order to make the network calculable? How many redundancies are there then?
6. If, in case 3, we fix one track, which one would you choose? Propose alternatively a solution where you do not have to make a choice.

Answers

1. As many as there are tracks: 8.
2. $16 - 8 = 8$.
3. No, because the absolute level of the whole network is indeterminate.
4. $16 - (8 - 1) = 9$. Now the network can be calculated.
5. If we assume that the tracks are “straight” in (x, y) coordinates, then the set of allowable transformations on the whole network is

$$\Delta h = a_{00} + a_{10}x + a_{01}y + a_{11}xy,$$

having four degrees of freedom. So, one needs to fix for example one bias and three trends, not all north- or all south-



going. Then there are $16 - (8 - 4) = 12$ redundancies.

6. Any such choice would be arbitrary. Rather use the method described above instead, Tikhonov regularisation.

13.2.4 Global crossover adjustment

In a global crossover adjustment, often a still more sophisticated model is used,

$$\Delta h = a + b \sin \tau + c \cos \tau, \quad (13.3)$$

in which now τ is an angular measure, for example the place along the track measured from the last south-north equator crossing or *ascending node*. See Schrama (1989), where this problem is treated more extensively. In this model, a represents the size of the orbit, while b and c denote the offset of the centre of the orbit from the geocentre. This model is three-dimensional: the orbital arcs with their crossovers form a spherical network surrounding the Earth. The degrees of freedom left by the crossover conditions are now the size of this sphere and the offset of its centre from the geocentre:

$$\Delta h = a_0 + a_1 \cos \phi \cos \lambda + a_2 \cos \phi \sin \lambda + a_3 \sin \phi \quad (13.4)$$

with four degrees of freedom.⁷

13.3 Choice of satellite orbit

In choosing a satellite orbit, Kepler's orbital laws are central. Kepler's third law says

$$GM_{\oplus} P^2 = 4\pi^2 a^3, \quad (13.5)$$

in which $a = a_{\oplus} + h$ is the satellite orbit's semimajor axis — the mean distance from the geocentre — while h is called the satellite's mean

⁷One could argue that, in equation 13.3, the parameter a should be zero, as Kepler's third law allows a very precise determination of the orbital size, see section 13.3. Then, also $a_0 = 0$ in equation 13.4.



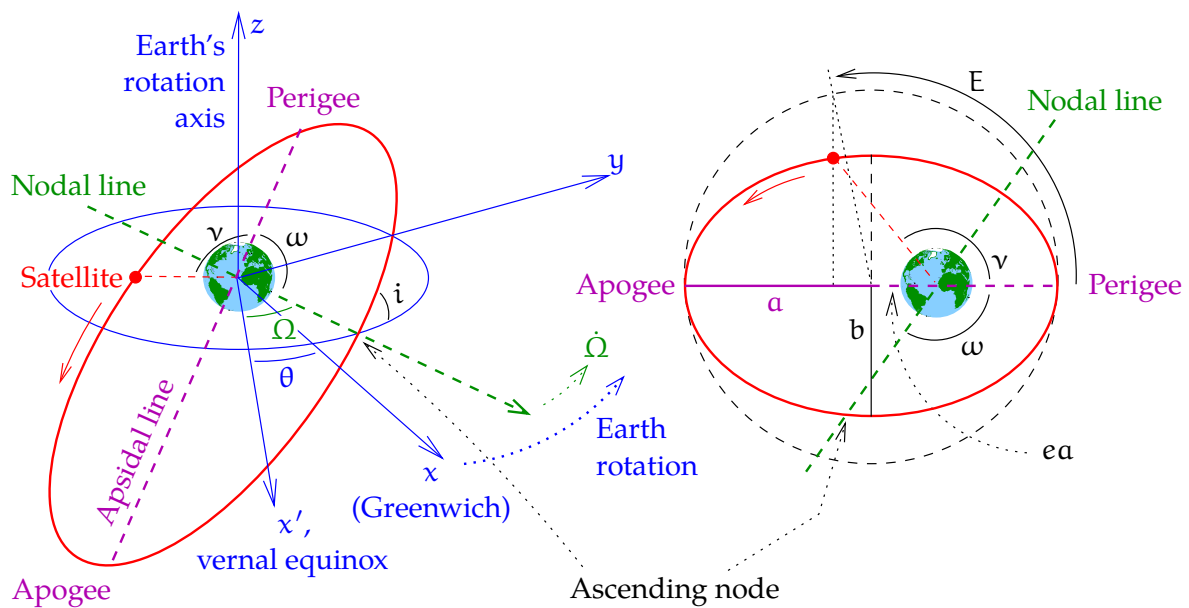


FIGURE 13.5. Kepler's orbital elements: a — semimajor axis, e — eccentricity, i — inclination, Ω — right ascension (celestial longitude) of the ascending node, ω — argument of perigee, and ν — true anomaly.

height. P is the orbital period; a_{\oplus} is the equatorial radius of the Earth ellipsoid.

From equation 13.5 one can already infer that using satellite observations one can precisely determine the quantity GM_{\oplus} , the mass of the Earth multiplied by Newton's universal gravitational constant.⁸ The period P can be precisely determined from long observation series, and the size of the orbit a can also be obtained very precisely, for example from satellite laser ranging (SLR) observations. For this purpose the well-known LAGEOS (Laser Geodynamic Satellite) satellites (1976-039A

⁸This is why it is said that Henry Cavendish was the first to "weigh the Earth"... Determining GM_{\oplus} was already straightforward back then using the orbital motion of the Moon, or even gravity on the Earth's surface. The challenge was separating G and the mass of the Earth M_{\oplus} from each other, obtaining the latter in ordinary units of mass.



and 1992-070B), which orbit the Earth at a height of 6000 km, have been used. Ranges are nowadays obtained with better than centimetre precision.

The orbits of altimetric satellites are chosen to be much lower, as is seen from table 13.1 at the start of the chapter. The height is fine-tuned using on-board thrusters, so that the satellite passes over the same place, for example once a day, after 14 orbital periods. Alternatively one chooses an orbit that flies over the same place every third, seventeenth, 168th day. . . This is called the *repeat period*.

rakettimoottorit

The choice of the repeat period depends on the mission objective:

- If one wishes to study the precise shape of the *mean sea surface*, one chooses a *long* repeat period, in order to get the tracks as close together as possible on the Earth's surface.
- If one wishes to study the *variability* of the sea surface, one chooses an orbit that returns to the same location after a *short* time interval. Then, the grid of tracks on the Earth's surface will be sparser.

Parameters describing the figure of the Earth also affect satellite motion, for example the quantity J_2 , the *dynamic flattening*, having a value of $J_2 = 1082.63 \cdot 10^{-6}$. It is the largest of the many spherical-harmonic coefficients that together represent the figure of the Earth and that affect satellite orbits. In the case of J_2 , the effect is that the plane of the satellite orbit rotates at a certain angular rate around the Earth's rotation axis: *orbital precession*. This makes the satellite, if it flies over the same location the next day, do so several minutes earlier. For a circular orbit of radius a , the equation is

$$\frac{d\Omega}{dt} = -\frac{3}{2} \sqrt{\frac{GM_{\oplus}}{a^3}} \frac{a_{\oplus}^2}{a^2} J_2 \cos i,$$

in which a_{\oplus} is the equatorial radius of the Earth reference ellipsoid, M_{\oplus} the mass of the Earth, and i the *inclination* of the orbital plane relative to the equator.



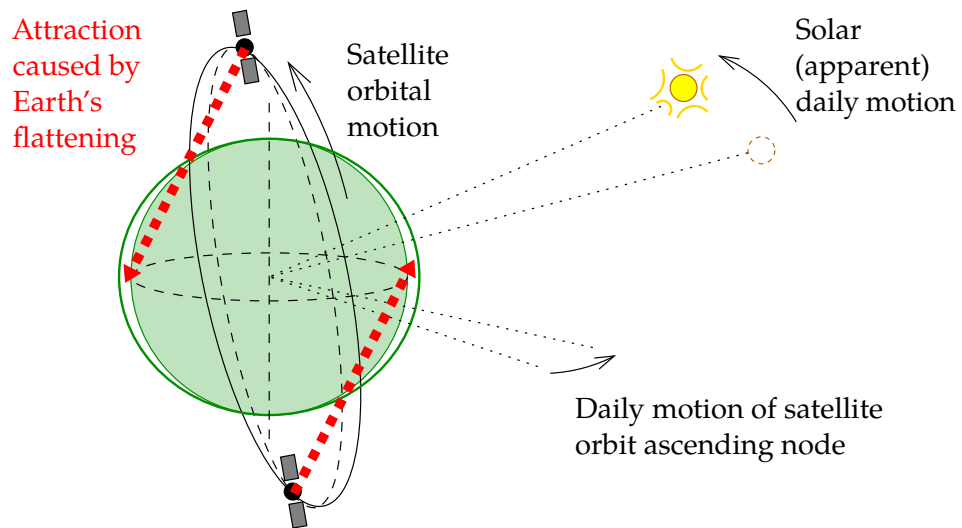


FIGURE 13.6. The mechanism of a Sun-stationary orbit.

Substituting numerical values into this yields

$$\frac{d\Omega}{dt} = -1.31895 \cdot 10^{18} \text{ m}^{3.5} \text{ s}^{-1} \cdot \frac{\cos i}{(a_{\oplus} + h)^{3.5}}$$

in which h is the *mean height* of the satellite orbit, conventionally above a sphere of size equatorial radius a_{\oplus} . If we substitute into this, say, the satellite height $h = 800$ km (and use $a_{\oplus} = 6\,378\,137$ m), we obtain

$$\frac{d\Omega}{dt} = -1.33103 \cdot 10^{-6} \text{ rad/s} \cdot \cos i = \left(-6^{\circ}.589 / \text{day} \right) \cdot \cos i.$$

For practical reasons — solar panels! — we often choose the satellite orbit such that the orbital plane turns along with the annual apparent motion of the Sun, $360^{\circ} / 365.25 \text{ days} = 0^{\circ}.9856 / \text{day}$. See figure 13.6.

If the inclination i is chosen in the range 96° – 102° , depending on the orbital height, then the Earth's dynamic flattening J_2 will cause just the suitable rotational motion of the orbital plane (“no-shadow / Sun-synchronous / Sun-stationary orbit”),⁹ see figure 13.7.

⁹If the height of the satellite orbit is less than 1400 km, it is not completely no-shadow. Either in midwinter or in midsummer, the satellite will fly through the Earth's shadow.



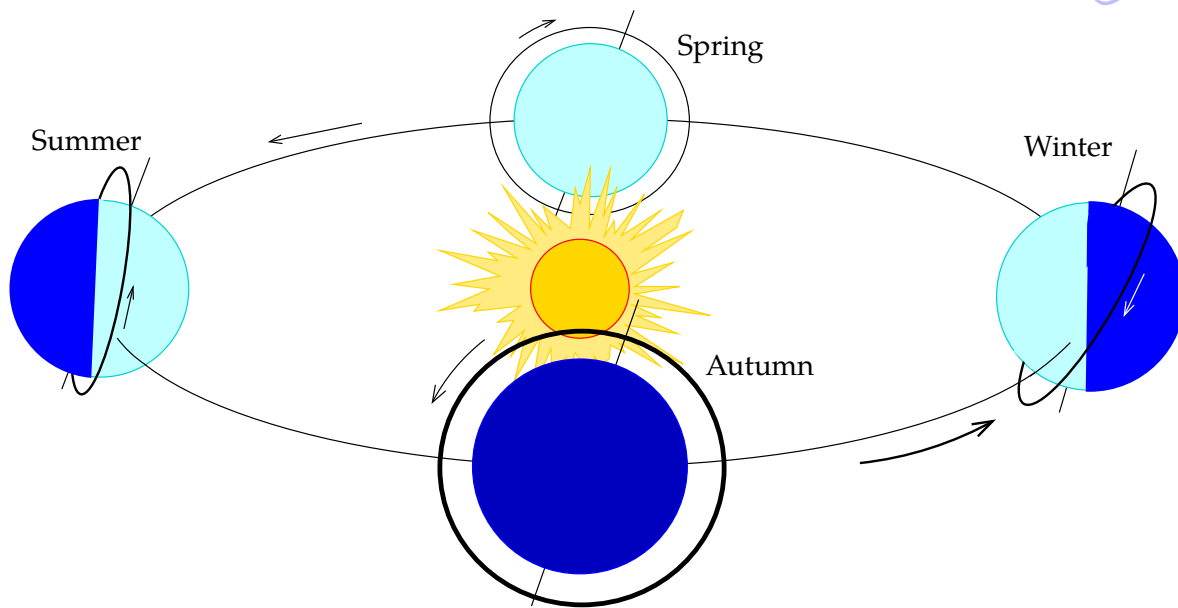


FIGURE 13.7. Geometry of a “no-shadow” orbit. Season names are boreal.

An orbit with an inclination $i > 90^\circ$ is called a *retrograde orbit*: the satellite is moving westwards in longitude, opposite to the direction of the Earth’s rotation, which is eastwards. The orbital inclination i , or for a retrograde orbit, its supplement $180^\circ - i$, is also the greatest northern or southern latitude a satellite can fly over. This means that, unless the inclination is precisely 90° , there will be areas around both poles that the satellite will never overfly: the “polar holes”.

A drawback of a Sun-stationary orbit is that the altimetric observations are always made at the same local time of day. For example, the diurnal and semidiurnal tides caused by the Sun will always have the same phase angle, and thus they cannot be observed with a satellite in this type of orbit (“resonance”). Therefore, the oceanographic satellite **TOPEX/Poseidon**, and the follow-up **Jason** satellites, were placed in non-Sun-stationary orbits.



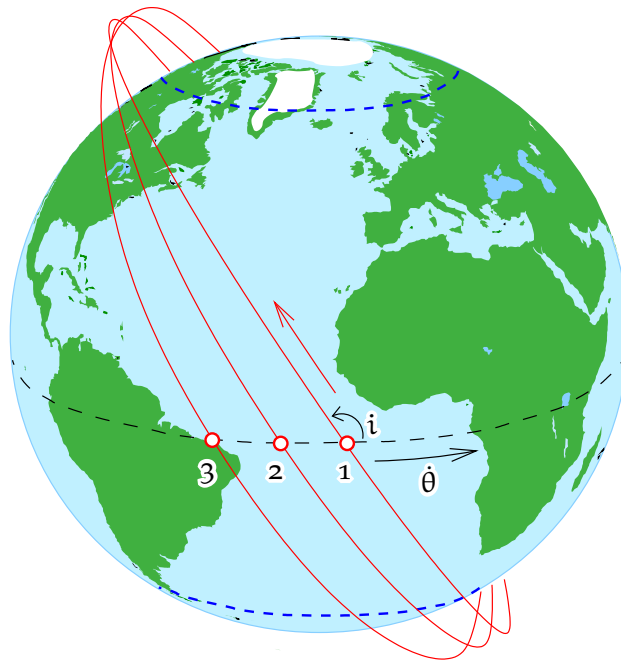


FIGURE 13.8. A satellite in a retrograde orbit around the rotating Earth, crossing the equator south to north three successive times. The angle between the orbit and the equator, the inclination i , or for a retrograde orbit, its supplement $180^\circ - i$, is also the highest northern or southern latitude that the satellite can fly over. The unreachable “polar holes” are indicated by blue dashed lines.



13.3.1 Example

A satellite moves in a Sun-stationary orbit, in other words, always, day after day, flies over the same latitude at the same local (mean) solar time.

Questions

1. What is the period of the satellite if it always flies again over the same spot after 14 revolutions?
2. The same question if the satellite always flies over the same spot after 43 revolutions (3 days)?



3. And after 502 revolutions (35 days)?
4. What is the height of the satellite in a “three-day orbit”? Use Kepler’s third law, equation 13.5. $GM_{\oplus} = 3\,986\,005 \cdot 10^8 \text{ m}^3/\text{s}^2$, and the height of the satellite is $h = a - a_{\oplus}$, with $a_{\oplus} = 6\,378\,137 \text{ m}$.
5. What is the satellite height in a “35-day orbit”? And the height *difference* from the previous question?
6. What is, for the three-day orbit, the mean separation between north-going orbital tracks (so, at what level of detail is the altimeter able to image the sea surface!)?
7. The same question for a 35-day orbit.
8. Questions for reflection:
 - (a) For what purpose would you use a 35-day orbit, for what purpose a three-day orbit?
 - (b) Would it be possible, or easy, to fly both orbits with the same satellite (see question 5)?

Answers

1. The satellite completes 14 orbits per day, i.e., per 1440 minutes: $P = 1440 \text{ min}/14 = 102.857 \text{ min}$.
2. The satellite completes 43 orbits in three days, i.e., per 3×1440 minutes: $P = 3 \times 1440 \text{ min}/43 = 100.465 \text{ min}$.
3. The satellite completes 502 orbits in 35 days, i.e., per 35×1440 minutes: $P = 35 \times 1440 \text{ min}/502 = 100.398 \text{ min}$.
4. Execute the octave code in tableau 13.2. The result is 780.604 km.
5. The same code, with $P=100.398 \cdot 60$, yields 777.421 km. The difference from the previous is 3.183 km.
6. There are 43 orbits with different ground tracks. That means a separation of $360^\circ/43 = 8.372$. At the equator this





TABLEAU 13.2. Calculating the height of a satellite from its period.

```
format long
GM=3986005e8;
ae=6378137;
P=100.465*60; % seconds
fac=4*pi*pi; % four pi square
a=(GM*P*P/fac)^0.33333333;
h = a - ae;
printf('\n\nOrbital height: %8.3f km.\n', h/1000);
```

is $40\,000\text{ km}/43 = 930\text{ km}$. The distance is shorter at higher latitudes.

7. $360^\circ/502 = 0.717^\circ$, or $40\,000\text{ km}/502 = 80\text{ km}$.
8. (a) The 35-day orbit would be excellent for detailed mapping. The three-day orbit would be able to see, for example, tides or weather-related phenomena, albeit at poor spatial resolution.
 - (b) The difference in height being only 3 km and in period 4 s, the change in orbit between the two repeat periods should be easily within reach of even small on-board thrusters. So, yes.



13.4 In-flight calibration

The highly precise, GNSS-positioned satellite radar altimeters in use today require proper *calibration*. The technique of choice for this is *in-flight calibration*, using an ocean area — or sometimes a lake area — the geocentric location of the water surface of which is known thanks to surrounding GNSS-positioned tide gauges combined with a precise geoid model of the area. An example of such measurements is [Vu et al.](#)



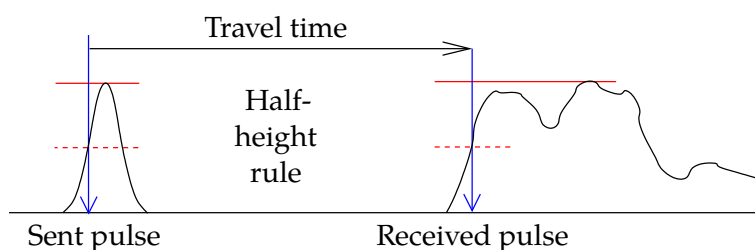


FIGURE 13.9. Analysing the altimeter return pulse. The classical return pulse time measurement uses the “half-height point”.

(2018).

One reason for in-flight calibration is the circumstance that radar altimeters not only have an unknown zero offset — due to the not precisely known signal paths through the electronic circuitry — but this offset may slowly change or drift over time, and may be temperature-dependent.

13.5 Retracking

The results of a satellite altimetry mission are published already during flight in the form of a *geophysical data record* (**GDR**) file, containing everything related to the measurement, such as atmospheric correction terms, tidal corrections, and sea-state parameters.

It is common practice today to re-process older altimetry measurements, applying improved methodologies in order to extract additional useful information. The complete return pulse is analysed again in a method called *retracking* (**Altimetry, Retracking**).

The method of analysis uses the point on the leading edge of the return pulse which is at half-height from the maximum value of the pulse. This is according to experience a good way to get the travel time associated with the point at the centre of the *footprint*, directly underneath the satellite. In the back part of the pulse are reflections from the further-away peripheral areas of the footprint.

There are three situations where the automatic analysis technique



applied during flight does not work properly, and a more careful *a posteriori* analysis of the pulse is worthwhile:

- Archipelagos like Indonesia or Åland. Here it may happen, for example, that the centre point of the footprint is on land. Then, the first strong bounces will come under an angle from the nearest coast. A precise coastline mask is then essential for processing. But already over open water close to coastlines the return pulse will be distorted.
- Sea ice areas in the Arctic and Antarctic Oceans. Bounces may come from the surface of the sea ice, in which case one should consider *freeboard* in the processing, i.e., how much the ice sticks out of the water.
- Over continental ice sheets. Here, the shape of the return pulse will be very different from that over open water. Furthermore, the travel time of the return pulse varies rapidly as the satellite flies on, and the reception window cannot keep track.¹⁰

In these cases the traditional real-time processing on-board produces erroneous measurements, or no measurements at all. With retracking, such measurements have been saved, and the area covered by altimetric measurements has been extended, especially into the Arctic and Antarctic areas.

Freeboard is an important quantity in determining the thickness of the ice. As the density of ice is about 920 kg/m^3 and the density of sea water about 1030 kg/m^3 , the ice thickness is about $8 \times$ freeboard.¹¹ If there is additional remote-sensing data on the area of ice cover, one can calculate the total volume and mass of sea ice.

The Arctic ice cover has diminished radically over recent decades.

¹⁰The newest satellites such as Sentinel-3 use a digital terrain model when not over the open ocean.

¹¹Assuming that there is no snow on the ice. Also, ice density varies, and differs between one-year and multi-year ice.



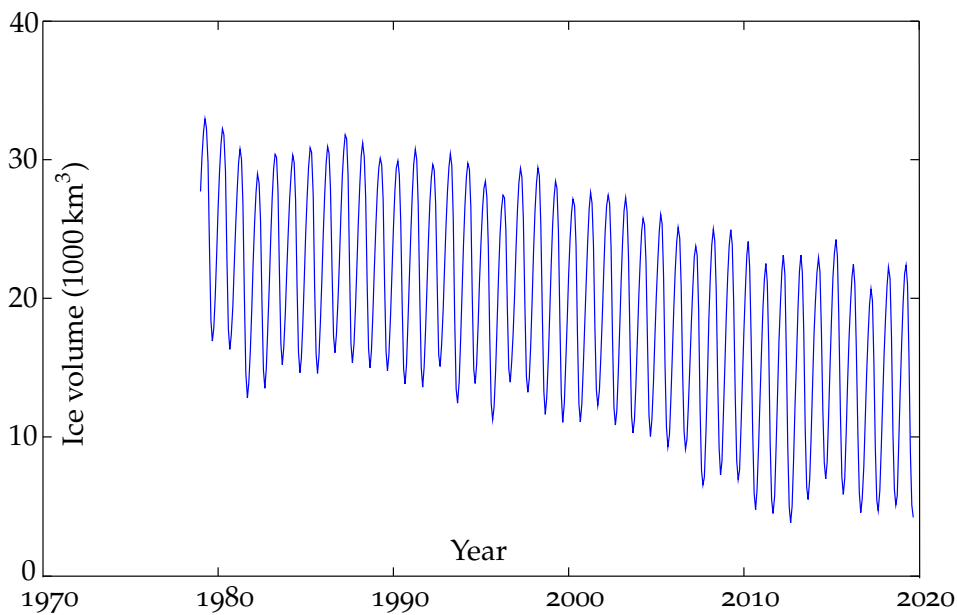


FIGURE 13.10. Ice volume on the Arctic Ocean. PIOMAS; Schweiger et al. (2011).

The most radical reduction has been that of ice volume, see figure 13.10. In addition to surface area, thickness is also decreasing: of the multi-year, thicker ice, a large part has already vanished.

13.6 Oceanographic research using satellite altimetry

The first geodetic application of satellite altimetry was geoid determination. Altimetric geoid determination works only if we assume that the sea surface

- is constant in time
- coincides with a level surface, i.e., is the same as the geoid.

In practice, however, the ocean surface is variable in time and is also not a level surface. Therefore, other approaches have been developed.

- Sea-surface variability can be studied by satellite altimetry using



three methods:

- Repeat tracks from the same satellite. The tracks can be stacked and adjusted together using a simple orbit-error correction model, and the remaining per-track residuals tell something (but not everything!) about the variability of the sea surface.
 - The crossovers may also provide information on sea-surface variability. When the sea surface varies, the results from the crossover adjustment will get poorer: the root-mean-square *a posteriori* (after calculation) crossover difference will grow. Using this method to actually *study* sea-surface variability is more difficult: it is mostly just able to establish that it exists, and estimate its magnitude.
 - Nowadays altimetric satellites always carry a **GNSS** positioning instrument, providing the absolute geocentric location of the microwave radar device at the moment of measurement. With it, the variations of sea level can be monitored by direct measurement, assuming that both temporal and spatial measurement densities are sufficient.
- The deviations of sea level from a level surface — the geoid — can be studied only if we have access to independent information on the true geoid surface. If dense, high-quality gravity measurements are available for an area, these may be used to estimate the geoid, and after that one may calculate the *sea-surface topography*. Collecting sufficiently precise and dense gravimetric data is possible with a sea gravimeter or *airborne gravimetry*. Measurement with a special satellite (gravitational gradiometry, **GOCE** satellite) has also long been planned and has finally been realised, see section 13.7.



13.7 Satellite gravity missions

During the early years of the 21st century, three satellite missions were launched to investigate the fine structure of the Earth's gravity field or geopotential; in other words, to determine a global high-resolution model of the geoid.

CHAMP (Challenging Minisatellite Payload for Geophysical Research and Applications, 2000-039B) was a German satellite project under the auspices of the German Research Centre for Geosciences **GFZ**. The satellite was launched into orbit from Plesetsk, Russia, in 2000. The orbit height was initially 454 km, coming down over the time of the mission to ~ 300 km due to atmospheric drag. The orbital inclination was 87°. On 19 September 2010, the satellite returned into the atmosphere. Project description: [CHAMP Mission](#).

CHAMP contained a **GPS** receiver in order to determine the satellite location in space $\mathbf{x}(t)$ for any moment in time t . From successive satellite locations one may calculate the geometric acceleration $\mathbf{a}(t)$ by differentiation:

$$\mathbf{a}(t) = \frac{d^2}{dt^2} \mathbf{x}(t).$$

The differentiation is done numerically as presented in the part on airborne gravimetry, equation 11.7.

The satellite also contained an accelerometer, which eliminated the satellite's accelerations caused by the atmosphere's aerodynamic forces, the deviations from free-fall motion. Then, only the accelerations caused by the Earth's gravitational field remain, from which a precise global geopotential or *geoid* model may be calculated using the techniques described earlier.

A number of global geopotential models based on **CHAMP** data have been calculated and published.

GRACE (Gravity Recovery And Climate Experiment Mission, 2002-012



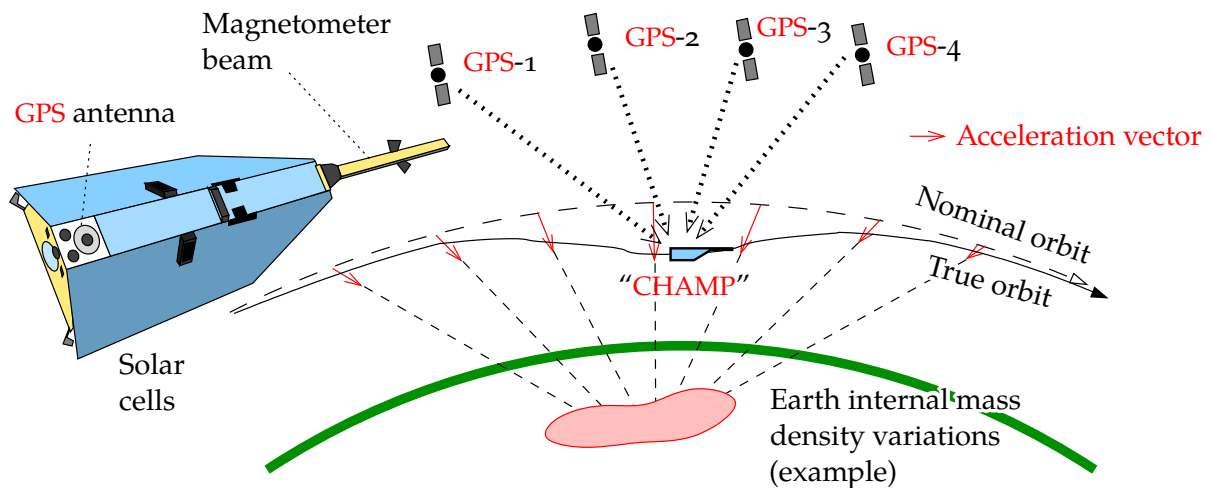


FIGURE 13.11. Determining the Earth's gravity field from GPS orbital tracking of a low flying satellite.

A and B) measured *temporal changes* in the Earth's gravity field extremely precisely, but at a rather crude geographic resolution. These temporal changes are caused by motions in the Earth's "blue film": her atmosphere and hydrosphere. The quantity measured is also called the "sea-floor pressure", a somewhat surprising expression, until one sees that it really represents the total mass of a column of air and water.

The effective time resolution was one complete mapping of the globe every month. Project description: [GRACE Mission](#). The project was a collaborative American-German undertaking under the leadership of the Center for Space Research, University of Texas at Austin.

GRACE was a *satellite pair* ("Tom and Jerry"): the satellites flew in the same orbit in a tandem configuration at initially about 500 km height, at an inter-satellite separation of 220 km. The orbital inclination was 89° , so the orbit was almost polar, providing complete global coverage. The changes in distance between the satellites were measured by a microwave link at a precision of



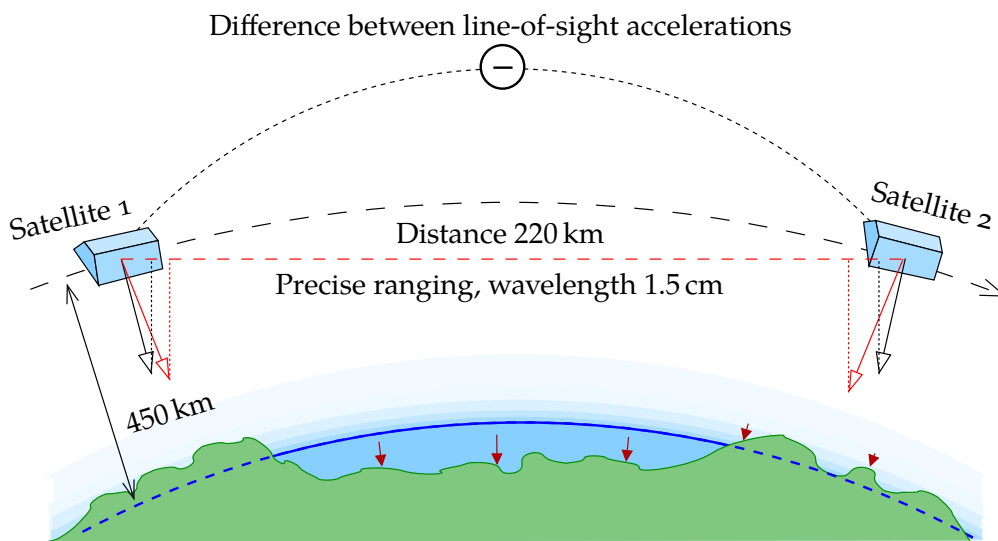


FIGURE 13.12. The principle of the **GRACE** satellites: measuring the minute variations in time of the gravity field using **SST** (satellite-to-satellite tracking). The changes are due to mass shifts in the “blue film” — the atmosphere and hydrosphere — and expressed as variations in “total sea-floor pressure” (\downarrow).

$\pm 1 \mu\text{m/s}$. Both satellites also carried sensitive accelerometers for measuring and eliminating the effect of atmospheric drag.

The measurement system was so sensitive that even the movement of a water layer of one millimetre thickness could be noticed, as long as the layer extended over an area the size of a continent (some 1000 km).

The published results show impressively, for example, the wet and dry monsoons, seasonal variations in opposite phases in the northern and southern hemispheres, in the great tropical river basins: Amazonas, Congo, the Mekong, India, Indonesia. . .

GRACE Mission, hydrology.

The mission ended in 2017 after 15 years, three times the planned mission duration. A **GRACE** follow-on mission was launched in 2018, **GRACE Follow-On Mission**.



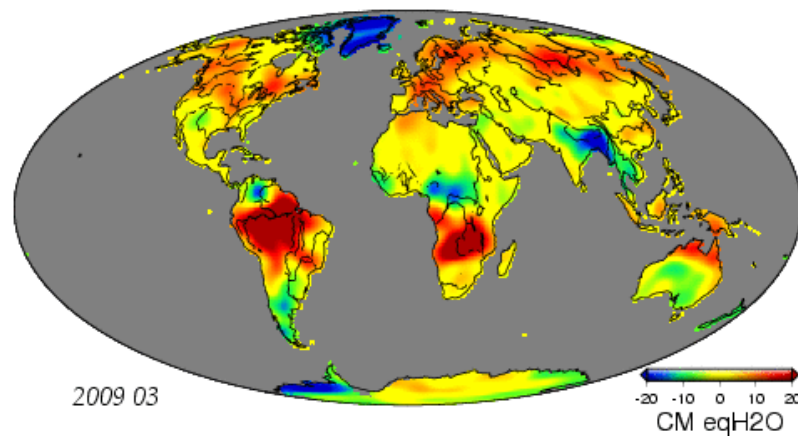


FIGURE 13.13. **GRACE** mission results: surface mass layer in centimetres of water equivalent. Click for animation (e-book).

GOCE (2009-013A, Geopotential and Steady-state Ocean Circulation Explorer) was the most ambitious of all the satellites. Built by the European Space Agency **ESA**, the satellite was launched successfully from Plesetsk in March 2009. The orbital height was only 270–235 km during the mission and the satellite contained an ionic rocket engine with a stock of propellant in order to maintain the orbit against atmospheric drag. The orbital inclination was $96^{\circ}.7$, so the orbit was Sun-stationary.¹²

GOCE carried a very sensitive *gravitational gradiometer*, a device that measured precisely components of the *gradient* of the Earth's attraction, the dependence of components of the attraction vector on the co-ordinates of place. The gradiometer consisted of six extremely sensitive, three-axes accelerometers mounted pairwise on a frame. The mission ended in 2013 and the satellite was seen to burn up in the atmosphere on 11 November over the Falkland

¹²Because of this inclination angle, there was a cap of radius $6^{\circ}.7$ at each pole within which no measurements were obtained. Over recent years these “poles of ignorance” have been gradually filled in by airborne gravimetry campaigns, for example [Forsberg et al. \(2017\)](#).



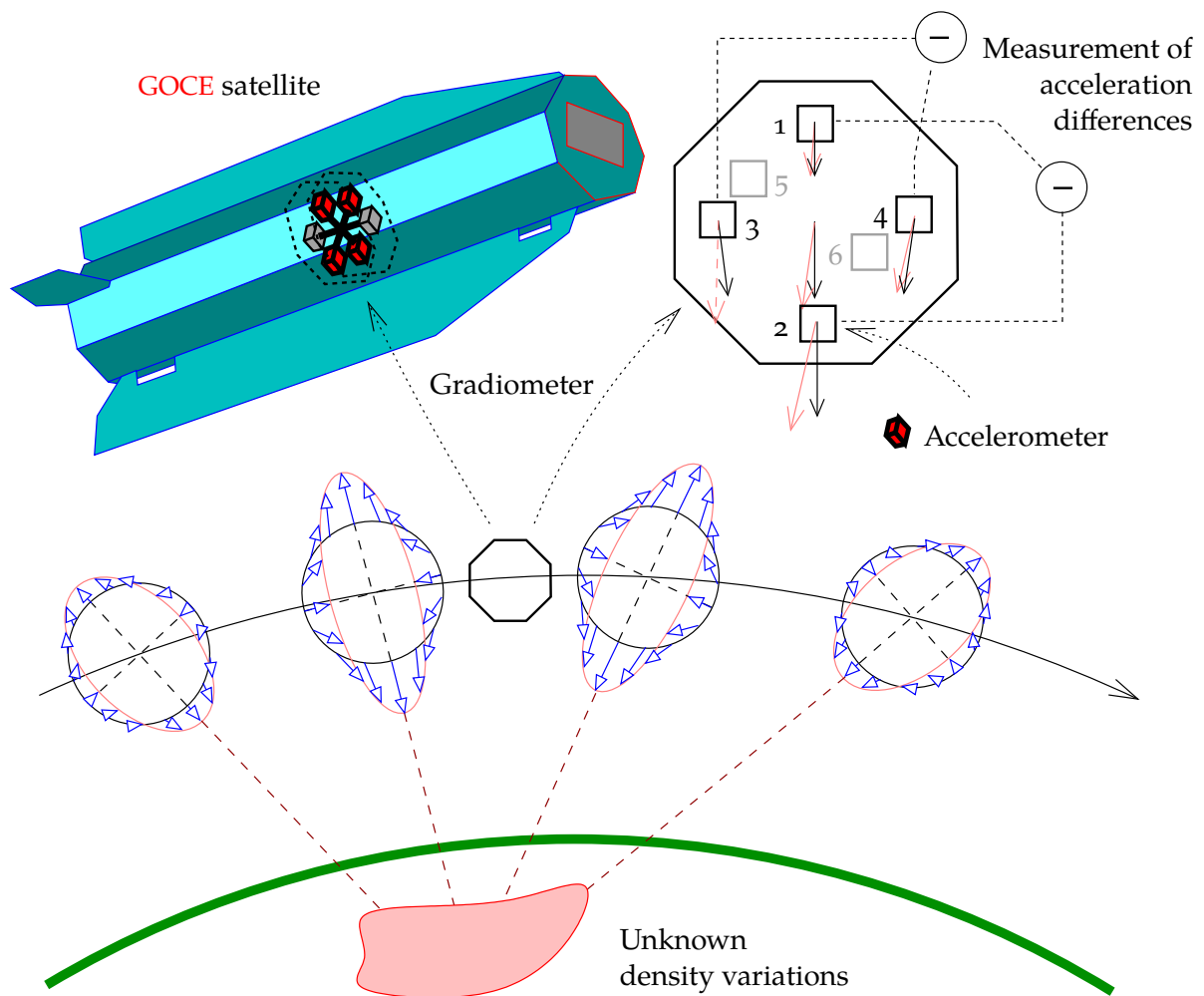


FIGURE 13.14. Determining the Earth's gravity field with the gravitational gradiometer on the GOCE satellite.

Islands (Scuka, 2013).

Theoretical analysis has shown that a gravitational gradiometer is the best way to measure the very local features of the Earth's gravity field, better than orbital tracking by GNSS. The smallest details in the geoid map seen by GOCE are only 100 km in diameter, and their precision is as good as ± 2 cm.

With a global geoid model this precise, we may calculate the



deviations of the sea surface from the geoid, an equipotential or level surface, at the same precision. We saw that the true location in space of the sea surface is obtained from satellite radar altimetry, also at a few centimetres' precision. This separation between sea surface and equipotential surface can again be *inverted* to *ocean currents*, see section 12.5 and figure 12.4. This is the background for the name of the **GOCE** satellite.



Self-test questions

1. What is the *footprint* of a radar altimeter? How does it depend on wave height?
2. What is the *freeboard* of ocean ice? How can it be used to determine the volume of the ice?
3. What three alternative models for the satellite orbit-error correction exist?
4. In satellite altimetry, what is a *datum defect*, and how can it be fixed?
5. How can Kepler's third law be used to determine the mean height of a satellite orbit if the satellite's period is given?
6. What is the repeat period of a satellite orbit?
7. What is J_2 , and how does it affect the motion of a satellite?
8. What is a Sun-synchronous orbit, and why is it useful?
9. What is a retrograde orbit?
10. Why are the orbits of the **TOPEX/Poseidon** and **Jason** satellites not Sun-synchronous?
11. In table 13.1 some satellites have a repeat period that is an integer number of days, some satellites do not. What do the satellites with integer repeat periods have in common?



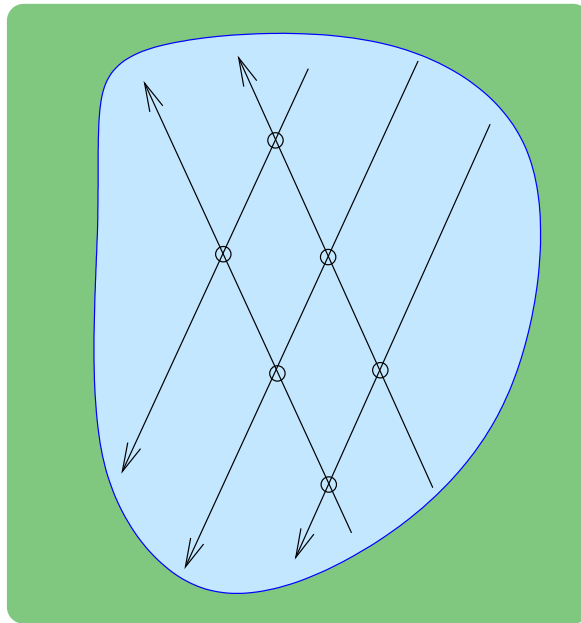


FIGURE 13.15. Example of a satellite altimetric track geometry.

12. With which three satellite altimetric methods can one study sea-surface variability?
13. Three satellite missions have been launched so far to study the fine structure of the Earth's gravity field and its temporal variability. Present them and the methods used by them.

Exercise 13 – 1: Altimetry, crossover adjustment

it is given that there are two north-going satellite tracks and three south-going ones. There are six crossover sites, see figure 13.15.

1. If the orbit-error corrections for every track are described as a linear function of place:

$$\Delta h = a + b\tau,$$

how many coefficients a and b are needed?



2. Write out the *observation equations*. The observations are the crossover differences, the unknowns are the coefficients a and b for the different tracks.
3. Can these observation equations give a unique solution? Why / why not?



Exercise 13 – 2: Satellite orbit

A satellite moves in a Sun-synchronous orbit, where after 419 orbits and 30 days, it again moves over exactly the same spot.

1. What is the period of the satellite?
2. How long is the distance (west to east), in kilometres, between the north-going tracks at the equator?
3. What is the highest northern latitude that the satellite can fly over?
4. *In what compass direction* is the satellite flying at that point?



Exercise 13 – 3: Kepler's third law

What is the satellite height h if the period is 98 minutes? Use Kepler's third law 13.5,

$$GM_{\oplus}P^2 = 4\pi^2a^3,$$

$GM_{\oplus} = 3\,986\,005 \cdot 10^8 \text{ m}^3/\text{s}^2$, and the height of the satellite is $h = a - a_{\oplus}$, in which $a_{\oplus} = 6\,378\,137 \text{ m}$.





Tides, the atmosphere, and Earth crustal movements

14



14.1 The theoretical tide

The tidal potential V can be written as follows:

$$V = \frac{GMR^2}{d^3} P_2(\cos \zeta) + \dots = \frac{GMR^2}{2d^3} (3 \cos^2 \zeta - 1) + \dots,$$

in which d is the distance to either the Moon or the Sun, R is the radius of the Earth, and ζ is the local *geocentric* zenith angle of the Sun or Moon, i.e., the local zenith angle ζ' corrected for parallax, see figure 14.1. $P_2(\cos \zeta)$ is the Legendre polynomial of degree two. GM is the mass of the Sun or Moon multiplied by Newton's gravitational constant. In the case of the Sun and Moon, the extra terms (...) can be neglected, because these are such remote bodies: $d \gg R$.

The cosine rule on the sphere tells us that

$$\cos \zeta = \sin \phi \sin \delta + \cos \phi \cos \delta \cos h,$$

in which ϕ is the latitude, δ is the declination¹ of the Moon, and h is the hour angle² of the Moon.

¹The declination of a celestial body is its latitude on the celestial sphere, its angular distance from the celestial equator ([Wikipedia, Declination](#)), in this case as seen from the geocentre.

²The hour angle is the angle, or difference in longitude, between the meridian of the

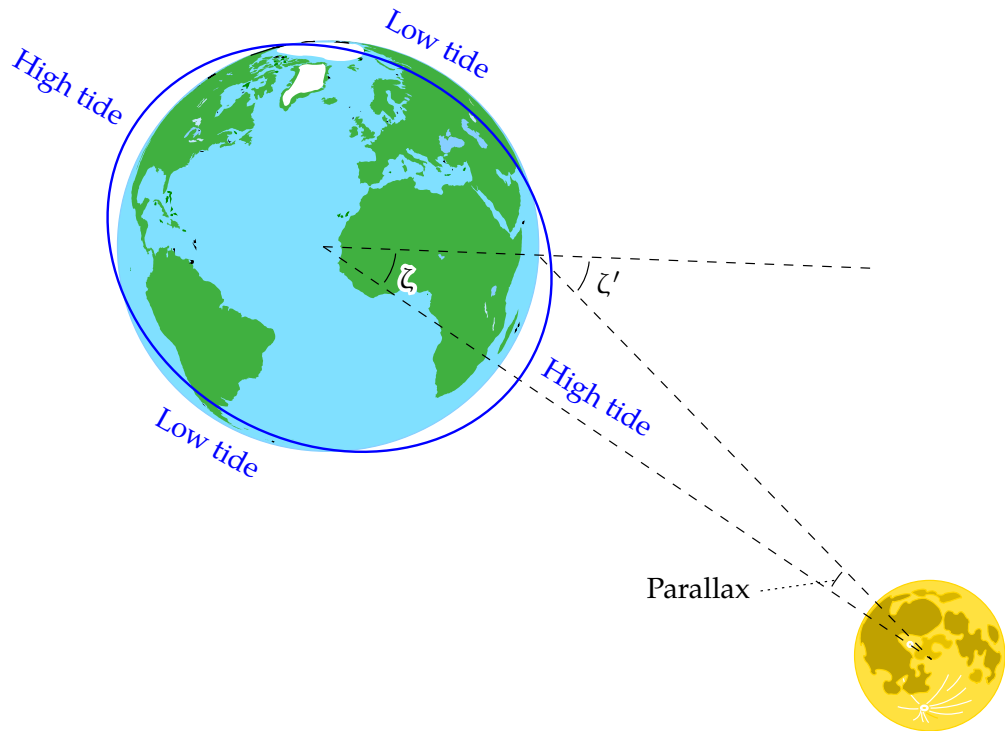


FIGURE 14.1. Theoretical tide. ζ' is the local zenith angle of the Moon (or Sun), ζ the corresponding geocentric angle.

According to the *spherical-harmonic addition theorem* ([Wolfram MathWorld, Spherical Harmonic Addition Theorem](#)) we have now

$$P_n(\cos \zeta) = P_n(\sin \phi)P_n(\sin \delta) + 2 \sum_{m=1}^n \frac{(n-m)!}{(n+m)!} P_{nm}(\sin \phi)P_{nm}(\sin \delta) \cos m\zeta,$$

or for $n = 2$,

$$P_2(\cos \zeta) = P_2(\sin \phi)P_2(\sin \delta) + \frac{1}{3}P_{21}(\sin \phi)P_{21}(\sin \delta) \cos \zeta + \frac{1}{12}P_{22}(\sin \phi)P_{22}(\sin \delta) \cos 2\zeta.$$

Moon and the local meridian measured along the celestial equator [Wikipedia, Hour angle](#), in this case as seen from the geocentre. It vanishes when the Moon is in *upper culmination*, in the local meridian due south when seen from northern non-tropical latitudes.



In this, according to table 3.2,

$$\begin{aligned} P_{21}(\sin \phi) &= 3 \sin \phi \cos \phi, & P_{21}(\sin \delta) &= 3 \sin \delta \cos \delta, \\ P_{22}(\sin \phi) &= 3 \cos^2 \phi, & P_{22}(\sin \delta) &= 3 \cos^2 \delta, \end{aligned}$$

and we obtain

$$\begin{aligned} P_2(\cos \zeta) &= P_2(\sin \phi)P_2(\sin \delta) + \\ &+ 3 \sin \phi \cos \phi \sin \delta \cos \delta \cos h + \frac{3}{4} \cos^2 \phi \cos^2 \delta \cos 2h = \\ &= \frac{1}{2} (3 \sin^2 \phi - 1) \frac{1}{2} (3 \sin^2 \delta - 1) + \frac{3}{4} \sin 2\phi \sin 2\delta \cos h + \\ &\quad + \frac{3}{4} \cos^2 \phi \cos^2 \delta \cos 2h. \end{aligned}$$

From this

$$V = \frac{GMR^2}{4d^3} \left(\begin{aligned} &(3 \sin^2 \phi - 1) (3 \sin^2 \delta - 1) + \\ &+ 3 \sin 2\phi \sin 2\delta \cos h + \\ &+ 3 \cos^2 \phi \cos^2 \delta \cos 2h \end{aligned} \right).$$

This is the *Laplace tidal decomposition equation*.

It has three parts:

- A slowly varying part,

$$V_1 = \frac{GMR^2}{4d^3} (3 \sin^2 \phi - 1) (3 \sin^2 \delta - 1),$$

that still depends on the lunar declination δ and is therefore periodic with a 14-day (half-month) period. Using spherical trigonometry:

$$\begin{aligned} \sin \delta &= \sin \epsilon \sin \ell \\ \implies \sin^2 \delta &= \sin^2 \epsilon \sin^2 \ell = \sin^2 \epsilon \left(\frac{1}{2} - \frac{1}{2} \cos 2\ell \right), \quad (14.1) \end{aligned}$$

in which ℓ is the longitude of the Moon in its orbit, reckoned from the ascending node (equator crossing), and ϵ is the inclination of



the Moon's orbital plane with respect to the equator, on average $23^\circ.5$ but rather variable, between $18^\circ.3$ and $28^\circ.6$. Thus we obtain

$$V_1 = \frac{GMR^2}{4d^3} (3 \sin^2 \phi - 1) \left(3 \sin^2 \epsilon \left(\frac{1}{2} - \frac{1}{2} \cos 2\ell \right) - 1 \right),$$

where we have used result 14.1. We split $V_1 = V_{1a} + V_{1b}$ into two parts, a constant³ and a periodic or semi-monthly ("fortnightly") part:

$$V_{1a} = \frac{GMR^2}{4d^3} (3 \sin^2 \phi - 1) \left(\frac{3}{2} \sin^2 \epsilon - 1 \right), \quad (14.2)$$

$$V_{1b} = -\frac{GMR^2}{4d^3} (3 \sin^2 \phi - 1) \left(\frac{3}{2} \sin^2 \epsilon \cos 2\ell \right).$$

- In addition, we have a couple of terms in which the hour angle h appears, periods roughly a day and roughly half a day:

$$V_2 = \frac{GMR^2}{4d^3} \cdot 3 \sin 2\phi \sin 2\delta \cos h,$$

$$V_3 = \frac{GMR^2}{4d^3} \cdot 3 \cos^2 \phi \cos^2 \delta \cos 2h.$$

In both, we have in addition to h , still δ as a "slow" variable. These equations could be written out as the sums of various functions of the longitude of the Moon ℓ .

Use basic trigonometry again, with equation 14.1:


$$\begin{aligned} \cos^2 \delta &= 1 - \sin^2 \delta = 1 - \sin^2 \epsilon \sin^2 \ell = \\ &= 1 - \sin^2 \epsilon \left(\frac{1}{2} - \frac{1}{2} \cos 2\ell \right), \end{aligned}$$

$$\cos 2\ell \cos 2h = \frac{1}{2} (\cos(2\ell + 2h) + \cos(2\ell - 2h)),$$

$$\begin{aligned} \sin 2\delta &= 2 \sin \delta \cos \delta = 2 \sqrt{\sin^2 \delta (1 - \sin^2 \delta)} = \\ &= 2 \sin \epsilon \sqrt{\left(\frac{1}{2} - \frac{1}{2} \cos 2\ell \right) \left(1 - \sin^2 \epsilon \left(\frac{1}{2} - \frac{1}{2} \cos 2\ell \right) \right)}, \end{aligned}$$

³Not precisely, because ϵ is (slowly) time-dependent.



 TABLE 14.1. The various periods in the theoretical tide. The widely used symbols were standardised by George Darwin.

| | Changing function | Period | | Darwin symbol | | Name |
|----------|-------------------|---------------------------------|------------------|---------------|------------|------------------|
| | | Moon | Sun | Moon | Sun | |
| V_{1a} | - | - | - | M_0 | S_0 | Permanent tide |
| V_{1b} | $\cos 2\ell$ | 14 ^d | 182 ^d | Mf^a | Ssa^b | Declination tide |
| V_2 | $\cos h$ | 24 ^h 50 ^m | 24 ^h | K_1, O_1 | S_1, P_1 | Diurnal |
| V_3 | $\cos 2h$ | 12 ^h 25 ^m | 12 ^h | M_2 | S_2 | Semidiurnal |

^aLunar fortnightly

^bSolar semi-annual

leading to a trigonometric expansion in lunar longitude ℓ , and so on. See for example Melchior’s⁴ famous book (1978).

The coefficient

$$D \stackrel{\text{def}}{=} \frac{3GM R^2}{4d^3}, \tag{14.3}$$

“Doodson’s⁵ constant” is often taken separately from the above equations. The value for the Moon equals $D = 26.8 \text{ cm} \times \gamma$ and for the Sun $12.3 \text{ cm} \times \gamma$, with $\gamma \approx 9.81 \text{ m/s}^2$. See figure 14.2.

The *periods* are listed in table 14.1 with their Darwin⁶ symbols.

In practice, the diurnal and semidiurnal tides can be divided further into many “spectral lines” close to each other, also because the lunar

⁴Paul Jacques Léon Camille baron Melchior (1925–2004) was an eminent Belgian geophysicist and Earth tides researcher and founder of the Walferdange underground laboratory for geodynamics in Luxembourg.

⁵Arthur Thomas Doodson FRS (1890–1968) was a British oceanographer, a pioneer of tidal theory, also involved in designing machines for computing the tides. He was completely deaf.

⁶Sir George Howard Darwin KCB FRS FRSE (1845–1912) was an English astronomer and mathematician, son of Charles Darwin of *Origin of Species* fame.



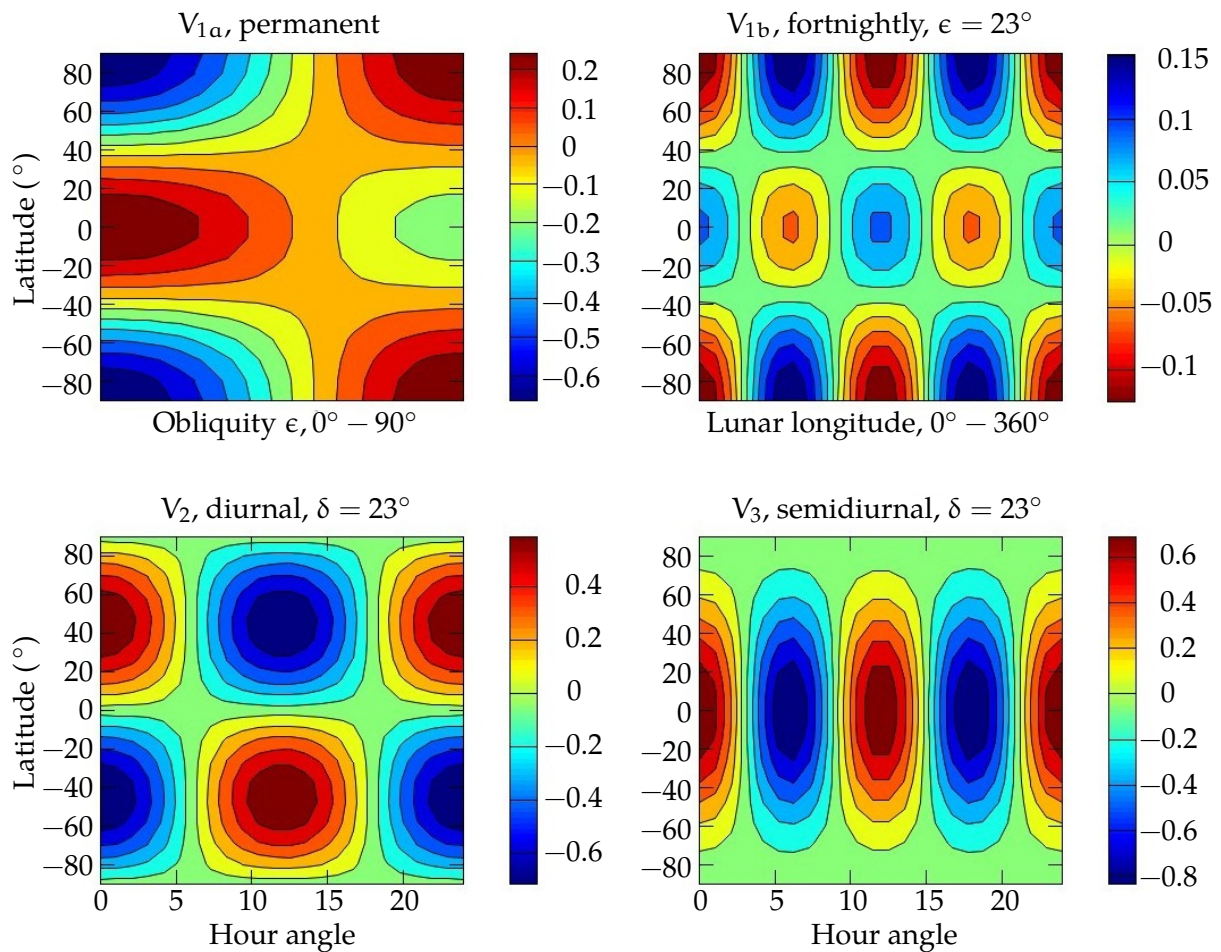


FIGURE 14.2. The main components of the theoretical tide. These values must still be multiplied by Doodson's constant D .

orbit (like the Earth's orbit) is an ellipse, not a circle.

14.2 Deformation caused by the tidal force

The tidal force, or theoretical tide, of which we spoke above, is not the same as the deformation it causes in the solid Earth. This deformation will depend upon the elastic properties inside the Earth. These elastic



properties are often characterised by *elastic Love⁷ numbers* (Love, 1909; Melchior, 1978).

Let us first write the external or tidal potential $V = V(\phi, \lambda, r)$ in the following way:

$$V(\phi, \lambda, r) = \sum_{n=2}^{\infty} \left(\frac{r}{R}\right)^n V_n(\phi, \lambda) = \sum_{n=2}^{\infty} \tilde{V}_n(\phi, \lambda, r),$$

in which the index n denotes the spherical-harmonic degree number. V_n is the degree constituent, $\tilde{V}_n = \left(\frac{r}{R}\right)^n V_n$ the solid spherical harmonic of potential V for degree number n .

Call the linear displacement of an element of matter of the solid Earth in the radial direction, u_r , in the north direction, u_ϕ , and in the east direction, u_λ . The following equations apply:

$$u_r(\phi, \lambda, r) = \frac{1}{\gamma} \sum_{n=2}^{\infty} H_n(r) \tilde{V}_n(\phi, \lambda, r) = \sum_{n=2}^{\infty} H_n(r) \zeta_n(\phi, \lambda, r),$$

$$u_\phi(\phi, \lambda, r) = \frac{1}{\gamma} \sum_{n=2}^{\infty} L_n(r) \frac{\partial}{\partial \phi} \tilde{V}_n(\phi, \lambda, r) = r \sum_{n=2}^{\infty} L_n(r) \xi_n(\phi, \lambda, r),$$

$$u_\lambda(\phi, \lambda, r) = \frac{1}{\gamma} \sum_{n=2}^{\infty} L_n(r) \frac{\partial}{\cos \phi \partial \lambda} \tilde{V}_n(\phi, \lambda, r) = r \sum_{n=2}^{\infty} L_n(r) \eta_n(\phi, \lambda, r).$$

All displacements are in length units. r is the distance from the geocentre. It is assumed here that the Love numbers H_n and L_n depend only on r , so that the elastic properties of the Earth are spherically symmetric. The symbols ζ_n , ξ_n and η_n represent the effect of the tidal potential of harmonic order n on the level of an equipotential surface and on the components of the direction of the plumb line.

The deformation of the Earth also causes a change, the “indirect effect” in addition to the Moon’s original tidal potential V , in the geopotential.

⁷Augustus Edward Hough Love **FRS** (1863–1940) was a British mathematician and student of Earth elasticity.



We write

$$\delta V(\phi, \lambda, r) = \sum_{n=2}^{\infty} K_n(r) \tilde{V}_n(\phi, \lambda, r),$$

in which we already use a third type of Love numbers.

On the Earth's surface $r = R$ we make the following specialisation:

$$h_n \stackrel{\text{def}}{=} H_n(R), \quad \ell_n \stackrel{\text{def}}{=} L_n(R), \quad k_n \stackrel{\text{def}}{=} K_n(R). \quad (14.4)$$

In practice, because of the large distances to Sun and Moon, the only important part of the tidal potential V is the part for the degree number $n = 2$, the “rugby-ball part” \tilde{V}_2 .

The Love numbers will still depend on the *frequency*, i.e., on the tidal *period* P :

$$h_n = h_n(P), \quad \ell_n = \ell_n(P), \quad k_n = k_n(P).$$

The tides offer an excellent means of determining all these Love numbers $h_2(P)$, $\ell_2(P)$, and $k_2(P)$ empirically, because, being periodic variations, they cause Earth deformations at the same periods, but with different amplitudes and phase angles. In this way we may determine at least those Love numbers that correspond to periods occurring in the theoretical tide.

The h and ℓ numbers are nowadays obtained for example by **GNSS** positioning. The **GNSS** processing software contains a built-in reduction for this phenomenon. From gravity measurements one obtains information on a certain linear combination of h and k , $\delta = 1 + h - \frac{3}{2}k$: lunar attraction changes gravity directly, vertical displacement changes gravity through its gradient, and deformation of the Earth, the shifting of masses, also changes gravity directly.

The long water-tube clinometer is also a useful research instrument, like the tube of the Finnish Geodetic Institute that has long been in use in the Tytyri limestone mine (**Tytyri Mine Experience**) in Lohja (**Kääriäinen and Ruotsalainen, 1989**). A modern, improved version of



this instrument is presented in [Ruotsalainen \(2017\)](#). The same applies for sensitive clinometers in general, like the Verbaandert–Melchior pendulum. A clinometer measures the changes in orientation between the Earth’s crust and the local plumb line. This can again provide information on a different linear combination of h and k , $\gamma = 1 - h + k$.

Measuring the *absolute* direction of the plumb line, for example with a zenith tube, can again provide information on the linear combination $\Lambda = 1 - \ell + k$, but only after various reductions (Earth orientation parameters like polar motion and variations in rotation rate), [Vondrák et al. \(2010\)](#). The Love number ℓ^8 comes in through the horizontal displacement of the zenith tube, to a location where the plumb-line direction is different.

14.3 The permanent part of the tide

As shown above, the theoretical tide equation contains a constant part that does not even vary in a long-period way. Of course the Earth also responds to this part of the tidal force. However, because the deformation is not periodic, it is not possible to measure it. And the mechanical theory of the solid Earth, and our knowledge of the state of matter inside the Earth, are just not good enough for a theoretical calculation of the response.

For this reason the understanding is generally accepted that the effect of the permanent part of the tide on the Earth’s state of deformation should not be included in any tidal reduction ([Ekman, 1992](#)). Many times, however, for example in the processing of [GNSS](#) observations or in defining spherical-harmonic expansions of the Earth’s gravity field, the tidal reduction does include this term which it is theoretically and practically impossible to know. See [Poutanen et al. \(1996\)](#).

More generally, the reduction of a geodetic quantity, for example the

⁸Also called the Shida number. Toshi Shida (1876–1936) was an eminent Japanese Earth tide researcher.

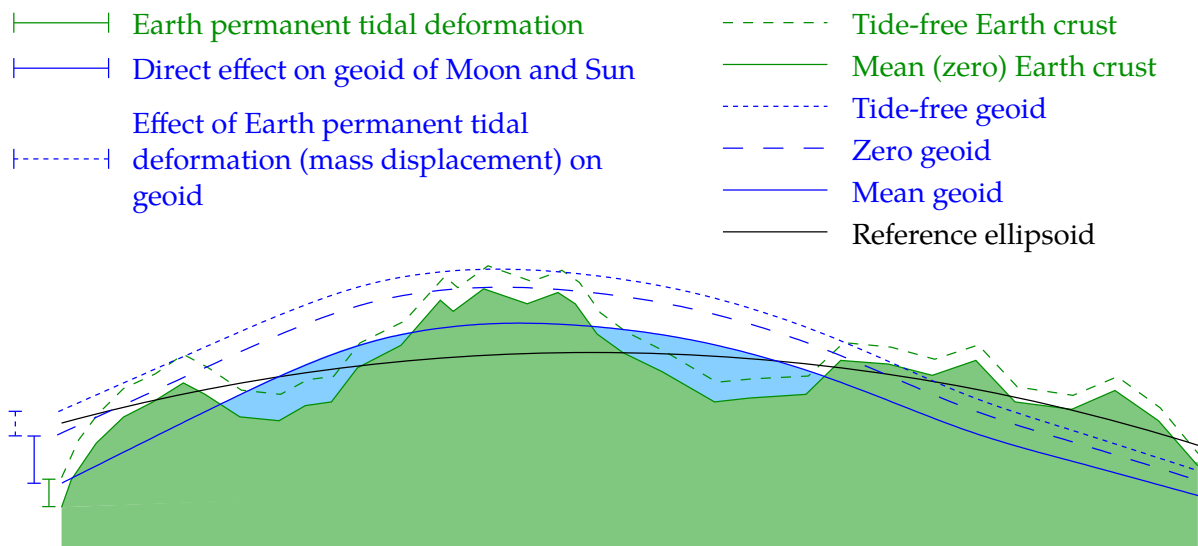


FIGURE 14.3. Conceptual diagram showing the constituents of the permanent tide.

height of the geoid, for the permanent part of the tide can be carried out *in three different ways*:

- No reduction whatever is made for the permanent part. The quantity thus obtained is called the “mean geoid”. The surface obtained is in the hydrodynamic sense an equilibrium surface, suitable for use in oceanography.
- The direct effect of the gravitational field emanating from celestial objects is removed in its entirety from the quantity, but the effect of the Earth’s deformation caused by it is left uncorrected. The quantity thus obtained is called the “zero geoid”.
- Both the gravitational effect of a celestial body, and the effect of the deformation it causes, can be calculated according to a certain deformation model (Love numbers), and removed. The result obtained is called the “tide-free geoid”. Its problem is, as explained, the empirical indeterminacy of the elasticity model used.



See figure 14.3. It is good to be critical and precisely analyse the way in which the data reduction has been done!

14.4 Tidal corrections between height systems

We see from equation 14.2 that, with $\epsilon = 23^\circ.5$, the permanent part of the tidal potential is equal to

$$\begin{aligned} V_{\text{perm}} &= \frac{GMR^2}{4d^3} (3 \sin^2 \phi - 1) \left(\frac{3}{2} \sin^2 \epsilon - 1 \right) \approx \\ &\approx -0.7615 \cdot \frac{3GMR^2}{4d^3} \left(\sin^2 \phi - \frac{1}{3} \right). \end{aligned}$$

With the combined Doodson's constant 14.3 for Sun and Moon equal to

$$\begin{aligned} D &= \frac{3GM_{\odot} R^2}{4d_{\odot}^3} + \frac{3GM_{\zeta} R^2}{4d_{\zeta}^3} = \\ &= (12.3 \text{ cm} + 26.8 \text{ cm}) \times \gamma = 39.1 \text{ cm} \times \gamma \end{aligned}$$

we obtain

$$V_{\text{perm}} = 29.77 \text{ cm} \times \left(\frac{1}{3} - \sin^2 \phi \right) \times \gamma.$$

We can express this, with Bruns equation 5.2, as a permanent tidal geoid effect:

$$N_{\text{perm}} = 29.77 \text{ cm} \times \left(\frac{1}{3} - \sin^2 \phi \right).$$

From this, $N_{\text{perm}}(0^\circ) = 9.92 \text{ cm}$ on the equator, and $N_{\text{perm}}(\pm 90^\circ) = -19.85 \text{ cm}$ on the poles.

This, the geoid effect of the permanent part of the external potential of the Sun and Moon is also equal to the difference between the mean geoid and the zero geoid as defined above:

$$\Delta_{\text{zero}}^{\text{mean}} N \stackrel{\text{def}}{=} N_{\text{mean}} - N_{\text{zero}} = 29.77 \text{ cm} \times \left(\frac{1}{3} - \sin^2 \phi \right).$$

For heights H above sea level, with $H = h - N$, we have

$$\Delta_{\text{zero}}^{\text{mean}} H \stackrel{\text{def}}{=} H_{\text{mean}} - H_{\text{zero}} = -29.77 \text{ cm} \times \left(\frac{1}{3} - \sin^2 \phi \right),$$



and for two different latitudes ϕ_1 and ϕ_2 we have for the effect on the height difference

$$\Delta_{\text{zero}}^{\text{mean}} H(\phi_2) - \Delta_{\text{zero}}^{\text{mean}} H(\phi_1) = 29.77 \text{ cm} \times (\sin^2 \phi_2 - \sin^2 \phi_1).$$

This is the value to be *added* when going from a zero-geoid to a mean-geoid height system, and *subtracted* when going from a mean-geoid to a zero-geoid height system.

When the *tide-free* geoid and Earth crust enter into the picture, we need values for the Love numbers h_2 and k_2 for the permanent tidal deformation, expressing this deformation and its potential as fractional parts of the original external tidal potential. As we have seen, these numbers cannot be empirically determined. Values often used are $h_2 \approx 0.6, k_2 \approx 0.3$. With this, the above equations apply with the coefficient 29.77 cm multiplied by $1 - h_2 + k_2$. This yields

$$\Delta_{\text{tidefree}}^{\text{mean}} H \stackrel{\text{def}}{=} H_{\text{mean}} - H_{\text{tidefree}} = -20.84 \text{ cm} \times \left(\frac{1}{3} - \sin^2 \phi\right),$$

$$\Delta_{\text{tidefree}}^{\text{mean}} H(\phi_2) - \Delta_{\text{tidefree}}^{\text{mean}} H(\phi_1) = 20.84 \text{ cm} \times (\sin^2 \phi_2 - \sin^2 \phi_1).$$

Any other correction equation can be obtained from these, like

$$\Delta_{\text{tidefree}}^{\text{zero}} H(\phi_2) - \Delta_{\text{tidefree}}^{\text{zero}} H(\phi_1) = -8.93 \text{ cm} \times (\sin^2 \phi_2 - \sin^2 \phi_1).$$



14.5 Loading of the Earth's crust by sea and atmosphere

In addition to the deformation caused by the tidal force, the Earth's crust also deforms due to the loading by sea and atmosphere. Especially close to the coast, the tidal motion of the sea causes a multi-period deformation that moves the Earth's crust up and down by as much as centimetres.

This phenomenon can be computationally modelled if the elastic properties of the solid Earth, the tidal motion of the sea, and the precise shape of the coastline are known. One known program for this purpose



is the package Eterna written by the German Wenzel,⁹ which also has been used in Finland.

On the other hand, when such tools exist, tidal loading offers also an excellent opportunity for *studying* precisely the very local elastic properties of the Earth's crust.

A registering gravimeter is generally used for measuring the deformation. The Earth's crust moves up and down elastically, which to first order changes gravity in proportion to the free-air gradient value -0.3 mGal/m . For a description of the method, see Torge (1992) section 4.2.

The use of GNSS for measuring the ocean tidal loading has not yet become common.

Like the ocean, the atmosphere also causes, through changes in air pressure, varying deformations of the Earth's crust. The phenomenon is very small, at most a couple of centimetres. Gravity measurement is not a very good way to study this phenomenon, because many more local, often poorly known, factors affect local gravity. Measurement by GNSS is promising but also challenging.

Self-test questions

1. Present *in words* the three components of the theoretical tide produced by the Laplace decomposition method.
2. How may the slowly varying part of the theoretical tide be further decomposed into two parts? Present the parts *in words*.
3. What are the declination and hour angle of a celestial body, for example the Moon?
4. What is Doodson's constant?
5. What do Love numbers express?

⁹Hans-Georg Wenzel (1945–1999) was a German physical geodesist and geophysicist.

6. Why is it not possible to empirically determine the deformation caused by the permanent part of the tide?
7. Present the three different ways to take the permanent part of the tide into account when defining the geoid.



Exercise 14 – 1: Tide

The equation for the permanent part of the tide is

$$W_{1a} = \frac{GM R^2}{4d^3} (3 \sin^2 \varphi - 1) \left(\frac{3}{2} \sin^2 \epsilon - 1 \right),$$

in which φ is latitude and ϵ is the *obliquity* of the Earth's axis of rotation, currently about $23^\circ 5'$.

1. For what value φ does the permanent part of the tide vanish? What is your interpretation?
2. For what value ϵ does the permanent part of the tide vanish? What is your interpretation?





Earth gravity field research

15



15.1 Internationally

In the framework of the **IAG**, the International Association of Geodesy, research into the Earth's gravity field is currently the responsibility of the International Gravity Field Service (**IGFS**). The **IGFS** was created in 2003 at the IUGG General Assembly in Sapporo, Japan, and it operates under the **IAG**'s new Commission 2 "Gravity Field". The United States National Geospatial-Intelligence Agency (**NGA**) serves as its technical centre.

An important and well-reputed **IAG** service is the International Gravity Bureau, the **BGI**, *Bureau Gravimétrique International* located in Toulouse, France (<http://bgi.omp.obs-mip.fr/>). The bureau works as an international broker to which countries can submit their gravimetric materials. If a researcher needs gravimetric material from another country, for example in order to do a geoid computation, they can request it from the **BGI**, who will provide it with the permission of the country of origin, provided the country of the researcher has in its turn submitted its own gravimetric materials for **BGI** use.

The French state has invested significant funds into this vital international activity.

Another important **IAG** service in this field is the **ISG**, the International Service for the Geoid. It has in fact been operating since as early as

1992 under the name International Geoid Service (**IGeS**), the executive arm of the International Geoid Commission (**IGeC**). The **ISG** office is located in Milan (<http://www.isgeoid.polimi.it/>), also with substantial support by the Italian state. The task of this service is to support geoid determination in different countries. Existing geoid solutions are collected into a common database, and international research schools are organised to develop awareness about and skills in the art of geoid computation, especially in developing countries.

Both services, **BGI** and **ISG**, are under the auspices of the **IGFS**, as two of the many official services of the **IAG**. Other **IGFS** services include the International Center for Earth Tides (**ICET**), the International Center for Global Earth Models (**ICGEM**), and the International Digital Elevation Model Service (**IDEMS**).



15.2 Europe

The **EGU**, the European Geosciences Union, operates in Europe, coordinating many publication and meeting activities relating to the gravity field and geoid. The **EGU** organises annual symposia, where sessions are always also included on subjects related to the gravity field and geoid. American scientists also participate. Conversely the American Geophysical Union's (**AGU**) fall and spring meetings¹ are also favoured by European researchers.

The Geodetic Institute (*"Institut für Erdmessung"*) of Leibniz University in Hannover, Germany has acted since 1990 as the computing centre of the International Geoid Commission's (**IGeC**) Subcommittee for Europe, and produced high-quality European geoid models (**Denker, 1998; European geoid calculations**). The work continues since 2011 within the framework of the **IAG** Subcommittee 2.4a *Gravity and Geoid in Europe*.

¹Fall (autumn) meetings are in San Francisco, spring meetings somewhere in the world. The **AGU**, although American, is a very cosmopolitan player.



15.3 The Nordic countries

In the Nordic countries, important work is being co-ordinated by the **NKG**, the *Nordiska Kommissionen för Geodesi*, and its Working Group for Geoid and Height Systems. Its activities include geoid determination, studying the preconditions for still more precise geoid models, new levelling technologies, and the study of post-glacial land uplift.

The group has for a long time computed high-quality geoid models at its computing centre in Copenhagen, the next to last one being **NKG2004** (Forsberg and Kaminskis, 1996; Forsberg and Strykowski, 2010). The newest model, **NKG2015**, is the result of calculations by the computing centres of several countries, including Sweden and Estonia. It was published in October 2016.

15.4 Finland

In Finland the study of the Earth's gravity field has mainly been in the hands of the Finnish Geodetic Institute, founded in 1918, one year after Finnish independence. The institute has been responsible for the national fundamental levelling and gravimetric networks and their international connections. In 2001 the Finnish Geodetic Institute's gravity and geodesy departments were joined into a new department of geodesy and geodynamics, to which gravity research also belongs.

Among topics studied are solid-Earth tides, the free oscillations of the solid Earth, post-glacial land uplift, and vertical reference or height systems.

Geoid models have been computed all the time, starting with Hirvonen's global model (Hirvonen, 1934) and ending, for now, with the Finnish model **FIN2005N00** (Bilker-Koivula, 2010). These geoid models are actually based on the Nordic **NKG2004** gravimetric geoid, and are fitted to a Finnish set of **GNSS** levelling control points through a transformation surface.

In 2015, the Finnish Geodetic Institute was merged into the National



Land Survey as its geospatial data centre and research facility. The English-language acronym continues as **FGI**, the Finnish Geospatial Research Institute (<http://www.fgi.fi/fgi>).

Helsinki University of Technology (today part of Aalto University) has also been active in research on the Earth's gravity field. Heiskanen, a professor at **HUT** in 1928–1949, acted in 1936–1949 as the director of the International Isostatic Institute. After moving to Ohio State University, he worked with many other, including Finnish and Finnish-born, geodesists on calculating the first major global geoid model, the “Columbus geoid” (Kakkuri, 2008).



15.5 Textbooks

There are many good textbooks on the study of the Earth's gravity field. In addition to the already mentioned classic, **Heiskanen and Moritz (1967)**, which is in large part obsolete, we may mention Wolfgang Torge's book (1989). **Moritz (1980)** is difficult but good. Similarly difficult is **Molodensky et al. (1962)**. Worth reading also from the perspective of physical geodesy is **Vaniček and Krakiwsky (1987)**. A newer book in the field is **Hofmann-Wellenhof and Moritz (2006)**.





Field theory and vector calculus — core knowledge



A.1 Vector calculus

In physics, many quantities are *vector quantities*; for example, force, velocity, electrostatic field, and many more. A vector behaves in the same way as the location difference between two neighbouring points. Let the location difference be $\Delta\mathbf{r} = \mathbf{r}_2 - \mathbf{r}_1$, in which \mathbf{r}_1 and \mathbf{r}_2 are the location vectors of points 1 and 2. In a co-ordinate transformation, the vector considered as an object does not change, but the numerical values of its *components*, subsection [A.2.2](#), are co-ordinate-system dependent and will change.

About notation In printed text, vectors are often written in **bold**. In _____ handwritten text one may use an arrow above the symbol: \vec{v} .



A.1.1 Scalar product

Between two vectors, a *scalar product* or dot product can be defined, which is itself a scalar value. A scalar is in physics a single numerical value; say, pressure or temperature. In the case of a scalar product of two vector *fields*, the value is tied to a location, but, even if a co-ordinate transformation changes the co-ordinate values of the location, the scalar itself remains unchanged.

An example of a scalar product: *work* ΔE is

$$\Delta E = \langle \mathbf{F} \cdot \Delta \mathbf{r} \rangle,$$

the scalar product of force \mathbf{F} and path $\Delta \mathbf{r}$. Often, we leave the angle brackets $\langle \cdot \rangle$ off.

Later we shall see that if the points 1 and 2, $\Delta \mathbf{r} = \mathbf{r}_2 - \mathbf{r}_1$, are very close to each other, we may write

$$dE = \langle \mathbf{F} \cdot d\mathbf{r} \rangle,$$

in which $d\mathbf{r}$ and dE are infinitesimal elements of path and energy. If now there is a curved path between points A and B, we may get from this an integral equation, the *work integral*:

$$\Delta E_{AB} = \int_A^B \langle \mathbf{F} \cdot d\mathbf{r} \rangle.$$

A.1.2 The scalar product, formally

Let

$$s \stackrel{\text{def}}{=} \langle \mathbf{a} \cdot \mathbf{b} \rangle$$

be the scalar product of the vectors \mathbf{a} and \mathbf{b} . It holds ($\mu \in \mathbb{R}$) that

$$\begin{aligned} \langle \mu \mathbf{a} \cdot \mathbf{b} \rangle &= \langle \mathbf{a} \cdot \mu \mathbf{b} \rangle = \mu \langle \mathbf{a} \cdot \mathbf{b} \rangle, \\ \langle \mathbf{a} \cdot \mathbf{b} \rangle &= \langle \mathbf{b} \cdot \mathbf{a} \rangle, \end{aligned}$$

and we call

$$\|\mathbf{a}\| \stackrel{\text{def}}{=} \sqrt{\langle \mathbf{a} \cdot \mathbf{a} \rangle}$$

the *norm* or length of vector \mathbf{a} .

The following also applies:

$$s = \|\mathbf{a}\| \|\mathbf{b}\| \cos \alpha,$$

where α is the angle between the directions of the vectors \mathbf{a} and \mathbf{b} .



A.1.3 Exterior or vectorial product

The exterior product, or cross product, of two vectors is itself a vector called the *vectorial product*, at least in three-dimensional Euclidean space. For example, the *angular momentum* \mathbf{q} :

$$\mathbf{q} = \langle \mathbf{r} \times \mathbf{p} \rangle,$$

where $\mathbf{p} = m\dot{\mathbf{r}}$ is linear momentum, \mathbf{r} the location vector of the body relative to some origin, m the mass of the body, and

$$\dot{\mathbf{r}} = \frac{d\mathbf{r}}{dt} \quad (\text{A.1})$$

is the time derivative of the location, or *velocity*. We write

$$\mathbf{q} = m \langle \mathbf{r} \times \dot{\mathbf{r}} \rangle.$$

A.1.4 The vectorial product, formally

Let

$$\mathbf{c} \stackrel{\text{def}}{=} \langle \mathbf{a} \times \mathbf{b} \rangle$$

be the vectorial product of the two vectors \mathbf{a} and \mathbf{b} . Then ($\mu \in \mathbb{R}$):

$$\langle \mu \mathbf{a} \times \mathbf{b} \rangle = \langle \mathbf{a} \times \mu \mathbf{b} \rangle = \mu \langle \mathbf{a} \times \mathbf{b} \rangle,$$

$$\langle \mathbf{a} \times \mathbf{b} \rangle = -\langle \mathbf{b} \times \mathbf{a} \rangle,$$

$$\text{and thus } \langle \mathbf{a} \times \mathbf{a} \rangle = 0.$$

The resulting vector \mathbf{c} is always *orthogonal* to the vectors \mathbf{a} and \mathbf{b} . The length of vector \mathbf{c} corresponds to the surface area of the parallelogram suunnikas spanned by vectors \mathbf{a} and \mathbf{b} :

$$\|\mathbf{c}\| = \|\mathbf{a}\| \|\mathbf{b}\| \sin \alpha, \quad (\text{A.2})$$

in which again α is the angle between the directions of vectors \mathbf{a} and \mathbf{b} . If the angle is zero, then the vectorial product is also zero (because then, $\mathbf{a} = \mu\mathbf{b}$ for some suitable value of μ).

If the angle is not zero we need in addition a *corkscrew rule* saying that, if a corkscrew is turned from vector \mathbf{a} to vector \mathbf{b} , it will move forward in the direction of the product vector $\mathbf{c} = \langle \mathbf{a} \times \mathbf{b} \rangle$.



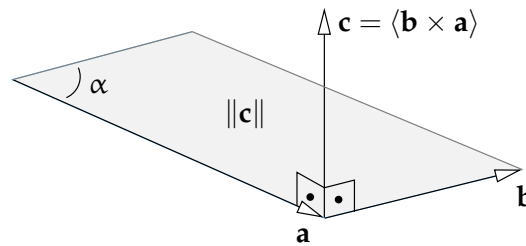


FIGURE A.1. Exterior or vectorial product.



A.1.5 Kepler's second law



Let \mathbf{r} be the location vector of the body (planet) relative to the centre of motion (the Sun), and $\dot{\mathbf{r}}$ (equation A.1) its velocity vector. Then, the vectorial product

$$\langle \mathbf{r} \times \dot{\mathbf{r}} \rangle = \left\langle \mathbf{r} \times \frac{d\mathbf{r}}{dt} \right\rangle \quad (\text{A.3})$$

is precisely twice the surface area of the triangle or “area” swept over in a unit of time.

Let us take the time derivative of this product, the expression A.3:

$$\frac{d}{dt} \langle \mathbf{r} \times \dot{\mathbf{r}} \rangle = \left\langle \frac{d\mathbf{r}}{dt} \times \frac{d\mathbf{r}}{dt} \right\rangle + \left\langle \mathbf{r} \times \frac{d^2\mathbf{r}}{dt^2} \right\rangle = \langle \dot{\mathbf{r}} \times \dot{\mathbf{r}} \rangle + \langle \mathbf{r} \times \ddot{\mathbf{r}} \rangle. \quad (\text{A.4})$$

Here, the first term vanishes, because for an arbitrary vector $\langle \mathbf{a} \times \mathbf{a} \rangle = 0$. In the second term, we can use our knowledge that the attractive force \mathbf{F} emanating from the Sun that causes planetary orbital motion, and also the acceleration it causes,

$$\ddot{\mathbf{r}} = \frac{d^2\mathbf{r}}{dt^2},$$

keskeisvoima are central:

$$\mathbf{F} = m\ddot{\mathbf{r}} = -\frac{GMm}{\|\mathbf{r}\|^3}\mathbf{r}.$$

G is the universal gravitational constant, M is the mass of the Sun, and m is the mass of the planet.

Substitute this into equation A.4:

$$\frac{d}{dt} \langle \mathbf{r} \times \dot{\mathbf{r}} \rangle = 0 - \frac{GM}{\|\mathbf{r}\|^3} \langle \mathbf{r} \times \mathbf{r} \rangle = 0.$$



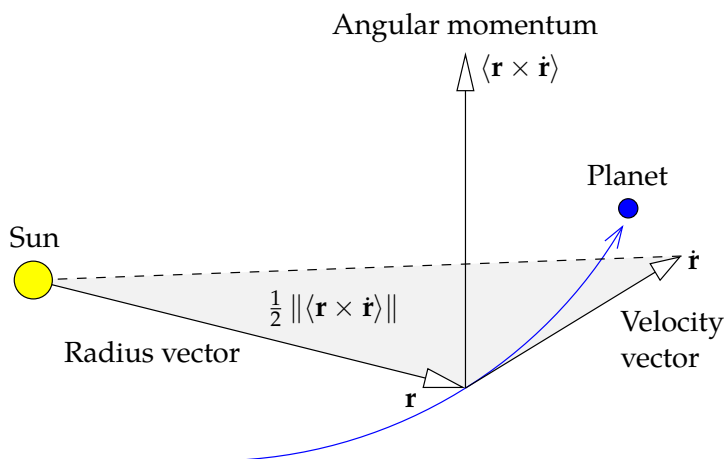


FIGURE A.2. Kepler’s second law. In the same amount of time, the radius vector of a planet will “sweep over” a same-sized area — conservation of angular momentum.



So: the quantity on the left-hand side, angular momentum \mathbf{q} per unit of mass m , is *conserved*:

$$\langle \mathbf{r} \times \dot{\mathbf{r}} \rangle = \frac{\mathbf{q}}{m}.$$

pyörähdyshetimitin säilyminen

Like, for example, the total amount of energy, electric charge and many other quantities, the amount of angular momentum in a closed system is also constant.

A.2 Scalar and vector fields

A.2.1 Definitions

In the Euclidean space we may define functions or *fields*.

A scalar field is a scalar-valued function, which is defined throughout the space (or a part of it), for example temperature $T(\mathbf{r})$. So, for every value of the location vector \mathbf{r} there is a temperature value $T(\mathbf{r})$.

A vector field is a vector-valued function that again is defined throughout space, for example the electrostatic field $\mathbf{E}(\mathbf{r})$.



A.2.2 A basis in space

In the space we may choose a *basis* made up of three vectors which *span* the space in question. Generally we choose three basis vectors \mathbf{i} , \mathbf{j} , \mathbf{k} , that are orthogonal to each other, and the norms, or lengths, of which are equal to 1, an *orthonormal basis*. Orthogonality of two vectors means that their scalar product vanishes; so

$$\mathbf{i} \perp \mathbf{j}, \quad \mathbf{i} \perp \mathbf{k}, \quad \mathbf{j} \perp \mathbf{k}$$

means that

$$\langle \mathbf{i} \cdot \mathbf{j} \rangle = \langle \mathbf{i} \cdot \mathbf{k} \rangle = \langle \mathbf{j} \cdot \mathbf{k} \rangle = 0. \quad (\text{A.5})$$

Orthonormality means in addition that

$$\|\mathbf{i}\| = \|\mathbf{j}\| = \|\mathbf{k}\| = 1. \quad (\text{A.6})$$

Now we may expand vectors in the space into their *components*:

$$\mathbf{a} = a_1\mathbf{i} + a_2\mathbf{j} + a_3\mathbf{k},$$

and scalar and vectorial products can now also be calculated with the aid of their components:

$$\begin{aligned} s = \langle \mathbf{a} \cdot \mathbf{b} \rangle &= \langle (a_1\mathbf{i} + a_2\mathbf{j} + a_3\mathbf{k}) \cdot (b_1\mathbf{i} + b_2\mathbf{j} + b_3\mathbf{k}) \rangle = \\ &= a_1b_1 + a_2b_2 + a_3b_3 = \sum_{i=1}^3 a_i b_i, \end{aligned}$$

using the identities stated above for the basis vectors [A.5](#) and [A.6](#).

For the vectorial product, the calculation is more involved. For orthogonal vectors, the angle α in equation [A.2](#) is 90° , so

$$\|\langle \mathbf{i} \times \mathbf{j} \rangle\| = \|\langle \mathbf{i} \times \mathbf{k} \rangle\| = \|\langle \mathbf{j} \times \mathbf{k} \rangle\| = 1.$$

The corkscrew rule now tells us that

$$\begin{aligned} \mathbf{k} &= \langle \mathbf{i} \times \mathbf{j} \rangle = -\langle \mathbf{j} \times \mathbf{i} \rangle, \\ \mathbf{i} &= \langle \mathbf{j} \times \mathbf{k} \rangle = -\langle \mathbf{k} \times \mathbf{j} \rangle, \\ \mathbf{j} &= \langle \mathbf{k} \times \mathbf{i} \rangle = -\langle \mathbf{i} \times \mathbf{k} \rangle. \end{aligned}$$



We get as the final outcome the determinant

$$\begin{aligned} \mathbf{c} = \langle \mathbf{a} \times \mathbf{b} \rangle &= \det \begin{bmatrix} \mathbf{i} & \mathbf{j} & \mathbf{k} \\ a_1 & a_2 & a_3 \\ b_1 & b_2 & b_3 \end{bmatrix} = \\ &= (a_2 b_3 - a_3 b_2) \mathbf{i} + (a_3 b_1 - a_1 b_3) \mathbf{j} + (a_1 b_2 - a_2 b_1) \mathbf{k}. \end{aligned}$$

So

$$c_1 = a_2 b_3 - a_3 b_2, \quad c_2 = a_3 b_1 - a_1 b_3, \quad c_3 = a_1 b_2 - a_2 b_1.$$

These expressions are determinants as well:

$$\begin{bmatrix} c_1 \\ c_2 \\ c_3 \end{bmatrix} = \begin{bmatrix} \det \begin{bmatrix} a_2 & a_3 \\ b_2 & b_3 \end{bmatrix} & \det \begin{bmatrix} a_3 & a_1 \\ b_3 & b_1 \end{bmatrix} & \det \begin{bmatrix} a_1 & a_2 \\ b_1 & b_2 \end{bmatrix} \end{bmatrix}^T.$$

A.2.3 The nabla operator

The *location vector* \mathbf{r} can be written on the $\{\mathbf{i}, \mathbf{j}, \mathbf{k}\}$ basis as follows:

$$\mathbf{r} = x\mathbf{i} + y\mathbf{j} + z\mathbf{k},$$

which defines (x, y, z) co-ordinates in space.

Let us define a vector operator called *nabla* (∇) as follows:

$$\nabla \stackrel{\text{def}}{=} \mathbf{i} \frac{\partial}{\partial x} + \mathbf{j} \frac{\partial}{\partial y} + \mathbf{k} \frac{\partial}{\partial z}.$$

The operator is on its own without meaning. It acquires meaning only when it *operates* on something, in which case the three partial derivatives on the right-hand side can be calculated.

A.2.4 The gradient

Let $V(\mathbf{r}) = V(x, y, z)$ be a scalar field in space. The nabla operator will give its *gradient* \mathbf{g} , a vector field in the same space:

$$\mathbf{g} = \text{grad } V = \nabla V = \mathbf{i} \frac{\partial V}{\partial x} + \mathbf{j} \frac{\partial V}{\partial y} + \mathbf{k} \frac{\partial V}{\partial z}.$$



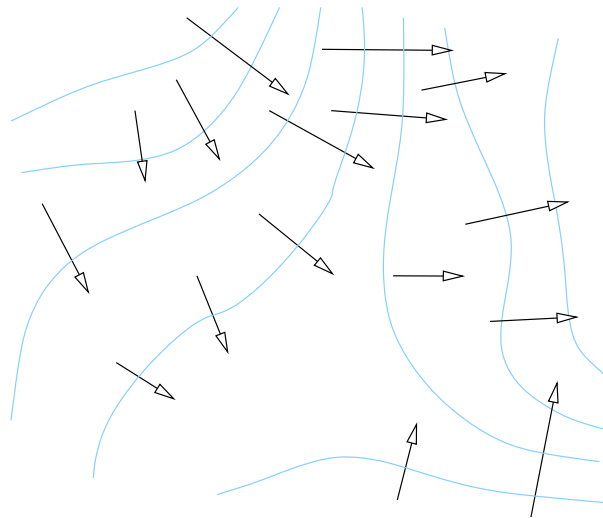


FIGURE A.3. The gradient. The level curves of the scalar field in blue.

So, the field $\mathbf{g}(\mathbf{r}) = \mathbf{g}(x, y, z)$ is the gradient field of V . In physics \mathbf{g} is often a force field and V its potential.

Interpretation The gradient describes the *slope* of the scalar field. The direction of the vector is the direction in which the value of the scalar field changes fastest, and its length describes the rate of change with location. Imaging a hilly landscape: the height of the ground above sea level is the scalar field, and its gradient is pointing *uphill* everywhere, away from the valleys towards the hilltops. The longer the \mathbf{g} arrows, the steeper the slope of the ground surface.

The gradient operator (like also the divergence and the curl, see later) is *linear*:

$$\text{grad} (U + V) = \text{grad} U + \text{grad} V.$$



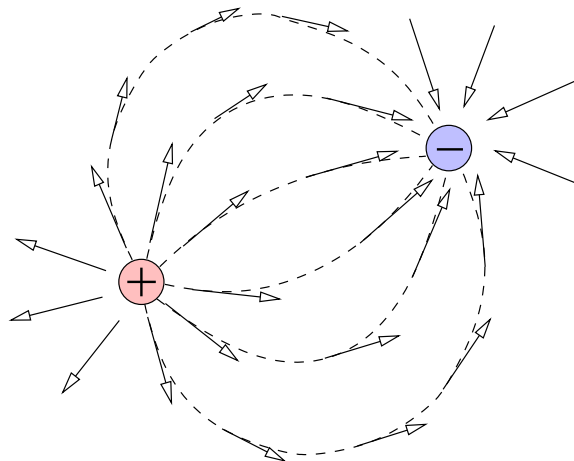


FIGURE A.4. The divergence. Positive divergences (“sources”) and negative ones (“sinks”). Field lines dashed.



A.2.5 The divergence



Given a vector field $\mathbf{a}(x, y, z) = a_1\mathbf{i} + a_2\mathbf{j} + a_3\mathbf{k}$, we form the *scalar product* s of this and the nabla operator:

$$s = \text{div } \mathbf{a} = \langle \nabla \cdot \mathbf{a} \rangle = \frac{\partial a_1}{\partial x} + \frac{\partial a_2}{\partial y} + \frac{\partial a_3}{\partial z}.$$

Interpretation The divergence describes the “sources” of a vector field, both the positive and negative ones. Imagine the velocity of the flow of water as a vector field. At the locations of the “sources” the divergence is positive, at the locations of the “sewer holes” or *sinks*, negative; everywhere else zero (because liquid cannot lähteet, nielut appear out of nothing or disappear into nothing).

A.2.6 The curl



Given again a vector field $\mathbf{a}(x, y, z)$, we form the *vectorial product* \mathbf{c} of this and the nabla operator, again producing a vector field:



$$\begin{aligned}
\mathbf{c} = \text{curl } \mathbf{a} &= \nabla \times \mathbf{a} = \det \begin{bmatrix} \mathbf{i} & \mathbf{j} & \mathbf{k} \\ \frac{\partial}{\partial x} & \frac{\partial}{\partial y} & \frac{\partial}{\partial z} \\ a_1 & a_2 & a_3 \end{bmatrix} = \\
&= \det \begin{bmatrix} \frac{\partial}{\partial y} & \frac{\partial}{\partial z} \\ a_2 & a_3 \end{bmatrix} \mathbf{i} - \det \begin{bmatrix} \frac{\partial}{\partial x} & \frac{\partial}{\partial z} \\ a_1 & a_3 \end{bmatrix} \mathbf{j} + \det \begin{bmatrix} \frac{\partial}{\partial x} & \frac{\partial}{\partial y} \\ a_1 & a_2 \end{bmatrix} \mathbf{k} = \\
&= \left(\frac{\partial a_3}{\partial y} - \frac{\partial a_2}{\partial z} \right) \mathbf{i} + \left(\frac{\partial a_1}{\partial z} - \frac{\partial a_3}{\partial x} \right) \mathbf{j} + \left(\frac{\partial a_2}{\partial x} - \frac{\partial a_1}{\partial y} \right) \mathbf{k},
\end{aligned}$$

using the evaluation rules for determinants.

Interpretation The curl describes the *eddy* or *turbulence* present in a _____ vector field.

Imagine a weather map, where low- and high-pressure zones are drawn. Our vector field is the wind field. The wind circulates (in the northern hemisphere) clockwise around the high-pressure zones, and anticlockwise around the low-pressure zones. We may say that the curl of the wind field is positive at the high pressures and negative at the low pressures.

(This is a poor metaphor, as it is two-dimensional. In \mathbb{R}^2 , the curl is a scalar, not a vector, just like we need only one angle to characterise a rotational motion, when in \mathbb{R}^3 we need the three Euler angles.)

A.2.7 Conservative fields

What happens if a vector field \mathbf{a} is the gradient of a scalar field V , and we try to calculate its curl \mathbf{b} , which is a vector as well? Write

$$\mathbf{b} = \text{curl } \mathbf{a} = \text{curl grad } V = \det \begin{bmatrix} \mathbf{i} & \mathbf{j} & \mathbf{k} \\ \frac{\partial}{\partial x} & \frac{\partial}{\partial y} & \frac{\partial}{\partial z} \\ \frac{\partial}{\partial x} & \frac{\partial}{\partial y} & \frac{\partial}{\partial z} \end{bmatrix} V$$

and let

$$\mathbf{b} = b_1 \mathbf{i} + b_2 \mathbf{j} + b_3 \mathbf{k}.$$



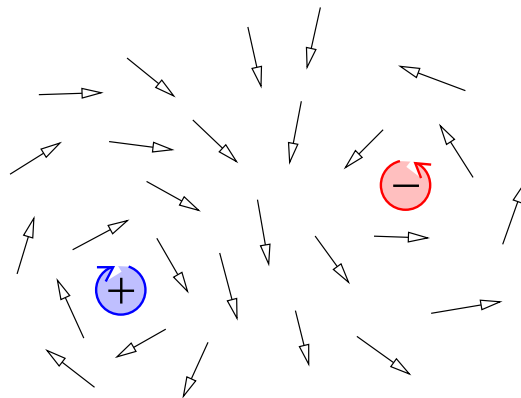


FIGURE A.5. The curl. Positive (clockwise) and negative (anticlockwise) eddies.

Then, expanding the determinant yields

$$\begin{aligned}
 b_1 &= \frac{\partial}{\partial y} \frac{\partial}{\partial z} V - \frac{\partial}{\partial z} \frac{\partial}{\partial y} V = 0, \\
 b_2 &= \frac{\partial}{\partial z} \frac{\partial}{\partial x} V - \frac{\partial}{\partial x} \frac{\partial}{\partial z} V = 0, \\
 b_3 &= \frac{\partial}{\partial x} \frac{\partial}{\partial y} V - \frac{\partial}{\partial y} \frac{\partial}{\partial x} V = 0,
 \end{aligned}$$

thus

$$\mathbf{b} = \text{curl } \mathbf{a} = \mathbf{0}!$$

In other words, if the vector field $\mathbf{a}(x, y, z)$ is the gradient of the scalar field $V(x, y, z)$, its curl will vanish:

$$\text{curl grad } V = \langle \nabla \times \nabla V \rangle = \langle \nabla \times \nabla \rangle V = \mathbf{0},$$

so the vectorial product of ∇ with itself vanishes just as if it were an ordinary vector!

Definition A vector field \mathbf{a} of which the curl vanishes is called *conservative*, and the corresponding scalar field V , $\mathbf{a} = \text{grad } V$, is called the *potential* of field \mathbf{a} .

We note immediately that, if

$$\mathbf{a}(x, y, z) = \text{grad } V(x, y, z),$$



then also

$$\mathbf{a}(x, y, z) = \text{grad}(V(x, y, z) + V_0),$$

with V_0 an arbitrary constant, because

$$\text{grad } V_0 = \mathbf{i} \frac{\partial V_0}{\partial x} + \mathbf{j} \frac{\partial V_0}{\partial y} + \mathbf{k} \frac{\partial V_0}{\partial z} = 0.$$

So the potential is *not uniquely defined*.

A.2.8 The Laplace operator

Assume a conservative field \mathbf{a} , so $\text{curl } \mathbf{a} = 0$. Then we may write

$$\mathbf{a} = \text{grad } V = \nabla V,$$

in which V is the potential.

Let us now express the *divergence* of field \mathbf{a} into the potential:

$$\begin{aligned} \text{div } \mathbf{a} = \langle \nabla \cdot \mathbf{a} \rangle &= \langle \nabla \cdot \nabla V \rangle = \frac{\partial}{\partial x} \frac{\partial}{\partial x} V + \frac{\partial}{\partial y} \frac{\partial}{\partial y} V + \frac{\partial}{\partial z} \frac{\partial}{\partial z} V = \\ &= \left(\frac{\partial^2}{\partial x^2} + \frac{\partial^2}{\partial y^2} + \frac{\partial^2}{\partial z^2} \right) V \stackrel{\text{def}}{=} \Delta V, \end{aligned}$$

where we have introduced a new *differential operator*, the Delta operator invented by the French Pierre-Simon Laplace,

$$\Delta = \frac{\partial^2}{\partial x^2} + \frac{\partial^2}{\partial y^2} + \frac{\partial^2}{\partial z^2} = \langle \nabla \cdot \nabla \rangle = \nabla^2.$$

When operating on the potential of a “source free” field — for example the gravitational potential in a vacuum or the electrostatic potential in an area of space free of electric charges — the result of this Delta, or Laplace, operator vanishes.

A.3 Integrals

A.3.1 The curve integral

We saw earlier that work ΔE can be written as the scalar product of force \mathbf{F} and path $\Delta \mathbf{r}$:

$$\Delta E = \langle \mathbf{F} \cdot \Delta \mathbf{r} \rangle.$$



The differential form of this is

$$dE = \langle \mathbf{F} \cdot d\mathbf{r} \rangle,$$

from which one obtains the integral form, the *work integral*

$$\Delta E_{AB} = \int_A^B \langle \mathbf{F} \cdot d\mathbf{r} \rangle.$$

Here, the amount of work needed to move a body from point A to point B is computed by integrating $\langle \mathbf{F} \cdot d\mathbf{r} \rangle$ along the path AB.

If we parametrise the path according to arc length s , and the tangent vector to the path is called

$$\mathbf{t} \stackrel{\text{def}}{=} \frac{dx}{ds} \mathbf{i} + \frac{dy}{ds} \mathbf{j} + \frac{dz}{ds} \mathbf{k},$$

we may also write

$$\Delta E_{AB} = \int_A^B \langle \mathbf{F} \cdot \mathbf{t} \rangle ds,$$

the parametrised version of the integral.

A.3.2 The surface integral

Assume we are given again a vector field \mathbf{a} and a surface in space S . Often, one seeks to integrate over surface S the *normal component* of a vector field, the projection of \mathbf{a} onto the normal vector of the surface.

Let the normal vector of the surface be \mathbf{n} . Then we must integrate

$$\iint_S \langle \mathbf{a} \cdot \mathbf{n} \rangle dS,$$

symbolically written

$$\iint_S \langle \mathbf{a} \cdot d\mathbf{S} \rangle,$$

in which the notation $d\mathbf{S}$ is called an *oriented surface element*. It is a vector pointing in the same direction as the normal vector \mathbf{n} .



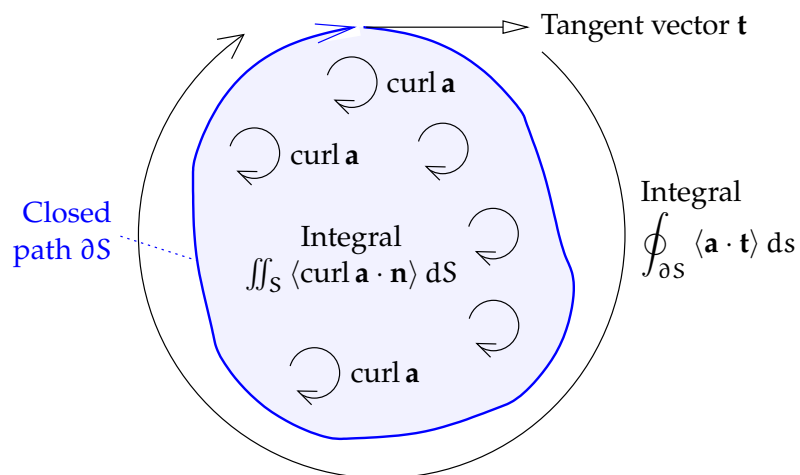


FIGURE A.6. The Stokes curl theorem.

Like a curve, a surface can also be *parametrised*. For example, the Earth's surface (assumed a sphere) can be parametrised by latitude ϕ and longitude λ : $\mathbf{r} = \mathbf{r}(\phi, \lambda)$. In this case we write as the surface element

$$dS = R^2 \cos \phi \, d\phi \, d\lambda,$$

in which $R^2 \cos \phi$ is *Jacobi's determinant* of the parameter pair (ϕ, λ) . In this parametrisation, the integral is calculated as follows:

$$\iint_S \langle \mathbf{a} \cdot d\mathbf{S} \rangle = \iint_S \langle \mathbf{a} \cdot \mathbf{n} \rangle dS = \iint_S \langle \mathbf{a} \cdot \mathbf{n} \rangle R^2 \cos \phi \, d\phi \, d\lambda.$$

Other surfaces and parametrisations have other Jacobi's determinants. The determinant always represents the *true* area of a "parameter surface element" $d\phi \, d\lambda$ "in nature". For example, on the Earth's surface, a degree times degree patch is largest near the equator. In polar coordinates (ρ, θ) in the plane ($x = \rho \cos \theta$, $y = \rho \sin \theta$), the determinant of Jacobi is ρ . In the ordinary (x, y) parametrisation in the plane, Jacobi's determinant is 1 and thus can be left out altogether.

A.3.3 The Stokes curl theorem

Let S be a surface in space (not necessarily flat) and ∂S its edge curve. Assume that the surface and its edge are well-behaved enough for all



necessary integrations and differentiations to be possible. Then (Stokes):

$$\iint_S \langle \text{curl } \mathbf{a} \cdot d\mathbf{S} \rangle = \oint_{\partial S} \langle \mathbf{a} \cdot d\mathbf{r} \rangle,$$

with \mathbf{r} the location vector of the edge curve. The parametrised form of the theorem is

$$\iint_S \langle \text{curl } \mathbf{a} \cdot \mathbf{n} \rangle dS = \oint_{\partial S} \langle \mathbf{a} \cdot \mathbf{t} \rangle ds,$$

with \mathbf{n} is the normal to surface S and \mathbf{t} the tangent vector of edge curve ∂S .

In words The surface integral of the curl of a vector field over a surface is the same as the closed path integral of the field around the edge of the surface.

Special case For a conservative vector field \mathbf{a} it holds that $\text{curl } \mathbf{a} = 0$ everywhere. Then

$$\oint_{\partial S} \langle \mathbf{a} \cdot d\mathbf{r} \rangle = 0,$$

so also

$$\int_{A, \text{path 1}}^B \langle \mathbf{a} \cdot d\mathbf{r} \rangle = \int_{A, \text{path 2}}^B \langle \mathbf{a} \cdot d\mathbf{r} \rangle.$$

Let \mathbf{a} be the force vector of a field, like the acceleration, or force per unit mass, caused by the gravity field. Then this has the following interpretation:

The work integral from point A to point B does not depend on the path chosen. And the work done by a body transported around a closed path is zero.

This perhaps explains better the essence of a conservative force field. A conservative field can be represented as the *gradient of a potential*: $\mathbf{a} = \text{grad } V$, in which V is the potential of the field. The Earth's gravity vector field $\mathbf{g}(x, y, z)$ is the gradient of the Earth's gravity potential $W(x, y, z)$. At mean sea level — more precisely,



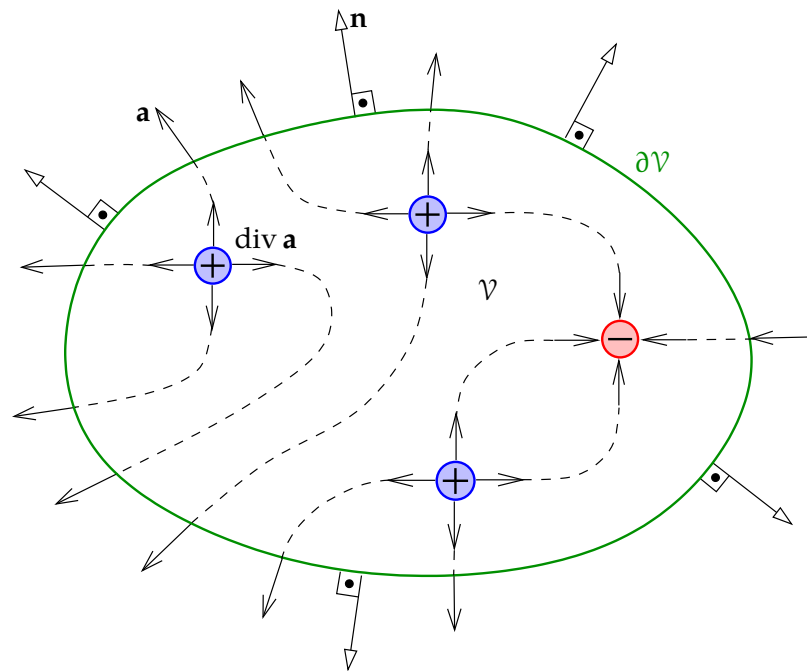


FIGURE A.7. The Gauss integral theorem. \mathbf{n} is the normal vector to the exterior surface. The Gauss integral theorem can also be presented with the aid of (Michael Faraday's) *field lines*: a field line starts or terminates on an electric charge (a place where $\operatorname{div} \mathbf{a} \neq 0$) or runs to infinity (through the surface $\partial\mathcal{V}$).



at the geoid — the gravity *potential* is constant; the gravity *vector* \mathbf{g} is everywhere perpendicular to the geoid.



A.3.4 The Gauss integral theorem

Let \mathcal{V} be a part of space, and $\partial\mathcal{V}$ its closed boundary, a union of surfaces. Assume again that both are mathematically well-behaved. Then the following theorem applies (Gauss):

$$\iiint_{\mathcal{V}} \operatorname{div} \mathbf{a} \, d\mathcal{V} = \iint_{\partial\mathcal{V}} \langle \mathbf{a} \cdot d\mathbf{S} \rangle = \iint_{\partial\mathcal{V}} \langle \mathbf{a} \cdot \mathbf{n} \rangle \, dS.$$



In words What is created inside a body (“sources”, divergence) must come out through its surfaces.

Usually, the orientation of surface $\partial\mathcal{V}$ is taken as positive on the outside: the normal vector \mathbf{n} of the surface points outwards.



A.4 The continuity of matter

An often-used equation in hydro- and aerodynamics is the *continuity equation*. This expresses that matter cannot just disappear or increase in amount. In the general case, the equation looks like this:

$$\operatorname{div}(\rho\mathbf{v}) + \frac{d}{dt}\rho = 0.$$

Here, the expression $\rho\mathbf{v}$ stands for *mass currents*, ρ is the matter density, \mathbf{v} is the velocity of flow. The term $\operatorname{div}(\rho\mathbf{v})$ expresses how much more matter, in a unit of time, exits the volume element than enters it, per unit of volume. The second term again, the time derivative of the density ρ , stands for the change in the amount of matter inside the volume element over time. The two terms must balance for the “matter accounting” to close.

If the moving fluid is incompressible, then ρ is constant:

$$\frac{d}{dt}\rho = 0 \implies \operatorname{div}(\rho\mathbf{v}) = \rho \operatorname{div} \mathbf{v} = 0 \implies \operatorname{div} \mathbf{v} = 0.$$

Remember, however, that $\operatorname{curl} \mathbf{v}$ does *not* necessarily vanish — so, the flow is not necessarily eddy-free — so a potential V for which $\mathbf{v} = \operatorname{grad} V$ does *not necessarily exist*.





Function spaces

B



B.1 An abstract vector space

In an *abstract vector space* we may create a *basis*, with the help of which kanta each vector can be written as a linear combination of the basis vectors: for example, if the basis, in a concrete three-dimensional space, is $\{\mathbf{e}_1, \mathbf{e}_2, \mathbf{e}_3\}$, we may write an arbitrary vector \mathbf{r} in the form

$$\mathbf{r} = r_1 \mathbf{e}_1 + r_2 \mathbf{e}_2 + r_3 \mathbf{e}_3 = \sum_{i=1}^3 r_i \mathbf{e}_i.$$

Precisely because three basis vectors (not in the same plane) are always enough, we call the ordinary (Euclidean) space three-dimensional.

In a vector space one can define a scalar product, which is a linear mapping from two vectors to one number (“bilinear form”):

$$\langle \mathbf{r} \cdot \mathbf{s} \rangle.$$

Linearity means that

$$\langle (\alpha \mathbf{r}_1 + \beta \mathbf{r}_2) \cdot \mathbf{s} \rangle = \alpha \langle \mathbf{r}_1 \cdot \mathbf{s} \rangle + \beta \langle \mathbf{r}_2 \cdot \mathbf{s} \rangle, \quad \alpha, \beta \in \mathbb{R}$$

and commutativity that

$$\langle \mathbf{r} \cdot \mathbf{s} \rangle = \langle \mathbf{s} \cdot \mathbf{r} \rangle.$$

vaihdannaisuus

If the basis vectors are *orthogonal* to each other, in other words, $\langle \mathbf{e}_i \cdot \mathbf{e}_j \rangle = 0$ if $i \neq j$, we may calculate the coefficients r_i in a simple way:

$$\mathbf{r} = \sum_{i=1}^3 r_i \mathbf{e}_i, \quad r_i = \frac{\langle \mathbf{r} \cdot \mathbf{e}_i \rangle}{\langle \mathbf{e}_i \cdot \mathbf{e}_i \rangle} = \frac{\langle \mathbf{r} \cdot \mathbf{e}_i \rangle}{\|\mathbf{e}_i\|^2}. \quad (\text{B.1})$$

If, in addition,

$$\langle \mathbf{e}_i \cdot \mathbf{e}_i \rangle = \|\mathbf{e}_i\|^2 = 1, \quad i \in \{1, 2, 3\},$$

in other words, the basis vectors are *orthonormal*, equation B.1 becomes simpler still:

$$\mathbf{r} = \sum_{i=1}^3 r_i \mathbf{e}_i, \quad r_i = \langle \mathbf{r} \cdot \mathbf{e}_i \rangle. \quad (\text{B.2})$$

The quantity

$$\|\mathbf{e}_i\| = \sqrt{\langle \mathbf{e}_i \cdot \mathbf{e}_i \rangle}$$

is called the *norm* of the vector \mathbf{e}_i .

Unlike ordinary space, which is three-dimensional, a function space is an infinite-dimensional, *abstract* vector space, that nevertheless helps us to make certain abstract, but very useful fundamentals of function theory more concrete!

B.2 The Fourier function space

B.2.1 Description

Functions can also be considered elements in a vector space. If we define the scalar product of two functions f and g as the following integral¹

$$\langle \vec{f} \cdot \vec{g} \rangle \stackrel{\text{def}}{=} \frac{1}{\pi} \int_0^{2\pi} f(x)g(x) dx, \quad (\text{B.3})$$

¹The arrows over the function designators try to psychologically instill the notion that they are “vectors”.



it is easily verified that the above requirements for a scalar product are met.

One basis in this vector space (a *function space*) is formed by the *Fourier basis functions*,

$$\begin{aligned}\vec{e}_0 &= \frac{1}{2}\sqrt{2}, \\ \vec{e}_k &= \cos kx, & k = 1, 2, 3, \dots \\ \vec{e}_{-k} &= \sin kx, & k = 1, 2, 3, \dots\end{aligned}\quad (\text{B.4})$$

This basis is *orthonormal* (proof: exercise). It is also a *complete* basis, which we shall not prove. As the number of basis vectors is countably infinite, we say that this function space is infinitely dimensional.

Now every function $f(x)$ meeting certain conditions can be expanded in the way of equation (B.2), as follows:

$$f(x) = \frac{1}{2}a_0\sqrt{2} + \sum_{k=1}^{\infty} (a_k \cos kx + b_k \sin kx),$$

— the familiar Fourier-series expansion — in which the coefficients are

$$\begin{aligned}a_0 &= \langle \vec{f} \cdot \vec{e}_0 \rangle = \frac{1}{2\pi}\sqrt{2} \int_0^{2\pi} f(x) dx = \sqrt{2} \cdot \overline{f(x)}, \\ a_k &= \langle \vec{f} \cdot \vec{e}_k \rangle = \frac{1}{\pi} \int_0^{2\pi} f(x) \cos kx dx, & k = 1, 2, 3, \dots \\ b_k &= \langle \vec{f} \cdot \vec{e}_{-k} \rangle = \frac{1}{\pi} \int_0^{2\pi} f(x) \sin kx dx, & k = 1, 2, 3, \dots\end{aligned}$$

This is the familiar way in which the coefficients of a Fourier series are calculated.

B.2.2 Example

As an example of Fourier analysis, we may take a step function on the interval $[0, 2\pi)$:

$$f(x) = \begin{cases} 0 & x \in [0, \pi) \\ 1 & x \in [\pi, 2\pi) \end{cases}.$$



We can calculate the Fourier coefficients of this function as follows:

$$\begin{aligned} a_0 &= \frac{1}{2\pi} \sqrt{2} \cdot \int_0^{2\pi} f(x) \, dx = \frac{1}{2\pi} \sqrt{2} \cdot \pi = \frac{1}{2} \sqrt{2}, \\ a_k &= \frac{1}{\pi} \int_0^{2\pi} f(x) \cos kx \, dx = \frac{1}{\pi} \int_{\pi}^{2\pi} \cos kx \, dx = \\ &= \frac{1}{\pi} \left[\frac{1}{k} \sin kx \right]_{\pi}^{2\pi} = \frac{1}{k\pi} (\sin 2k\pi - \sin k\pi) = 0, \\ b_k &= \frac{1}{\pi} \int_0^{2\pi} f(x) \sin kx \, dx = \frac{1}{\pi} \int_{\pi}^{2\pi} \sin kx \, dx = \\ &= \frac{1}{\pi} \left[-\frac{1}{k} \cos kx \right]_{\pi}^{2\pi} = \frac{1}{k\pi} (\cos k\pi - \cos 2k\pi) = \\ &= \frac{1}{k\pi} \left((-1)^k - 1 \right) = \begin{cases} 0 & \text{if } k \text{ even,} \\ -\frac{2}{k\pi} & \text{if } k \text{ odd.} \end{cases} \end{aligned}$$

In numbers: $a_0 = \frac{1}{2} \sqrt{2} = 0.70710\dots$, $b_1 = -2/\pi = -0.63662\dots$, $b_3 = -2/3\pi = -0.21220\dots$, $b_5 = -0.12732\dots$, and so forth. The expansion now becomes

$$f(x) = \frac{1}{2} \sqrt{2} a_0 + \sum_{k=1}^{\infty} b_k \sin kx = \frac{1}{2} - \frac{2}{\pi} \sum_{\substack{k=1 \\ \text{odd}}}^{\infty} \frac{\sin kx}{k}.$$

We see that it only contains sines, no cosines. This is a consequence of the function's symmetry properties.

In figure B.1 we show truncated expansions for this function:

$$f^{(K)}(x) \stackrel{\text{def}}{=} \frac{1}{2} a_0 \sqrt{2} + \sum_{k=1}^K b_k \sin kx = \frac{1}{2} - \frac{2}{\pi} \sum_{\substack{k=1 \\ \text{odd}}}^K \frac{1}{k} \sin kx, \quad (\text{B.5})$$

with K the truncation parameter.

B.2.3 Convergence

The Fourier expansion converges in the square integral sense: if we define the truncated expansion

$$f^{(K)}(x) \stackrel{\text{def}}{=} \frac{1}{2} a_0 \sqrt{2} + \sum_{k=1}^K (a_k \cos kx + b_k \sin kx),$$



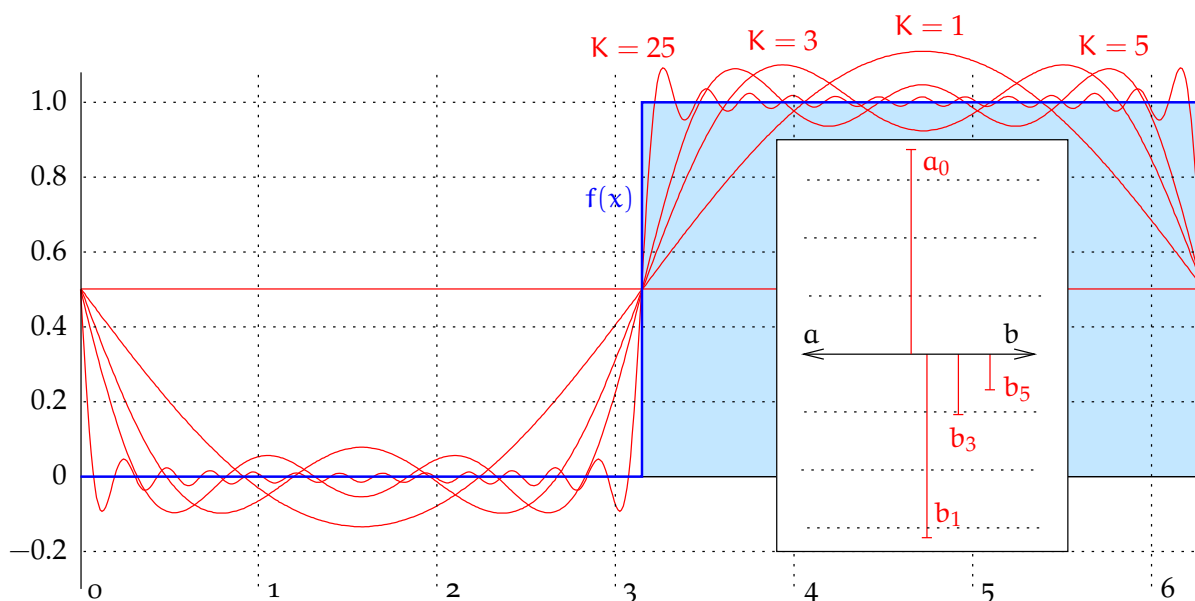


FIGURE B.1. Fourier analysis on a step function. Plotted are the truncated Fourier expansions $f^{(K)}(x)$, equation B.5, for values of K of 1, 3, 5, and 25. The inset gives the spectrum of the function.

then

$$\lim_{K \rightarrow \infty} \frac{1}{\pi} \int_0^{2\pi} (f^{(K)}(x) - f(x))^2 dx = 0.$$

This does *not* mean that, for every $x \in [0, 2\pi)$, $f^{(K)}(x) \rightarrow f(x)$ when $K \rightarrow \infty$. Looking at figure B.1, there will always remain a small neighbourhood of $x = \pi$ where the absolute difference $|f^{(K)}(x) - f(x)|$ will reach 0.5, even for arbitrarily large values of K . We say that the Fourier expansion is *convergent*, but not *uniformly* convergent.

tasainen
suppeneminen

The Fourier expansion converges pointwise “almost everywhere” in $x \in [0, 2\pi)$: at all points except for the two special points $x = 0$ and $x = \pi$. By defining $f(0) = f(\pi) = 0.5$, the expansion is made pointwise convergent everywhere.

Also, note the “shoulder” of the expansion, even for $K = 25$. This shoulder will get narrower for higher K , but not any lower, remaining at approximately 0.09. This is known as the Gibbs phenomenon.



B.3 Sturm–Liouville differential equations

B.3.1 The eigenvalue problem

In an abstract vector space we may formulate an eigenvalue problem: given a linear operator (mapping) L , we may write

$$Lx - \lambda x = 0,$$

where the problem consists of determining the *eigenvalues* λ_p for which one or more solutions or *eigenvectors* x_p exist.

In a concrete n -dimensional vector space in which there is an orthonormal basis $\{\mathbf{e}_i, i = 1, \dots, n\}$ we may write the vector

$$\mathbf{x} = \sum_{i=1}^n x_i \mathbf{e}_i,$$

and, thanks to linearity,

$$L\mathbf{x} = L\left(\sum_{i=1}^n x_i \mathbf{e}_i\right) = \sum_{i=1}^n x_i \cdot L\mathbf{e}_i.$$

On the other hand, we may write n different vectors $L\mathbf{e}_i$ on the basis $\{\mathbf{e}_j\}$ in the following way:

$$L\mathbf{e}_i = \sum_{j=1}^n a_{ij} \mathbf{e}_j, \quad i = 1, \dots, n.$$

This defines the coefficients a_{ij} , which may be collected into a size $n \times n$ matrix A .

Now substitution yields

$$L\mathbf{x} = \sum_{j=1}^n \left(\sum_{i=1}^n a_{ij} x_i\right) \mathbf{e}_j. \quad (\text{B.6})$$

Also

$$\lambda \mathbf{x} = \lambda \sum_{i=1}^n x_i \mathbf{e}_i = \sum_{j=1}^n (\lambda x_j) \mathbf{e}_j. \quad (\text{B.7})$$



By combining equations B.6 and B.7, of which all coefficients must be identical, we obtain

$$\sum_{i=1}^n a_{ij} x_i - \lambda x_j = 0, \quad j = 1, \dots, n,$$

or, as a matrix equation,

$$A\bar{x} - \lambda\bar{x} = 0, \quad (\text{B.8})$$

in which A is a matrix consisting of the coefficients a_{ji} , and \bar{x} a column vector consisting of the coefficients x_i : $\bar{x} = \begin{bmatrix} x_1 & x_2 & \cdots & x_n \end{bmatrix}^T$.

Of course equation B.8 also represents an eigenvalue problem, but now in the linear vector space \mathbb{R}^n consisting of all *coefficient vectors* \bar{x} . Every \bar{x} is the numerical representation of a vector \mathbf{x} on the chosen basis $\{\mathbf{e}_i\}$. Matrix A is again the numerical representation of operator L on the same basis.²

B.3.2 A self-adjoint operator

Let L be a linear operator in a vector space where there exists a *scalar product*, i.e., a bilinear form $\langle \mathbf{x} \cdot \mathbf{y} \rangle$ which is symmetric or commutative. vaihdannaisuus

Then L is *self-adjoint*, if for each pair of vectors \mathbf{x}, \mathbf{y} it holds that

$$\langle \mathbf{x} \cdot L\mathbf{y} \rangle = \langle L\mathbf{x} \cdot \mathbf{y} \rangle.$$

If the corresponding *matrix* A is self-adjoint, that means that

$$\langle \bar{\mathbf{x}} \cdot A\bar{\mathbf{y}} \rangle = \langle A\bar{\mathbf{x}} \cdot \bar{\mathbf{y}} \rangle,$$

i.e.,

$$\sum_{i=1}^n x_i \left(\sum_{j=1}^n a_{ij} y_j \right) = \sum_{i=1}^n \left(\sum_{j=1}^n a_{ij} x_j \right) y_i,$$

²An advantage of the numerical representations is of course that one can actually calculate with them.



which is trivially true if

$$a_{ij} = a_{ji}, \quad i, j \in 1, \dots, n \iff A = A^T.$$

In other words,

A symmetric matrix is a self-adjoint operator.

From linear algebra it is undoubtedly familiar that *the eigenvectors* x_p, x_q *belonging to different eigenvalues* $\lambda_p \neq \lambda_q$ *of a symmetric, size* $n \times n$ *matrix are mutually orthogonal:* $x_p \perp x_q$. If all eigenvalues λ_p , $p = 1, \dots, n$ are different, then the eigenvectors x_p , $p = 1, \dots, n$ will constitute a *complete orthogonal basis*³ in the vector space \mathbb{R}^n .

The proof is not hard. We start from the equation for the eigenvalue problem for eigenvectors and -values x_p, λ_p :

$$Lx_p = \lambda_p x_p,$$

and multiply from the left by vector x_q :

$$\langle x_q \cdot Lx_p \rangle = \lambda_p \langle x_q \cdot x_p \rangle.$$

Similarly for eigenvectors and -values x_q, λ_q multiplied from the left by vector x_p :

$$\langle x_p \cdot Lx_q \rangle = \lambda_q \langle x_p \cdot x_q \rangle.$$

If L is self-adjoint, then

$$\langle x_q \cdot Lx_p \rangle = \langle Lx_q \cdot x_p \rangle = \langle x_p \cdot Lx_q \rangle \implies \lambda_p \langle x_q \cdot x_p \rangle = \lambda_q \langle x_p \cdot x_q \rangle.$$

It follows that

$$(\lambda_p - \lambda_q) \langle x_p \cdot x_q \rangle = 0.$$

Remember that the scalar product is symmetric. If $\lambda_p \neq \lambda_q$, we thus must have $\langle x_p \cdot x_q \rangle = 0$, or $x_p \perp x_q$, what was to be proven.

³Actually the eigenvectors may be arbitrarily re-scaled: if x is an eigenvector, then also $e \stackrel{\text{def}}{=} x/\|x\|$ is. Thus we obtain an *orthonormal basis*.



Example *The variance matrix of location in the plane.* The variance matrix of the co-ordinates of point P in the plane is

$$\text{Var}\{\bar{\mathbf{x}}_P\} = \text{Var}\left\{\begin{bmatrix} \bar{x}_P \\ \bar{y}_P \end{bmatrix}\right\} = \Sigma_{PP} = \begin{bmatrix} \sigma_x^2 & \sigma_{xy} \\ \sigma_{xy} & \sigma_y^2 \end{bmatrix},$$

a *symmetric* matrix. Here, σ_x^2 and σ_y^2 are the variances, or squares of the mean errors, of the x and y co-ordinates, whereas σ_{xy} is the covariance between the co-ordinates.

The eigenvalues of this matrix Σ_{PP} are the solutions of the *characteristic equation*

$$\det \begin{bmatrix} \sigma_x^2 - \lambda & \sigma_{xy} \\ \sigma_{xy} & \sigma_y^2 - \lambda \end{bmatrix} = 0,$$

or

$$(\sigma_x^2 - \lambda)(\sigma_y^2 - \lambda) - \sigma_{xy}^2 = 0.$$

This yields

$$\begin{aligned} \lambda_{1,2} &= \frac{1}{2}(\sigma_x^2 + \sigma_y^2) \pm \frac{1}{2}\sqrt{[\sigma_x^2 + \sigma_y^2]^2 - 4[\sigma_x^2\sigma_y^2 - \sigma_{xy}^2]} = \\ &= \frac{1}{2}(\sigma_x^2 + \sigma_y^2) \pm \frac{1}{2}\sqrt{[\sigma_x^2 - \sigma_y^2]^2 + 4\sigma_{xy}^2}. \end{aligned}$$

The variance matrix has a *variance or error ellipse*. The semi-lengths of its principal axes are $\sqrt{\lambda_1}$ and $\sqrt{\lambda_2}$, and the directions of the principal axes are the eigenvectors of Σ_{PP} : $\bar{\mathbf{x}}_1$ and $\bar{\mathbf{x}}_2$, mutually orthogonal. If the co-ordinate axes are turned into the directions of $\bar{\mathbf{x}}_{1,2}$, the matrix Σ_{PP} will assume the form

$$\Sigma'_{PP} = \begin{bmatrix} \sigma_{x'}^2 & 0 \\ 0 & \sigma_{y'}^2 \end{bmatrix} = \begin{bmatrix} \lambda_1 & 0 \\ 0 & \lambda_2 \end{bmatrix}.$$

The sum of the eigenvalues (and the *trace* of the matrix), $\lambda_1 + \lambda_2 = \sigma_x^2 + \sigma_y^2$, is an *invariant* called the *point variance*.



B.3.3 Self-adjoint differential equations

A function space also features self-adjoint or “symmetric” differential equations. In fact, the most famous equations of physics are of this type.

Take a good look at, for example, the oscillation equation, in which $x(t)$ is the position as a function of time:

$$\frac{d^2}{dt^2}x(t) + \omega^2x(t) = 0. \quad (\text{B.9})$$

The solution has the general form (α amplitude, ϕ phase constant)

$$x(t) = \alpha \sin(\omega t - \phi).$$

On the interval $t \in [0, T]$ we require *periodicity*:

$$x(0) = x(T), \quad \left. \frac{d}{dt}x \right|_{x=0} = \left. \frac{d}{dt}x \right|_{x=T}.$$

These *boundary conditions* are an essential part of being self-adjoint. Then, a solution is found only for certain values of ω — *quantisation*.

Equation B.9 is an *eigenvalue problem*, form-wise:

$$Lx + \omega^2x = 0,$$

in which the operator is

$$L = \frac{d^2}{dt^2}.$$

We first show that this operator is on the interval $[0, T]$ *self-adjoint*. If the scalar product is defined as follows:

$$\langle \vec{x} \cdot \vec{y} \rangle \stackrel{\text{def}}{=} \int_0^T x(t)y(t) dt,$$



it holds that (integration by parts):

$$\begin{aligned}\langle \vec{x} \cdot L \vec{y} \rangle &= \int_0^T x(t) \frac{d^2 y(t)}{dt^2} dt = \\ &= \left[x(t) \frac{dy(t)}{dt} \right]_0^T - \int_0^T \frac{d}{dt} x(t) \frac{d}{dt} y(t) dt, \\ \langle L \vec{x} \cdot \vec{y} \rangle &= \int_0^T \frac{d^2 x(t)}{dt^2} y(t) dt = \\ &= \left[\frac{dx(t)}{dt} y(t) \right]_0^T - \int_0^T \frac{d}{dt} x(t) \frac{d}{dt} y(t) dt.\end{aligned}$$

As, on the right-hand side, the first terms vanish and the second terms are identical, it follows that

$$\langle \vec{x} \cdot L \vec{y} \rangle = \langle L \vec{x} \cdot \vec{y} \rangle,$$

which was to be proven.

Self-adjoint operators have eigenvalues and eigenvectors, in this case *functions*, that are mutually orthogonal for different values of ω .⁴ For the oscillation equation with the above periodicity conditions they are just the solution functions

$$\sin(\omega_k t - \phi) = \sin\left(\frac{2\pi k}{T} t - \phi\right), \quad (\text{B.10})$$

in which the frequency

$$\omega_k = \frac{2\pi k}{T}$$

is quantised by a “quantum number” $k \in \mathbb{N}$.

If we let $T \rightarrow \infty$, the frequencies ω_k get closer and closer to each other, and in the end morph into a continuum.

⁴In fact, for the same value ω_k there exist two mutually orthogonal periodic solutions,

$$\sin \omega_k t = \sin \frac{2\pi k t}{T}, \quad \cos \omega_k t = \cos \frac{2\pi k t}{T}.$$

Any linear combination of these is a valid solution as well, and is of the general form **B.10**.



In physics there is a broad class of differential equations that are self-adjoint in some function space. The class is known as “Sturm⁵–Liouville⁶ type problems”. It includes the oscillation equation, Legendre’s equation, Bessel’s equation, and many more. Every one of them generates, in a natural way, its own set of mutually orthogonal functions that serve as the basis functions for the general solution of many partial differential equations.



B.4 Legendre polynomials

The ordinary Legendre polynomials $P_n(t)$ also constitute a basis in a function space, with the scalar product definition

$$\langle \vec{f} \cdot \vec{g} \rangle \stackrel{\text{def}}{=} \int_{-1}^{+1} f(t)g(t) dt.$$

They do not however constitute an *orthonormal* basis, but only an *orthogonal* one:

$$\|\vec{P}_n\|^2 = \langle \vec{P}_n \cdot \vec{P}_n \rangle = \int_{-1}^{+1} P_n^2(t) dt = \frac{2}{2n+1}.$$



B.5 Spherical harmonics

On the surface of a *sphere*, all functions can also be considered elements of a function space. Every function meeting certain well-behavedness requirements — like integrability — is an element. The functions

$$\begin{aligned} R_{nm}(\phi, \lambda) &= P_{nm}(\sin \phi) \cos m\lambda, & n &= 0, 1, 2, \dots, m = 0, \dots, n, \\ S_{nm}(\phi, \lambda) &= P_{nm}(\sin \phi) \sin m\lambda, & n &= 0, 1, 2, \dots, m = 1, \dots, n, \end{aligned}$$

together form a *complete basis* for this vector space in such a way that every function can be written as an — if necessary infinite — linear

⁵Jacques Charles François Sturm **FRS FAS** (1803–1855) was an eminent French mathematician, one of the 72 names engraved on the Eiffel Tower. [Eiffel Tower, 72 names.](#)

⁶Joseph Liouville **FRS FRSE FAS** (1809–1882) was an eminent French mathematician.



combination of these basis functions. The situation is analogous to three-dimensional space, where a complete basis consists of three vectors not in the same plane.

An alternative, more compact way of writing this is

$$Y_{nm}(\phi, \lambda) = \begin{cases} P_{nm}(\sin \phi) \cos m\lambda & \text{if } m \geq 0, \\ P_{n|m|}(\sin \phi) \sin |m|\lambda & \text{if } m < 0, \end{cases}$$

for values $n = 0, 1, 2, \dots$, $m = -n, \dots, n$.

In this function space, a *scalar product* is defined:

$$\langle \vec{V} \cdot \vec{W} \rangle = \frac{1}{4\pi} \iint_{\sigma} V(\phi, \lambda) W(\phi, \lambda) d\sigma,$$

in which σ is the surface of the unit sphere (“directional sphere”, or even “celestial sphere”), $d\sigma = \cos \phi d\phi d\lambda$ is a surface element of the sphere, and $\cos \phi$ is the determinant of Jacobi of the co-ordinates (ϕ, λ) .

According to this definition, we can show that two different functions, Y_{nm} and Y_{sr} , are orthogonal with respect to each other:

$$\langle \vec{Y}_{nm} \cdot \vec{Y}_{sr} \rangle = \frac{1}{4\pi} \iint_{\sigma} Y_{nm}(\phi, \lambda) Y_{sr}(\phi, \lambda) d\sigma = 0$$

if $n \neq s$ or $m \neq r$.

The basis $\{ \vec{Y}_{nm}, n = 0, 1, 2, \dots, m = -n, \dots, n \}$, is *orthogonal* but not *orthonormal*: the “length” of the vectors differs from unity.

$$\begin{aligned} \|\vec{Y}_{nm}\|^2 &= \langle \vec{Y}_{nm} \cdot \vec{Y}_{nm} \rangle = \\ &= \frac{1}{4\pi} \iint_{\sigma} Y_{nm}^2(\phi, \lambda) d\sigma = \begin{cases} \frac{1}{2n+1} & \text{if } m = 0, \\ \frac{1}{2(2n+1)} \frac{(n+|m|)!}{(n-|m|)!} & \text{if } m \neq 0, \end{cases} \end{aligned}$$

see [Heiskanen and Moritz \(1967, equation 1-69\)](#). Proving this orthogonality is not straightforward.



If we now divide the functions Y_{nm} (or, equivalently, R_{nm}, S_{nm}) by the square roots of the above factors, we obtain the *fully normalised* surface spherical harmonics \bar{Y}_{nm} , for which it holds that

$$\left\| \vec{\bar{Y}}_{nm} \right\|^2 = \frac{1}{4\pi} \iint_{\sigma} \bar{Y}_{nm}^2(\phi, \lambda) d\sigma = 1.$$

With those it is again easy to calculate the coefficients \bar{f}_{nm} of a given general function on the sphere $f(\phi, \lambda)$ (the overline means that these are fully normalised coefficients):

$$\bar{f}_{nm} = \left\langle \vec{f} \cdot \vec{\bar{Y}}_{nm} \right\rangle = \frac{1}{4\pi} \iint_{\sigma} f(\phi, \lambda) \bar{Y}_{nm}(\phi, \lambda) d\sigma. \quad (\text{B.11})$$

This is a straightforward *projection* on the unit vectors of the basis (geometric analogue).

In the above integral, $f(\phi, \lambda)$ is the function f on the Earth's surface: if the radius of the spherical Earth is R , then $f(\phi, \lambda) = f(\phi, \lambda, R)$.

The fully normalised equation corresponding to expansion 2.11 is

$$V(\phi, \lambda, r) = \sum_{n=0}^{\infty} \frac{1}{r^{n+1}} \sum_{m=0}^n \bar{P}_{nm}(\sin \phi) (\bar{a}_{nm} \cos m\lambda + \bar{b}_{nm} \sin m\lambda).$$

We may also write

$$\bar{Y}_{nm}(\phi, \lambda) = \begin{cases} \bar{P}_{nm}(\sin \phi) \cos m\lambda & \text{if } m \geq 0, \\ \bar{P}_{n|m|}(\sin \phi) \sin |m|\lambda & \text{if } m < 0, \end{cases}$$

which corresponds to the definition of the fully normalised Legendre functions:

$$\begin{aligned} \bar{P}_{n0}(\sin \phi) &= \sqrt{2n+1} P_{n0}(\sin \phi), \\ \bar{P}_{nm}(\sin \phi) &= \sqrt{2(2n+1) \frac{(n-m)!}{(n+m)!}} P_{nm}(\sin \phi), \quad m > 0. \end{aligned}$$



Now, the above equation for the potential becomes

$$V(\phi, \lambda, r) = \sum_{n=0}^{\infty} \frac{1}{r^{n+1}} \sum_{m=-n}^n \bar{v}_{nm} \bar{Y}_{nm}(\phi, \lambda),$$

in which

$$\bar{v}_{nm} = \begin{cases} \bar{a}_{nm} & \text{if } m \geq 0, \\ \bar{b}_{n|m|} & \text{if } m < 0. \end{cases}$$

On the sphere $r = R$ this becomes

$$V(\phi, \lambda, R) = \sum_{n=0}^{\infty} \frac{1}{R^{n+1}} \sum_{m=-n}^n \bar{v}_{nm} \bar{Y}_{nm}(\phi, \lambda),$$

from which by orthogonal projection (equation B.11) follows

$$\bar{v}_{nm} = R^{n+1} \left\langle \vec{V} \cdot \vec{Y}_{nm} \right\rangle = \frac{R^{n+1}}{4\pi} \iint_{\sigma} V(\phi, \lambda, R) \bar{Y}_{nm}(\phi, \lambda) d\sigma$$

or

$$\begin{aligned} \bar{a}_{nm} &= \frac{R^{n+1}}{4\pi} \iint_{\sigma} V(\phi, \lambda, R) \bar{P}_{nm}(\phi, \lambda) \cos m\lambda d\sigma, \\ \bar{b}_{nm} &= \frac{R^{n+1}}{4\pi} \iint_{\sigma} V(\phi, \lambda, R) \bar{P}_{nm}(\phi, \lambda) \sin m\lambda d\sigma. \end{aligned}$$



Self-test questions

1. The identity $\langle \mathbf{r} \cdot \mathbf{s} \rangle = \langle \mathbf{s} \cdot \mathbf{r} \rangle$, for two elements \mathbf{r} and \mathbf{s} of a vector space, expresses the property of linearity | commutativity | associativity.



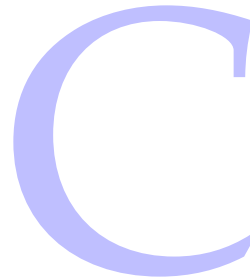
Exercise B – 1: Orthonormality of the Fourier basis functions

Show the orthonormality of the Fourier basis functions, equation B.4 by deriving their scalar products by equation B.3.





Why does FFT work?



FFT is a factorisation method for computing the discrete Fourier transform that spectacularly reduces the number of calculations needed and speeds up the calculation. It requires the number of grid points to be a factorisable number.

There are alternatives in choosing precisely which **FFT** method to use. The fastest **FFT** requires a grid the number of points of which is a power of 2. The size of the grid is then $2^n \times 2^m$. Alternative, “mixed-radix” methods may also be considered and perform well if the grid size is something like 360×480 , for example $N = 360 = 2 \times 2 \times 2 \times 3 \times 3 \times 5$. If the grid size is a prime number, **FFT** is no better than the ordinary discrete Fourier transform.

If the function $f(x)$ is given on the interval $x \in [0, L)$, on an equi-spaced grid, $x_k = kL/N$, as values $f_k = f(x_k)$, $k = 0, \dots, N - 1$, the discrete Fourier transform in one dimension is

$$\mathcal{F}\{f(x)\} = F(\tilde{\nu}),$$

in which

$$F(\tilde{\nu}_j) = \frac{1}{N} \sum_{k=0}^{N-1} f(x_k) \exp\left(-2\pi i \frac{j k}{N}\right), \quad j = 0, \dots, N - 1. \quad (\text{C.1})$$

The frequency argument, spatial frequency or wave number, $\tilde{\nu}_j =$

j/L , $j = 0, \dots, N-1$ is defined on the interval¹ $[0, (N-1)/L]$. i is the imaginary unit: $i^2 = -1$. We use $\exp(x)$ to denote e^x .

Correspondingly, the inverse discrete Fourier transform,

$$\mathcal{F}^{-1}\{F(\tilde{v})\} = f(x),$$

is

$$f(x_k) = \sum_{j=0}^{N-1} F(\tilde{v}_j) \exp\left(2\pi i \frac{jk}{N}\right), \quad k = 0, \dots, N-1. \quad (\text{C.2})$$

FFT is just a brutally efficient way of computing both these equations **C.1** and **C.2**. A brute-force calculation of these formulas requires an order of N^2 “standard operations”, each of them a single multiplication plus a single addition or subtraction. If N is even, we may write

$$\begin{aligned} F(\tilde{v}_j) &= \frac{1}{N} \left(\sum_{k=0}^{\frac{1}{2}N-1} f_k \exp\left(-2\pi i \frac{jk}{N}\right) + \sum_{k=\frac{1}{2}N}^{N-1} f_k \exp\left(-2\pi i \frac{jk}{N}\right) \right) = \\ &= \frac{1}{N} \left(\sum_{k=0}^{\frac{1}{2}N-1} f_k \exp\left(-2\pi i \frac{jk}{N}\right) + \exp\left(-2\pi i j \frac{1}{2} \frac{N}{N}\right) \sum_{k'=0}^{\frac{1}{2}N-1} f_{k'+\frac{1}{2}N} \exp\left(-2\pi i \frac{jk'}{N}\right) \right) = \\ &= \frac{1}{N} \left(\sum_{k=0}^{\frac{1}{2}N-1} f_k \exp\left(-2\pi i \frac{jk}{N}\right) + \exp(-\pi i j) \sum_{k=0}^{\frac{1}{2}N-1} f_{k'+\frac{1}{2}N} \exp\left(-2\pi i \frac{jk}{N}\right) \right) = \\ &= \frac{1}{N} \sum_{k=0}^{\frac{1}{2}N-1} \left[f_k \pm f_{k+\frac{1}{2}N} \right] \exp\left(-2\pi i \frac{jk}{N}\right), \quad \left\{ \begin{array}{l} + \text{ if } j \text{ even} \\ - \text{ if } j \text{ odd} \end{array} \right\} \quad (\text{C.3}) \end{aligned}$$

the computation of which sum requires only $N \cdot \frac{1}{2}N$ multiplications and additions, not counting pre-calculations.

¹Alternatively, the interval of definition could be chosen as $[-\frac{1}{2}N/L, (\frac{1}{2}N-1)/L]$. This is done by mapping $\tilde{v}_j \rightarrow \tilde{v}_j - N/L$, or $j \rightarrow j - N$, for $j > \frac{1}{2}N-1$. This has the merit of placing the frequency zero in the middle. It does not materially change anything, as it simply multiplies $F(\tilde{v}_j)$ with unity: $\exp(-2\pi i Nk/N) = \exp(-2\pi i k) = 1$, the periodicity property of the discrete Fourier transform.



Here we used Euler's identity $\exp(-\pi i) = -1$, so $e^{-\pi i j} = (e^{-\pi i})^j = (-1)^j$, either $+1$ or -1 .² The expression in square brackets, for each $k = 0, 1, \dots, \frac{1}{2}N - 1$, is either a summation, for even values of j , or a subtraction, for odd values of j . In total, $\frac{1}{2}N$ sums and $\frac{1}{2}N$ differences are pre-calculated. Also the \exp expressions are pre-calculated into a lookup table.

Altogether some $\frac{1}{2}N^2$ standard operations are needed, half the original number.

Equation C.3 is itself recognised as a Fourier series, but the number of support points is only $\frac{1}{2}N$ instead of N . If $\frac{1}{2}N$ is also even, we may repeat the above trick, resulting in an expression requiring only an order of $\frac{1}{4}N^2$ operations. Lather, rinse, repeat, and the number of operations becomes $\frac{1}{8}N^2, \frac{1}{16}N^2, \frac{1}{32}N^2$, etc. . . . A more precise analysis shows that if N is a power of 2, the whole discrete Fourier transform may be computed in order $N \times \log N$ operations!

In the literature, smart algorithms are found implementing the method described, for example `fftw` ("Fastest Fourier Transform in the West", [FFTW Home Page](#); Frigo and Johnson, 2005).

²These values are called the "twiddle factors".





Helmert condensation

D

In order to derive the equation for Helmert condensation, we derive the equation for the potential of the topography:

$$V_{\text{top}}(\phi, \lambda, r) = G \iiint_{\text{top}} \frac{\rho(\phi', \lambda', r')}{\ell(\psi, r, r')} dV' \approx G\rho \iiint_{\text{top}} \frac{1}{\ell(\psi, r, r')} dV',$$

in which ψ is the geocentric angular distance between the evaluation point (ϕ, λ, r) and the data point (ϕ', λ', r') . We assume a standard density ρ .

We similarly derive the equation for the potential of the condensation layer:

$$V_{\text{cond}}(\phi, \lambda, r) = G\rho \iiint_{\text{cond}} \frac{1}{\ell(\psi, r, R)} dV'.$$

We integrate in spherical co-ordinates:

$$\begin{aligned} \iiint_{\text{top}} \frac{1}{\ell(\psi, r, r')} dV' &= \int_{\sigma} \int_R^{R+H(\phi', \lambda')} \frac{1}{\ell(\psi, r, r')} (r')^2 dr' d\sigma', \\ \iiint_{\text{cond}} \frac{1}{\ell(\psi, r, R)} dV' &= \int_{\sigma} \frac{1}{\ell(\psi, r, R)} \int_R^{R+H(\phi', \lambda')} (r')^2 dr' d\sigma' \approx \\ &\approx R^2 \int_{\sigma} \frac{1}{\ell(\psi, r, R)} H(\phi', \lambda') \left(1 + \frac{H(\phi', \lambda')}{R} + \frac{H^2(\phi', \lambda')}{3R^2} \right) d\sigma', \end{aligned}$$

with H the height of the topography.

D.1 The exterior potential of the topography

In order to derive the exterior potential of the topography, we use the expansion of the inverse distance (equation 8.6):

$$\frac{1}{\ell} = \sum_{n=0}^{\infty} \frac{1}{r'} \left(\frac{r'}{r} \right)^{n+1} P_n(\cos \psi) = \sum_{n=0}^{\infty} \frac{1}{r} \left(\frac{r'}{r} \right)^n P_n(\cos \psi).$$

This expansion converges uniformly¹ with respect to ψ if $r > r'$. In the following, we shall assume convergence throughout, dangerous as that may be especially close to a jagged topographic surface. For the philosophically inclined, see [Moritz \(1980\)](#).

Substitution yields

$$\begin{aligned} V_{\text{top}}^{\text{ext}}(\phi, \lambda, r) &= G\rho \iiint_{\text{top}} \sum_{n=0}^{\infty} \frac{1}{r} \left(\frac{r'}{r} \right)^n P_n(\cos \psi) dV' = \\ &= G\rho \iint_{\sigma} \left(\int_{\text{R}}^{\text{R}+\text{H}(\phi', \lambda')} \sum_{n=0}^{\infty} \frac{1}{r} \left(\frac{r'}{r} \right)^n (r')^2 dr' \right) P_n(\cos \psi) d\sigma' = \\ &= G\rho \iint_{\sigma} \left[\sum_{n=0}^{\infty} \frac{1}{r^{n+1}} \frac{1}{n+3} (r')^{n+3} \right]_{r'=R}^{\text{R}+\text{H}} P_n(\cos \psi) d\sigma' = \\ &= G\rho \iint_{\sigma} \sum_{n=0}^{\infty} \frac{1}{r^{n+1}} \frac{1}{n+3} \left((\text{R}+\text{H})^{n+3} - \text{R}^{n+3} \right) P_n(\cos \psi) d\sigma'. \end{aligned}$$

Here, we shall expand the following term into a Taylor series:

¹Uniform convergence means that, given r and r' , for every $\epsilon > 0$ there is an N_{min} for which

$$\left| \frac{1}{\ell} - \frac{1}{r} \sum_{n=0}^N \left(\frac{r'}{r} \right)^n P_n(\cos \psi) \right| < \epsilon$$

for all $N > N_{\text{min}}$, and for all values of ψ . This is a stronger property than mere convergence.



$$\begin{aligned}
 (R + H)^{n+3} &= \\
 &= R^{n+3} \left(1 + (n+3) \frac{H}{R} + \frac{(n+3)(n+2)}{2} \frac{H^2}{R^2} + \frac{(n+3)(n+2)(n+1)}{2 \cdot 3} \frac{H^3}{R^3} + \dots \right).
 \end{aligned}
 \tag{D.1}$$

Substitution yields

$$\begin{aligned}
 V_{\text{top}}^{\text{ext}}(\phi, \lambda, r) &= G\rho R^2 \cdot \\
 &\cdot \iint_{\sigma} \sum_{n=0}^{\infty} \left(\frac{R}{r} \right)^{n+1} \left(\frac{H}{R} + \frac{1}{2}(n+2) \frac{H^2}{R^2} + \frac{1}{6}(n+2)(n+1) \frac{H^3}{R^3} + \dots \right) P_n(\cos \psi) \, d\sigma'.
 \end{aligned}
 \tag{D.2}$$

This is thus the *exterior potential* of the topography, or, inside the topographic masses, the *harmonic downwards continuation* of the exterior potential, assuming that this is mathematically possible (in the case of mountainous topography, generally not) and does not diverge.

D.2 The interior potential of the topography

In the same way we may derive the equation for the interior potential of the topography, i.e., the masses between the sea level and terrain surface. For the spatial distance ℓ between those points we use the *interior expansion*, equation 8.6, valid for $r < r'$:

$$\frac{1}{\ell} = \frac{1}{r} \sum_{n=0}^{\infty} \left(\frac{r}{r'} \right)^{n+1} P_n(\cos \psi).$$

Substitute:



$$\begin{aligned}
V_{\text{top}}^{\text{int}}(\phi, \lambda, r) &= G\rho \iiint_{\text{top}} \frac{1}{r} \sum_{n=0}^{\infty} \left(\frac{r}{r'}\right)^{n+1} P_n(\cos \psi) dV' = \\
&= G\rho \iint_{\sigma} \left(\int_R^{R+H(\phi', \lambda')} \frac{1}{r} \sum_{n=0}^{\infty} \left(\frac{r}{r'}\right)^{n+1} (r')^2 dr' \right) P_n(\cos \psi) d\sigma' = \\
&= G\rho \iint_{\sigma} \left[\sum_{\substack{n=0 \\ n \neq 2}}^{\infty} r^n \left(-\frac{(r')^{-(n-2)}}{n-2} \right) + r^2 \ln r' \right]_{r'=R}^{R+H(\phi', \lambda')} P_n(\cos \psi) d\sigma' = \\
&= G\rho \iint_{\sigma} \sum_{\substack{n=0 \\ n \neq 2}}^{\infty} \frac{r^n}{n-2} \left(R^{-(n-2)} - (R+H)^{-(n-2)} + r^2 \ln \frac{R+H}{R} \right) P_n(\cos \psi) d\sigma'.
\end{aligned}$$

Here we use the Taylor expansion

$$\begin{aligned}
(R+H)^{-(n-2)} &= \\
&= R^{-(n-2)} \left(1 - (n-2) \frac{H}{R} + \frac{(n-2)(n-1)H^2}{2R^2} - \frac{(n-2)(n-1)nH^3}{2 \cdot 3R^3} + \dots \right).
\end{aligned}$$

Also, the special case $n = 2$,

$$\begin{aligned}
r^2 \ln \frac{R+H}{R} &= r^2 \left(\frac{H}{R} - \frac{1}{2} \frac{H^2}{R^2} + \frac{1}{3} \frac{H^3}{R^3} - \frac{1}{4} \frac{H^4}{R^4} + \dots \right) = \\
&= \frac{r^n}{R^{n-2}} \left(\frac{H}{R} - \frac{n-1}{2} \frac{H^2}{R^2} + \frac{(n-1)n}{2 \cdot 3} \frac{H^3}{R^3} - \frac{(n-1)n(n+1)}{2 \cdot 3 \cdot 4} \frac{H^4}{R^4} + \dots \right),
\end{aligned}$$

is cleanly included into the following expression obtained by substitution:

$$\begin{aligned}
V_{\text{top}}^{\text{int}}(\phi, \lambda, r) &= \\
&= G\rho \iint_{\sigma} \sum_{n=0}^{\infty} \frac{r^n}{R^{n-2}} \left(\frac{H}{R} - \frac{1}{2} (n-1) \frac{H^2}{R^2} + \frac{1}{6} (n-1)n \frac{H^3}{R^3} - \dots \right) P_n(\cos \psi) d\sigma'. \quad (\text{D.3})
\end{aligned}$$

D.3 The exterior potential of the condensation layer

This is derived by specialising equation D.2 to the case $H \rightarrow 0$, but nevertheless $\rho \rightarrow \infty$, so that $\kappa = \rho H$ remains finite. In this limit, all



terms containing H^2 , H^3 and higher powers go to zero. The result is then

$$\begin{aligned} V_{\text{cond}}^{\text{ext}}(\phi, \lambda, r) &= G\rho R^2 \iint_{\sigma} \sum_{n=0}^{\infty} \left(\frac{R}{r}\right)^{n+1} \frac{H}{R} P_n(\cos \psi) d\sigma' = \\ &= GR \iint_{\sigma} \sum_{n=0}^{\infty} \left(\frac{R}{r}\right)^{n+1} \kappa P_n(\cos \psi) d\sigma'. \end{aligned}$$

Earlier on we had a more precise formula 6.4 for κ on the surface of a spherical Earth:

$$\kappa = \rho H \left(1 + \frac{H}{R} + \frac{1}{3} \frac{H^2}{R^2}\right).$$

By substituting this into the previous, we obtain

$$V_{\text{cond}}^{\text{ext}} = G\rho R^2 \iint_{\sigma} \sum_{n=0}^{\infty} \left(\frac{R}{r}\right)^{n+1} \left(\frac{H}{R} + \frac{H^2}{R^2} + \frac{1}{3} \frac{H^2}{R^2}\right) P_n(\cos \psi) d\sigma'. \quad (\text{D.4})$$



D.4 Total potential of Helmert condensation

This is obtained by subtracting equations D.4 and D.2 from each other. The result — which applies in the *exterior* space² — is

$$\begin{aligned} \delta V_{\text{Helmert}}^{\text{ext}}(\phi, \lambda, r) &= V_{\text{cond}}^{\text{ext}}(\phi, \lambda, r) - V_{\text{top}}^{\text{ext}}(\phi, \lambda, r) = -G\rho R^2 \cdot \\ &\cdot \iint_{\sigma} \sum_{n=0}^{\infty} \left(\frac{R}{r}\right)^{n+1} \left(\left(\frac{1}{2}(n+2) - 1\right) \frac{H^2}{R^2} + \left(\frac{1}{6}(n+2)(n+1) - \frac{1}{3}\right) \frac{H^3}{R^3} + \dots \right) \cdot \\ &\cdot P_n(\cos \psi) d\sigma' = \\ &= -G\rho \iint_{\sigma} \sum_{n=0}^{\infty} \left(\frac{R}{r}\right)^{n+1} \left(\frac{1}{2}nH^2 + \frac{1}{6}n(n+3) \frac{H^3}{R} + \dots \right) P_n(\cos \psi) d\sigma'. \end{aligned}$$

Often, we define the *degree constituents* of powers of height H (compare the degree constituent equation 3.8), as follows:

$$H_n^{\nu}(\phi, \lambda) = \frac{2n+1}{4\pi} \iint_{\sigma} H^{\nu}(\phi', \lambda') P_n(\cos \psi) d\sigma', \quad (\text{D.5})$$

²Theoretically speaking, the exterior space is the space outside a geocentric sphere that encloses all of the Earth's topography. Practice is less restrictive.



with which it holds that

$$H^v(\phi, \lambda) = \sum_{n=0}^{\infty} H_n^v(\phi, \lambda).$$

Then

$$\begin{aligned} \delta V_{\text{Helmert}}^{\text{ext}} &= \\ &= -4\pi G\rho \sum_{n=0}^{\infty} \left(\frac{R}{r}\right)^{n+1} \frac{1}{2n+1} \left(\frac{1}{2}nH_n^2 + \frac{1}{6}n(n+3)\frac{H_n^3}{R} + \dots\right). \end{aligned}$$

If the topography is *constant*, all terms vanish for which $n \neq 0$. In the above expansion, in that case the first and second terms also vanish. In this case $n = 0$, the following terms do not even exist: the expansion **D.1** is the binomial expansion

$$(R + H)^3 = R^3 + 3R^2H + 3RH^2 + H^3.$$

So

$$\delta V_{\text{Helmert}}^{\text{ext}} = 0$$

as was to be expected according to section 1.4: condensing a spherical shell will not change the exterior field.

D.4.1 The gravity effect of Helmert condensation

Let us calculate the effect of the Helmert condensation potential on *gravity anomalies*:

$$\begin{aligned} \Delta g_{\text{Helmert}}^{\text{ext}} &= -\frac{\partial}{\partial r} \delta V_{\text{Helmert}}^{\text{ext}} - \frac{2}{r} \delta V_{\text{Helmert}}^{\text{ext}} \approx \\ &\approx 4\pi G\rho \sum_{n=0}^{\infty} \frac{1}{2n+1} \left(\frac{-(n+1)}{r} + \frac{2}{r}\right) \left(\frac{R}{r}\right)^{n+1} \left(\frac{1}{2}nH_n^2 + \frac{1}{6}n(n+3)\frac{H_n^3}{R} + \dots\right) = \\ &= -4\pi G\rho \cdot \frac{1}{r} \sum_{n=0}^{\infty} \frac{n-1}{2n+1} \left(\frac{R}{r}\right)^{n+1} \left(\frac{1}{2}nH_n^2 + \frac{1}{6}n(n+3)\frac{H_n^3}{R} + \dots\right). \quad (\text{D.6}) \end{aligned}$$

Now, $n = 1$ also gives a zero result, expected as gravity anomalies do not contain any constituents of degree number 1.



Result D.6 is approximate and not to be used on or close to the topography. Note the strong dependence upon n : the gravity effect of Helmert condensation is dominated by short wavelengths, i.e., the local features of the topography.

D.4.2 The interior potential of Helmert condensation

This quantity is evaluated *on the level of the geoid*. It represents the *indirect effect* of Helmert condensation, the shift of the geoid surface in space caused by the mass shifts. Subtract equations D.4 and D.3 from each other:

$$\begin{aligned} \delta V_{\text{Helmert}}^{\text{int}}(\phi, \lambda, R) &= V_{\text{cond}}^{\text{ext}}(\phi, \lambda, R) - V_{\text{top}}^{\text{int}}(\phi, \lambda, R) = \\ &= G\rho R^2 \iint_{\sigma} \sum_{n=0}^{\infty} \left(\frac{H}{R} + \frac{H^2}{R^2} + \frac{1}{3} \frac{H^3}{R^3} \right) P_n(\cos \psi) d\sigma' - \\ &\quad - G\rho R^2 \iint_{\sigma} \sum_{n=0}^{\infty} \left(\frac{H}{R} - \frac{1}{2} (n-1) \frac{H^2}{R^2} + \frac{1}{6} (n-1) n \frac{H^3}{R^3} - \dots \right) P_n(\cos \psi) d\sigma' = \\ &= G\rho \iint_{\sigma} \sum_{n=0}^{\infty} \left(\frac{1}{2} (n+1) H^2 - \frac{1}{6} (n-2) (n+1) \frac{H^3}{R} + \dots \right) P_n(\cos \psi) d\sigma'. \end{aligned}$$

Using again the definition of the degree constituents of the powers of height H , equation D.5, we obtain

$$\delta V_{\text{Helmert}}^{\text{int}} = 4\pi G\rho \sum_{n=0}^{\infty} \frac{n+1}{2n+1} \left(\frac{1}{2} H_n^2 - \frac{1}{6} (n-2) \frac{H_n^3}{R} + \dots \right),$$

from which one obtains with Bruns equation 5.2 the *indirect effect* of Helmert condensation:

$$\begin{aligned} \delta N_{\text{Helmert}} &= \frac{\delta V_{\text{Helmert}}^{\text{int}}}{\gamma} = \\ &= \frac{4\pi G\rho}{\gamma} \sum_{n=0}^{\infty} \frac{n+1}{2n+1} \left(\frac{1}{2} H_n^2 - \frac{1}{6} (n-2) \frac{H_n^3}{R} + \dots \right). \quad (\text{D.7}) \end{aligned}$$

The term $n = 0$ yields the indirect effect of a constant terrain $H = \bar{H} = H_0$:



using only the first term inside the parentheses yields

$$\delta N_{\text{Helmert, const}} = \frac{2\pi G \rho}{\gamma} \bar{H}^2,$$

which *cannot* be neglected.

D.5 The dipole method

As a sanity test, we may describe the effect of Helmert condensation in first approximation as a *dipole-density layer field* μ . The topographic mass, surface density $\kappa = \rho H$, moves downwards by on average $\frac{1}{2}H$. The effect would be the same if the mean sea level³ were covered by a double mass-density layer

$$\mu = \frac{1}{2}\rho H^2. \quad (\text{D.8})$$

The potential of this layer is, in spherical approximation (equation 1.18):

$$V = G \iint_S \mu \frac{\partial}{\partial n} \left(\frac{1}{\ell} \right) dS \approx GR^2 \iint_\sigma \mu \frac{\partial}{\partial n} \left(\frac{1}{\ell} \right) d\sigma.$$

Written more explicitly

$$V_P = GR^2 \iint_\sigma \mu_Q \frac{\partial}{\partial r_Q} \left(\frac{1}{\ell_{PQ}} \right) d\sigma_Q.$$

We use the expansion into Legendre polynomials, equation 8.6:

$$\frac{1}{\ell_{PQ}} = \frac{1}{r_Q} \sum_{n=0}^{\infty} \left(\frac{r_Q}{r_P} \right)^{n+1} P_n(\cos \psi_{PQ}),$$

differentiate with respect to r_Q , and substitute:

$$V_P = GR^2 \iint_\sigma \frac{1}{r_Q^2} \mu_Q \sum_{n=0}^{\infty} n \left(\frac{r_Q}{r_P} \right)^{n+1} P_n(\cos \psi_{PQ}) d\sigma_Q.$$

³In fact, a better place for this replacement layer would be the $\frac{1}{4}H$ level.



By substituting into this equation D.8 for the double mass-density layer μ_Q we obtain, by taking the limit $r_P, r_Q \downarrow R$:

$$\begin{aligned} V &= \frac{1}{4\pi} \sum_{n=0}^{\infty} n \iint_{\sigma} (2\pi G\rho H) HP_n(\cos \psi) d\sigma' = \\ &= \frac{1}{4\pi} \sum_{n=0}^{\infty} n \iint_{\sigma} A_B HP_n(\cos \psi) d\sigma'. \end{aligned}$$

Here, we have left off the designations P and Q again as they are no longer needed for clarity.

The symbol A_B denotes the attraction of a Bouguer plate of thickness H and matter density ρ .

Let us develop the quantity $(A_B H)$ into a spherical-harmonic expansion. According to degree constituent equation 3.8:

$$(A_B H)_n = \frac{2n+1}{4\pi} \iint_{\sigma} (A_B H) P_n(\cos \psi) d\sigma',$$

yielding

$$V = \sum_{n=0}^{\infty} \frac{n}{2n+1} (A_B H)_n \approx \frac{1}{2} (A_B H),$$

at least for the higher n values, i.e., regionally though not globally. The term $n = 0$ vanishes, which is not realistic.

Thus we obtain again an estimate for the indirect effect of Helmert condensation. In geoid computation by means of this method this represents the shift in geoid surface caused by the condensation, which must be undone, i.e., accounted for with the opposite algebraic sign. In other words, when looked upon as a *remove-restore* method, it constitutes its “restore” step:

$$\delta N_{\text{Helmert}} = \frac{V}{\gamma} \approx \frac{1}{2} \frac{A_B H}{\gamma} = \frac{\pi G \rho H^2}{\gamma}.$$

For comparison, the more precise expansion D.7 yields in approximation for larger n values

$$\delta N_{\text{Helmert}} \approx \frac{4\pi G \rho}{\gamma} \cdot \frac{1}{2} \sum_{n=0}^{\infty} \frac{n+1}{2n+1} H_n^2 \approx \frac{\pi G \rho}{\gamma} \sum_{n=0}^{\infty} H_n^2 \approx \frac{\pi G \rho H^2}{\gamma},$$



essentially the same result.





The Laplace equation in spherical co-ordinates

E



E.1 Derivation

Consider a small volume element with sizes in co-ordinate directions of $\Delta\phi$, $\Delta\lambda$, and Δr . Look at the difference in flux of vector field $\mathbf{a} \stackrel{\text{def}}{=} \nabla V$ between what comes in and what goes out through opposite faces.

We do the analogue of what was shown in subsection 1.12.4, using a body or volume element with surfaces aligned along co-ordinate lines, allowing the size of the element to go to zero in the limit, and exploiting integral theorem 1.19 of Gauss. The quantity $\text{div } \mathbf{a} = \Delta V$ is a *source density* in space, and its average value multiplied by the volume of an element must equal the total flux through the surfaces of the element.

Define at the location of the body an orthonormal basis $\{\mathbf{e}_1, \mathbf{e}_2, \mathbf{e}_3\}$ of type “north east up”. The vector \mathbf{e}_1 points to the local north, the vector \mathbf{e}_2 to the east, and the vector \mathbf{e}_3 “up”, in the radial direction. Now we may write

$$\mathbf{a} = a_1 \mathbf{e}_1 + a_2 \mathbf{e}_2 + a_3 \mathbf{e}_3.$$

Part of the difference in flux f between opposing faces is due to a change in the normal component of \mathbf{a} between the faces, part is due to a difference in face surface area ω :

$$f^+ - f^- \approx \overbrace{\omega (a^+ - a^-)}^{\text{I}} + \overbrace{a (\omega^+ - \omega^-)}^{\text{II}}.$$

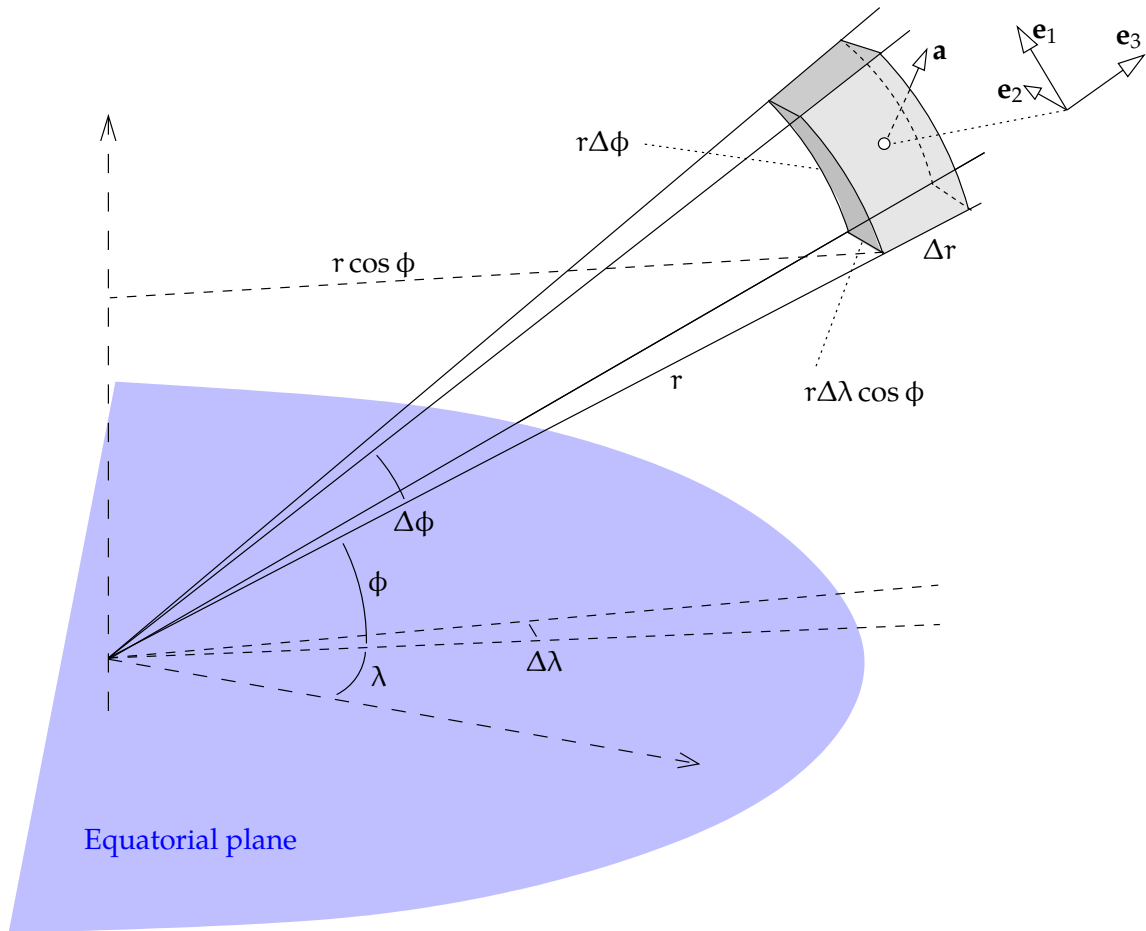


FIGURE E.1. Gauss integral theorem applied to a co-ordinate aligned volume element.



See figure E.1.

- o Latitudinal direction, ϕ , "south–north":

$$\omega_{\phi}^{-} = r \cos \phi \Delta r \Delta \lambda, \quad \omega_{\phi}^{+} = r \cos(\phi + \Delta \phi) \Delta r \Delta \lambda,$$

difference

$$\omega_{\phi}^{+} - \omega_{\phi}^{-} \approx -r \sin \phi \Delta \phi \cdot \Delta r \Delta \lambda.$$

Multiply by

$$a_1 = \frac{\partial V}{\partial (r\phi)} = \frac{1}{r} \frac{\partial V}{\partial \phi}$$



and divide by element volume $r^2 \cos \phi \Delta r \Delta \phi \Delta \lambda$, yielding

$$\Delta_{\phi}^{\text{II}} V = -\frac{\tan \phi}{r^2} \frac{\partial V}{\partial \phi}.$$

This of course in addition to the first contribution

$$\Delta_{\phi}^{\text{I}} V = \langle \nabla \mathbf{a}_1 \cdot \mathbf{e}_1 \rangle = \frac{\mathbf{a}_1^+ - \mathbf{a}_1^-}{r \cdot \Delta \phi},$$

with

$$\mathbf{a}_1^+ - \mathbf{a}_1^- = \left[\frac{\partial \mathbf{V}}{\partial (r\phi)} \right]_{-}^{+} = \frac{1}{r} \left[\frac{\partial \mathbf{V}}{\partial \phi} \right]_{-}^{+},$$

yielding

$$\Delta_{\phi}^{\text{I}} V = \frac{1}{r} \cdot \frac{1}{r} \cdot \frac{\left[\frac{\partial}{\partial \phi} V \right]_{-}^{+}}{\Delta \phi} \approx \frac{1}{r^2} \frac{\partial^2 V}{\partial \phi^2}.$$

- Longitudinal direction, λ , “west–east”: no change in surface area $\omega_{\lambda} = r \Delta r \Delta \phi$ because of rotational symmetry:

$$\Delta_{\lambda}^{\text{II}} V = 0.$$

We only have

$$\Delta_{\lambda}^{\text{I}} V = \langle \nabla \mathbf{a}_2 \cdot \mathbf{e}_2 \rangle = \frac{\mathbf{a}_2^+ - \mathbf{a}_2^-}{r \cos \phi \cdot \Delta \lambda},$$

with

$$\mathbf{a}_2^+ - \mathbf{a}_2^- = \left[\frac{\partial \mathbf{V}}{\partial (\lambda r \cos \phi)} \right]_{-}^{+} = \frac{1}{r \cos \phi} \left[\frac{\partial \mathbf{V}}{\partial \lambda} \right]_{-}^{+}.$$

Substitution yields

$$\Delta_{\lambda}^{\text{I}} V = \frac{1}{r \cos \phi} \cdot \frac{1}{r \cos \phi} \cdot \frac{\left[\frac{\partial}{\partial \lambda} V \right]_{-}^{+}}{\Delta \lambda} \approx \frac{1}{r^2 \cos^2 \phi} \frac{\partial^2 V}{\partial \lambda^2}.$$

- In the radial direction, the surface areas of opposing faces — “inner–outer” — are

$$\omega_r^- = r^2 \cos \phi \Delta \phi \Delta \lambda, \quad \omega_r^+ = (r + \Delta r)^2 \cos \phi \Delta \phi \Delta \lambda,$$



the difference being

$$\omega_r^+ - \omega_r^- \approx 2r\Delta r \cdot \cos \phi \Delta \phi \Delta \lambda.$$

Multiply by

$$a_3 = \frac{\partial V}{\partial r}$$

and divide by the volume of the element $r^2 \cos \phi \Delta r \Delta \phi \Delta \lambda$, yielding for the second contribution to the Laplace operator

$$\Delta_r^{\text{II}} V = \frac{2}{r} \frac{\partial V}{\partial r}.$$

This in addition to the first contribution

$$\Delta_r^{\text{I}} V = \langle \nabla a_3 \cdot \mathbf{e}_3 \rangle = \frac{a_3^+ - a_3^-}{\Delta r} = \frac{\left[\frac{\partial V}{\partial r} \right]_+^+}{\Delta r} \approx \frac{\partial^2 V}{\partial r^2},$$

in which

$$a_3^+ - a_3^- = \left[\frac{\partial V}{\partial r} \right]_-^+.$$

All of this gives us the end result

$$\begin{aligned} \Delta V &= \Delta_r^{\text{I}} V + \Delta_\lambda^{\text{I}} V + \Delta_\phi^{\text{I}} V + \Delta_r^{\text{II}} V + \Delta_\phi^{\text{II}} V = \\ &= \frac{\partial^2 V}{\partial r^2} + \frac{1}{r^2 \cos^2 \phi} \frac{\partial^2 V}{\partial \lambda^2} + \frac{1}{r^2} \frac{\partial^2 V}{\partial \phi^2} + \frac{2}{r} \frac{\partial V}{\partial r} - \frac{\tan \phi}{r^2} \frac{\partial V}{\partial \phi}, \end{aligned}$$

equivalent to equation 2.8.

E.2 Solution

E.2.1 Separating the radial dependency

Let us attempt separation of variables as follows:

$$V(\phi, \lambda, r) = R(r)Y(\phi, \lambda).$$

Substitution into equation 2.8 and multiplication by $r^2/R Y$ yields

$$\frac{1}{R} \left(r^2 \frac{\partial^2 R}{\partial r^2} + 2r \frac{\partial R}{\partial r} \right) = -\frac{1}{Y} \left(\frac{1}{\cos^2 \phi} \frac{\partial^2 Y}{\partial \lambda^2} + \frac{\partial^2 Y}{\partial \phi^2} - \tan \phi \frac{\partial Y}{\partial \phi} \right).$$



This must again apply for all values r , ϕ , and λ and thus can only be a constant, p . This yields two equations:

$$\begin{aligned} \left(r^2 \frac{\partial^2 R}{\partial r^2} + 2r \frac{\partial R}{\partial r} \right) - pR &= 0, \\ \left(\frac{1}{\cos^2 \phi} \frac{\partial^2 Y}{\partial \lambda^2} + \frac{\partial^2 Y}{\partial \phi^2} - \tan \phi \frac{\partial Y}{\partial \phi} \right) + pY &= 0. \end{aligned}$$

For the first equation we try a power law,

$$R(r) = r^q,$$

yielding

$$q(q-1)r^q + 2qr^q - pr^q = 0 \implies (q(q+1) - p)r^q = 0$$

with the solution

$$p = q(q+1).$$

Solving the second equation for $Y(\phi, \lambda)$,

$$\left(\frac{1}{\cos^2 \phi} \frac{\partial^2 Y}{\partial \lambda^2} + \frac{\partial^2 Y}{\partial \phi^2} - \tan \phi \frac{\partial Y}{\partial \phi} \right) + q(q+1)Y = 0, \quad (\text{E.1})$$

is trickier. It turns out that q must be an integer. One finds, for $n \in \mathbb{N}_0$, that there are non-negative solutions $q = n$ and negative solutions $q = -(n+1)$, with $n = 0, 1, 2, \dots$. With this, the full set of special solutions is

$$\tilde{V}_{n,1} = r^n Y_n(\phi, \lambda), \quad \tilde{V}_{n,2} = \frac{Y_n(\phi, \lambda)}{r^{n+1}}, \quad n \in \mathbb{N}_0,$$

equations 2.9.

E.2.2 Solving for surface harmonics

Both solutions q , the non-negative and the negative one, yield on substitution into equation E.1 the same equation for n :

$$\left(\frac{1}{\cos^2 \phi} \frac{\partial^2 Y}{\partial \lambda^2} + \frac{\partial^2 Y}{\partial \phi^2} - \tan \phi \frac{\partial Y}{\partial \phi} \right) + n(n+1)Y = 0.$$



We attempt separation of variables:

$$Y(\phi, \lambda) = F(\phi)L(\lambda).$$

Substitution and multiplication by $\cos^2 \phi / FL$ yields

$$\frac{\cos^2 \phi}{F} \left(\frac{\partial^2 F}{\partial \phi^2} - \tan \phi \frac{\partial F}{\partial \phi} + n(n+1)F \right) = -\frac{1}{L} \frac{\partial^2 L}{\partial \lambda^2}.$$

Both sides must be again equal to the same constant, which we shall assume positive and call m^2 :

$$\begin{aligned} \frac{\partial^2 F}{\partial \phi^2} - \tan \phi \frac{\partial F}{\partial \phi} + \left(n(n+1) - \frac{m^2}{\cos^2 \phi} \right) F &= 0, \\ \frac{\partial^2 L}{\partial \lambda^2} + m^2 L &= 0. \end{aligned}$$

The first equation is known as Legendre's equation. Its solutions are the Legendre functions $P_{nm}(\sin \phi)$, with the integer $m = 0, 1, \dots, n$. The second is the classical *harmonic oscillator*, with solutions¹

$$L_{m,1}(\lambda) = \cos m\lambda, \quad L_{m,2}(\lambda) = \sin m\lambda.$$

With this, we find for the surface spherical harmonics the linear combinations

$$Y_n(\phi, \lambda) = \sum_{m=0}^n P_{nm}(\sin \phi) (a_{nm} \cos m\lambda + b_{nm} \sin m\lambda).$$

The general solution is now formed as follows:

$$\begin{aligned} V_1(\phi, \lambda, r) &= \sum_{n=0}^{\infty} r^n \sum_{m=0}^n P_{nm}(\sin \phi) (a_{nm} \cos m\lambda + b_{nm} \sin m\lambda), \\ V_2(\phi, \lambda, r) &= \sum_{n=0}^{\infty} \frac{1}{r^{n+1}} \sum_{m=0}^n P_{nm}(\sin \phi) (a_{nm} \cos m\lambda + b_{nm} \sin m\lambda). \end{aligned}$$

¹This also explains why m must be an integer: the longitude λ is circular with a period of 2π .



Here, a_{nm} and b_{nm} are the spherical-harmonic coefficients specifying the linear combination of special solutions. Only the second solution is physically realistic for representing the Earth's gravitational field, going to zero at infinity $r \rightarrow \infty$.



Bibliography

- M. Abrehdary, L. E. Sjöberg, and M. Bagherbandi. The spherical terrain correction and its effect on the gravimetric-isostatic Moho determination. *Geophysical Journal International*, 204(1):262–273, 2016. URL <https://doi.org/10.1093/gji/ggv450>. 139
- G. d’Agostino, S. Desogus, A. Germak, C. Origlia, D. Quagliotti, G. Berrino, G. Corrado, V. d’Errico, and G. Ricciardi. The new IMG-C-02 transportable absolute gravimeter: Measurement apparatus and applications in geophysics and volcanology. *Annals of Geophysics*, 51(1):39–49, 2008. URL <https://doi.org/10.4401/ag-3038>. 308
- Altimetry, Retracking. Radar altimetry tutorial & toolbox. ESA and CNES. URL <http://www.altimetry.info/radar-altimetry-tutorial/data-flow/data-processing/retracking/>. Accessed 1 March 2022. 365
- O. B. Andersen, P. Knudsen, and P. Berry. The DNSCo8GRA global marine gravity field from double retracked satellite altimetry. *Journal of Geodesy*, 84: 191–199, 2010. URL <https://doi.org/10.1007/s00190-009-0355-9>. 245
- M. de Angelis, A. Bertoldi, L. Cacciapuoti, A. Giorgini, G. Lamporesi, M. Prevedelli, G. Saccorotti, F. Sorrentino, and G. M. Tino. Precision gravimetry with atomic sensors. *Measurement Science and Technology*, 20(2): 022001, 2009. URL <http://dx.doi.org/10.1088/0957-0233/20/2/022001>. 308
- G. Balmino, N. Vales, S. Bonvalot, and A. Briais. Spherical harmonic modeling to ultra-high degree of Bouguer and isostatic anomalies. *Journal of Geodesy*,

- 86:499–520, 2012. URL <https://www.doi.org/10.1007/s00190-011-0533-4>.
62, 138
- T. B. Bedada. *Absolute geopotential height system for Ethiopia*. PhD thesis, University of Edinburgh, 2010. URL https://www.era.lib.ed.ac.uk/bitstream/1842/4726/3/Bedada2010_small.pdf. Accessed 11 May 2019. 247
- N. Benitez, T. J. Broadhurst, H. C. Ford, M. Clampin, G. Hartig, G. D. Illingworth, et al. *Hubble Looks Through Cosmic Zoom Lens*, 2003. URL <https://www.spacetelescope.org/images/op00301a/>. © 2003 ESA/Hubble (CC BY 4.0). Accessed 15 May 2019. 3
- BGI, EGM2008. EGM2008 anomaly maps visualization. URL <http://bgi.omp.obs-mip.fr/data-products/Toolbox/EGM2008-anomaly-maps-visualization>. Accessed 10 May 2019. 124, 134
- BGI, WGM2012. WGM2012 maps visualization/extraction. URL <http://bgi.omp.obs-mip.fr/data-products/Toolbox/WGM2012-maps-vizualisation-extraction>. Accessed 10 May 2019. 151
- M. Bilker-Koivula. Development of the Finnish Height Conversion Surface FIN2005Noo. *Nordic Journal of Surveying and Real Estate Research*, 7(1):76–88, 2010. URL <http://ojs.tsv.fi/index.php/njs/article/download/3663/3432>. Accessed 11 May 2019. 393
- M. Bilker-Koivula and M. Ollikainen. Suomen geoidimallit ja niiden käyttäminen korkeuden muunnoksissa. *Tiedote 29*, Geodeettinen laitos, 2009. URL <https://www.maanmittauslaitos.fi/sites/maanmittauslaitos.fi/files/fgi/GLtiedote29.pdf>. Accessed 11 May 2019. 245, 326
- G. P. Bottoni and R. Barzaghi. Fast collocation. *Bulletin géodésique*, 67(2): 119–126, 1993. URL <https://www.doi.org/10.1007/BF01371375>. 287
- V. V. Brovar, M. I. Yurkina, M. Heifets, M. S. Molodensky, and H. Moritz. M. S. Molodensky In Memoriam. Online PDF, *Mitteilungen der geodätischen Institute der Technischen Universität Graz Folge 88*, 2000. URL <http://www.helmut-moritz.at/SciencePage/Molodensky.pdf>. Helmut Moritz and Maria I. Yurkina, editors. Accessed 1 March 2020. 168



- J. M. Brozena. The Greenland Aerogeophysics Project: Airborne gravity, topographic and magnetic mapping of an entire continent. *International Association of Geodesy Symposia*, 110, pages 203–214, Vienna, Austria, 20 August 1992. Springer, New York, NY. URL https://doi.org/10.1007/978-1-4613-9255-2_19. 316
- J. M. Brozena and M. F. Peters. State-of-the-art airborne gravimetry. *International Association of Geodesy Symposia*, 113, pages 187–197, Graz, Austria, 1994. Springer-Verlag. URL https://doi.org/10.1007/978-3-642-79721-7_20. 316
- J. M. Brozena, M. F. Peters, and R. Salman. Arctic airborne gravity measurements program. In [Segawa et al. \(1996\)](#), pages 131–146. URL https://doi.org/10.1007/978-3-662-03482-8_20. 316
- H. Bruns. *Die Figur der Erde: Ein Beitrag zur europäischen Gradmessung*. Stankiewicz, Berlin, 1878. URL <https://play.google.com/books/reader?id=DPo-AAAAYAAJ&hl=en&pg=GBS.PP5>. Accessed 31 January 2020. 92
- B. Bucha, C. Hirt, and M. Kuhn. Cap integration in spectral gravity forward modelling: near- and far-zone gravity effects via Molodensky’s truncation coefficients. *Journal of Geodesy*, 93:65–83, 2019. URL <https://doi.org/10.1007/s00190-018-1139-x>. 220
- L. Caesar, S. Rahmstorf, A. Robinson, G. Feulner, and V. S. Saba. Observed fingerprint of a weakening Atlantic Ocean overturning circulation. *Nature*, 556:191–196, 2018. URL <https://doi.org/10.1038/s41586-018-0006-5>. 333
- H. Cavendish. Experiments to determine the density of the earth. *Philosophical Transactions of the Royal Society*, 88, 1798. URL <https://doi.org/10.1098/rstl.1798.0022>. 4
- CHAMP Mission. CHAMP – CHALLENGING Minisatellite Payload. Deutsches Geoforschungszentrum, Helmholtz-Zentrum Potsdam. URL <https://www.gfz-potsdam.de/champ/>. Accessed 1 March 2020. 369
- B. J. Coakley, S. C. Kenyon, and R. Forsberg. Updating the Arctic Gravity Project grid with new airborne and Extended Continental Shelf data. *AGU Fall Meeting Abstracts*, page C3, December 2013. URL



- <https://ui.adsabs.harvard.edu/abs/2013AGUFM.G13C..03C/abstract>. Accessed 17 January 2020. 316
- J. J. O'Connor and E. F. Robertson. George Green (1793–1841). MacTutor History of Mathematics archive, School of Mathematics and Statistics, University of St Andrews, Scotland, 1998. URL <http://www-history.mcs.st-and.ac.uk/Biographies/Green.html>. Accessed 2 March 2020. 29
- B. D. DeJong, P. R. Bierman, W. L. Newell, Tammy, M. Rittenour, S. A. Mahan, G. Balco, and D. H. Rood. Pleistocene relative sea levels in the Chesapeake Bay region and their implications for the next century. *GSA Today*, 25(8): 4–10, 2015. URL <https://doi.org/10.1130/GSATG223A.1>. 336
- H. Denker. Evaluation and improvement of the EGG97 quasigeoid model for Europe by GPS and leveling data. In *Vermeer and Ádám (1998)*, pages 53–61. 392
- Eiffel Tower, 72 names. List of the 72 names on the Eiffel Tower. URL https://en.wikipedia.org/wiki/List_of_the_72_names_on_the_Eiffel_Tower. Accessed 7 April 2019. 16, 17, 34, 45, 55, 88, 424
- M. Ekman. Postglacial rebound and sea level phenomena with special reference to Fennoscandia and the Baltic Sea. In *Kakkuri (1993)*, pages 7–70. 331, 385
- Encyclopaedia Britannica, Moho. URL <https://www.britannica.com/science/Moho>. Accessed 22 January 2020. 156
- L. Eötvös. *Three Fundamental Papers of Loránd Eötvös*. Loránd Eötvös Geophysical Institute of Hungary, 1998. ISBN 963-7135-02-2. Editor Zoltán Szabó. 319
- European geoid calculations. Leibniz Universität Hannover, Institute of Geodesy. URL <https://www.ife.uni-hannover.de/en/research/main-research-focus/regional-gravity-field-and-geoid-modelling/european-geoid-calculations/>. Accessed 11 May 2019. 392
- G. Farmelo. *The Strangest Man*. Basic Books, reprint edition, 2011. ISBN 978-0-4650-2210-6. 27



- W. E. Farrell and J. A. Clark. On postglacial sea level. *Geophysical Journal of the Royal Astronomical Society*, 46(3):647–667, 1976. URL <https://doi.org/10.1111/j.1365-246X.1976.tb01252.x>. 336
- W. E. Featherstone. Software for computing five existing types of deterministically modified integration kernel for gravimetric geoid determination. *Computers and Geosciences*, 29:183–193, 2003. URL [https://doi.org/10.1016/S0098-3004\(02\)00074-2](https://doi.org/10.1016/S0098-3004(02)00074-2). 222
- FFTW Home Page. URL <https://www.fftw.org>. Accessed 15 May 2019. 431
- R. Forsberg. A study of terrain reductions, density anomalies and geophysical inversion methods in gravity field modelling. Report 355, Ohio State University, Department of Geodetic Science and Surveying, 1984. URL <https://earthsciences.osu.edu/sites/earthsciences.osu.edu/files/report-355.pdf>. Accessed 17 February 2020. 248
- R. Forsberg and J. Kaminskis. Geoid of the Nordic and Baltic region from gravimetry and satellite altimetry. In [Segawa et al. \(1996\)](#), pages 540–547. URL https://doi.org/10.1007/978-3-662-03482-8_72. 393
- R. Forsberg and G. Strykowski. NKG Gravity Data Base and NKG Geoid. Technical University of Denmark, DTU Space, National Space Institute, 2010. URL http://www.nordicgeodeticcommission.com/wp-content/uploads/2014/10/8-WG_geoid_2010_March_presentation_ForsbergStrykowski.pdf. Accessed 11 May 2019. 393
- R. Forsberg, A. V. Olesen, F. Ferraccioli, T. Jordan, H. Corr, and K. Matsuoka. PolarGap 2015/16 - Filling the GOCE polar gap in Antarctica and ASIRAS flight around South Pole. Final report, European Space Agency, 2017. URL <https://earth.esa.int/documents/10174/134665/PolarGap-2015-2016-final-report>. Accessed 8 January 2020. 372
- R. Forsberg and C. C. Tscherning. An overview manual for the GRAVSOFIT Geodetic Gravity Field Modelling Programs, 2008. URL https://www.academia.edu/9206363/An_overview_manual_for_the_GRAVSOFIT_Geodetic_Gravity_Field_Modelling_Programs. Accessed 11 May 2019. 244



- R. Forsberg and M. Vermeer. A generalized Strang van Hees approach to fast geopotential inversion. *Manuscripta geodaetica*, 17:302–314, 1992. 241
- J.-P. Friedelmeyer. Du côté des lettres (2) : une lettre de Sophie Germain à Carl Friedrich Gauss (20 février 1807), et la réponse de celui-ci (30 avril 1807), 2014. URL <https://images.math.cnrs.fr/Du-cote-des-lettres-2-une-lettre-de-Sophie-Germain-a-Carl-Friedrich-Gauss-20.html>. Accessed 14 May 2019. 92
- M. Frigo and S. G. Johnson. The design and implementation of FFTW3. *Proceedings IEEE*, 93(2):216–231, 2005. URL <http://www.fftw.org/fftw-paper-ieee.pdf>. Accessed 14 February 2020. 431
- E. S. Garcia, D. T. Sandwell, and W. H. Smith. Retracking CryoSat-2, Envisat and Jason-1 radar altimetry waveforms for improved gravity field recovery. *Geophysical Journal International*, 2014. URL <https://doi.org/10.1093/gji/ggt469>. 245
- A. Gatti, M. Reguzzoni, F. Sansò, and F. Migliaccio. Space-wise grids of gravity gradients from GOCE data at nominal satellite altitude. Presented at the 5th International GOCE User Workshop, UNESCO, Paris, France, 25–28 November 2014. URL https://www.researchgate.net/publication/275029640_SPACE-WISE_GRIDS_OF_GRAVITY_GRADIENTS_FROM_GOCE_DATA_AT_NOMINAL_SATELLITE_ALTITUDE. Accessed 11 May 2019. 284
- O. R. Godø, A. Samuelsen, G. J. Macaulay, R. Patel, S. S. Hjøllø, J. Horne, S. Kaartvedt, and J. A. Johannessen. Mesoscale eddies are oases for higher trophic marine life. *PLoS One*, 7(1):e30161, 2012. URL <https://doi.org/10.1371/journal.pone.0030161>. 334
- GRACE Follow-On Mission. Jet Propulsion Laboratory. URL <https://gracefo.jpl.nasa.gov/mission/overview/>. Accessed 1 March 2020. 371
- GRACE Mission. Measuring Earth’s Surface Mass and Water Changes. Jet Propulsion Laboratory. URL <https://grace.jpl.nasa.gov/>. Accessed 1 March 2020. 370
- GRACE Mission, hydrology. NASA. URL <https://commons.wikimedia.org/wiki/File:>



- [Global_Gravity_Anomaly_Animation_over_LAND.gif](#). Accessed 1 March 2020. 371
- G. Green. *An Essay on the Application of Mathematical Analysis to the Theories of Electricity and Magnetism*. 1828. URL <https://play.google.com/books/reader?id=GwYXAAAAYAAJ>. Accessed 23 April 2019. 29
- Green's Windmill. Green's windmill and science centre. URL <https://www.greensmill.org.uk/>. Accessed 10 May 2019. 29
- GWR Instruments, Inc., iGRAV® Gravity Sensors. URL <http://www.gwrinstruments.com/igrav-gravity-sensors.html>. Accessed 27 May 2019. 312
- R. Haagmans, E. de Min, and M. van Gelderen. Fast evaluation of convolution integrals on the sphere using 1D FFT, and a comparison with existing methods for Stokes' integral. *Manuscripta geodaetica*, 18:227–241, 1993. 241
- P. Häkli, J. Puupponen, H. Koivula, and M. Poutanen. Suomen geoidimallit ja niiden käyttäminen korkeuden muunnoksissa. Tiedote 30, Geodeettinen laitos, 2009. URL <https://www.maanmittauslaitos.fi/sites/maanmittauslaitos.fi/files/fgi/GLtiedote30.pdf>. Accessed 26 January 2020. 326
- J. C. Harrison and M. Dickinson. Fourier transform methods in local gravity modelling. *Bulletin Géodésique*, 63:149–166, 1989. URL <https://doi.org/10.1007/BF02519148>. 248, 249
- M. Heikkinen. Solving the shape of the Earth by using digital density models. *Report 81:2*, Finnish Geodetic Institute, Helsinki, 1981. 99, 100, 103, 314
- W. A. Heiskanen. The latest achievements of physical geodesy. *Journal of Geophysical Research*, 65(9):2827–2836, 1960. URL <https://doi.org/10.1029/JZ065i009p02827>. 153
- W. A. Heiskanen and H. Moritz. *Physical Geodesy*. W. H. Freeman and Company, San Francisco, London, 1967. 35, 53, 55, 66, 68, 76, 77, 78, 92, 95, 96, 102, 103, 104, 110, 113, 116, 152, 154, 175, 177, 178, 183, 191, 192, 198, 199, 204, 208, 289, 394, 425



- W. F. Hermans. *Beyond Sleep*. Harry N. Abrams, reprint edition, 2007. ISBN 978-1-5856-7583-8. 144
- C. Hirt and M. Kuhn. Band-limited topographic mass distribution generates full-spectrum gravity field: Gravity forward modeling in the spectral and spatial domains revisited. *Journal of Geophysical Research Solid Earth*, 119, 2014. URL <https://doi.org/10.1002/2013JB010900>. 138
- R. A. Hirvonen. *The continental undulations of the geoid*. PhD thesis, Helsinki University of Technology, 1934. Finnish Geodetic Institute Publication 19. 393
- R. A. Hirvonen. *Relative Bestimmungen der Schwerkraft in Finnland in den Jahren 1931, 1933 und 1935*. Publication 23, Finnish Geodetic Institute, Helsinki, 1937. 296
- B. Hofmann-Wellenhof and H. Moritz. *Physical Geodesy*. Springer-Verlag Wien GmbH, 2006. Second, revised edition. 394
- Humboldt University Berlin. Friedrich Robert Helmert with a relative pendulum, 2017. URL https://www.researchgate.net/publication/318994932_Friedrich_Robert_Helmert_founder_of_modern_geodesy_on_the_occasion_of_the_centenary_of_his_death/figures. © 2017 Humboldt-Universität zu Berlin, Universitätsbibliothek (CC BY 3.0). Accessed 19 May 2019. 142
- E. Hytönen. *Absolute gravity measurement with long wire pendulum*. PhD thesis, University of Helsinki, 1972. Finnish Geodetic Institute Publication 75. 297
- International Intercomparison of Absolute Gravimeters. University of Luxembourg, European Center for Geodynamics and Seismology. URL <http://www.ecgs.lu/international-intercomparison-of-absolute-gravimeters/>. Accessed 6 February 2020. 310
- ISG, Geoid Schools. International Service for the Geoid. URL <http://www.isgeoid.polimi.it/Schools/schools.html>. Accessed 1 March 2020. 244
- E. Kääriäinen. *The Second Levelling of Finland in 1935–1955*. Publication 61, Finnish Geodetic Institute, Helsinki, 1966. 163, 164, 179



- J. Kääriäinen and H. Ruotsalainen. *Tilt Measurements in the Underground Laboratory Lohja 2, Finland, in 1977–1987*. Publication 110, Finnish Geodetic Institute, Helsinki, 1989. 384
- J. Kakkuri, editor. *Geodesy and Geophysics, lecture notes, NKG Autumn School 1992*, Finnish Geodetic Institute Publication 115, 1993. 454, 464, 465
- J. Kakkuri. *Surveyor of the Globe – Story of the Life of V. A. Heiskanen*. National Land Survey of Finland, 2008. URL <https://readymag.com/u95015526/508134>. Accessed 13 May 2019. 144, 394
- S. C. Kenyon, R. Forsberg, A. V. Olesen, and S. A. Holmes. NGA's use of aerogravity to advance the next generation of Earth Gravitational Models. *AGU Fall Meeting Abstracts*, page A4, December 2012. URL <https://ui.adsabs.harvard.edu/abs/2012AGUFM.G12A..04K/abstract>. Accessed 11 May 2019. 316
- M. G. Kogan, M. Diament, A. Bulot, and G. Balmino. Thermal isostasy in the South Atlantic Ocean from geoid anomalies. *Earth and Planetary Science Letters*, 74:280–290, 1985. URL [https://doi.org/10.1016/0012-821X\(85\)90028-7](https://doi.org/10.1016/0012-821X(85)90028-7). 153
- M. Kuhn, W. Featherstone, and J. Kirby. Complete spherical Bouguer gravity anomalies over Australia. *Australian Journal of Earth Sciences*, 56(2):213–223, 2009. URL <https://espace.curtin.edu.au/handle/20.500.11937/34751>. Accessed 1 March 2020. 138, 139
- A. Kuivamäki, P. Vuorela, and M. Paananen. Indications of postglacial and recent bedrock movements in Finland and Russian Karelia. *Report YST-99*, Geological Survey of Finland, 1998. URL http://tupa.gtk.fi/julkaisu/ydinjate/yst_099.pdf. Accessed 17 January 2020. 341
- A. E. H. Love. The Yielding of the Earth to Disturbing Forces. *Proceedings of the Royal Society A*, 82(551):73–88, 1909. URL <https://royalsocietypublishing.org/doi/pdf/10.1098/rspa.1909.0008>. 383
- B. Lu, F. Barthelmes, S. Petrovic, C. Förste, F. Flechtner, Z. Luo, K. He, and M. Li. Airborne gravimetry of GEOHALO mission: Data processing and



- gravity field modeling. *Journal of Geophysical Research: Solid Earth*, 122: 10 586–10 604, 2017. URL <https://doi.org/10.1002/2017JB014425>. 316
- J. Mäkinen, A. Engfeldt, L. Engman, B. G. Harsson, T. Oja, S. Rekkedal, K. Røthing, P. Rouhiainen, H. Ruotsalainen, H. Skatt, G. Strykowski, H. Virtanen, K. Wiczerkowski, and D. Wolf. The Fennoscandian Land Uplift Gravity Lines: comparison of observed gravity change with observed vertical motion and with GIA models. *Report, Nordiska Kommissionen för Geodesi*, 2010. URL http://www.nordicgeodeticcommission.com/wp-content/uploads/2014/10/1-Makinen_et_al_land_uplift_gravity_lines.pdf. Accessed 11 May 2019. 329
- S. Märdla. *Regional Geoid Modelling by the Least Squares Modified Hotine Formula Using Gridded Gravity Disturbances*. PhD thesis, Tallinn University of Technology, 2017. URL <https://digi.lib.ttu.ee/i/file.php?DLID=9130&t=1>. Accessed 11 May 2019. 128, 212
- P. J. Melchior. *The Tides of the Planet Earth*. Pergamon Press, Oxford, 1978. ISBN 978-0-0802-6248-2. 381, 383
- J. X. Mitrovica, M. E. Tamisiea, J. L. Davis, and G. A. Milne. Recent mass balance of polar ice sheets inferred from patterns of global sea level change. *Nature*, 409:1026–1029, February 2001. URL <https://doi.org/10.1038/35059054>. 339
- M. S. Molodensky, V. F. Eremeev, and M. I. Yurkina. *Methods for the Study of the External Gravitational Field and Figure of the Earth*. Israel Program of Scientific Translations, Jerusalem, 1962. (Transl. from Russian). 127, 171, 220, 394
- D. Monniaux. Autograv CG5, 2011. URL https://commons.wikimedia.org/wiki/File:Autograv_CG5_P1150838.JPG. © 2011 David Monniaux (GFDL). Accessed 13 May 2019. 297
- H. Moritz. *Advanced Physical Geodesy*. H. Wichmann Verlag, Karlsruhe, 1980. ISBN 978-3-87-907106-7. 394, 434
- W. H. Munk. The U.S. Commission on Ocean Policy, Testimony, 12 April 2002. URL https://govinfo.library.unt.edu/oceancommission/meetings/apr18_19_02/munk_statement.pdf. Accessed 14 May 2019. 345



- R. S. Nerem, D. P. Chambers, C. Choe, and G. T. Mitchum. Estimating mean sea level change from the TOPEX and Jason altimeter missions. *Marine Geodesy*, 33(1):435, 2010. URL <https://doi.org/10.1080/01490419.2010.491031>. 346
- NOAA, Ocean currents. How does the ocean affect climate and weather on land? NOAA Ocean Exploration and Research. URL <https://oceanexplorer.noaa.gov/facts/climate.html>. Accessed 1 March 2020. 335
- P.-A. Olsson, K. Breili, V. Ophaug, H. Steffen, M. Bilker-Koivula, E. Nielsen, T. Oja, and L. Timmen. Postglacial gravity change in Fennoscandia – three decades of repeated absolute gravity observations. *Geophysical Journal International*, 217:1141–1156, 2019. URL <https://doi.org/10.1093/gji/ggz054>. 330
- R. L. Parker. The rapid calculation of potential anomalies. *Geophysical Journal of the Royal Astronomical Society*, 31:447–455, 1972. URL <https://doi.org/10.1111/j.1365-246X.1973.tb06513.x>. 250
- M. K. Paul. A method of evaluating the truncation error coefficients for geoidal height. *Bulletin Géodésique*, 110:413–425, 1973. URL <https://doi.org/10.1007/BF02521951>. 221
- N. K. Pavlis, S. A. Holmes, S. C. Kenyon, and J. K. Factor. An Earth Gravitational Model to degree 2160: EGM2008. In *EGU General Assembly 2008*, Vienna, Austria, 13–18 April 2008. URL <http://earth-info.nga.mil/GandG/wgs84/gravitymod/egm2008>. Accessed 11 May 2019. 74
- N. K. Pavlis, S. A. Holmes, S. C. Kenyon, and J. K. Factor. The development and evaluation of the Earth Gravitational Model 2008 (EGM2008). *Journal of Geophysical Research*, 117(B4), 2012. URL <https://doi.org/10.1029/2011JB008916>. 74
- W. R. Peltier. Closure of the budget of global sea level rise over the GRACE era: the importance and magnitudes of the required corrections for global glacial isostatic adjustment. *Quaternary Science Reviews*, 28(17–18): 1658–1674, 2009. URL <https://doi.org/10.1016/j.quascirev.2009.04.004>.



- Special issue: Quaternary Ice Sheet-Ocean Interactions and Landscape Responses. 336
- W. R. Peltier, FRSC, Home Page. URL <http://www.atmosp.physics.utoronto.ca/~peltier/data.php>. Accessed 15 May 2019. 336
- U. Pesonen. *Relative Bestimmungen der Schwerkraft in Finnland in den Jahren 1926–1929*. Publication 13, Finnish Geodetic Institute, Helsinki, 1930. 296
- PIOMAS. Polar Science Center, PIOMAS Arctic Sea Ice Volume Reanalysis. URL <http://psc.apl.washington.edu/research/projects/arctic-sea-ice-volume-anomaly/>. Accessed 11 May 2019. 367
- M. Poutanen, M. Vermeer, and J. Mäkinen. The Permanent Tide in GPS Positioning. *Journal of Geodesy*, 70:499–504, 1996. URL <https://doi.org/10.1007/BF00863622>. 385
- J. H. Pratt. II. On the attraction of the Himalaya mountains, and of the elevated regions beyond them, upon the plumb-line in India. *Philosophical Transactions of the Royal Society of London*, 145:53–100, 1855. URL <https://doi.org/10.1098/rstl.1855.0002>. 143
- J. H. Pratt. II. On the deflection of the plumb-line in India caused by the attraction of the Himalaya mountains and the elevated regions beyond, and its modification by the compensating effect of a deficiency of matter below the mountain mass. *Proceedings of the Royal Society of London*, 9:493–496, 1859. URL <https://doi.org/10.1098/rspl.1857.0096>. 143
- J. H. Pratt. On the degree of uncertainty which local attraction, if not allowed for, occasions in the map of a country, and in the mean figure of the earth as determined by geodesy ; a method of obtaining the mean figure free from ambiguity by a comparison of the Anglo-Gallic, Russian, and Indian Arcs ; and speculations on the constitution of the earth's crust. *Proceedings of the Royal Society of London*, 13:253–276, 1864. URL <https://doi.org/10.1098/rspl.1863.0061>. 143
- K. Predehl, G. Grosche, S. M. Raupach, S. Droste, O. Terra, J. Alnis, Th. Legero, T. W. Hänsch, Th. Udem, R. Holzwarth, and H. Schnatz. A 920 km Optical Fiber Link for Frequency Metrology at the 19th Decimal Place. *Science*, 27 April 2012. URL <https://doi.org/10.1126/science.1218442>. 185, 186



- I. Prutkin. Gravitational and magnetic models of the core-mantle boundary and their correlation. *Journal of Geodynamics*, 45:146–153, 2008. URL https://www.researchgate.net/publication/257097255_Gravitational_and_magnetic_models_of_the_core-mantle_boundary_and_their_correlation. Accessed 1 March 2020. 153
- R. H. Rapp. The decay of the spectrum of the gravitational potential and the topography for the Earth. *Geophysical Journal International*, 99(3):449–455, 1989. URL <https://doi.org/10.1111/j.1365-246X.1989.tb02031.x>. 282
- J. Richer. Observations astronomiques et physiques faites en l’isle de Caienne. In *Ouvrages de Mathematique de M. Picard*. P. Gosse and J. Neaulme, 1731. URL <http://www.e-rara.ch/zut/content/pageview/815403>. Accessed 11 May 2019. 296
- R. A. Rohde. Post-glacial sea level rise, 2005. URL https://commons.wikimedia.org/wiki/File:Post-Glacial_Sea_Level.png. © 2005 Robert A. Rohde (GFDL). Accessed 21 July 2019. 339
- R. Rummel and F. Sansó, editors. *Satellite Altimetry in Geodesy and Oceanography. Proceedings, International Summer School of Theoretical Geodesy*, Lecture Notes in Earth Sciences, 50, Trieste, Italy, 25 May – 6 June 1992. Springer-Verlag. URL <https://doi.org/10.1007/BFb0117924>. 334
- H. Ruotsalainen. Interferometric water level tilt meter development in Finland and comparison with combined earth tide and ocean loading models. *Pure and Applied Geophysics*, 2017. URL <https://www.doi.org/10.1007/s00024-017-1562-6>. 385
- O. Sacks. Henry Cavendish: An early case of Asperger’s syndrome? *Neurology*, 57(7):1347–1347, 2001. URL <https://doi.org/10.1212/WNL.57.7.1347>. 4
- E. J. O. Schrama. *The Role of Orbit Errors in Processing of Satellite Altimeter Data*. PhD thesis, Delft University of Technology, 1989. URL <https://www.ncgeo.nl/downloads/33Schrama.pdf>. Accessed 11 May 2019. 357
- A. R. Schweiger, R. Lindsay, L. Zhang, M. Steele, H. Stern, and R. Kwok. Uncertainty in modeled Arctic sea ice volume. *Journal of Geophysical Research*, 116(C00D06), 2011. URL <http://dx.doi.org/10.1029/2011JC007084>. 367



- D. Scuka. GOCE burning: Last orbital view. ESA blog, 2013. URL <http://blogs.esa.int/rocketscience/2013/11/11/goce-burning-last-orbital-view/>. Accessed 1 March 2020. 373
- Sea Level Research Group. University of Colorado. URL <http://sealevel.colorado.edu/>. Accessed 12 April 2019. 346
- J. Segawa, H. Fujimoto, and S. Okubo, editors. *Proceedings, IAG International Symposium on Gravity, Geoid and Marine Geodesy (GraGeoMar96)*, International Association of Geodesy Symposia, 117, Tokyo, Japan, 30 September – 5 October 1996. Springer-Verlag. 453, 455
- SourceForge, Maxima. Maxima, a computer algebra system. URL <http://maxima.sourceforge.net/>. Accessed 11 May 2019. 352
- G. Spada and D. Melini. SELEN: a program for solving the “Sea Level Equation”. User manual for version 2.9, Computational Infrastructure for Geodynamics (CIG), 2015. URL <http://geodynamics.org/cig/software/selen/selen-manual.pdf>. Accessed 1 March 2020. 336
- W. Torge. *Gravimetry*. de Gruyter, Berlin, New York, 1989. ISBN 978-3-11-010702-9. 394
- W. Torge. Gravity and tectonics. In Kakkuri (1993), pages 131–172. 389
- C. C. Tscherning and R. H. Rapp. Closed covariance expressions for gravity anomalies, geoid undulations, and deflections of the vertical implied by anomaly degree variances. *Report 208*, Dept. of Geodetic Science and Surveying, The Ohio State University, Columbus, OH, USA, 1974. URL <https://earthsciences.osu.edu/sites/earthsciences.osu.edu/files/report-208.pdf>. Accessed 17 January 2020. 283
- Tytyri Mine Experience. URL <https://www.tytyrielamyskaivos.fi/en/experiencemine/>. Accessed 29 February 2020. 384
- P. Vaníček and E. Krakiwsky. *Geodesy – The Concepts*. Elsevier Science Publishers, second edition, 1987. ISBN 978-0-4448-7777-2. 394



- F. A. Vening Meinesz. Gravity survey by submarine via Panama to Java. *The Geographical Journal*, 71(2):144–156, 1928. URL <https://doi.org/10.2307/1782700>. 296
- M. Vermeer. Chronometric levelling. *Report 83:2*, Finnish Geodetic Institute, 1983a. 185, 308
- M. Vermeer. A new Seasat altimetric geoid for the Baltic. *Report 83:4*, Finnish Geodetic Institute, 1983b. 343
- M. Vermeer. *Geoid studies on Finland and the Baltic*. PhD thesis, University of Helsinki, 1984. Report 84:3, Finnish Geodetic Institute. 34, 112
- M. Vermeer. Geoid determination using frequency domain techniques. In *Kakkuri (1993)*, pages 183–200. 232
- M. Vermeer. FGI studies on satellite gravity gradiometry. 3. Regional high resolution geopotential recovery in geographical coordinates using a Taylor expansion FFT technique. *Report 92:1*, Finnish Geodetic Institute, 1992b. 241
- M. Vermeer and J. Ádám, editors. *Proceedings, Second Continental Workshop on the Geoid in Europe*, Report 98:4, Finnish Geodetic Institute, Masala, 10–14 March 1998. 454, 466
- H. Virtanen. On superconducting gravimeter observations above 8 mHz at the Metsähovi station. *Report 98:5*, Finnish Geodetic Institute, Masala, 1998. 311
- H. Virtanen. *Studies of Earth dynamics with superconducting gravimeter*. PhD thesis, University of Helsinki, 2006. URL <http://ethesis.helsinki.fi/julkaisut/mat/fysik/vk/virtanen/studieso.pdf>. Publication 133, Finnish Geodetic Institute. Accessed 11 May 2019. 311
- H. Virtanen and J. Kääriäinen. The installation and first results from the superconducting gravimeter GWR20 at the Metsähovi station, Finland. *Report 95:1*, Finnish Geodetic Institute, Helsinki, 1995. 311
- J. Vondrák, C. Ron, and V. Štefka. Earth orientation parameters based on EOC-4 astrometric catalog. *Acta Geodynamica et Geomaterialia*, 7(3):245–251, 2010. URL https://www.irsm.cas.cz/materialy/acta_content/2010_03/2_Vondrak.pdf. Accessed 20 February 2020. 385



- P. Vu, F. Frappart, J. Darrozes, V. Marieu, F. Blarel, G. Ramillien, P. Bonnefond, and F. Birol. Multi-satellite altimeter validation along the French Atlantic Coast in the Southern Bay of Biscay from ERS-2 to SARAL. *Remote Sensing*, 93(10), 2018. URL <http://dx.doi.org/10.3390/rs10010093>. 364
- D. Watts. Fourifier, 2004. URL <http://www.ejectamenta.com/Imaging-Experiments/fourierimagefiltering.html>. Accessed 10 May 2019. 243
- L. Wen and D. L. Anderson. Layered mantle convection: A model for geoid and topography. *Earth and Planetary Science Letters*, 146(3-4):367-377, 1997. ISSN 0012-821X. URL <http://222.195.83.195/wen/Reprints/WenAnderson97EPSL.pdf>. Accessed 4 March 2020. 153
- H.-G. Wenzel. Ultra high degree geopotential model GPM3E97A to degree and order 1800 tailored to Europe. In *Vermeer and Ádám (1998)*, pages 71-80. 79
- K. Wiczerkowski, J. X. Mitrovica, and D. Wolf. A revised relaxation-time spectrum for Fennoscandia. *Geophysical Journal International*, 139:69-86, 1999. URL <https://doi.org/10.1046/j.1365-246X.1999.00924.x>. 340
- Wikipedia, Declination. URL <https://en.wikipedia.org/wiki/Declination>. Accessed 29 February 2020. 377
- Wikipedia, Dislocation. URL <https://en.wikipedia.org/wiki/Dislocation>. Accessed 23 April 2019. 303
- Wikipedia, Double-slit experiment. URL https://en.wikipedia.org/wiki/Double-slit_experiment. Accessed 18 February 2020. 308
- Wikipedia, Earth normal modes. URL https://en.wikipedia.org/wiki/Seismic_wave#Normal_modes. Accessed 16 March 2020. 312
- Wikipedia, Hour angle. URL https://en.wikipedia.org/wiki/Hour_angle. Accessed 29 February 2020. 378
- Wikipedia, John Pratt. URL [https://en.wikipedia.org/wiki/John_Pratt_\(Archdeacon_of_Calcutta\)](https://en.wikipedia.org/wiki/John_Pratt_(Archdeacon_of_Calcutta)). Accessed 23 April 2019. 143



- Wikipedia, Mu-metal. URL <https://en.wikipedia.org/wiki/Mu-metal>. Accessed 23 April 2019. 310
- Wikipedia, Pendulum clock. URL https://en.wikipedia.org/wiki/Pendulum_clock. Accessed 23 April 2019. 295
- Wikipedia, Saros. URL [https://en.wikipedia.org/wiki/Saros_\(astronomy\)](https://en.wikipedia.org/wiki/Saros_(astronomy)). Accessed 23 April 2019. 325
- Wikipedia, Sea level rise. URL https://en.wikipedia.org/wiki/Sea_level_rise. Accessed 23 April 2019. 335
- Wikipedia, Seasat conspiracy theory. URL https://en.wikipedia.org/wiki/Seasat#Conspiracy_theory. Accessed 23 April 2019. 343
- Wikipedia, Strengthening mechanisms of materials. URL https://en.wikipedia.org/wiki/Strengthening_mechanisms_of_materials. Accessed 10 May 2019. 303
- Wikipedia, Sverdrup. URL <https://en.wikipedia.org/wiki/Sverdrup>. Accessed 23 April 2019. 333
- Wikipedia, The Aerospace Corporation. URL https://en.wikipedia.org/wiki/The_Aerospace_Corporation. Accessed 23 April 2019. 218
- Wikipedia, Zero-length springs. URL [https://en.wikipedia.org/wiki/Spring_\(device\)#Zero-length_springs](https://en.wikipedia.org/wiki/Spring_(device)#Zero-length_springs). Accessed 23 April 2019. 300
- Wolfram Demonstrations, Difference formula for cosine. URL <http://demonstrations.wolfram.com/DifferenceFormulaForCosine/>. Accessed 7 April 2019. 195
- Wolfram Functions, $\sum_{k=1}^{\infty} \frac{\cos kx}{k}$. URL <http://functions.wolfram.com/ElementaryFunctions/Cos/23/02/0001/>. Accessed 25 February 2020. 196



- Wolfram MathWorld, Spherical Harmonic Addition Theorem. URL <http://mathworld.wolfram.com/SphericalHarmonicAdditionTheorem.html>. Accessed 11 May 2019. 378
- L. Wong and R. Gore. Accuracy of geoid heights from modified Stokes kernels. *Geophysical Journal of the Royal Astronomical Society*, 18(1):81–91, 1969. URL <https://doi.org/10.1111/j.1365-246X.1969.tb00264.x>. 218
- G. Wöppelmann, C. Letetrel, A. Santamaría-Gómez, M.-N. Bouin, X. Collilieux, Z. Altamimi, S. D. Williams, and B. Martín-Míguez. Rates of sea-level change over the past century in a geocentric reference frame. *Geophysical Research Letters*, 36(12), 2009. URL <https://doi.org/10.1029/2009GL038720>. 327
- YouTube, Hammer vs. Feather, 2010. URL https://www.youtube.com/watch?feature=player_embedded&v=KDp1tiUsZw8#! Accessed 7 April 2019. 4
- D.-N. Yuan, W. L. Sjogren, A. S. Konopliv, and A. B. Kucinskis. Gravity field of Mars: A 75th degree and order model. *Journal of Geophysical Research*, 106 (E10):23377–23401, 2001. URL <https://doi.org/10.1029/2000JE001302>. 282



Index

ABCDEFGHIJKLMNOPQRSTUVWXYZ

A

- a priori* information, 356
- a priori* variance, 355
- Aalto University, 394
- Abell 1689, 3
- acceleration
 - geometric, 369
 - measured by GNSS, 315
 - measured by gravimeter, 315
 - of aircraft, 315
 - of free fall, 304
 - satellite, 369
- accelerometer, 317, 369, 372
 - on GRACE, 370
- action at a distance, 1
- adjustment, least-squares, 355
- Agulhas Stream, 323
- air pressure, variations, 313
- airborne gravimetry, 245, 368
 - description*, 314
 - flight height, 316
 - homogeneity, 316
- Airy, George Biddell, 142
- Airy–Heiskanen hypothesis, 143, 149
- Airy–Heiskanen model, 142
- Åland, 366
- Alaska (USA), 146
- algebraic-sign domain, 83
- algebraic-sign interval, 57, 58
- altimetric satellite, 344, 359
- Amazonas (Brazil), 245, 371
- American Geophysical Union (AGU), 392
- amplifier, in fibreoptic cable, 184
- Amsterdam (The Netherlands), 161, 325
- analysis, *a posteriori*, 366
- angular distance, geocentric
 - definition*, 257
 - covariance function, 258, 263
 - degree constituent equation, 68
 - forward geodetic problem, 257
 - generating function, 198
 - Helmert condensation, 433
 - Stokes kernel, 188, 233
 - tangent plane, 228
- anisotropy, 197
- anomalous quantity, 85, 107, 109
- Antarctic Ocean, 366
- Antarctica, 126, 245, 316, 335, 339
- antimatter, 27
- anti-root, under sea, 145
- Apollo project, 4, 304
- Arabelos, Dimitris, 242
- Archimedes' law, 144
- Arctic, 245, 316
- Arctic Ocean, 366
 - ice cover, 366
 - ice volume, 366, 367
- argument of perigee, 358
- arrest (gravimeter), 303
- ascending node, 357, 358

- of the Moon, 379
- Asperger syndrome, 4
- associated Legendre function, 57
 - fully normalised, 66
 - symmetry, 62, 82
- associated Legendre functions
 - figure, 58
 - table, 58
- astatisation, 303
- astatisation ratio, 300, 301
- asthenosphere, 329, 335
- Atlantic Ocean
 - North, 334
 - salinity, 331
- atmosphere
 - attraction, 312
 - surface mass density, 312
 - total mass, 313
- atmospheric drag, 369, 370, 372
 - compensation, 316
- atmospheric loading, 388, 389
- atmospheric refraction, 159
- atomic clock, 182
- attenuation factor, 80, 81
- attenuation with height, 47, 54
- attraction, 5
 - exterior, 19
 - interior, 19
 - of a spherical shell, 8, 9
- autocovariance, 254
- autoregressive process, 265
- average density, of the Earth's crust, 129
- averaging over ocean surface, 338
- axial vector, 332
- azimuth, 197, 227, 228, 257, 258
 - definition, 257
- B**
- Baltic Sea
 - airborne gravimetry, 316
 - mean sea surface, 343
 - salinity, 331
 - sea-surface topography, 325, 331
- barometric heighting, 113
- Barzaghi, Riccardo, 242
- base network measurement, 309
- basis
 - complete, 415, 424, 425
 - in a function space, 424
 - in a vector space, 413, 419
- basis vector, 413–415
- bathymetry, 129, 136, 137
- Bergensbanen (Norway), 145
- Bessel's equation, 424
- BGI, 122, 132, 149, 391
- bias, of measurement, 347
- bilinear form, 413, 419
- Bjerhammar sphere, 283
- Bjerhammar, Arne, 283
- blue film, of the Earth, 369
- Blue Road Geotraverse project, 330
- bordering, 240
- Bose–Einstein condensate, 183, 308
- Bothnian Bay (Finland, Sweden), 331
- Bouguer anomaly, 129, 156
 - bias, 130, 132
 - calculation, 178
 - calculation steps, 134
 - example, 134
 - interpolation, 130
 - prediction, 130
 - properties, 130
 - simple, 130
 - Southern Finland, 132
 - spherical, 136
 - bias, 137
 - terrain corrected, 131
- Bouguer hypothesis, of land uplift, 328, 329
- Bouguer plate
 - as approximation, 129, 172
 - attraction, 127, 128, 130, 441
 - double, 175
 - half, 135
 - of air, 312
- Bouguer reduction, 127, 207, 213
 - simple, 130
- Bouguer shell, attraction, 136
- Bouguer, Pierre, 126, 140
- Boulder, University of Colorado at, USA, 304, 346
- boundary condition, 44, 45, 117
 - periodicity, 422



- boundary surface, choice, 125
 boundary-value problem, 35, 42, 125
 definition, 34
 free, 113
 of Dirichlet, 35, 117, 200
 of Neumann, 71, 72, 117
 of physical geodesy, 117
 spectral solution, 118
 third, 114, 117
 bounded support, 229
 box, rectangular, 24, 25
 Brovelli, Maria, 242
 Bruns equation, 111, 124, 172, 188, 387
 Bruns vertical-gradient equation, 92
 Bruns, Ernst Heinrich, 92, 111
 bulldozer, 208
 Bureau Gravimétrique International, *see* BGI
- C**
 cage, in absolute gravimeter, 304
 Calgary (Canada), 240
 calibration
 gravimeter, 312
 in-flight, 348, 364
 radar altimeter, 348, 364
 calibration certificate, 312
 cannon, 83
 carbon dioxide, 331
 Cavendish, Henry, 4, 358
 celestial mechanics, 13
 celestial sphere, *see* unit sphere
 central force field, 398
 centrifugal acceleration, 88
 centrifugal force, 87, 106
 divergence, 319
 centrifugal potential, 86
 expression, 88
 CHAMP (satellite), 74, 244, 369
 characteristic equation, 421
 Chasles theorem, 2, 34, 36
 Chasles, Michel, 34
 checkerboard, 59
 chlorophyll, 331
 circular disk, attraction, 128
 climate research, 336
 climate, of Earth, 334
 clinometer, 384
 clinometer, long water-tube, 384
 clock, 182
 pendulum, 295
 closing error, 303
 coastline, 388
 coastline mask, 366
 coefficient vector, 419
 co-geoid, 126
 of isostatic reduction, 150, 155
 coherence, of matter waves, 183
 collocation, least-squares (LSC), 150, 242, 263, 265, 269
 description, 258, 266
 FFT, 284
 flexibility, 270
 Columbus geoid (model), 142, 394
 commutative diagram, 46, 71, 213, 214, 232
 comparison point, for geoid
 determination, 326
 compensation depth, 149, 151
 component, of a vector, 400
 Congo (Africa), 371
 conservative field, 159, 180
 definition, 5, 405
 curl, 409
 potential, 405, 409
 continental ice sheet, 146, 147, 327, 335
 continental ice sheets, total mass, 336
 continental shelf, 145
 continuity equation, 411
 convection, in the Earth's mantle, 151
 convolution, 15, 46, 237, 286
 calculation, 237
 linear combination, 235
 notation, 229
 sea-level equation, 337
 terrain correction, 246
 two-dimensional, 229
 convolution theorem, 229, 230, 240
 co-ordinate conversion, 51
 co-ordinate reference system
 co-rotating, 87, 319
 inertial, 87
 co-ordinate time, 182
 co-ordinate transformation, 395



- co-ordinates
 - cylindrical, 42
 - ellipsoidal, 52
 - geodetic, 50
 - definition, 52
 - geographical, 50, 234
 - natural, 94, 95
 - polar, 408
 - rectangular, 5, 50
 - spherical, 30, 42, 50, 55
 - definition, 51
 - topocentric, 317
 - toroidal, 42
 - Copenhagen (Denmark), 240, 393
 - coral, 336
 - Coriolis acceleration, 332
 - direction, 332
 - Coriolis effect, 331
 - Coriolis force, 88, 324, 332
 - Coriolis, Gaspard-Gustave, 88
 - corkscrew rule, 397, 400
 - correlation, 261
 - correlation length, 263, 264, 293
 - correlation, quasi-geoid & topography, 170, 171
 - correspondence, integral & spectral equations, 189
 - cosine rule, 233, 377
 - half-angle, 233
 - cosine taper, 240
 - covariance function, 256, 269
 - definition, 257
 - empirical, 282
 - Gauss–Markov, 269
 - global, 283
 - isotropic, 274
 - of gravity anomalies, 280
 - of Hirvonen, 263, 264, 266
 - of the disturbing potential, 273, 291
 - in space, 278, 280
 - on the Earth's surface, 279
 - spectral representation, 274
 - cross covariance, 254
 - cross product, *see* vectorial product
 - crossover adjustment, 355, 368, 375
 - global, 357
 - crossover condition, 357
 - crossover difference, 356, 368, 375
 - crossover point, 350, 354, 355
 - crustal density, 143, 245
 - Cryosat-2 (satellite), 345
 - curl (operator), 404, 405
 - interpretation, 404
 - linearity, 402
 - of gradient, 404
 - of wind field, 404
 - curvature
 - of a level surface, 90, 91, 318
 - of field line, 93, 108, 167
 - of plumb line, 92, 93
 - of the Earth, 133, 144, 229
 - cyclone, tropical, 323
- D**
- damping, of gravimeter, 304, 314, 315
 - Danish straits, 331
 - Darwin, Sir George, 381
 - datum, 354
 - datum defect, 354
 - datum point, 161
 - datum transformation, 354, 356
 - Dead Sea (Levant), 152
 - declination, of the Moon, 377
 - Defense Mapping Agency, US (DMA), 73
 - deformation
 - of the Earth, 382
 - viscous, 340
 - deglaciation, last, 148, 327, 340
 - degree constituent
 - of powers of height, 437, 439
 - of the disturbing potential, 104
 - of the gravity anomaly, 115
 - degree constituent equation, 68–70, 118, 187
 - data point, 68
 - evaluation point, 68
 - harmonic field, 199
 - degree number, of tidal force, 384
 - degree of freedom, 356, 357
 - degree variance
 - notation, 276
 - of gravity anomalies, 281, 282
 - of the disturbing potential, 274, 276



- on the Earth's surface, 280
 - degree variance formula, 282
 - degree, harmonic, 54, 57, 61, 216
 - definition, 53
 - Delft (The Netherlands), 240
 - delta function, Dirac's, 27, 202, 285, 340
 - Denker, Heiner, 242
 - density
 - ice, 147, 337, 366
 - mantle, 144
 - rock, 95, 176
 - sea water, 144, 146, 337, 366
 - standard crustal, 176
 - topography, 172, 210
 - upper mantle, 148
 - density model, 36
 - density profile, 36
 - density, SI unit, 11
 - developing country, education, 392
 - dice throw, 254
 - difference, geoid – free-air geoid, 173
 - difference, height anomaly – free-air geoid, 172
 - difference, height anomaly – geoid height, 172
 - difference, orthometric height – normal height, 174
 - difference, quasi-geoid – geoid, 173, 178
 - differential operator, 406
 - digital terrain model (DTM), 131, 208, 366
 - dipole, 20, 67, 68
 - dipole field, 105
 - dipole moment, 67
 - definition, 20
 - of the Earth, 67
 - vanishing, 76
 - dipole surface density, 20
 - dipole-density layer, 20, 440
 - dipole-layer element, 20
 - Dirac, Paul, 27
 - directional sphere, *see* unit sphere
 - Dirichlet, Peter Gustav Lejeune, 35
 - Dirichlet's problem, 2
 - dislocation (crystal), 302
 - disturbing potential, 107, 123
 - definition, 103
 - at terrain level, 211
 - local, 230
 - spherical-harmonic expansion, 104
 - surface harmonics, 54
 - divergence (operator), 16, 22, 403, 406, 411
 - interpretation, 403
 - linearity, 402
 - Doodson, Arthur Thomas, 381
 - Doodson's constant, 381, 387
 - DORIS (positioning instrument), 345
 - dot product, *see* scalar product
 - downwards continuation, harmonic, 172, 207, 209, 210, 245, 435
 - existence, 200, 208
 - of $r\Delta g$, 201
 - drift (gravimeter), 302, 311
- E**
- Earth
- centre of mass, 50, 67, 74, 105, 115
 - flattening, 50, 51, 74, 98
 - gravitational field, 41, 369
 - spectral representation, 2
 - gravity field, 74
 - radius, 18
 - rotation rate, 88, 98, 385
- earthquake, 311, 340
- eccentricity, orbital, 358
- eddiness, in a vector field, 404
- eddy, 345
- eddy phenomenon, 88
- eddy-free flow, 411
- EGM96 (geopotential model), 73
 - coefficients, mean errors, 75
- EGM2008 (geopotential model), 61, 74, 122, 132
- Eiffel Tower, 92
 - 72 names, 16, 17, 34, 45, 55, 88, 424
- eigenvalue problem, 418–420
- eigenvectors of a symmetric matrix, 420
- eight-unit cube, 27
- Einstein summation convention, 261
- Einstein, Albert, 4
- El Niño Southern Oscillation (ENSO), 323
- elasticity, 92, 302
 - of the Earth, 382, 383, 388
 - of the Earth's crust, 388



- elasticity model, 386
 electric charge, conservation, 399
 electric currents, in the Earth's core, 151
 electrostatic compensation, 314
 electrostatic potential, 406
 ellipsoid of revolution, 50
 ellipsoidal harmonic, 95
 ellipsoidal-harmonic expansion, 77
 definition, 76
 centrifugal potential, 95
 computation, 79
 convergence, 79
 normal potential, 78
 RMS *Empress of Ireland*, 161
 energy
 conservation, 399
 of place, 161
 Envisat (satellite), 344
 Eötvös (unit), 116, 318
 Eötvös tensor, 317
 Eötvös, Loránd, 89
 epoch
 of land uplift, 326
 of measurement, 306
 equations of motion, of satellites, 67
 equatorial radius, *see* semimajor axis,
 Earth ellipsoid
 equilibrium length, of spring, 298, 299
 equipotential surface, 19
 as boundary, 33, 34
 figure, 111
 equivalence principle, 4, 89
 ergodicity, 256
 error ellipse, 421
 ERS-1 (satellite), 344
 ERS-2 (satellite), 344
 escape velocity, 83
 estimation, 259
 estimator, 260
 mean error, 266
 optimal, 261
 Eterna (software), 388
 Ethiopia, 245
 Euclidean space, 5, 10, 413
 Euler angle, 404
 Euler notation, 92
 Euler's identity, 431
 Eurajoki (Finland), 309
 European climate, 334
 European Geosciences Union (EGU), 392
 European Space Agency (ESA), 344, 345,
 371
 eustatic rise, of mean sea level, 327, 328,
 337
 evaluation functional, 252
 evaluation latitude, 234
 Everest, Mount, 146
 expectancy
 of a stochastic process, 256
 statistical, 255
 exterior product, *see* vectorial product

F
 factorial, 55
 Falkland Islands, 372
 Faller, James E., 304
 Faraday, Michael, 23, 410
 Fast Collocation, 150, 287
 Fast Fourier Transform (FFT), 15, 150, 232
 algorithms, 431
 and convolution, 230
 and tapering, 241
 collocation, 284, 286
 mixed-radix, 429
 radix 2, 429
 terrain correction, 245, 248
 Fastest Fourier Transform in the West
 (fftw, software), 431
 Father Point / Pointe-au-Père (Rimouski,
 Quebec, Canada), 161
 Fennoscandia, 147, 326, 339
 Fennoscandian Shield, 149
 fibreoptic cable, 184
 field equations
 of electromagnetism, 17
 of gravitation, 1, 17
 field line, 23, 403, 410
 field theory
 of electromagnetism, 42
 of gravitation, 1
 field, the concept, 41
 figure of the Earth, 85, 89, 126, 141, 359
 FIN2000 (geoid model), 243, 244, 326



- precision, 244
 - FIN2005Noo (geoid model), 244, 393
 - precision, 244
 - finite element method (FEM), 150
 - Finland, 160, 175, 244, 304
 - Finnish climate, 334
 - Finnish Geodetic Institute (FGI), 304, 310, 384, 393
 - Finnish Geospatial Research Institute (FGI), 394
 - first eccentricity, 51
 - flat Earth model, 144
 - flattening, of a planet, 13
 - flow velocity, 23, 403, 411
 - vector field, 333
 - fluid motion in gravity field, 161
 - flux, 23
 - fluxion, 328
 - footprint, radar altimeter, 347, 365, 366
 - footscrews, 300
 - Forsberg, René, 240, 242
 - Fourier basis function, 46, 55, 63, 415
 - Fourier coefficient, 45, 53
 - Fourier series, 415, 431
 - Fourier sine expansion, 45
 - Fourier theory, 192
 - Fourier transform, 46
 - artefacts, 240
 - discrete, 230, 232, 429, 431
 - periodicity, 239, 240
 - reverse, 430
 - forward, 230
 - of l^{-3} , 247
 - notation, 229
 - reverse, 230, 247
 - Fourier, Joseph, 45
 - France (funding), 391
 - free oscillations, of the solid Earth, 311, 393
 - periods, 311
 - free-air anomaly
 - definition, 120
 - calculation, 121, 178
 - linearisation, 120
 - Southern Finland, 122
 - use, 121
 - free-air hypothesis, of land uplift, 329
 - free-air reduction, 134
 - freeboard, 345, 366
 - French Academy of Sciences, 126
 - frequency domain, 46, 231, 232
 - fresh water, 323, 331
 - fulcrum, of a pendulum, 297
 - function space, 252, 253, 414, 415, 422, 424
 - on the sphere, 424
 - function theory, 414
 - functional, 276
 - definition, 252
 - linear, 35, 253, 276, 282
 - definition, 252
 - of the disturbing potential, 253
 - of the disturbing potential, 252
 - fundamental equation of physical geodesy, 114, 117, 211
- G**
- Galilei, Galileo, 4
 - gauge invariance, 17
 - Gauss integral theorem, 2, 28, 30, 33, 410, 443, 444
 - figure, 23, 410
 - presentation, 22
 - book-keeping, 24
 - in terms of potential, 24
 - Gauss, Carl Friedrich, 22
 - Gauss–Markov process, 265
 - Gelderens, Martin van, 240
 - general relativity, 17, 182
 - generating function
 - geometry, 197
 - of the Legendre polynomials, 151, 198
 - geodetic forward problem on the sphere, 257
 - Geodetic Reference System 1967 (GRS67), 100
 - geographic mean, 256–258, 270
 - definition, 255
 - geographic variance, 255
 - geoid, 116, 151, 164, 323, 324
 - definition, 89, 163
 - classical, 324
 - fake, 176



- free-air, 172
- true, 368
- geoid determination, 34, 73, 214, 367, 391, 392
- 1D-FFT, 239
- classical, 126
- FFT, 240, 242
- gravimetric, 189, 220, 330, 331
 - principle, 188
 - computational framework, 191
- NKG, 393
- precise, 176
- software, 242
- spherical FFT
 - multi-band, 234
 - Taylor expansion, 235
- geoid height, 107, 117, 172, 178, 345, 349
 - definition, 108
 - from satellite altimetry, 244
 - reduced, 214
- geoid map, 372
- geoid model, 150
 - computation, 242
- global
 - high resolution, 369
 - precise, 369, 373
 - gravimetric, 326
 - local, 325
 - of Finland, 110
- geoid rise, 327, 328
- geoid undulation, 108
 - global, 108
 - in Finland, 108
- geological map, 177
- geometric geodesy, 103
- geophysical data record (GDR), 348, 365
- geophysical reduction, 126
- geopotential, 95
 - gradient, 317
 - level surface, 89
 - on the tangent plane, 91
 - spectral expansion, 70
- geopotential image, sharpness, 61
- geopotential model, global, 369
- geopotential number, 161, 163
 - definition, 160
- GEOS-3 (satellite), 343
- Geosat (satellite), 343
- geostrophic equilibrium, 332
- Germain curvature, 91
- Germain, Marie-Sophie, 91
- German Research Centre for Geosciences (GFZ), 369
- Gibbs phenomenon, 217, 240, 417
- Gibbs, Josiah Willard, 217
- glacial isostatic adjustment (GIA), 327, 339
- glacial maximum, last, 147
- glacier, 152, 327, 337
 - retreat, 146
- global warming, 335
- GM_{\oplus} , best value, 6
- GNSS
 - height of gravimetric stations, 126
 - in airborne gravimetry, 315
 - in aircraft, 315
 - in altimetric satellite, 368
 - in height determination, 242
 - measuring atmospheric, ocean tidal loading, 389
 - orbital tracking, 372
 - positioning of tide gauges, 327, 330
- GNSS levelling, 326
- GOCE, 74, 244, 316, 333, 334, 373
 - description, 371
 - name, 374
- GPS
 - on satellite, 344, 369
 - orbital tracking, 370
 - reference system, 99
- GRACE (satellite pair), 74, 244
 - description, 369, 371
- GRACE follow-on mission, 371
- grade measurement, 126
- gradient
 - of Earth attraction, 372
 - of gravity disturbance, 291
 - of potential, normal direction, 34
- gradient (operator), 9, 12, 402, 404
 - interpretation, 402
 - linearity, 402
 - of scalar field, 401



- gravimeter
- absolute, 304, 330
 - principle of operation*, 305
 - airborne, 304, 314
 - astatized, 299, 301
 - atomic, 308
 - principle of operation*, 309
 - ballistic, 297, 304
 - FG5, 304, 306
 - IMGC-02, 307
 - JILA, 304
 - LaCoste-Romberg, 299, 301, 305
 - pendulum, 296
 - quantum, *see* gravimeter, atomic
 - registering, 389
 - relative, 330
 - sea, 303, 368
 - spring, 296, 297, 300, 302, 309
 - superconducting, 310, 311
- gravimetry, 74
- airborne, *see* airborne gravimetry
 - satellite, 316
 - study of Earth interior, 36
- gravitation, 3
- gravitational acceleration, 4, 11, 13, 34, 89
- measurements, 73
- gravitational acceleration vector, 9–11, 16
- gravitational constant, universal, 2, 337, 358, 377, 398
- gravitational field, 5, 22
- of celestial objects, 386
- gravitational force, 41
- gravitational gradiometer (GOCE), 368
- description*, 372, 373
- gravitational lens, 3
- gravitational potential, 1
- in a vacuum, 406
 - rotationally symmetric, 95
- gravitational vector, 11
- gravitational wave, 17
- gravity, 127, 296, 314, 330
- definition*, 304
 - absolute measurement, Finland, 309
 - along levelling line, 182
 - equatorial, 100
 - in airborne gravimetry, 314
 - in the tropics, 295
 - local, 165, 295, 315
 - measurement, 116
 - on the rotating Earth, 88
 - prediction, 213
 - total, 314
- gravity acceleration, 89
- from pendulum, 296
 - on the plumb line, 95
- gravity anomaly, 113, 273
- a priori* estimate, 268
 - definition*, 117
 - as a boundary condition, 117
 - as a functional, 253
 - at sea level, 201, 206
 - at topography level, 206
 - atmospheric reduction, 313
 - availability, 251
 - block average, 220, 222, 270
 - calculation, 113, 120
 - change, 328
 - estimate, 267, 268
 - from satellite altimetry, 244
 - global average, 255
 - horizontal gradient, 222
 - in the external space, 200
 - mean error, 267
 - observations, 266
 - reduced, 214
 - surface harmonics, 54
- gravity disturbance, 291
- definition*, 112
 - observing, 113
 - spectral representation, 112
- gravity field, 2, 85, 163
- change, 339
 - determination, 282, 370, 373
 - exterior, 121, 211
 - fine structure, 368
 - GOCE resolution, 317
 - observation density, 251
 - oceanic, 343
 - of mountains, 140
 - research in Europe, 392
 - research in Finland, 393
 - research in HUT, 394



- research internationally, 391
 - residual, 213
 - spatial variability, 229
 - statistical behaviour, 263
 - temporal change, 369
 - textbooks, 394
 - very local features, 372
 - gravity formula, 85, 98, 100, 121
 - gravity gradient, 116, 318, 384
 - free air, 389
 - gravity mapping survey, 309
 - gravity potential
 - as sum of gravitational and centrifugal potentials, 88
 - gradient, 409
 - in spherical harmonics, 103
 - of falling atoms, 308
 - gravity vector, 163
 - gravity vector field, 409
 - gravity versus gravitation, 87
 - gravity-gradient field of Sun and Moon, *see* tidal field
 - gravity-gradient tensor, 317, 318
 - GRAVSOF (software), 242
 - Green equivalent-layer theorem, 34
 - Green, George, 29
 - Greenland, 126, 245, 335, 339
 - Greenland Aerogeophysics Project (GAP), 316
 - Green's first theorem, 29
 - Green's function, 337, 339
 - of sea level, 338
 - of the geopotential, 338
 - of vertical displacement, 338
 - partial, of deformation, 338
 - Green's second theorem, 29
 - Green's theorems, 2
 - Green's third theorem, 29, 125
 - exterior point, 30
 - external space, 32
 - interior point, 31
 - Greenwich meridian, 50
 - grid
 - of gravity anomalies, 230
 - of the disturbing potential, 231
 - of the Stokes kernel, 231
 - grid integration, 150
 - grid matrix calculation, 238
 - grid representation, 230
 - GRS80
 - definition, 99
 - GM_{\oplus} , 6
 - spherical-harmonic coefficients, 102
 - Gulf of Finland, 331
 - airborne gravimetry, 316
 - Gulf Stream, 323, 332–334
 - Guyana, French, 295
 - GWR *i*Grav (gravimeter), 312
 - GWR20 (gravimeter), 310
- ## H
- Haagmans, Roger, 240
 - Hannover (Germany), 242
 - Hardanger plateau (Norway), 145
 - harmonic continuation
 - of gravity anomalies, 202
 - of the potential, 276
 - harmonic field
 - definition, 16
 - $r\Delta g$, 200
 - harmonic oscillator, 44, 448
 - hat notation, of estimator, 269
 - Hayford ellipsoid, 100, 121
 - Hayford, John Fillmore, 141
 - heat transport, 331, 334
 - height
 - above mean sea level, 163, 164
 - above the geoid, 163
 - above the reference ellipsoid, 51, 109, 166, 345
 - height anomaly, 119, 120, 166, 169, 171
 - definition, 165
 - height system, 393
 - national, 325, 326, 354
 - Heiskanen, Veikko Aleksanteri, 142, 394
 - helicopter, 315
 - helium, liquid, 310, 312
 - Helmert condensation, 2, 138, 139, 207, 213, 433, 439, 440
 - gravity effect, 439
 - Helmert ellipsoid, 100
 - Helmert height, 172, 326
 - definition, 175



- as approximation, 175
 - Helmert, Friedrich Robert, 138
 - Helsinki (Finland), 325
 - Helsinki astronomical observatory, 161, 162
 - Helsinki harbour, 160, 325, 354
 - Helsinki University of Technology (HUT, TKK), 394
 - Himalayas, 140
 - Hirvonen, Reino Antero, 263
 - Hirvonen's geoid model, 393
 - Hofmann-Wellenhof, Bernhard, 394
 - homogeneity
 - of data precision, 287
 - of gravimetric data, 316
 - homogeneity assumption, 255, 256
 - horizon plane, 332
 - hour angle, of the Moon, 377
 - Hubble Space Telescope, 3
 - Huygens, Christiaan, 295
 - HY-2A (satellite), 345
 - hydrodynamics, 385
 - hydrosphere, 369
- I**
- ice age, last, 329, 335, 339
 - ice cap, 327
 - ice load, 329, 339
 - history, 338
 - ice sheet, 337, 340
 - Laurentide, 335
 - ice, multi-year, 367
 - identity matrix, 285
 - ill-posed problem, 208
 - inclination, orbital, 358, 359, 361, 362
 - of the Moon, 379
 - incompressibility, 23, 411
 - independence, statistical, 266
 - India, 345
 - indirect effect, 126
 - of Bouguer reduction, 150, 207
 - of Helmert condensation, 207, 439, 441
 - constant terrain, 439
 - of isostatic reduction, 150, 154, 207
 - of residual terrain modelling (RTM), 209
 - of the tidal potential, 383, 386
 - Indonesia, 366, 371
 - inertial tensor, 68
 - instantaneous length, of spring, 301
 - Institut für Erdmessung* (Hannover, Germany), 242, 392
 - integrability, 424
 - integral equation, 2
 - integration by parts, 423
 - intercomparison, of absolute gravimeters, 307, 309, 310
 - International Association of Geodesy (IAG), 242, 391
 - International Center for Earth Tides (ICET), 392
 - International Center for Global Earth Models (ICGEM), 392
 - International Digital Elevation Model Service (IDEMS), 392
 - International Geodynamics and Earth Tide Service (IGETS), 310
 - International Geoid Commission (IGeC), 392
 - International Geoid Service (IGeS), 392
 - International Gravimetric Bureau, *see* BGI
 - International Gravity Field Service (IGFS), 391, 392
 - International Isostatic Institute, 394
 - International Service for the Geoid (ISG), 391
 - International Union of Geodesy and Geophysics (IUGG), 391
 - interpolation from grid, 231, 232
 - invariant, 421
 - inversion calculation, 232, 238
 - inverted barometer, 323
 - isostasy, 1, 141, 142
 - modern understanding, 146, 147
 - isostasy hypothesis, 140
 - isostatic anomaly
 - definition, 148
 - interpolation, 148
 - prediction, 148
 - Southern Finland, 149
 - isostatic compensation, 142, 143
 - definition, 140



- percentage, 151
- isostatic equilibrium, 296
- isostatic geoid, 150, 151
- isostatic hypothesis, 141, 143, 150
- isostatic reduction, 148, 149, 213
 - description, 151
 - and density layers, 153
 - residual field, 148
- isotropic density distribution, 9
- isotropic process, 263
- isotropy, 197
 - and spectral representation, 197
 - of the disturbing potential, 273
 - of the viscosity, 338
- isotropy assumption, 258
- Italy (funding), 392
- iteration
 - calculation of normal height, 177
 - calculation of orthometric height, 164, 175
- J**
- J_2 (dynamic flattening), 74, 99, 359, 360
- Jacobi, Carl Gustav Jacob, 65
- Jacobi's determinant, 127
 - definition, 408
 - map projection co-ordinates, 229
 - polar co-ordinates, 225, 408
 - spherical co-ordinates, 65, 197, 227, 258, 408, 425
- Jason (satellites), 345, 361
- Java Sea (Dutch Indies, Indonesia), 296
- Jerry (GRACE satellite), 370
- Joensuu (Finland), 309
- K**
- Kääriäinen, Jussi, 316
- Kaivopuisto (Helsinki, Finland), 161, 162, 325
- Kater, Henry, 296
- Kater's reversion pendulum, 296
- Kaula, William, 282
- Kepler, Johannes, 221, 357
- Kepler's laws, 357
- Kepler's orbital elements, 358
- Kepler's second law, 398, 399
- Kepler's third law, 357, 363, 376
- kernel modification
 - advanced, 218
 - coefficients, 218
 - degree, 216
 - sharp cut-off, 216
 - soft, 217
 - Wong–Gore, 216, 218
- Kevo (Finland), 309
- Kirkkonummi (Finland), 310, 325
- KKJ, 121
- Knudsen, Per, 242
- Kolkata (India), 141
- Krasovsky ellipsoid, 100
- Kronecker delta, 285
- Kronstadt (Russia), 161
- Kuusamo (Finland), 309
- L**
- LaCoste, Lucien, 301
- LAGEOS (satellite), 358
- land uplift
 - absolute, 327, 328
 - Fennoscandian, 340
 - post-glacial, 325, 327, 393
 - mechanism, 329
 - relative, 327, 328
- Laplace equation, 16, 41, 319
 - definition, 41
 - basis solutions, 53
 - in ellipsoidal co-ordinates, 75
 - in polar co-ordinates, 47
 - in rectangular co-ordinates, 43
 - in spherical co-ordinates, 52, 443
 - linearity, 42, 43
 - solution, 41
 - transformation, 42
- Laplace operator (Δ), 406
 - definition, 16, 41
 - linearity, 252
- Laplace, Pierre-Simon, 16, 406
- Lapland (Northern Europe), 127
- laser interferometer, 304
- latitude
 - astronomical, 94, 107, 121
 - geocentric, 50, 52, 98
 - geodetic, 98, 106, 107, 234
 - geographic, 98



- reduced, 52, 98, 106
 - types, 97
 - least-squares method, 307, 326
 - ordinary, 351
 - Legendre function, 53, 55, 448
 - fully normalised, 426
 - of the second kind, 76, 78
 - Legendre polynomial, 55
 - fully normalised, 65
 - Legendre polynomials
 - as a basis, 424
 - figure, 56
 - orthogonality on the interval $[-1, +1]$, 64
 - orthogonality on the unit sphere, 65
 - orthonormality on the unit sphere, 66
 - table, 56
 - Legendre, Adrien-Marie, 55
 - Legendre's equation, 424, 448
 - Lego™ brick, 26
 - Leibniz University (Hannover, Germany), 392
 - Leibniz, Gottfried Wilhelm, 1
 - level surface, 90, 163, 324, 373
 - definition, 89
 - level, bull's eye, 300
 - levelling, 94, 163
 - principle, 159, 160
 - geostrophic, 331
 - new technologies, 393
 - relativistic, 183
 - steric, 331
 - levelling instrument, 159
 - levelling line, 181
 - levelling staff, 159
 - levelling, of gravimeter, 300
 - lever beam, 299, 303
 - lever motion, 336
 - linear partial differential equations,
 - theory of, 42
 - linear regression, 347
 - Liouville, Joseph, 424
 - localised kernel, 203, 211
 - location vector of a mass element, 67
 - Lohja (Finland), 384
 - longitude
 - astronomical, 94, 107
 - geodetic, 108
 - of the Moon, 379, 380
 - lookup table, 431
 - Love number, 383, 384, 386, 388
 - determination, 384
 - by GNSS, 384
 - elastic, 340, 383
 - viscous, 340
 - Love, Augustus, 383
 - LSC, *see* collocation, least-squares
 - lunar laser ranging (LLR), 304
- M**
- magnetic field, 310
 - of the Earth, 151, 310
 - Mäkinen, Jaakko, 165
 - Maldives (Indian Ocean), 336
 - map projection co-ordinates, 227, 228
 - map projection plane, 214
 - mareograph, *see* tide gauge
 - Mars (planet), gravity field, 282
 - mass density, 16
 - mass distribution inside the Earth, 35
 - mass point, underground, 239, 293
 - mass surface density, 18, 138
 - mass-density layer, 1, 207
 - double, 20, 33, 440
 - single, 18, 33, 138, 151, 189
 - matter density, 11, 12, 411
 - matter, conservation, 23
 - Mauna Kea, 157
 - Maupertuis, Pierre de, 126
 - Maxwell, James Clerk, 17
 - mean error of unit weight, 307, 355
 - mean geoid, 385
 - mean sea level, 116, 163, 324
 - definition, 323, 324
 - global, 325, 327
 - location, 115
 - mean sea surface, 359
 - measurement axis, 304
 - measuring telescope, 159
 - mechanics, of the solid Earth, 385
 - Meissner effect, 310
 - Mekong (river), 371



- Melchior, Paul, 381
 meridian convergence, 232
 meridian ellipse, 97
 mesoscale eddy, 323, 334
 metal fatigue, 302
 metallurgy, 302
 Metsähovi research station (Finland), 161, 309–311, 325
 microgal (μGal), 115
 microseismicity, effect on gravimeter, 302, 304
 microwave link (GRACE), 370
 mid-Holocene highstand, 336
 Milan (Italy), 240, 392
 milligal (mGal), 115
 Min, Erik de, 240
 minimum energy state, 161
 mirror antisymmetry, 57
 mirror symmetry, 57, 63
 missile, submarine-launched ballistic, 343
 mixed covariance, 281
 modal strength, 340
 Mohorovičić, Andrija, 154
 Mohorovičić discontinuity (“Moho”), 154, 248
 Molodensky theory, 34, 119
 Molodensky, Mikhail Sergeevich, 34, 119, 125, 164–166, 394
 Molodensky’s method, 206
 height anomaly, 212
 linearisation, 210
 linearisation error, 212
 Molodensky’s realisation, 166, 169, 170
 momentum
 angular, 397
 conservation, 399
 per unit of mass, 399
 linear, 397
 Mongolia, 245
 monopole, 67, 68
 monsoon, 371
 Moritz, Helmut, 394
 mosaic, 59
 mu-metal, 310
 Munk, Walter, 345
- N**
 N60 (height system), 160, 244, 325
 N2000 (height system), 161, 244, 325
 nabla (∇ , operator), 10, 401
 National Geospatial-Intelligence Agency, US (NGA), 73, 391
 National Imagery and Mapping Agency, US (NIMA), 73
 National Land Survey of Finland, 310, 393
 National Map Grid Co-ordinate System, *see* KKJ
 NAVD88, North American Vertical Datum 1988, 161
 Navy, United States, 343
 network densification, stepwise, 308
 network hierarchy, 308
 Neumann, Carl Gottfried, 71
 Newton, Isaac, 2, 13
 Newton’s law of gravitation, 1, 246
 definition, 2
 for a spherical Earth, 317
 Newton’s law of motion, 4
 Newton’s theory of gravitation, 1, 17
 Niethammer, Theodor, 176
 Niethammer’s method, 176
 NKG Working Group for Geoid and Height Systems, 393
 NKG2004 (geoid model), 393
 NKG2015 (geoid model), 393
 NN (height system), 161
 noise
 definition, 260
 in altimetry observations, 349
 observational, 260
 noise variance matrix, 260, 270
 Nordiska Kommissionen för Geodesi (NKG), 393
 norm, of a vector, 5, 396, 414
 Normaal Amsterdams Peil (NAP), 161
 normal component, of a vector field, 407
 normal correction (NC), 181
 equation, 181
 for staff interval, 181
 normal derivative, 19
 existence, 31
 of potential, 19



- on surface of sphere, 26
- normal direction, 19
 - existence, 31
- normal equation, 307
- normal gravitational potential, 86
- normal gravity
 - definition, 85
 - at sea level, 121
 - calculation, 113
 - GRS80, 99
 - linearity along the plumb line, 166, 169, 177
 - on the equator, 97
 - on the poles, 97
 - on the reference ellipsoid, 97, 98
- normal gravity field, 86
 - and reference ellipsoid, 108
 - choice, 177
 - ellipsoidal, 98
 - GRS80, 313
- normal gravity vector, 108, 111, 167
- normal height, 164, 169, 171
 - calculation, 177, 178, 181
 - precise calculation, 177
- normal matrix, 351
- normal plumb line, 108, 109, 167
- normal potential, 85, 86, 96
 - definition, 85
 - global average, 115
 - gradient, 85
 - GRS80, 99
 - in a co-rotating system, 100
 - in spherical harmonics, 103
 - on the reference ellipsoid, 96, 98, 167
 - over the equator, 100, 101
- normal vector, of a surface, 407, 411
- Norwegian Sea, 145
- Nottingham (Great Britain), 29
- Nouvel, Henri SJ, 161
- O**
- obliquity, of the Earth's rotation axis, 390
- observation equation, 270
 - adjustment constraint, 351
 - of ballistic gravimetry, 306, 307
 - of crossover adjustment, 349, 353, 375
- of levelling, 351
- of satellite altimetry, 349
- ocean current, 333, 334
 - GOCE mission, 333
 - inversion problem, 373
 - measurements, 331
 - permanent, 324
 - tilt, 332
 - unit, 333
 - variation, 334
- ocean loading, 388
- oceanography, 385
- octave (programming language), 63, 363
- Ohio (USA), 142, 264
- Ohio State University, 73, 74, 394
- one-Earth problem, 255
- operator
 - linear, 35, 418, 419
 - self-adjoint, 419, 420, 423
 - spectral representation, 277
- optical lattice clock, 183
- optimality, least-squares, 262
- orbit
 - 35-day, 364
 - no-shadow, 360, 361
 - retrograde, 361, 362
 - Sun-stationary, 360–362, 372
 - Sun-synchronous, 360, 376
 - three-day, 364
- orbit correction, 346, 349, 353
 - bias, 356
 - trend, 354, 356
- orbit error, 348
 - correction, 368
- orbit prediction, 354
- order, harmonic, 53
- orientation, of a surface, 411
- orthogonal basis, 414, 425
 - complete, 420
 - Legendre polynomials, 424
- orthogonality
 - of degree constituents, 275
 - of functions, 424
- orthometric correction (OC), 179, 181
 - equation, 180
 - for staff interval, 181



- orthometric height, 108, 163, 172
definition, 94, 163
 calculation, 164, 178, 179
 precise calculation, 174, 176
- orthonormal basis, 10, 67, 87, 90, 414, 415, 420
definition, 5, 400
- orthonormality, 192
- oscillation equation, 298, 302, 422, 424
 as an eigenvalue problem, 422
- Ostrobothnia (Finland), 326
- OSU model, 74
- P**
- paleo-research, 146
- parallax, 377
- parallelogram, 397
- path integral, 9, 409
- Peltier effect, 335
- Peltier, W. Richard, 336
- pendulum clock, 295
- pendulum equation, 295
- penplain, 145
- period
 fortnightly tide, 379
 orbital, 358
 oscillation, 298, 302
 pendulum, 295
 theoretical tide, 381, 384
- Peru (South America), 126
- petroleum extraction industry, 242
- phase angle
 of an atom, 308
 of matter waves, 308
- phase angle, tidal, *see* tide
- phase, of water, 335
- physical geodesy
 geometry and physics, 50
 potential convention, 10
 textbook, 394
- physical modelling, 331
- physical theory, nature of, 1
- phytoplankton, 331
- Pizzetti, Paolo, 98
- planet as a mass point, 13
- plasma, 183
- plasticity, 302
- plate tectonics, 147
- Plesetsk Cosmodrome (Russia), 369, 371
- plumb line, 90
definition, 85
 bending, 141
- plumb-line deflection, 107, 108, 123, 140, 196
definition, 86, 107
 and the geoid, 108
 as a functional, 253
 at sea, 343
 in Finland, 108
 local contribution, 222
 observed, 110
- plumb-line direction, 107, 112, 315
 absolute, 385
 measurement, 94
- point mass, underground, 34
- point variance, 421
- Poisson equation, 26, 176
definition, 17
 data point, 199, 200
 evaluation point, 199
 for computing a harmonic field from surface values, 199
 for $r\Delta g$, 201
 gravity potential, 89
 spectral form, 201
- Poisson kernel for gravity anomalies, 201–203
- Poisson, Siméon Denis, 17
- polar hole, 361, 362
- polar motion, Earth, 385
- polar radius, *see* semimajor axis, Earth ellipsoid
- poles of ignorance, 372
- polynomial fit, of geoid surface, 326
- potential
definition, 5
 at a terrain point, 160
 exterior, 21, 36, 43, 115, 125, 150
 of the topography, 434
 interior, 21
 of the topography, 435
 of a mass line, 14
 of a point mass, 10, 16, 35, 66



- of a pointlike body, 6
 - of a set of mass points, 11
 - of a solid body, 11
 - of a spherical shell, 6, 7, 9
 - of an extended body, 6
 - of the topography, 15
 - origin of word, 29
 - uniqueness, 406
 - potential difference, 17, 94, 160
 - potential energy, 10
 - potential field, 2, 41
 - local behaviour, 42
 - of a dipole, 67
 - of a mass-density layer, 1
 - vertical shift, 46, 47, 71
 - potential theory, 2
 - Potsdam system, 297, 309
 - PRARE (positioning instrument), 344
 - Pratt, John Henry, 141
 - Pratt–Hayford hypothesis, 141, 142
 - precession, orbital, 359
 - precise levelling, 160, 325, 331
 - prediction, 240, 259
 - homogeneous, 269, 270
 - Prey reduction, 175
 - Prey, Adalbert, 175
 - principal axes, of error ellipse, 421
 - Principia* (book), 2
 - prism method of terrain correction, 133
 - propagation delay
 - ionospheric, 348
 - tropospheric
 - dry, 348
 - wet, 348
 - propagation of covariances, 280, 281
 - propagation of variances, 261, 271
 - propellant (GOCE), 317, 371
 - propeller aircraft, 315
 - proper time, 182
 - pseudo-force
 - aircraft motions, 315
 - Earth's rotation, 86
 - moving on a rotating Earth, 88
 - Päijänne, Lake (Finland), 165
 - Pythagoras theorem, 5
- Q**
- quadrature, 221
 - quadrupole, 68
 - quadrupole moment, of the Earth, 68
 - quantisation, 422
 - quantum mechanics, 42
 - quantum number, 423
 - quantum state, 183, 308
 - quantum theory, 308
 - quasi-geoid, 119, 120, 164, 170, 171
 - quasi-geoid height, 166, 171
 - quasi-geoid model, 119, 150
 - computation, 242
- R**
- radar, microwave, 343, 368
 - radio energy, 348
 - radius of curvature
 - transversal, 51
 - Raman effect, 308
 - Rapp, Richard H., 74, 283
 - recursion
 - calculation of normal height, 169
 - calculation of orthometric height, 175
 - computation of Fourier basis functions, 57
 - computation of Legendre polynomials, 63
 - recursive algorithm, 55
 - reduction to sea level, 206
 - redundancy, 356
 - reference benchmark, 162
 - N60, 325
 - N2000, 325
 - reference ellipsoid, 51, 116
 - as a level surface, 85, 98
 - reference latitude, 233, 235, 236
 - reference radius, 104
 - reference-surface thinking, 120
 - regularisation, 208, 248
 - relativity theory, 1
 - relaxation time, 340
 - remote sensing of sea ice, 366
 - “remove” step, 208, 229
 - remove–restore method, 126, 213, 214, 441



- renormalisation, 248
 repeat track, 367
 research school, international, 242, 392
 residual terrain modelling (RTM), 208, 210
 resolution, of measurement, 251
 resonance, 361
 rest length, of spring, 297, 299
 “restore” step, 207, 209, 230, 441
 rheology, 338
 Richer, Jean, 295
 rising dough model, 329
 Robin, Victor Gustave, 117
 rocket engine (GOCE), 371
 Romberg, Arnold, 301
 Romberg, Werner, 221
 root, of mountain, 140, 141, 149
 density, 141, 142
 depth, 144
 rotational potential, 86
 rotational symmetry, 82, 236, 284, 445
 Royal Society of Edinburgh, 17
 Royal Society of London, 2, 4, 17, 118
- S**
 Sacks, Oliver, 4
 salinity (sea water), 324, 331
 salinity gradient (Baltic Sea), 331
 sampling, spatial, 251
 San Francisco (USA), 392
 Sandwell, David, 244
 Sansò, Fernando, 240
 SARAL/AltiKa (satellite), 345
 saros (lunar motion periodicity), 325
 satellite altimetry, 74, 330, 343
 concepts, 347
 geoid, 367
 in archipelagos, 366
 location of sea surface, 373
 measured range, 345
 measurement method, 345
 orbital geometry, 355
 results, 365
 retracking, 365, 366
 return pulse
 analysis, 365
 half-height point, 365
 time measurement, 365
 travel time, 366
 sea-surface variability, 367
 satellite geodesy, 282
 satellite laser ranging (SLR), 358
 satellite orbit, 357
 mean height, 358, 360
 perturbation, 74, 251
 repeat period, 359
 Sun-stationary, 360
 satellite-to-satellite tracking (SST), 371
 Saturn (planet), ring, 295
 scalar field, definition, 399
 scalar product, 219
 definition, 395
 commutativity, 413
 in a function space, 422
 in a vector space, 5, 413, 419
 linearity, 413
 of force and path, 396
 of Legendre polynomials, 64, 424
 of operator and vector, 403
 of two functions, 414
 of vector fields, 395
 of vectors, 396
 on the sphere, 425
 Schrödinger equation, 42
 Schrödinger, Erwin, 42
 Schrödinger’s cat, 42
 Schwarz, Klaus Peter, 240
 Schwarzschild metric, 182
 Schwarzschild, Karl, 182
 sea ice, 366
 sea-floor pressure, 369
 sea-level equation, 336, 337
 angular distance, geocentric, 337
 convolution, 337, 338
 data point, 337, 338
 evaluation point, 337, 338
 sea-level oscillation, 331
 sea-level rise, 327
 global, 345
 Holocene, 339
 Seasat (satellite), 343
 sea-surface residual variation, 349
 sea-surface topography, 324, 332, 333, 345,



- 349, 368
- definition, 325
- change, 328
- determination, 330
- global, 331
- map, 334
- mapping, 344
- sea-surface variability, 359, 367
- secular effect, in sea level, 324
- seismicity, 340
- seismology, 36, 141
- seismometer, 311
- self-adjoint differential equation, 422, 424
- semimajor axis, Earth ellipsoid, 52, 98, 106
- semimajor axis, orbital, 357, 358
- semiminor axis, Earth ellipsoid, 52, 98, 106
- sensitivity, instrument, 298, 299
- Sentinel-3A (satellite), 345
- separation of variables, 43, 48, 53, 446, 448
- shoebox world, 44, 45, 245
- Sideris, Michael, 240
- sight axis, of a level, 159
- signal covariance matrix, 260
- signal variance, 263
- signal variance matrix, 259
 - gravity anomalies, 265
- signal, definition, 260
- significant wave height (SWH), 347, 348
- Simpson integration, 222
- Simpson, Thomas, 221
- Simpson's rule, 221
- singularity, of normal matrix, 351, 354
- sink (vector field), 22, 23, 403
- Skylab (space station), 343
- slowing-down ratio, of time, 182
- snow clearing, 311
- Sodankylä (Finland), 309
- solar panel, 360
- solar time, 362
- Solheim, Dag, 242
- solid body, 11
- solid spherical harmonic, 53
- Somigliana, Carlo, 98
- Somigliana–Pizzetti equation, 98
- source (vector field), 10, 22, 23, 403
- source function, 22
- space domain, 46, 231
- space geodesy, 74
- spatial frequency, 231, 247
- spatial wavelength, 231
- spectral coefficients, 53
- spectral constituent function, 69
- spherical Bouguer reduction, 138
 - mass effect, 137
- spherical cap, 214
- spherical harmonic
 - algebraic sign, 60
 - sectorial, 59, 60
 - semi-wavelength, 61, 79
 - tesseral, 59, 60
 - wavelength, 59
 - zonal, 59, 60
- spherical shell, 7, 9
- spherical symmetry, 339, 383
 - of mass distribution, 36
 - of the Earth, 255, 258
- spherical-cap integration, 150
- spherical-harmonic coefficient, 276, 359
 - as a linear functional, 253
 - fully normalised, 73, 426
- spherical-harmonic expansion, 2, 62, 229, 230
 - coefficients, 53
 - degree-one, 67
 - first terms, 102
 - global, 73
 - high-degree, 79
 - model, 73, 215
 - of the normal gravitational potential, 101
 - of the topography, 61
 - resolution, 61
 - rotational symmetry, 63, 64
- spheroid
 - Bruns, 103
 - Helmert, 103
- spirit level, 159
- Spitsbergen (island), 146
- spline, 240
- spring balance, linear, 297



- spring constant, 297
 spring lengthening, 298
 stabilised platform, 304, 314
 stability (gravimeter), 311
 staff-reading difference, 179
 stationarity, of a stochastic process, 258
 stationary field, 5
 steel manufacture, 302
 stereographic map projection, 228
 Sterneck, Robert von, 296
 stochastic process
 definition, 253
 ergodic, 256
 of location, 254
 on the Earth's surface, 255
 stochastic quantity, 253
 realisation, 254
 Stokes curl theorem, 408
 Stokes equation, 118, 189, 214, 227, 328
 at sea level, 211
 data point, 189
 differentiation, 196
 evaluation point, 189, 227
 exterior space, 189
 geoid height, 188
 in collocation, 269
 in plane co-ordinates, 229
 inner zone, 221
 integration, 189
 spectral form, 187
 Stokes equation and harmonicity, 207
 Stokes kernel, 118, 188, 190, 235
 closed expression, 190
 modified, 216, 217
 on the Earth's surface, 190
 re-written, 234
 smoothness, 219
 spectral form, 189
 Taylor-series expansion, 235
 two-dimensional, 194
 Stokes, George Gabriel, 34, 118
 Strang van Hees, Govert, 234, 240
 Sturm, Jacques, 424
 Sturm-Liouville problem, 424
 submarine measurements, 296
 subsidence, land, 335
 superconduction, 310
 superspring, 304
 support latitude, 234
 surface element, oriented, 407
 surface normal
 Earth, 117
 ellipsoidal, 112
 exterior, 85
 exterior, 22
 surface spherical harmonic, 53, 59, 448
 as a map, 60
 fully normalised, 426
 plotting, 63, 64
 surface spherical harmonics
 linear combination of, 215
 orthogonality, 215
 orthonormality, 276
 sverdrup (unit), 333
 swinging time (pendulum), 295
 symbolic algebra software, 204
 Synthetic Aperture Radar Altimeter
 (SRAL), 345
- T**
- tangent plane, 227, 228
 to a level surface, 90
 tapering, 241
 tapering function, 240
 Taylor-series expansion, 14, 15, 21
 Helmert condensation, 434, 436
 tea break, 311
 telluroid, 119, 170
 definition, 119
 telluroid mapping, 119, 171
 temperature (sea water), 324
 terrain correction (TC), 130–132, 135, 157,
 176, 245
 bias, 132
 calculation, 131, 133
 data point, 246
 equation, 132
 evaluation point, 245–247
 example, 134
 in spherical geometry, 137
 in the exterior space, 248
 prism method, 131, 246
 values, 133



- terrain effect, local, 316
 thermal expansion
 of a pendulum, 295
 of sea water, 327
 thermostat (gravimeter), 303
 thruster, on-board, 359, 364
 tidal decomposition equation of Laplace, 379
 tidal field, 319
 tidal force, 382, 385
 tidal loading, ocean, 388, 389
 tidal potential, 377, 384
 tidal reduction, permanent deformation, 385
 tide, 13, 323, 345, 349
 amplitude, 384
 diurnal, 361, 380, 381
 fortnightly, 380
 frequency, 384
 ocean, 348, 388
 period, 384
 permanent part, 385, 386, 390
 deformation, 385
 effect on height difference, 387
 effect on the geoid, 387
 phase angle, 384
 semidiurnal, 361, 380, 381
 solid-Earth, 348, 393
 theoretical, 378, 382, 385
 tide gauge, 324, 327, 337
 tide-free Earth crust, 388
 tide-free geoid, 386, 388
 Tikhonov regularisation, 355, 357
 Tikhonov, Andrey Nikolayevich, 355
 Toeplitz circulant matrix, 285
 Toeplitz, Otto, 285
 Tom (GRACE satellite), 370
 tomography, seismic, 150
 TOPEX/Poseidon (satellite), 325, 344, 346, 361
 topographic-potential integral
 data point, 433
 evaluation point, 433
 topography, 129, 136
 topography shift to inside geoid, 207
 Torge, Wolfgang, 394
 torque, 299
 torsion balance, 4, 318
 total mass
 of a body, 13
 of a column of air and water, 370
 of a column of matter, 143
 of the Earth, 73, 99, 105, 115
 Toulouse (France), 391
 trace, of a matrix, 421
 transformation surface, geoidal, 326, 393
 trench, ocean, 296
 triangle inequality, 12, 13
 Trieste (Italy), 161
 true anomaly, 358
 Tscherning, Carl Christian, 242, 283
 Tscherning-Rapp formula, 283
 Tukey taper, 240
 turbulence, in a vector field, 404
 Turku (Finland), harbour, 354
 Tuvalu (Pacific Ocean), 336
 twiddle factor (FFT), 431
 Tytyri limestone mine (Lohja, Finland), 384

U
 uncertainty
 a priori, 354
 inside the Earth, 251
 of co-ordinate measurement, 315
 of estimate, 258, 268
 of observation, 251, 266, 270
 of vertical acceleration, 315
 uniform convergence, 417, 434
 unit matrix, 285
 unit sphere, 65, 197, 206, 275, 425
 unknown (adjustment parameter), 306, 356
 upper culmination, of the Moon, 378

V
 Vaasa (Finland), 309
 variance, 254
 variance function, of a stochastic process, 254
 variance matrix of location, 421
 variance of prediction, 266, 268, 271, 289
 definition, 261



- minimisation, 262
 - vector, 395
 - vector field
 - definition, 399
 - differentiable, 22
 - vector space, 415
 - abstract, 413, 414
 - n-dimensional, 418
 - vector sum, 89
 - vectorial product, 397, 398
 - of operator and vector, 403
 - Vening Meinesz equations, 197, 222
 - Vening Meinesz, Felix Andries, 150, 197
 - submarine measurements, 296
 - Verbaandert–Melchior pendulum, 384
 - vertical displacement, of test mass, 302
 - vertical gravity gradient, 100, 121, 306
 - anomalous, 206, 211, 232
 - at sea level, 206
 - kernel, 203, 204
 - free-air, 175, 176, 317
 - inside-rock, 175
 - on the Earth's surface, 116
 - vertical normal gravity gradient, 120, 134, 172
 - vertical reference system, *see* height system
 - viscosity, 338
 - viscous relaxation mode, 340
 - Von Sterneck device, 296
- W**
- water flowing upwards, 165
- water vapour radiometer, 348
- wave equation
 - of matter, 42
 - relativistic, for the electron, 27
- weighing visitors, 311
- weightlessness, 316
- Wenzel, Hans-Georg, 388
- wind field, 404
- wind pile-up, 323
- wire pendulum, very long, 297
- wire-frame model, 354
- work integral, 396, 407, 409
- world aether, 1
- World Geodetic System 1984 (WGS84), 68, 99
- Z**
- zenith angle, of the Moon, 377, 378
- zenith tube, 385
- zero geoid, 386
- zero potential
 - at infinity, 18
 - at mean sea surface, 18
- zero topography compensation level, 144
- zero-length spring, 300, 301, 303
 - how to build, 300



